

Diagnostic Imaging of the
Tympanic Bulla and Temporomandibular Joint
in the Dog, Cat and Rabbit.

by

Alison Margaret King

B.V.M.S., M.V.M., D.V.R., Dip. E.C.V.D.I., M.R.C.V.S.

A thesis submitted for the Degree of
Doctor of Philosophy
in the
Faculty of Veterinary Medicine
of the
University of Glasgow

June, 2008

© Alison M. King 2008

Declaration

I declare that the work presented in this thesis is original and has been carried out solely by the author or with due acknowledgement.

Alison Margaret King

Summary

The area of the skull incorporating the tympanic bulla (TB) and temporomandibular joint (TMJ) is significant clinically in the dog, cat, and more recently the rabbit. Diagnostic imaging is important in the assessment of disease of these structures but there is a relative lack of comparative anatomical information relating to the normal that may be used to understand the abnormal features encountered when using currently available diagnostic imaging modalities.

A review of conventional radiography demonstrated that views for imaging the canine and feline TB could be extrapolated for use in the rabbit but the same did not apply to the TMJ. Plastinated multiplanar anatomical sections proved useful for the identification of anatomical features on corresponding tomographic images. Ultrasound imaging of this region has not been widely reported but allowed evaluation of the TB in all three species, although the information obtained regarding the TMJ was limited. Directly acquired computed tomography (CT) and Magnetic Resonance (MR) images were of better quality than previous publications due to technological advances in the equipment available. Directly acquired images were still better than reconstructed ones and reduced image acquisition times are likely to make this viable in clinical cases. CT produced optimal imaging of the TB but only allowed assessment of the bony elements of the TMJ. Little information was obtained regarding the normal TB using MR imaging due to the indistinguishable signal voids produced by the bone wall and gas lumen. However, T1 weighted sequences allowed identification of intra-articular TMJ soft tissue structures in the dog and rabbit. While opening the mouth altered the areas of the TMJ examined using each modality, it did not improve visualisation of the intra-articular structures.

The introduction of fluid into the middle ear cavity of dog, cat and rabbit cadavers aided identification of the TB and acted as a model of one of the major features of acute otitis media, or inflammation of the middle ear cavity. CT was most accurate at identifying middle ear material in cadavers and clinical cases, while ultrasound produced better results than radiography in cadavers but not clinical cases. These imaging modalities also proved useful in the characterisation of the unexpected anatomical anomalies that were encountered during the study.

The results of this study indicate that the optimal imaging technique will vary with the species and area being examined, and that extrapolation between species is not always appropriate. Continual improvements in technology and image quality make studies such as this necessary to allow selection of the most appropriate single or combination of imaging techniques and to obtain the maximum amount of information from the resulting images.

List of publications arising from this work

(Please note author's maiden name of Dickie)

King AM, Hall J, Cranfield F, Sullivan M. (2007) Anatomy and ultrasonographic appearance of the tympanic bulla and associated structures in the rabbit. *The Veterinary Journal* 173, 638-644.

King A.M., Weinrauch S A, Doust R, Hammond G, Sullivan M. (2007) Comparison of ultrasonography, radiography and a single computed tomography slice for fluid identification within the feline tympanic bulla. *The Veterinary Journal* 173, 512 – 521.

Doust R, King A, Hammond G, Cave T, Weinrauch S, Mellor, D, Sullivan M. (2007) Assessment of middle ear disease in the dog: A comparison of diagnostic imaging modalities. *Journal of Small Animal Practice*, 48: 188-192.

King A.M. (2006) Development, advances and applications of diagnostic ultrasound in animals. *The Veterinary Journal*, 171: 408-420.

Hammond G J C, Sullivan M, Weinrauch S, King A.M. (2005) A comparison of the rostro-caudal open mouth and rostro 10° ventro-caudodorsal oblique radiographic views for imaging fluid in the feline tympanic bulla. *Veterinary Radiology & Ultrasound* 46: 205-209.

Dickie A M, Doust R, Cromarty L, Johnson V S, Sullivan M, Boyd J S. (2003) Comparison of ultrasonography, radiography and a single computed tomography slice for the identification of fluid within the canine tympanic bulla. *Research in Veterinary Science*, 75: 209-216.

Dickie A M, Doust R, Cromarty L, Johnson V S, Sullivan M, Boyd J S. (2003) Ultrasound imaging of the canine tympanic bulla. *Research in Veterinary Science*, 75: 121-126.

Dickie A M, Schwarz T, Sullivan M. (2002) Temporomandibular joint morphology in Cavalier King Charles Spaniels. *Veterinary Radiology & Ultrasound*, 43: 260-266.

Dickie A M, Sullivan M. (2001). The effect of obliquity on the radiographic appearance of the temporomandibular joint in dogs. *Veterinary Radiology & Ultrasound*, 42: 205-217.

Acknowledgements

I would like to express sincere gratitude to my supervisors, Professor Martin Sullivan, who has guided me through all my academic imaging achievements, culminating in the production of this thesis and Professor Jack Boyd, who first introduced me to the field of diagnostic imaging and fostered my interest in ultrasound.

This work could not have been performed without the support of the University of Glasgow Small Animal Hospital and all its staff. In particular, I am very grateful to diagnostic imaging residents past and present, Tobias Schwarz, Vicky Johnson, Gawain Hammond, Tim Trevail and Ines Carrera, and also Ross Doust, for their help with the clinical aspects of the study and subsequent publications. I would also like to thank radiologists Gill Cameron and Nicola Milne, and imaging technician Iain McNaught for their technical support. Much of the comparative imaging work was carried out in association with summer vacation undergraduate research students Steve Weinrauch, Fiona Cranfield, Jason Hall and Jamie Posthumus.

The University of Glasgow Veterinary Anatomy Unit and Biological Services were invaluable in sourcing the cadaver material for this work. In particular, I would like to acknowledge the assistance I received from anatomy technicians David Newham, Alan Purvis and Pat Wilson with subsequent storage and processing of the material. I would also like to thank Jim Mullin of the 7Tesla MRI unit for his patience and persistence in the acquisition of the MRI images, and Richard Irvine from the Division of Pathological Sciences for his help with photography of the anatomical sections.

Funding for various components of the work was very generously provided by the Petplan Charitable Trust, the Royal College of Veterinary Surgeons Trust, the British Small Animal Veterinary Association Petsavers grants and the University of Glasgow Veterinary School Summer Vacation Scholarship programme. I am also grateful to Ramsay MacIver of Dynamic Imaging for the loan of the Diasus ultrasound machine.

Finally, I have to thank 'Baby' King for the non-negotiable deadline for completion of this thesis and my husband George for single handedly running the farm and renovating the house while I have been glued to the laptop. I am also indebted to my long suffering parents for their continuing help and support in all my endeavours.

Table of Contents	Page
List of figures	xii
List of tables	xviii
Chapter 1. General Introduction	1
1.1 Companion animal species	1
1.2. Relationship between anatomy and diagnostic imaging	1
1.3. Anatomy of the temporal region of the skull	4
1.4. Radiography	6
1.5. Ultrasound	8
1.6. Computed Tomography	11
1.7. Magnetic Resonance Imaging	14
1.8. Clinical conditions affecting the TB	17
1.9. Conditions affecting the TMJ	22
Chapter 2. Anatomy of the tympanic bulla, temporomandibular joint and associated structures in the dog, cat and rabbit.	25
2.1 Introduction	
2.1.1. Comparison between diagnostic images and cadaver material	25
2.1.2. Plastination	26
2.1.3. Anatomy of the TB	27
2.1.4. Anatomy of the TMJ	30
2.1.5. Skull measurements	33
2.1.6. Aims	34
2.2 Materials and Methods	
2.2.1. Cadaver material	35
2.2.2. Bony anatomy of the TB and TMJ in the dog, cat and rabbit.	35
2.2.3. Soft tissue anatomy of the TB, TMJ and surrounding areas in the dog, cat and rabbit.	36
2.2.4. Multiplanar anatomy of the TB and TMJ in the dog, cat and rabbit.	36
2.2.5. Image production	37
2.2.6. Preservation of material using plastination	37
2.2.7. Skull measurements	37

2.3 Results	
2.3.1. Bony anatomy of the TB and TMJ in the dog, cat and rabbit	40
2.3.2. Soft tissue anatomy of the TB, TMJ and surrounding areas in the dog, cat and rabbit.	59
2.3.3. Multiplanar sections of the TB and TMJ in the dog, cat and rabbit	73
2.3.4. Plastination	102
2.3.5. Facial index in the dog, cat and rabbit	102
2.3.6. Rotational angle of the canine mandibular condyle	103
2.4 Discussion	
2.4.1. Bony anatomy of the TB and TMJ	106
2.4.2. Soft tissue anatomy of the TB and TMJ	108
2.4.3. Multiplanar anatomy	110
2.4.4. Plastination	111
2.4.5. Facial index	112
2.4.6. Rotational angle	113
Chapter 3. Radiography of the tympanic bulla, temporomandibular joint and associated structures in the dog, cat and rabbit.	115
3.1 Introduction	
3.1.1. Radiography of the head	115
3.1.2. Radiography of the TB and associated structures	117
3.1.3. Radiography of the TMJ and associated structures	120
3.1.4. Aims	123
3.2 Materials and Methods	
3.2.1 Cadaver material	124
3.2.2 Radiographic equipment	124
3.2.3. Radiographic views.	126
3.2.4. Additional procedures	127
3.2.5. Image production	127
3.3 Results	
3.3.1. Radiography	131
3.3.2. Lateral rotational angles in emascerated skulls	131
3.3.3. Long axis rotational angles in emascerated skulls	151
3.3.4. Ventral rotational angles in emascerated skulls	168
3.3.5. Cadaver heads	171

3.4 Discussion	
3.4.1. Material and technical considerations	189
3.4.2. Radiography of the TB in the dog, cat and rabbit.	192
3.4.3. Radiography of the TMJ in the dog, cat and rabbit	196
Chapter 4. Ultrasound of the tympanic bulla, temporomandibular joint and associated structures in the dog, cat and rabbit.	201
4.1 Introduction	
4.1.1. Technical aspects of ultrasound image production	201
4.1.2. Applications of ultrasound relating to the TB and TMJ	203
4.1.3. Aims	205
4.2 Materials and Methods	
4.2.1. Equipment	206
4.2.2 Image production and processing	206
4.2.3. Preparation of cadaver material	206
4.2.4. Ultrasound examination	206
4.2.5. Additional Procedures	207
4.3 Results	
4.3.1. Optimum equipment for imaging the TB	209
4.3.2. Optimum transducer position for imaging the TB	210
4.3.3. Sonographic appearance of the TB and associated structures	210
4.3.4. Optimum equipment for imaging the TMJ	226
4.3.5. Optimum transducer position for imaging the TMJ	226
4.3.6. Sonographic appearance of the TMJ	227
4.3.7. Additional procedures	234
4.4 Discussion	
4.4.1. Ultrasound of the TB in the dog, cat and rabbit	253
4.4.2. Ultrasound of the TMJ in the dog, cat and rabbit	258
Chapter 5. Computed tomography of the tympanic bulla, temporomandibular joint and associated structures in the dog, cat and rabbit.	264
5.1 Introduction	
5.1.1 Technical aspects regarding CT of the temporal region	264
5.1.2. Clinical applications of CT relating to the TB	266

5.1.3. Applications of CT relating to the TMJ	267
5.1.4. Aims	268
5.2 Materials and Methods	
5.2.1. Cadaver material	269
5.2.2. CT equipment and procedure	269
5.2.3. Image analysis and reproduction	270
5.3 Results	
5.3.1. CT appearance of the gas and fluid-filled TB in the dog, cat and rabbit	272
5.3.2. CT appearance of the open and closed TMJ in the dog, cat and rabbit	289
5.3.3. Effect of windowing	293
5.4 Discussion	
5.4.1. Material and technical considerations	311
5.4.2. CT of the TB in the dog ,cat and rabbit	315
5.4.3. CT of the TMJ in the dog, cat and rabbit	317
Chapter 6. Magnetic resonance imaging of the tympanic bulla, temporomandibular joint and associated structures in the dog, cat and rabbit.	320
6.1 Introduction	
6.1.1. Technical aspects of MR image production	320
6.1.2. MRI of the TB and associated structures	322
6.1.3. MRI of the TMJ and associated structures	323
6.1.4. Aims	324
6.2 Materials and Methods	
6.2.1. Cadaver material	325
6.2.2. MRI equipment	325
6.2.3. Image analysis and reproduction	326
6.3 Results	
6.3.1. Technical considerations	327
6.3.2. MRI appearance of the gas and fluid-filled TB in the dog, cat and rabbit	328
6.3.3. MRI appearance of the closed and open TMJ in the dog, cat and rabbit	361

6.4 Discussion	
6.4.1. Material and technical considerations	392
6.4.2. MRI of the TB in the dog, cat and rabbit	396
6.4.3. MRI of the TMJ in the dog, cat and rabbit	398
Chapter 7. Comparison of imaging modalities for the investigation of otitis media in the dog, cat and rabbit.	
7.1 Introduction	
7.1.1 Otitis media	401
7.1.2. Radiography in the investigation of otitis media	401
7.1.3. Sonographic investigation of otitis media.	403
7.1.4. CT in the investigation of otitis media	404
7.1.5. MRI in the investigation of otitis media	405
7.1.6. Aims	407
7.2 Materials and Methods	
7.2.1. Comparison of imaging techniques in cadavers	408
7.2.2. Comparison of imaging techniques in canine otitis media cases	415
7.2.3. Investigation of the TB in two Cavalier King Charles Spaniels	417
7.3 Results	
7.3.1. Cadaver study	418
7.3.2. Clinical case series study	429
7.3.3. Investigation of the TB in two Cavalier King Charles Spaniel	436
7.4 Discussion	
7.4.1. Material and technical considerations	439
7.4.2. Technical considerations of the diagnostic imaging procedures	440
7.4.3. Comparison between the imaging modalities in cadavers	443
7.4.4. Comparison between imaging techniques in canine otitis media cases	449
7.4.5. Investigation of the TB in two Cavalier King Charles Spaniels	453
Chapter 8. Anatomical anomalies of the rabbit skull and canine temporomandibular joint.	455
8.1 Introduction	455
8.1.1. Aims	456
8.2 Materials and Methods	

8.2.1. CKCS cadaver material	457
8.2.2. Diagnostic imaging of CKCS cadavers	457
8.2.3. Review of CKCS cases	457
8.2.4. Rabbit cadaver material and diagnostic imaging	458
8.3 Results	
8.3.1. Anatomy and radiography of emascerated CKCS skulls	459
8.3.2. Radiography, CT and MRI of the CKCS cadavers	460
8.3.3. Review of clinical cases	462
8.3.4. Rotational angles	464
8.3.5. Anatomical observations in the emascerated rabbit skulls.	483
8.3.6. CT and MRI appearance of anatomical variations in the rabbit skull.	483
8.4 Discussion	
8.4.1. TMJ dysplasia in CKCS	489
8.4.2. Variations in rabbit skull anatomy	496
Chapter 9. General discussion.	498
Reference List	510

List of Figures

Page

Chapter 2

Figure 2.2.1.	Features used to measure facial width and length in dog, cat and rabbit skulls for calculation of the facial index.	39
Figure 2.2.2.	Measurement of the rotational angle of the mandibular condyles.	39
Figure 2.3.1	Bony components of a typical canine TB.	48
Figure 2.3.2.	Bony components of a typical feline TB.	49
Figure 2.3.3.	Bony components of a typical rabbit TB.	50
Figure 2.3.4.	Bony components of a typical canine TMJ.	52
Figure 2.3.5.	Regions of the articular surfaces of the canine TMJ.	53
Figure 2.3.6.	Bony components of a typical feline TMJ.	54
Figure 2.3.7.	Regions of the articular surfaces of the feline TMJ.	55
Figure 2.3.8.	Bony components of a typical rabbit TMJ.	56
Figure 2.3.9.	Regions of the articular surfaces of the rabbit TMJ.	58
Figure 2.3.10.	Soft tissue structures associated with the TB and TMJ in the dog.	65
Figure 2.3.11.	Soft tissue structures associated with the TB and TMJ in the cat.	67
Figure 2.3.12.	Soft tissue structures associated with the TB and TMJ in the rabbit.	70
Figure 2.3.13.	Transverse sections through the region of the TB and TMJ in the dog.	75
Figure 2.3.14.	Transverse sections through the region of the TB and TMJ in the cat	78
Figure 2.3.15.	Transverse sections through the region of the TB and TMJ in the rabbit.	81
Figure 2.3.16.	Sagittal sections through the region of the TB and TMJ in the dog.	84
Figure 2.3.17.	Sagittal sections through the region of the TB and TMJ in the cat.	87
Figure 2.3.18.	Sagittal sections through the region of the TB and TMJ in the rabbit.	92
Figure 2.3.19.	Dorsal sections through the region of the TB and TMJ in the dog.	95
Figure 2.3.20.	Dorsal sections through the region of the TB and TMJ in the cat.	97
Figure 2.3.21.	Dorsal sections through the region of the TB and TMJ in the rabbit.	100
Figure 2.3.22.	Examples of plastinated transverse sections through the region of the TB and TMJ in the dog.	102

Chapter 3

Figure 3.2.1.	V.R 30/90T (S.M.R) X-Ray machine.	128
Figure 3.2.2.	Radiographic cassettes.	128

List of Figures continued

Page

Figure 3.2.3.	Equipment designed and constructed to allow repeatable positioning of the skull for radiographic examination.	128
Figure 3.2.4.	Canine skull mounted in the equipment using a single clamp and in a lateral position prior to the lateral rotational series.	129
Figure 3.2.5.	Feline skull mounted in the equipment using an additional clamp and in a lateral position prior to the lateral rotational series.	129
Figure 3.2.6.	Rabbit skull mounted using a plastic cup and packed with cotton wool in a lateral position prior to the lateral rotational series.	129
Figure 3.2.7.	Canine skull mounted in the equipment in a lateral position prior to the long axis rotational series.	130
Figure 3.2.8.	Canine skull mounted in the equipment in a rostrocaudal position prior to the dorsal and ventral rotational series.	130
Figure 3.2.9.	Modification of the equipment to allow positioning of rabbit cadaver heads for radiography.	130
Figure 3.3.1.	Mesaticephalic dog skull. Radiographs taken at lateral rotational angles from 0 (lateral) to 70 and 90 degrees (rostrocaudal).	138
Figure 3.3.2.	Lateral rotation of 15° in a dolichocephalic dog skull.	143
Figure 3.3.3.	Lateral rotation of 30° in a brachycephalic dog skull.	143
Figure 3.3.4.	Cat skull. Radiographs taken at lateral rotational angles from 0 (lateral) to 90 degrees (rostrocaudal).	144
Figure 3.3.5.	Rabbit skull. Radiographs taken at lateral rotational angles from 0 (lateral) to 90 degrees (rostrocaudal).	148
Figure 3.3.6.	Mesaticephalic dog skull. Radiographs taken at long axis rotational angles from 10 – 90 degrees (ventrodorsal).	156
Figure 3.3.7.	Long axis rotation of 20° in a dolichocephalic dog skull.	161
Figure 3.3.8.	Long axis rotation of 30° in a brachycephalic dog skull.	161
Figure 3.3.9.	Cat skull. Radiographs taken at long axis rotational angles from 10 to 90 degrees (ventrodorsal).	162
Figure 3.3.10.	Rabbit skull. Radiographs taken at long axis rotational angles from 10 to 90 degrees (ventrodorsal).	165
Figure 3.3.11.	Mesaticephalic dog skull. Radiographs taken at ventral rotational angles of 10 and 30 to 80 degrees with the mouth closed and 0 (rostrocaudal view) to 30 degrees with the mouth open.	172

List of Figures continued

Page

Figure 3.3.12.	Cat skull. Radiographs taken at ventral rotational angles of 10 and 30 to 80 degrees with the mouth closed and 0 (rostrocaudal view) to 30 degrees with the mouth open.	177
Figure 3.3.13.	Rabbit skull. Radiographs taken at ventral rotational angles of 10 and 30 to 80 degrees with the mouth closed and 0 (rostrocaudal view) to 30 degrees with the mouth open.	181
Figure 3.3.14.	Rabbit skull. Radiographs taken at dorsal rotational angles of 10 and 30 to 80 degrees with the mouth closed and 0 (rostrocaudal view) to 30 degrees with the mouth open.	185
Figure 3.3.15.	Radiographs produced in cadaver heads.	188
Chapter 4		
Figure 4.2.	Ultrasound machines and transducers.	208
Figure 4.3.1.	Transducer positions for imaging the TB and associated structures in the dog, cat and rabbit.	214
Figure 4.3.2.	Ultrasound appearance of the gas-filled external ear canal in the dog and rabbit from a lateral approach with corresponding line diagrams.	216
Figure 4.3.3.	Ultrasound appearance of the gas-filled TB in the dog and rabbit from a lateral approach with corresponding line diagrams.	218
Figure 4.3.4.	Ultrasound appearance of the gas and fluid-filled TB from a ventral approach in the dog with corresponding line diagrams.	219
Figure 4.3.5.	Ultrasound appearance of the gas and fluid-filled TB from a ventral approach in the cat with corresponding line diagrams.	220
Figure 4.3.6.	Ultrasound appearance of the gas and fluid-filled TB from a ventral approach in the rabbit with corresponding line diagrams.	223
Figure 4.3.7.	Transducer positions for imaging the TMJ in the dog, cat and rabbit.	235
Figure 4.3.8.	Ultrasound appearance of the TMJ in the dog and cat from a lateral approach and vertical transducer orientations with corresponding line diagrams.	238
Figure 4.3.9.	Ultrasound appearance of the TMJ in the dog and cat from a lateral approach and horizontal transducer orientations with corresponding line diagrams.	241

List of Figures continued

Page

Figure 4.3.10.	Ultrasound appearance of the TMJ in the dog and cat from a caudal approach and vertical transducer orientation with corresponding line diagrams.	245
Figure 4.3.11.	Ultrasound appearance of the TMJ in the dog and cat from a rostral approach and rostrodorsal – caudoventral transducer orientation with corresponding line diagrams.	249
Figure 4.3.12.	Ultrasound appearance of the TMJ in the rabbit with corresponding line diagrams.	251
 Chapter 5		
Figure 5.2.1.	Elscent Twin Flash CT scanner.	271
Figure 5.2.2.	Rabbit cadaver head demonstrating positioning in the CT scanner.	271
Figure 5.3.1.	Transverse CT images of the gas and fluid-filled canine TB.	276
Figure 5.3.2.	Transverse CT images of the gas and fluid-filled feline TB.	277
Figure 5.3.3.	Transverse CT images of the gas and fluid-filled rabbit TB.	278
Figure 5.3.4.	Sagittal CT images of the gas and fluid-filled canine TB.	279
Figure 5.3.5.	Sagittal CT images of the gas and fluid-filled feline TB.	282
Figure 5.3.6.	Sagittal CT images of the gas and fluid-filled rabbit TB.	283
Figure 5.3.7.	Dorsal CT images of the gas and fluid-filled canine TB.	284
Figure 5.3.8.	Dorsal CT images of the gas and fluid-filled feline TB.	286
Figure 5.3.9.	Dorsal CT images of the gas and fluid-filled rabbit TB.	287
Figure 5.3.10.	Transverse CT images of the closed and open canine TMJ.	295
Figure 5.3.11.	Transverse CT images of the closed and open feline TMJ.	297
Figure 5.3.12.	Transverse CT images of the closed and open rabbit TMJ.	299
Figure 5.3.13.	Sagittal CT images of the closed and open canine TMJ.	301
Figure 5.3.14.	Sagittal CT images of the closed and open feline TMJ.	303
Figure 5.3.15.	Sagittal CT images of the closed and open rabbit TMJ.	305
Figure 5.3.16.	Dorsal CT images of the closed and open canine TMJ.	306
Figure 5.3.17.	Dorsal CT images of the closed and open feline TMJ.	308
Figure 5.3.18.	Dorsal CT images of the closed and open rabbit TMJ.	309
Figure 5.3.19.	Transverse CT images of the empty and fluid-filled rabbit TB and TMJ viewed using different windows.	310

List of Figures continued

Page

Chapter 6

Figure 6.2.1.	Bruker Biospin Avance 7T (300MHz) Magnetic Resonance Imaging system.	326
Figure 6.2.2.	Gradient set and radiofrequency resonator combinations.	326
Figure 6.3.1.	Transverse MR images through the TB in the dog.	330
Figure 6.3.2.	Transverse MR images through the TB in the cat.	334
Figure 6.3.3.	Transverse MR images through the TB in the rabbit.	337
Figure 6.3.4.	Sagittal MR images through the TB in the dog.	341
Figure 6.3.5.	Sagittal MR images through the TB in the cat.	345
Figure 6.3.6.	Sagittal MR images through the TB in the rabbit.	349
Figure 6.3.7.	Dorsal MR images through the TB in the dog.	353
Figure 6.3.8.	Dorsal MR images through the TB in the cat.	355
Figure 6.3.9.	Dorsal MR images through the TB in the rabbit.	358
Figure 6.3.10.	Transverse MR images through the TMJ in the dog.	364
Figure 6.3.11.	Transverse MR images through the TMJ in the cat.	368
Figure 6.3.12.	Transverse MR images through the TMJ in the rabbit.	372
Figure 6.3.13.	Sagittal MR images through the TMJ in the dog.	376
Figure 6.3.14.	Sagittal MR images through the TMJ in the cat.	379
Figure 6.3.15.	Sagittal MR images through the TMJ in the rabbit.	381
Figure 6.3.16.	Dorsal MR images through the TMJ in the dog.	383
Figure 6.3.17.	Dorsal MR images through the TMJ in the cat.	387
Figure 6.3.18.	Dorsal MR images through the TMJ in the rabbit.	389

Chapter 7

Figure 7.2.1.	Radiographic positioning of the canine cadaver head for the rostral-caudal open mouth view.	413
Figure 7.2.2.	Radiographic positioning of the rabbit head using foam wedges.	413
Figure 7.3.1.	Radiographs of canine, feline and rabbit cadaver heads with a fluid-filled left TB and a gas-filled right TB.	421
Figure 7.3.2.	Ultrasound images of canine, feline and rabbit cadaver heads with a fluid-filled left TB and a gas-filled right TB.	423
Figure 7.3.3.	CT images of cadaver heads with a fluid-filled left TB and a gas-filled right TB.	424

List of Figures continued

Page

Figure 7.3.4.	Images of the TB in CKCS undergoing MRI examination for the investigation of neurological signs	437
Figure 7.3.5	Ultrasound images of the left TB of a CKCS with fluid in the TB lumen identified during an MRI examination.	438
Chapter 8		
Figure 8.3.1.	Gross appearance of the TMJ in CKCS skulls.	465
Figure 8.3.2.	Radiographic appearance of the TMJ in emascerated CKCS skulls.	466
Figure 8.3.3.	Radiographic appearance of the TMJ in CKCS cadavers.	468
Figure 8.3.4.	CT images through the TMJ in a CKCS cadaver viewed using a bone window.	470
Figure 8.3.5.	T1 weighted MRI sections through the TMJ of a CKCS cadaver.	474
Figure 8.3.6.	Examples of typical radiographs obtained in live CKCS dogs undergoing radiography of the head for the investigation of a variety of clinical conditions.	479
Figure 8.3.7.	Examples of typical transverse sections through the TMJ of live CKCS dogs undergoing CT of the head for the investigation of a variety of clinical conditions.	480
Figure 8.3.8.	Examples of typical MR images through the TMJ of live CKCS dogs undergoing MRI of the head for the investigation of a variety of clinical conditions.	481
Figure 8.3.9.	Anatomical variations observed in rabbit skulls.	485
Figure 8.3.10.	Sagittal CT images through a rabbit cadaver, viewed using a bone window.	487
Figure 8.3.11.	Sagittal T1 weighted MR images through a rabbit cadaver.	488

	List of Tables	Page
Chapter 2		
Table 2.3.1.	Key for the bony components of the typical canine, feline and rabbit TB, demonstrated in Figures 2.3.1. to 2.3.3.	47
Table 2.3.2.	Dimensions of the TB in the dog, cat and rabbit.	51
Table 2.3.3.	Key for the bony components of the typical canine, feline and rabbit TMJ, demonstrated in Figures 2.3.4., 2.3.6 and 2.3.8.	51
Table 2.3.4.	Key for anatomical features demonstrated in the dog and cat in figures 2.3.10 and 2.3.11.	64
Table 2.3.5.	Key for anatomical features demonstrated in the rabbit in figures 2.3.12.	69
Table 2.3.6.	Key for anatomical features demonstrated in Figures 2.3.13 to 2.3.21	74
Table 2.3.7.	Facial index calculated in 50 canine skulls	104
Table 2.3.8.	Rotational angles of the mandibular condyles in 38 canine skulls.	105
Chapter 3		
Table 3.3.1.	Key for anatomical features demonstrated in Figures 3.3.1 to 3.3.14 depicting the radiographic appearance of the TB and associated structures in the dog, cat and rabbit.	137
Chapter 4		
Table 4.3.1.	Key for anatomical features demonstrated in Figures 4.3.2. 4.3.6. depicting the ultrasound appearance of the TB and associated structures in the dog, cat and rabbit.	215
Table 4.3.2.	Key for anatomical features demonstrated in Figures 4.3.8. to 4.3.12. depicting the ultrasound appearance of the TMJ and associated structures in the dog, cat and rabbit.	237
Chapter 5		
Table 5.1.	Anatomical features associated with the TB. Key for figures 5.3.1. to 5.3.9.	275
Table 5.2.	Anatomical features associated with the TMJ. Key for figures 5.3.10 to 5.3.18.	294

List of Tables continued

Page

Chapter 6

Table 6.1.	Anatomical features associated with the TB. Key for figures 6.3.1. to 6.3.9.	329
Table 6.2.	Anatomical features associated with the TMJ. Key for figures 6.3.10 to 6.3.18.	363

Chapter 7

Table 7.1.	Results from previous imaging studies of canine otitis media.	403
Table 7.2.1.	The formulae used to calculate the accuracy, sensitivity, specificity, positive and negative predictive values for each of the techniques.	414
Table 7.2.2.	The levels of agreement for Kappa analysis (k) performed to determine the inter-observer variance in interpretation of the imaging procedures performed.	414
Table 7.3.1.	Accuracy, sensitivity, specificity, positive (PPV) and negative predictive values (NPV), and interobserver agreement (k=kappa) calculated for each of the techniques used to identify fluid within the TB in canine cadavers	427
Table 7.3.2.	Accuracy, sensitivity, specificity, positive (PPV) and negative predictive values (NPV), and interobserver agreement (k=kappa), calculated for each of the techniques used to identify fluid within the TB in feline cadavers.	427
Table 7.3.3.	Accuracy, sensitivity, specificity, positive (PPV) and negative predictive values (NPV), and interobserver agreement (k=kappa), calculated for each of the techniques used to identify fluid within the TB in rabbit cadavers.	428
Table 7.3.4.	Sensitivity, specificity, positive (PPV) and negative predictive values (NPV), and interobserver agreement (k=kappa), calculated for each of the techniques used to examine the TB in clinical cases of canine otitis media cases.	431
Table 7.3.5.	Interobserver agreement (k=kappa), calculated for the independent identification of TB wall and lumen changes using each of the imaging techniques	431

List of Tables continued

Page

Table 7.3.6.	Univariable binary logistic regression analysis of the association between consensual CT and radiographic interpretation	432
Table 7.3.7.	Univariable binary logistic regression analysis of the association between consensual CT and radiologist A's interpretation of each radiographic view.	432
Table 7.3.8.	Univariable binary logistic regression analysis of the association between consensual CT and radiologist B's interpretation of each radiographic view.	433
Table 7.3.9.	Univariable binary logistic regression analysis of the association between consensual CT and sonographers A's interpretation	433
Table 7.3.10.	Univariable binary logistic regression analysis of the association between consensual radiographic and sonographers A's interpretation.	434
Table 7.3.11.	Multivariable binary logistic regression analysis of the association between consensual CT, and consensual radiographic and sonographers A's interpretation.	434
Table 7.3.12.	Univariable ordinal regression analysis of the association between increasing CT grade and radiographic and sonographers A's results interpretation.	435
Chapter 8		
Table 8.3.1.	Details of adult CKCS that had undergone a radiographic examination of the skull between 1991 and 2001.	478
Table 8.3.2.	The rotational angles measured from the dorsoventral radiographs of CKCS.	482

Chapter 1. General Introduction

1.1 Companion animal species

Dogs and cats are the most common companion animals species in the United Kingdom and since 2002 their numbers have remained relatively constant at 6.1 and 7.5 million respectively (PFMA 2006). With pet insurance now commonplace, owners have an increased expectation of the level of clinical investigation and management available for their pet.

However, there has recently been a marked increase in the popularity of rabbits as companion animals, making these the third most popular mammalian pet in the United Kingdom (Nicholson 2001, Meredith 2006). The domestic rabbit *Oryctolagus cuniculus*, is a descendent of the European wild rabbit (Shively 1979). Rabbits differ from rodents in that they have an extra pair of incisor teeth known as peg teeth, which are reduced in size and located immediately caudal to the large central pair in the upper arcade (Shively 1979). They are therefore members of the order Lagomorpha along with hares and pikas (Shively 1979, Crossley 2003). In addition to being kept as pets, rabbits are also used by man for biomedical research and the production of meat and fur. (Shively 1979). The study of the rabbit is therefore of great economic, scientific and clinical interest, so further investigations in this species are warranted (Barone and others 1973).

1.2. Relationship between anatomy and diagnostic imaging

An image is a likeness or representation of a person or thing. To image is to produce a pictorial representation of a part of the body for diagnostic medical purposes (Schwarz 1993). In the medical professions, diagnostic imaging is the science that produces and records images of structures located within the intact body, to assist in the diagnosis and treatment of disease (Tidwell 1999).

All imaging modalities rely on the interaction of energy with body tissue and the detection and recording of the resulting alterations in signal. The complex mathematical equations involved are converted into a pictorial format and displayed as images for interpretation. This relies on computing power and therefore image quality depends heavily on the equipment available (Tidwell 1999). Older publications will typically tend to have poorer quality images simply due to equipment limitations (Feeney and others 1991). Image

quality depends on many factors including resolution, which is the ability to distinguish between two points. Spatial resolution relates to the distinction between objects according to their physical location while contrast resolution relates to their differences in density (Curry and others 1990).

Anatomy is the science of the physical structure of an animal (Schwarz 1993). In the earlier phases of its development, anatomy signified the cutting apart or disassociation of parts of the body and was purely a descriptive science based on what could be observed with the naked eye. Dissection still remains an important anatomical technique although the introduction of the microscope and other technological advances have allowed development beyond macroscopic or gross anatomy and there are now many specialised fields and methods of work. Once such area is applied anatomy, the consideration of anatomical facts in relation to surgery and physical diagnosis (Ellenport 1975).

Accurate interpretation of diagnostic images depends directly on the differentiation between normal and abnormal anatomy (Nyland and others 1995). Radiography is currently the most widely available diagnostic imaging modality and requires an understanding of topographic anatomy, the position of various parts of the body relative to each other (Ellenport 1975). Computed tomography (CT), Magnetic Resonance Imaging (MRI) and ultrasound are all forms of tomography and therefore depict a section through the body free from superimposition by overlying structures. Planes can be transverse or transaxial, dorsal or coronal, sagittal and oblique (Tidwell 1999). This has altered the way in which anatomical structures are perceived on images (Assheuer and Sager 1997, Zook and others 1981) and interpretation requires an appreciation of how the structures should appear in each of these planes (Tidwell 1999). A paucity of illustrations of normal transverse sections of the canine body was reported (Assheuer and Sager 1997, Zook and others 1981) but now that CT and MRI are becoming much more widely available in the veterinary field, this is rapidly being redressed in the dog (Assheuer and Sager 1997, Zook and others 1981, George and Smallwood 1992).

When interpreting diagnostic images, it is often useful to have normal images or specimens available for comparison (Harcourt-Brown 2003). Cadavers have been used for comparison with diagnostic images to determine normal morphological detail and sections through a cadaver have been compared with corresponding tomographic images (Zook and others

1981, George and Smallwood 1992, Tasaki and Westesson 1993, Weller and others 1999a, Morrow and others 2000). However, decay is an impediment to morphological studies (Miklošová and Sivrev 1999). Information must therefore be recorded pictorially using photography before the specimen is discarded (Zook and others 1981, George and Smallwood 1992) or alternatively a suitable technique must be found to preserve the material allowing re-examination at a later date (Miklošová and Sivrev 1999). This can be achieved in a variety of ways (Gillbe 1973, Zook and others 1981, Ström and others 1988, Morrow and others 2000, Rodriguez and others 2002). Aquatic formalin solutions have good display, preserving, disinfecting and deodorant qualities and are used in various forms in most anatomical and preparatory laboratories throughout the world (Gillbe 1973, Zook and others 1981, Miklošová and Sivrev 1999, Morrow and others 2000). Material can also be frozen at temperatures varying from -25° to -70° (Ström and others 1988, Rodriguez and others 2002). Plastination is a relatively new preservation technique that has several advantages over traditional methods. The material produced has been reported as an excellent adjunct for studying sectional anatomy and for correlation with images produced by ultrasonography, CT or MRI (Miklošová and Sivrev 1999).

Ethical, financial or logistic reasons may necessitate cadavers being used in place of live animals to produce images of normal structures (Jones and others 1995, Weller and others 1999a, Morrow and others 2000) and to investigate imaging phenomenon (Barthez and others 1996). This is a well established technique in the medical literature with advantages being ease of procurement and storage, use of lower technical factors and therefore less equipment wear, the ability to maximise the use of animals already scheduled for euthanasia (Jones and others 1995) and the absence of motion artefacts (Tasaki and Westesson 1993). In addition, the images generated can then be compared directly with the structure that produced them although care must be taken that the position of cadaver is maintained between imaging and sectioning (George and Smallwood 1992).

However, problems with cadavers can include a lack of clinical history and a difference in age and sex compared with patient material (Tasaki and Westesson 1993). Care must be taken when using fresh material due to the occurrence of post mortem degeneration that may alter the appearance of the area of interest, or mimic anatomical structures or pathology (Weller and others 1999a). The ultrasonographic images of canine stifles obtained immediately before and after euthanasia were reported to be unchanged (Reed and

others 1995, Long and Nyland 1999). However, post mortem changes have been observed in studies involving sonographic evaluation of the equine temporomandibular joint (TMJ) (Weller and others 1999a), CT of the equine head (Morrow and others 2000), CT of the canine vertebral column (Jones and others 1995) and MRI of human TMJ (Tasaki and Westesson 1993). Consequently, most examinations in fresh cadavers should be performed as soon after death as possible (Rodriguez and others 2002, Soler and others 2002).

1.3. Anatomy of the temporal region of the skull

The skull of the domestic dog demonstrates a variation in size and shape that is far greater than any other mammalian species (Evans 1993). Cat and rabbit skulls also demonstrate breed and individual variations in shape, although not as marked as in dogs (Harcourt-Brown 2003). Craniometry has been used to objectively differentiate between canine skull types with a range of parameters being measured and indices calculated to take into account the absolute differences in size between breeds (Evans 1993, Schwarz and others 2000). However, the effect of these variations on the anatomy of the temporal region of the skull and in particular the tympanic bulla (TB) and temporomandibular joint (TMJ) is not well reported.

The anatomy of the temporal region in the dog is well documented (Evans 1993). The feline anatomy is reasonably well documented (Crouch 1969, Barone and others 1973) but not as well as the dog and there appears to be some extrapolation. Although there are several atlases documenting rabbit anatomy (Barone and others 1973, Popesko 1977, Popesko and others 1992) there seems to be only one anatomical text (Barone 1989). New terms have been established according to the rules of the *Nomina Anatomica Veterinaria* for features present in the rabbit for which no official veterinary terms existed. Articles in scientific journals are usually restricted to particular points of interest and fail to place these in a more general context (Barone and others 1973).

The temporal bone (in the dog) forms a large part of the ventrolateral wall of the cranium and comprises three sections. The petrosal part is pyramidal in shape and is located entirely within the skull, housing the cochlea and semicircular canals of the inner ear, which are responsible for hearing and balance (Evans 1993).

The tympanic part is the largest component and forms a hemispherical protuberance called the tympanic bulla (TB), which projects ventral to the base of the skull. Its gas-filled lumen, combined with the epitympanic recess located on the ventral surface of the petrous temporal bone, forms the middle ear cavity (Evans 1993). In humans, the middle ear cavity lacks this large ventral protrusion and takes the form of a rectangular cleft in the temporal bone. It communicates with various spaces within the temporal bone called the mastoid air cells (Holliday and Reede 1989), which are absent in the dog, cat and rabbit. The presence of a TB in these species is thought to improve the perception of very low or high frequency sound (Huang and others 1997).

The third component of the temporal bone is the squamous part, which consists of a plate of bone with a lateral extension called the zygomatic process. The ventral surface of this process houses the mandibular fossa that articulates with the condyloid process of the mandible (Evans 1993). In evolutionary terms, this is a new joint that formed at the point where the increasingly large dentary bone came in contact with the cranium and is located lateral to the original articulation between the articular and quadrate bones, which has subsequently been incorporated into the middle ear. This new articulation was known as the mandibular joint (*articulatio mandibularis*) but in 1955, the International Congress of Anatomists renamed it as temporomandibular joint (*articulatio temporomandibularis*) (Gillbe 1973). While its new name was considered more informative in humans, it did not adequately describe the joint in all mammals (Gillbe 1973, Ström and others 1988) and so the craniomandibular joint was suggested as an alternative name that could be correctly applied to all mammals (Sicher 1962, Gillbe 1973, Tanaka and others 1999). Since the term temporomandibular joint (TMJ) remains anatomically correct in the dog, cat and rabbit, it will be used throughout this thesis (Crouch 1969, Barone 1989, Evans 1993).

In the development of the head, the embryonic precursors of the mandible and temporal bones (including the TB) form by a process of endochondral ossification from Meckel's cartilage or the periotic capsule and its surrounding bone. This is different to other bones of the skull that form by endomembranous ossification in a pre-osseous membranous sheet (Riser and others 1967).

The masticatory apparatus of animals has been classified into generalised and specialised groups with the specialised group being further subdivided into three. Dogs and cats are

carnivores with a predominantly vertical masticatory movement and a hinge action at the TMJ therefore they belong in specialised group 1 (Gillbe 1973). Herbivores belong in group 2 and rodents in group 3 (Gillbe 1973) with rabbits being intermediate between these two groups (Weijs and Dantuma 1981, Crossley 2003). The rabbit TMJ permits four movements. These are a hinge action, caudal retraction, rostral protrusion and a complex lateral swinging motion with one condyle held stationary while the other moves in a rostroventral – dorsocaudal direction (Crossley 2003). The TMJ contains an intra-articular disc or meniscus that is better developed in herbivores than carnivores. However, a feature common to all mammalian joints that contain a disc or meniscus is that translatory movement occurs in addition to other movement (Gillbe 1973).

1.4. Radiography

X-rays were first discovered by Wilhelm Conrad Roentgen in 1895. They are part of the electromagnetic spectrum, a group of radiations that convey energy through space as a combination of electric and magnetic fields (Curry and others 1990). Visible light is also part of this group although it has a longer wavelength than X-rays (Thrall 2002). Within 6 months of their discovery, X-rays were being used by physicians on the battlefield to locate bullets in wounded soldiers (Anon 2006) and the first veterinary radiograph, of an equine foot, was published in the *Veterinary Record* in 1896 (Williamson 1978, Kealy 1992). Since then X-rays have been used extensively in the medical profession for diagnostic imaging (Anon 2006). However, the veterinary field was slow to embrace the potential of this technique due to the high cost of equipment resulting in charges that animal owners were not prepared to bear, long exposure times (20 to 40 minutes for a human hand) making movement blur a problem, insufficient penetration, soft tissue structures not being differentiated and the disappointment associated with unrealistic expectations (Williamson 1978, Kealy 1992).

Until 1930, there were therefore few references to veterinary radiology in the literature but subsequent improvements in equipment lead to investigation into its uses in equine lameness and small animal practice (Pryer 1931, Kirk 1932, Williamson 1978) and the first veterinary radiology textbook was published in 1944 (Schnelle 1944). Although the safety implications regarding the use of radiography were widely known and an international recommendation for radiological protection published in 1928, these were frequently ignored by veterinary radiologists resulting in radiation burns being common among

practitioners. Financial constraints meant that practices and veterinary schools initially relied on local medical radiographers and their equipment. However, following World War II, the sale of surplus army units at affordable prices resulted in the more widespread distribution of X-ray equipment and in 1948, it was one of these machines that provided the first X-ray facilities at the Glasgow Veterinary College, then located in Buccleuch Street (Williamson 1978).

Literature regarding veterinary radiology was still relatively sparse in 1957, with only one text and few articles in the veterinary literature. At this time, the American Veterinary Radiology Society was set up and consisted primarily of veterinary practitioners who were interested in learning more and contributing new knowledge to this discipline. In 1958, as a result of growing interest and increased awareness of the value of radiography, they published the proceedings of their meetings as a set of mimeographed, non-illustrated notes (Rhodes 1960). In 1960, they published again as the Journal of the American Veterinary Radiology Society (to become Veterinary Radiology in 1979), producing the first journal dedicated exclusively to the subject of veterinary radiology (Rhodes 1960). The College of Veterinary Radiologists in the USA was founded in 1961 to determine the competence of voluntary candidates in veterinary radiology and to encourage the development of teaching personnel and training facilities in veterinary radiology (American College of Veterinary Radiology 2006). Although the suggested formation of a similar UK veterinary radiology association at this time was regarded as premature (Kealy 1992), the British Veterinary Radiology Association was eventually formed in 1963 (Williamson 1978), (to become the European Veterinary Radiology Association in 1991 (EAVDI - British and Irish Division website 2006)). The Royal College of Veterinary Surgeons also instituted the Diploma in Veterinary Radiology about the same time (Williamson 1978). By this stage, the 'best and finest' equipment for radiology departments in veterinary teaching establishments was being planned (Lewis 1960) and although still in its infancy, radiology had become a routine part of veterinary undergraduate teaching (Hall 1966).

Radiography remains the most common imaging technique in veterinary practice due to equipment availability and familiarity with the procedure (Herring and Bjornton 1985). Most patients undergoing imaging will have radiographs taken as the first and often the only imaging method, especially in a general practice setting (Thrall 1994). The principles, equipment and image interpretation of radiographs are therefore well documented (Curry

and others 1990, Thrall 2002). The static images produced are permanently recorded on film and are therefore available for interpretation either during the examination or after it has been completed. This allows input from multiple interpreters and also the potential for remote diagnosis.

The quality of radiographs, the ability of the observer to interpret them and the irrevocable physical limitations of what can and cannot be recorded on the film limit their value (Rhodes 1960). Radiography depicts the three dimensional body as a two dimensional image so superimposition of structures is inevitable (Thrall 1994). It is therefore necessary to be familiar with the normal radiographic appearance of the area to allow accurate interpretation of the images. A series of standard views are employed to facilitate this. Incorrect positioning of the animal relative to the film can result in magnification or distortion of the structures causing confusion or lead to misinterpretation (Thrall 1994). Accurate patient positioning is therefore essential to reduce these problems (Rose 1977) meaning heavy sedation or general anaesthesia is usually necessary (Wolvekamp and Oschwald 1991, Hoskinson 1993, Sullivan 1995, Harcourt Brown 2003a). In addition, an endotracheal tube may obscure the region of interest in some projections and require removal immediately prior to making the exposure (Gibbs 1978). The involvement of ionising radiation means radiography must be carried out within the legal requirements of the Ionising Radiation Regulations Act 1998 (Health and Safety Executive 1998).

1.5. Ultrasound

The piezo-electric properties of certain crystals were discovered in 1880 (Curie and Curie 1991) leading to the production of ultrasound. Sound is a longitudinal wave with audible sound having a frequency of 15 to 20,000 cycles per second and ultrasound greater than 20,000 cycles per second. One cycle per second is called a Hertz therefore ultrasound has a frequency of greater than 20kHz (Curry and others 1990). The commercial applications of ultrasound are diverse and include use as a therapeutic aid to stimulate tissue healing (Porter 1991, Steiss 2000), food sterilisation (Piyasena and others 2003) and vaccination of fish (Zhou and others 2002).

The pulse-echo principle was originally developed as a shipping aid to identify submerged objects, allow fog bound ships to identify potential hazards and to determine water depth (Richardson 1912a, Richardson 1912b, Langevin 1924). It was also employed in

unsuccessful attempts to locate the sunken Titanic. Improvements in these systems during World War II resulted in SONAR (Sound Navigation and Ranging) (Curry and others 1990). Current applications include detecting flaws in metals (Curry and others 1990), wood (Lemattre and others 1999) and cheese (Cho and Irudayaraj 2003), foreign material in food (Cho and Irudayaraj 2003), and drinks (Zhao BoSen, Basir and Mittal 2003), and to measure bone density in humans (Toyras and others 2002) and animals (Buckingham and Jeffcott 1991, Toyras and others 2002, Sandersen and others 2003).

The use of ultrasound as a diagnostic aid was first proposed by Dussik in 1942 and early applications of 'A' Mode ultrasound in humans included imaging the head (Dussik and others 1947), the abdomen to identify gallstones and foreign material (Ludwig and Struthers 1949), in obstetrics and the eye (Henry and others 1956). Although the analysis of small echoes arising from within organs to produce an actual image was originally proposed in 1950 (Wild 1950), it was not until the introduction of computer systems that this became possible in the early 1970s (Kossof and others 1971, Milan 1972). The ability to store, process and present large amounts of data allowed the production of static two dimensional grey scale images and by 1973, real time imaging was also possible (Griffith and Henry 1973). This real time Brightness or 'B' Mode imaging is the form of ultrasound now most commonly used while the original A-Mode is restricted to use in basic fluid detection equipment such as that for detecting pregnancy in pigs (Holtz 1982) and fluid in the human maxillary sinus (Hilbert and others 2001). The beams used in diagnostic imaging have frequencies ranging from 1 to 20 million cycles per second or MHz (Curry and others 1990).

Ultrasound was first used in animals as a means of determining back fat thickness in relation to carcass quality (Temple and others 1956), and a review of the current veterinary literature indicates that this remains its most common application. In addition to the common food producing species, this procedure has also been employed to determine body condition in Alaskan moose (Keech and others 1998) and elephant seals (Crocker and others 1998, Field and others 2002) as a conservation tool, and also in sumo wrestlers (Saito and others 2003). Ultrasound can be used to assess carcass quality and detect abscesses and this has been applied in avians (Konig and others 1998, Pym and others 1998, Cywa-Benko and others 1999, Farhat and Chavez 2000) and pigs (Bergan and Langanke 1996).

The first reported use of ultrasound as a veterinary diagnostic aid was for the identification of pregnancy in sheep in 1966 (Lindahl 1966). Subsequently more veterinary applications emerged, with a review of the literature up until 1986 identifying 492 references (Lamb and others 1988). Fifty percent (248) of these were related to large animal applications with farm animal reproductive examinations accounting for 25% (126). The 169 (34%) small animal references were divided evenly between cardiac and abdominal examinations, while the remaining references related to applications including blood pressure measurement, guided biopsy procedures and the imaging of more diverse species including gorillas and fish (Lamb and others 1988). It was also around 1986 that the University of Glasgow Veterinary School purchased its first ultrasound machine. In recognition of the increased contribution that ultrasound was making to veterinary imaging the journal, *Veterinary Radiology*, underwent a name change in 1992 to *Veterinary Radiology and Ultrasound* to emphasise its role in providing state-of-the-art information to the profession. Ultrasound examinations are now a routine part of small animal and equine diagnostic workups with cardiac, thoracic, abdominal, reproductive, ocular and musculoskeletal applications all being well documented and many texts are available (Nyland and others 1995, Green 1996, Reef 1998).

Ultrasound has many benefits as a veterinary diagnostic imaging procedure. The images are tomographic, representing a single slice through a three dimensional structure and are produced in real time. Routine examinations have been shown to have no harmful biological effects making it a safe procedure for the patient, the operator and nearby personnel, and allowing it to be performed in any location without the need for specific safety precautions (Preston and Shaw 2001). It is non-invasive and therefore well tolerated in unsedated animals making serial examinations to monitor progression of the condition, response to treatment or to practice scanning techniques possible (Nyland and others 1995). Ultrasound machines are now readily available in general veterinary practice and the information is obtained instantaneously (Nyland and others 1995; Green 1996). It is better suited to imaging soft tissue structures than radiography, being able to distinguish fluid from soft tissue and differentiate between soft tissue types (Nyland and others 1995).

However, ultrasound is limited by its inability to penetrate gas filled or bony structures (Herring and Bjornton 1985, Nyland and others 1995, Green 1996). Interpretation is

required at the time of the study, and it can be difficult to render meaningful information from another sonographer's images or videotape (Nyland and others 1995) so the results are dependent on the experience and skill of the operator (Reed and others 1995, Long and Nyland 1999). It is therefore necessary to have a thorough knowledge of the relevant regional anatomy (Long and Nyland 1999) since accurate interpretation of images depends directly on the differentiation between normal and abnormal anatomy at the time of the examination (Nyland and others 1995).

1.6. Computed Tomography

CT utilises X-rays to produce a tomographic slice of a specified thickness through an object. Multiple projections are obtained allowing subsequent reproduction of the object. These mathematical principles, on which CT image production is based, are known as back projection and were first described in 1917. They were subsequently applied in many fields unrelated to diagnostic imaging with the first mechanical CT scanner not being constructed until 1968 (Curry and others 1990). In 1972, Godfrey Newbold Hounsfield, working at the Thorn EMI Central Research Laboratories, created the first medical CT system and demonstrated its diagnostic imaging capabilities (Curry and others 1990). Allan McLeod Cormack based at Tufts University in Boston, independently invented a similar process and they shared a Nobel Prize in medicine in 1979 (Wikipedia 2006a). The equipment was originally known as the EMI-Scanner and it is claimed that this was the greatest legacy of the Beatles due to the massive profits from their record sales going to EMI as their record label (Wikipedia 2006a).

The first CT scanner was installed in Atkinson Morley's Hospital in Wimbledon in 1972, and was limited to scanning the brain taking approximately 4 minutes to scan a section and 7 minutes to reconstruct the image (Wikipedia 2006a). These 'first generation' machines consisted of an X-ray tube producing a pencil shaped beam and a detector with movement occurring in a semicircle around the patient involving both linear and rotary motion, known as translate – rotate. 'Second generation' scanners still involved translate – rotate motion but the use of a fan shaped beam and multiple detectors reduced the scan time to approximately 60 – 90 seconds per section. In 1975, the General Electric Company introduced a CT system that eliminated the translation motion allowing the tube and multiple detectors to move around the patient reducing scan times to around 4.9 seconds a section (Curry and others 1990). Systems with this rotate – rotate configuration are known

as ‘third generation’ and currently are the most common type available. A rotate – fixed system has also been developed using a moving tube and a large number of static detectors and has produced scan times of 1second per section. Although known as ‘fourth generation’ systems, this configuration is not necessarily superior to ‘third generation’ ones as the larger number of detectors makes them more expensive and the non-fixed relationship with the tube makes them more susceptible to artifacts (Curry and others 1990). The introduction of ‘slip ring’ technology allowed the tube and detectors to spin continuously without interference from cabling and this combined with the ability to move the patient continuously through the scanner on a gantry is know as ‘helical’ or ‘spiral’ CT (Wikipedia 2006a). Multi-detector row systems allow several images to be acquired at once thereby reducing scan times even further (Wikipedia 2006a).

The principles of CT imaging including physics, equipment evolution, patient preparation, procedure, and interpretation have been described (Hathcock and Stickle 1993, Forrest 1999, Jones and others 1995, Tidwell 1999). Between 1980 and 1992, there were over 250 publications in which CT had been utilised in the dog although many involved research rather than clinical applications (George and Smallwood 1992). It has also been employed in horses and a range of other animals including cats, goats, llamas, calves, birds, fish and turtles. CT has been used to investigate many areas of the body including the musculoskeletal system, thorax and abdomen but it is most commonly used to image the central nervous system (Kraft 2002) and has gained acceptance in the veterinary field for musculoskeletal and neural imaging (Widmer and others 1991). In 1992, the European Veterinary Radiology Association (EVRA) underwent another name change to the Eurpoean Association of Veterinary Diagnostic Imaging (EAVDI) to demonstrate its encompassment of all aspects of diagnostic imaging, including radiography, ultrasonography, computerised x-ray tomography, magnetic resonance imaging and nuclear medicine (EAVDI - British and Irish Division website 2006). It was in 1999 that the University of Glasgow Veterinary School first installed a CT scanner.

Advantages of CT over radiography include the visualisation of cross sectional anatomy free from the confusing superimposed opacities of overlying structures (Hathcock and Stickle 1993, Hoskinson 1993, Seitz and others 1996) allowing clearer visualisation of areas such as the base of the skull (Hoskinson 1993d). CT also provides superior image contrast resolution (Love and others 1995, Dvir and others 2000) being able to discriminate

between physical density differences as small as 0.5% compared to the 10% required for visual detection with conventional radiographs (Curry and others 1990). This allows the differentiation of fluid from soft tissue and increases the visibility of subtle soft tissue opacities (Hathcock and Stickle 1993). High resolution CT is capable of producing an in-plane spatial resolution of less than 1mm (Hoskinson 1993b). Radiographic contrast media can be administered to enhance visualisation of structures and determine the extent and vascularity of lesions (Forrest 1999).

Merging the data from adjacent slices makes it possible to reformat acquired images in alternative planes (Seitz and others 1996) and produce three dimensional reconstructions (Tidwell 1999). Elimination of the soft tissue CT numbers then allows the bone surface to be depicted as a three dimensional image that can be viewed with different degrees of rotation (Kraus and others 1997) allowing the extent of bony lesions to be determined (Seitz and others 1996, Kraus and others 1997). However, the quality of these images depends on the acquired images, the computer performing the reconstruction (Koblick and Berry 1990) and accurate patient positioning (Hathcock and Stickle 1993) therefore it appears to be infrequently used in veterinary medicine (Kraus and others 1997).

Although high resolution CT images have better spatial resolution than MRI, they are currently less than radiographs (Hoskinson 1993, Tidwell 1999). Precise positioning is required to ensure the symmetry that is important for assessment of bilateral structures such as the TB (Hoskinson 1993c) and TMJ (Schwarz and others 2002). This, and the need for patient immobility throughout the scan, necessitates general anaesthesia (Love and others 1995, Seitz and others 1996), although heavy sedation may be adequate for imaging areas such as the elbow (Carerra and Trevail 2007). Reconstructed images are of poorer quality than the original in-plane ones. Equipment cost (Seitz and others 1996) and significantly larger radiation doses than with conventional radiography are other factors that require consideration (Dixon 1991). Although CT is becoming increasingly available, it is currently still restricted to use in referral centres (Forrest 1999).

1.7. Magnetic Resonance Imaging

Nuclear magnetic resonance or NMR, was independently described by two scientists in 1946 (Bloch and others 1946, Purcell and others 1946), for which both were awarded a Nobel Prize in Physics in 1952. NMR is the resonance transition between nuclear spin states of certain nuclei in an external magnetic field and allows investigation of chemical and physical properties at the molecular level (Curry and others 1990). A wide range of applications were subsequently developed for this technology, including the determination of rock permeability to hydrocarbons and the non-destructive analysis of small samples of various materials including produce and timber (European Magnetic Resonance Forum website 2003, Wikipedia 2006b). Work in human and animal tissue samples was also performed culminating in the first reports of its use in living humans and animals (Budinger and Lauterbur 1984, Jackson and Langham 1968). In 1972, it was discovered that cancer tissue produced a different signal to normal tissue resulting in the filing of a patent for an 'Apparatus and Method for Detecting Cancer in Tissue (Damadian 1974) although this was never actually used diagnostically (Anon 2003).

Up until this point, it was not possible to determine where the signal originated within the sample so all NMR examinations were one- dimensional and lacked spatial information (European Magnetic Resonance Forum website 2003). The first actual NMR images (of two tubes of water) were published in 1973 and were produced by the application of magnetic field gradients in all three dimensions combined with the back projection technique used to create CT images (Lauterbur 1973). This was then followed by images of a living clam then the thoracic cavity of a living mouse (Lauterbur 1974). This technique was initially known as 'zeugmatography' from the Greek word meaning that which joins together to highlight the interaction between the static and the gradient magnetic fields that are critical to image formation, although this nomenclature never caught on (Wikipedia 2006b). The term NMR imaging was used until the 'nuclear' was dropped due to its associations with radiation leaving the term MR imaging or MRI that is used today (Wikipedia 2006b).

In 1975, an alternative method of image formation was proposed that involved the application of both phase and frequency encoding (European Magnetic Resonance Forum website 2003, Wikipedia 2006b). This, in combination with Fourier transformation, as described at the beginning of the nineteenth century, produced the technique that is the

basis of current MRI formation (Kumar and others 1975). In 1978, the first transverse MRI image through a human head was published (Clow and Young 1978) and the first MRI scanners for use in the medical profession were available around 1980 (Wikipedia 2006b).

However, the development of the various different types of MR imaging sequences that are used today took several years to develop. Echo-planar imaging (EPI) was first proposed in 1977 but for technical reasons took a long time to be adopted commercially. RARE (rapid acquisition with relaxation enhancement), also known by the commercial names of fast or turbo spin-echo, was introduced in 1986. At about the same time, FLASH (fast low angle shot) appeared, opening the way to similar gradient-echo sequences and was very rapidly adopted commercially. However, early clinical imaging was extremely difficult, time-consuming, and often disappointing. Although today spin-echo (SE) imaging, is taken for granted and has helped MR imaging immensely to become a routine technique, it was a big step to develop (Anon 2003)

Early MR images were mainly based upon proton-density differences and later upon differences in T1-weighting. In 1982, it was reported that long heavily T2-weighted spin echo sequences were better at highlighting pathology (Bydder and others 1982, Rinck and others 1984). However, many companies claimed that long echo time was neither possible nor necessary and so it took many years until this was generally accepted (Anon 2003).

MRI uses a magnet and applied radiofrequencies to produce a tomographic slice of a specified thickness through the body. The principals of MRI imaging including physics, patient preparation, procedure, equipment and principles of interpretation have been described (Shores 1993, Thomson and others 1993, Assheuer and Sager 1997, Tidwell 1999).

Most of the work in animals relates to experimental investigations with the dog being employed as a research model for a variety of conditions (Widmer and others 1991). Most publications therefore involve this species, although MRI has been applied in a range of other animals including cats, horses and birds (Kraft 2002). Investigation of many areas of the body has been performed, including the musculoskeletal system, thorax and abdomen, but it is most commonly used for evaluation of the central nervous system (Widmer and

others 1991, Shores 1993, Thomson and others 1993, Kraft 2002), and is emerging as an important diagnostic and research tool for animals (Widmer and others 1991).

In 2002, there were approximately 22,000 medical MRI units were in use worldwide, and more than 60 million MRI examinations were performed (Wikipedia 2006b). The first dedicated veterinary MRI scanner in the UK was installed at the Animal Health Trust in Newmarket in 1992 (Onslow 2007) and there are now many veterinary referral centres worldwide equipped with an MRI unit. Many of those without a permanent facility, like the University of Glasgow Veterinary School, make use of a mobile service. This means that despite being a newer technology, MRI is currently more widely available to veterinary patients in the UK than CT (Dennis 2006). The mobile service was introduced in Glasgow in 2003. Also in 2003 a permanent 7 Tesla MRI unit was installed in the University of Glasgow Institute for Comparative Medicine. It is used mainly for research purposes and was used in the present study.

MRI has no known detrimental biological effects (Larheim 1995) and unlike CT and radiography, does not use ionising radiation (Widmer et al. 1991). Like CT, the production of individual slices allows examination of structures free from superimposition making it ideal for imaging the base of the skull (Dvir and others 2000). In addition, it has superior contrast resolution to CT, which compensates for its poorer spatial resolution (Shores 1993, Tidwell 1999). Tissues imaged by MRI vary according to their hydrogen content, optimising soft tissue detail (Shores 1993) and making it more sensitive for identifying soft tissue changes than either CT or radiography (Shores 1993, Forrest 1999). Unlike CT, areas surrounded by bone can be visualised without artefacts (Thomson and others 1993) and it is also possible to directly acquire multiple imaging planes without repositioning the patient (Widmer and others 1991, Shores 1993, Forrest 1999).

The lack of mobile hydrogen protons in compact bone means that MRI depicts cortices as signal void and is therefore less suitable for bone imaging than CT (Forrest 1999). However, bone can usually be visualised indirectly with trabecular bone being outlined by the intense signal from the marrow fat and cortical bone outlined by the marrow and surrounding soft tissue (Widmer and others 1991). Anatomical structures may be geometrically less precise on MRI scans compared to CT due to reduced spatial resolution (Forrest 1999) and the cost and availability of equipment has limited the use of MRI in

veterinary medicine (Dixon 1991, Widmer and others 1991). Each sequence takes much longer to acquire than a CT scan (Dennis 2006), so anaesthesia is required to reduce patient movement and prevent blurring of the image (Assheuer and Sager 1997, Allgoewer and others 2000). However, the presence of the magnetic field means that care must be taken with the positioning of conventional anaesthetic and monitoring equipment (Dennis 2006). As with CT, MRI examinations should also be preceded by a standard clinical and radiological workup (Dvir and others 2000).

1.8. Clinical conditions affecting the TB

Conditions affecting the middle ear that warrant diagnostic imaging include otitis media, inflammatory polyps, craniomandibular osteopathy and neoplasia (White 2003, Thrall 2002).

Otitis media can arise via three routes (Neer and Howard 1982, Shell 1988). The most common in the dog is via the spread of inflammation across the tympanic membrane secondary to chronic or severe external ear canal disease (Neer and Howard 1982, Shell 1988, Little and others 1991a). Otitis media may occur in up to 50% of dogs with chronic otitis externa (Shell 1988) although it can also result from trauma or the presence of foreign material within the external ear canal (Neer and Howard 1982, Shell 1988). Otitis media can occur independently of otitis externa and vice versa (Lawson 1957) although the incidence of primary otitis media is relatively low in dogs (Shell 1988). An alternative route of infection is via the auditory tube (Shell 1988). Although this is uncommon in the dog (Neer and Howard 1982, Shell 1988), auditory tube obstruction has been suggested as a factor in the pathophysiology of otitis media in some dogs (Tojo and others 1985). Primary ciliary dyskinesia is a congenital condition resulting in depressed function of the mucociliary system that serves to remove debris from the middle ear cavity down the auditory tube (White 2003). The result is a sterile secretory otitis media known as 'glue ear' in children and has been reported to occur in Cavalier King Charles Spaniel dogs (White 2003). The third route, via blood borne pathogens appears to be uncommon in all species (Neer and Howard 1982, White 2003).

Otitis media in the rabbit may also occur secondary to the presence of otitis externa and ear parasites (Gao and others 1995, Kumar and others 2000), (detected in 91.2% of rabbits demonstrating clinical signs of ear disease (Mishra 1995) and 90% rabbits with otitis media

(Rai and others 1986.) However, by far the most common route in this species is secondary to respiratory infection with *Pasteurella multocida* (Kpodekon 1983). In one study otitis media was present in 32% of rabbits with rhinitis (Smith and Webster 1925, Snyder and others 1973) and in another, *Pasteurella* was isolated from 80 – 100% of rabbits with otitis media (Smith and Webster 1925, Fox and others 1971, Snyder and others 1973, Flatt and others 1977). The pathogenesis is thought to be similar to children whereby pharyngeal inflammation leads to dysfunction of the auditory tube so the middle ear cavity is not drained properly (Flatt and others 1977). Infection passing from the upper respiratory tract to the TB via the auditory tube (Deeb 1997, Percy and Barthold 2001) can then result in suppurative otitis media (Flatt and others 1977) and this has been reproduced experimentally (Smith and Webster 1925). The reasons for the spread of infection to the middle ear are not clear but genetic factors, environmental stress and chronicity of infection appear to be involved (Fox and others 1971, Flatt and others 1977). Even if any respiratory signs subside, infection remains harboured in TB (Deeb 1997). A variety of other organisms have also been identified in association with *Pasteurella* but their significance could not be determined (Snyder and others 1973, Rai and others 1986).

Acute pathological changes observed in dogs with experimentally induced otitis media and in rabbits with naturally occurring disease were mucosal inflammation and the presence of intraluminal fluid (Smith and Webster 1925, Tojo and others 1985). More chronic changes include mucosal hypertrophy, the presence of pus or soft tissue within the TB lumen and new bone formation resulting in thickening of the TB wall (Geary 1965, Flatt and others 1977, Gibbs 1978, Little and others 1991a, White 2003). In severe cases this can extend to the petrous temporal bone (Gibbs 1978). Less commonly, progression to osteomyelitis may result in lysis and thinning of the TB wall (Geary 1965) and this is associated with a poorer prognosis (Farrow 1985). The condition was bilateral in 61% of affected young rabbits and 70% (Flatt and others 1977) and 82% of affected adults (Snyder and others 1973).

There are several potential complications associated with the presence of otitis media. Spread to the external ear canal can occur if the tympanic membrane ruptures (Bjotvedt and Geib 1981, Deed 1997). Concurrent suppurative otitis externa was identified in 17% (5/29) of young rabbits with otitis media and 34% (94/278) of adult rabbits (Flatt and others 1977). Involvement of the facial or sympathetic nerves as they pass through the TB may cause neurological dysfunction (Bruyette and Lorenz 1993), being demonstrated in 26%

(5/19) of animals in one study (Remedios and others 1991). Damage to the facial nerve may result in a lost or diminished palpebral reflex, wide palpebral fissure, drooping of the ear and lips, excessive drooling and muscle contracture (Neer and Howard 1982, Bruyette and Lorenz 1993). Damage to the sympathetic trunk may result in Horner's Syndrome characterised by ptosis, miosis, endophthalmos and protrusion of the nictitating membrane third eyelid (Neer and Howard 1982, Bruyette and Lorenz 1993).

The round window membrane is the only soft tissue barrier between the middle and inner ears, and in the presence of otitis media it can become permeable to macromolecules allowing progression to otitis interna (Neer and Howard 1982). Although unusual in the dog, it is often encountered in association with Pasteurellosis in rabbits (Kpodekon 1983). Inner ear involvement affects the vestibular mechanism (Fox and others 1971, Snyder and others 1973, Bjotvedt and Geib 1981), resulting in peripheral vestibular signs including head tilt, torticollis, nystagmus and ataxia (Fox and others 1971, Neer and Howard 1982, Shell 1988, Bruyette and Lorenz 1993, Deeb 1997, Garosi and others 2001, Suckow and others 2002), which can be a diagnostic challenge to distinguish from central vestibular syndrome (Dvir and others 2000). Complications affecting the brain are becoming increasingly important in rabbits and can arise either from the spread of infection along the meninges that follow the 8th cranial nerve into the internal ear (Kpodekon 1983, Deeb 1997, Suckow and others 2002), or directly from the nasal cavity along the nerve trunks in rabbits (Kpodekon 1983) causing a suppurative meningioencephalitis (Fox and others 1971) or brain stem abscesses that result in motor deficits to the limbs and other cranial nerve involvement (Neer and Howard 1982). This intracranial extension is the most serious complication of middle ear infection in humans (Martin and others 1990).

Another potential complication reported in dogs is the formation of a cholesteatoma (Little and others 1991b). These are a form of epidermoid cyst that result when a pocket of tympanic membrane becomes adhered to the inflamed middle ear mucosa. They are aggressive lesions associated with extensive bone resorption and remodelling and may be responsible for an increased incidence of neurological signs or temporomandibular joint pain. They carry a poorer prognosis and therefore must be differentiated from uncomplicated otitis media and neoplasia (Little and others 1991a, Little and others 1991b).

Otitis media has few specific clinical signs making it difficult to diagnose (Harcourt-Brown 2003) and has been identified in 4% young and 32% adult rabbits in the absence of clinical signs (Smith and Webster 1925, Snyder and others 1973, Flatt and others 1977). The only signs present may be those caused by the secondary complications (Little and others 1991a). Diagnosis used to rely on otoscopic examination of the tympanic membrane but visualisation of the membrane is not always possible (Spruell 1964) and perforations are not always evident in association with otitis media (Spruell 1964, Little and others 1991a, Bruyette and Lorenz 1993). Therefore otitis media is a condition that warrants diagnostic imaging (Thrall 2002).

In cats, otitis media rarely occurs secondary to otitis externa but is more likely due to ascending infection through the auditory tubes from nasopharyngeal viral infections (White 2003). It tends to affect middle aged animals and may be bilateral (Trevor & Martin 1993). In younger cats inflammatory polyps are the most common cause of middle ear disease (Trevor and Martin 1993). However, they are also often associated with the presence of otitis media although it is not clear whether they are the cause or sequel (Parker and Binnington 1985, Kapatkin and others 1990, Trevor and Martin 1993). Polyps are benign pedunculated growths that originate from the epithelium of the middle ear cavity or auditory tube (White 2003). They can either remain within the TB, extend out through the tympanic membrane into the external ear canal or down the auditory tube into the nasopharynx (White 2003). The aetiology is unknown although an association with poor auditory tube function is suspected (Kapatkin and others 1990, White 2003) and since they are inflammatory lesions, it is possible that they form in response to local tissue irritation (Bradley and others 1985). There has been a single report of a nasopharyngeal polyp arising in a 7 month old Shar Pei dog (Fingland and others 1993). Most occur as unilateral lesions (Harvey and Goldschmidt 1978, Trevor and Martin 1993) but bilateral polyps have been reported (Kapatkin and others 1990).

Otoliths are stone-like bodies embedded in inflammatory soft tissue within the TB (Farrow 1992) representing mineralised necrotic material and are reported to be associated with chronic otitis although as yet there is no firm evidence to confirm this (Ziemer and others 2003). The underlying aetiology of their formation is not clear (Ziemer and others 2003) although spicules of new bone have been identified within the connective tissue of clinical cases of otitis media (Little and others 1991a). It is thought to be unlikely that they

represent mineralised cholesteatomas or polyps but that they may be related to the formation of chondroids in equine guttural pouch mycosis (Ziemer and others 2003).

Neoplasia involving the middle ear cavity of dogs and cats is uncommon but slightly more prevalent in cats than dogs. In one study, they were present in only 2.6% of dogs referred for aural surgery over a 10 year period (Little and others 1989) but in 21% of cats undergoing surgery over a 7 year period (Trevor and Martin 1993). Adnexal and ceruminous gland tumours were responsible for the majority of the reported cases in dogs (Little and others 1989) with squamous cell carcinomas also represented in cats (Indrieri and Taylor 1984). However, primary tumours arising from the middle and inner ear are considered rare (Gibbs 1978) although there are sporadic reports (Little and others 1989, Indrieri and Taylor 1984). Malignant neoplasia involving the middle ear in cats tended to affect older animals (Trevor and Martin 1993).

Craniomandibular osteopathy has been reported mainly in Scottish and West Highland White Terriers although it also occurs sporadically in other breeds (Riser and others 1967, Hudson and others 1994). The cause is unknown but typically it involves the bones of the skull that form by endochondral ossification, particularly the occipital bone, mandible and TB, although may also involve other bones of the skull and long bones (Riser and others 1967, Hudson and others 1994). The condition is characterised by bilateral irregular osseous proliferation and although it is usually self limiting with the changes regressing with time, in severe cases, it can lead to changes that cannot be resolved including fusion of the mandible with the TB (Riser and others 1967).

Bilateral sclerosis of the TB walls may be seen on radiographs in normal aged animals especially cats and is considered to be an incidental finding (Hoskinson 1993a). However, other changes may be encountered that are not associated with clinical signs and the significance of which cannot be determined. Fluid within the TB is occasionally observed unexpectedly in dogs undergoing CT of the brain (Barthez and others 1996). A soft tissue opacity was identified on CT in the dorsolateral TB compartment of a cat with a nasopharyngeal polyp affecting the contralateral ear, the aetiology of which was never determined (Seitz and others 1996). A hyperintense focus was identified on T2 weighted images that corresponded to the site of the ipsilateral vestibular nerve in two dogs with MR findings compatible with otitis media and one with otitis interna of which the clinical

importance was unknown (Garosi and others 2001). These examples demonstrate that we are still a long way from being able to interpret all the changes identified on diagnostic images.

1.9. Conditions affecting the TMJ

Conditions affecting the TMJ that warrant diagnostic imaging include craniomandibular osteopathy, TMJ dysplasia, fractures, luxation, degenerative joint disease and neoplasia (Stewart and others 1975, Robins and Grandage 1977, Johnson 1979, Hoppe and Svalastoga 1980, Lane 1982, Bennet and Prymak 1986, Hudson and others 1994, Schwarz and others 2002). With conditions such as myositis, retrobulbar abscessation, tetanus or neoplasia of the surrounding tissue, a normal appearance to the TMJ on diagnostic images can help rule out its association with the clinical signs (Sullivan 1989, Thrall 2002).

Dysplasia is the abnormal development or growth of a cell, tissue or organ (Schwarz 1993). Congenital dysplasia of the TMJ has been reported in the Irish Setter, Basset Hound, Boxer, Golden Retriever, Labrador and Bernese Mountain Dog as isolated cases with most of the population demonstrating normal TMJ anatomy (Stewart and others 1975, Robins and Grandage 1977, Johnson 1979, Lane 1982, Stead 1984, Bennet and Prymak 1986). The majority of these dogs presented clinically with open mouth jaw locking that was most commonly due to the existing joint laxity allowing the coronoid process to impinge upon the zygomatic arch and become trapped in a position lateral to it (Stewart and others 1975, Robins and Grandage 1977, Johnson 1979). However, in the Boxer, Retriever and Labrador this was not observed and the jaw locking was thought to have arisen from secondary osteoarthritic changes associated with the joints (Bennet and Prymak 1986). In one dog, the presenting signs were of jaw pain and dysphagia, with open mouth jaw locking not being a feature (Bennet and Prymak 1986). Radiographic changes consistent with temporomandibular joint dysplasia have also been described in American Cocker Spaniels and Dachshunds in the absence of clinical signs (Hoppe and Svalastoga 1980, Vollmerhaus and others 1996, Vollmerhaus and Roos 2003). In addition, open mouth jaw locking has been reported in other breeds in the absence of noticeable radiographic abnormalities (Lantz and Cantwell 1986, Hazewinkel and others 1993).

The underlying cause of TMJ dysplasia in the dog is not known although many theories have been suggested including it being a primary problem with either congenital or

acquired aetiologies or that the dysplastic changes develop as a result of other factors such as the effect of rapid growth in chondrodystrophied breeds, inferior prognathism or laxity of the mandibular symphysis (Robins and Grandage 1977, Johnson 1979).

Measurement of the angle between the long axis of the mandibular condyle and the axis of rotation has been performed (Hazewinkel and others 1993). An increase in the obliquity of the condyloid processes has been associated with temporomandibular joint dysplasia and open mouth jaw locking (Robins and Grandage 1977, Johnson 1979, Bennet and Prymak 1986, Lantz and Cantwell 1986, Hazewinkel and others 1993). The shape of the condyloid process associated with large angles was reported to result in excessive movement of the lateral aspect of the condyle leading to stretching of the lateral ligament and in turn predisposing to subluxation (Robins and Grandage 1977, Lantz and Cantwell 1986). However, there do not appear to be any standard values for these measurements published although one study including 35 dogs representing 18 different breeds found mean angles of the right and left condyloid processes of 13.8 and 15.2° (Hazewinkel and others 1993) while another suggested that the rotational angle of a normal joint should be 0° (Lantz and Cantwell 1986).

Fractures secondary to head trauma may involve any of the TMJ components (Schwarz and others 2002). However, extra-articular fractures are identified more frequently than intra-articular ones, suggesting that the latter are either less common or under diagnosed (Schwarz and others 2002). Fractures may result in luxation of the TMJ and this is usually in a rostradorsal direction although fracture of the retromandibular process can result in caudal displacement (Ticer and Spencer 1978, Stead 1984, Hoskinson 1993). Unilateral luxation is usually only possible in association with a mandibular fracture (Gibbs 1977). However, it may occur in cats without a fracture due to the wider angle between the mandibles in this species (Schwarz and others 2002). Subluxation may result from dysplastic, degenerative, traumatic and idiopathic conditions, can be unilateral or bilateral and is usually difficult to identify (Schwarz and others 2002).

Untreated intra- or extra-articular fractures may result in ankylosis of the joint (Sullivan 1989), although this may also result from extensive secondary new bone formation associated with otitis media or craniomandibular osteopathy (Lane 1982). Mandibular or

zygomatic masses and aural or retrobulbar abscesses can also cause restriction of the TMJ (Schwarz and others 2002).

Infection of the TMJ is rare but may result from the extension of osteomyelitis from the ipsilateral TB or local abscess (Schwarz and others 2002). This may be more common in cats due to the closer anatomical association of the TMJ and TB, but also the increased incidence of infected bite wounds in this species (Stead 1984). Osteoarthritis and primary neoplasia affecting the canine and feline TMJ are both rare (Schwarz and others 2002). However, the TMJ may become invaded following extension of neoplasia arising from adjacent structures. These appear most commonly to be osteosarcomas, osteochondrosarcomas or osteomas (Liu and others 1974, Stead 1984) although a fibrosarcoma and a squamous cell carcinoma have also been reported (Anderson and Orsini 1996, Whitelock and others 1997).

Dental disease is a common problem in pet rabbits and is usually the result of an inappropriate diet (Harcourt-Brown 1995). Diet has been shown experimentally to have an effect on the function of the rabbit TMJ and the articular disc (Block and others 1988), so it is also probable that malocclusion resulting from dental disease will have an impact on the TMJ. As with the dog and cat, it is likely that trauma and extension from adjacent inflammatory, infectious or neoplastic processes have the potential to affect the TMJ although there do not appear to be many specific reports in the literature at this time.

Chapter 2. Anatomy of the tympanic bulla and temporomandibular joint in the dog, cat and rabbit.

2.1 Introduction

2.1.1. Comparison between diagnostic images and cadaver material

Diagnostic images depict structures located within the intact body, therefore these regions must be exposed to allow visual identification for comparison and this can be achieved in several ways. Extraneous tissue can be removed using gross dissection (Gillbe 1973, Ström and others 1988) or assisted by a dissecting microscope (Gillbe 1973). Techniques for post mortem examination of the canine ear (Getty and others 1956, Rose 1977) and TMJ including the disc (Gillbe 1973, Shengyi and Yinghua 1991) and joint capsule have been described (Scapino 1965, Ström and others 1988, Bermejo Fenoll and other 1992). However, it is also beneficial to compare tomographic images with the corresponding section through a cadaver and this can be achieved by freezing the material and then slicing it using a bandsaw (Zook and others 1981, George and Smallwood 1992, Weller and others 1999a, Morrow and others 2000). Cross sectional anatomical sections of the canine head and neck have been produced in this way (Zook and others 1981) and compared with transverse CT and MRI images (Zook and others 1981, George and Smallwood 1992, Assheuer and Sager 1997, Morrow and others 2000). Oblique sections have also been produced for comparison with ultrasound images obtained in the corresponding plane (Weller and others 1999a). The thickness of the anatomical slices is usually selected to correspond with those of the imaging technique in question (George and Smallwood 1992, Morrow and others 2000) and correlation with the images depends on how carefully the location of the slices is matched (George and Smallwood 1992). It is often difficult to slice cadavers exactly perpendicular to the long axis resulting in one side being cut slightly deeper than the other (Zook and others 1981). A variety of techniques have been employed in an attempt to overcome this including mounting material on boards (Patrick 2002) or embedding it in blocks of ice (Valente and others 2007). However, these mildly uneven slices may reveal more anatomical relationships than would have been apparent otherwise and therefore facilitate identification and labelling of tissues (Zook and others 1981).

In the UK, radiographs are generally displayed using a standard orientation. However, although it has been stated in the literature that radiographs should always be hung the same way (Thrall 2002), there does not appear to be any specific mention of what this is,

therefore this seems to happen by consensus. A similar situation exists with ultrasound, CT and MR images (George and Smallwood 1992). In a study of the canine spine, dorsal recumbency was selected to ensure consistent positioning between animals and the CT images were orientated with the dorsal aspect at bottom of the image to match. This was reported to correspond with images presented in the human literature and conform to existing veterinary precedents in abdominal imaging (Jones and others 1995). However, in another publication, dorsal was positioned to the top of the image to correspond with the nomination of slice orientation decided by the American College of Veterinary Radiology, although there was no specific mention of what these nominations were (Assheuer and Sager 1997). Most clinical publications appear to have adopted this approach for transverse CT and MR images with the right side of the animal towards the left of the image (Assheuer and Sager 1997, Tidwell 1999, Russo and others 2002, Schwarz and others 2002, Thrall 2002, Dennis 2006), although one anatomical study using cadavers placed right to the right (George and Smallwood 1992). Dorsal sections of the head tend to be displayed with rostral to the top of the image (Assheuer and Sager 1997, Tidwell 1999, Russo and others 2002, Schwarz and others 2002). However, there is variation in how sagittal sections are presented with dorsal to the top and rostral to the left (Tidwell 1999, Dennis 2006), rostral to the right (Forrest 1999) and with rostral to the top and dorsal to the left (Assheuer and Sager 1997).

2.1.2. Plastination

Plastination is a method of preserving perishable biological specimens by replacing water and fat within the tissue with a curable, plastic polymer (Whittaker 2007). The technique was invented at Heidelberg University by Professor Gunther von Hagens in 1978 and is now being carried out in institutions worldwide with many new applications being found. There are four variations with the class of polymer determining the optical (transparent or opaque) and mechanical properties (flexible or firm) of the resulting specimen (Miklošová and Sivrev 1999). Plastinated specimens are dry, odourless, non-toxic, durable, can be handled without gloves and have no specialised storage requirements. They retain their original surface relief and cellular identity down to microscopic level, and can be practically indistinguishable from the original specimen. They therefore have many advantages over traditionally preserved material and have great flexibility of use in the classroom or as material for review or assessment (Miklošová and Sivrev 1999, Whittaker 2007). Transparent body slices allow detailed study of anatomical and pathological

structures in their topographical context and can be easily correlated with diagnostic images. This makes them excellent adjuncts for studying sectional anatomy and for correlation with ultrasonographic, CT or MRI images (Miklošová and Sivrev 1999). Plastinated specimens have been used in the investigation of the equine TMJ (Rodriguez and others 2002) and have proved to be valuable tools when teaching interpretation of MR images of the canine stifle (Soler and others 2002).

2.1.3. Anatomy of the TB

2.1.3.1. Dog and cat

Anatomy of the canine (Getty and others 1956, Spruell 1964, Evans 1993) and feline ear have been described (Little and Lane 1986, Farrow 1994).

The external ear consists of the pinna that is formed by the auricular cartilage. This directs sound along the vertical and short horizontal sections of the external auditory canal and into the osseous external acoustic meatus. In the dog, this takes the form of a dorsolateral – ventromedially orientated, bone canal less than 1cm long with the external opening dorsal to the middle ear. A bone extension from around its ventral margin forms a ledge projecting into the middle ear. In the cat, the external acoustic meatus is shallower, wider and orientated horizontally with its external opening located further ventrally than in the dog. It is surrounded by the bone of the tympanic ring or ectotympanum. The meatus in both species terminates at the obliquely orientated tympanic membrane. The middle and inner ears are both housed within the temporal bone of the skull.

The middle ear is an air-filled cavity bounded by the ventrally located tympanic part of the TB and the lateroventral or tympanic surface of the petrous temporal bone that forms its roof. It is pear shaped and comprises the tympanic cavity proper or mesotympanum, a small dorsal epitympanic recess and a larger ventral region called the fundus or hypotympanum that occupies the TB (White 2003).

The tympanic cavity proper lies adjacent to the tympanic membrane, which separates it from the external ear canal and forms the major component of its lateral wall. This compartment is approximately 15mm long, 8-10 mm wide and high in the dog, and orientated at an angle of about 45° with the sagittal plane in a caudolateral direction. It contains three auditory ossicles, the malleus, incus and stapes, which transmit air vibrations

from the tympanic membrane across the middle ear to the inner ear. These are located with the malleus in contact with the tympanic membrane, the articulation between the malleus and incus located in the epitympanic recess and the base of the stapes occluding the vestibular or oval window medially. Beyond this window lies the vestibule of the inner ear. A second window, the cochlear or round window, is located further ventrally in the caudal portion of the tympanic cavity proper facing rostrally. This is covered by the secondary tympanic membrane that forms a thin soft tissue barrier between the tympanic cavity proper of the middle ear and the vestibule of the inner ear. Ventral to the cochlear window, the medial wall of the tympanic cavity proper bulges over the cochlea of the inner ear to form the promontory, a barrel or oval shaped bony prominence lying opposite the tympanic membrane (Little and Lane 1986, Evans 1993).

At the rostral extremity of the tympanic cavity proper is the ostium of the auditory tube. This short canal extends dorsomedially through the bony musculotubal canal and continues as a membranous structure supported medially by a hyaline cartilage plate. It runs to the lateral wall of the nasopharynx where it opens dorsal to the middle of the soft palate. The walls of the tube are usually collapsed but the lumen opens during the process of swallowing, yawning and chewing thus balancing the pressure of the air in the middle ear with atmospheric pressure (Junqueira and others 1986).

The ventrally located TB forms a smooth bulbous protuberance lying ventral to the mastoid process of the temporal bone and between the retroarticular process and the jugular or paracondylar process of the occipital bone. In the dog it is approximately 15mm in diameter with a flattened lateral wall and slightly pointed ventral margin while in the cat, it is hemispherical and approximately 10mm in diameter (Riser and others 1967). The wall is smooth in both the cat and dog, despite variations in the thickness of the bone wall and is thinnest ventrally (White 2003). In the dog, the thin ledge of bone that extends from the ventral margin of the opening of the external acoustic meatus is situated between the hypotympanum and the tympanic cavity proper. In older animals this may have fine, knobbled spicules projecting from its border.

In the cat, each TB is almost completely separated by a thin osseous septum known as the septum bullae that arises along its rostral aspect and curves to attach to the midpoint of the lateral wall (Fossum 2002). The location of this septum is marked by the presence of a

shallow groove on the external surface of the TB and represents the fusion of the tympanic ring (ectotympanum) and TB (endotympanum) during foetal development (Crouch 1969). The septum creates a large ventro-caudo-medial compartment that corresponds with the hypotympanum (fundus) in the dog and a smaller dorso-rostro-lateral one that incorporates the tympanic cavity proper (mesotympanum) and the recess of the epitympanum (Little and Lane 1986, White 2003). There still appears to be some confusion in the literature as to the location of these compartments relative to each other (Garosi and others 2003), despite this being documented definitively (Little and Lane 1986). The septum is incomplete on its dorsomedial aspect, allowing the compartments to communicate via a narrow fissure that enlarges into a triangular foramen towards its caudal edge. This opening overlies the promontory and the round window and there is a ventral lip to the septum in this area that shields these structures within the dorsal compartment (Little and Lane 1986). The actual function of the TB is not fully understood although it is thought to improve the perception of very low or high frequency sound.

Most of the middle ear is lined by cuboidal, ciliated epithelium (Spruell 1964, Neer and Howard 1982, Bruyette and Lorenz 1993), which is continuous with the respiratory epithelium of the auditory tube and the nasopharynx (Neer and Howard 1982, White 2003). Columnar cells and the largest proportion of ciliated cells are found in the tympanic cavity proper (White 2003) while simple squamous epithelium covers the most ventral portion of the fundus, the tympanic membrane, the membrane covering the cochlear or round foramen and the auditory ossicles (Spruell 1964, Neer and Howard 1982). Ciliated and secretory cells are more abundant in the chamber lining of the cat than in the dog (White 2003). The muco-ciliary apparatus of the middle ear and auditory tube actively clears foreign material and bacteria therefore acting as a defence mechanism to decrease the likelihood of infection (Neer and Howard 1982, Bruyette and Lorenz 1993). In addition, a surface tension lowering agent has been identified in the auditory tube of dogs, which helps maintain its patency. Loss of this substance through infection or inflammation can result in apposition of the walls leading to poor aeration and drainage (Bruyette and Lorenz 1993).

The inner ear is located within the petrosal part of the temporal bone and contains the bony and membranous labyrinths, which are responsible for hearing and balance (Evans 1993, Farrow 1994).

2.1.3.2. Rabbit

Although the bone elements of the TB of the rabbit have been documented (Barone 1989, Popesko and others 1992) there do not appear to be many other reports regarding the anatomy of this region. It is formed by the tympanic part of the temporal bone and continues dorsally into the short, wide, bony tube of the external auditory meatus (Popesko and other 1992). In the natural state, this large opening would be continued into the aperture of the external ear. The auditory ossicles of the rabbit have been described and although they generally resemble those of the dog, there are some distinctive features (Arnautovic and Osman 1985). The histology of the mucosal lining of the middle ear of the rabbit has been described (Flatter and others 1977) but there do not appear to be any further detailed reports.

2.1.4. Anatomy of the TMJ

2.1.4.1. Dog and cat

The canine (Scapino 1965, Ström and others 1988, Evans 1993) and feline (Caporn 1995) TMJ have been described, as has the histology of the canine inter-articular disc (Gillbe 1973, Shengyi and Yinghua 1991, Tanaka and others 1999). It is a condylar joint that is located dorsal and lateral to the molar teeth.

The squamous part of the temporal bone possesses a long curved zygomatic process that extends rostrolaterally and overlies the caudal half of the zygomatic bone to form the zygomatic arch. The ventral part of the base of this process expands to form a transversely elongated smooth area called the mandibular fossa or glenoid fossa that receives the condyle of the mandible to form the TMJ. At the rostrolateral margin of the mandibular fossa is a pronounced, roughened articular tubercle or eminence that is particularly well developed in the cat.

The retroarticular or post glenoid process is a curved, spade-like ventral extension of the squamous temporal bone at the caudal medial half of the mandibular fossa. Its rostral surface combines with the medial part of the mandibular fossa to form a funnel shaped articular surface while the narrower lateral section of the mandibular fossa remains open caudally.

The condyloid or articular process of the mandible is reported to be transversely elongated, sagittally convex and caudally directed to articulate with the mandibular fossa of the temporal bone in forming the TMJ. The condyloid process is inclined so that in a coronal plane its lateral pole is dorsal to the medial one, and in a transverse plane the lateral pole is caudal to the medial one. In the dog, the articular region of the condyle has been divided into a horizontal surface on the rostradorsal aspect and another on the caudal medial surface. It has also been divided into medial and lateral components with the medial part being a truncated cone that tapers medially with dorsal, caudal and ventral articular surfaces and a narrow lateral part with dorsal and slightly caudal articular surfaces. The condyloid process is virtually encircled by the temporal components and fits snugly into the mandibular fossa, with the exception of the caudolateral margin of the condyloid process, which is not bounded by bony parts. The lateral pole of the condyle is located dorsal and rostral to the axis of rotation. In cats, the condyloid processes are also transversely elongated and narrower in the sagittal plane but unlike the dog, are almost perfectly in line with the common axis of the TMJ (Caporn 1995).

The transversely elongated condyle of the mandible does not correspond entirely to the articular surface of the mandibular fossa and in the dog, a thin articular disc lies between the cartilage covered articular surfaces (Shengyi and Yinghua 1991). This is a roughly triangular shaped connective tissue plate that follows the outline of the articular surfaces (Scapino 1965, Ström and others 1988), so the lower surface of the disc is concave to correspond with the shape of the condyloid process while the dorsal surface is convex (Gillbe 1973, Shengyi and Yinghua 1991). It is thinner centrally than peripherally, where it is attached to the capsule (Shengyi and Yinghua 1991). The rostral margin of the disc is firmly attached to the condyle and skull (Gillbe 1973). Tendons of the lateral pterygoid muscle perforate the capsule and attach to the disc at its rostromedial margin (Scapino 1965). Medially the disc is attached to the mandibular fossa, retroarticular process and squamous part of the temporal bone (Ström and others 1988) by a stout ligamentous extension into the pit at the base of the retroarticular process (Scapino 1965, Gillbe 1973), which is thought to represent the remains of the primitive attachment of the lateral pterygoid muscle to the malleus in the middle ear. Laterally the disc is strongly attached to the condyle (Scapino 1965). These peripheral attachments mean that little movement of the disc over the skull can occur (Gillbe 1973). They also mean that the joint is divided into two separate synovial chambers that are completely unconnected histologically (Caporn

1995). The upper or dorsal meniscotemporal component is located between the disc and the temporal bone and the lower or ventral condylomeniscal component between the disc and the condyle. Therefore, as well as acting as a shock absorber and joint stabiliser, the resulting double synovial film reduces friction within the joint (Shengyi and Yinghua 1991, Tanaka and others 1999). The presence of a thick membrane was reported in cats but no disc (Gillbe 1973).

The entire TMJ is surrounded by a thin, loose, fibrous capsule (Ström and others 1988) that attaches to the retroarticular process and extends from the articular cartilage of the mandibular fossa to the condyloid process, fusing with the periphery of the disc as it crosses the joint (Evans 1993). Fibrous bands span the joint medially and laterally providing stability against excessive joint excursions (Caporn 1995). Laterally these bands are very well developed and referred to as the lateral ligament of the TMJ or temporomandibular ligament, running from the caudoventral border of the zygomatic arch to the lateral aspect of the condyle and the adjacent region of the condyloid process (Scapino 1965, Evans 1993, Caporn 1995). The mandibular fossa and retroarticular process resist dorsal, caudal and ventral displacement of the condyle while these ligaments limit medial, lateral and rostral displacement (Caporn 1995). In the cat, the well developed articular tubercle also resists rostral luxation of the condyle. Bony structures assume more responsibility for stability in the feline than the canine TMJ and therefore it is inherently more stable (Caporn 1995).

2.1.4.2. Rabbit

There appears to be only two publications providing a description of the anatomy of the rabbit TMJ (Barone 1989, Weijs and Dantuma 1981). The TMJ is located lateral to and high above the cheek teeth (Weijs and Dantuma 1981). The glenoid fossa is a longitudinal gutter (Barone 1989) formed by the narrow root of the zygomatic process (Weijs and Dantuma 1981). It is the shape of an inverted V in transverse section and its fibrocartilage covered articular facet faces caudoventrally with the medial slope of the articular surface being longer and steeper than the lateral one (Weijs and Dantuma 1981). The rostral articular tubercle is concave in the transverse plane but convex rostrocaudally, and there is no retroarticular process to prevent retropulsion of the condyle (Barone 1989).

From the dorsal aspect, the condyle is circular rostrally and tapers caudally being smaller and more rounded than the fossa (Weijs and Dantuma 1981). The articular disc is saddle shaped being relatively thick laterally and medially with a central indentation (Barone 1989, Weijs and Dantuma 1981). Although it conforms to the condyloid and glenoid articular surfaces (Weijs and Dantuma 1981), it does not cover the rostral portion of the condyloid process (Barone 1989). The rostral margin of the disc merges with loose areolar tissue adjacent to the joint while caudally it joins a strongly reinforced portion of the capsule to form a strong lateral ligament extending horizontally from the zygomatic arch where it commences a little below the external acoustic meatus and ends caudal to the condyloid process. The ventral synovial compartment is much larger than the dorsal one (Barone 1989). Part of the caudal portion of the deep masseter muscle has its origin on the articular capsule and this muscle also has a muscular insertion on the lateral aspect of the articular process (Weijs and Dantuma 1981).

The condyle can slide 6-7mm rostroventrally along the sloping articular eminence and is limited by the capsule. Transverse shift is limited to 1-2mm by the close fit of the condyle, disc, fossa and the tight capsule (Weijs and Dantuma 1981). Maximal gape amounts to 20-25° and can only be achieved with the condyles in a maximally rostral location, being limited by the capsule and soft tissue compression between the mastoid region of the skull and the mandible. Maximal horizontal deviation from the mid-sagittal plane is 10° and achieved with the condyles in an extreme caudal position (Weijs and Dantuma 1981).

2.1.5. Skull measurements

The skull of the domestic dog demonstrates a variation in size and shape far greater than any other mammalian species (Evans 1993). The majority of breeds demonstrate a mesaticephalic skull type and include the German Shepherd Dog and Border Collie. Those with long narrow heads including the Rough Collie and Greyhound are classified as dolichocephalic and those with short wide heads such as the Boxer and Cavalier King Charles Spaniel are brachycephalic. Craniometry has been used to objectively differentiate between canine skull types with a range of parameters being measured and indices calculated to take into account the absolute differences in size between breeds (Evans 1993). The most useful parameter to determine between these skull types appears to be the facial index with brachycephalic breeds reported to demonstrate an average of 215, mesaticephalic 111 and dolichocephalic 81 (Evans 1993). However, the effect of these

variations on the anatomy of the temporal region of the skull and in particular the TB and TMJ is not well reported.

Measurement of the angle between the long axis of the mandibular condyle and the axis of rotation of the TMJ on dorsoventral radiographs has been performed in dogs. The shape of the condyle associated with large angles was reported to result in excessive movement of the lateral aspect of the condyle and stretching of the lateral ligament, thereby leading to laxity of the joint (Robins and Grandage 1977, Lantz and Cantwell 1986). A variety of values have been suggested in association with normal joints, but there do not appear to be any standard values published (Robins and Grandage 1977, Lantz and Cantwell 1986, Hazewinkel and others 1993).

2.1.6. Aims

The aims of the work presented in this chapter were to:

- Review the normal anatomy of the TB and TMJ of the dog and cat and describe that of the rabbit
- Determine a system to allow accurate description of these structures for use with different imaging techniques
- Prepare and preserve multiplanar canine, feline and rabbit anatomical specimens for comparison with the diagnostic images produced in Chapters 4 and 5
- Determine the facial index in a variety of dog breeds, domestic breed cats and New Zealand White rabbits
- Determine the normal rotational angle of the canine mandibular condyle in a variety of breeds
- Investigate the influence of skull type on anatomy of the TB and TMJ in the dog

2.2. Materials and Methods

2.2.1. Cadaver material

The material used through this entire study was sourced from cadavers donated to the University of Glasgow Veterinary Anatomy unit. Prior to selection, material was checked to ensure there was no visible external evidence of ear, respiratory or dental disease and no abnormalities associated with the external ear, mouth or temporomandibular region. Border Collie canine cadavers, domestic breed feline cadavers and New Zealand White rabbit cadavers of similar size and age were selected. The heads were removed at the mid cervical region and stored at -20°C until required.

Emascerated canine, feline and rabbit skulls from the collection held in the University of Glasgow Veterinary Anatomy unit were used. Additional emascerated feline and rabbit skulls were prepared by thawing the stored material, removing as much superficial soft tissue as possible by gross dissection and then boiling in water for 2 to 10 hours depending on the size of the specimen. Any remaining soft tissue was removed and the skull boiled for a further 1 hour with detergent (Persil washing powder). The mandibles were glued at the rostral symphysis. The skulls and mandibles were labelled and stored together until required. Three of these skulls were selected for use in the radiography section of the study in Chapter 3 (Rough Collie, German Shepherd and Boxer as indicated in Table 2.3.7.).

The number of cadavers studied in this and subsequent chapters reflected the availability of material. At the end of the study, selected material was preserved using plastination and retained in the University of Glasgow Veterinary Anatomy unit for teaching purposes. The rest was disposed of via the appropriate recommended channels for biological waste.

2.2.2. Bony anatomy of the TB and TMJ in the dog, cat and rabbit.

The bony conformation of the TB and TMJ was assessed in 50 canine (48 known breed, two unknown), 10 domestic breed feline and 10 New Zealand White rabbit skulls.

Calipers were used to measure the following features in all of the skulls:

- the length (in a rostrocaudal direction) and width (in a mediolateral direction) of the external margins of the TB
- the depth of the TB (dorsal aspect of the external acoustic meatus to the ventral TB wall)
- the width (in a rostrocaudal direction) and the depth (in a dorsoventral direction) of the external acoustic meatus
- the length of the external acoustic meatus was measured in the cat and rabbit skulls

In the rabbit skulls, the following features were also measured:

- the length and width of the articular surface of the mandibular fossa
- the length of the condyloid process
- the length of the articular surface of the condyloid process
- the length and width of the rostral component of the articular surface of the condyloid process

2.2.3. Soft tissue anatomy of the TB, TMJ and surrounding areas in the dog, cat and rabbit.

Cadaver heads from five Border Collie dogs, five domestic breed cats and five New Zealand White rabbits were thawed and gross dissection of the areas surrounding the TB and TMJ performed.

2.2.4. Multiplanar anatomy of the TB and TMJ in the dog, cat and rabbit.

Frozen cadaver heads from six Border Collie dogs, six domestic breed cats and six New Zealand White rabbits were selected. A bandsaw was used to produce serial sections in two heads of each species in transverse, two in sagittal and two in dorsal planes. A metal guide plate was mounted parallel with the blade at a distance of 0.6cm. Care was taken to ensure that the first slice was parallel with the appropriate plane through the head (transverse, sagittal or dorsal). The application of pressure to keep the head in firm contact with the plate while advancing it through the bandsaw ensured that subsequent slices were as parallel as possible and an even 0.6cm thickness. Appropriate health and safety measures were observed while using the bandsaw.

Both sides of each slice were labelled and stored at -20°C until photographed. A damp cloth was used to remove frosting from the surface of each slice prior to photography.

2.2.5. Image production

Dissection material was photographed at various stages throughout the procedure using a digital camera (Olympus Camedia C-21002 ultras zoom). Where the zoom function was not sufficient to produce adequate resolution images, photography was performed through a magnifying light (Daylight™). Images of the multiplanar slices were obtained using a digital camera (Nikon D200) with a 105mm lens.

Images were transferred digitally to a desk top personal computer. Paint Shop Pro 7 software (Microsoft) was used to manipulate and label the resulting images. Anatomical texts were used to aid in the identification of the structures (Crouch 1969, Barone and others 1973, Popesko 1977, Barone 1989, Popesko and others 1992, Evans 1993).

2.2.6. Preservation of material using plastination

The transverse, sagittal and dorsal sections from one canine, feline and rabbit skull were preserved using plastination. While still frozen, the sections were placed in a 4% formaldehyde solution for 48 hours then moved into 100% acetone and stored at ambient winter outdoor temperature in a secure fireproof container. The acetone was monitored and replenished over a period of 3 to 4 weeks until the concentration remained static. The sections were then submerged in silicon (Biodur S10 Silicone Polymer; FOB, Heidelberg) and placed in a vacuum chamber at -20°C for a further 2 weeks. On removal, the sections were placed in a sealed chamber and exposed to gas cure (S6 silicone hardener 2; FOB, Heidelberg). Although they were dry to the touch after 2 days, they were left for 2 weeks to cure completely.

2.2.7. Skull measurements

2.2.7.1. Facial index in the dog, cat and rabbit.

The facial index was determined in 50 known breed canine, 10 domestic breed feline and 10 New Zealand White rabbit emasculated skulls. Calipers were used to measure the facial width and length as demonstrated in Figure 2.2.1. The facial width was defined as the widest interzygomatic distance and the facial length as the distance from the nasion (junction on the median plane of the right and left nasofrontal sutures) to the prosthion

(rostral end of interincisive suture between the roots of upper central incisors). The facial index was calculated as facial width x 100/ facial length.

2.2.7.2. Rotational angle of the canine mandibular condyle

The rotational angle of the mandibular condyles was measured in 38 known breed emasculated canine skulls with normal TMJ anatomy. The mandibular condyles were photographed from the ventral aspect to produce the same projection as that of a dorsoventral radiograph. A line was drawn through both condyles along the common long axis and a second line was drawn along the articular surface (Figure 2.2.2). The angle between the two lines was measured using a protractor.



Figure 2.2.1. Features used to measure facial width and length in dog, cat and rabbit skulls for calculation of the facial index. Facial width = white arrow. Facial length (nasion to prosthion) = black arrow.

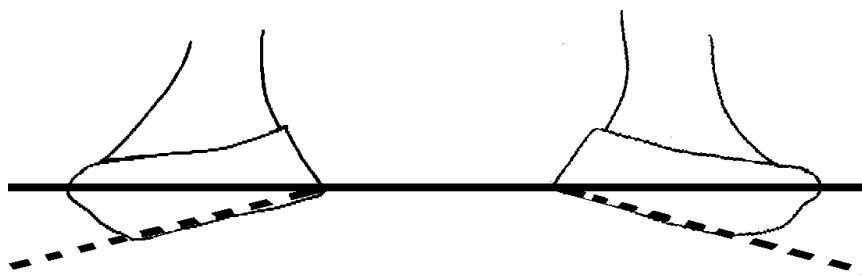


Figure 2.2.2. Measurement of the rotational angle of the mandibular condyles. Solid line = common long axis through the condyles. Dotted line = articular surface of the condyles. The angle between these lines was measured.

2.3. Results

2.3.1. Bony anatomy of the TB and TMJ in the dog, cat and rabbit

2.3.1.1. Canine TB

An emascerated skull from a German Shepherd dog with a facial index of 110 (mesaticephalic) was selected as being representative of a typical (mesaticephalic) canine skull type according to the criteria presented by (Evans 1993) and was used to produce the images of the TB and TMJ in the dog. The appearance of the bony components of the TB in the dog is demonstrated in Figure 2.3.1. and the key in Table 2.3.1. The dimensions measured in the TB are demonstrated in Table 2.3.2.

The TB appeared similar in all of the skulls that were examined. They were located on the ventral aspect of the squamous temporal bone and projected ventral to the level of the basioccipital bone. There was a prominent muscular tubercle on the basioccipital bone adjacent to the rostral half of the tympani-occipital suture, which varied in size between skulls. The TB were bilaterally symmetrical and their flattened caudomedial border gave them a rhomboidal appearance when viewed from the ventral aspect. There was a subtle depression on the external surface of the TB running from the ventral aspect of the external acoustic meatus to the middle of the tympano-occipital suture. Caudal to the TB, the paracondylar / jugular process of the occipital bone extended in a caudoventral direction. The mastoid process of the temporal bone was a smaller bony protuberance immediately caudodorsal to the external acoustic meatus. The bone tube that formed the external acoustic meatus ran horizontally with the caudal wall being longer than the rostral one and in mature skulls, often demonstrated an irregular lateral margin. The length of the external acoustic meatus could not therefore be accurately measured.

The promontory was a distinctive tubular shaped area of bone with the larger cochlear or round window at its caudal border and the slightly smaller vestibular or oval window dorsal to it. Ventral to the promontory, the boundary between the squamous temporal bone and the medial wall of the TB was visible as an irregular concave line. From the caudal aspect of this suture line, a more well developed ridge of bone extended in rostral and lateral directions to divide the rostral region of the lumen into dorsal and ventral areas. The internal ostium of the auditory tube was located at the rostral extremity of the dorsal area. The internal margin of the ventral region of the external acoustic meatus projected into the

lumen above the bone ridge producing a bone shelf under which the rostral and lateral areas of the lumen were located. This resulted in the lateral wall of the TB being thickest while the ventral wall was the thinnest.

2.3.1.2. Feline TB

The appearance of bony components of the TB in the cat is demonstrated in Figure 2.3.2 and the key in Table 2.3.1. The dimensions measured in the TB are demonstrated in Table 2.3.2. The TB appeared similar in all of the skulls that were examined.

The TB were bilaterally symmetrical structures located on the ventral surface of the squamous temporal bone, projecting ventral to the level of the basioccipital bone. There was no muscular tubercle associated with the basioccipital bone. The TB bone surface was very smooth and the TB had a bulbous appearance with an oval shaped outline when viewed from the ventral aspect. There was a marked depression on the external surface of the TB running ventral to the external acoustic meatus and extending to the rostral end of the tympano-occipital suture. The external acoustic meatus took the form of a horizontally orientated shallow bone ring in the cat. In older animals, the external margin was occasionally irregular but in the rest of the skulls it remained smooth. Caudodorsal to the external ear canal, the mastoid process was a very small bony bump and the paracondylar / jugular process almost non-existent.

The dorsal half of the promontory was visible through the external acoustic meatus as a cylindrical, smooth walled bony structure. The small vestibular window could be seen dorsal to the promontory while the cochlear window was visible as a distinctive round hole at its caudal margin. A prominent ridge of bone ran in a rostro-medial caudo-lateral direction across the lateral aspect of the promontory and bridged the space between the promontory and the lateral TB wall, obscuring the ventral part of the promontory and cochlear window from view. This ridge was continuous with the lateral aspect of the TB wall where it was accompanied by the corresponding depression on the external surface of the bone previously mentioned. This resulted in a complete, concave bone septum separating the small rostradorsal compartment from the larger caudoventral area of the lumen. The only communication between the two compartments was through the space produced by the bridging of the bone ridge in the region of the cochlear window previously mentioned.

Removal of the ventral TB wall allowed the smooth convex ventral surface of the bone septum to be visualised along with the ventral compartment of the TB. The ventral half of the promontory and cochlear windows could be visualised and the boundary between the squamous temporal bone and the medial wall of the TB produced a concave line immediately ventral to the promontory. The rostral part of this line merged with the rostral medial margin of the bone septum. There was a small bone ridge at the internal margin of the external acoustic meatus resulting in the lateral wall being the thickest and the ventral surface the thinnest.

2.3.1.3. Rabbit TB

The appearance of bony components of the TB in the rabbit is demonstrated in Figure 2.3.3. and the key in Table 2.3.1. The dimensions measured in the TB are demonstrated in Table 2.3.2. The TB appeared similar in all of the skulls that were examined.

The TB in the rabbit were located on the ventrolateral aspect of the skull, caudal to the squamous temporal bone. They had a smooth convex outer bone surface, appeared relatively rounded and did not project as far ventrally as the adjacent occipital bone. The bone wall of the TB was thinnest ventrally and thickest laterally, at the boundary between the external acoustic meatus and the TB wall, which was marked by a smooth internal bony rim and a rough external one. The external acoustic meatus was formed by a prominent bony tube, extending from the lateral aspect of the TB in a caudodorsal direction. The retrotympenic process was a fine finger of bone projecting from the caudal margin of the squamous temporal bone immediately dorsal to the external acoustic meatus and extending over the surface of the petrous temporal bone in a caudoventral direction terminating dorsal to the mastoid process. The mastoid process was an elongated bony structure arising from the petrous temporal bone caudal to the external acoustic meatus and extending ventrally to project below the level of the TB. Caudal and parallel to this ran the paracondylar or jugular process of the occipital bone.

Removal of the ventral bone wall of the TB exposed the bone ledge at the internal margin of the external acoustic meatus. Further removal of the lateral bone wall exposed the middle ear cavity. There do not appear to be any anatomical descriptions of these internal

features in the rabbit so they were identified by extrapolating from the features in other species (Little and Lane, 1986; Barone, 1989; (Evans 1993); Farrow, 1994).

The smooth bone wall of the semicircular shaped promontory was visible on the medial wall with the vestibular and cochlear windows located at its dorsal and caudal aspects respectively. The vestibular window was the same size or even slightly larger than the cochlear one. The internal opening of the auditory tube was immediately rostral to the promontory. The large epitympanic recess was located dorsal to the vestibular window and extended medial to the bone ledge at the internal margin of the external acoustic meatus. The suture between the TB wall and the petrous temporal bone was visible as a horizontal line ventral to the promontory and extending in a dorsal direction rostral to the promontory. There was no bone ridge present so the TB lumen was a single compartment. However, the carotid canal was present as a hollow ridge of bone running down the medial wall of the TB ventral to the promontory. It emerged at the external carotid foramen on the external surface of the ventromedial aspect of the TB.

The middle ear cavity proper occupied the space between the base of the external acoustic meatus and promontory, while the hypotympanum was located within the confines of the TB ventrally and extended rostr dorsally around the ostium of the auditory tube. The auditory ossicles were lost during the preparation process but would have been located within the middle ear cavity and epitympanic recess.

2.3.1.4. Canine TMJ

Three of the 50 canine skulls were from Cavalier King Charles Spaniels and in each, marked conformational variations were noted in the anatomy of the TMJ when compared with those of the other skulls. They were therefore excluded from the TMJ studies in this chapter but the results of further investigation into the variations observed are presented in Chapter 8. The anatomy of the TMJ in the remaining 47 skulls was very similar and the appearance of the bony components is demonstrated in Figure 2.3.4. with the key in Table 2.3.3. Each articular surface was divided into regions for descriptive purposes as demonstrated in Figure 2.3.5.

The condyloid process was mildly angled in a laterodorsal rostroventral direction. The articular surface was made up of a medial and lateral aspect, each occupying approximately

half of the condyloid process. The lateral surface occupied the dorsal and caudal aspects of the condyloid process and was convex in all directions. The medial surface extended in a curve occupying the dorsal, caudal and ventral aspects of the condyloid process, reflecting the shape of the corresponding retroarticular process and was more flattened in a mediolateral direction. The medial margin of the condyloid process was produced by the angular shape of the edge of the medial articular surface and the most laterally placed protrusion of the condyloid process was rounded in shape and located in a rostradorsal position. However, this extremity was non-articular as the lateral articular surface terminated just medial to it.

The mandibular fossa occupied the ventral surface of the zygomatic process of the temporal bone and was also mildly angled in a laterodorsal rostroventral direction. There was a small non-articular bony protrusion at the rostrrolateral margin of the mandibular fossa on the rostroventral aspect of the zygomatic process. Both the lateral and medial articular surfaces of the mandibular fossa were concave in a rostrocaudal direction and the medial half of the articular surface was continuous caudally and ventrally with that of the retroarticular process. This bony protrusion was broadest dorsally and tapered to a blunt end ventrally formed by the meeting of the well-defined lateral and medial margins. The ventral margin was slightly oblique, being angled at a mediodorsal - lateroventral angle. The articular surface of the retroarticular process was concave in a dorsoventral direction but slightly convex in a lateromedial one. At the medial aspect of the retroarticular process was a well-defined, conical shaped pit in the bone surface.

Variations in the shape of the TMJ components were noted mainly between the different breeds but there was also some variation between individuals within a breed. The most obvious was in the overall length of the condyloid process and mandibular fossa, which was related to the length of the caudal portion of the zygomatic process and this was therefore affected by the breed of dog. When viewed from a dorsoventral direction, there was a variation in the angle formed between the medial and lateral condylar articular surfaces with German Shepherd dogs having the flattest margin and Boxers the most acute. Closer examination of the Boxer mandibular fossa revealed a matching caudolateral angulation of the medial aspect of the mandibular fossa and its rostral margin. The shape of the retroarticular process also varied between breeds with the Boxer having a more vertically orientated process while in other breeds such as the Mastiff, the medial margin of

the retroarticular process was markedly convex in outline and extended further medially than in other breeds such as the German Shepherd dog.

2.3.1.5. Feline TMJ

The appearance of the bony components of the feline TMJ is demonstrated in Figure 2.3.6. with the key in Table 2.3.3. Each articular surface was divided into regions for descriptive purposes as demonstrated in Figure 2.3.7. The components of the TMJ appeared similar in all of the skulls that were examined

The condyloid process was horizontally orientated. The articular surfaces extended to the medial and lateral margins of the condyloid process, being convex dorsoventrally and flat mediolaterally. They were relatively smooth and featureless so there was no clear distinction between the medial and lateral parts of the articular surface. The dorsal and caudal parts of the articular surface were both very narrow and occupied the dorsal and caudal aspects of the condyloid process respectively. The lateral part of the caudal surface tapered laterally in some cats giving it an almost triangular shape. The ventral articular surface was also triangular in shape with an upright medial margin and tapering lateral one that merged with the tapering margin of the caudal articular surface. This resulted in poor distinction between the ventral and caudal lateral articular surfaces but reflected the corresponding shape of the retroarticular process.

The mandibular fossa in the cat was located on the ventral surface of the transversely orientated caudal portion of the zygomatic process and was also orientated horizontally. The medial and lateral articular surfaces were concave but there was no bony prominence at the rostrolateral aspect of the articular surface as in the dog. However, there was a ridge of bone projecting from the ventral surface of the zygomatic process of the temporal bone along the rostral margin of the articular surface, which was most prominent laterally and in some cats terminated laterally in a bony tubercle. This ridge was continuous with the medial and lateral articular surfaces of the mandibular fossa. The medial articular surface was also continuous ventrally with the retroarticular process as in the dog. This was a finer structure than in the dog with a more vertical medial margin, a curved lateral one and a horizontally orientated ventral one. Its articular surface was concave dorsoventrally but relatively flat mediolaterally. When viewed from the lateral aspect the combination of the rostral bone ridge, the mandibular fossa and the retroarticular process produced a

semicircular shape to the articular surface. When the mandible was rearticulated this conformed well to the shape of the condyloid process resulting in a closely fitting joint. The pit at the medial aspect of the retroarticular process was not as well-defined in the cat as it was in the dog.

2.3.1.6. Rabbit TMJ

The appearance of the bony components of the rabbit TMJ are demonstrated in Figure 2.3.8 with the key in Table 2.3.3. Each articular surface was divided into regions for descriptive purposes as demonstrated in Figure 2.3.9. The components of the TMJ appeared similar in all of the skulls that were examined

The mandibular condyle was the most dorsal component of the mandible, extending dorsal to the level of the poorly developed coronoid process. The condyle was elongated in a rostrocaudal direction with a mean length of 1.11cm (SD 0.07). The convex articular surface occupied approximately three quarters of the dorsal aspect having a mean length of 0.83 cm (SD 0.06). The rostral section of the articular surface (mean length 0.355cm (SD 0.04), therefore making up approximately 40% of the articular surface) was particularly wide (mean 0.49cm (SD 0.02)) with a very marked convex surface. The caudal section of the articular surface then tapered to a point dorsomedially.

The articular surface of the temporal bone was located on the ventral aspect of the zygomatic part of the temporal bone and was short (mean 0.375cm; SD 0.03), narrow (mean 0.62cm; SD 0.04) and very deep. The rostral component of the articular area was formed by the articular process and had a convex articular surface. The caudal component was formed by the mandibular fossa and had a concave surface. There was no retroarticular process in the rabbit.

Rearticulation of the TMJ components was difficult due to the poor congruity between the joint surfaces and the large range of potential positions the condyle could occupy relative to the fossa in a rostrocaudal direction. In general, the condyloid process sat best just caudoventral to the mandibular fossa. Lateral positioning was restricted by the narrow mandibular fossa and the caudal projection of the zygomatic bone that extended alongside the condyle. The TMJ was located dorsal and caudal to the molar arcade.

Although the anatomy of the TB and TMJ was similar in all of the rabbit skulls examined, variations were noted in the anatomy of the base of the skull. These are described further in Chapter 8.

<u>Label</u>	<u>Description</u>
1	retroarticular process
2	mastoid process
3	paracondylar / jugular process
4	external acoustic meatus
5	TB (lateral wall)
6	TB (ventral surface)
7	Tympano-occipital fissure
8	muscular tubercle
9	TB (caudal surface)
10	TB lumen
11	bone ridge (dog) / septum (cat) within TB
12	promontory
13	epitympanic recess
14	suture line between squamous temporal bone and medial wall of TB
15	bone ledge at the internal margin of the external acoustic meatus
16	external carotid foramen (rabbit)
17	retrotympanic process (rabbit)
a	vestibular / oval window
b	cochlear / round window
c	internal opening of the auditory tube
*	depression in bone surface

Table 2.3.1. Key for the bony components of the typical canine, feline and rabbit TB demonstrated in Figures 2.3.1. to 2.3.3.

Figure 2.3.1. Bony components of a typical canine tympanic bulla (TB). For key see Table 2.3.1.

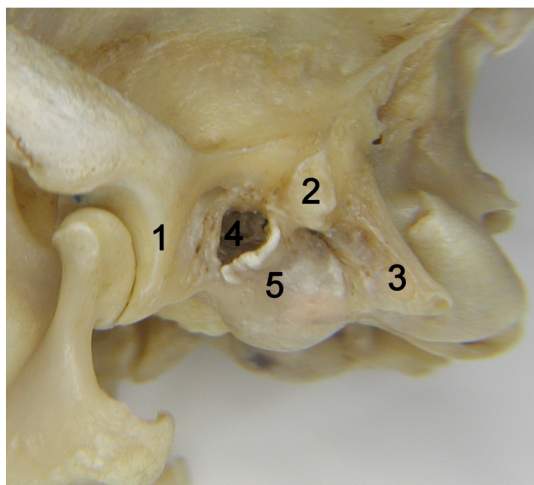


Figure 2.3.1.1. The left TB of the dog viewed from a lateral perspective. Rostral = left.

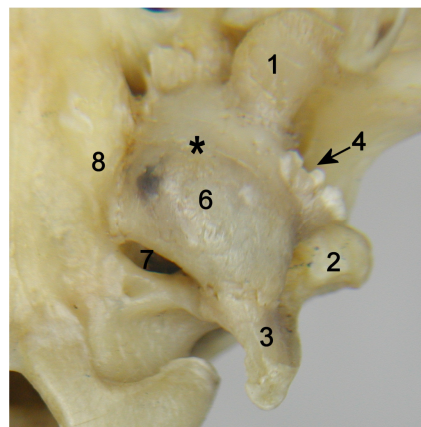


Figure 2.3.1.2. The left TB of the dog viewed from a ventral perspective. Rostral = top.

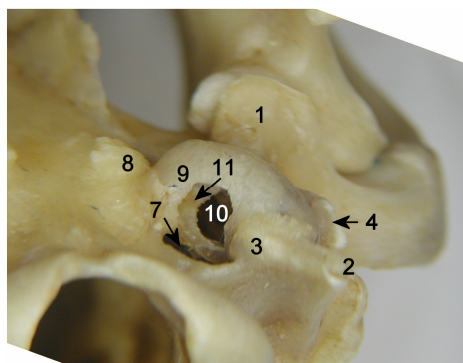


Figure 2.3.1.3. The left TB of the dog viewed from a caudal perspective through a hole created in the caudomedial wall. Ventral = top.

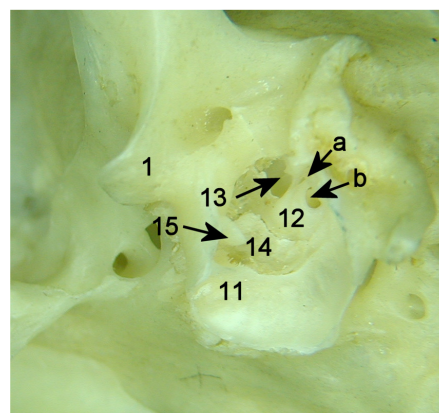


Figure 2.3.1.4. The left TB of the dog viewed from a lateral and slightly ventral perspective with the wall removed. Rostral = top left.

Figure 2.3.2. Bony components of a typical feline tympanic bull (TB). For key see Table 2.3.1.

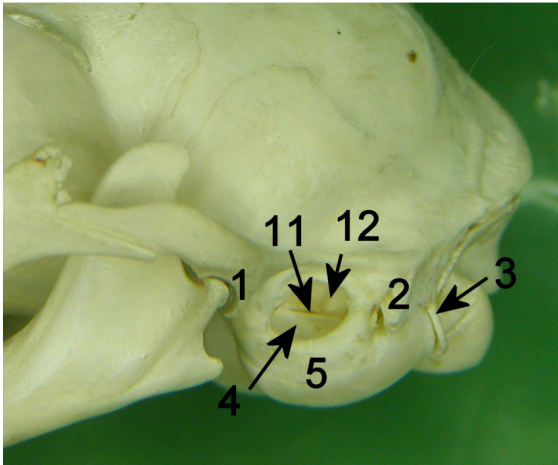


Figure 2.3.2.1. The left TB of the cat viewed from a lateral perspective. Rostral = left.

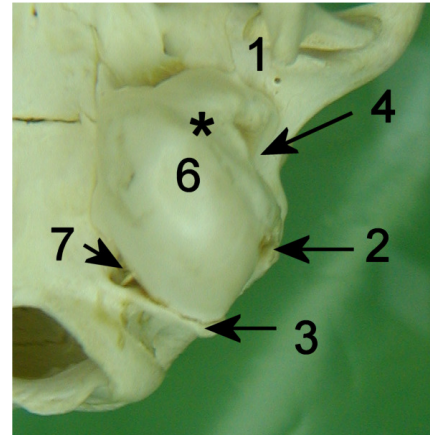


Figure 2.3.2.2. The left TB of the cat viewed from a ventral perspective. Rostral = top.

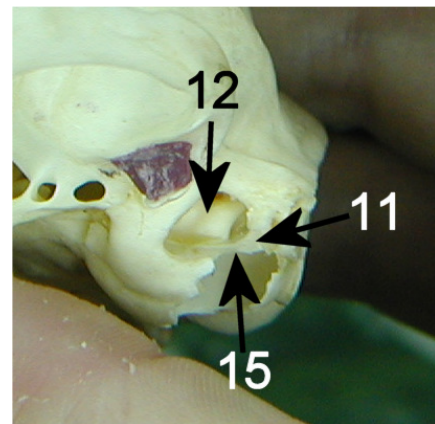
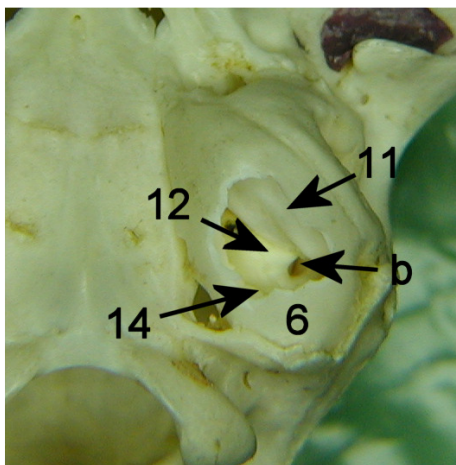


Figure 2.3.3. Bony components of a typical rabbit tympanic bulla (TB). For key see Table 2.3.1.

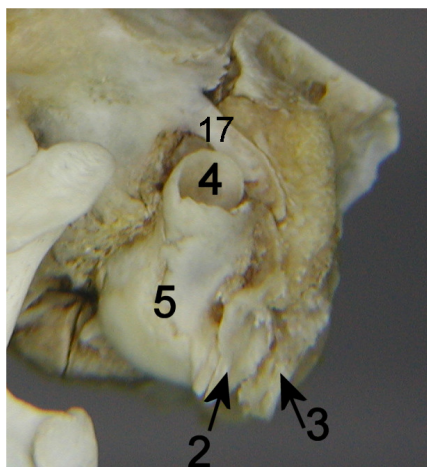


Figure 2.3.3.1. The left TB of the rabbit viewed from a lateral perspective. Rostral = left

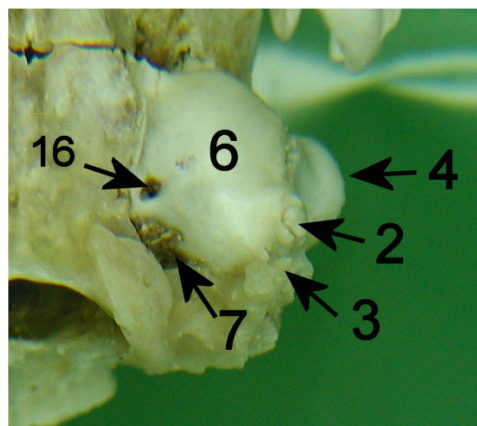


Figure 2.3.3.2. The left TB of the rabbit viewed from a ventral perspective. Rostral = top.

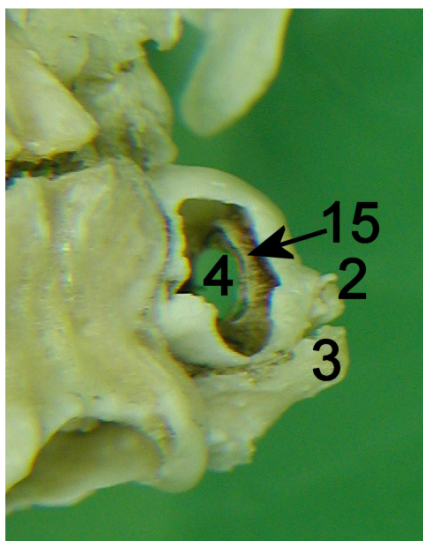


Figure 2.3.3.3. The left TB of the rabbit viewed from a caudo-medial perspective with the ventral wall removed. Rostral = top.

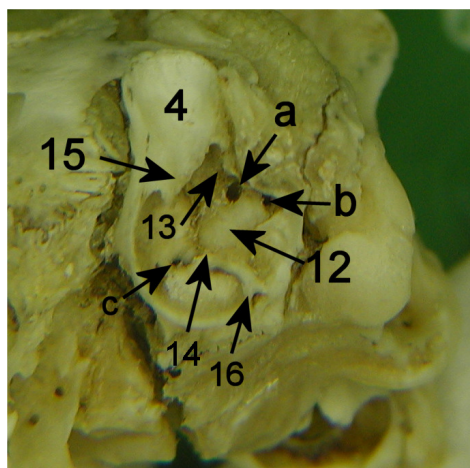


Figure 2.3.3.4. The left TB of the rabbit viewed from a lateral perspective with the lateral and ventral walls removed. Rostral = left.

	Dog Mean	SD	Cat Mean	SD	Rabbit Mean	SD
<u>Tympanic Bulla</u>						
Length	2	0.4	1.87	0.11	1.13	0.06
Width	1.58	0.4	1.28	0.06	0.9	0.04
Depth	1.6	0.4	1.16	0.08	0.96	0.08
<u>External Acoustic Meatus</u>						
Length	NP	NP	0.24	0.03	0.76	0.04
Width	0.49	0.09	0.43	0.03	0.68	0.06
Depth	0.77	0.1	0.75	0.04	0.62	0.04

Measurements all in cm

SD = standard deviation

NP = not performed

Table 2.3.2. Dimensions of the TB in the dog, cat and rabbit.

<u>Label</u>	<u>Description</u>
1	condyloid process of mandible
2	neck of the condyloid process
3	angular process of mandible
4	coronoid process of mandible
5	mandibular fossa
5a	ridge at rostral margin of mandibular fossa - cat
6	protrusion at rostralateral aspect of mandibular fossa
7	retroarticular process
8	zygomatic process of the temporal bone
9	molar arcade
10	caudal extension of the temporal process of the zygomatic bone
11	external acoustic meatus

Table 2.3.3. Key for the bony components of the typical canine, feline and rabbit TMJ demonstrated in Figures 2.3.4., 2.3.6 and 2.3.8.

Figure 2.3.4. Bony components of a typical canine temporomandibular joint (TMJ).
For key see Table 2.3.3.

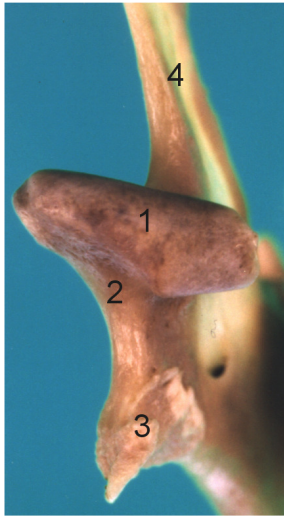


Figure 2.3.4.1. The left condyloid process viewed from a caudal perspective. Dorsal = top.

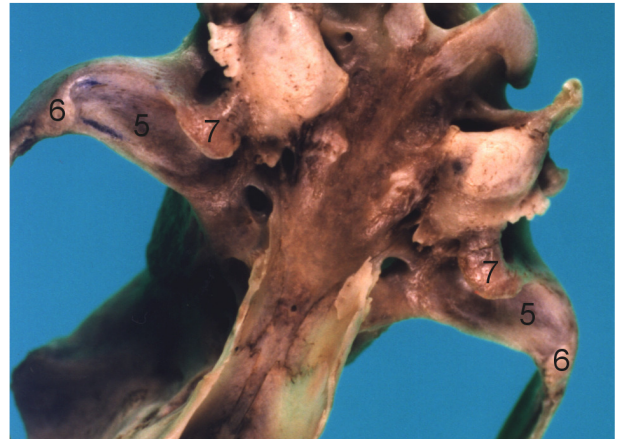
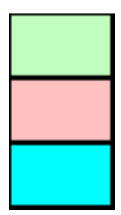
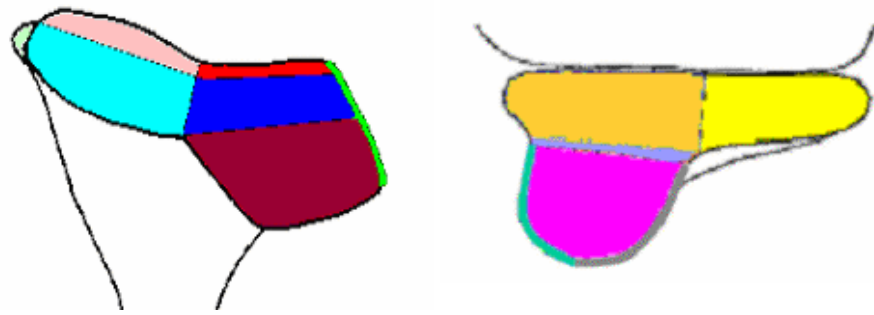


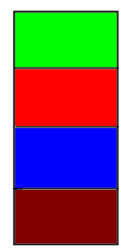
Figure 2.3.4.2. The mandibular fossae viewed from an oblique ventral perspective. Rostral = bottom left.



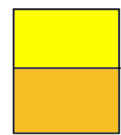
Figure 2.3.4.3. The articulation between the condyloid process, mandibular fossa and retromandibular process forming the left TMJ, viewed from a ventrolateral perspective. Rostral = left.



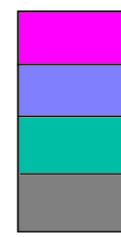
Lateral aspect of mandibular condyle
 Lateral protrusion
 Dorsal articular surface
 Caudal articular surface



Medial aspect of mandibular condyle
 Medial margin
 Dorsal articular surface
 Caudal articular surface
 Ventral articular surface



Mandibular Fossa
 Lateral aspect
 Medial aspect



Retroarticular process
 Articular surface
 Base
 Medial margin
 Lateral margin

Figure 2.3.5. Regions of the articular surfaces of the canine TMJ for descriptive purposes.

Figure 2.3.6. Bony components of a typical feline temporomandibular joint (TMJ).
For key see Table 2.3.3.



Figure 2.3.6.1. The left condyloid process viewed from a caudal perspective. Dorsal = top.

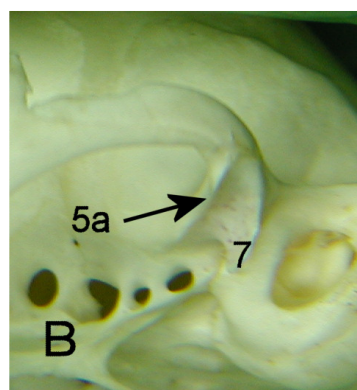
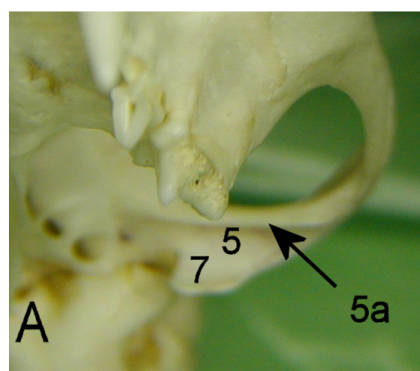


Figure 2.3.6.2. The left mandibular fossa.

A. Viewed from a rostral perspective. Dorsal = top.

B. Viewed from an oblique lateral perspective. Rostral = left.

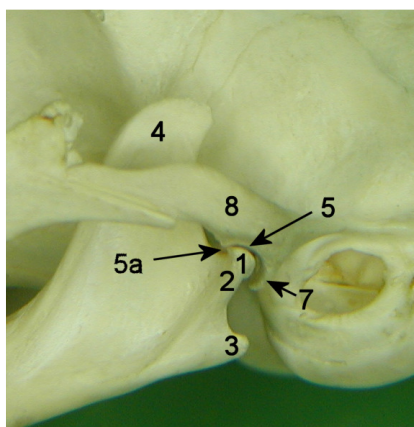
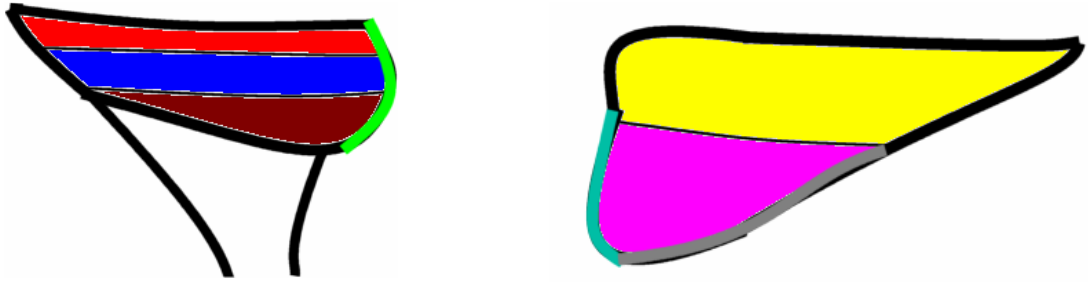
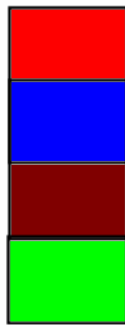


Figure 2.3.6.3. The articulation between the condyloid process, mandibular fossa and retroarticular process forming the left TMJ, viewed from a lateral perspective. Rostral = left.



Mandibular condyle



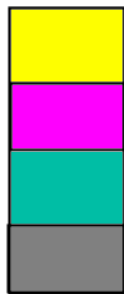
Dorsal articular surface

Caudal articular surface

Ventral articular surface

Medial margin

Mandibular fossa



Dorsal articular surface

Ventral articular surface (retroarticular process)

Medial margin of retroarticular process

Lateral margin of retroarticular process

Figure 2.3.7. Regions of the articular surfaces of the feline TMJ for descriptive purposes.

Figure 2.3.8. Bony components of a typical rabbit temporomandibular joint (TMJ).
For key see Table 2.3.3.

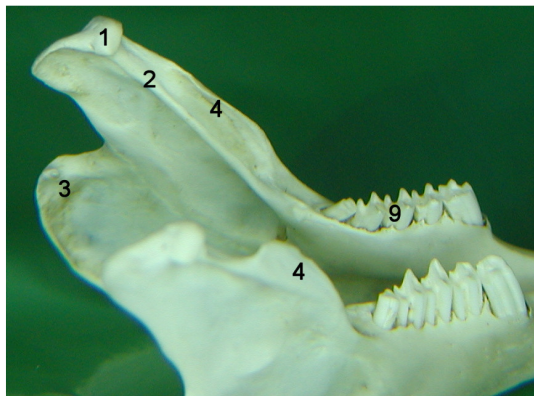


Figure 2.3.8.1. The left condyloid process viewed from a medial perspective. Rostral = right.



Figure 2.3.8.2. The left condyloid process viewed from a caudal dorsal perspective. Rostral = top right.

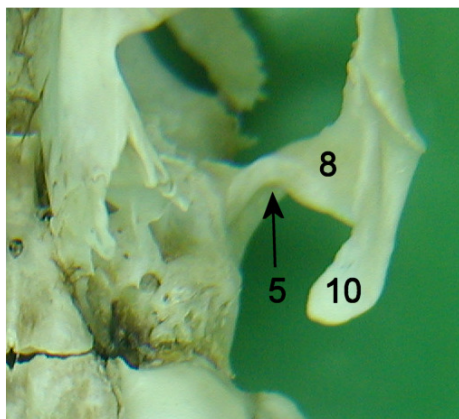


Figure 2.3.8.3. The left mandibular fossa viewed from a ventral perspective. Rostral = top.

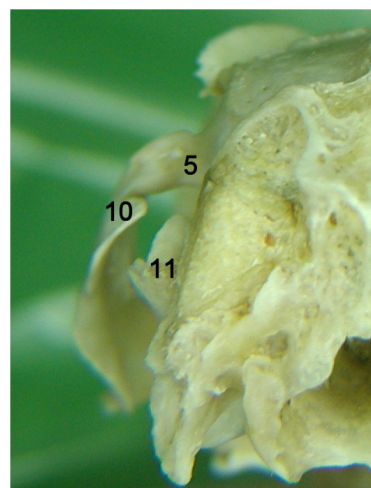


Figure 2.3.8.4. The left mandibular fossa viewed from a caudoventral perspective. Dorsal = top.

Figure 2.3.8. continued. Bony components of a typical rabbit temporomandibular joint (TMJ) . For key see Table 2.3.3.

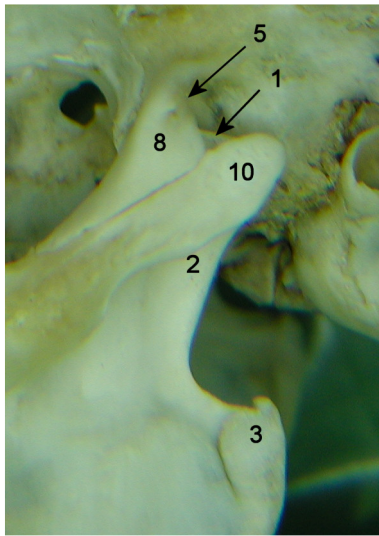


Figure 2.3.8.5. The articulation between the condyloid process, mandibular fossa and retroarticular process forming the left TMJ, viewed from a lateral perspective. Rostral = left.

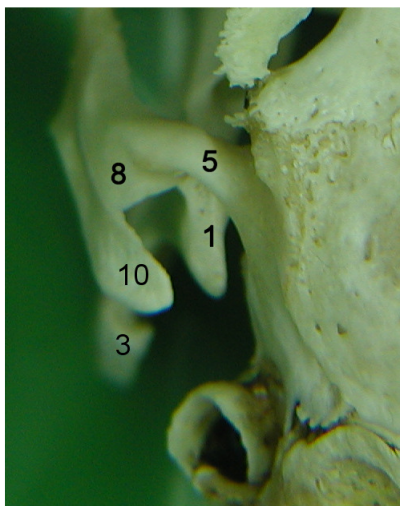


Figure 2.3.8.6. The left TMJ viewed from a dorsal perspective. Rostral = top.

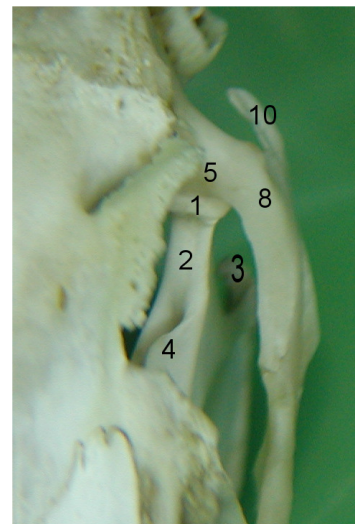
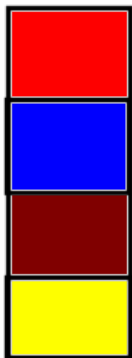
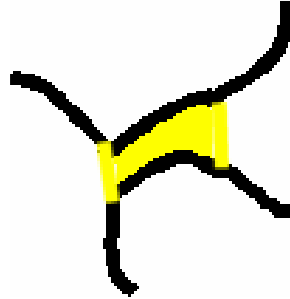


Figure 2.3.8.7. The left TMJ viewed from a rostradorsal perspective. Rostral = bottom.



- Rostral articular surface of mandibular condyle
- Dorsal articular surface of mandibular condyle
- Dorsal non-articular area of mandibular condyle
- Ventral articular surface of mandibular fossa

Figure 2.3.9. Regions of the articular surfaces of the rabbit TMJ for descriptive purposes.

2.3.2. Soft tissue anatomy of the TB, TMJ and surrounding areas in the dog, cat and rabbit.

2.3.2.1. Dog and cat TB, TMJ and surrounding area

The anatomical features observed in the dog and cat are demonstrated in Figures 2.3.10. and 2.3.11. with the key in Table 2.3.4. The soft tissue anatomy of the dog and cat were similar and so have been described together.

Immediately beneath the skin surface was the superficial and intermediate portions of the deep sphincter coli muscle that took the form of delicate transverse fibres. The platysma was a sheet of muscle running rostrally from the dorsal tendinous raphe of the neck across the cheek to the commissure of the lips. These structures were particularly fine in the cat and difficult to separate from the skin. The parotidoauricular muscle was a well developed vertical band of muscle in the dog overlying the parotid salivary gland and extending ventrally towards midline, while in the cat, it was much less well defined. Subcutaneous fascia and fat then separated the skin and these superficial structures from the parotid salivary gland, which overlay the lateral aspect of the vertical ear canal. The mandibular salivary gland in both species was located within the fat caudal to the mandible. The lingual and facial veins ran across the surface of the gland and converged to form the linguofacial vein before running caudally to join the maxillary vein in forming the external jugular vein. Lymph nodes of varying size and shape were embedded in the fascia and fat adjacent to these vessels around the caudal aspect of the mandible in both species, with the cat also demonstrating a parotid lymph node located caudal to the parotid salivary gland.

The caudal aspect of the digastricus muscle was associated with the caudal aspect of the mandible and was located rostromedial to the salivary glands. In the cat, it had a distinctive transverse band running across it at the level of the TB. Following its caudomedial border, blunt dissection allowed separation from the more medially located mylohyoideus muscle in both species. This exposed the lateral aspect of the horizontally orientated hyoglossus muscle and the rostroventrally orientated styloglossus muscle, which covered that lateral aspect of the hyoid apparatus. The presence of the hypoglossal nerve (Cranial Nerve XII) running across the surface of the hyoglossus muscle prior to entering the base of the tongue confirmed its identity and these structures required medial retraction. Digital palpation then located the TB deep to the styloglossus muscle and hyoid apparatus, and guided further blunt dissection to expose the ventral aspect. The shape of the cat skull meant the TB was

closer to the skin surface and a large area of the ventral surface could be easily exposed whereas deep dissection was required in the dog resulting in exposure of a smaller area.

The TMJ was accessed by dissecting between the masseter muscle and the external ear canal, and resulted in exposure of the caudal aspect of the joint. Further sectioning of the fibrous attachment between the masseter muscle and the zygomatic process allowed exposure of the lateral aspect of the joint and the medial portion of the masseter muscle. The caudolateral aspect of the joint space, between the lateral aspect of the zygomatic process and retroarticular process, and the corresponding areas of the condyloid process, could be visualised through the intact joint capsule. In the cat, the mandibuloauricularis muscle overlay the caudal aspect of the joint, running from the caudal margin of the tragus of the ear to the caudal aspect of the mandible between the angular and condyloid processes. This structure was not well represented in the dog.

Incision through the lateral and caudal aspects of the TMJ capsule allowed visualisation of the joint space that contained a small volume of synovial fluid. In the dog, the disc was identified as a thick fibrous pad that appeared to be most intimately associated with the condyloid process, although incision through the joint capsule between these two structures revealed the presence of synovial fluid in this area also. In the cat, only a thin fold of fibrous tissue running across the joint space could be identified as representing the disc. The lateral ligament in the dog was identified between the zygomatic arch and the non-articular lateral extremity of the condyloid process and sectioned. This was not very distinct in the cat.

Disarticulation of the joint required dissection of the muscles attaching to the coronoid process of the mandible, including the masseter and temporalis muscles, and its displacement to the lateral aspect of the zygomatic process. The disc was attached firmly to all aspects of the surrounding joint capsule, therefore dissection of these attachments was required to allow its removal. Its shape in the dog closely mirrored that of the joint components while in the cat, it did not appear to have a distinctive form.

2.3.2.2. Rabbit TB, TMJ and surrounding structures

The soft tissue structures associated with the region of the TB and TMJ in the rabbit are demonstrated in Figure 2.3.12. with the key in Table 2.3.5.

The sphincter coli muscle was not easily identifiable and removed with the skin. The next muscle layer was very fine and difficult to separate from the skin and fascia. There was some disagreement in the literature as to the arrangement and naming of these muscles (Barone, 1989; Popesko et al. 1992) but they appeared to comprise the zygomatic or zygomatic-auricular; zygomatic-auricular or zygomatic-mandibular; zygomatic-scutular or zygomatic; parotidoauricular; various sections of the scutulo-auricular; fronto-scutular and platysma muscles.

The parotid salivary gland was embedded in the fat on the lateral aspect of the head, caudal to the mandible and deep to the vertically orientated parotidoauricular muscle. Dorsally, it overlay the external ear canal and external acoustic meatus but further ventrally it was separated from the lateral aspect of the TB by the muscles attaching to the mastoid process. The gland was very diffuse in nature and difficult to distinguish from the surrounding fat. Reflection of these superficial muscles and removal of the fat allowed the maxillary and linguofacial veins to be identified. The caudal mandibular lymph nodes were located between these vessels as they converged to form the jugular vein.

Removal of the fat from the lateral aspect of the neck revealed the cervical muscles. The sternohyoid muscle ran along the ventral midline over the larynx. The sternocephalic / sternomastoid muscle attached to the distal end of the mastoid process and also the jugular / paracondylar process running in a caudoventral direction. The cleidomastoid muscle, part of the brachiocephalic group, attached to the proximal section of the mastoid process and also ran caudoventrally. The trapezius muscle covered the dorsal aspect of the neck and attached cranially to the external occipital protuberance, where its fibres merged with those of the cleidomastoid muscle. Deep to the trapezius ran the third head of the rhomboideus muscle, which attached to the nuchal crest of the skull, and the splenius muscle (attached to the wing of the atlas and then the mastoid process, deep to the attachment of the cleidomastoid muscle). Further ventrally ran the omotransversarius muscle (attached onto the basilar area of the occipital bone) and the cleidobasilar muscle (also part of the brachiocephalic group and attached at the junction between the basioccipital and sphenoid

bones). Reflection of these structures revealed the muscles associated with the cervical vertebrae. The most prominent component was the long muscle of the head that attached to the junction between the basal area of the occipital bone and the sphenoid bone along with the cleidobasilar muscle.

From a ventral approach, removal of fat and fascia revealed the submandibular salivary glands and the maxillary and linguofacial veins. The salivary gland was located medial to the mandible and being a more well defined structure than the parotid salivary gland, was easier to identify. The rostral mandibular lymph nodes were also located in this region. Removal of these structures revealed the structures ventral to the TB. The rabbit does not have a stylohyoid or epihyoid bone in its hyoid apparatus. The thyrohyoid bones were visible extending in a caudolateral direction from the ventral surface of the larynx. The stylohyoid muscle was a small structure running rostroventrally from the jugular process to the thyrohyoid bone. Immediately deep to it was the tendon of origin of the digastricus muscle, which also arose from the jugular process and ran in a rostral direction to insert onto the ventral surface of the mandible. Deep again was the styloglossus muscle, which also appeared to originate from the region of the jugular or mastoid process. It ran rostro-ventro-medially and featured a prominent longitudinal tendinous component. Section of this structure revealed mineralised fragments at its origin. The digastricus muscle in the rabbit also has a distinct second part called the mandibular retractor muscle that was located along the ventral surface of the mandibular angle and also had a lateral attachment on the jugular process. Sectioning of these structures and removal of the associated fat revealed the ventral surface of the TB that extended laterally to the external acoustic meatus.

From the dorsal aspect, the frontal muscle occupied the most superficial position. Removal of the frontal muscle revealed the superficial part of the temporal muscle below. This occupied the temporal fossa and ran under the orbital ligament and cranial to the TMJ before inserting onto the coronoid process of the mandible. The deeper part originated within the orbit and was therefore not relevant to the current description. Lateral to the temporal muscle lay the styloauricular muscle. This was a prominent band running caudally and then proximally along the medial aspect of the external ear canal. Rostrally, it was attached to caudal aspect of the TMJ capsule and also the caudal extension of the zygomatic bone.

The TMJ had a strong lateral ligament running to the zygomatic process that was continuous with the articular disc rostrally. With the mouth closed, the caudal part of the mandibular condyle was orientated approximately horizontally. However, opening the mouth drew it rostrally and ventrally (compare figures 2.3.12.9 and 2.3.12.10). The lateral ligament of the TMJ was sectioned and the attachments of the styloauricular muscle were clearly visible. The medial and lateral pterygoid muscles originated in the pterygoid fossa and inserted onto the medial aspect of the mandible, occupying the area medial to the TMJ from the ventral aspect.

Disarticulation of the TMJ required extensive dissection. The joint capsule was extensive, and closely associated with the surrounding fascia, the zygomatic process laterally, the temporal muscle rostrally, the pterygoid muscles medially and the styloauricular muscle caudally. The articular disc was located within the mandibular fossa and attached to the surrounding joint capsule creating a small dorsal compartment and larger ventral compartment. This arrangement was reflected in the observation that the disc remained more closely associated with the fossa despite extreme movement of the mandibular condyle. On removal, the disc appeared saddle shaped, being oval in outline with a thin centre and thicker periphery producing convex indentations dorsally and ventrally to accommodate the articular surfaces of the fossa and the condyle respectively.

<u>Label</u>	<u>Description</u>
1	frontal muscle
2	platysma muscle
3	sphincter coli muscle
4	parotidoauricular muscle
5	lingual vein
6	facial vein
7	linguofacial vein
8	maxillary vein
9	jugular vein
10	parotid salivary gland
11	mandibular salivary gland
12	caudal mandibular lymph nodes
12a	parotid lymph node (cat)
13	temporal muscle
14	masseter muscle- superficial portion
14a	masseter muscle – medial portion
15	sternocephalic / sternomastoid muscle
16	digastricus muscle
*	location of tendinous band in the digastricus muscle (cat)
17	mylohyoid muscle
18	hyoglossus muscle
19	sternohyoid muscle
20	thyrohyoid muscle
21	pharyngeal muscles
22	styloglossus muscle (surrounding stylohyoid bone)
23	TB – exposed ventral surface
24	external ear canal
25	zygomatic process
26	retroarticular process
27	neck of condyloid process
28	TMJ - capsule
29	TMJ – lateral ligament
30	mandibuloauricularis muscle
Arrow	TMJ – intra-articular disc

Table 2.3.4. Key for anatomical features demonstrated in the dog and cat in figures 2.3.10 and 2.3.11.

Figure 2.3.10. Soft tissue structures associated with the tympanic bulla (TB) and temporomandibular joint (TMJ) in the dog. For key see Table 2.3.4. Rostral is to the left in all images.

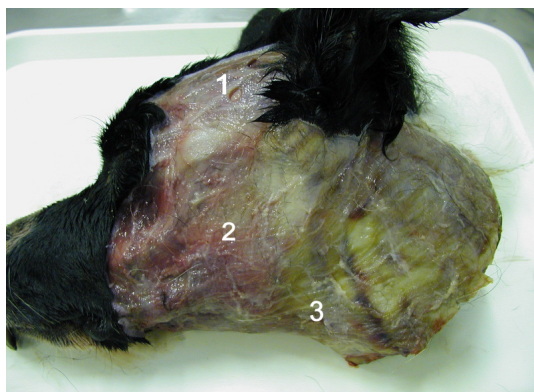


Figure 2.3.10.1. Superficial muscles of the canine head from a lateral approach with the skin and some fat and fascia removed.

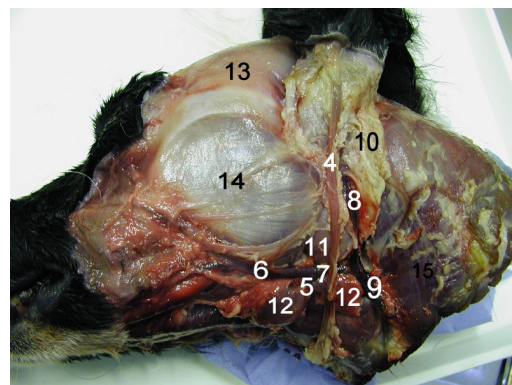


Figure 2.3.10.2. Superficial muscles removed to reveal deeper structures.

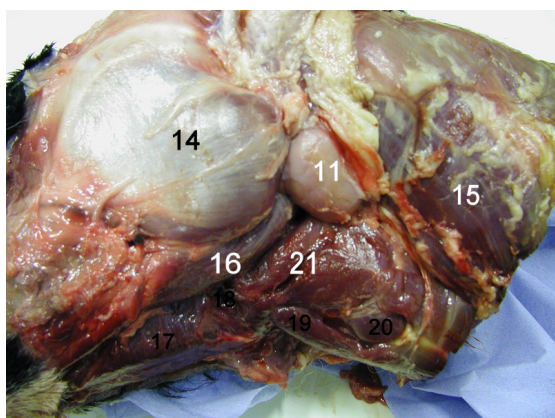


Figure 2.3.10.3. Superficial and vascular structures removed to reveal deeper structures of the pharyngeal region.

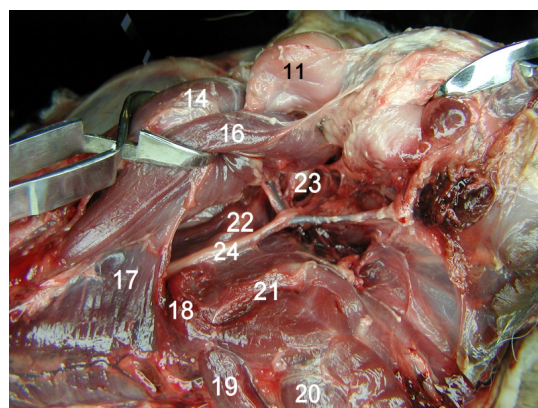


Figure 2.3.10.4. Structures overlying the ventral aspect of the canine TB.

Figure 2.3.10. continued. Soft tissue structures associated with the TB and TMJ in the dog.
For key see Table 2.3.4. Rostral is to the left in all images.

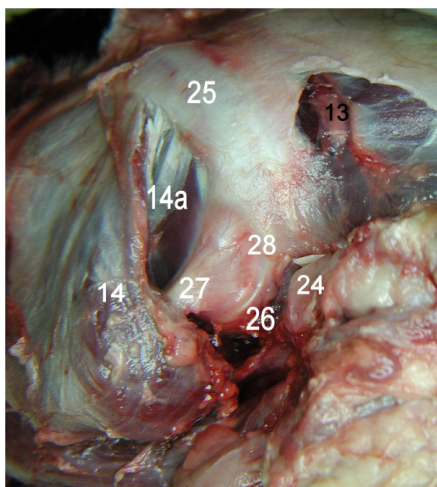


Figure 2.3.10.5. Canine TMJ with the joint capsule intact, viewed from a caudolateral aspect.

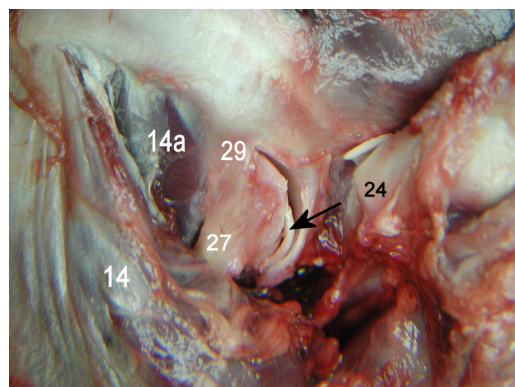


Figure 2.3.10.6. Canine TMJ viewed from a caudolateral aspect. An incision has been made through the joint capsule but the lateral ligament remains intact.

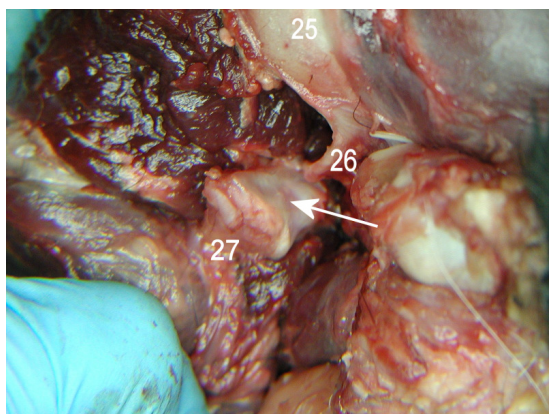


Figure 2.3.10.7. Disarticulated canine TMJ viewed from a caudolateral aspect.

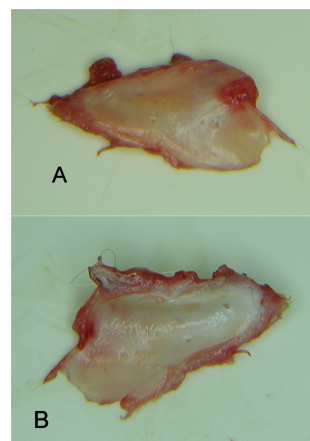


Figure 2.3.10.8. Canine intra-articular TMJ disc.
A: viewed from the dorsal aspect
B: viewed from the ventral aspect

Figure 2.3.11. Soft tissue structures associated with the tympanic bulla (TB) and temporomandibular joint (TMJ) in the cat. For key see Table 2.3.4. Rostral is to the left in all images.



Figure 2.3.11.1. Superficial muscles of the feline head from a lateral approach with the skin and some fat and fascia removed.

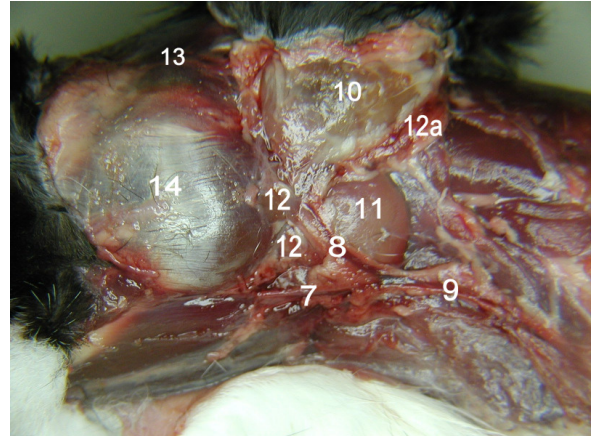


Figure 2.3.11.2. Superficial muscles removed to reveal deeper structures.

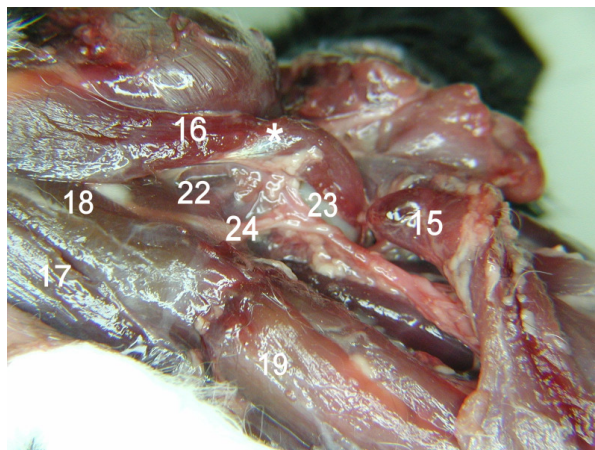


Figure 2.3.11.3. Structures overlying the ventral aspect of the feline TB.

Figure 2.3.11. continued. Soft tissue structures associated with the TB and TMJ in the cat. For key see Table 2.3.4. Rostral is to the left in all images.

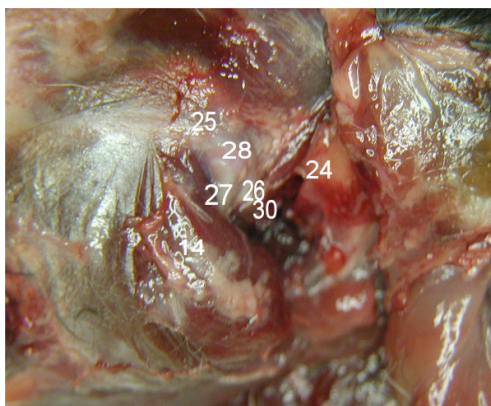


Figure 2.3.11.4. Feline TMJ with the joint capsule intact, viewed from a lateral aspect.

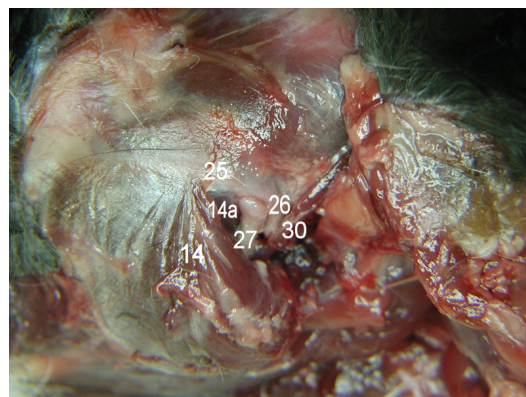


Figure 2.3.11.5. Feline TMJ viewed from a lateral aspect. An incision has been made through the joint capsule.

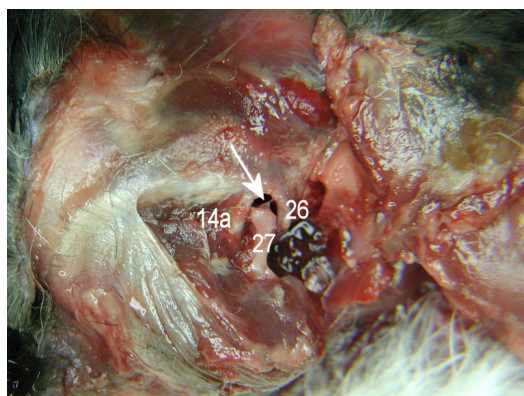


Figure 2.3.11.6. Partially disarticulated feline TMJ viewed from a lateral aspect demonstrating the intra-articular disc.

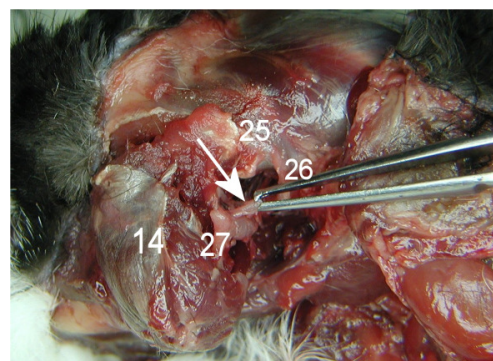


Figure 2.3.11.7. Completely disarticulated feline TMJ viewed from a lateral aspect demonstrating the intra-articular disc.

<u>Label</u>	<u>Description</u>
1	zygomatic muscle – labial part
2	zygomatic muscle – auricular part
3	zygomatic muscle – mandibular part
4	parotidoauricular muscle
5	platysma muscle
6	frontoscutular muscle – temporal part
7	frontal muscle
8	external jugular vein
9	linguofacial vein
10	maxillary vein
11	parotid salivary gland
12	submandibular salivary gland
13	caudal mandibular lymph nodes
14	sternohyoid muscle
15	sternocephalic / sternomastoid muscle
16	long muscle of the head
17	cleidomastoid muscle (part of brachiocephalic group)
18	cleidobasilar muscle (part of brachiocephalic group)
19	omotransversarius muscle
20	splenius muscle
21	trapezius muscle
22	masseter muscle
23	vertebral muscles
24	larynx
25	stylohyoid muscle
26	hyoid bone
27	mandibular retractor muscle
28	styloglossus muscle
29	ventral surface of TB
30	external acoustic meatus
31	temporalis muscle
32	styloauricular muscle

Table 2.3.5. Key for anatomical features demonstrated in the rabbit in figures 2.3.12.

Figure 2.3.12. Soft tissue structures associated with the tympanic bulla (TB) and temporomandibular joint (TMJ) in the rabbit. For key see Table 2.3.5. Rostral is to the left in all images.

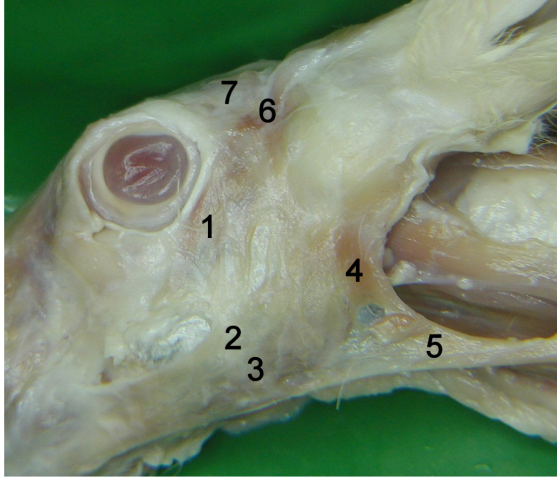


Figure 2.3.12.1. Superficial muscles of the rabbit head from a lateral approach with the skin and some fat and fascia removed.

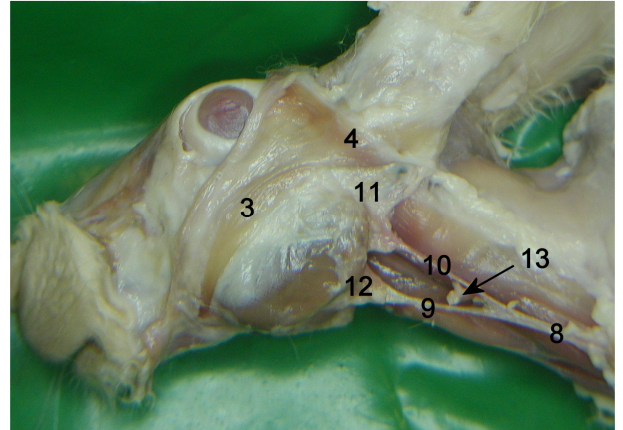


Figure 2.3.12.2. Superficial muscles reflected to reveal deeper structures

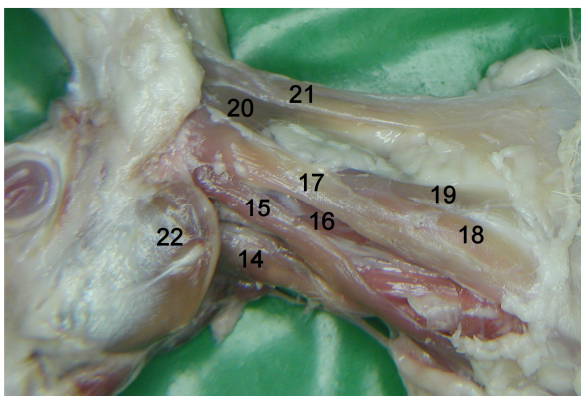


Figure 2.3.12.3. Muscles of the cervical region of the rabbit from a lateral approach.



Figure 2.3.12.4. Superficial structures of the rabbit head from a ventral approach with fat and fascia removed.

Figure 2.3.12. continued. Soft tissue structures associated with the TB and TMJ in the rabbit. For key see Table 2.3.5. Rostral is to the left in all images.

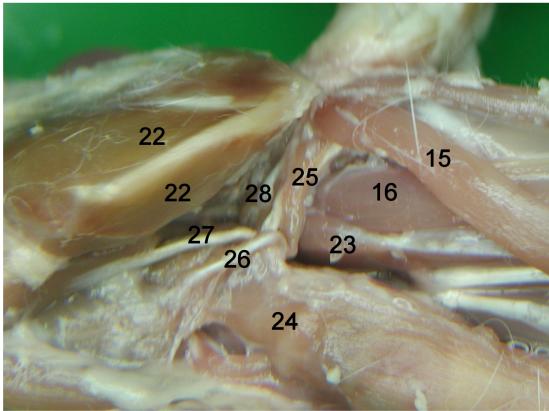


Figure 2.3.12.5. Structures overlying the ventral aspect of the rabbit TB.

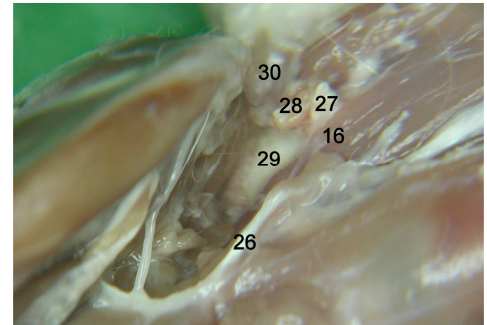


Figure 2.3.12.6. Rabbit TB viewed from the ventral aspect with the overlying structures removed.



Figure 2.3.12.7. Superficial structures of the rabbit head from a dorsal approach with fat and fascia removed.



Figure 2.3.12.8. Superficial structures of the rabbit head from a lateral approach with fat and fascia removed.

Figure 2.3.12. continued. Soft tissue structures associated with the TMJ and TMJ in the rabbit. For key see Table 2.3.5. Rostral is to the left in all images.

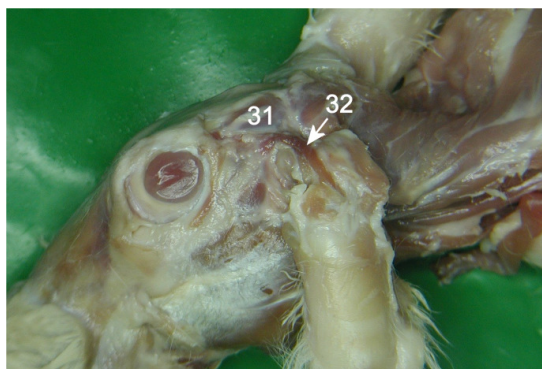


Figure 2.3.12.9. Deep dissection of the muscles attaching to the external ear with the mouth closed.

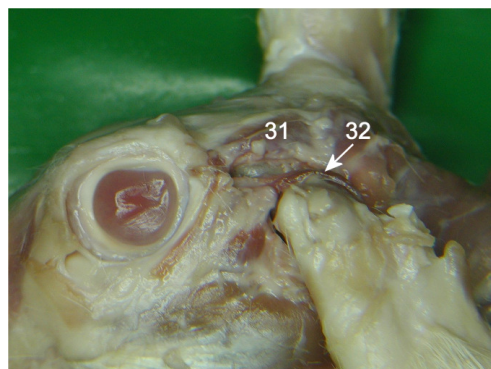


Figure 2.3.12.10. Deep dissection of the muscles attaching to the external ear with the mouth open. Removal of the lateral ligament of the TMJ reveals the attachments of the styloauricular muscle to the TMJ capsule and zygomatic bone.

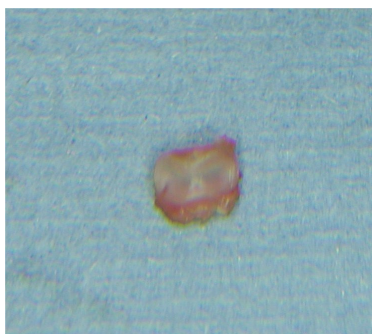


Figure 2.3.12.11. Intra-articular TMJ disc in the rabbit.

2.3.3. Multiplanar sections of the TB and TMJ in the dog, cat and rabbit

The multiplanar sections obtained are demonstrated in Figures 2.3.13. to 2.3.21 with the key in Table 2.3.6.

Although care was taken to ensure the slices were as parallel as possible with the relevant plane through the head and each other, some deviation of the bandsaw blade proved unavoidable in all three species. This was mainly due to the marked differences in density of the structures encountered during each slice. In particular, the high density of the molar teeth and the base of the skull caused increased resistance to passage of the blade and in some instances the heat generated by the friction caused discolouration of the adjacent tissues, which can be seen in some of the images. The resulting non-uniform slice thickness was most evident in the transverse and dorsal sections where bilateral symmetry was affected. However, all of the areas of interest were still identified on both sides of the head and often demonstrated different regions of the structure.

A slice thickness of 0.6cm was the minimum that could be obtained using the equipment available with attempts to produce thinner slices resulting in greater variability in slice thickness and sections that were too friable to handle for photography. Problems with friability were also encountered at the edge of some slices, particularly in the sagittal plane, where the tissue thickness tapered markedly. Slight overall size differences between the 2 heads in each series meant that slightly different slices were produced. During sectioning, hair from the skin was drawn across the surface of the sections. This proved impossible to completely remove prior to photography and so is visible in the images. During photography, sections thawed to varying degrees as evidenced by ice crystals being visible in some close up images while others appear more moist.

The transverse and dorsal sections allowed comparison between sides while the sagittal sections exposed each side independently. The transverse section only allowed visualisation of the dorsal aspect of the TMJ space in the dog and cat. The sagittal sections allowed visualisation of the entire articulation between the condyloid process and mandibular fossa in the dog and cat at a series of levels through the joint. The dorsal sections allowed only the caudal aspect of the TMJ space to be assessed in the dog and cat while the rostral area was visible in the rabbit.

<u>Label</u>	<u>Description</u>
1	condyloid process
2	zygomatic arch
3	zygomatic extension of the temporal bone
4	squamous temporal bone
5	hyoid apparatus
6	soft tissue components of the TMJ
7	retroarticular process
8	pit at the medial aspect of the retroarticular process
9	retroarticular foramen
10	TB lumen
11	bone ridge – dog septum bulla – cat caudal extension of the zygomatic arch - rabbit
12	tympanic cavity
13	external ear canal
14	tympanic membrane
15	incus
16	stapes
17	vestibular / oval window
18	promontory
19	cochlear / round window
20	mastoid process
21	epitympanic recess

Table 2.3.6. Key for anatomical features demonstrated in the multiplanar images of the dog, cat and rabbit in Figures 2.3.13 to 2.3.21.

Figure 2.3.13. Transverse anatomical sections through the region of the tympanic bulla (TB) and temporomandibular joint (TMJ) in the dog progressing from rostral to caudal. For key see Table 2.3.6. Dorsal is to the top and left is to the right in all images.



Figure 2.3.13.1. Rostral aspect of section 1.

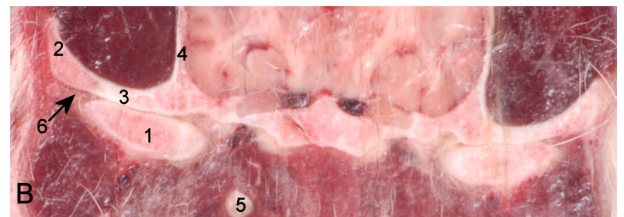
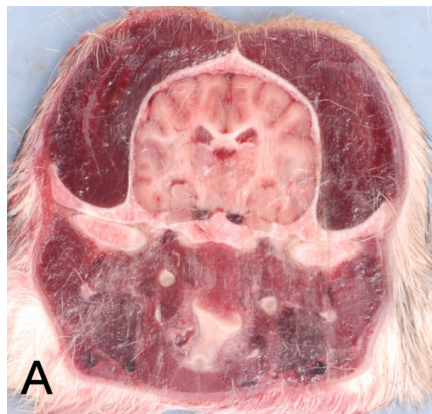


Figure 2.3.13.2. A. Caudal aspect of section 1. B. Magnified view of both TMJ

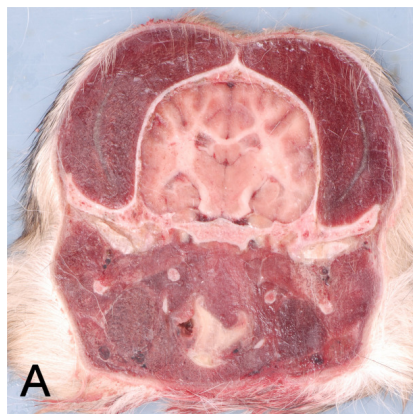


Figure 2.3.13.3. A. Rostral aspect of section 2. B. Magnified view of both TMJ

Figure 2.3.13. continued. Transverse anatomical sections in the dog.

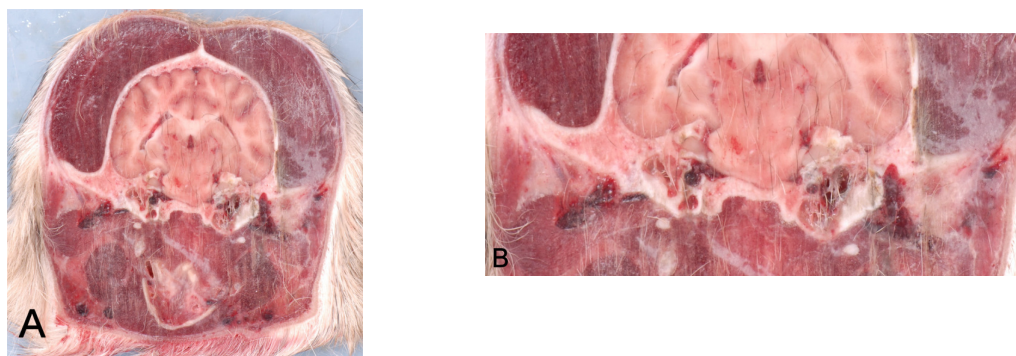


Figure 2.3.13.4. A. Caudal aspect of section 2. B. Magnified view of both TB

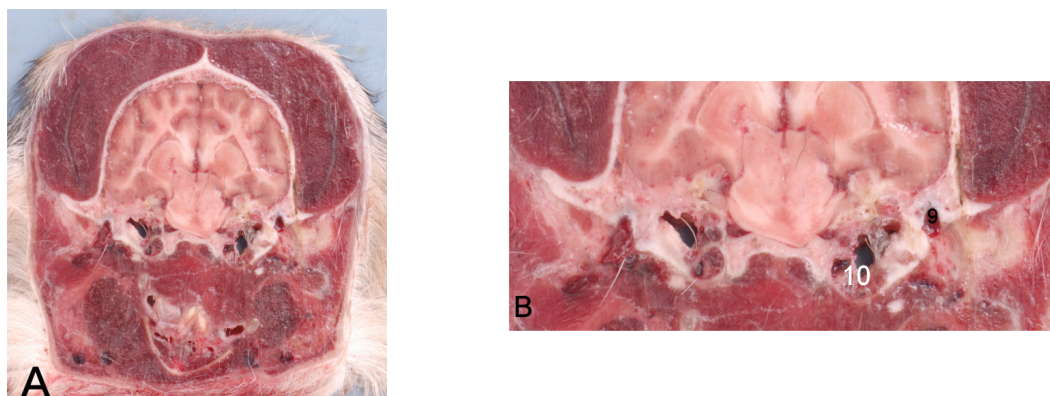


Figure 2.3.13.5. A. Rostral aspect of section 3. B. Magnified view of both TB

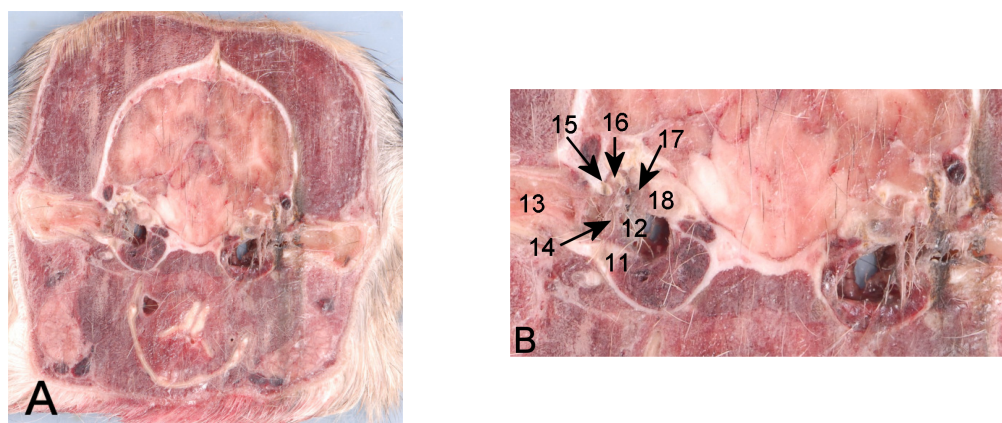


Figure 2.3.13.6. A. Caudal aspect of section 3. B. Magnified view of both TB

Figure 2.3.13. continued. Transverse anatomical sections in the dog.

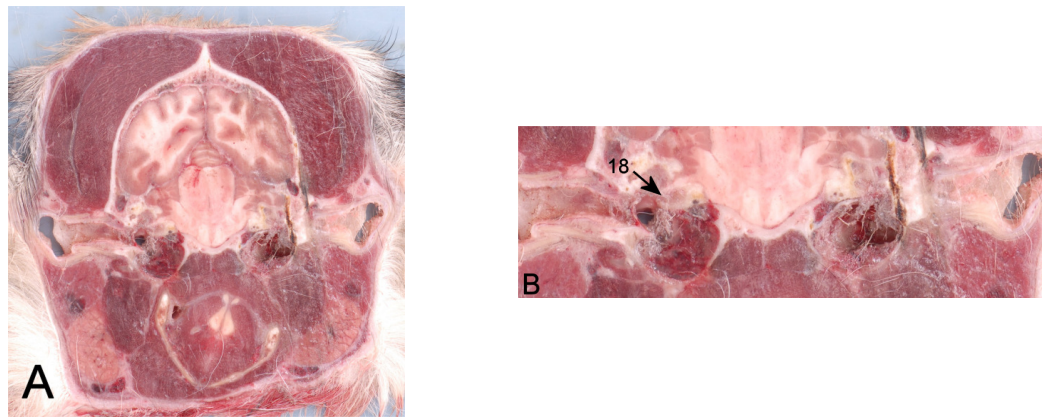


Figure 2.3.13.7. A. Rostral aspect of section 4. B. Magnified view of both TB

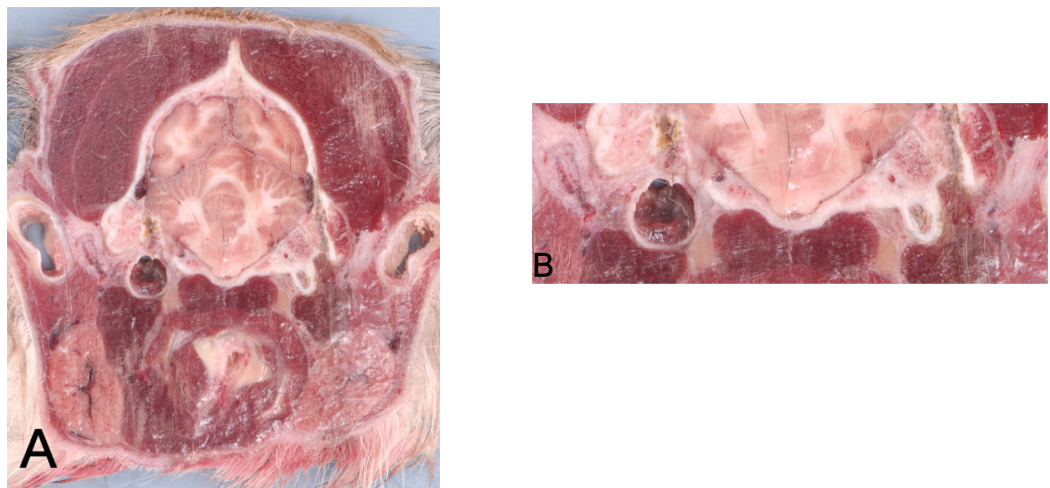


Figure 2.3.13.8. A. Caudal aspect of section 4. B. Magnified view of right TB

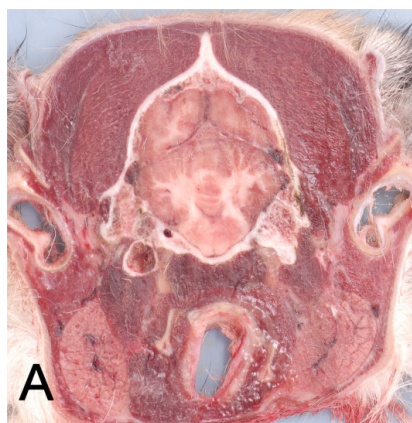


Figure 2.3.13.9. Rostral aspect of section 5.

Figure 2.3.14. Transverse anatomical sections through the region of the tympanic bulla (TB) and temporomandibular joint (TMJ) in the cat progressing from rostral to caudal. For key see Table 2.3.6. Dorsal is to the top and left is to the right in all images.

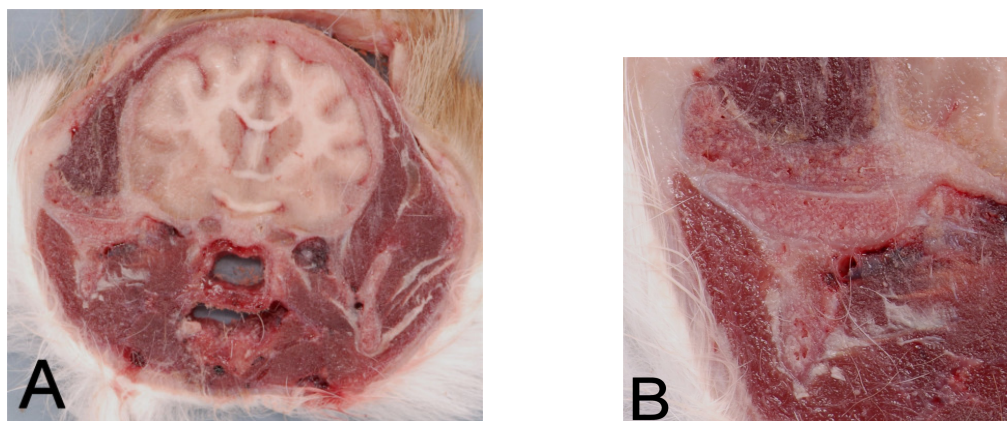


Figure 2.3.14.1. A. Caudal aspect of section 1. B. Magnified view of right TMJ.

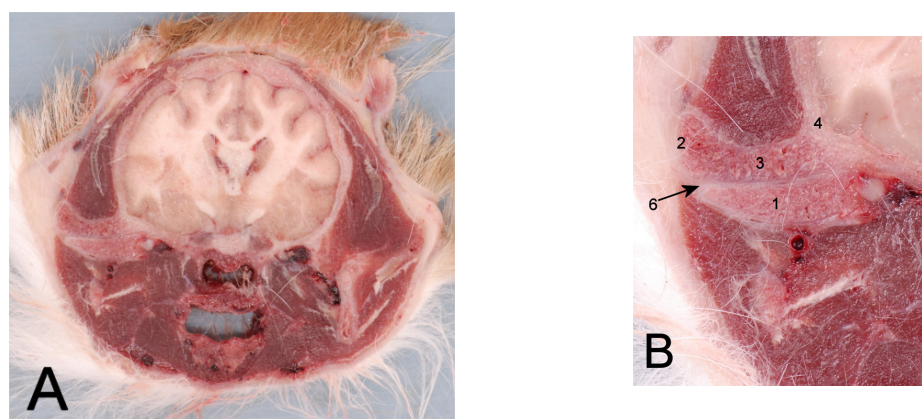


Figure 2.3.14.2. A. Rostral aspect of section 2. B. Magnified view of right TMJ.

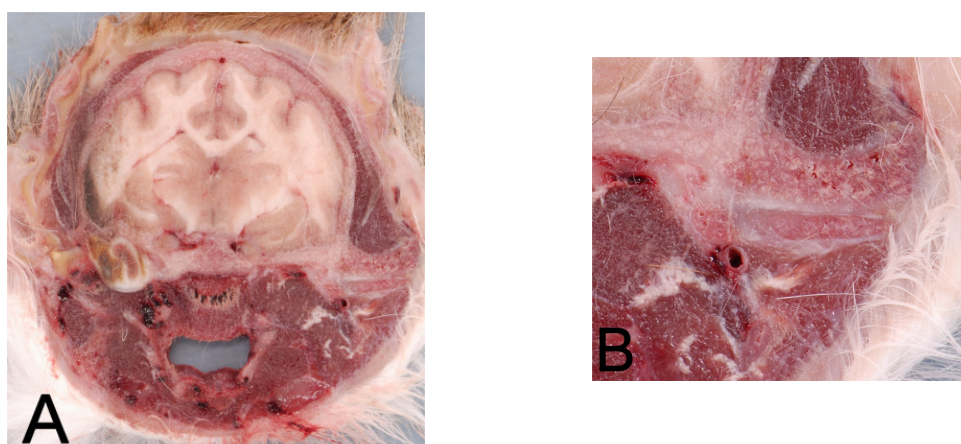


Figure 2.3.14.3. A. Caudal aspect of section 2. B. Magnified view of left TMJ.

Figure 2.3.14. continued. Transverse anatomical sections in the cat

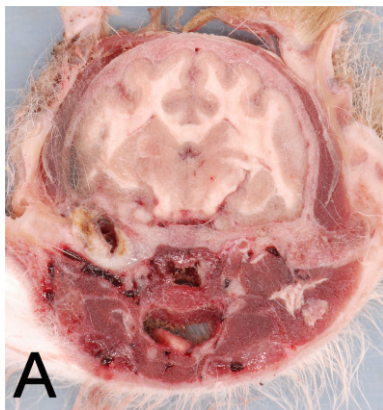


Figure 2.3.14.4. Rostral aspect of section 3

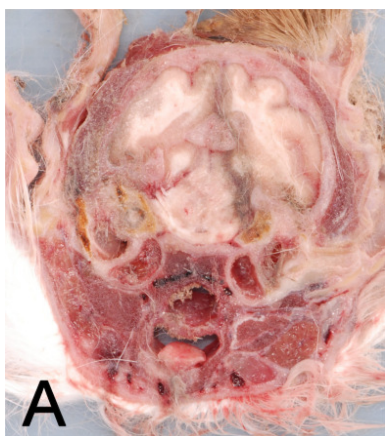


Figure 2.3.14.5. A. Caudal aspect of section 3. B. Magnified view of both TB

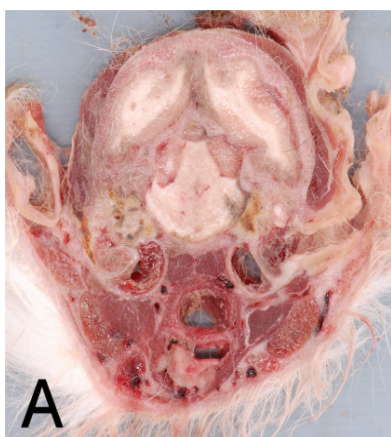


Figure 2.3.14.6. A. Rostral aspect of section 4. B. Magnified view of both TB

Figure 2.3.14. continued. Transverse anatomical sections in the cat

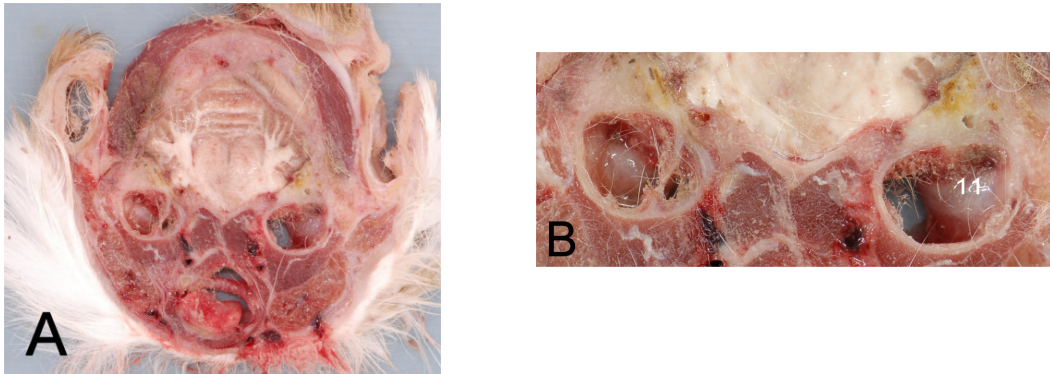


Figure 2.3.14.7. A. Caudal aspect of section 4. B. Magnified view of both TB

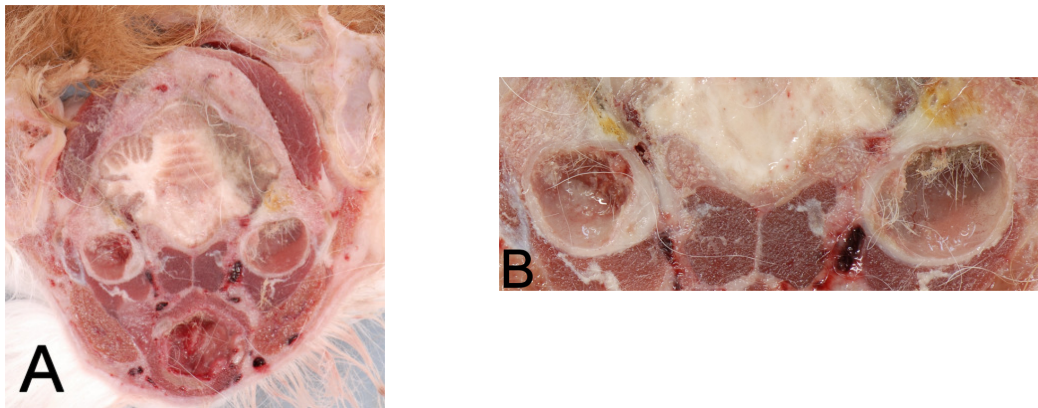


Figure 2.3.14.8. A. Rostral aspect of section 5. B. Magnified view of both TB

Figure 2.3.15. Transverse anatomical sections through the region of the tympanic bulla (TB) and temporomandibular joint (TMJ) in the rabbit progressing from rostral to caudal. For key see Table 2.3.6. Dorsal is to the top and left is to the right in all images

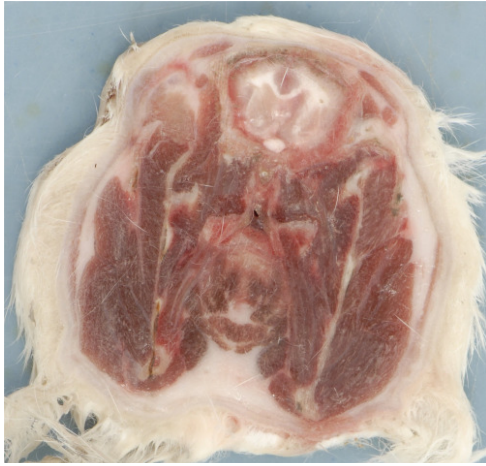


Figure 2.3.15.1. Caudal aspect of section 1.

Figure 2.3.15.2. Rostral aspect of section 2.

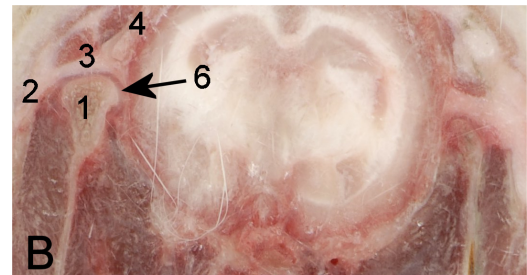
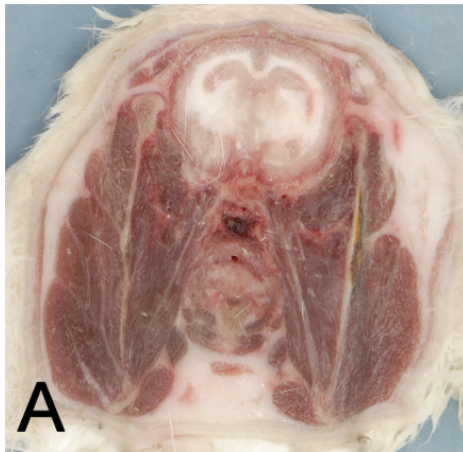


Figure 2.3.15.3. A.Caudal aspect of section 2. B. Magnified view of both TMJ

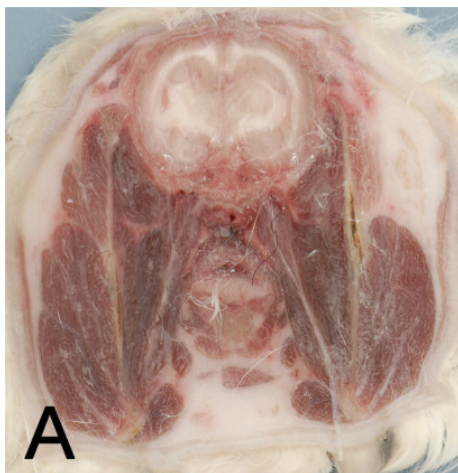


Figure 2.3.15.4. A.Rostral aspect of section 3. B. Magnified view of both TMJ

Figure 2.3.15. continued. Transverse anatomical sections in the rabbit.

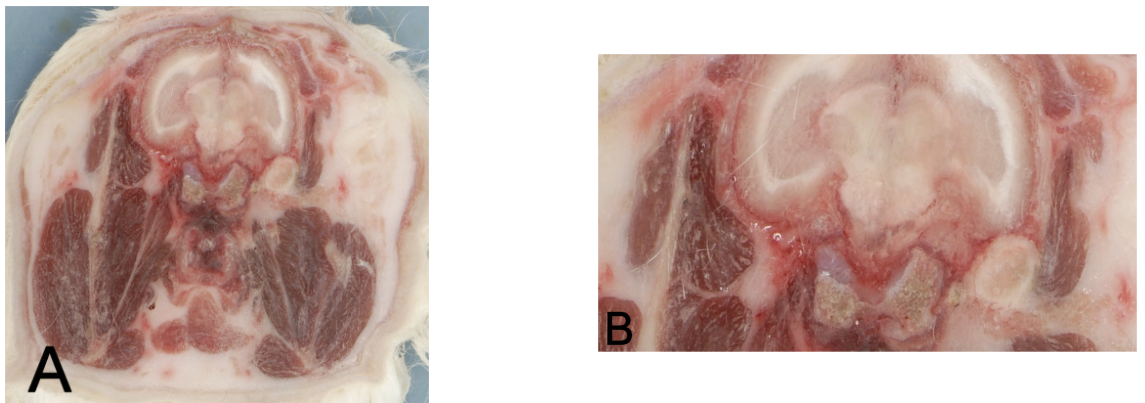


Figure 2.3.15.5. A.Caudal aspect of section 3. B. Magnified view of right TMJ and left TB

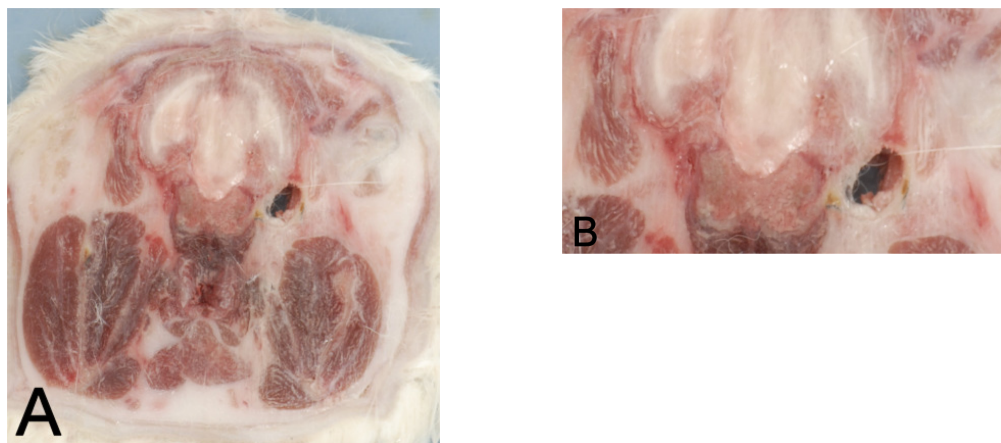


Figure 2.3.15.6. A.Rostral aspect of section 4. B. Magnified view of left TB

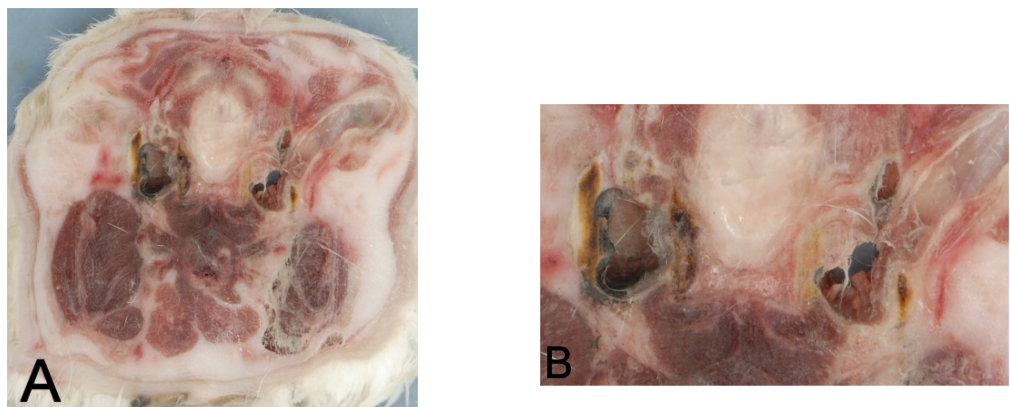


Figure 2.3.15.7. A.Caudal aspect of section 4. B. Magnified view of both TB

Figure 2.3.15. continued. Transverse anatomical sections in the rabbit.

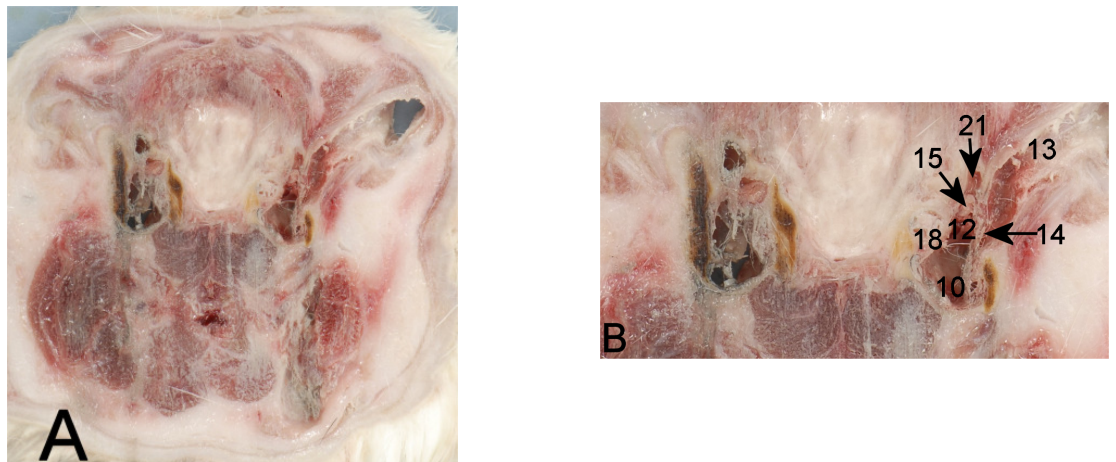


Figure 2.3.15.6. A.Rostral aspect of section 5. B. Magnified view of both TB

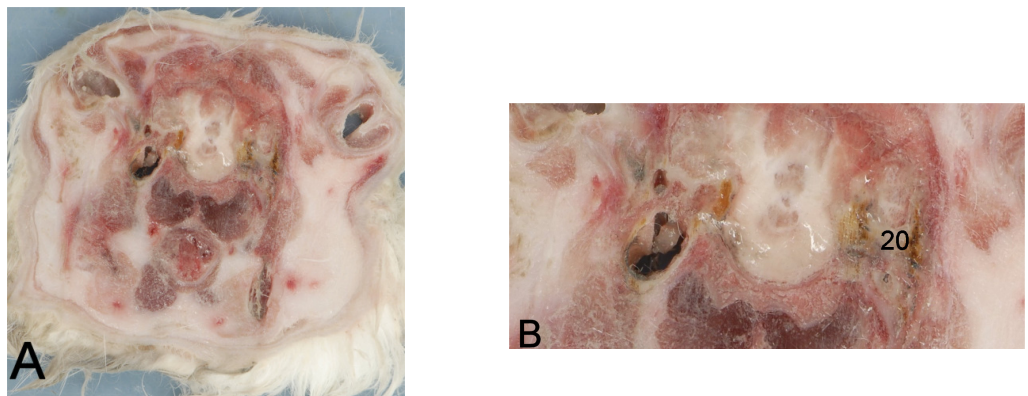


Figure 2.3.15.7. A.Caudal aspect of section 5. B. Magnified view of right TB

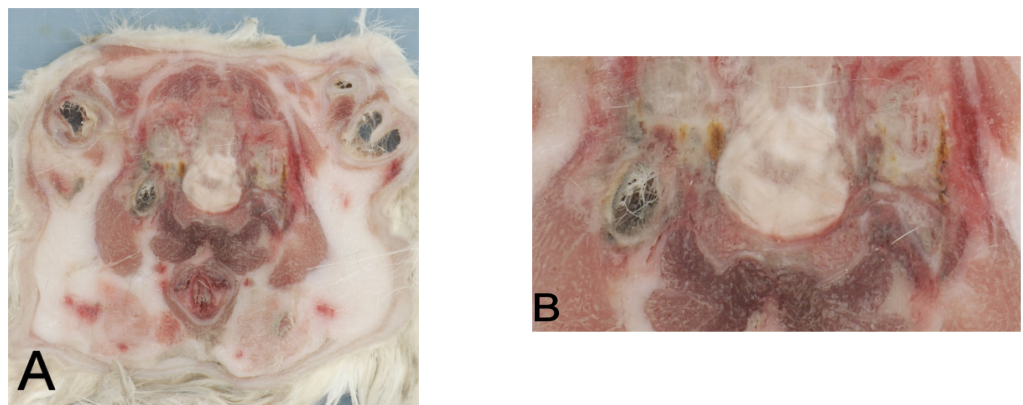


Figure 2.3.15.8. A.Rostral aspect of section 6. B. Magnified view of right TB

Figure 2.3.16. Sagittal anatomical sections through the region of the tympanic bulla (TB) and temporomandibular joint (TMJ) in the dog progressing from midline towards left. For key see Table 2.3.6. Dorsal is to top and rostral is to the left in all images.



Figure 2.3.16.1. Medial aspect of section 1



Figure 2.3.16.2. Lateral aspect of section 1

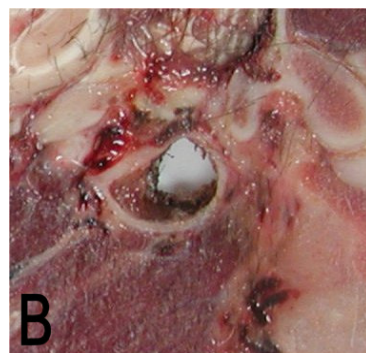


Figure 2.3.16.3. A. Medial aspect of section 2. B. Magnified view of left TB

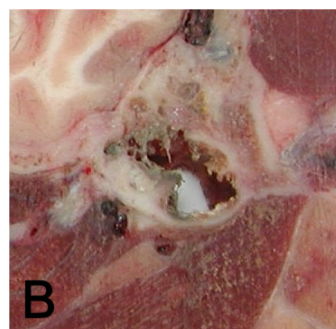


Figure 2.3.16.4. A. Lateral aspect of section 2. B. Magnified view of left TB

Figure 2.3.16. continued. Sagittal anatomical sections in the dog

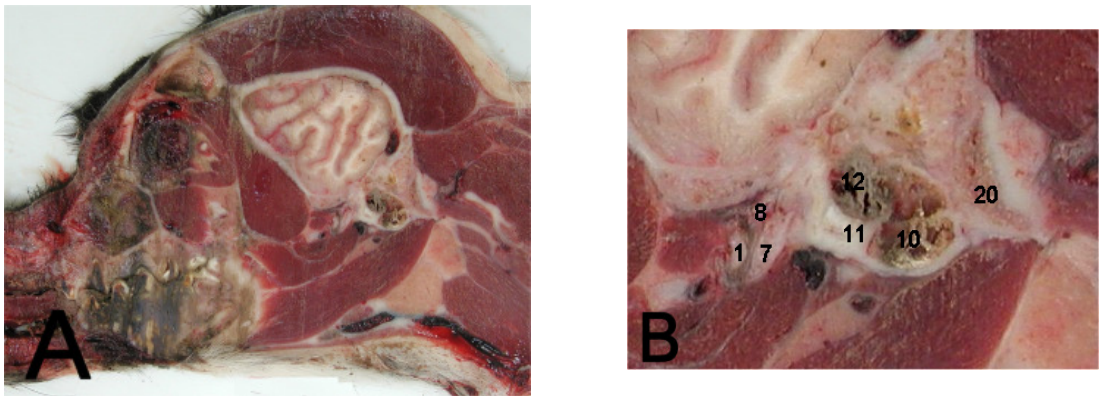


Figure 2.3.16.5. A. Medial aspect of section 3. B. Magnified view of left TB and TMJ

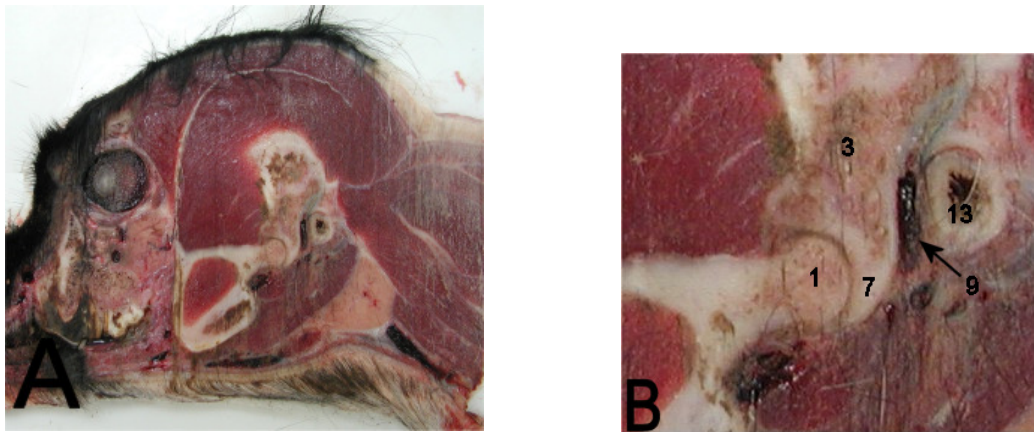


Figure 2.3.16.6. A. Lateral aspect of section 3. B. Magnified view of left TMJ



Figure 2.3.16.7. Medial aspect of section 4.

Figure 2.3.16. continued. Sagittal anatomical sections in the dog

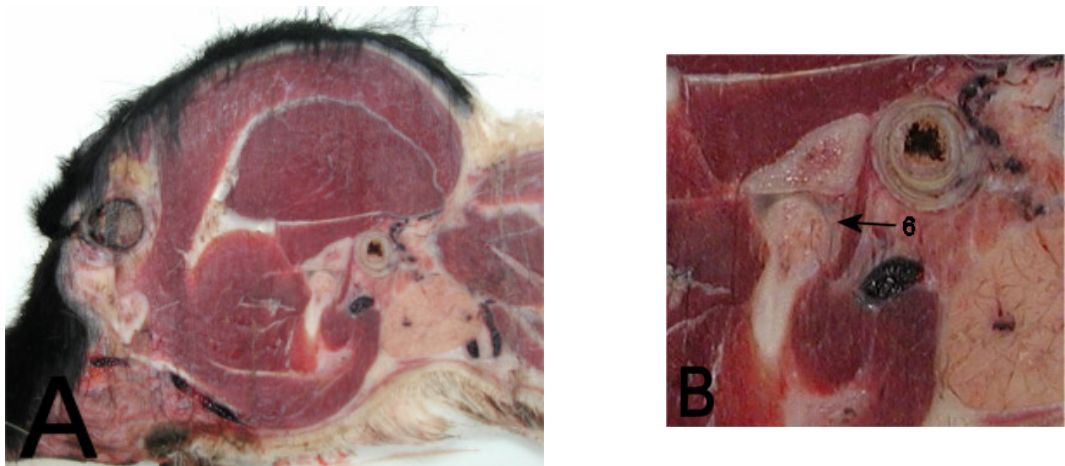


Figure 2.3.16.8. A. Lateral aspect of section 4. B. Magnified view of left TMJ

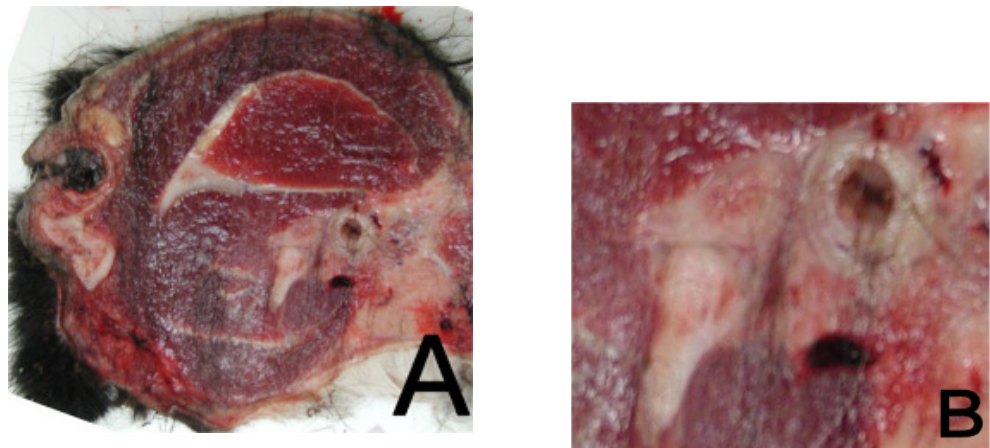


Figure 2.3.16.9. A. Medial aspect of section 5. B. Magnified view of left TMJ

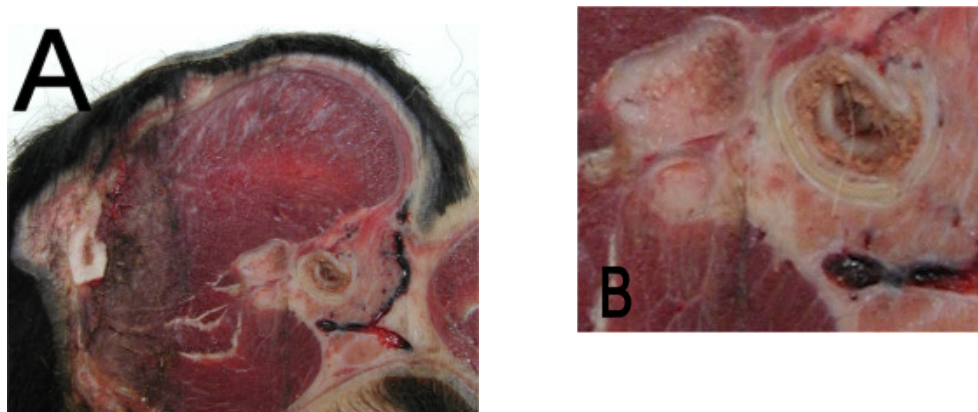


Figure 2.3.16.10. A. Lateral aspect of section 5. B. Magnified view of left TMJ

Figure 2.3.17. Sagittal anatomical sections through the region of the tympanic bulla (TB) and temporomandibular joint (TMJ) in the cat progressing from right towards left. For key see Table 2.3.6. Dorsal is to top and rostral is to the left in all images.

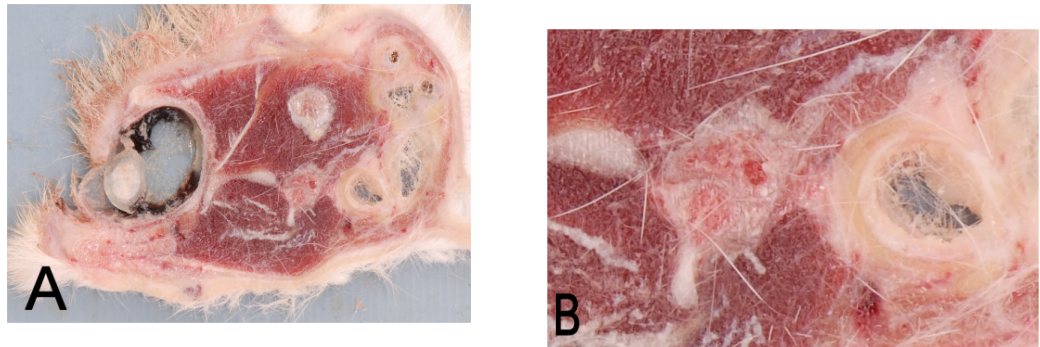


Figure 2.3.17.1. A. Left aspect of section 1. B. Magnified view of right TMJ

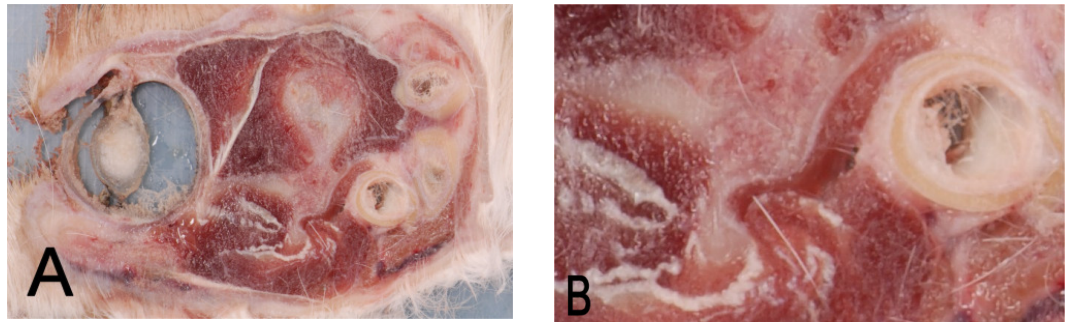


Figure 2.3.17.2. A. Right aspect of section 2. B. Magnified view of right TMJ

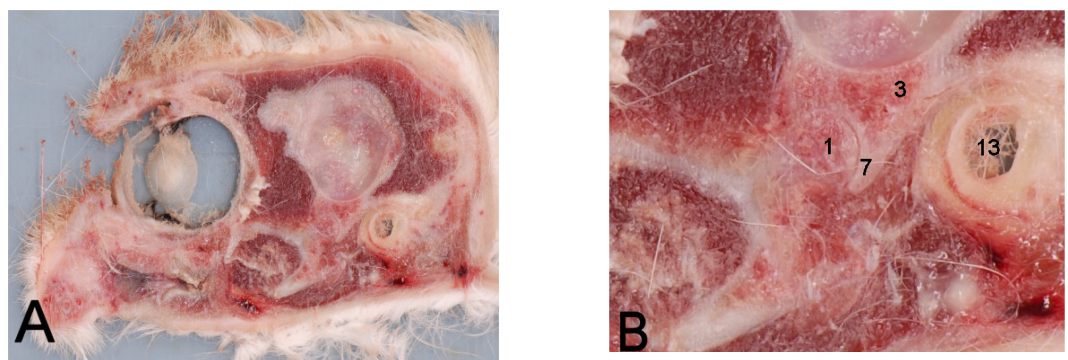


Figure 2.3.17.3. A. Left aspect of section 2. B. Magnified view of right TMJ

Figure 2.3.17. continued. Sagittal anatomical sections in the cat.

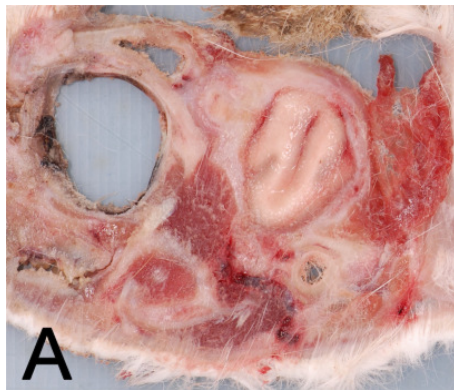


Figure 2.3.17.4. A. Right aspect of section 3. B. Magnified view of right TMJ

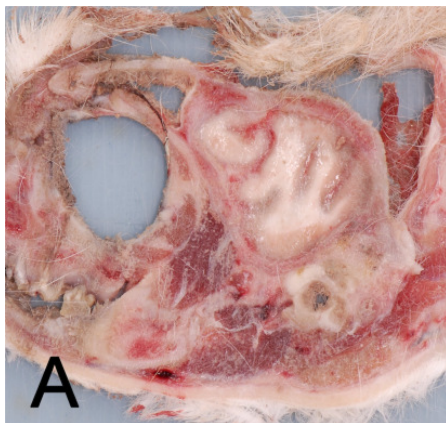


Figure 2.3.17.5. A. Left aspect of section 3. B. Magnified view of right TB and TMJ

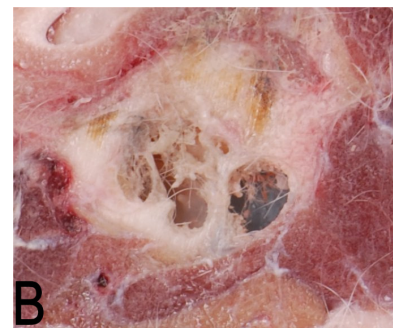
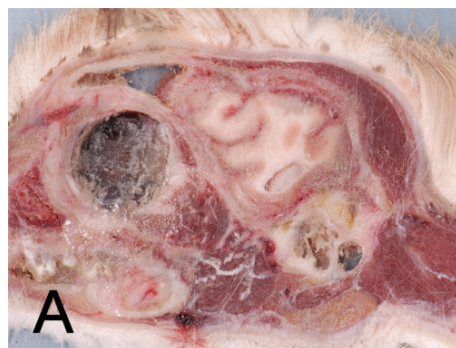


Figure 2.3.17.6. A. Right aspect of section 4. B. Magnified view of right TB

Figure 2.3.17. continued. Sagittal anatomical sections in the cat.

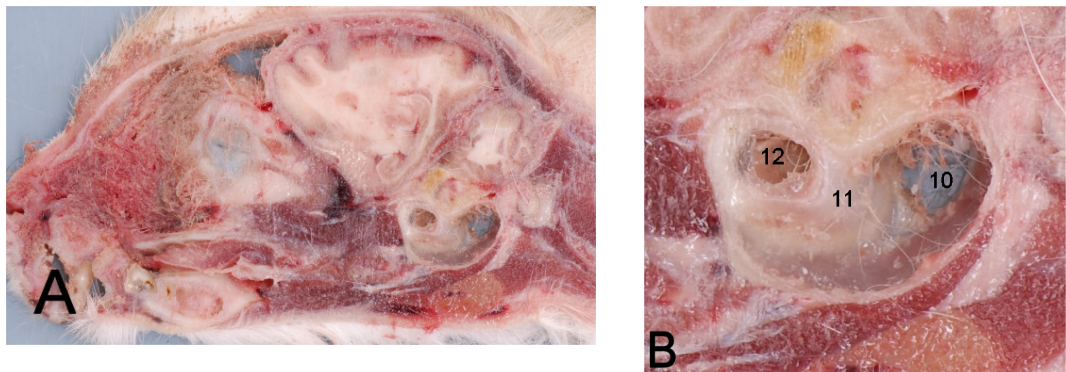


Figure 2.3.17.7. A. Left aspect of section 4. B. Magnified view of right TB

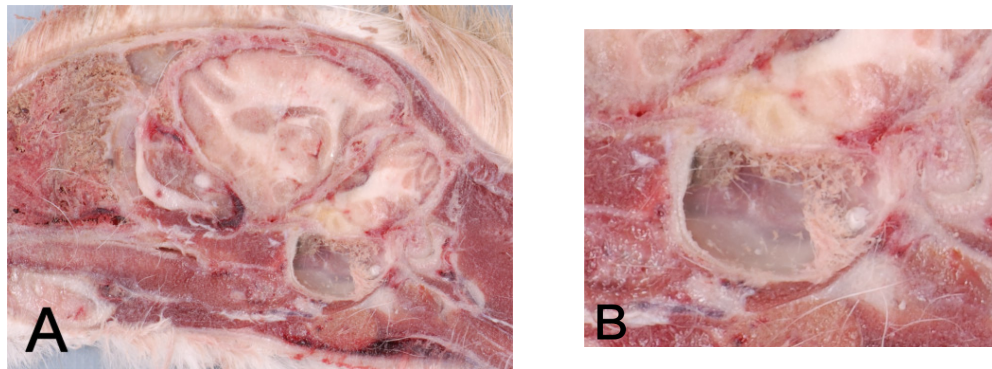


Figure 2.3.17.8. A. Right aspect of section 5. B. Magnified view of right TB



Figure 2.3.17.9. Left aspect of section 5.

Figure 2.3.17. continued. Sagittal anatomical sections in the cat.



Figure 2.3.17.10. Left aspect of section 7. B. Magnified view of left TB

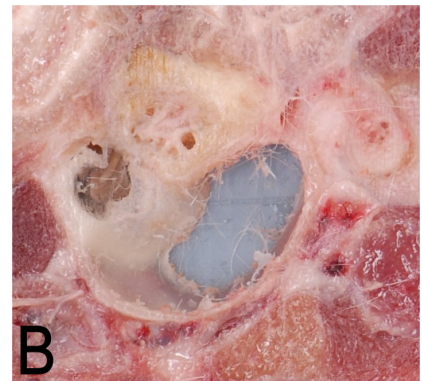
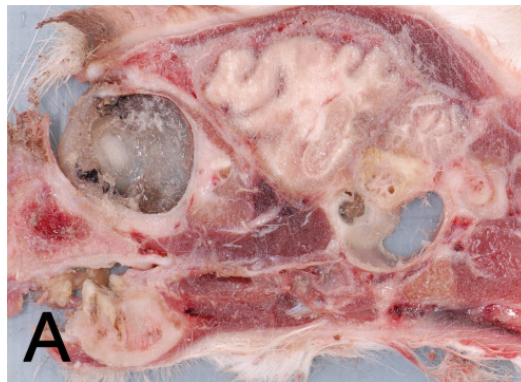


Figure 2.3.17.11. Right aspect of section 8. B. Magnified view of left TB

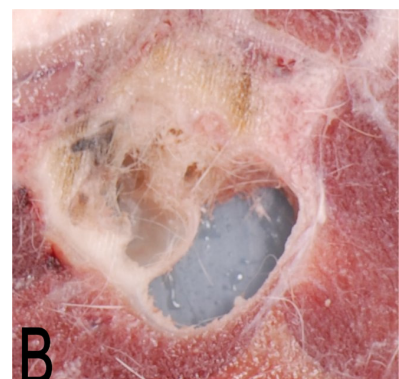
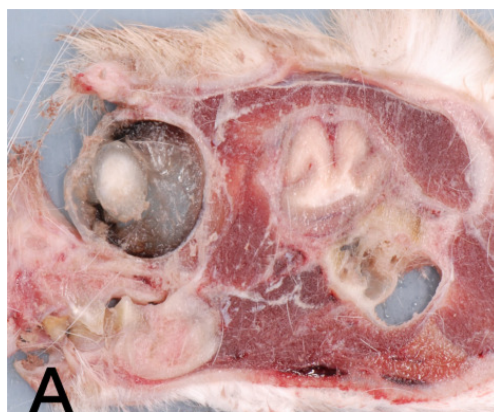


Figure 2.3.17.12. Left aspect of section 8. B. Magnified view of left TB

Figure 2.3.17. continued. Sagittal anatomical sections in the cat.

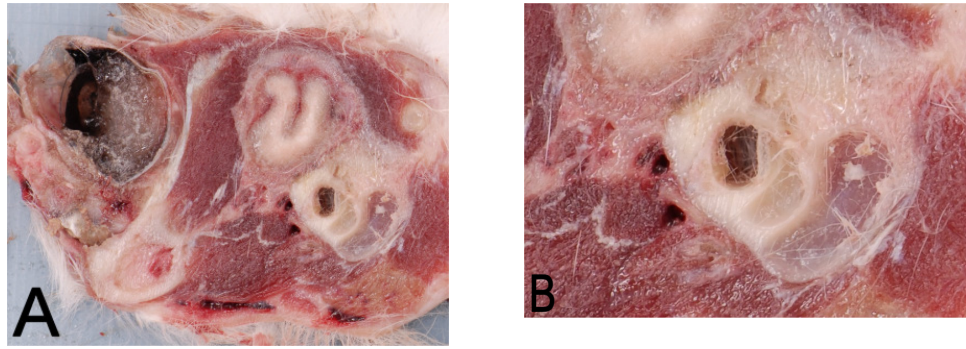


Figure 2.3.17.13. Right aspect of section 9. B. Magnified view of left TB

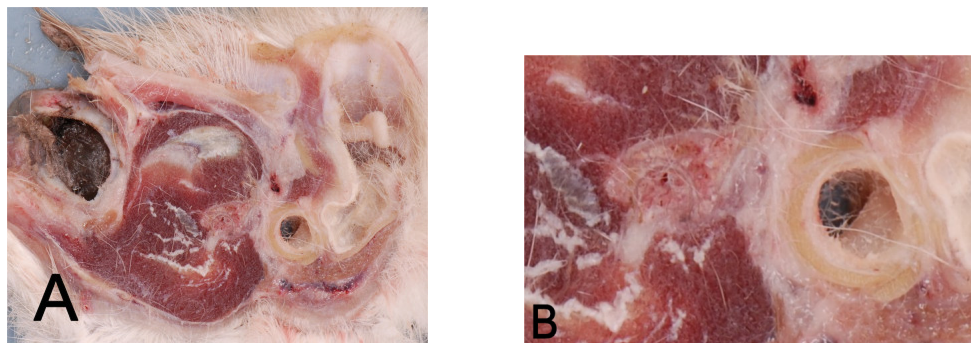


Figure 2.3.17.14. Left aspect of section 9. B. Magnified view of left TMJ

Figure 2.3.18. Sagittal anatomical sections through the region of the tympanic bulla (TB) and temporomandibular joint (TMJ) in the rabbit progressing from right towards left. For key see Table 2.3.6. Dorsal is to top and rostral is to the left in all images.

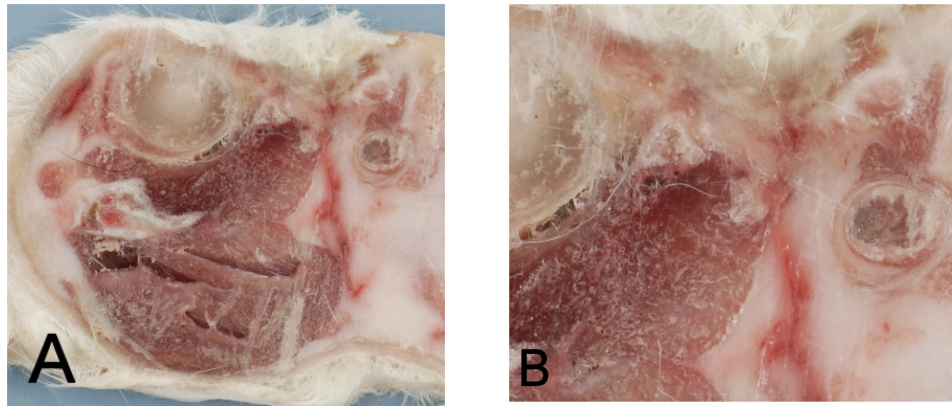


Figure 2.3.18.1. Right aspect of section 1. B. Magnified view of right TMJ

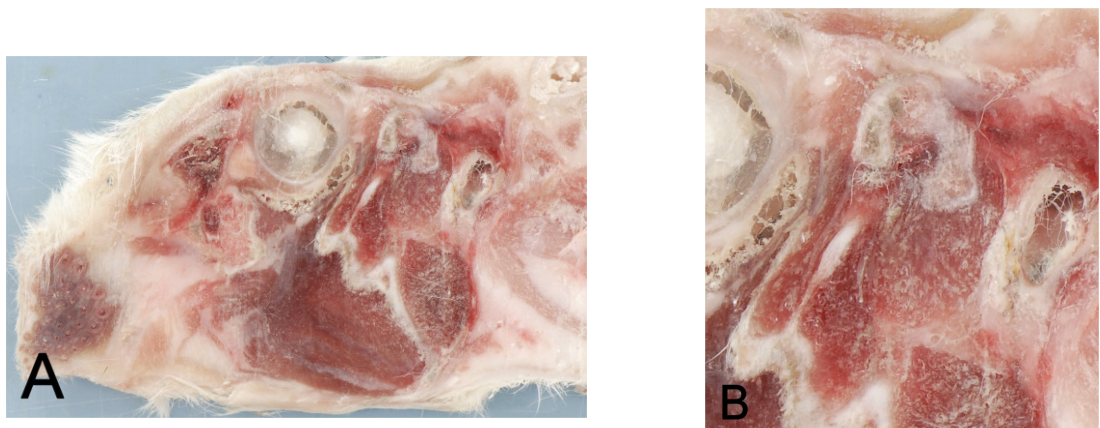


Figure 2.3.18.2. Left aspect of section 1. B. Magnified view of right TMJ



Figure 2.3.18.3. Right aspect of section 2.

Figure 2.3.18. continued. Sagittal anatomical sections in the rabbit.

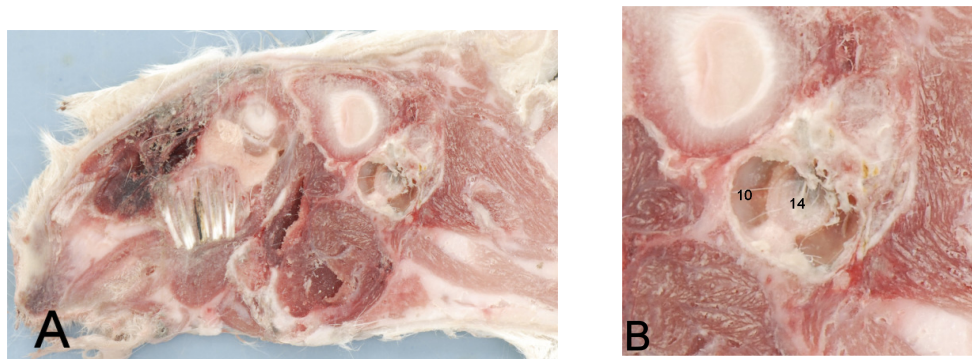


Figure 2.3.18.4. Left aspect of section 2. B. Magnified view of right TB



Figure 2.3.18.5. Right aspect of section 3. B. Magnified view of right TB

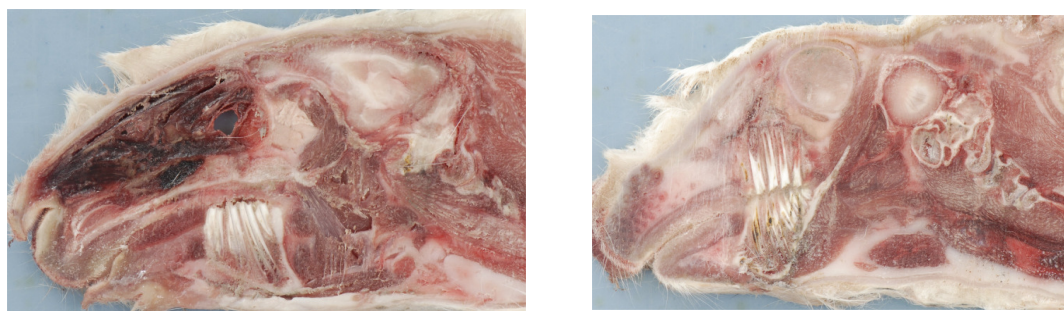


Figure 2.3.18.6. Left aspect of section 3.

Figure 2.3.18.7. Left aspect of section 6

Figure 2.3.18. continued. Sagittal anatomical sections in the rabbit.

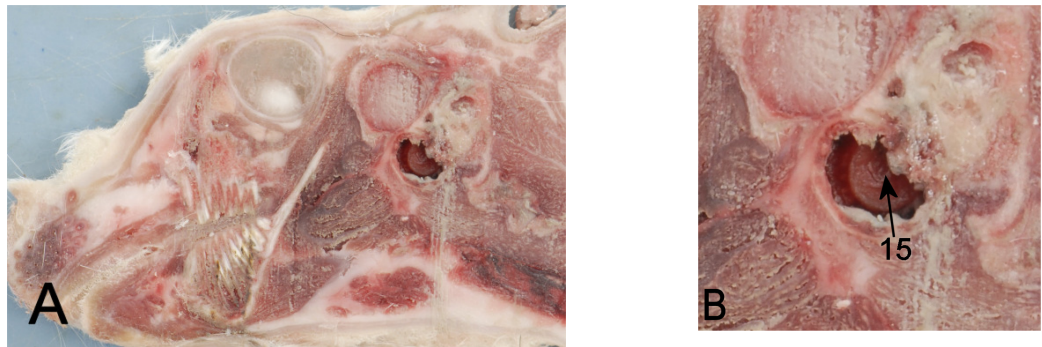


Figure 2.3.18.8. Right aspect of section 7. B. Magnified view of left TB

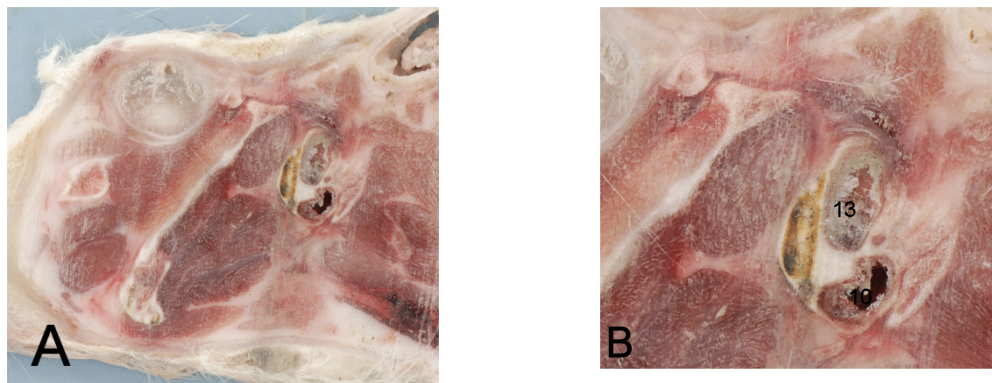


Figure 2.3.18.9. Left aspect of section 7. B. Magnified view of left TB and TMJ

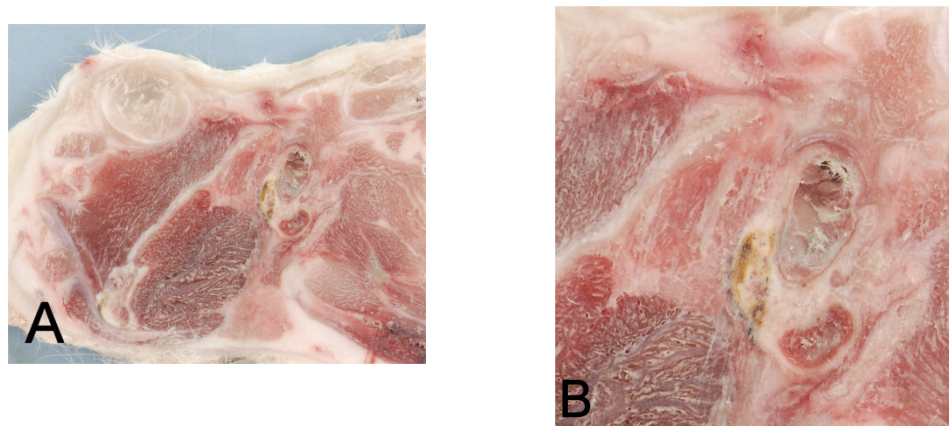


Figure 2.3.18.10. Right aspect of section 8. B. Magnified view of left TB and TMJ

Figure 2.3.19. Dorsal anatomical sections through the region of the tympanic bulla (TB) and temporomandibular joint (TMJ) in the dog progressing from dorsal to ventral. For key see Table 2.3.6. Rostral is to top and left is to the right in all images.



Figure 2.3.19.1. Dorsal aspect of section 1

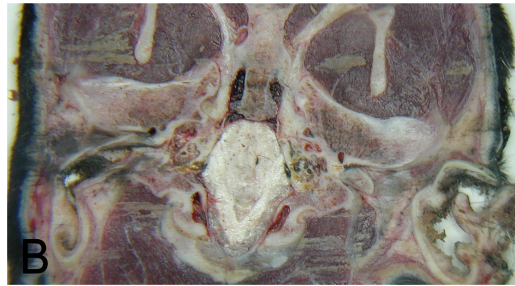


Figure 2.3.19.2. A. Ventral aspect of section 1. B. Magnified view of both TMJ.

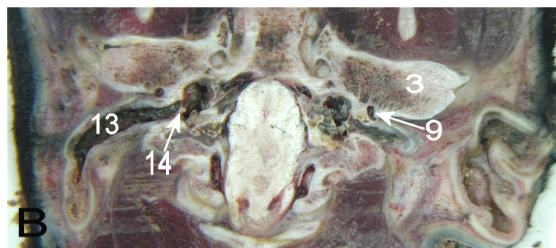


Figure 2.3.19.3. A. Dorsal aspect of section 2. B. Magnified view of both TMJ.

Figure 2.3.19. continued. Dorsal anatomical sections in the dog.

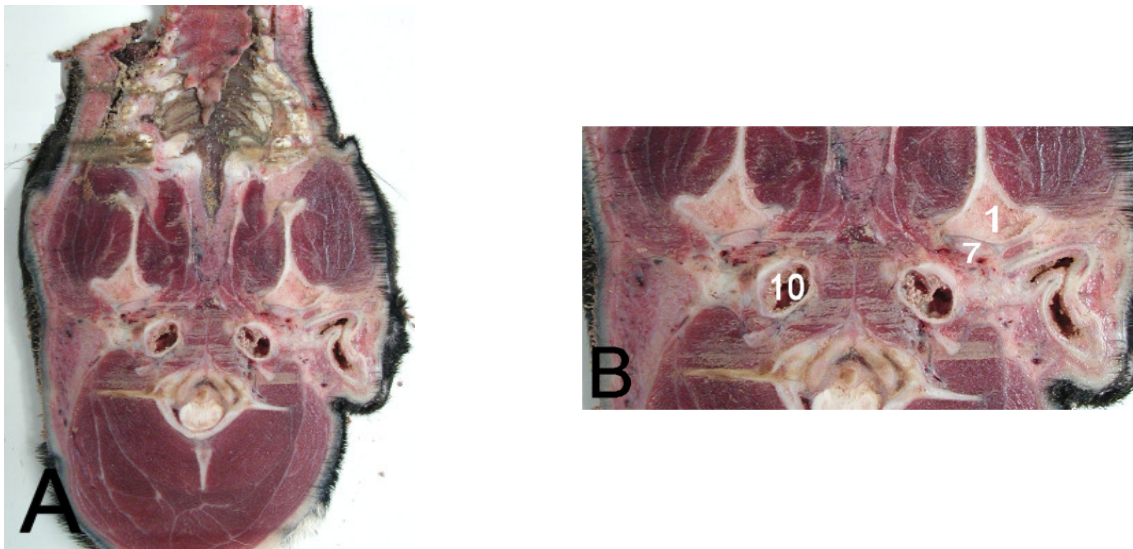


Figure 2.3.19.4 A. Ventral aspect of section 2. B. Magnified view of both TB and TMJ.

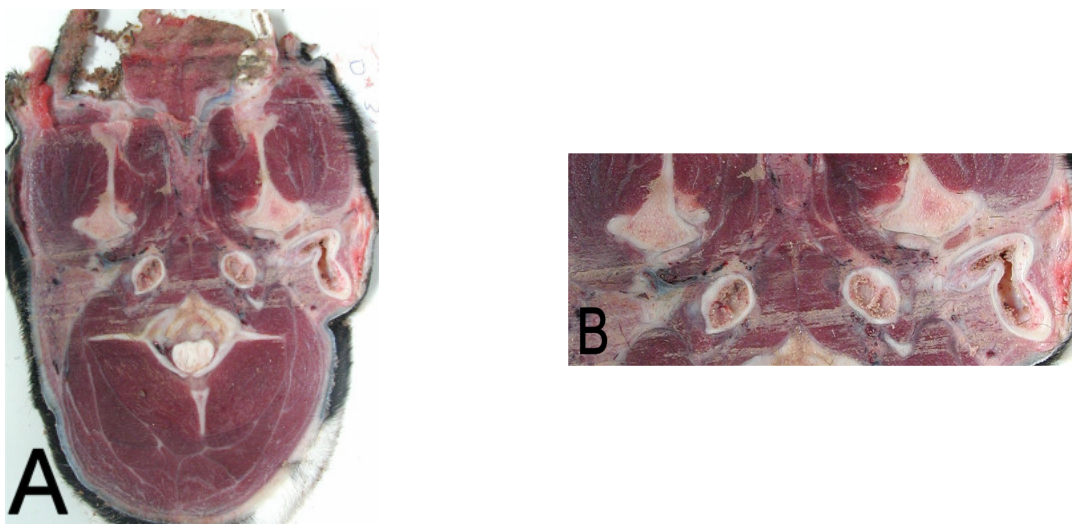


Figure 2.3.19.5. A. Dorsal aspect of section 3. B. Magnified view of both TB and TMJ.



Figure 2.3.19.6. Ventral aspect of section 3

Figure 2.3.20. Dorsal anatomical sections through the region of the tympanic bulla (TB) and temporomandibular joint (TMJ) in the cat progressing from dorsal to ventral. For key see Table 2.3.6. Rostral is to top and left is to the right in all images.

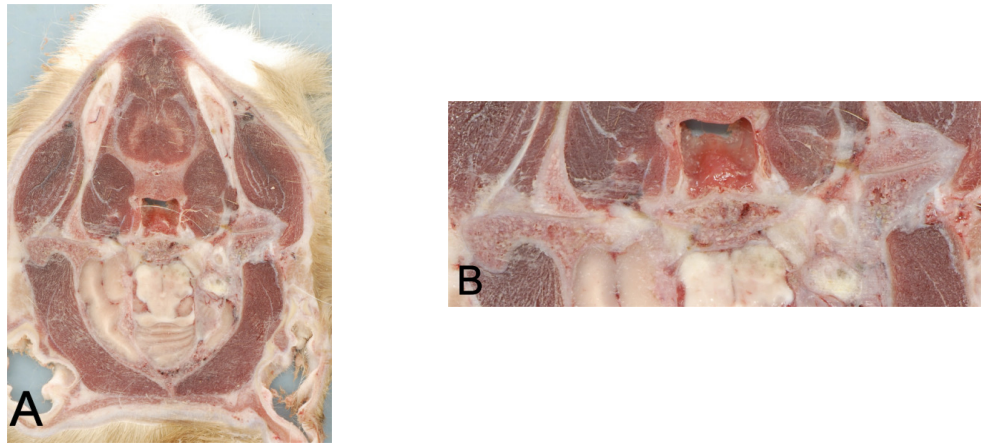


Figure 2.3.20.1. A. Ventral aspect of section 1. B. Magnified view of both TMJ

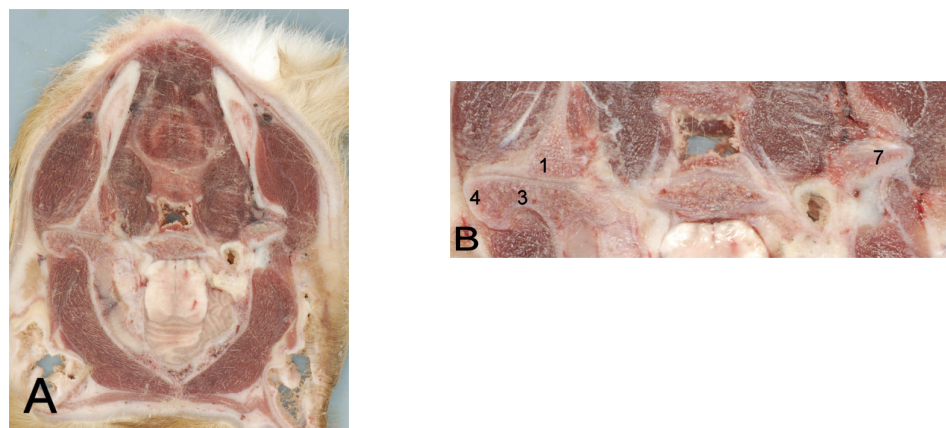


Figure 2.3.20.2. A. Dorsal aspect of section 2. B. Magnified view of both TMJ

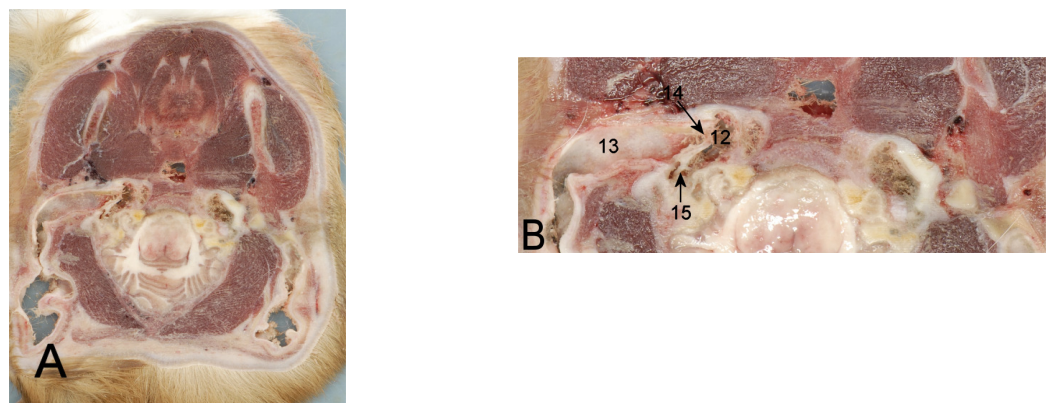


Figure 2.3.20.3. A. Ventral aspect of section 2. B. Magnified view of both TB

Figure 2.3.20. continued. Dorsal anatomical sections in the cat.

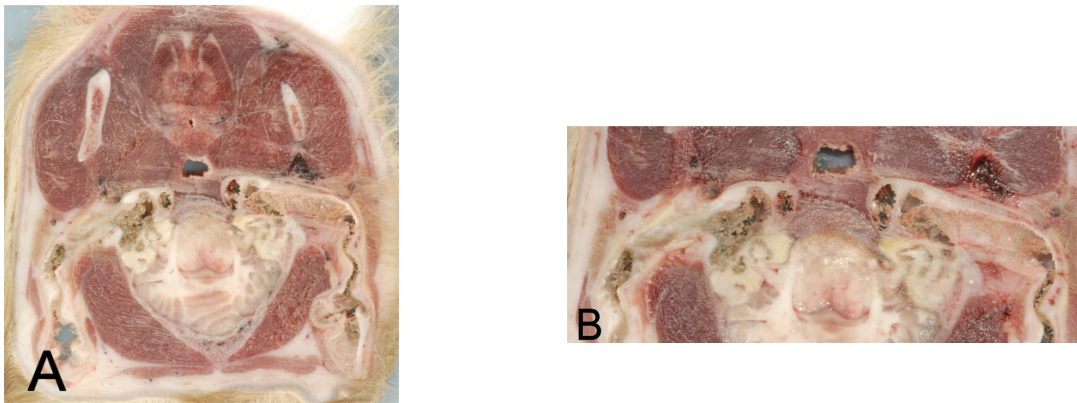


Figure 2.3.20.4. A. Dorsal aspect of section 3. B. Magnified view of both TB

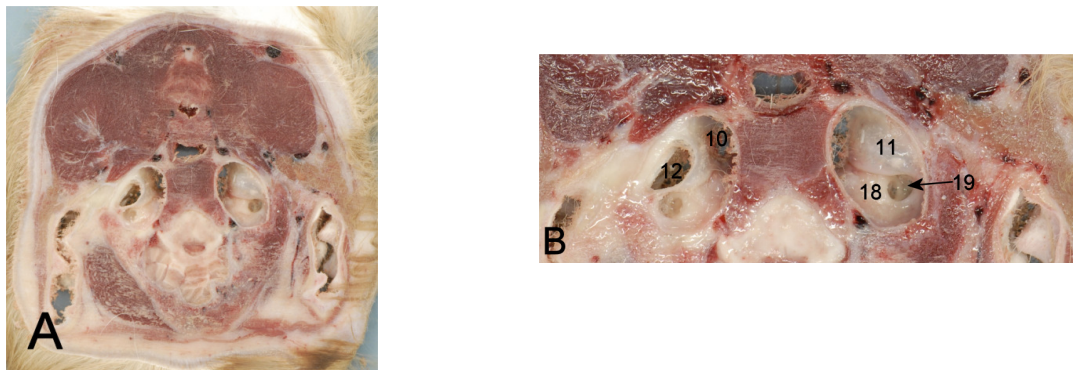


Figure 2.3.20.5. A. Ventral aspect of section 3. B. Magnified view of both TB

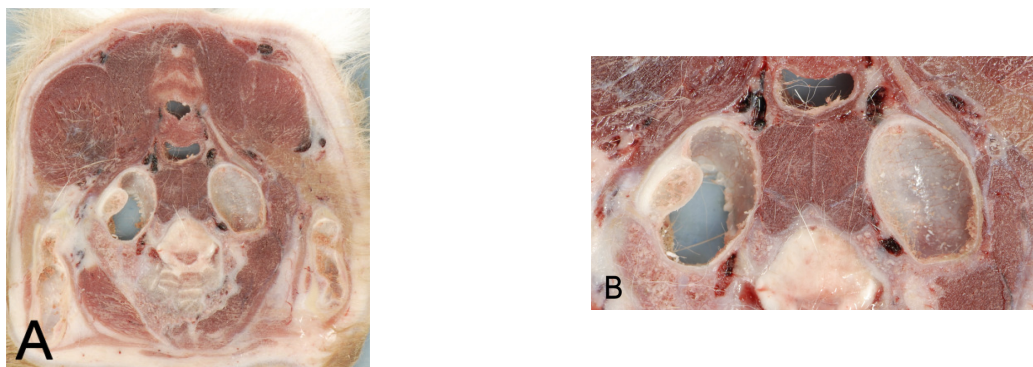


Figure 2.3.20.6. A. Dorsal aspect of section 4. B. Magnified view of both TB

Figure 2.3.20. continued. Dorsal anatomical sections in the cat.

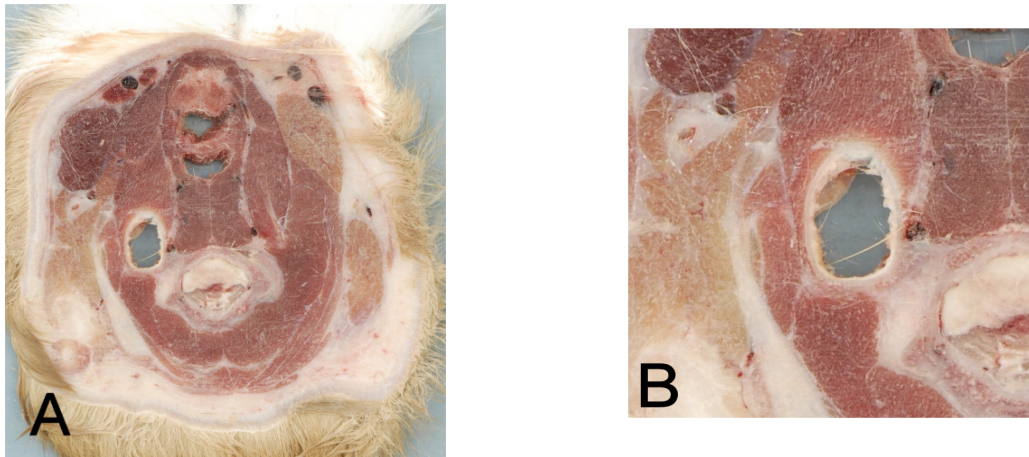


Figure 2.3.20.7. A. Ventral aspect of section 4. B. Magnified view of right TB

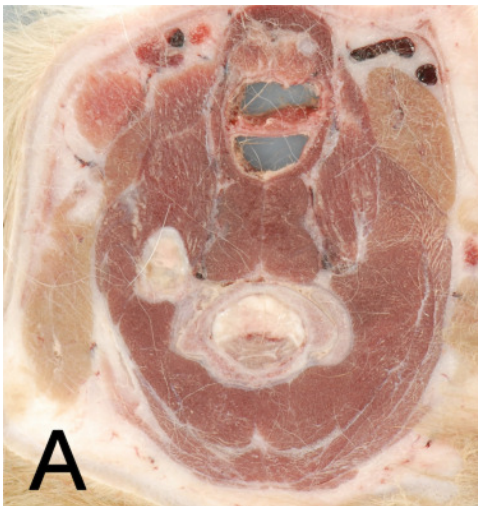


Figure 2.3.20.8. Dorsal aspect of section 5.

Figure 2.3.21. Dorsal anatomical sections through the region of the tympanic bulla (TB) and temporomandibular joint (TMJ) in the rabbit progressing from dorsal to ventral. For key see Table 2.3.6. Rostral is to top and left is to the right in all images.

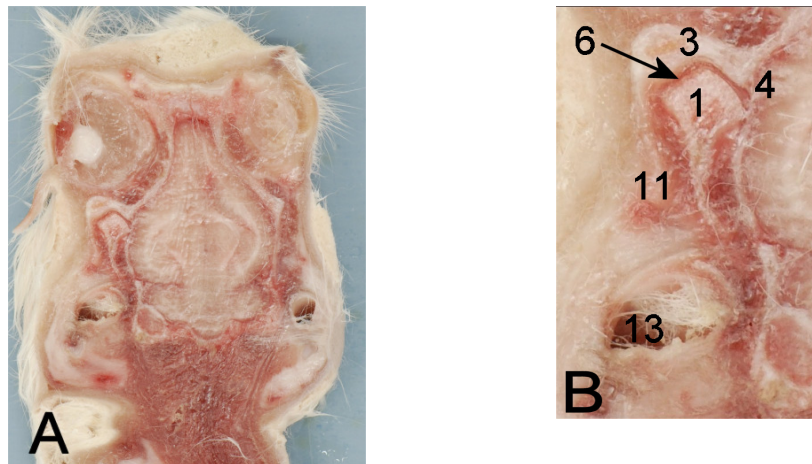


Figure 2.3.21.1. A. Ventral aspect of section 1. B. Magnified view of right TMJ.

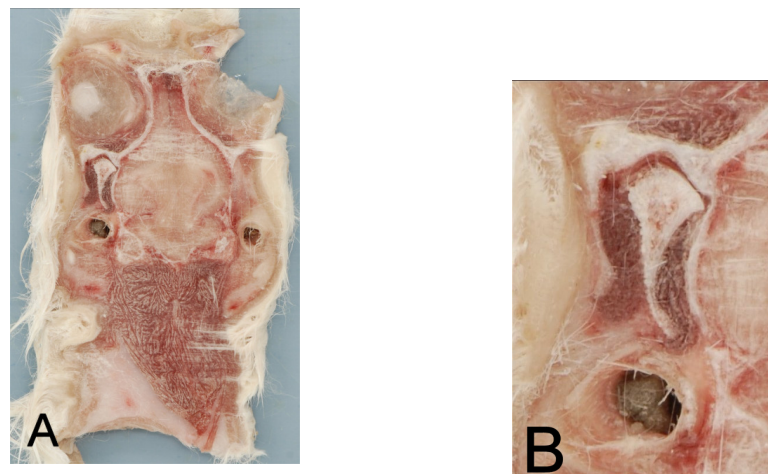


Figure 2.3.21.2. A. Dorsal aspect of section 2. B. Magnified view of right TMJ.

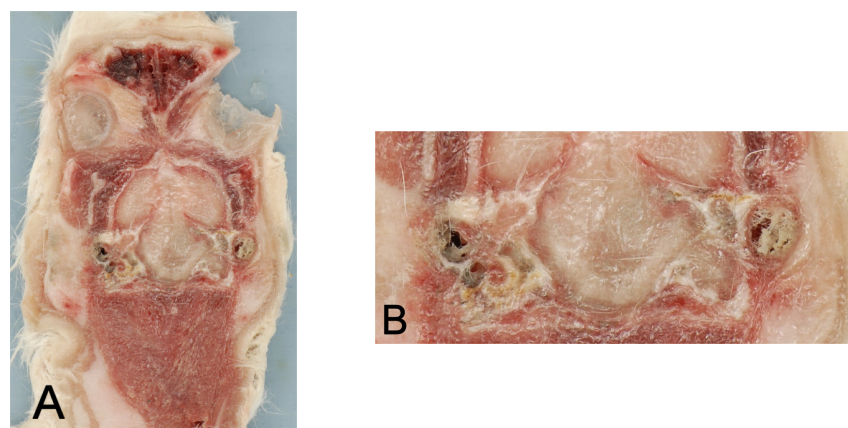


Figure 2.3.21.3. A. Ventral aspect of section 2. B. Magnified view of both TB.

Figure 2.3.21. continued. Dorsal anatomical sections in the rabbit. .

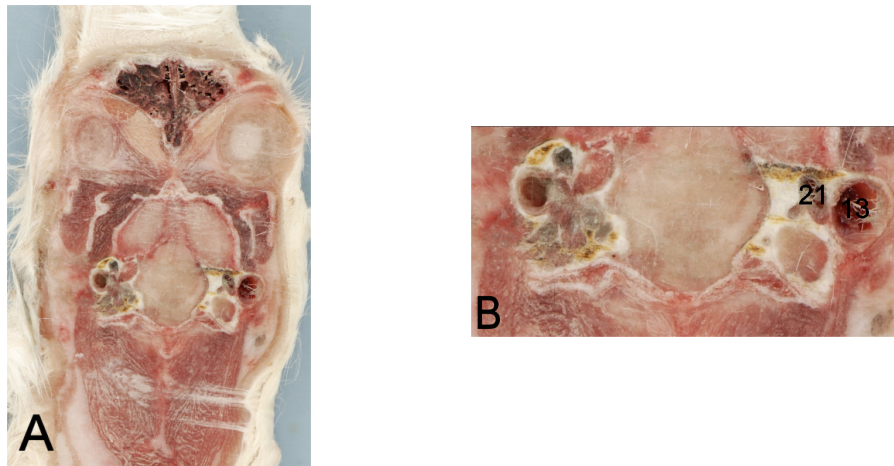


Figure 2.3.21.4. A. Dorsal aspect of section 3. B. Magnified view of both TB.

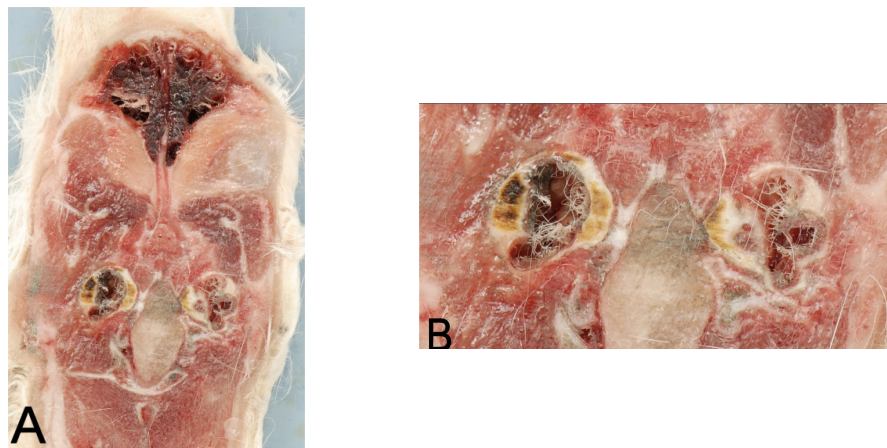


Figure 2.3.21.5. A. Ventral aspect of section 3. B. Magnified view of both TB.

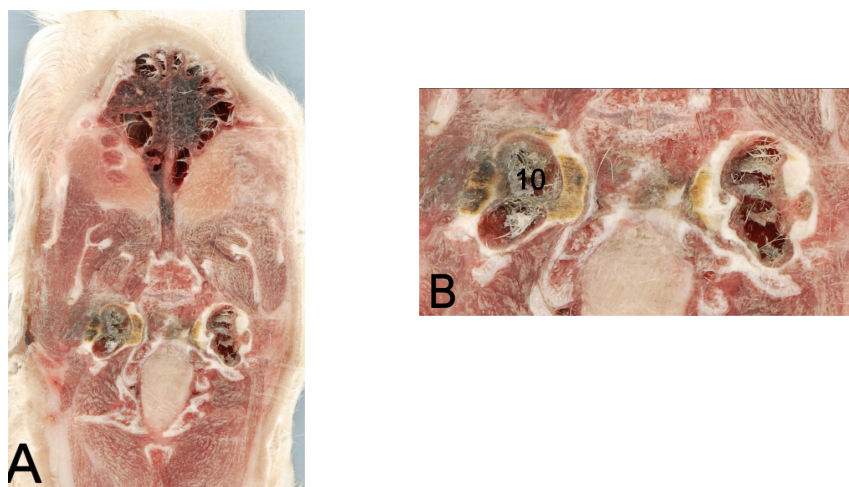


Figure 2.3.21.6. A. Dorsal aspect of section 4. B. Magnified view of both TB.

2.3.4. Plastination

The transverse section from the dog, cat and rabbit heads were successfully plastinated and retained within the veterinary anatomy unit for teaching purposes. Examples are demonstrated in Figure 2.3.22.

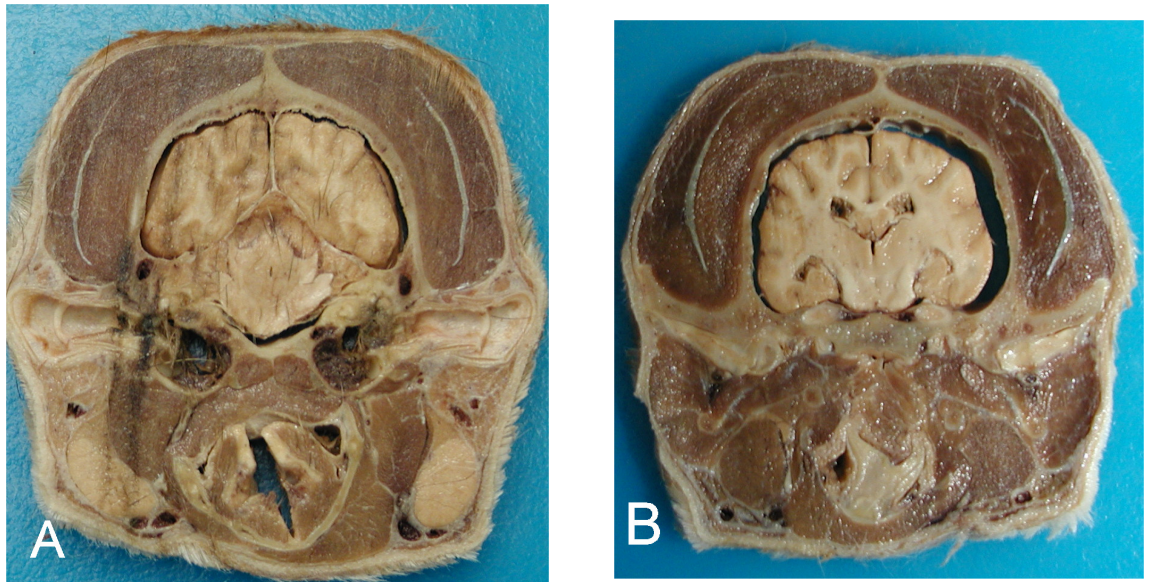


Figure 2.3.22. Examples of plastinated transverse anatomical sections through the region of the tympanic bulla and temporomandibular joint in the dog.

2.3.5. Facial index in the dog, cat and rabbit

The facial index calculated for 50 canine skulls (Table 2.3.7.) ranged from 79 to 480 (mean 150.8; SD 72.6). Most of the breeds represented were of a mesaticephalic skull type (n=30; range 100-147; mean 121.1; SD 14.5). Only five dolichocephalic skulls were present and of these, the specific breed was only known in three (Rough Collie, Great Dane and Deer Hound). They produced values of 95 or less (mean 89.2; SD 6.6).

A larger number of brachycephalic skulls were present (n=15) representing a number of breeds and these produced facial indices of 158 or greater (mean 231; SD 88.7). However, within this group, the larger breeds (Boxer and Mastiff n=8) were observed to produce lower facial indices (range 159-190, mean 172; SD 12.5) than the smaller breeds (Cavalier King Charles Spaniel, Pekingese, Chihuahua n=7) (range 215-480, mean 298; SD 91.4).

In 10 cats the facial length ranged from 1.8 to 2.4cm (mean 2.11; SD 0.19) and the facial width from 5.3 to 6.7cm (mean 5.99; SD 0.46). The resulting facial indices ranged from 241 to 331.25 (mean 285.9; SD 27.9).

In rabbits, the rostral margin of the nasal bone was located immediately dorsal to the prosthion and therefore provided a more convenient landmark for the measurement of facial length. The nasofrontal suture in the rabbit formed a 'V' or 'U' shape rather than the '∧' shape observed in the dog and cat. However, the nasion could still be easily identified at the bottom of the trough on midline and was located level with the rostral margin of the orbit while in the dog and cat it extended further caudally.

In 10 rabbits the facial length ranged from 3.45 to 4.15cm (mean 3.82; SD 0.18) and facial width from 4.2 to 4.6 cm (mean 4.4; SD 0.14). The resulting facial indices ranged from 103.6 to 124.3 (mean 115.5; SD 6.05).

2.3.6. Rotational angle of the canine mandibular condyle

The rotational angles measured for the condyloid processes in 38 canine skulls ranged from 5 to 30°, (mean 16.1°; SD 4.99) (Table 2.3.8.). The left and right condyles of each mandible had angles within 3° of each other (left condyle mean 15.9°; SD 5.2: right condyle mean 16.3°; SD 4.8). Although there was no direct correlation between the rotational angle and facial index, there was grouping of some breeds particularly the Labrador and Boxer, the latter also producing the highest results (n=6; mean 22.8°; SD 3.9).

Breed	Facial Index	Breed	Facial Index
Unknown	79	Corgi	129
Unknown	88	West Highland Terrier	130
Rough Collie *	89	Poodle	135
Great Dane	95	Cairn Terrier	137
Deerhound	95	Poodle	140
Collie	100	Keeshund	140
Scottish Terrier	104	Cairn Terrier	141
German Shepherd	105	Jack Russell Terrier	144
Fox terrier	106	Skye Terrier	144
Fox terrier	107	Cairn Terrier	147
Labrador	107	Mastiff	158
Old English Sheepdog	107	Boxer	159
Labrador	108	Boxer	160
German Shepherd	109	Boxer	169
German Shepherd *	110	Mastiff	180
Spaniel	110	Boxer	180
Kerry Blue	110	Boxer	183
German Shepherd	111	Boxer *	190
Pointer	117	CKCS	215
Labrador	118	CKCS	237
Staffordshire Bull Terrier	120	Chihuahua	250
Lakeland Terrier	121	CKCS	257
Yorkshire Terrier	124	Pekingese	300
Springer Spaniel	124	Chihuahua	347
Labrador	127	Pekingese	480

Table 2.3.7. Facial index calculated in 50 canine skulls

* indicates skulls used for the radiographic study in Chapter 3

CKCS = Cavalier King Charles Spaniel.

Breed	Rotational Angle		Facial
	Left	Right	Index
Jack Russell Terrier	5	6.5	144
Chihuahua	6	6.5	347
German Shepherd	7	9	111
Lakeland Terrier	8.5	9	121
Scottish Terrier	9.5	10	104
West Highland Terrier	11	12	130
Cairn Terrier	12	12	147
Chihuahua	12	15	250
Yorkshire Terrier	12.5	11.5	124
Rough Collie	13	14	89
Skye Terrier	14	13	144
Pointer	14	14	117
German shepherd	14	17	109
Corgi	14	17	129
Cairn Terrier	15	14	141
Cairn Terrier	15	14.5	137
Boxer	15	17	159
Fox terrier	16	14	106
Poodle	16	17	140
Kerry Blue	16	18	110
Mastiff	16	18	158
German Shepherd	16	19	110
Labrador	17	14	107
Labrador	17	15	127
Labrador	17	18	118
Labrador	17	19	108
Keeshund	18.5	17	140
Fox terrier	19	17.5	107
Staffordshire Bull Terrier	20	19	120
German Shepherd	20	20	105
Old English Sheepdog	20	21	107
Mastiff	20	22	180
Great Dane	21	20	95
Boxer	21	24	183
Boxer	23	21	180
Boxer	24	24	190
Boxer	25	24	160
Boxer	29	27	169

Table 2.3.8. Rotational angles of the mandibular condyles in 38 canine skulls.

2.4. Discussion

2.4.1. Bony anatomy of the TB and TMJ

The anatomy of canine and feline TB observed in the present study corresponded with that of previous descriptions (Little and Lane 1986, Evans 1993, Farrow 1994) although the dimensions recorded were greater than previous reports of 15mm long and 8-10 mm wide in dogs (Evans 1993) and 10mm diameter in cats (Riser and others 1967). The small standard deviations for the feline and rabbit measurements were presumably due to the uniformity of the structures within these species when compared with the greater variation observed between the dogs. The mean measurements of TB size recorded reflected the overall size differences between the three species and the proportions, the subtle variations in shape. The rabbit demonstrated similar values in all dimensions reflecting a rounder shape than the other species and this was also evident visually when viewing the TB from a ventral aspect. The length was the greatest measurement in both the dog and cat, with similar values suggesting that the cat has a disproportionately long TB for its size.

The basic anatomy of the rabbit TB was similar to the dog and cat although it did not project ventrally beyond the level of the occipital bone, as it does in both these species. The external acoustic meatus of the rabbit was a long prominent tube of bone compared to the short bone canal of the dog, while the cat has little more than a bone ring. The meatus in the rabbit was also vertically rather than horizontally orientated. The dimensions of the external acoustic meatus were very similar between the dog and cat despite the overall size difference between the species and both were narrower than they were tall. The rabbit TB was smaller in all dimensions than the dog and cat but was more cylindrical.

In all three species, the ventral wall of the TB was thinnest and the lateral wall thickest due to the presence of an internal bone rim at the boundary between the external acoustic meatus and the TB wall. In the rabbit, this was also marked by a roughened external rim, which is absent in the dog and cat. The mastoid and jugular processes were very prominent in the rabbit overlying the caudolateral aspect of the TB and extending ventral to it. The mastoid process in the dog and cat is present as a small bone protrusion caudal to the external acoustic meatus. The jugular process is poorly developed in the cat but in the dog is located caudal to the TB and projects in a caudoventral direction although still much less prominent than in the rabbit.

Although the margin between the TB wall and the petrous temporal bone was visible in the rabbit, there was no bone ridge as present in the dog and no bone septum separating the tympanic cavity proper from the hypotympanum as in the cat. There do not appear to be any descriptions of the internal structures of the middle ear cavity in this species, suggesting further work would be indicated to further document the anatomy of this area.

The anatomy of dog and cat TMJ observed in the present study also corresponded with that of previous descriptions (Scapino 1065, Ström and others 1988, Evans 1993, Caporn 1995), although there does not appear to be any mention of breed variation. In the canine skulls in the present study, some variation in the size and shape of the TMJ components was observed between and within breeds although insufficient numbers of any particular breed were present to allow characteristics to be determined. The dolichocephalic and mesaticephalic type skulls had very similar TMJs and most of the variations were noted in the brachycephalic skulls. The variation noted in the large brachycephalic breeds (Boxer, Mastiff) were not sufficiently marked as to render the gross anatomy of the joints incomparable with those of the other skulls and they were therefore regarded as normal anatomic variations. This was not the case however with the small brachycephalic breeds examined (Cavalier King Charles Spaniel), where the differences were considered too marked to allow direct comparison with the other skulls. This indicates that there can be an association between dog breed and TMJ anatomy. The observations on these skulls will be further investigated in Chapter 8.

Since dogs and cats are both carnivores, they have similar TMJ anatomy reflecting the predominantly vertical masticatory movement and hinge action typical of specialised group 1 (Gillbe 1973). The canine condyloid process has distinctive medial and lateral components, a feature that seems particularly prominent in some breeds such as the Boxer. This is not the case in the cat, which lacks many of the features observed in the dog including the non-articular lateral extremity of the condyloid process and the tubercle at the lateral aspect of the mandibular fossa. This simplicity is reflected in the fewer regions that were defined for descriptive purposes in Figure 2.3.7. However, one significant feature the cat has that is lacking in the dog is the ridge of bone at the rostral margin of the mandibular fossa. This creates a more enclosed joint space and therefore better congruity between the components of the joint in this species

Practicing veterinary surgeons are likely to be familiar with the TMJ anatomy of the dog and cat since they are encountered on a daily basis. However, rabbits are lagomorphs and their masticatory apparatus has been classed as intermediate between herbivores (group 2) and rodents (group 3) (Gillbe 1973, Wiejs and Dantuma 1981, Crossley 2003) so their TMJ anatomy is different to most of the commonly encountered companion animals species. The TMJ is located caudal and dorsal to the molar arcade in the rabbit while it is level with it in the dog and cat (Wiejs and Dantuma 1981, Evans 1993, Caporn 1995). In carnivores, the joint is orientated in the transverse plane with the mandibular condyle and fossa being of complimentary shapes compared with the rabbit TMJ that is orientated in a paramedian plane with an elongated condyle and a short, deep fossa (Wiejs and Dantuma 1981, Evans 1993, Caporn 1995). The condyle is the most dorsal extension of the mandible in the rabbit, sitting above the level of the coronoid process but in the dog and cat the coronoid process extends dorsal to the condyloid process and TMJ in a position medial to the zygomatic arch. The TMJ is located level with the caudal aspect of the zygomatic arch while in the rabbit, the caudal end of the zygomatic arch is elongated, projecting alongside the lateral aspect of the condyloid process. There is no retroarticular process in the rabbit as there is in the dog and cat and so nothing to prevent retropulsion of the condyle (Barone 1989). This combined with the poor congruity between components permits the rabbit a much greater range of movement than the carnivores (Crossley 2003). The reported 6-7mm range of movement in a rostrocaudal direction (Weijs and Danuma 1981) corresponded with the length of the articular surface of the condyloid process observed in the present study and the resulting range of potential positions the condyloid process could occupy relative to the mandibular fossa. The limited transverse shift (Weijs and Dantuma 1981) also fitted with the narrow mandibular fossa and corresponding articular surface of the condyloid process, and the caudal extension of the zygomatic arch.

2.4.2. Soft tissue anatomy of the TB and TMJ

The superficial structures in the cat and rabbit were much more difficult to visualise than in the dog, and often were removed inadvertently with the skin. The main structures surrounding the TB and TMJ were similar in all three species with a few exceptions. The parotidoauricularis muscle was well developed in the dog but was not well represented in the cat, while the opposite was true of the mandibuloauricularis or tragicus lateralis muscle. This was reported to be greatly reduced in the dog and may only be present as tendinous remains (Evans 1993), which would explain why it was not readily identified in any of the

dogs in the present study. No mention of this muscle in the rabbit could be found in the literature although an equivalent muscle called the styloauricularis muscle was reported (Barone 1989). Although there was no mention of its attachments, a diagram of its location in the horse suggested an attachment to the caudal aspect of the TMJ (Barone 1989). In the present study of the rabbit, it was well developed with attachments to the caudal extension of the zygomatic process as well as the caudal aspect of the condyloid process.

In keeping with a previous report, an extra parotid lymph node was observed in the cat (Crouch 1969), which was absent in the dog and rabbit. Although the digastricus muscle was divided into rostral and caudal parts in all three species, the division was particularly prominent in the cat and was represented by a fibrous band, again in keeping with previous reports (Crouch 1969). The caudal retractor muscle was observed in the rabbit as an additional component to this muscle that was absent in the other species.

Access to the TB was obtained by similar approaches in all three species although the more superficial position of the feline TB made it easier to expose a larger area of the ventral wall than that allowed by the deeper position in the other species. The absence of some of the bony components of the styloid apparatus also facilitated exposure in the rabbit.

Exposure of the lateral aspect of the TMJ capsule was straightforward in the dog and cat with the dog demonstrating a well defined lateral ligament between the rostral aspects of the mandibular fossa and condyloid process, as has been previously described (Evans 1993, Caporn 1995). A corresponding structure was not obvious in the cat. In the rabbit, more extensive dissection was required to reveal the joint and the lateral aspect was guarded by the caudal projection of the zygomatic arch meaning only the dorsal aspect could be exposed. Although the rabbit also has a well defined lateral ligament (Barone 1989), it was located between the condyloid process and the caudal projection of the zygomatic process and therefore was not as readily visible.

The TMJ disc in the dog was visible from the lateral aspect of the joint and could be easily separated from both the condyloid process and the mandibular fossa, reflecting the fact that it divides the joint into two separate synovial chambers (Gillbe 1973, Capron 1995). Its appearance corresponded with that of previous reports (Shengyi and Yinghua 1991). The fibrous sheet observed in the cat corresponded with the thick membrane rather than a disc

that has been reported in this species (Gillbe 1973). The disc in the rabbit was not readily accessible due to its location ventral to the mandibular fossa, to which it was firmly attached, corresponding with reports that the ventral synovial compartment is much larger than the dorsal one (Barone 1989). Extensive dissection was required to expose it and its saddle shaped appearance corresponded with that of previous reports (Weijs and Dantuma 1982, Barone 1989). It has been suggested that in grazing animals, the disc functions to allow both hinge movements between the mandible and disc and a sliding motion between the disc and the fossa so the mandible can move sideways relative to the skull. Hinge like movements predominate in the dog therefore the presence of a thinner, more poorly developed disc probably reflects the reduced amount of lateral movement in this species (Evans 1993).

2.4.3. Multiplanar anatomy

The tomographic sections produced in this study allowed visualisation of the structures associated with the TB and TMJ, assessment of the topographical anatomy and comparison with images produced using CT and MRI in Chapters 5 and 6. In previous studies, the cranial (Zook and others 1981) or caudal (George and Smallwood 1992) surfaces of the cadaver slices have been presented. Although the appearance of contiguous surfaces was similar, the appreciation of three dimensional variations between the sections was thought to warrant presentation of both surfaces in the present study.

The small size of the TB and TMJ in the cat and rabbit meant that the slice thickness of 0.6cm was not adequate to allow complete examination of these structures and many areas went unobserved. The thickness of the anatomical sections should also ideally be selected to correspond with those of the imaging technique being compared (George and Smallwood 1992, Morrow and others 2000) but in this case could not match the 1.1 mm slices obtainable using CT and MRI. Although a more rigid blade could be used to produce thinner slices, the structural integrity of the cadaver material and safety considerations when using the bandsaw will dictate the minimum slice thickness obtainable. One way to ensure sections through enough areas of these structures to allow a complete examination would be to section a greater number of similar heads and rely on the fact that each series is likely to be at a slightly different level through the relevant structure to generate a more complete database of images. This was outwith the scope of

the present study but may form the basis for further work if such an image bank was required.

It is often difficult to slice cadavers exactly perpendicular resulting in one side being cut slightly deeper than the other (Zook and others 1981). This problem was also encountered in the present study because of the marked difference in density of tissue within the head being sectioned simultaneously and therefore mounting on a board or in ice, as has been suggested, is unlikely to have helped (Patrick 2002, Valente and others 2007). However, this did not hinder identification of the relevant structures in the present study and has been reported in many instances to reveal more anatomical relationships than would otherwise have been apparent (Zook and others 1981).

The quality of some images was affected by tissue discoloration, resulting from the heat generated by the blade passing through dense bone structures, and was unavoidable. Likewise, it proved impossible to remove all the hair from the surface of the sections and this is a recognised problem when photographing post mortem material (Thompson and Irvine 2007).

2.4.4. Plastination

The plastination process involved a series of stages. In preparation for plastination, the sections had to be fixed, which was achieved using formalin to stabilise the tissue and prevent autolysis (Whittaker 2007). They then had to be dehydrated and this was achieved using acetone, which slowly replaced the water within the tissue over a period of weeks (Whittaker 2007). This part of the procedure is also known as freeze substitution as it is usually performed at a temperature of -25°C to reduce distortion of the tissue during the dehydration process (Whittaker 2007). However, due to its flammable nature, compliance with the University of Glasgow health and safety requirements meant the acetone used in the present study had to be stored outside the building in a fireproof container and prevented it being placed in the freezer. The temperature of this part of the process was therefore dependent on environmental conditions and was not controllable. Performance over the winter months meant the temperature was likely to be low but was unlikely to have been below zero degrees for any length of time. Problems with tissue distortion were therefore anticipated during this stage due to the inability to freeze the material. However, apart from an overall reduction in the size of the brain, which resulted in the presence of a

space between its external margin and the cranium, little tissue distortion was noted in the resulting sections.

The next stage was forced impregnation where the dehydrated specimens were placed in a vacuum that drew out the acetone and replaced it with the polymer (Whittaker 2007). There are no specific temperature requirements for this part of the process and in the present study this was performed at sub-zero temperatures due to the vacuum unit being located within the freezer. This should have prevented any further distortion of the sections. The final stage involved gas curing the sections to harden the polymer throughout the tissue (Whittaker 2007).

The S10 silicon polymer in this study is the most frequently used as it is the easiest of the techniques to implement (Whittaker 2007). It produced excellent preservation of the soft tissue structures surrounding the TB and TMJ in all three species. Thinner polymers are better suited to preservation of brain tissue to allow rapid penetration and reduce distortion (Whittaker 2007), although apart from shrinkage, little distortion of the brain tissue was observed in this study. The time taken for each stage of the process will vary depending on the material being processed and the thin nature of the sections in the present study meant that each stage was completed relatively quickly. Nevertheless, the entire procedure still took approximately 9 weeks making it time consuming. The cost of the specialist equipment and consumables also makes it relatively expensive. However, the advantages of the resulting material over traditionally preserved equivalents make this a worthwhile procedure although further work with this equipment will be required to develop optimum procedures to cater for a range of specimens.

2.4.5. Facial index

The facial index as described by (Evans 1993) was useful for classifying the skull types used in this study. The range of values present reflected the wide range of skull shapes present within the canine population. The skulls examined were determined by availability of material and most were of the mesaticephalic type, which is not surprising as most breeds fall into this group. There were more brachycephalic breeds represented than dolichocephalic ones, which presumably reflects the relative popularity of various breeds. The different values within breeds presumably reflected variation in cranial conformation

between different familial lines although there were insufficient numbers of each breed examined to draw any conclusions.

The average facial indices calculated for the dolichocephalic and mesaticephalic skulls in the present study were larger than the previously reported values (Evans 1993) (89 compared to the published 81 and 121 compared with 111 respectively) while those of the brachycephalic group were smaller (215 compared with 231). In the present study, the large and small brachycephalic breeds appeared to form two distinct groups with the larger breeds demonstrating lower indices than the smaller breeds. Only skulls from this latter group (Cavalier King Charles Spaniels, Pekingese and Chihuahua) reached and exceeded the previously reported value. The use of indices rather than actual measurements should remove the effect of physical size from the calculation so it may be more appropriate to group large and small breed brachycephalics separately although further investigations with larger numbers would be required to determine if this is the case. The numbers and breeds of dog involved in the original determination of these values was not clear, nor whether live animals, cadavers or emasculated skulls were used, all of which would have an influence on the results.

Compared with the dog, the range of facial indices demonstrated in the cat and rabbit were much more limited, reflecting the much smaller range of skull shape demonstrated in these species. The TB and TMJ anatomy was therefore very similar among the cats and rabbits examined. Although relatively dolichocephalic cats (Oriental breeds) and brachycephalic cat (Persian) and rabbit (Netherland Dwarf) breeds do exist (Pond and Raleigh 1979, Mettler 1992), availability of material meant they were not included in the present study. Further work would therefore be warranted to determine whether there are similar variations in the TMJ anatomy in these breeds as observed in small brachycephalic dog breeds. The lack of literature in this area may reflect an absence of changes or a lack of investigation.

2.4.6. Rotational angle

A range of rotational angles of the condyloid process were observed both between and within breeds although the left and right values in an individual were relatively constant. Normal breed ranges could not be determined due to insufficient numbers of any one breed in the sample although some grouping was observed. The majority of the skulls had values

less than 20°. The general exception was the Boxer, which had higher values and this presumably corresponded with the increased angulation of the caudal margin observed grossly.

In a study measuring the rotational angle in 35 dogs representing 18 different breeds, the mean angle of the right condyloid process was 13.8° (SD 5.0) and the left was 15.2° (SD 5.1) (Hazewinkel and others 1993). The large number of Boxers in the present study may account for the increased mean values observed as when they are removed from the calculations, the mean value for the right condyle becomes 15.1° (SD 4.1) and for the left 14.6° (SD 4.1), which are very similar. Another study also measured the rotational angle in five dogs and reported a range from 0 to 12° with a value of 0° considered to be indicative of normal TMJs (Lantz and Cantwell 1986). However, only 6 dogs in the present study demonstrated values below 12° and none were 0°, despite the TMJs being grossly normal. It was not clear exactly what measurements were made in obtaining the results for this previous report therefore an alternative methodology may have account for the different ranges observed (Lantz and Cantwell 1986). Interestingly though, it was a Boxer which produced the highest values in that study also.

Chapter 3. Radiography of the tympanic bulla and temporomandibular joint in the dog, cat and rabbit.

3.1 Introduction

3.1.1. Radiography of the head

Radiographic images are produced according to the density and atomic number of the structures being interrogated (Curry and others 1990). The high density of bone results in attenuation of a large portion of the X-ray beam by a combination of the photoelectric effect and Compton scatter. The radiographic film beyond bony structures is therefore relatively underexposed and depicted as a radio-opaque or white area following processing. Conversely, gas has a very low density so the beam passes through relatively unattenuated and the resulting exposed area of film is depicted as black. This produces a clear distinction from adjacent tissue making radiography well suited for the investigation of bone or gas filled structures. Soft tissue and fluid have very similar densities and atomic numbers, and so attenuate a similar proportion of the beam making them indistinguishable on radiographs. Radiography more limited for the investigation of these areas and the ability to locate soft tissue structures depends on the presence of adjacent fat, which has a lower atomic number and density, therefore appears darker on the radiograph (Curry and others 1990).

Diagnostic imaging of the canine head has historically centred around the use of radiography (Douglas 1987, Hoskinson 1993, Schwarz and others 2002) although the base of the skull is a complex anatomical region that can be difficult to evaluate using this method (Love and others 1995). Radiographic evaluation of the head of the dog, cat (Gibbs 1978, Douglas 1987, Kapatkin and others 1990, Remedios and others 1991, Hoskinson 1993, Farrow 1994, Love and others 1995, Sullivan 1995, Owens and Biery 1998) and rabbit (Gibbs and Hinton 1981, Wolvekamp and Oswald 1991, Crossley 1995, Harcourt-Brown 1995, Harcourt-Brown 2003) has been described. For the most accurate three dimensional assessment of changes, several different views should be taken (Rose 1977) but although there are a large number of projections described, some are more useful for the investigation of specific areas than others (Douglas 1987). Skull type in the dog also influences the recommended views for examination of these regions (Douglas 1987, Morgan and Silverman 1987). Radiographic views are generally named according to the

direction that the beam penetrates the body and the standardized nomenclature, with correct abbreviations, has been described (Smallwood and others 1985).

True lateral views of the head are often performed, using foam wedges and tape as positioning aids, but result in superimposition of the two halves of the head (Douglas 1987, Harcourt-Brown 2003). Since disease processes are often unilateral, it may be beneficial to produce views that allow comparison between the two sides as this should facilitate the identification of abnormalities (Gibbs 1978, Bruyette and Lorenz 1993, Thrall 2002). Dorsoventral, ventrodorsal and rostrocaudal views project both sides of the skull onto a single film making comparison easy. The latter can be performed with the mouth closed or open. Dorsoventral views are easy to position and so may be possible to produce in conscious or lightly sedated animals (Sullivan 1989). Placing the mandibles flat on the cassette or table top ensures symmetry, although raising them on a block may be more comfortable for conscious patients (Douglas 1987). In rabbits, extension of the head and neck can be achieved by placing a tie round the upper incisors to anchor the head in position but care must be taken when placing the animal as, in this position, the mandible may move to one side so it is no longer aligned with the maxilla (Harcourt-Brown 2003). Ventrodorsal views will produce a similar appearance but are more difficult to position to ensure symmetry and therefore usually require heavy sedation or general anaesthesia (Douglas 1987). However, they may be easier to produce in the presence of extensive mandibular trauma that compromises symmetrical positioning for a dorsoventral view (Ticer and Spencer 1978). Rostrocaudal views, particularly open mouth ones, require general anaesthesia (Douglas 1987). They are acquired with the animal in dorsal recumbency and the head positioned either perpendicular to the beam or at an angle depending on which structures are being investigated (Douglas 1987).

Oblique views are used to project individual structures free from superimposition onto the skull and each other. The shape, position and anatomic relationship of the various components can therefore be assessed, enabling the detection of more subtle changes (Lane 1982, Sullivan 1989, Schwarz and others 2002). However, since each structure requires a separate exposure, it is important to ensure that the same degree of angulation has been applied to each side and that the views are clearly labelled to avoid confusion (Douglas 1987). This means they may be difficult to reliably reproduce between or within animals (Sullivan 1995), thereby hindering comparison of bilateral symmetry (Hoskinson 1993). With the exception of dorsoventral views in the dog, most radiographic investigations of

the head require sedation or general anaesthesia, due to the accurate patient positioning necessary to obtain repeatable, diagnostic quality radiographs (Wolvekamp and Aschwald 1991, Hoskinson 1993, Sullivan 1995, Harcourt-Brown 2003).

Rare-earth, high-detail screen-film combinations should be used for radiography of the head (Hoskinson 1993, Schwarz and others 2002) with a table-top technique (no grid) in small breeds of dogs, cats (Schwarz and others 2002) and rabbits (Gibbs and Hinton 1981). In medium to large breed dogs where the region being examined is greater than 10cm thick, a fast screen-film combination with a grid should be used (Sullivan 1995, Schwarz and others 2002). In general, exposure factors for the cat are appropriate for the rabbit (Gibbs and Hinton 1981) but should be varied depending on the area of interest as it is not usually possible to satisfactorily examine all areas of skull on a single film.

3.1.2. Radiography of the TB and associated structures

Prior to the advent of CT, plain radiography and pleuridirectional tomography or polytomography were used to evaluate human patients with temporal bone disease (Holliday and Reede 1989). Both techniques gave information regarding the bony anatomy of the ear (Twemlow 1991) with tomography allowing many important features to be identified (Wright and others 1982). These techniques were used to evaluate trauma in the region of the ear (Owens and Biery 1998) and radiolucent fracture lines with or without displacement could be identified (Hoskinson 1993). However, they did not demonstrate soft tissue components and so negative results did not exclude the presence of a lesion, while positive results were not informative enough to permit surgery (Twemlow 1991). The sensitivity of radiography for identifying fractures in the temporal region of the human skull was considered to be too low for it to be used for this purpose (Robinson and others 2003).

The routine radiographic evaluation of the canine and feline TB usually includes a combination of dorsoventral or ventrodorsal; rostrocaudal open mouth (RCdOM); ventrodorsal oblique or latero 20° ventral - laterodorsal (Le20° V-RtDO & Rt20° V-LLtDO), which is also referred to as a 'lateral oblique'; and lateral 'tilted-up' or 'nose up' views (Gibbs 1978, Douglas 1987, Kapatkin and others 1990, Remedios and others 1991, Hoskinson 1993, Farrow 1994, Love and others 1995, Sullivan 1995, Owens and Biery 1998).

In dorsoventral and ventrodorsal views, the TB are superimposed onto the dense petrous temporal bone (Hoskinson 1993) and therefore appear denser and thicker walled than in other views (Sullivan 1995). The walls produce bilaterally symmetrical, fine, crisp, distinct linear bone opacities although there is a large amount of variation in the exact bone pattern between breeds (Hoskinson 1993). In true lateral views, the crisply margined TB should have a smooth external surface and the external acoustic meatus should be rounded with distinct smooth margins (Hoskinson 1993). The inner and outer compartments of the feline TB can also be appreciated (Sullivan 1995). However, this view superimposes the TB over one another and so is generally considered to be of limited value for investigation of these structures.

The rostrocaudal open mouth view is generally considered best for demonstrating the TB in dogs (Gibb 1978). In dorsal recumbency, the mouth is opened, the tongue taped to the lower jaw and the endotracheal tube can either be removed (Douglas 1987, Gibbs 1978) or taped to the mandible (Hoskinson 1993). The head is positioned so the hard palate is perpendicular to the cassette (Douglas 1987) and the beam directed vertically, centred on the base of the tongue or the free edge of the soft palate (Sullivan 1995). To avoid superimposition of the TB onto the wings of the atlas in some breeds, it may be necessary to angle the hard palate away from the central X-Ray beam. An angle varying from approximately 10° in mesaticephalic breeds up to 20° in brachycephalics has been recommended (Douglas 1987), although another author suggests that all dogs should be radiographed at an angle of 30° (Hoskinson 1993).

On rostrocaudal open mouth views, the air filled cavity surrounded by the thin bony shell of the TB wall produces good radiographic contrast (Lawson 1957). The TB therefore appear as air filled structures of equal opacity surrounded by a sharply defined, smooth, complete thin line of uniform thickness ventral to the base of the skull (Lawson, 1957, Sullivan 1995). The radiolucent background of the air filled oropharynx enhances the radiographic contrast in this region therefore improving visualisation (Gibbs 1978), although care should be taken not to mistake overlying oral soft tissue structures for abnormal increases in opacity of the TB (Hoskinson 1993).

This rostrocaudal open mouth view can be difficult to perform in the cat due to the positioning involved and only slight obliquity resulting in a loss of symmetry (Hofer and others 1995). A rostro 10° ventral-dorsocaudal oblique or 10° ventrodorsal view may be

used in this species instead (Hofer and others 1995, Owens and Biery 1998). The animal is placed in dorsal recumbency and the head is extended 10-20° beyond the vertical with the mouth remaining closed. The beam is centred approximately 1cm ventral to the nares or on the chin (Hofer and others 1995, Owens and Biery 1998). Extension of the head allows projection of the TB free from superimposition onto the occipital bone or the mandible (Hofer and others 1995). The septum bullae is clearly visible in this view, creating distinct dorsolateral and ventromedial compartments (Little and Lane 1986) and the resulting double walled appearance has been described as resembling that of a snail shell (Farrow 1994).

The 'lateral oblique' view is achieved by positioning the head as if for a true lateral view with the side under investigation nearest the cassette (Douglas 1987). The head is then rotated about the long axis until the sagittal plane of the skull is at approximately 10-20° (Geary 1965, Hoskinson 1993) to the horizontal in dogs or 10-15° in cats (Bistner 1967). The beam is centred on the base of the ear (Hoskinson 1993) and results in the ventral surface of the skull and the lower TB being exposed (Douglas 1987, Hoskinson 1993). The mouth should remain closed to prevent superimposition of the mandible (Hoskinson 1993). The lateral 'tilted-up' or 'nose up' view can be achieved in conscious animals by placing the head in a lateral position and then elevating the nose using a foam pad so the sagittal plane of the skull is approximately 15° (Sullivan 1995) or 45° to the film (Gibbs 1978).

These views project each TB free from superimposition onto the other or the skull. However, since a separate exposure is required to visualise each TB, it is important to ensure that the same degree of angulation has been applied to each side in order to produce comparable projections (Douglas 1987). However, oblique views are not easy to reliably reproduce between or within animals (Sullivan 1995) and inability to precisely reproduce the angle of obliquity hinders comparison of bilateral symmetry (Hoskinson 1993). Each side must also be clearly labelled to avoid confusion (Douglas 1987).

Lateral and dorsoventral or ventrodorsal radiographs of the normal rabbit skull have been published (Shively 1979, Gibbs and Hinton 1981, Wolvekamp and Oschwald 1991, Harcourt-Brown 2003); (Gibbs & Hinton 1981). Despite the petrous temporal bone of the rabbit being relatively large and very dense (Gibbs and Hinton 1981), the bony structures of the middle ear remain well visualised (Wolvekamp and Oschwald 1991). The TB are well developed, hollow and thin walled, although the walls are relatively thicker than those

of the cat and dog (Beed 1997). The bony collar surrounding the external auditory meatus is visible lateral to each TB (Shively 1979). On dorsoventral or ventrodorsal views, the zygomatic arch extends caudally beyond its junction with the temporal bone (Shively 1979). In lateral and dorsoventral views superimposition of the teeth and mandibles can be a problem, making interpretation difficult (Harcourt-Brown 1995).

3.1.3. Radiography of the TMJ and associated structures

Transcranial radiography for evaluating the human TMJ has a long and much studied history although its popularity has derived partially from its cost effectiveness (Dixon 1991). The procedure for plain and arthrographic views of the TMJ have been described (Dixon 1991). However they are technically difficult to obtain due to the relevant anatomy and its relationship with the dense osseous structures in the surrounding cranial base (Suarez and others 1980, Dixon 1991) so the images are often distorted (Suarez and others 1980). Only a limited area of the joint can be examined (Dixon 1991) subtle abnormalities are not well visualised (Suarez and others 1980) and there may be an absence of detectable changes in the acute phase of disease (Payne and Nakielny 1996) so the value of plain radiographs in the evaluation of TMJ disorders has been questioned (Payne and Nakielny 1996).

A minimum of one dorsoventral and two lateral oblique views have been recommended in order to investigate the canine and feline TMJ and that both the affected and contralateral joint should be examined for comparison and to confirm the presence of unilateral abnormalities (Ticer and Spencer 1978, Lane 1982, Douglas 1987). The VD has been reported as not allowing evaluation of the TMJs (Gibbs 1977). True lateral views superimpose the TMJs and so are of limited value (Schwarz and others 2002).

The dorsoventral is often the most informative view (Schwarz and others 2002) providing information about the position of the various aspects of the joint and the mandibles relative to each other (Douglas 1987) and permitting comparison of the two joints (Sullivan 1989). However, the TMJ is superimposed onto the bones of the skull. The important area in this view is the thin, smoothly margined, curved, relatively radiolucent band between the caudal edge of the condyloid process and the rostral margin of the mandibular fossa that represents the joint space (Schwarz and others 2002). The medial portion of the joint space appears narrower than the lateral portion and is often more difficult to recognise due to superimposition from the retroarticular process and petrous temporal bone (Schwarz and

others 2002). The angular process is a bony protrusion on the caudoventral aspect of each mandible and was superimposed over the centre of the TMJ while the coronoid process was visible rostral to the TMJ and medial to the zygomatic arch (Schwarz and others 2002). In the cat, the TMJ space appears as a thin, sharply marginated, radiolucent band of uniform width. The angular processes are smaller than in the dog so often do not extend as far caudally as the joint space and the coronoid processes are projected more obliquely due to the greater angle between the mandibles (Schwarz and others 2002).

A variety of oblique views may be obtained with rotation of the skull about the long axis, in a lateral direction or in a combination of different planes depending on the region of the joint under investigation (Ticer and Spencer 1978, Douglas 1987, Morgan and Silverman 1987, Meomartino and others 1999, Schwarz and others 2002). However, the long axis of the TMJ is neither exactly along the axial nor dorsal plane of the skull. The differences in skull shape mean that no single projection will consistently result in perfect positioning in the dog, explaining the difficulty in repeatedly achieving satisfactory oblique views of the TMJ (Lane 1982, Sullivan 1989, Vollmerhaus and others 1996, Schwarz and others 2002).

A 45° rotation of the head along its median axis, resulting in a 45° dorsoventral oblique projection, can be achieved in sedated animals using a trough and enables visualisation of the both TMJs on the same view. However, both are superimposed onto skull structures and are projected at different angles of obliquity, and therefore are not directly comparable (Douglas 1987, Schwarz and others 2002). The same view in the open mouth position has been advocated for the assessment of TMJ dislocation (Gibbs 1977). Other rotational angles in this direction include 'slightly tilted', 20° and 25° (Douglas 1987, Ticer and Spencer 1978).

'Nose-up' or 'tilted-up' views are reported to be the most useful of the oblique views (Schwarz and others 2002) and are achieved by placing a foam pad beneath the nose resulting in a rostro-caudal oblique with different angles from 15-35° being recommended for different skull types (Morgan and Silverman 1987). The TMJ nearest the cassette will be projected ventral to the opaque base of the skull (Morgan and Silverman 1987, Schwarz and others 2002). Other authors advocate an additional 10° rotation along the median axis of the head to project the lower TMJ free of the skull ventrally or alternatively, projecting the upper TMJ free from superimposition by placing the lower maxilla and mandible flat on a cassette in an open mouth position (Morgan and Silverman 1987). The appearance of

the TMJ space varies slightly with the breed but should appear as a sharply demarcated, curved, radiolucent band of constant width between the convex condyloid process and the concave mandibular fossa (Schwarz and others 2002). Incomplete ossification in young dogs (less than 6 months) causes the joint space to appear wider, slightly less curved and with less well defined margins and is a normal finding that should not be confused with TMJ dysplasia (Schwarz and others 2002).

The most commonly advocated oblique view of the feline TMJ is a Le20°V-RtDO projection, where the head is rotated along its median-axis and the lower right TMJ is projected clear of the skull ventrally (Rt20°V-LeDO for a lower left TMJ) (Ticer and Spencer 1978). To image the TMJ from a more ‘end-on’ orientation, an additional 7-10° lateral “nose-up” rotation has been suggested, resulting in a complex Rt10°R20°V-LCdDO projection for a lower left TMJ (Meomartino and others 1999).

Lateral and dorsoventral views are reported to be the most useful for imaging the region of the TMJ in the rabbit (Wolvekamp and Oschwald 1991, Harcourt-Brown 1995, Harcourt-Brown 2003). However, a potential problem of placing the rabbit in sternal recumbency is that the mandible may move to one side so it is no longer aligned with the maxilla and this must be taken into account when positioning the animal (Harcourt-Brown 2003). Slightly oblique lateral, open mouth, rostrocaudal extra-oral and intraoral views can also be beneficial to ensure a complete examination of the oral structures (Crossley 1995, Harcourt-Brown 1995, Harcourt-Brown 2003). However, interpretation of these additional views is only possible with the appropriate anatomical and physiological knowledge (Crossley 1995).

3.1.4. Aims

The appearance of the canine TMJ and TB on radiographs varies considerably depending on the beam angle and it is often unclear which regions of these structures are actually being interrogated. In addition, there are no reports detailing the radiographic examination or appearance of the rabbit TMJ or TB.

The aims of the work presented in this chapter were therefore to:

- Investigate the effect of altering the angle of the skull relative to the central beam on the radiographic appearance of the TMJ and TB in the dog, cat and rabbit.
- Demonstrate the anatomical features depicted in each view.

- Identify any views likely to be of benefit in live animals for the investigation of disease processes affecting the TMJ or TB.

3.2 Material and Methods

3.2.1 Cadaver material

A pair of German Shepherd canine, domestic breed feline and New Zealand White breed rabbit cadavers that were of similar age, weight, cranial conformation and facial index were selected. They were checked to ensure there was no external evidence of ear, respiratory or dental disease and no abnormalities associated with the external ear, mouth or temporomandibular region. The heads were removed at the mid-cervical region and one of each was placed into cold storage at -20°C while the other was emascerated, as described in Chapter 2.

The mandibles from the emascerated skulls were then glued at the rostral symphysis. In the dog and cat, they were re-articulated with the skull in a closed position using an elastic band. In the rabbit, re-articulation was more difficult due to the incongruity between the articular surfaces of the condyloid process and mandibular fossa. However, it could be achieved by careful positioning of the mandible and then wrapping the entire skull in cellophane film. In all three species, the mandible could also be held in the open position by inserting a plug of cotton wool or a syringe case between the incisor teeth prior to placement of the elastic band or cellophane film.

An additional two canine skulls were selected from the anatomical collection held by the University of Glasgow anatomy unit. These were a Boxer and a Rough Collie, which represented a brachycephalic (facial index 190) and dolichocephalic (facial index 89) skull type respectively. The mandibles were again re-articulated with the corresponding skull using an elastic band. Further information regarding the skulls used in this study is presented in Chapter 2.

3.2.2 Radiographic equipment

The X-ray machines used were a Heliophos (Siemens), a V.R 30/90T (S.M.R) (Figure 3.2.1) and a Villa Sistemi Medicali Genius HF depending on availability. Eighteen x 24cm and 24 x 30cm Ultravision cassettes and screens with CEA film, or Quanta Detail cassettes and screens with AGFA Cronex 10T film, were used (Figure 3.2.2). A table-top technique without a grid was used throughout and the height of the machine adjusted to ensure a constant film focal distance of 1m. Films were developed using a DuPont Cronex CX-130 (Accessorio Radiogra Co, Bernareggio, Italy) automatic processor. Lateral and

dorsoventral views of the canine, feline and rabbit emascerated skulls and cadaver heads were made and used in conjunction with the exposure chart for the machines to determine the optimum settings. The exposure setting used for the emascerated canine skulls was 57kV and 3.2mAs and for the cadaver heads 66kV and 20mAs. The feline skulls required 47kV and 2mAs and the cadaver heads 53kV and 4mAs while the rabbit skulls were 47kV and 2mAs with the cadaver heads being 57kV and 3.2mAs.

A piece of equipment was designed and constructed to allow repeatable positioning of the skulls for radiographic examination (Figure 3.2.3). This consisted of a wheel that was fixed at its hub to a shaft of wood and mounted on a platform that was placed on the X-ray table. A clamp was attached to the periphery of the wheel to hold the skull in a position with the TB and TMJ level with the hub of the wheel. To achieve this, the rostral portion of the canine skull was either placed directly into the clamp (Figure 3.2.4) or into a second clamp that was held in the first, depending on the position required (Figure 3.2.7.). With the cat skull, it was necessary to place the rostral portion into an additional clamp for most of the views (Figure 3.2.5.). Surgical tape was also used to stabilise the skull in the clamp. For the rabbit skull and some views in the cat, the skull was placed into a radiolucent, plastic cup and packed in place with cotton wool (Figure 3.2.6.). A length of wood was attached to the cup and the end placed in the clamp with the length adjusted to ensure that again, the TB and TMJ were level with the hub of the wheel. Rotation of the wheel therefore resulted in rotation of the skull around the level of these structures. A protractor was attached to the shaft of wood and allowed the angle between the shaft of the clamp and the horizontal to be determined.

The same equipment was used to produce radiographs of the entire cadaver heads although the additional weight required some modifications. Sandbags were used as a counterbalance and a spirit level was placed on the shaft to ensure it remained horizontal (Figure 3.2.3.). When imaging the rabbit cadaver, the plastic cup was replaced by a 2 litre plastic bottle that was cut in half (Figure 3.2.9.). The head placed in the top half and the bottom half pushed up into the top half to keep the head in place. The neck of the bottle was placed in the clamp and a piece of bandage was threaded through holes in the bottle and tied to the hub of the wheel to ensure it did not rotate.

3.2.3. Radiographic views.

The beam was not repositioned so it effectively remained centred at the midpoint between the two TB and TMJ throughout each series.

3.2.3.1. Lateral rotational angles

Each skull was mounted in a true lateral position with the long axis of the head parallel with the wheel, the hard palate in a vertical position and the upper and lower angular processes in alignment with each other (Figure 3.2.4. to 3.2.6.) The wheel was then rotated and a series of radiographs were made at known angles of upward rotation from 0 to 90° at 5° increments in the dog and 10° in the cat and rabbit to end with a true rostrocaudal view. This created a series of latero (10-80°) rostral-latero-caudal oblique views.

In the dog, downward rotation from 0 to 40° was also performed, producing a series of latero (10-40°) caudal-latero-rostral oblique views. These were possible because the depth of the base of the positioning device allowed room for the nose of the skull to be moved below horizontal towards the table top. Rotation beyond 40° was not performed though as this would have required the object–film distance to be increased to accommodate the length of the skull between the areas of interest and the cassette.

3.2.3.2. Long axis rotational angles

Each skull was then mounted in a true lateral position with the TB and TMJ level with the centre of the wheel, but this time with the long axis of the skull perpendicular to the wheel (Figure 3.2.7.). A lateral view of the skull was made and then a series of radiographs were made at known angles of rotation about the long axis of the skull from 0 to 90° at 10° increments, ending with a true ventrodorsal view. This created a series of latero (10-80°) ventral-laterodorsal oblique views. In the dog, rotation from 0 to 90° in the opposite direction was also performed, producing a series of latero (10-80°) dorsal-lateroventral oblique views and ending in a true dorsoventral view.

3.2.3.3. Ventral and dorsal rotational angles

Each skull was then mounted in a true rostrocaudal position (Figure 3.2.6.). Radiographs were made at known angles of ventral rotation from 0° to 90° at 10° increments, producing a series of rostro (10-80°) ventral-caudodorsal oblique views and ending in a true ventrodorsal view. These views were then repeated with the mandible in an open position. In the rabbit, rotation was also performed in a dorsal direction to produce a series of rostro (10-80°) dorsal-caudoventral oblique views and ending in a true dorsoventral view.

3.2.4. Additional procedures

Small, malleable lead markers were then taped to various anatomic features associated with the TB and TMJ and the views repeated. Anatomical atlases (Crouch 1969, Barone 1989, Popesko and others 1992, Evans 1993) in conjunction with the anatomical information and digital images obtained in Chapter 2, were used to aid in orientation of the images and identification of the structures visualized.

The lateral and long axis rotational views were repeated using the Boxer and Rough Collie skulls and selected views from all the series performed using the entire cadaver heads.

3.2.5. Image production

The resulting radiographs were photographed using a digital camera (Olympus Camedia C-21002 ultras zoom). Images were transferred digitally to a desk top personal computer. Paint Shop Pro 7 software (Microsoft) was used to manipulate and label the resulting images.



Figure 3.2.1. V.R 30/90T (S.M.R) X-Ray machine

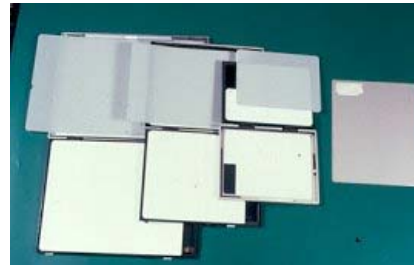


Figure 3.2.2. Examples of radiographic cassettes and film used

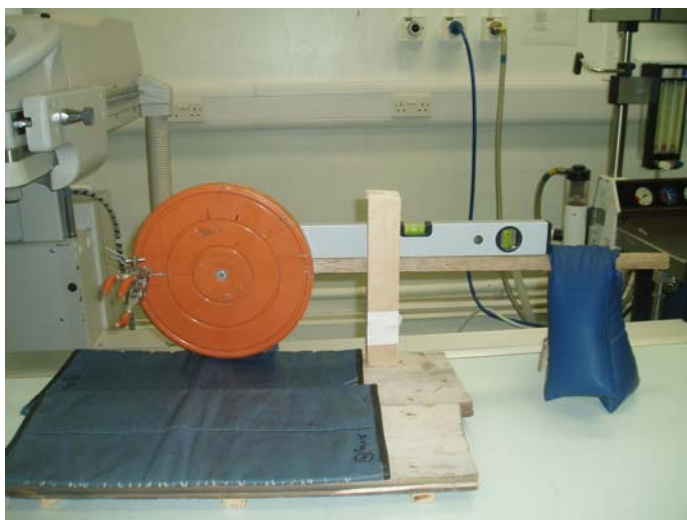


Figure 3.2.3. Equipment designed and constructed to allow repeatable positioning of skulls for radiographic examination



Figure 3.2.4. Canine skull mounted in the equipment using a single clamp and in a lateral position prior to the lateral rotational series.



Figure 3.2.5. Feline skull mounted in the equipment using an additional clamp and in a lateral position prior to the lateral rotational series.

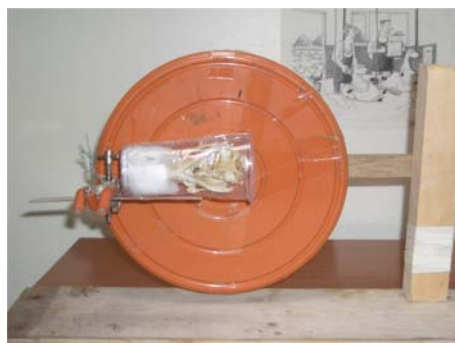


Figure 3.2.6. Rabbit skull mounted using a plastic cup and packed with cotton wool in a lateral position prior to the lateral rotational series.

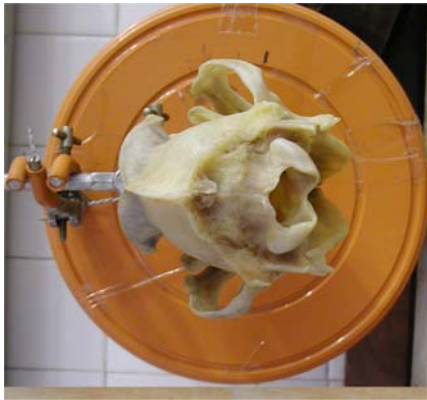


Figure 3.2.7. Canine skull mounted in the equipment in a lateral position prior to the long axis rotational series.



Figure 3.2.8. Canine skull mounted in the equipment in a rostrocaudal position prior to the dorsal and ventral rotational series.



Figure 3.2.9. Modification of the equipment to allow positioning of rabbit cadaver heads for radiography.

3.3 Results

3.3.1. Radiography

The radiographic views obtained using the apparatus described were repeatable to within 5°. The term 'lower' was used to describe structures nearest the cassette and 'upper' to describe those furthest from it. All of the canine images have been labelled but only representative feline and rabbit ones.

3.3.2. Lateral rotational angles in emascerated skulls

In the lateral view (0°), the two halves of the skull were superimposed in all three species as confirmed by the close proximity and similar orientation of a number of features including the zygomatic arches, the TB, the TMJ, the coronoid processes and the angular processes in the dog and cat (Figures 3.3.1.1., 3.3.4.1. and 3.3.5.1.). However, complete superimposition of these structures was not observed due to the effects of magnification on the upper half of the skull. The upper and lower TMJ and TB were projected directly onto each other, limiting the amount of information obtained about each. Upward lateral rotations through 0 to 90° (rostrocaudal view) caused the lower TB and TMJ to move rostrally and the upper ones to move caudally in all species. As the skull was progressively rotated, the angular processes were observed to move apart although they remained in the same axis and this provided a good indication of the degree of angulation.

Downward rotation of 0 to -40° was performed in the dog and resulted in the lower TB and TMJ moving caudally and the upper ones moving rostrally, therefore allowing better visualization of the upper structures. The views achieved using these downwards rotational angles were identical to the corresponding upward rotations but positioning was only possible due to design of the positioning device. Since they would be more difficult to reproduce in live animals than the upward rotations, these results were disregarded and these views not repeated in the other species.

3.3.2.1. Lateral rotational angles in the dog

The radiographs produced at lateral rotational angles in the mesaticephalic skull are presented in Figure 3.3.1. Neither the TB nor the TMJ could be visualised at a rotation of 80° and so this image has been omitted from the Figure.

3.3.2.1.1. Appearance of the TB in the mesaticephalic canine skull

The ventral areas of both TB lumen and walls were projected ventral to the basioccipital bone while the dorsal areas were superimposed onto the dense bones at the base of the skull throughout this series. Lateral rotation of more than 20° was required to project the lower and upper TB free from each other. Beyond this, the lower TB lumen remained visible while the upper one became superimposed onto the occipital condyles and therefore was poorly visualized. At 50°, the lower TB became superimposed onto the molar teeth and could no longer be discerned. At 60°, the upper TB briefly emerged and became visible ventral to the ipsilateral zygomatic arch but then also became obscured by the molar teeth so neither were visible in the rostrocaudal view at 90°

3.3.2.1.2. Appearance of the TMJ in the mesaticephalic canine skull

Lateral rotation of 10° was required to project the lower joint independently of the upper one and the joint space became clearly visualized as a lucent curve with the caudal margin produced by the centre of the articular surface of the retroarticular process and the rostral margin by the ventral articular surface of the condyloid process. The joint space tapered slightly dorsally to where its dorsal region was overlain by the base of the skull. At 15°, the joint space remained clearly visible and the condyloid process changed in outline from a rounded to a more oval shape due to the lateral aspect of the dorsal articular surface becoming increasingly projected beyond its medial aspect. This elongation of the condyloid process became more pronounced as the angle of rotation increased. The medial half of the mandibular fossa was visible on the ventral margin of the caudal portion of the zygomatic process and dorsal to the radio-opaque line of the dorsal medial articular surface of the condyloid process.

Although the joint space remained visible at 20°, a small amount of superimposition of the condyloid process and retroarticular process was noted, with the lateral aspect of the articular surface of the retroarticular process profiled as a curved line running over the caudoventral border of the condyle. The entire length of the mandibular fossa was skylined immediately ventral to the base of the skull. The medial aspect was located dorsal to the caudal aspect of the condyloid process and the obliquely skylined lateral half was observed dorsal to the rostral aspect of the condyle and immediately caudal to the curved line representing the rostral border of the caudal portion of the zygomatic process.

At 25°, the condyloid process was located immediately caudal to the vertical radio-opaque line produced by the rostral portion of the upper coronoid process while the caudal portion

of the coronoid process was overlying the TB. Despite increased superimposition, the condyloid process was still visible through the reduced thickness of the obliquely projected body of the retroarticular process. The joint space was obscured with the exception of a short section in the centre which corresponded with the division between the medial and lateral portions of the dorsal articular surface of the condyloid process and the medial half of the mandibular fossa skylined dorsal to it. Rotation through 30° and 35° moved the condyloid process across the rostral portion of the upper coronoid process and caused further superimposition onto the retroarticular process. Beyond 35°, the lower TMJ became superimposed onto the molars and was therefore no longer visible.

Neither TMJ could be visualized due to superimposition onto the skull until 60°, when the lateral aspect of the upper joint became visible projected beyond the temporal bone. The amount of the joint visualized increased until 75° when the entire condyloid process lateral to the coronoid process was visible. Superimposition of the rostral portion of the zygomatic arch then reduced the amount visible until 90° (rostrocaudal view) when only the lateral regions were projected beyond the skull. The lateral aspect of the dorsal articular surface of the condyloid process was skylined ventral to the corresponding rostral margin of the mandibular fossa. The caudal margin of the mandibular fossa could be seen as an oblique line running across the condyloid process in a medioventral direction. The other features of the joint were superimposed and not visible.

3.3.2.1.3. Appearance of the TB and TMJ in the dolichocephalic canine skull

The TB in the dolichocephalic skull (Rough Collie) appeared similar to those in the mesaticephalic skull. The joint space of the lower TMJ was best visualized between 10 and 15° (Figure 3.3.2.). Beyond 20°, a marked depression was visible in the dorsal articular surface representing the transition from medial to lateral aspects. The condyloid process did not become superimposed onto the coronoid process until 35° and was still not superimposed onto the molars at 40°. The lateral aspect of the upper TMJ did not become visible until 75° and the entire condyloid process lateral to the coronoid process was visible at 80° before reducing in size again. However, at 90° a larger proportion of the lateral aspect of the condyloid process remained visible than in the mesaticephalic skull. Otherwise, the areas of the TMJ visualized in each view were similar.

3.3.2.1.4. Appearance of the TB and TMJ in the brachycephalic canine skull

The caudal portion of the brachycephalic skull (Boxer) was noticeably shorter than in the other skull types and this could be appreciated in the lateral view (Figure 3.3.3.). The TB in the brachycephalic skull did not project as far ventral to the basioccipital bone as in the other skull types and the TB walls appeared thicker therefore the gas filled lumen was not as clearly visible. It remained superimposed onto the petrous temporal bone and upper TMJ at all angles of rotation in this series and therefore was poorly visualised.

The lower TMJ was not well visualized free from the base of skull until 20° and the joint space did not become visible until 25 and 30°. The condyloid process also had a marked depression on dorsal surface. This skull had retroarticular processes which were shorter, narrower and less concave than those of the mesaticephalic or dolichocephalic skulls resulting in superimposition of condyloid process and retroarticular process not starting until 35°. The lower TMJ overlay the upper coronoid process from 25 to 35° and was superimposed onto the molars at 40°.

The lateral extremity of the upper TMJ was first visible at 60° but was visualized free from superimposition of the zygomatic arch between 65° and 75° after which the amount visible reduced in size till both joints were completely obscured at 90°. Otherwise the areas of the TMJ visualized in each view were similar to those of the mesaticephalic skull.

3.3.2.2. Lateral rotational angles in the cat

The radiographs produced at lateral rotational angles in the feline skull are presented in Figure 3.3.4.

3.3.2.2.1. Appearance of the TB in the feline skull

The dorsal half of the external acoustic meatus, the promontory and epitympanic recess were superimposed onto the basisphenoid, basioccipital and petrous temporal bones but the rest of the TB components were projected ventral to them. Lateral rotation of more than 30° was required to project the lower and upper TB completely free from each other. Beyond this, the upper TB became progressively superimposed onto the occipital condyles while beyond 50°, the lower one overlay the molar teeth, although the ventral components of each were discernible through the skull throughout the series.

3.3.2.2.2. Appearance of the TMJ in the feline skull

In the lateral view, only the ventral part of the condyloid process and the retroarticular process were visible, projected ventral to the base of the skull and the ventral part of the joint space appeared as a lucent curve. Rotation of 10° caused the medial half of the lower condyloid process to move over the obliquely projected retroarticular process although it remained visible through it. The joint space was obscured with the exception of a short section in the centre which corresponded with the division between the medial and lateral portions of the dorsal articular surface of the condyloid process and the medial half of the mandibular fossa skyline dorsal to it. Rotation of 20° caused more of the medial half of the lower condyloid process to become superimposed over the retroarticular process. However, a larger portion of the joint space became visible representing the lateral and part of the medial halves of the dorsal surface of the condyloid process and the corresponding areas of the mandibular fossa. At 30° the lower TMJ moved over the molar teeth and was therefore obscured throughout the rest of the series.

Rotation of 10° moved the upper TMJ over the base of the skull and the petrous temporal bone so it was no longer visible until the lateral components were projected free from the skull beyond 60° .

3.3.2.3. Lateral rotational angles in the rabbit

The radiographs produced at lateral rotational angles in the rabbit skull are presented in Figure 3.3.5.

3.3.2.3.1. Appearance of the TB in the rabbit skull

In the lateral view, a series of circular lucencies resulting from the dorsal extension of the epitympanic recess medial to the external acoustic meatus were visible. A second circular lucency level with the external margin of the external acoustic meatus resulted from the overlying cerebellar fossa of the petrous temporal bone.

At 10° rotation, the lower TB was still partially superimposed over the upper one but was visible, while the upper one was superimposed over the base of the skull and therefore poorly visualised. At 20° the lower TB was projected free from superimposition and ventral to the base of the skull. It remained so until 50° at which point it overlay the upper molar arcade. Between 60 and 70° the most ventral areas of it became visible between the dental arcades but beyond this it was completely superimposed over the ipsilateral dental arcade. The upper TB was not well visualised at any of these angles of rotation, being

superimposed onto the cranium and then the occipital condyle, although its most ventral areas were visible at 70° before its superimposition onto the upper molar arcade. At 90° rotation (true rostrocaudal), both TB were completely obscured by the ipsilateral molar arcades.

3.3.2.3.2. Appearance of the TMJ in the rabbit skull

The TMJ was located dorsal to the level of the base of the skull and the molar arcade so remained free from superimposition onto these dense structures throughout all these angles of rotation. From 10 to 30°, it overlay the less dense bone of the cranium, from 40 to 50° the orbit and from 60 to 70° the maxilla after which it was projected lateral to the skull, free from superimposition. Although the dorsal border of the mandibular condyle was visible in the lateral view, the rostral section of the articular surface was obscured by the overlying zygomatic process of the temporal bone. This articular surface first became free from superimposition at 40 to 50° of rotation while 80 and 90° (true rostrocaudal) allowed the joint space itself to be skylined. The upper TMJ remained superimposed over the cranium until it too was projected lateral to the skull and therefore free from superimposition at 80 and 90°.

<u>Label</u>	<u>Description</u>
Solid line	outer margins of TB
Diamond line	bone ridge at junction between TB and petrous temporal bone - dog bone septum – cat internal margin of external acoustic meatus - rabbit
Dashed line	external acoustic meatus
Dotted line	promontory
Hairy line	route of bone prominences - rabbit
*	epitympanic recess
D	dorsal region of TB lumen - dog / ventral compartment - cat
V	ventral region of TB lumen - dog / ventral compartment - cat
L	lateral region of TB lumen - dog / ventral compartment - cat
M	medial region of TB lumen - dog / ventral compartment - cat
R	rostral region of TB lumen ventral to bone ridge dog / septum cat
R2	rostral region of TB lumen dorsal to bone ridge - dog rostral region of dorsal compartment - cat
C	caudal region of TB lumen - dog / ventral compartment - cat
C2	caudal region of dorsal compartment - cat
@	communication between dorsal and ventral compartments - cat
1	mastoid process
2	paracondylar / jugular process
3	retroarticular process
4	neck of the condyloid process of the mandible
5	angular process of the mandible
6	coronoid process of the mandible
7	molar tooth root
8	tubercle at lateral aspect of mandibular fossa
9	retroarticular foramen
10	tympano-occipital fissure
11	ramus of mandible
12	muscular tubercle (at tympano-occipital suture – dog)
13	spheno-occipital fissure –rabbit
14	temporal process of the zygomatic bone
15	caudal extension of the temporal process of the zygomatic bone-rabbit
16	temporo-zygomatic suture
17	zygomatic process of the temporal bone
18	temporal fossa
19	carotid canal / external carotid foramen – rabbit
20	retrotympanic process (rabbit)
21	occipital condyle
a	stylomastoid foramen
b	foramen lacerum
c	musculotubal canal
d	carotid canal / caudal carotid foramen
e	trigeminal nerve canal
f	internal acoustic meatus
g	cerebellar fossa

Table 3.3.1. Key for anatomical features demonstrated in Figures 3.3.1 to 3.3.14 depicting the radiographic appearance of the TB and associated structures in the dog, cat and rabbit.

Figure 3.3.1. Radiographs of the tympanic bulla (TB) and temporomandibular joint (TMJ) of a mesaticephalic dog skull taken at lateral rotational angles from 0 (lateral) to 70 and 90 degrees (rostrocaudal). For key see Table 3.3.1 and Figure 2.3.5.

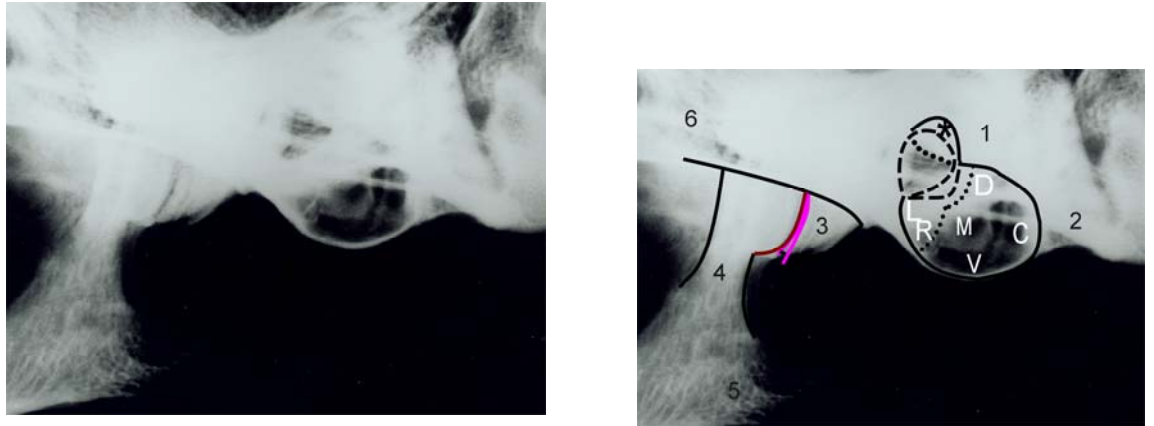


Figure 3.3.1.1. Mesaticephalic dog. Rotational angle = 0 degrees (true lateral)

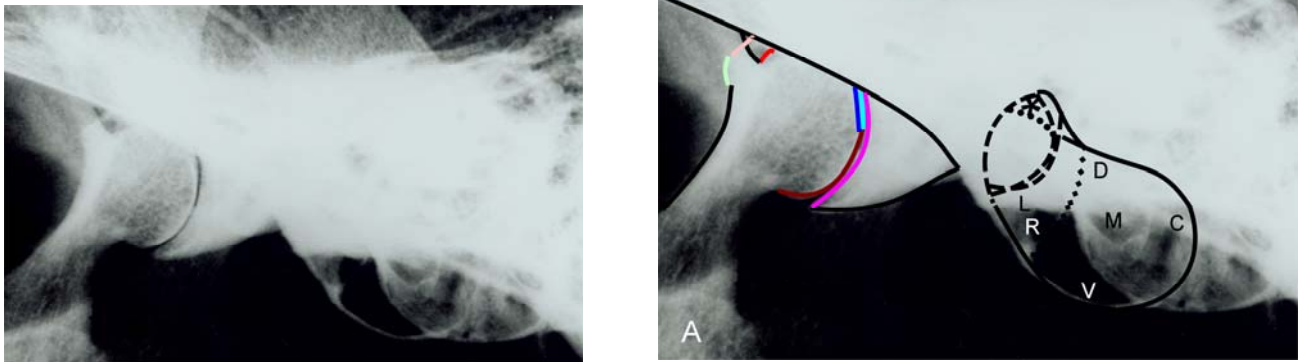


Figure 3.3.1.2. Mesaticephalic dog.
 Rotational angle = 10 degrees.
 A- Lower TMJ and TB. B- upper TB.

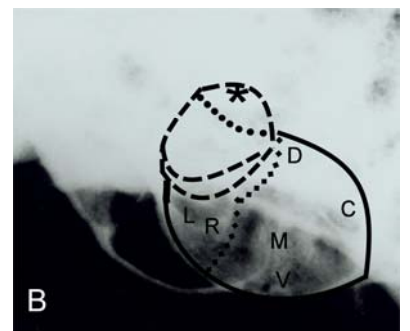


Figure 3.3.1. continued. Lateral rotations in a mesaticephalic dog skull.

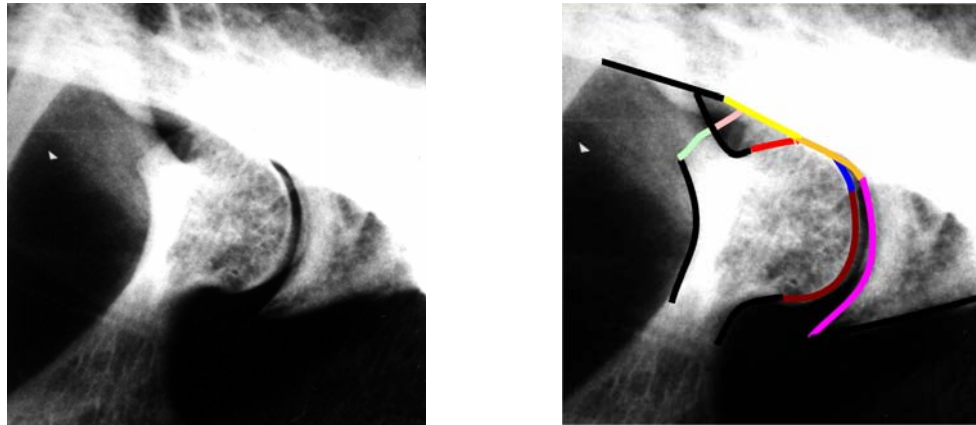


Figure 3.3.1.3. Mesaticephalic dog. Rotational angle = 15 degrees demonstrating lower TMJ.

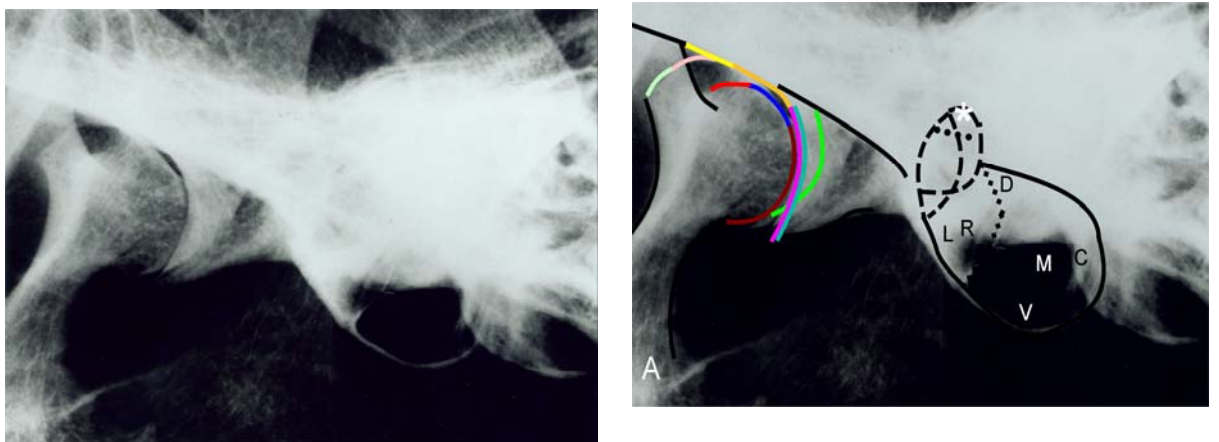


Figure 3.3.1.4. Mesaticephalic dog.
Rotational angle = 20 degrees.
A- lower TMJ and TB. B- upper TB.

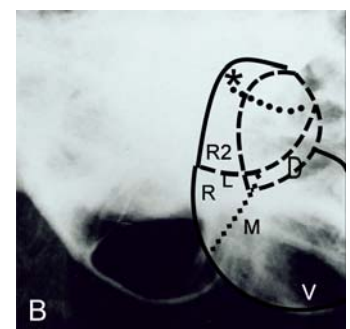


Figure 3.3.1. continued. Lateral rotations in a mesaticephalic dog skull

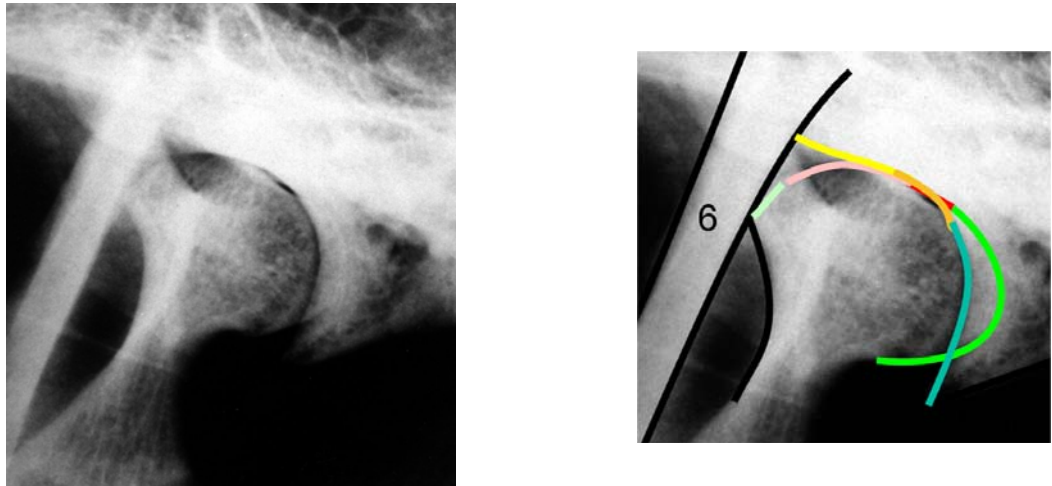


Figure 3.3.1.5. Mesaticephalic dog. Rotational angle = 25 degrees demonstrating the lower TMJ.

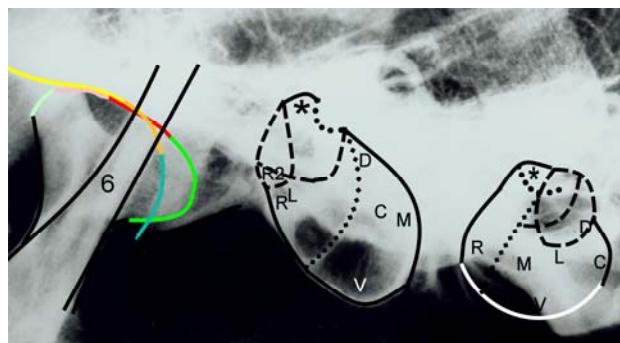


Figure 3.3.1.6. Dog. Rotational angle = 30 degrees demonstrating the lower TMJ, lower TB (middle of image) and the upper TB (right of image).

Figure 3.3.1. continued. Lateral rotations in a mesaticephalic dog skull

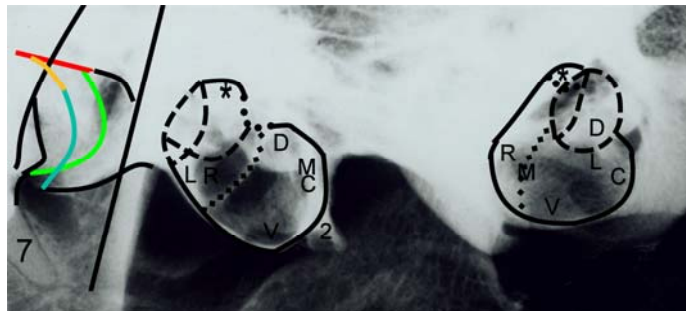
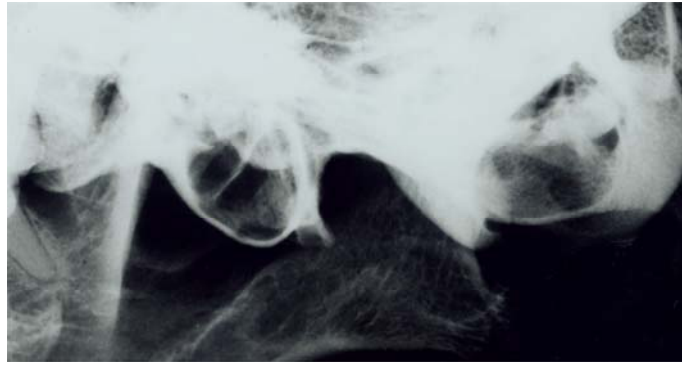


Figure 3.3.1.7. Mesaticephalic dog. Rotational angle = 40 degrees demonstrating the lower TMJ, lower TB (middle of image) and the upper TB (right of image).

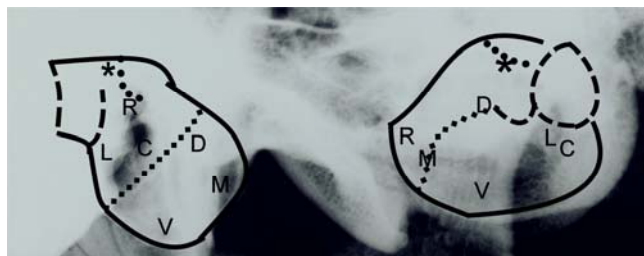


Figure 3.3.1.8 Mesaticephalic dog. Rotational angle = 50 degrees demonstrating the lower TB (left of image) and the upper TB (right of image).

Figure 3.3.1. continued. Lateral rotations in a mesaticephalic dog skull

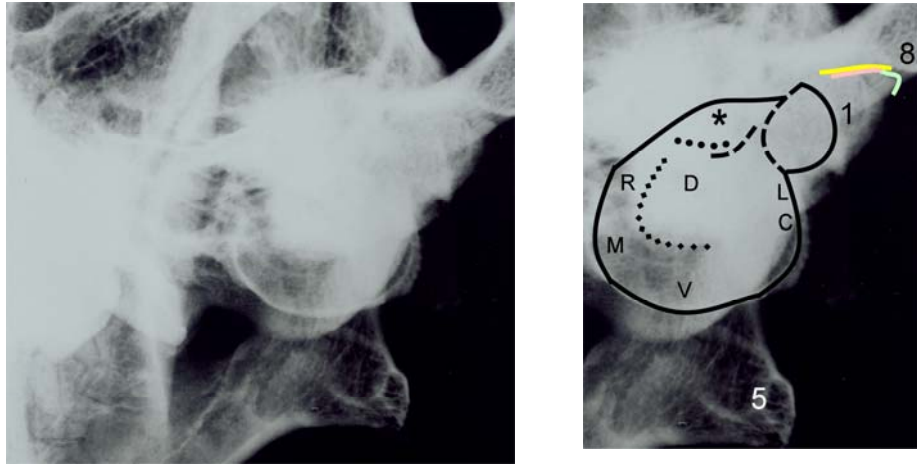


Figure 3.3.1.9. Mesaticephalic dog. Rotational angle = 60 degrees demonstrating the upper TB and TMJ.

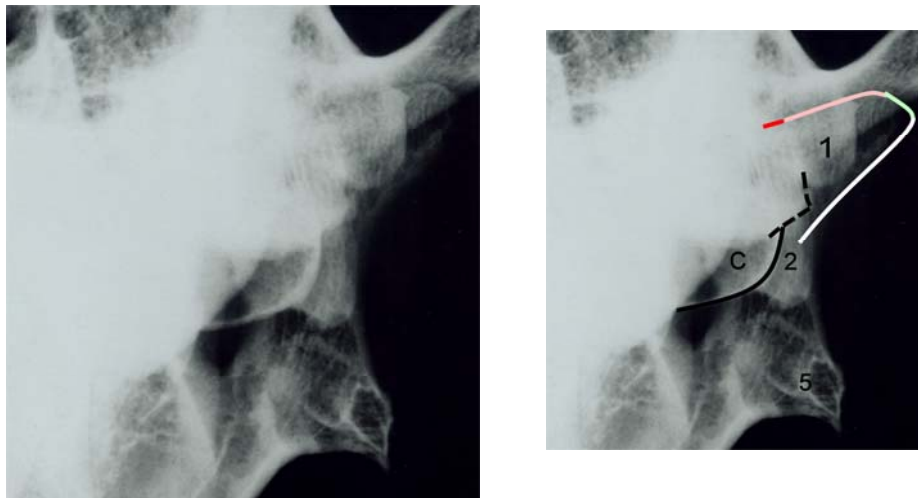


Figure 3.3.1.10. Mesaticephalic dog. Rotational angle = 70 degrees demonstrating the upper TB and TMJ.

Figure 3.3.1. continued. Lateral rotations in a mesaticephalic dog skull

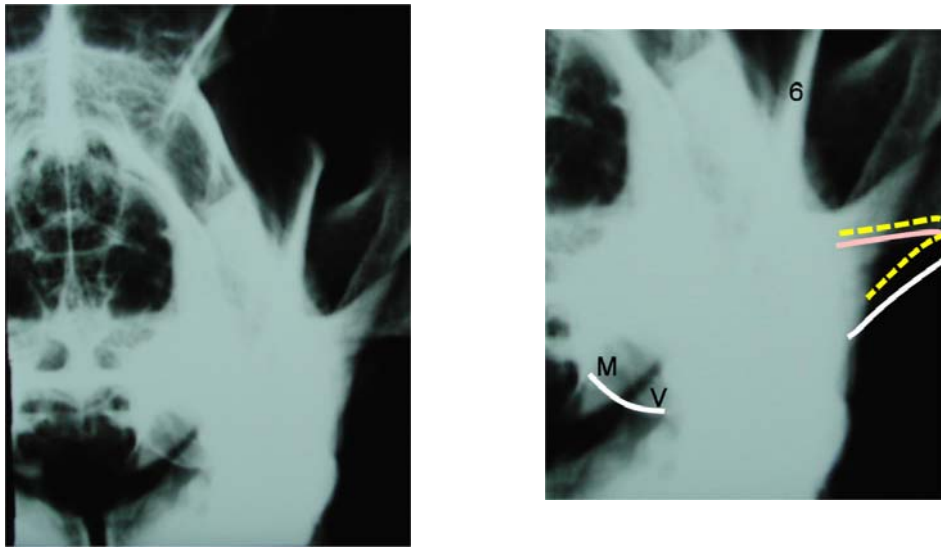


Figure 3.3.1.11. Mesaticephalic dog. Rotational angle = 90 degrees (true rostrocaudal) demonstrating the upper TMJ.



Figure 3.3.2.
Dolichocephalic dog skull.
Rotational angle = 15 degrees



Figure 3.3.3.
Brachycephalic dog skull.
Rotational angle = 30 degrees

Figure 3.3.4. Radiographs of the tympanic bulla (TB) and temporomandibular joint (TMJ) of a cat skull taken at lateral rotational angles from 0 (lateral) to 90 degrees (rostrocaudal). For key see Table 3.3.1 and Figure 2.3.7.

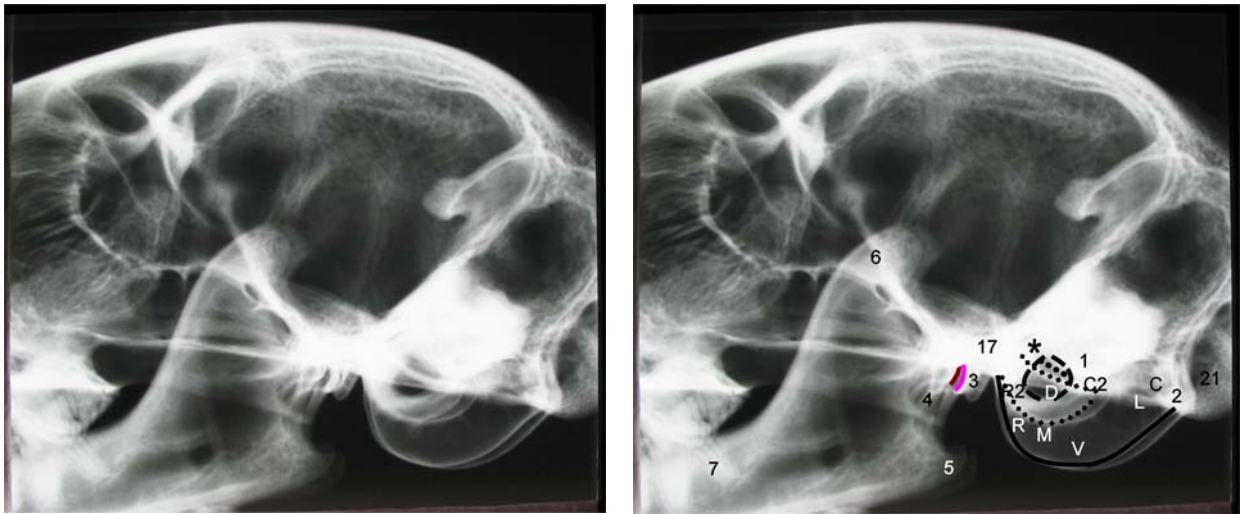


Figure 3.3.4.1. Cat. Rotational angle = 0 degrees (true lateral).



Figure 3.3.4.2. Cat. Rotational angle = 10 degrees.

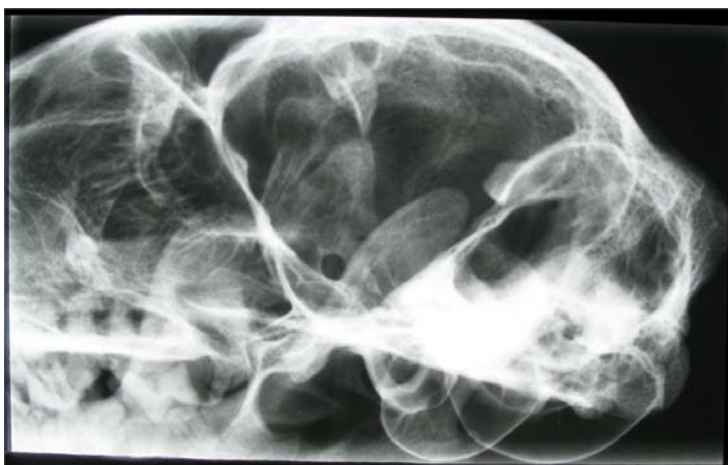


Figure 3.3.4.3. Cat. Rotational angle = 20 degrees.

Figure 3.3.4. continued. Lateral rotations in a cat skull.

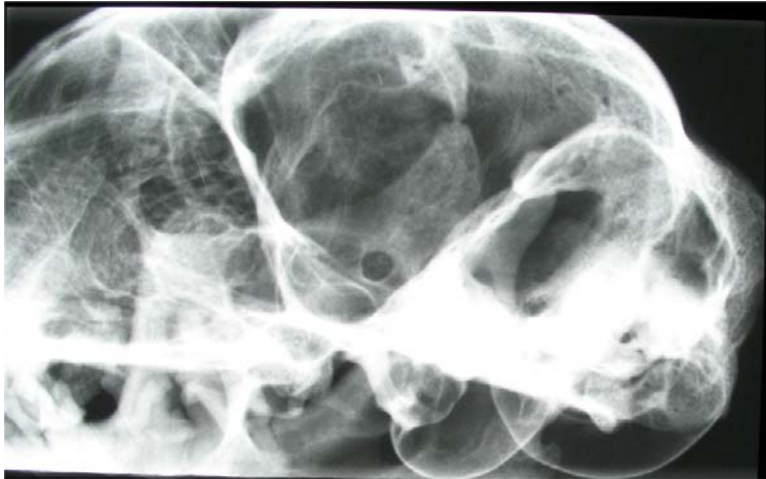


Figure 3.3.4.4. Cat.
Rotational angle = 30
degrees

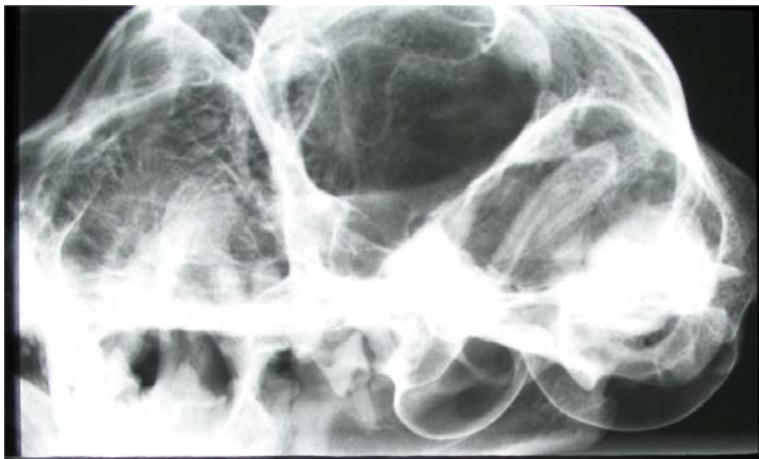


Figure 3.3.4.5. Cat.
Rotational angle = 40
degrees.



Figure 3.3.4.6. Cat.
Rotational angle = 50
degrees.

Figure 3.3.4. continued. Lateral rotations in a cat skull.



Figure 3.3.4.7. Cat.
Rotational angle = 60
degrees.



Figure 3.3.4.8. Cat.
Rotational angle = 70
degrees.



Figure 3.3.4.9. Cat.
Rotational angle = 80
degrees.

Figure 3.3.4. continued. Lateral rotations in a cat skull.

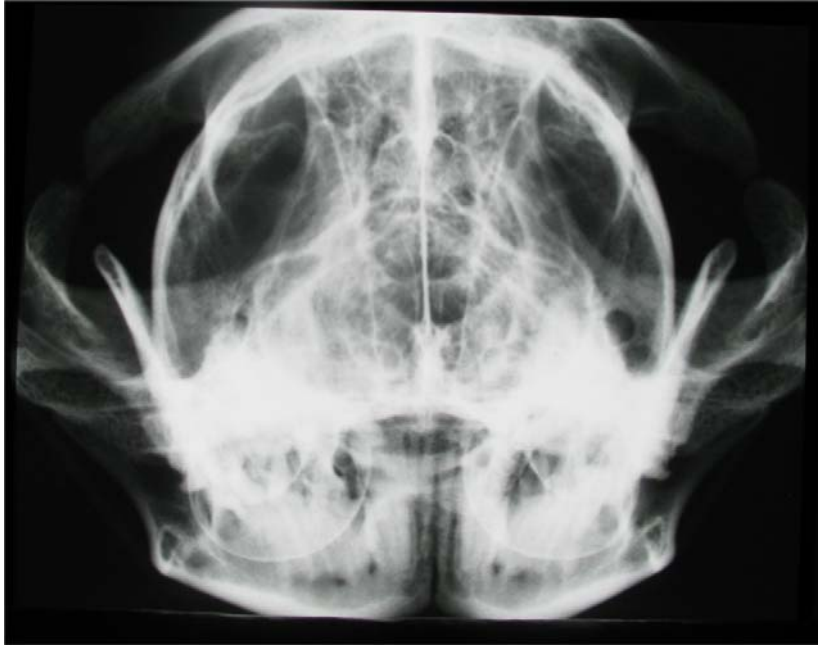


Figure 3.3.4.10. Cat.
Rotational angle = 90
degrees (true
rostrocaudal)

Figure 3.3.5. Radiographs of the tympanic bulla (TB) and temporomandibular joint (TMJ) of a rabbit skull taken at lateral rotational angles from 0 (lateral) – 90 degrees (rostrocaudal). For key see Table 3.3.1 and Figure 2.3.9.

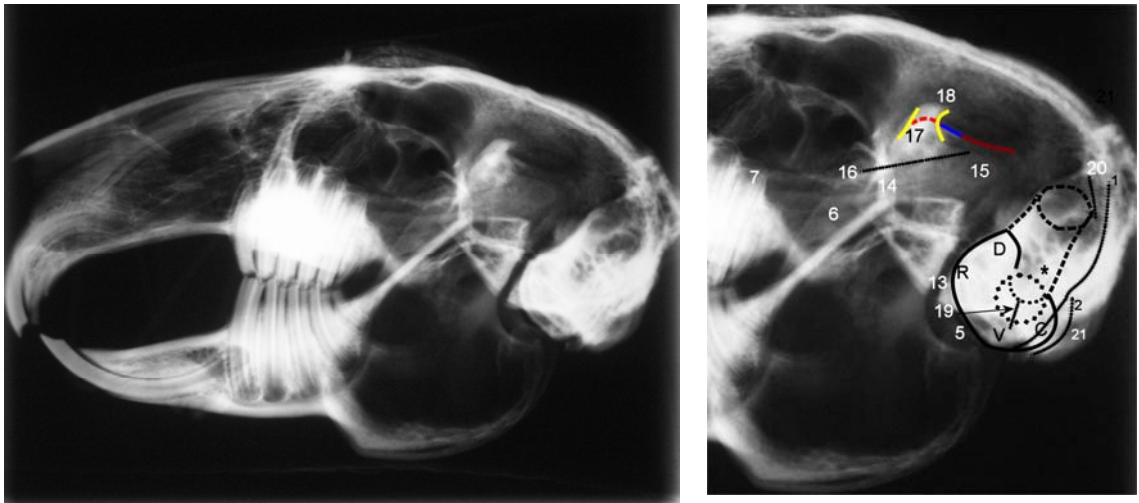


Figure 3.3.5.1. Rabbit skull. Rotational angle = 0 degrees (true lateral)



Figure 3.3.5.2. Rabbit skull.
Rotational angle = 10 degrees.



Figure 3.3.5.3. Rabbit skull.
Rotational angle = 20 degrees

Figure 3.3.5. continued. Lateral rotations in a rabbit skull.

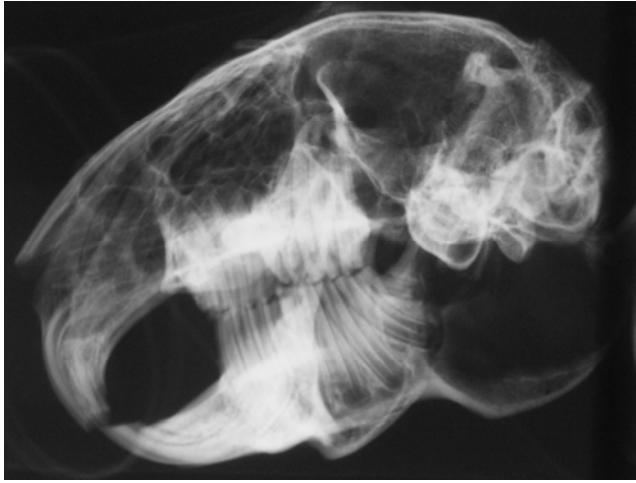


Figure 3.3.5.4. Rabbit skull.
Rotational angle = 30 degrees.



Figure 3.3.5.5. Rabbit skull.
Rotational angle = 40 degrees.

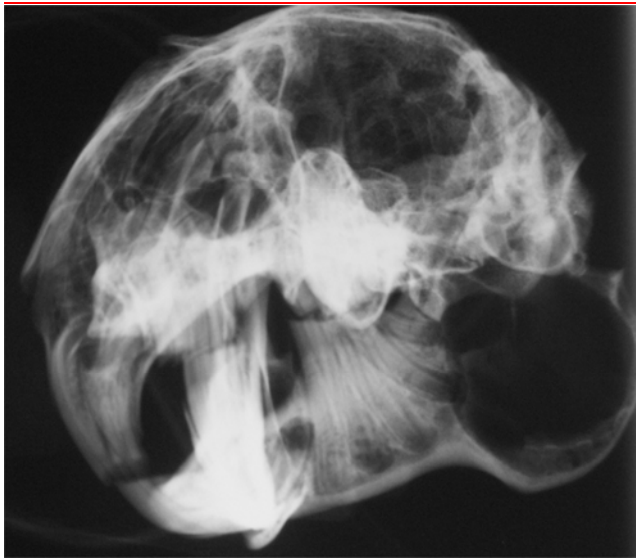


Figure 3.3.5.6. Rabbit skull.
Rotational angle = 50 degrees.

Figure 3.3.5. continued. Lateral rotations in a rabbit skull.

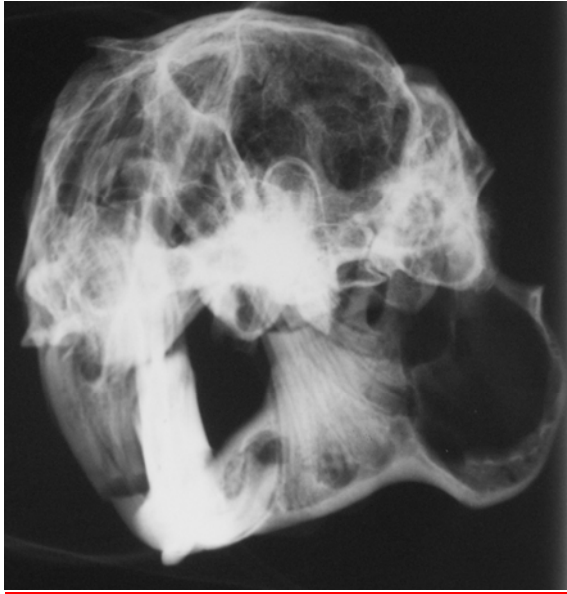


Figure 3.3.5.7. Rabbit skull.

Rotational angle = 60 degrees.

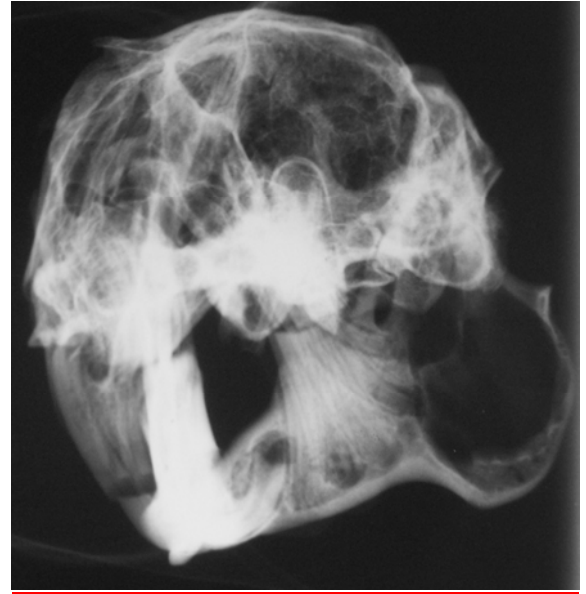


Figure 3.3.5.8. Rabbit skull.

Rotational angle = 70 degrees.

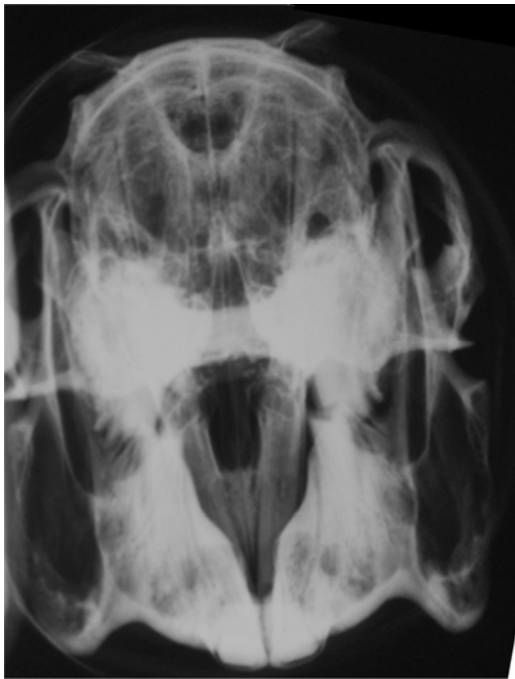


Figure 3.3.5.9. Rabbit skull.

Rotational angle = 80 degrees.

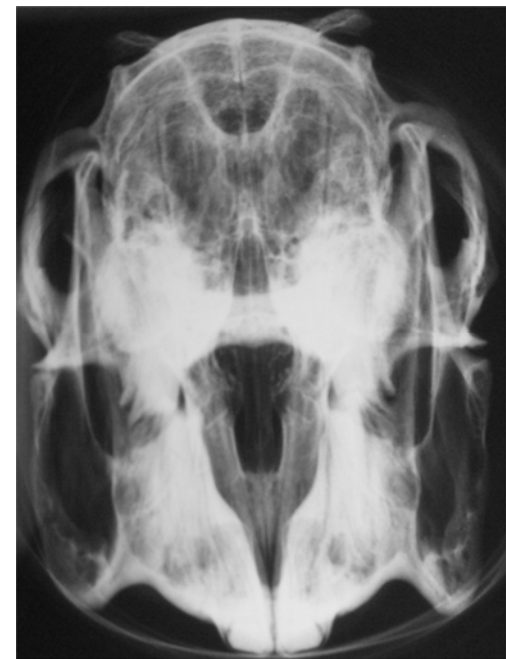


Figure 3.3.5.10. Rabbit skull.

Rotational angle = 90 degrees
(true rostrocaudal).

3.3.3. Long axis rotational angles in emascinated skulls

The lateral view (0°) in all species was the same as previously described. Rotating the skull through 90° from a lateral to a ventrodorsal position moved the lower TB and TMJ in a ventral direction. The upper ones moved dorsally to overlie the skull and so were less well visualised in all species.

Rotation in the opposite direction, to a dorsoventral position, was performed in the dog. This produced corresponding views of the upper joint, as it was moved ventrally while the lower moved dorsally to overlie the skull. Although the views achieved were identical, the increased object-film distance of the upper structures resulted in a loss of edge sharpness. These results have therefore been disregarded and these views were not repeated in the other species. There is a horizontal radio-opaque linear structure visible in the feline radiographs that is an artefact produced by part of the positioning equipment.

3.3.3.1. Long axis rotational angles in the dog

The radiographs produced at long axis rotational angles in the mesaticephalic skull are presented in Figure 3.3.6.

3.3.3.1.1. Appearance of the TB in the mesaticephalic canine skull

Rotation of 20° was required to move the TB apart but at this angle the entire lower TB was visible ventral to the basioccipital bone. The upper one was partially superimposed onto the basioccipital bone but the dorsal areas were visible through the calvarium. The lower TB became increasingly superimposed onto the temporal bones until 50° when no portion was projected free. From 30° to 50° , the upper TB was overlying the thinner bones of the calvarium and therefore was visible through them. From 60° onwards, both TB moved across the petrous temporal bone until 90° when a ventrodorsal view was produced in which the TB were bilaterally symmetrical and overlying the petrous temporal bone.

3.3.3.1.2. Appearance of the TMJ in the mesaticephalic canine skull

Rotation of at least 10° was required to move the TMJs apart and project the lower one free from the base of the skull. The lateral and medial aspects of the mandibular condyle of the lower TMJ were aligned producing a round appearance. At 20° the lower condyloid process began to change shape as the medial aspect was projected beyond the lateral and at 30° , a concavity became apparent in the caudal margin representing the division between

the medial and lateral caudal articular surfaces. The retroarticular process became superimposed onto the 'end-on' projection of the caudal portion of the zygomatic process. Its lateral margin and the caudal margin of the lateral aspect of the mandibular fossa became skylined in the region immediately caudal to the lateral aspect of the condyloid process.

There was a progressive increase in the length of the lower condyloid process as the medial aspect was projected further beyond the lateral half and by 40°, a further shape change was noted due to the medial edge of the articular surface becoming projected beyond the dorsal articular surface and replacing the rounded medial outline with a more angular one. Also, the lateral prominence was no longer superimposed onto the neck of the condyloid process and appeared as a curved protrusion at the rostral end of the rounded lateral margin. The entire retroarticular process and mandibular fossa were now superimposed onto the condyloid process and the caudal portion of the zygomatic process. An opaque, curved line became visible immediately caudal to the condyloid process representing the thick region of bone at the base of the retroarticular process.

Continued rotation produced progressive elongation of the lower condyloid process until between 60 and 75°, its entire length was projected overlying the caudal portion of the zygomatic process. The angular process was located laterally and overlay the lateral prominence of the condyloid process making the margin in this region less clearly defined. Beyond 75°, the medial aspect of the condyloid process became increasingly superimposed onto the calvarium until 90° when a ventrodorsal view of the skull was achieved.

The upper TMJ was superimposed onto the lower joint and the base of the skull until a rotational angle of 20°, when it was visualized through the calvarium of the emascerated skull. The upper condyloid process was elongated in shape and the entire caudal articular surface was visible with the medial edge of the articular surface producing the angled medial margin. The rostral part of the lateral margin was produced by the lateral prominence and the extreme lateral aspect of the dorsal articular surface was profiled immediately caudal to it.

The upper retroarticular process became clearly visible after 20° with the distal end of the process projected free from the condyloid process and the adjacent joint space was visible. The tip of the retroarticular process became increasingly superimposed across the

condyloid process until 35° where it was overlying the medial articular surface of the condyloid process with the its lateral margin highlighted. Further rotation resulted in the retroarticular process being no longer visible due to superimposition. However, the rest of the joint could be visualized through the calvarium until 70° when superimposition onto the lateral aspect of the calvarium reduced its visibility with the exception of the lateral margin which was projected beyond the margin of the skull. The lateral prominence became projected beyond the dorsal articular surface producing a rounded protrusion on the lateral margin although the edge of the dorsal articular margin was still visible medial to it.

The ventrodorsal view (90°) was bilaterally symmetrical as confirmed by the identical 'end-on' appearance of the coronoid processes. The entire length of both condyloid processes were visible in a transverse position overlying the caudal portions of the zygomatic processes and the medial margins were visible through the empty calvarium with the lateral walls of the bony case forming rostromedial - caudolaterally orientated radio-opaque lines across them. There was a mild curvature of the caudal margin of the condyloid process and the entire length of the caudal articular surface was visible with the exception of the medial extremity where the dorsal articular surface overlay it. The base of the body of the retroarticular process was visible as an opaque curved line immediately caudal to the condyloid process and the angular processes of the mandible were visible as opaque rectangles overlying the middle of the condyloid processes.

3.3.3.1.3. Appearance of the TB and TMJ in the dolichocephalic and brachycephalic canine skulls

The shortened caudal aspect of the brachycephalic skull was particularly evident in this series. The areas of the TB and TMJ visualised in the dolichocephalic and brachycephalic skulls using this rotational series were similar to these observed in the mesaticephalic skull (Figures 3.3.7 and 3.3.8). In the brachycephalic skull, the lower TB did not project as far beyond the basioccipital bone and this combined with the thicker TB wall resulted in less of the lumen being visible. The increased angulation of the caudal border of the upper condyloid process in the brachycephalic skull (described in Chapter 2) was visible from 30 to 90°.

3.3.3.2. Long axis rotational angles in the cat

The radiographs produced at long axis rotational angles in the feline skull are presented in Figure 3.3.9.

3.3.3.2.1. Appearance of the TB in the feline skull

Rotation of 30° was required to move the lower TB completely free from the upper one and at this angle, the entire lower TB was visible ventral to the basioccipital bone. The upper one was also partially superimposed onto the basioccipital bone but the dorsal areas were visible through the calvarium.

The lower TB became increasingly superimposed onto the temporal bones until 80° when no portion of it was projected free. From 40 to 60° the upper TB was overlying the thinner bones of the calvarium and therefore was visible through them. From 70° onwards, both TB moved across the petrous temporal bone until 90° when a ventrodorsal view was produced in which the TB were bilaterally symmetrical and overlying the petrous temporal bone.

3.3.3.2.2. Appearance of the TMJ in the feline skull

The appearance of the TMJ throughout this rotational series in the cat was very similar to that of the dog and therefore the same description applies.

3.3.3.3. Long axis rotational angles in the rabbit

The radiographs produced at long axis rotational angles in the rabbit skull are presented in Figure 3.3.10.

3.3.3.3.1. Appearance of the TB in the rabbit skull

The TB began to separate at 10° but were not completely free from superimposition onto each other until 30°. The upper TB overlay the cranium throughout the series but remained visible. From 30 to 60°, varying areas of the lower TB were projected ventral to base of the skull allowing it to be well visualised. The bone tube of the external acoustic meatus was particularly prominent in these views and was projected 'end-on', appearing as a radio-opaque circle with a lucent centre. From 70°, the lower TB once more became superimposed onto the cranium, but remained visible. Although the TB were superimposed onto the dense petrous temporal bone at the base of the skull in the ventrodorsal view, they

were both still clearly visible. The external acoustic meatus was also clearly visible as a prominent bone tube extending laterally from them.

3.3.3.3.2. Appearance of the TMJ in the rabbit skull

Rotation of 10° was required to move the TMJ apart but beyond this, the lower TMJ became increasingly superimposed onto the dense bone structures at the base of the skull so was poorly visualised. The upper TMJ was superimposed onto the cranium and viewed 'side-on' so the temporal process of the zygomatic bone interfered with visualisation until 60°, when it was projected free from this and also beyond the margin of the skull. The lateral aspect of the TMJ components were visible until 70°, and after this, the angular process of the mandible and then the 'end-on' projection of the vertical ramus of the mandible moved across and obscured it. After 70°, the lower TMJ also emerged from beyond the skull but its visualisation was also influenced by the vertical ramus of the mandible and the angular process.

Rotation of 90° to a ventrodorsal view resulted in both of the mandibular fossae being projected clear of the cranium but the vertical ramus of the mandible obscured the articular portion of the mandibular condyle, although its caudal extremity could be discerned. The angular processes were clearly visible overlying the lateral aspect of the mandibular fossae.

Figure 3.3.6. Radiographs of the tympanic bulla (TB) and temporomandibular joint (TMJ) of a mesaticephalic dog skull taken at long axis rotational angles from 10 to 90 degrees (ventrodorsal). For key see Table 3.3.1 and Figure 2.3.5.

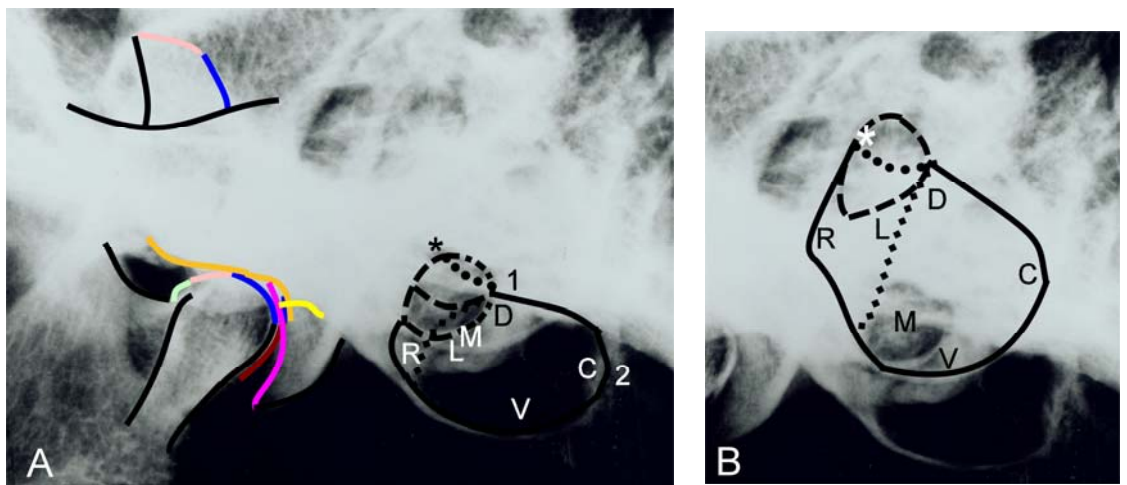


Figure 3.3.6.1. Mesaticephalic dog. Rotational angle = 10 degrees. A- Both TMJ and lower TB. B- upper TB.

Figure 3.3.6. continued. Long axis rotations in a mesaticephalic dog skull.

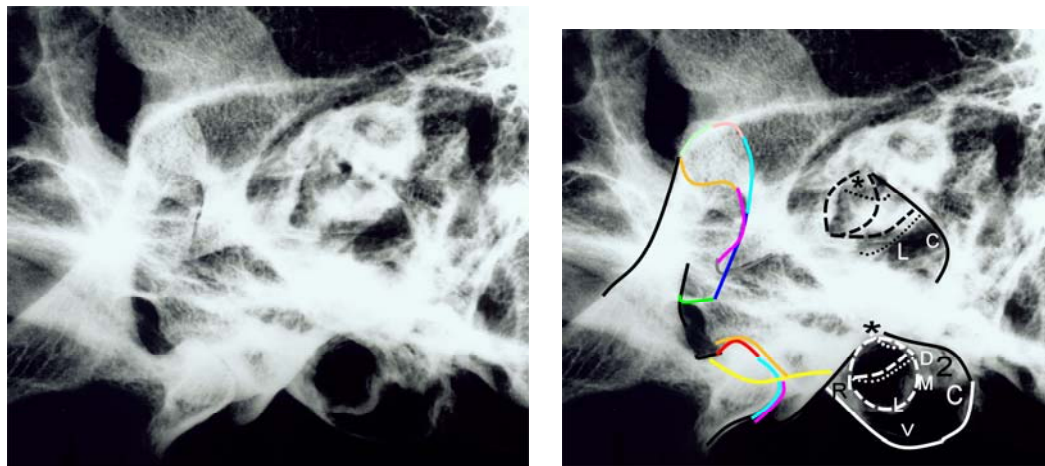


Figure 3.3.6.2. Mesaticephalic dog. Rotational angle = 20 degrees.

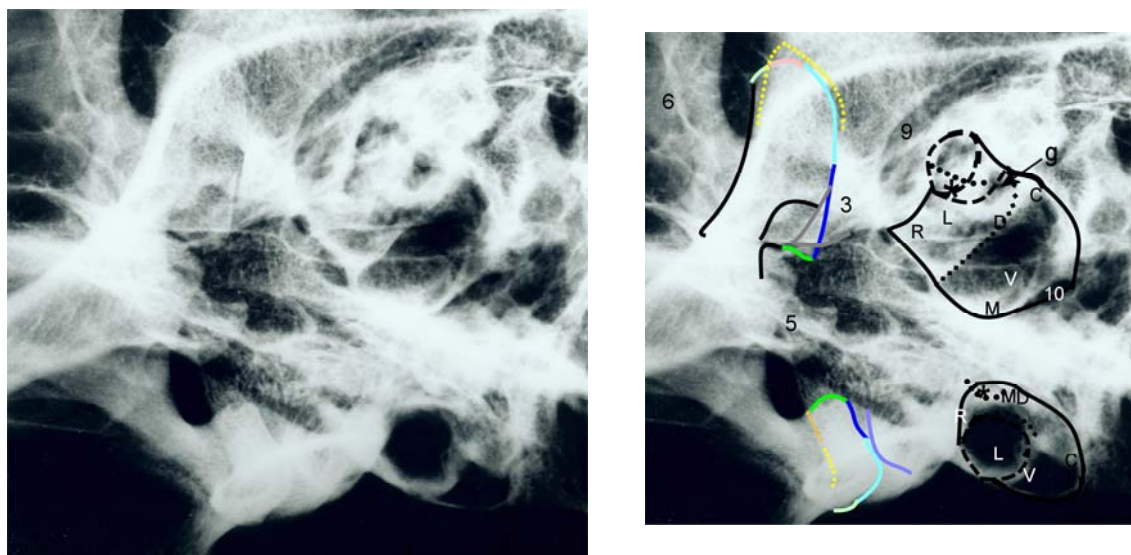


Figure 3.3.6.3. Mesaticephalic dog. Rotational angle = 30 degrees.

Figure 3.3.6. continued. Long axis rotations in a mesaticephalic dog skull.

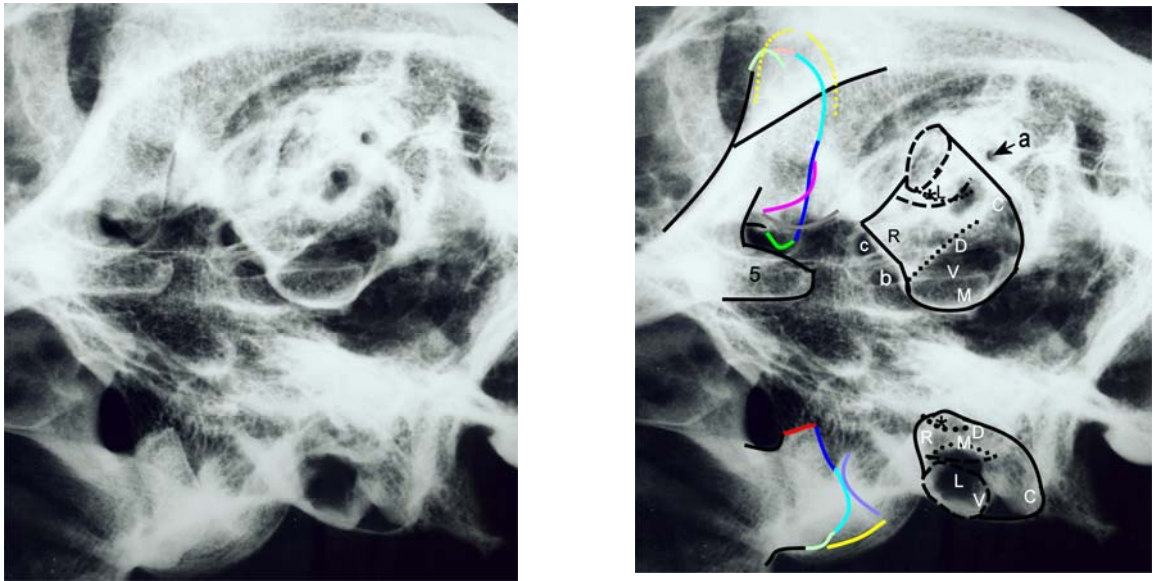


Figure 3.3.6.4. Mesaticephalic dog. Rotational angle = 40 degrees.

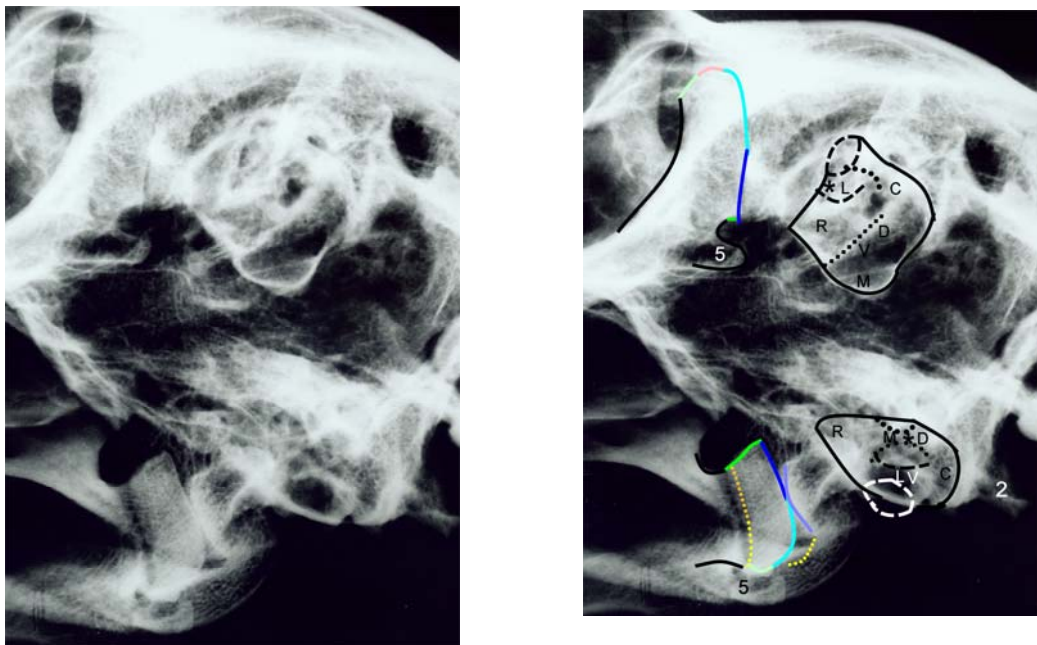


Figure 3.3.6.5. Mesaticephalic dog. Rotational angle = 50 degrees.

Figure 3.3.6. continued. Long axis rotations in a mesaticephalic dog skull.

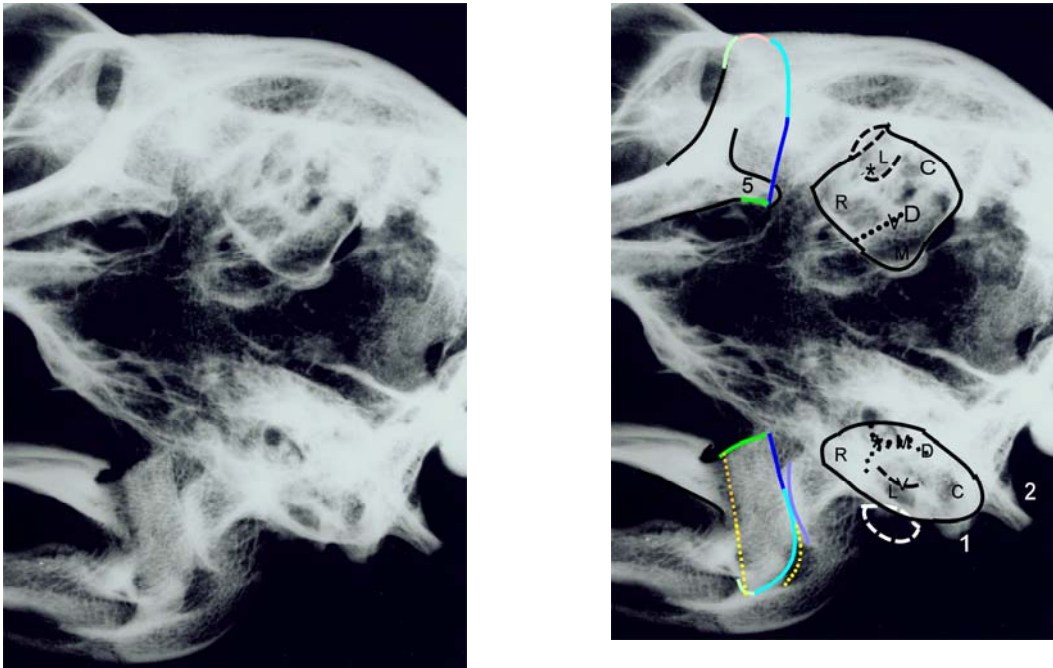


Figure 3.3.6.6. Mesaticephalic dog. Rotational angle = 60 degrees.

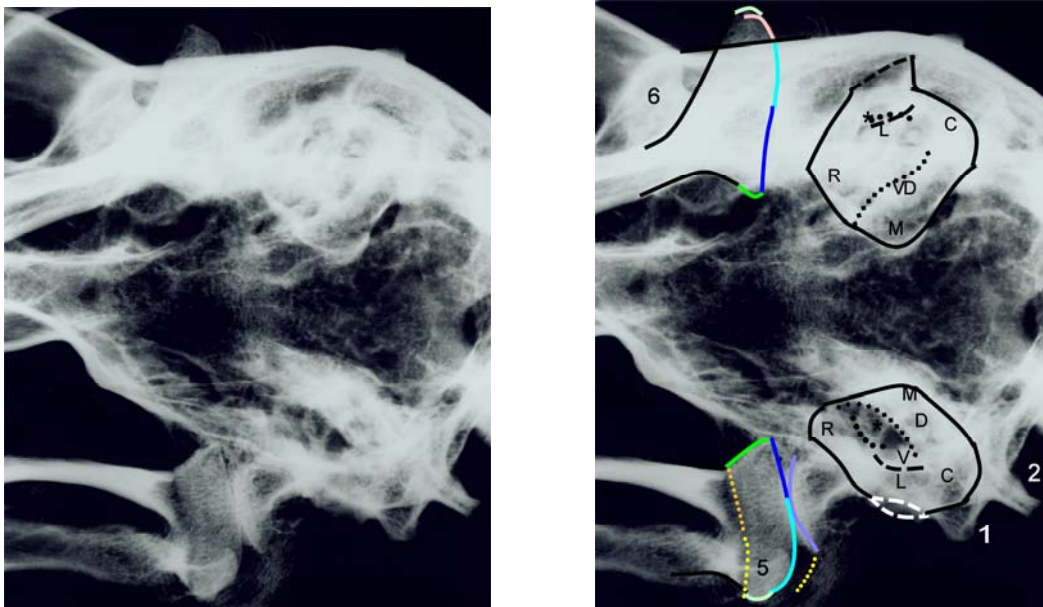


Figure 3.3.6.7. Mesaticephalic dog. Rotational angle = 70 degrees.

Figure 3.3.6. continued. Long axis rotations in a mesaticephalic dog skull.

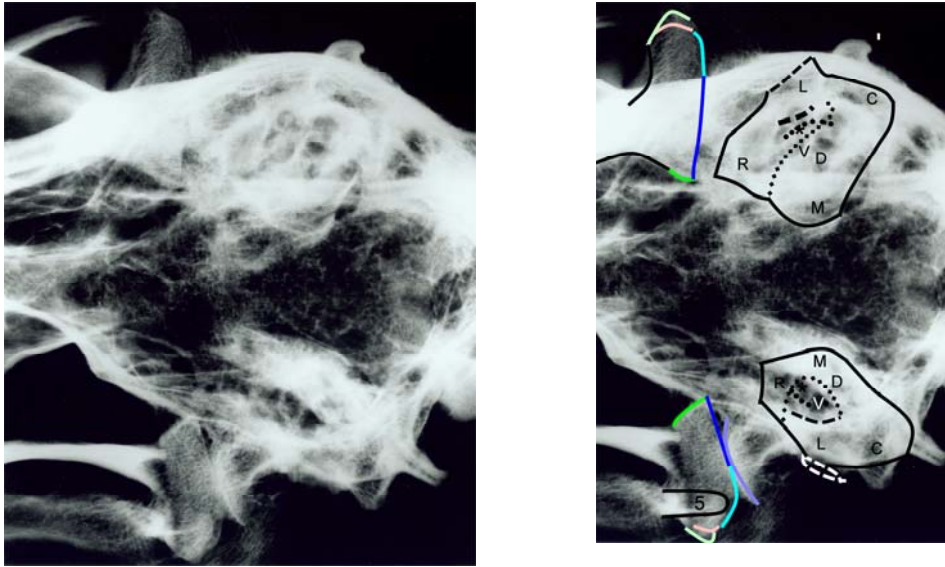


Figure 3.3.6.8. Mesaticephalic dog. Rotational angle = 80 degrees.

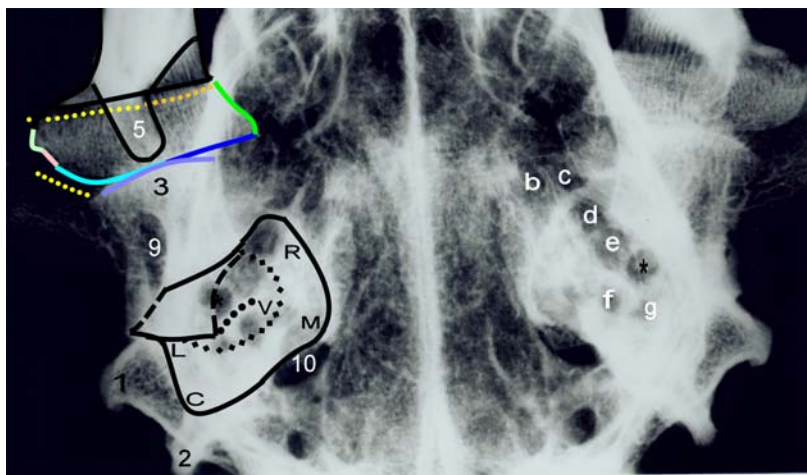
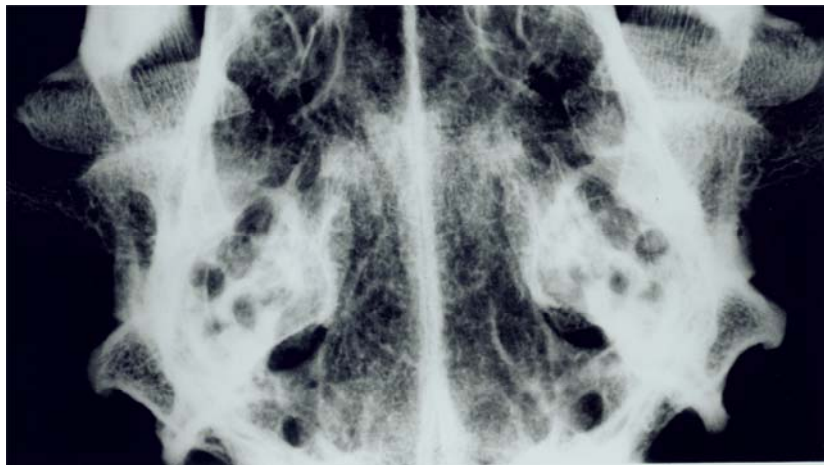


Figure 3.3.6.9. Mesaticephalic dog. Rotational angle = 90 degrees (true ventrodorsal).

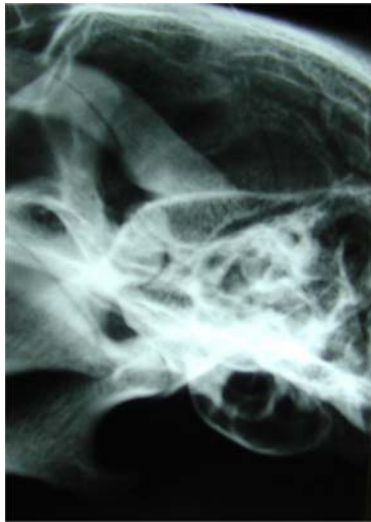


Figure 3.3.7.
Dolichocephalic dog skull.
Rotational angle = 20 degrees



Figure 3.3.8.
Brachycephalic dog skull.
Rotational angle = 30 degrees

Figure 3.3.9. Radiographs of the tympanic bulla (TB) and temporomandibular joint (TMJ) of a cat skull taken at long axis rotational angles from 10 to 90 degrees (ventrodorsal). For key see Table 3.3.1 and Figure 2.3.7.



Figure 3.3.9.1. Cat.
Rotational angle = 10
degrees



Figure 3.3.9.2. Cat.
Rotational angle = 20
degrees

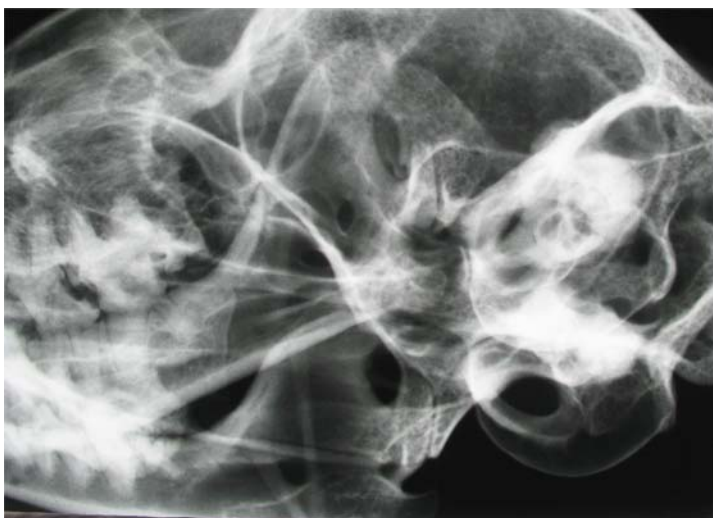


Figure 3.3.9.3. Cat.
Rotational angle = 30
degrees

Figure 3.3.9. continued. Long axis rotations in a cat skull.



Figure 3.3.9.4. Cat. Rotational angle = 40 degrees



Figure 3.3.9.5. Cat. Rotational angle = 50 degrees



Figure 3.3.9.6. Cat. Rotational angle = 60 degrees

Figure 3.3.9. continued. Long axis rotations in a cat skull.



Figure 3.3.9.7. Cat. Rotational angle = 70 degrees



Figure 3.3.9.8. Cat. Rotational angle = 80 degrees

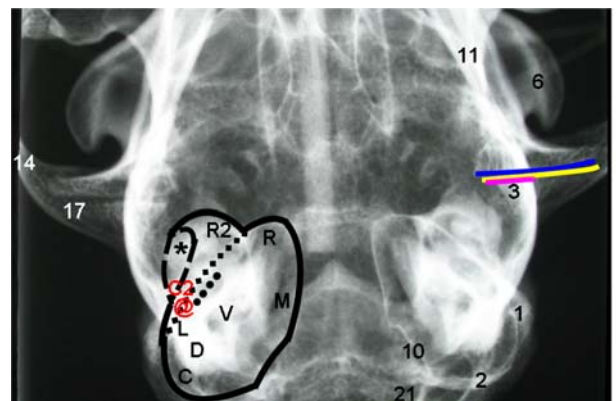


Figure 3.3.9.9. Cat. Rotational angle = 90 degrees (ventrodorsal)

Figure 3.3.10. Radiographs of the tympanic bulla (TB) and temporomandibular joint (TMJ) of a rabbit skull taken at long axis rotational angles from 10 to 90 degrees (ventrodorsal). For key see Table 3.3.1 and Figure 2.3.9.



Figure 3.3.10.1. Rabbit skull.
Rotational angle = 10 degrees

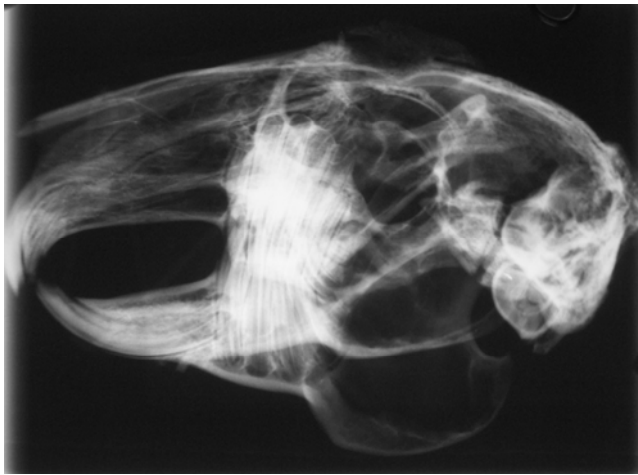


Figure 3.3.10.2. Rabbit skull.
Rotational angle = 20 degrees.



Figure 3.3.10.3. Rabbit skull.
Rotational angle = 30 degrees.

Figure 3.3.10. continued. Long axis rotations in a rabbit skull.



Figure 3.3.10.4. Rabbit skull.
Rotational angle = 40 degrees.



Figure 3.3.10.5. Rabbit skull.
Rotational angle = 50 degrees.



Figure 3.3.10.6. Rabbit skull.
Rotational angle = 60 degrees.

Figure 3.3.10. continued. Long axis rotations in a rabbit skull.



Figure 3.3.10.7. Rabbit skull.
Rotational angle = 70 degrees.

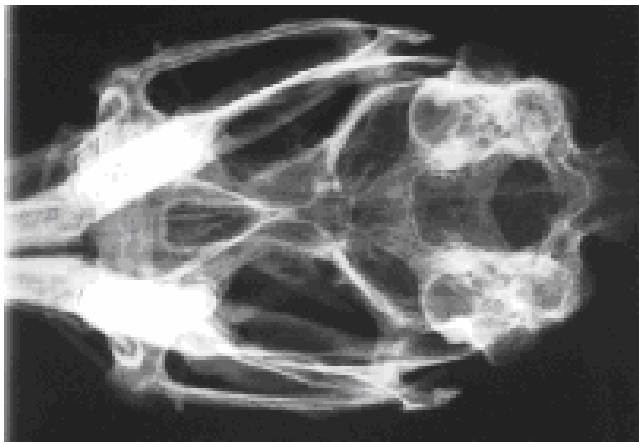


Figure 3.3.10.8. Rabbit skull.
Rotational angle = 80 degrees.

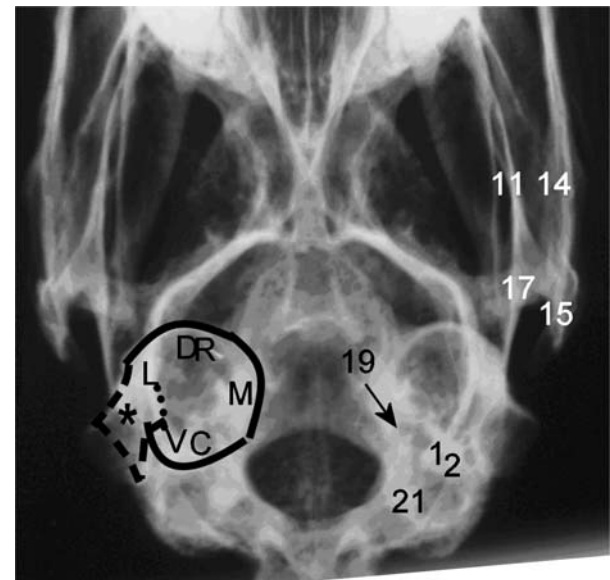


Figure 3.3.10.9. Rabbit skull. Rotational angle = 90 degrees (ventrodorsal).

3.3.4. Ventral rotational angles in emascerated skulls

The features visible in the rostrocaudal (0°) and ventrodorsal views (90°) have already been described in all three species. The TMJ and TB appeared bilaterally symmetrical at all the rotational angles in this series in all three species.

3.3.4.1. Ventral rotational angles in the dog

The radiographs produced at ventral rotational angles in the mesaticephalic skull are presented in Figure 3.3.11. Neither the TB nor the TMJ were visible at a rotational angle of 20° and so this image has been omitted. Only the open-mouth images from 0 to 30° rotation have been presented as beyond this the images obtained were similar to the equivalent closed mouth views, with the exception that a slightly different area of the condyloid process was visible.

3.3.4.1.1. Appearance of the TB in the mesaticephalic canine skull

The TB were superimposed over the maxilla and then the ramus of the mandible so they were not visible until a rotation of 30° had been reached when they were visible between the mandible and the occipital condyle. They subsequently became superimposed onto the skull and then the dense petrous temporal bone but remained visible right through to 90° (ventrodorsal view).

With the mouth open, only the ventral extremity of the TB was visible at 0° in the rostrocaudal view and the rest was superimposed onto the hard palate and molar teeth. Rotation through 10 and 20° allowed the TB to be clearly visualised between the hard palate and mandible but rotation to 30° and beyond resulted in superimposition onto the mandible and therefore inadequate visualisation.

3.3.4.1.2. Appearance of the TMJ in the mesaticephalic canine skull

The lateral half of the dorsal articular surface of the condyloid process and its lateral non-articular extremity were visible lateral to the maxilla at rotations of 10 to 20°. However, the medial components of the TMJ, including the retroarticular process were superimposed over the maxilla and therefore not visible. At 40° rotation the dorsal articular surface was still just visible and the caudal articular surface was emerging beyond the neck of the condyloid process. The medial margin of the condyloid process and the ventral aspect of the medial articular surface were just visible medial to the ramus of the mandible. At 50°, the dorsal articular surface was no longer visible. However, the TMJ was also no longer

superimposed onto the ramus of the mandible and was only overlain by the angular process so the caudal border of the lateral half of the condyle was visible along with the ventral portion of the medial half. The 'end-on' projection of the retroarticular process produced a distinctive curved opacity caudal to the medial articular surface. The same features were visible until 70° when the dorsal aspect of the medial articular surface became visible along with the base of the retroarticular process.

In the rostrocaudal view with the mouth open, the caudodorsal surface of the condyloid process was skylined. The lateral half of this surface was visible and also part of medial section between coronoid process and maxilla along with corresponding sections of the mandibular fossa. Rotation to 10° resulted in only the most lateral areas of dorsal articular surface being skylined. The tip of the retroarticular process was visible overlying the rostro-lateral aspect of TB, but all other features of the TMJ were superimposed over the maxillary molar teeth and therefore not visible. At 20° of rotation, the TMJ moved ventral to the level of the maxillary molar and therefore visibility improved. This time it was the rostral margin of lateral half of the dorsal articular surface that was skylined. The medial half of the condyloid process and the retroarticular process were superimposed over the coronoid process of mandible. By 30° rotation, the medial portion of the condyloid process was now superimposed over the mandibular molar teeth and therefore poorly visible. The lateral half of the dorsal articular surface was superimposed over the body of the condyloid process so only the non-articular areas at the rostral edge of the condyloid process are skylined.

3.3.4.2. Ventral rotational angles in the cat

The radiographs produced at ventral rotational angles in the feline skull are presented in Figure 3.3.12. Only the open-mouth images from 0 to 30° rotation have been presented as beyond this the images obtained were similar to the equivalent closed mouth views, with the exception that a slightly different area of the condyloid process was visible.

3.3.4.2.1. Appearance of the TB in the feline skull

At 10° rotation, the ventral margin of each TB began to emerge beyond the ventral aspect of the mandible and by 20°, the entire ventral compartment and part of the dorsal compartment were visible free from superimposition. The petrous temporal bone emerged from behind the mandible at 30° and increasingly overlay the dorsal and then ventral compartments of the TB as progression was made towards 90°.

With the mouth open, the ventral aspect of the TB was visible ventral to the base of the skull between the mandibles. Both the ventral and dorsal compartments were visible at 10°, but by 20° the petrous temporal bone overlay the dorsal compartment. By 30°, the lateral region of the ventral compartment was obscured by the mandibles and beyond this the TB was no longer visible until it emerged beyond the mandibles, after which the appearance was the same as in the views with the mouth closed.

3.3.4.2.2. Appearance of the TMJ in the feline skull

The appearance of the TMJ throughout this rotational series in the cat was very similar to that of the dog and therefore the same description applies.

3.3.4.3. Ventral and dorsal rotational angles in the rabbit

The radiographs produced at ventral rotational angles in the rabbit skull are presented in Figure 3.3.13 and at dorsal rotational angles in Figure 3.3.14.

3.3.4.3.1. Appearance of the TB in the rabbit skull

The TB were obscured by the dental arcades until 20°, only emerging completely free from them between 30 and 40° when they were visible between the mandible and the occipital condyle. However, the TB lumen was not projected free from superimposition onto the base of the skull at any of these angles. The TB remained visible through to 90° (ventrodorsal view) but were increasingly superimposed onto the petrous temporal bone and the base of the skull. With the mouth open, there were no angles that the TB were visible between the mandibles and ventral to the base of the skull. They were not visible completely free from the mandible until between 40 and 50°, after which they appeared the same as in the closed mouth views.

In the dorsal rotational series, the TB were not visible until 40° due to superimposition onto the maxilla and teeth. Subsequently, the lumen was clearly visible through the thin bones of the calvarium until rotation of 60° moved the TB over the occipital region and the petrous temporal bone.

3.3.4.3.2. Appearance of the TMJ in the rabbit skull

The condyloid process overlay the zygomatic process of the temporal bone at a rotation of 10° but various aspects of the TMJ were then skylined from 20° to between 40 and 50°,

after which they were superimposed onto the vertical ramus of the mandible and therefore were no longer visible. Other than skylining slightly different aspects of the TMJ, opening the mouth did not significantly alter the appearance of the TMJ.

In the dorsal rotational views, the TMJ was skylined from the rostrocaudal view (0°) through to 20°. The caudal non-articular section of the mandibular condyle overlay the TMJ until 40° when the TMJ was projected dorsal to the external acoustic meatus. Beyond this they became superimposed onto the external acoustic meatus and the vertical ramus of the mandible was projected 'end-on' and so prevented much information being obtained regarding the joints.

3.3.5. Cadaver heads

The lateral, long axis, ventral and dorsal rotational views were all reproducible in the cadaver heads and the appearance of the TB and TMJ was similar to that obtained using the skulls (Figure 3.3.15). Areas that were projected free from the bony components of the skull were well visualised but those overlying the skull were less well visualised than in the skulls due to the increased beam attenuation resulting from the presence of soft tissue.

Figure 3.3.11. Radiographs of the tympanic bulla (TB) and temporomandibular joint (TMJ) of a mesaticephalic dog skull taken at ventral rotational angles of 10 and 30 to 80 degrees with the mouth closed and 0 (rostrocaudal view) to 30 degrees with the mouth open.

For key see Table 3.3.1 and Figure 2.3.5

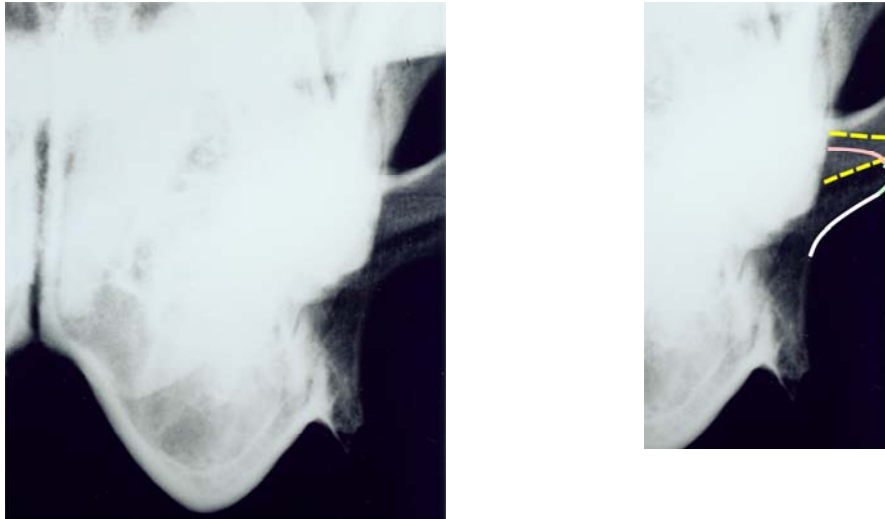


Figure 3.3.11.1. Mesaticephalic dog. Rotational angle = 10 degrees with the mouth closed.



Figure 3.3.11.2. Mesaticephalic dog. Rotational angle = 30 degrees with the mouth closed.

Figure 3.3.11. continued. Ventral rotational angles in a mesaticephalic dog skull.

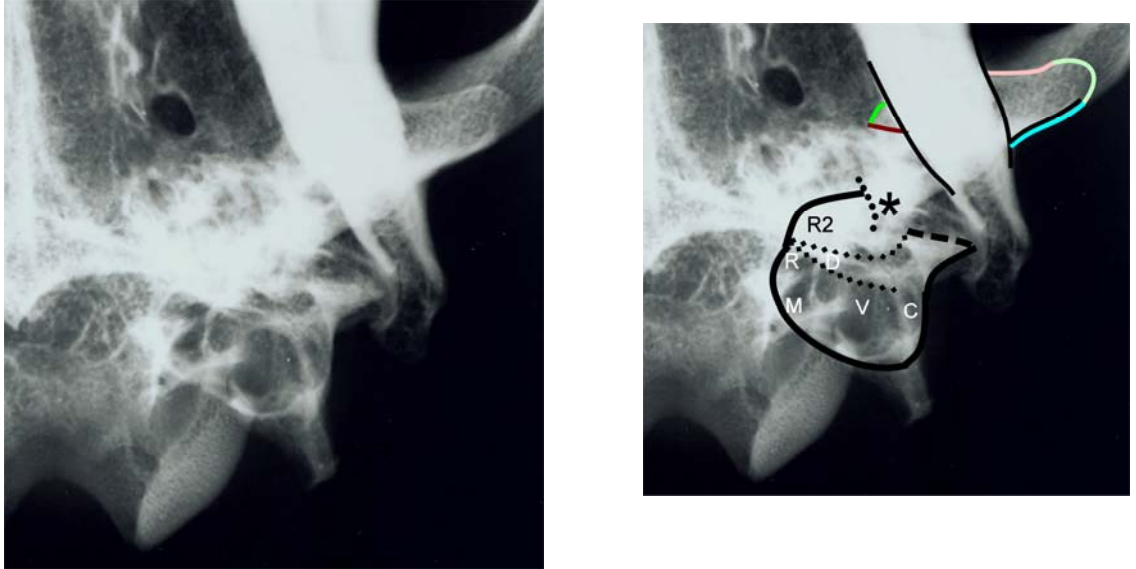


Figure 3.3.11.3. Mesaticephalic dog. Rotational angle = 40 degrees with the mouth closed.

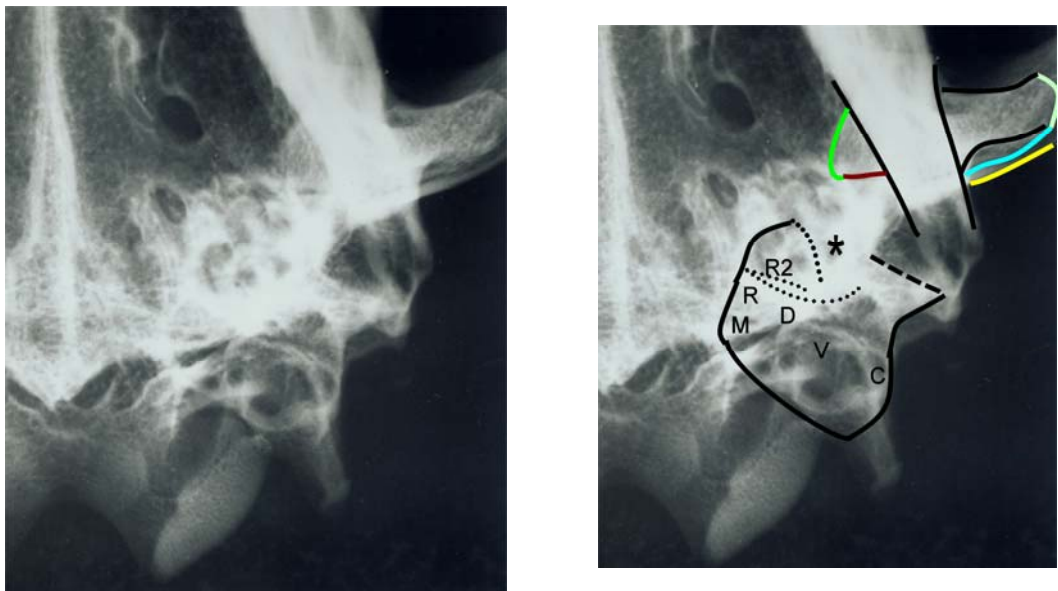


Figure 3.3.11.4. Mesaticephalic dog. Rotational angle = 50 degrees with the mouth closed.

Figure 3.3.11. continued. Ventral rotational angles in a mesaticephalic dog skull

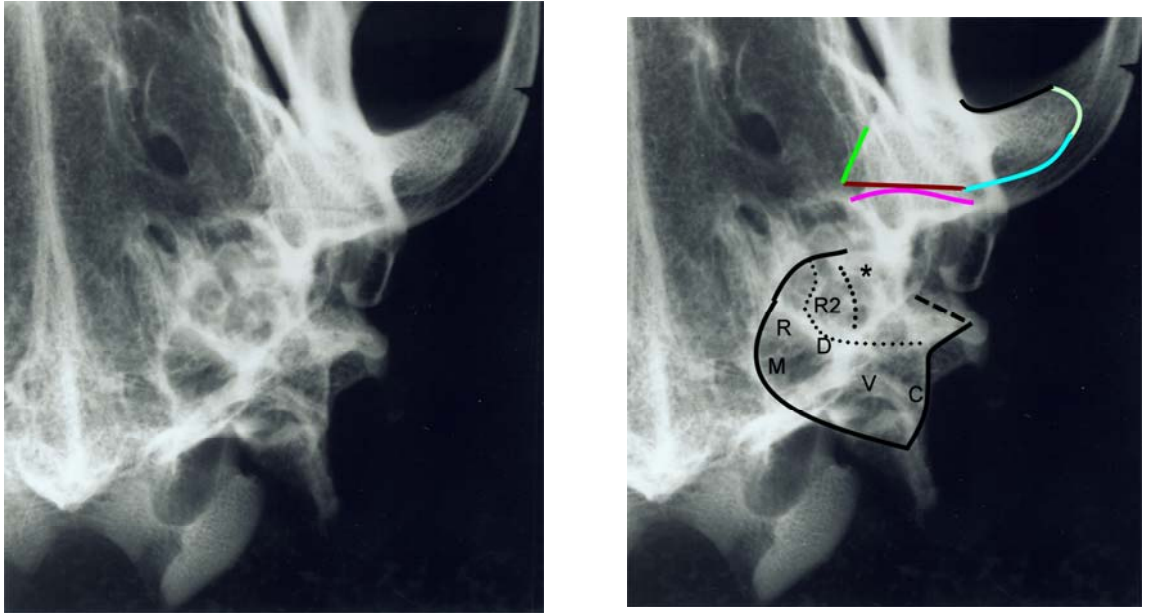


Figure 3.3.11.5. Mesaticephalic dog. Rotational angle = 60 degrees with the mouth closed.

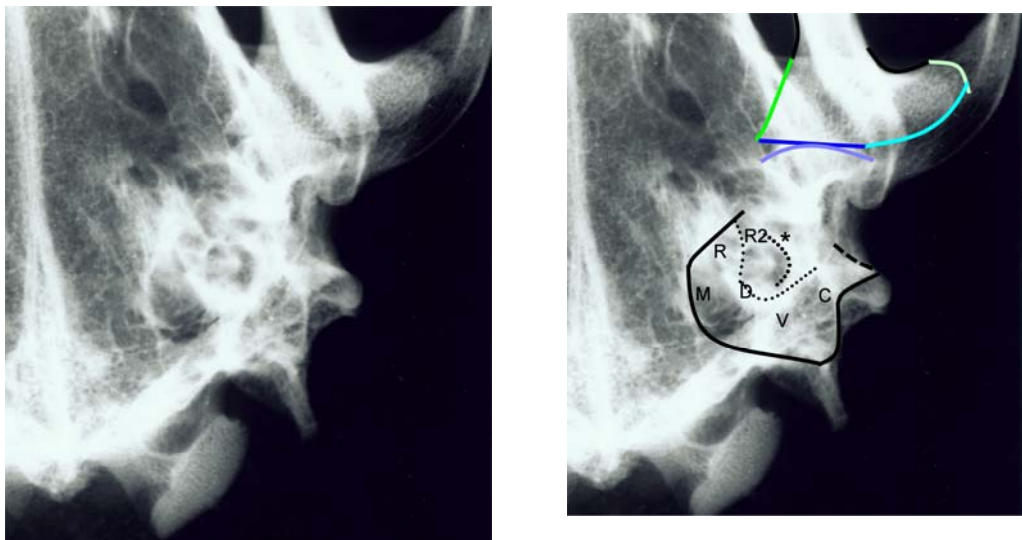


Figure 3.3.11.6. Mesaticephalic dog. Rotational angle = 70 degrees with the mouth closed.

Figure 3.3.11. continued. Ventral rotational angles in a mesaticephalic dog skull

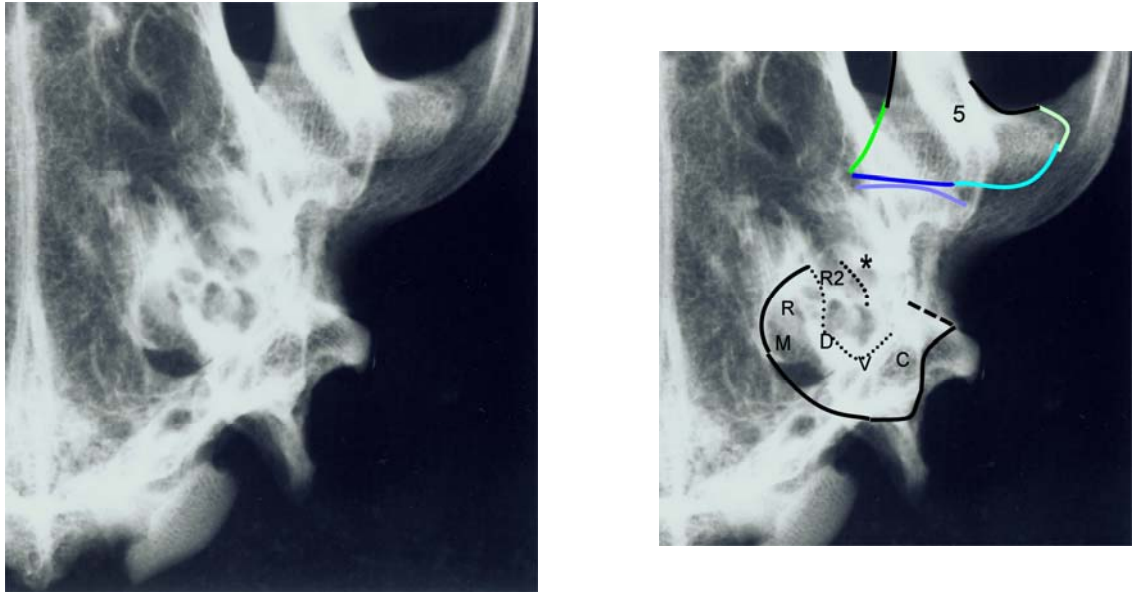


Figure 3.3.11.7. Mesaticephalic dog. Rotational angle = 80 degrees with the mouth closed.

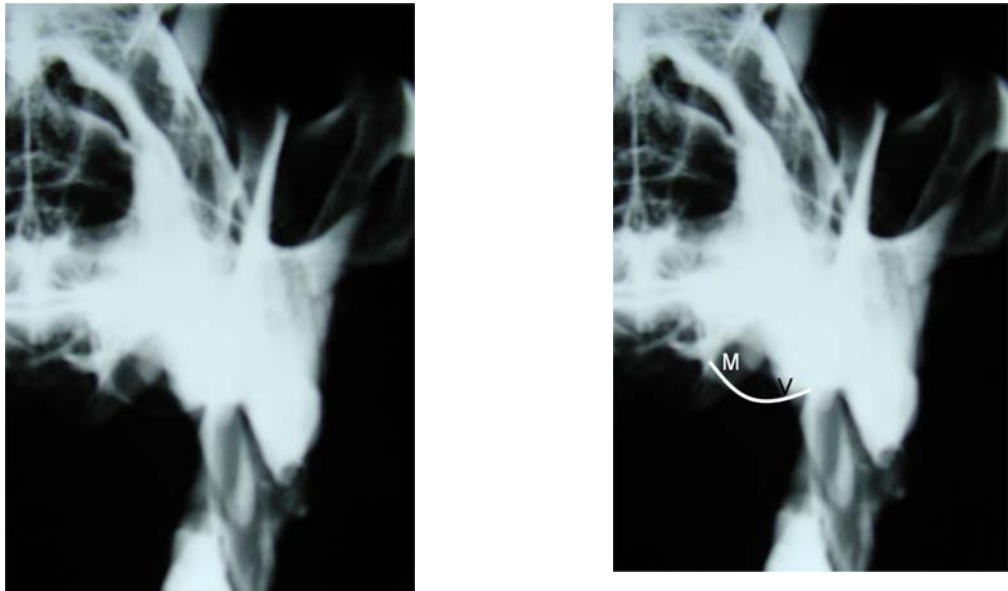


Figure 3.3.11.8. Mesaticephalic dog with the mouth open. Rotational angle = 0 degrees (rostrocaudal view).

Figure 3.3.11. continued. Ventral rotational angles in a mesaticephalic dog skull

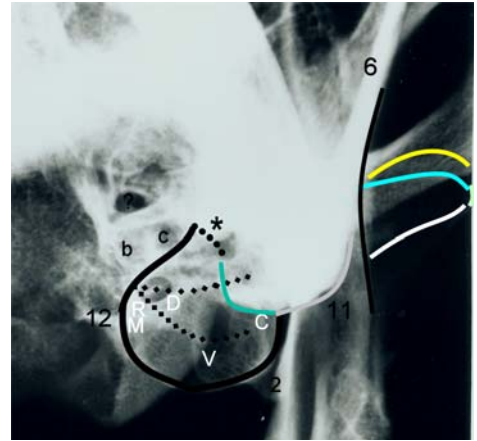


Figure 3.3.11.9. Mesaticephalic dog with the mouth open. Rotational angle = 10 degrees.

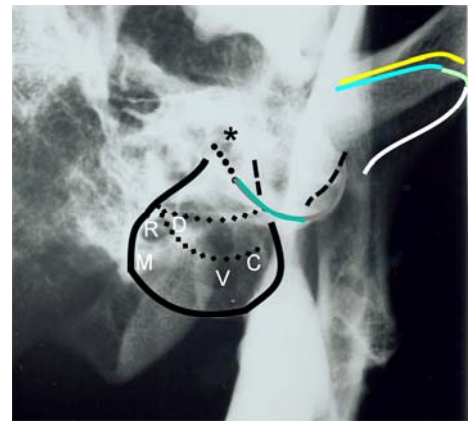


Figure 3.3.11.10 Mesaticephalic dog with the mouth open. Rotational angle = 20 degrees.



Figure 3.3.11.11. Mesaticephalic dog with the mouth open.

Rotational angle = 30 degrees

Figure 3.3.12. Radiographs of the tympanic bulla (TB) and temporomandibular joint (TMJ) of a cat skull taken at ventral rotational angles of 10 to 80 degrees with the mouth closed and 0 (rostrocaudal view) to 30 degrees with the mouth open.

For key see Table 3.3.1 and Figure 2.3.7



Figure 3.3.12.1. Cat.
Rotational angle = 10 degrees

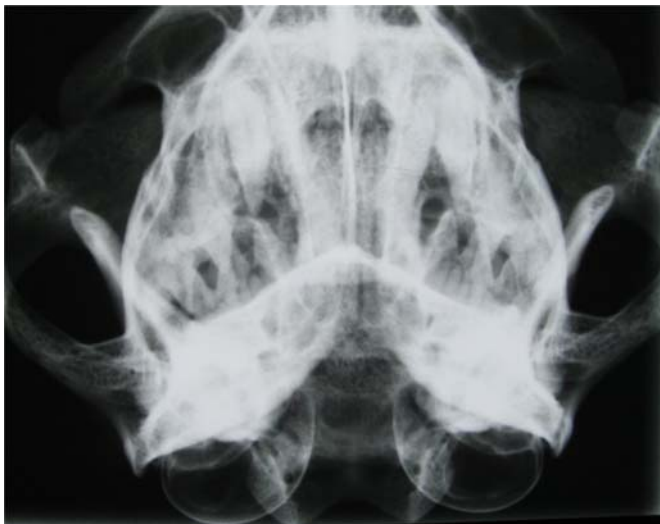


Figure 3.3.12.2. Cat.
Rotational angle = 20 degrees



Figure 3.3.12.3. Cat. Rotational angle = 30 degrees

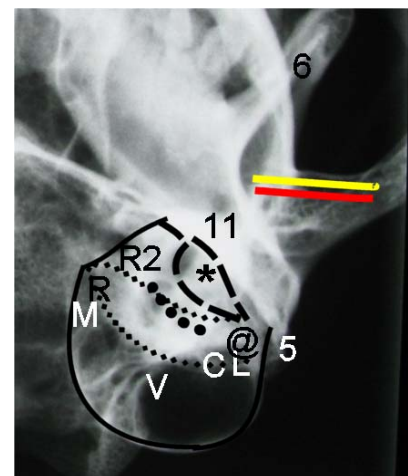


Figure 3.3.12. continued. Ventral rotations in a cat skull.



Figure 3.3.12.4. Cat.
Rotational angle = 40
degrees



Figure 3.3.12.5. Cat.
Rotational angle = 50
degrees

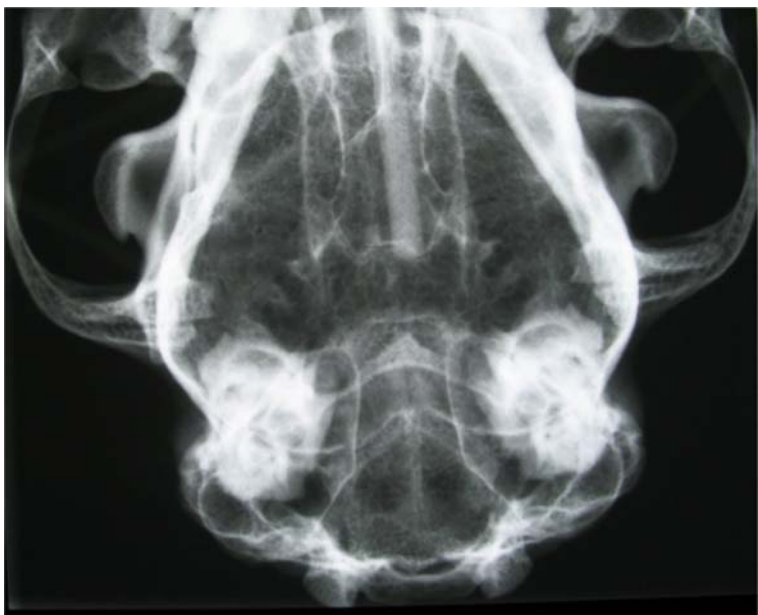


Figure 3.3.12.6. Cat.
Rotational angle = 60
degrees

Figure 3.3.12. continued. Ventral rotations in a cat skull.

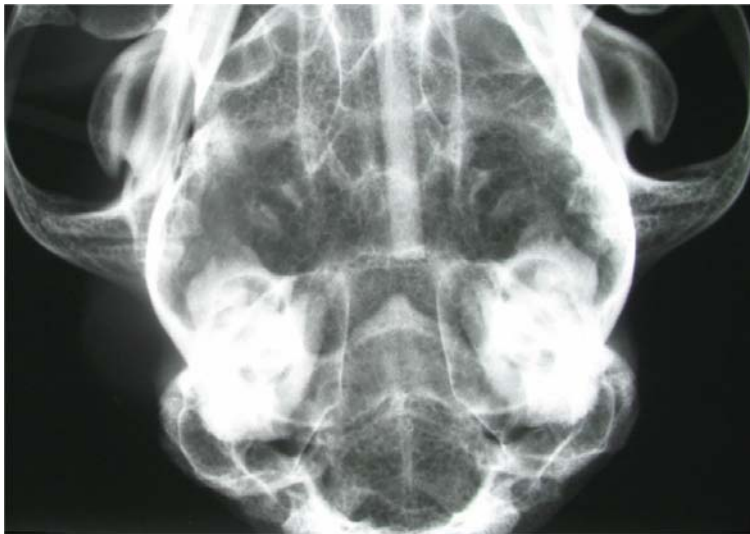


Figure 3.3.12.7. Cat.
Rotational angle = 70
degrees

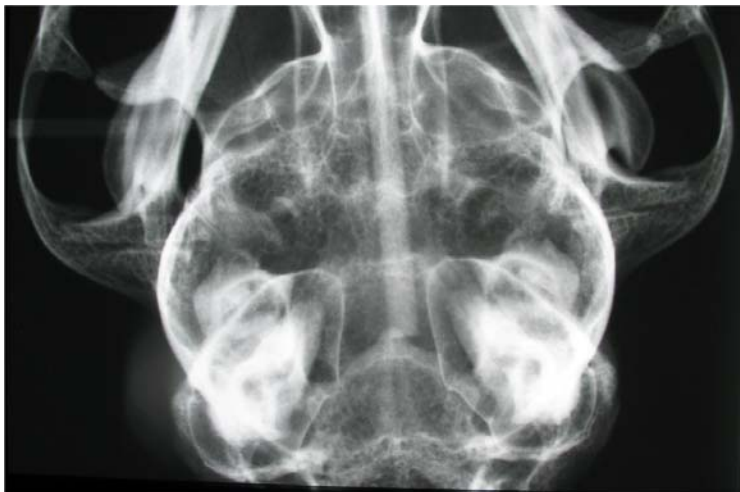


Figure 3.3.12.8. Cat.
Rotational angle = 80
degrees



Figure 3.3.12.9. Cat with
mouth open. Rotational
angle = 0 degrees (true
rostrocaudal).

Figure 3.3.12. continued. Ventral rotations in a cat skull.



Figure 3.3.12.10. Cat with mouth open. Rotational angle = 10 degrees.



Figure 3.3.12.11. Cat with mouth open. Rotational angle = 20 degrees.



Figure 3.3.12.12. Cat with mouth open. Rotational angle = 30 degrees.

Figure 3.3.13. Radiographs of the tympanic bulla (TB) and temporomandibular joint (TMJ) in a rabbit skull taken at ventral rotational angles from 10 to 80 degrees with the mouth closed and from 10 to 70 degrees with the mouth open. For key see Table 3.3.1 and Figure 2.3.9.

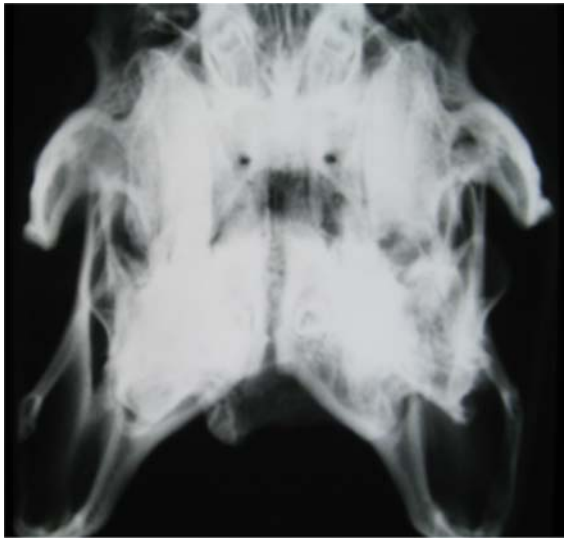


Figure 3.3.13.1. Rabbit skull.

Rotational angle = 10 degrees.

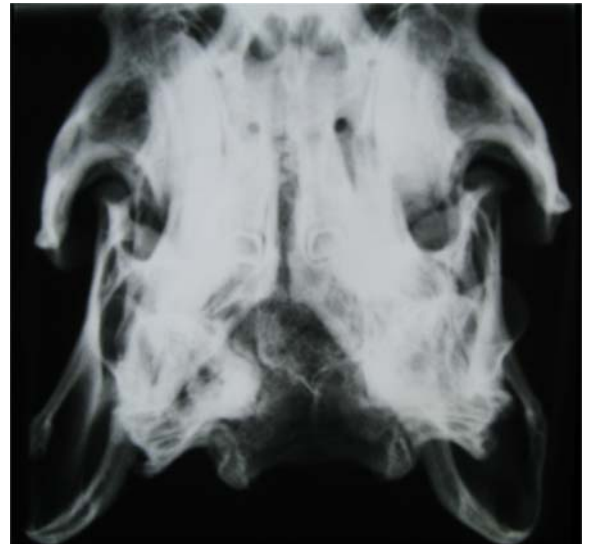


Figure 3.3.13.2. Rabbit skull.

Rotational angle = 20 degrees.



Figure 3.3.13.3. Rabbit skull. Rotational angle = 30 degrees.

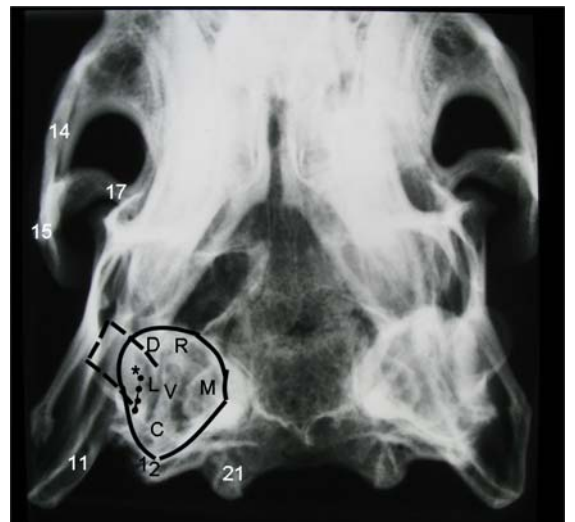


Figure 3.3.13. continued. Ventral rotations in a rabbit skull.

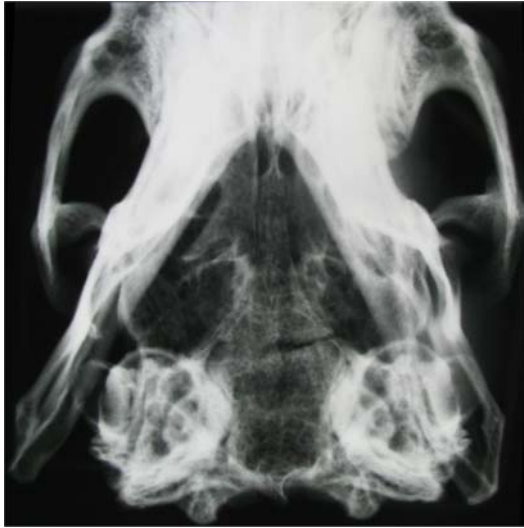


Figure 3.3.13.4. Rabbit skull.
Rotational angle = 40 degrees.



Figure 3.3.13.5. Rabbit skull.
Rotational angle = 50 degrees.



Figure 3.3.13.7. Rabbit skull.
Rotational angle = 70 degrees.



Figure 3.3.13.8. Rabbit skull.
Rotational angle = 80 degrees.

Figure 3.3.13. continued. Ventral rotations in a rabbit skull.



Figure 3.3.13.9. Rabbit skull with the mouth open. Rotational angle = 0 degrees (true rostrocaudal).



Figure 3.3.13.10. Rabbit skull with the mouth open. Rotational angle = 10 degrees.



Figure 3.3.13.11. Rabbit skull with the mouth open. Rotational angle = 20 degrees.



Figure 3.3.13.11. Rabbit skull with the mouth open. Rotational angle = 30degrees.

Figure 3.3.13. continued. Ventral rotations in a rabbit skull.



Figure 3.3.13.12. Rabbit skull with the mouth open. Rotational angle = 40 degrees.



Figure 3.3.13.13. Rabbit skull with the mouth open. Rotational angle = 50 degrees.



Figure 3.3.13.14. Rabbit skull with the mouth open. Rotational angle = 60 degrees.



Figure 3.3.13.15. Rabbit skull with the mouth open. Rotational angle = 70 degrees.

Figure 3.3.14 . Radiographs of the tympanic bulla (TB) and temporomandibular joint (TMJ) in a rabbit skull taken at dorsal rotational angles from 10 to 80 degrees.
For key see Table 3.3.1 and Figure 2.3.9.

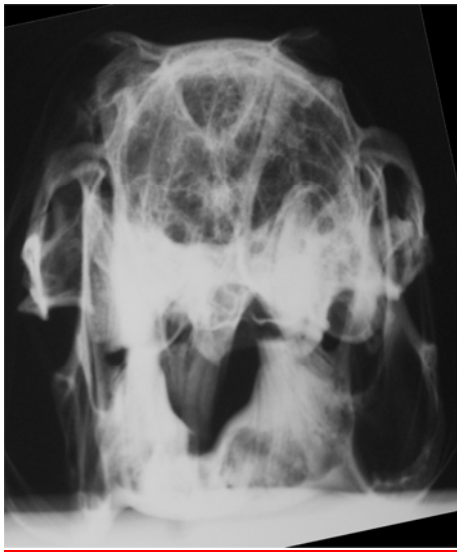


Figure 3.3.14.1. Rabbit skull.
Rotational angle = 10 degrees.

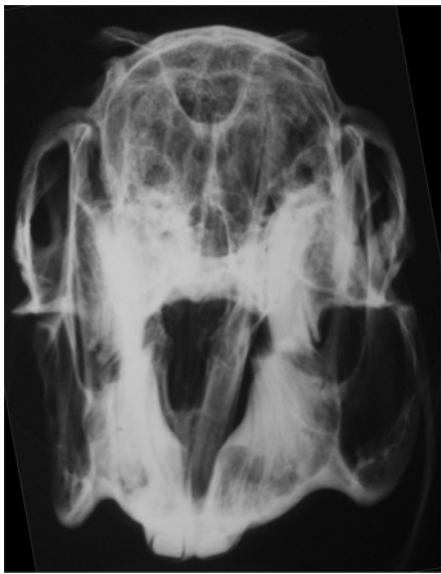


Figure 3.3.14.2. Rabbit skull. Rotational angle = 20 degrees.

Figure 3.3.14. continued. Dorsal rotations in a rabbit skull.

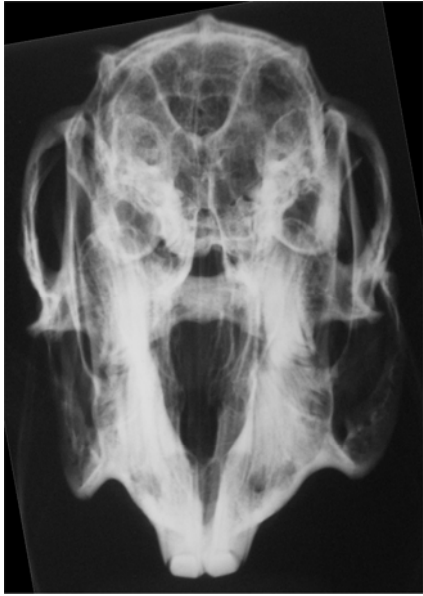


Figure 3.3.14.3. Rabbit skull.
Rotational angle = 30 degrees



Figure 3.3.14.4. Rabbit skull.
Rotational angle = 40 degrees.



Figure 3.3.14.5. Rabbit skull.
Rotational angle = 50 degrees.

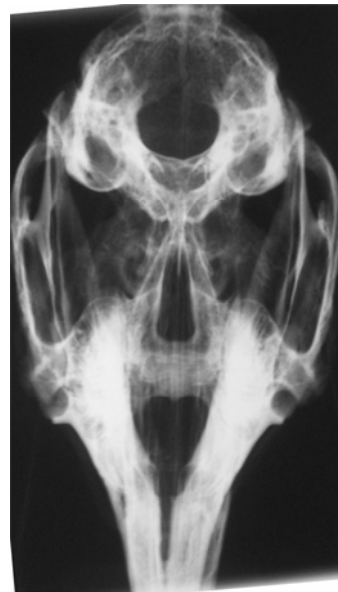


Figure 3.3.14.6. Rabbit skull.
Rotational angle = 60 degrees.

Figure 3.3.14. continued. Dorsal rotations in a rabbit skull.



Figure 3.3.14.7. Rabbit skull.
Rotational angle = 70 degrees.



Figure 3.3.14.8. Rabbit skull.
Rotational angle = 80 degrees.

Figure 3.3.15. Radiographs produced in cadaver heads.



Figure 3.3.15.1. Canine cadaver at a lateral rotational angle of 15 degrees.



Figure 3.3.15.2. Canine cadaver at a long axis rotational angle of 20 degrees.



Figure 3.3.15.3. Feline cadaver at a ventral rotational angle of 10 degrees with the mouth open.



Figure 3.3.15.4. Rabbit cadaver at a ventral rotational angle of 30 degrees.

3.4 Discussion

3.4.1. Material and technical considerations

The canine skulls were selected from the material in Chapter 2 as being typical of their type using reported criteria and the calculation of facial indices (Evans 1993). The dolichocephalic skull (Rough Collie) had a slightly higher facial index value than that reported but was the lowest value available of a known breed. The mesaticephalic skull (German Shepherd) closely matched the reported value (Evans 1993) but was lower than the average determined in Chapter 2. However, the absence of a correlation between facial index, and TB and TMJ anatomical variations in mesaticephalic skull types, as determined in Chapter 2, meant it remained an appropriate choice. The brachycephalic skull (Boxer) selected was lower than both the published value and the average determined in Chapter 2. However, skulls with a higher facial index demonstrated abnormal TMJ anatomy and were therefore deemed unsuitable for use in this part of the study. Unfortunately, time and technical constraints meant that it was only possible to radiograph one skull of each type. While each one was considered to be a typical representative of its type, further work involving larger numbers of skulls would be required to confirm that the observations made from the skulls in this study were in fact real and not due to natural variation.

The TB and TMJ are both complex three dimensional anatomical structures as determined in Chapter 2. It was therefore necessary to divide these structures into regions for descriptive purposes, especially since it was not possible to examine every region on each radiographic view. The terms ‘lower’ to indicate the structures nearest the cassette and ‘upper’ to indicate those furthest from it were deliberately used as these can refer to both right and left sides, depending on the side of recumbency of the animal prior to radiography.

The equipment used in the present study was designed to allow specific angles of rotation to be obtained about the level of the TB and TMJ and therefore standardize the images produced between the different skulls. This was necessary to allow an objective comparison between the views obtained. The beam was centred and collimated between the TMJ and TB to ensure both were visible on each film and the beam was not re-positioned throughout each series of rotations to avoid inadvertent alteration of the beam angle. This was a slightly artificial situation as when positioning a live animal, the pivotal point would be at the occipito-atlanto-axial complex. However, rotation about this area

would have required constant repositioning of the beam which was undesirable and in clinical cases the beam should always be centred over the specific region of interest (Douglas 1987). Likewise, downward lateral rotations in the canine skulls were deemed as undesirable due to the need to increase the film-object distance to accommodate the length of the nose between the areas of interest and the cassette. This distance should ideally be as small as possible to prevent magnification and distortion of structures on the resulting radiograph and is usually achieved by placing the area of interest nearest the cassette (Curry and others 1990).

The equipment was easily modified to accommodate skulls of the different species despite variations in size and shape. It also allowed the same views to be reproduced in cadaver heads, although some problems were encountered due to the additional weight and relative weakness of the material used in its construction. This was also the reason for the 5° variation between views observed. In clinical cases, the degree of angulation is determined subjectively by the radiographer (Douglas 1987, Morgan and Silverman 1987) and is therefore likely to vary by more than 5°. With suitable construction, the equipment described in this study could potentially be used to position anaesthetized patients with a high degree of accuracy. However, in clinical cases positioning aids including foam wedges, troughs, tapes and ropes are more commonly used than stereotactic devices (Douglas 1987, Morgan and Silverman 1987). Projections from all of the series in this chapter could be easily positioned in cadavers or clinical cases using foam wedges with the exception of the dorsal rotational series performed in the rabbit. These views would be difficult to obtain in a live animal using a vertical X-ray beam due to the need to either hyperflex the neck when the animal was placed in dorsal recumbency or hyperextend it with the animal in sternal recumbency. An alternative approach would be to position the animal in sternal recumbency as for a dorsoventral view and then alter the angle of the beam, although this may prove to be inconvenient or impossible in practice. There are also safety issues that must be considered when using a primary X-ray beam that is not vertical (Health and Safety Executive 1998) and when using a grid, the potential for cut-off if the beam and grid are not in alignment (Curry and others 1990).

Ideally a single set of radiographic equipment would have been used throughout the entire study but this was not possible due to a series of upgrades. This meant that the exposure factors required for the cat in the present study were slightly different to those used for the rabbit, despite it being reported that the same factors can be used (Gibbs and Hinton 1981).

It was not surprising that the cadaver heads required higher exposure factors than the emascerated skulls, due to the increased beam attenuation resulting from the presence of soft tissue structures (Curry and others 1990). It was also not surprising that this increased attenuation resulted in the TB and TMJ being more poorly visualised in the cadaver heads than the emascerated skulls. However, the marked contrast between the bone wall and gas lumen of the TB resulted in it remaining more clearly defined than the TMJ, where the contrast between the bone and adjacent soft tissue was poorer (Curry and others 1990). Although the images from the emascerated skulls were artificially enhanced due to the absence of soft tissue, their use was necessary to allow the accurate placement of markers and the resulting radiographic location of these anatomical structures will enhance interpretation of images obtained in cadavers or live animals.

Only selected views were performed in the cadaver heads so it could not be determined whether the same exposure factors would be suitable for all views in live animals. However, it is not advisable to attempt to examine all areas of skull on a single film (Gibbs and Hinton 1981). Therefore it would be prudent to measure the region of interest and select an appropriate exposure factor based on the thickness of the tissue present and the individual machine rather than relying on a specific Figure, particularly in larger patients. A grid was not used in the present study as the emascerated specimens did not require it and none of the views of the cadaver heads involved a region greater than 10cm thick (Sullivan 1995, Schwarz and others 2002). The heads of cats and rabbits are rarely more than 10cm in any dimension but larger dogs may exceed this and so a grid may be required.

The lateral and long axis rotational series projected each TB and TMJ independently therefore two separate exposures would be required to allow examination of both sides. The same degree of angulation must be applied to produce comparable projections, which is not always easy (Douglas and others 1987, Hoskinson 1993, Sullivan 1995). This would increase the time associated with the examination and inaccurate positioning would increase the number of exposures required. The ventral and dorsal rotational projections produced the only series of images where both TB were present on one film. Careful positioning was required at the outset to ensure bilateral symmetry but this allowed direct comparison between these structures and therefore had the potential to reduce the examination time.

3.4.2. Radiography of the TB in the dog, cat and rabbit.

The location of the TB at the base of the skull make their radiographic examination a challenge due to the large potential for superimposition (Crossley 1995, Garosi and others 2003, Bischoff and Kneller 2004). This can arise from neighbouring structures which include the temporal bone and the base of the skull, the mandible and teeth, the contralateral TB and TMJ, and also from within the structures themselves due to their complex nature. The routine radiographic evaluation of the canine and feline TB should involve a combination of projections including dorsoventral or ventrodorsal ; rostrocaudal open mouth (RCdOM); ventrodorsal oblique or latero 20° ventral - laterodorsal (Le20° V-RtDO & Rt20° V-LLtDO), which is also referred to as a 'lateral oblique'; and lateral 'tilted-up' or 'nose up' views (Gibbs 1978, Douglas 1987, Kapatkin and others 1990, Hoskinson 1993, Farrow 1994, Remedios and others 1991, Love and others 1995, Sullivan 1995, Owens and Biery 1998). True lateral projections of the skull produced the greatest amount of superimposition and were regarded as being of limited value for investigation of these structures in all three species (Schwarz and others 2002, Garosi and others 2003). The findings of the present study support these observations.

The lateral rotational series in the present study produced latero (10-80°) rostral-laterocaudal oblique projections that were equivalent to the lateral 'tilted-up' or 'nose up' views recommended in the dog and cat (Gibbs 1978, Douglas 1987, Hoskinson 1993, Farrow 1994). The ventral regions of the canine, feline and rabbit TB all extended beyond the level of the base of the skull and it was only these regions that were clearly visible in this series. Rotation of at least 20° was required to completely separate the TB of the dog and rabbit while 40° was required in the cat. This presumably reflected the disproportionately long TB in this species, as observed in Chapter 2. The lower TB was imaged best since the upper TB very rapidly became superimposed over the occipital condyles in all three species. However, the lower TB only remained visible until 50°, after which it became superimposed onto the upper mandible and molar teeth. This meant that the window of observation in the cat was particularly limited and careful positioning would be required in this species while some variation would be tolerated in the other two. An advantage of this view is that it can be achieved in conscious dogs by placing the head in a lateral position and then elevating the nose using a foam pad (Gibbs 1978, Sullivan 1995). However, given the precise positioning required for the cat, this is unlikely to be an option in this species.

The TB of the mesaticephalic and dolichocephalic skulls were similar radiographically but differences were observed in the appearance of the brachycephalic skull. It had thicker walls and did not project as far ventrally as in the other specimens therefore was not well visualised in these views. The external appearance of the TB in that particular skull was the same as the others and no association between skull type and TB anatomy was observed in Chapter 2. However, variations in the radiographic appearance of the TB between dog breeds has been reported, with the Cavalier King Charles Spaniel (CKCS) being cited as an example where the TB were small and thick walled (Dennis 2006). Both the CKCS and the Boxer are brachycephalic breeds so it is possible they will demonstrate similar TB anatomy. Increased thickness of the TB wall could not be determined by external visual inspection alone and so may account for the apparent normal external appearance of the Boxer skull in the present study. Due to their TMJ abnormalities, no CKCS skulls were examined in this part of the study. The radiographic appearance of the TB in the CKCS is reported to be a normal variation and unassociated with disease therefore comparison between both TB on well positioned radiographs is necessary to diagnose abnormalities with certainty (Dennis 2006). Further work would be indicated to determine whether this is a repeatable observation in the Boxer and other brachycephalic dog breeds.

The long axis rotational series in the present study produced latero (10-80°) ventral-laterodorsal oblique projections that were equivalent to the recommended 'ventrodorsal oblique' or 'lateral oblique' views in the dog and cat (Gibbs 1978, Douglas 1987, Kapatkin and others 1990, Remedios and others 1991, Hoskinson 1993, Farrow 1994, Love and others 1995, Sullivan 1995, Owens and Biery 1998). Rotation of 20° in this series was required to separate the TB of the dog and 30° for the cat and rabbit. However, in all three the entire lower TB was then visible free from superimposition therefore it was these lower rotational angles that were deemed to be potentially the most useful views in this series for imaging the TB. Subsequent superimposition onto the temporal bones occurred at 50° in the dog, 70° in the rabbit and 80° in the cat. This reflected the variations in skull shape and relative TB size between the different species. The bone tube of the external acoustic meatus was a prominent feature in these views in the rabbit.

The upper TB in all three species was visible through the thin bones of the calvarium throughout most of the rotational angles. At the higher angles, both TB progressively overlay the dense petrous temporal bone so by 90°, the true ventrodorsal view, they

appeared bilaterally symmetrical. Despite the superimposition, the ability to compare both sides on a single film makes the dorsoventral or ventrodorsal view one of those recommended views for assessing the TB in the dog, cat and rabbit (Douglas 1987, Harcourt-Brown 2003). Another advantage is the potential to produce this projection in conscious dogs (Douglas 1987). The petrous temporal bone of the rabbit was reported as being relatively large and very dense (Gibbs and Hinton 1981), but the bony structures of the middle ear remained well visualised (Wolvekamp and Oshwald 1991) as confirmed in the present study. In this projection, the TB were reported to appear as bilaterally symmetrical, fine, crisp, distinct linear bone opacities (Hoskinson 1993), although denser and thicker walled than in other views (Sullivan 1995). A large amount of variation in the exact bone pattern has been reported between breeds (Hoskinson 1993) and this also appears to apply to the different species in the present study which corresponds with a report that the TB walls in the rabbit are relatively thicker than those of the cat and dog (Beed 1997). The external acoustic meatus and ear canal can be assessed using this view in all three species (Shively 1979, Gibbs 1978, Farrow 1994). However, the vertical nature of the external ear canal in the rabbit meant its route was not as clear as in the dog and cat.

The ventral rotational series in the present study produced rostro (10-80°) ventral-caudodorsal oblique projections that included the '10° ventrodorsal' view recommended for investigation of the feline TB (Hofer and others 1995). The projections with the mouth open corresponded with the rostrocaudal open mouth views recommended in the dog and cat (Gibbs 1978, Douglas 1987, Hoskinson 1993, Sullivan 1995). The dorsal rotational series produced rostro (10-80°) dorsal-caudoventral oblique projections in the rabbit that have not been previously reported in any species.

In the rostrocaudal views with the mouth closed, the TB in all three species were not visible due to superimposition onto the mandible and teeth. Ventral rotation resulted in their emergence at 30° in the dog, 20° in the cat and 40° in the rabbit. This reflected the deeper TB in the cat compared with the other species and the longer vertical ramus of the mandible in the rabbit. The deep TB in the cat also resulted in it being projected free from superimposition onto the base of the skull until 40°, while in the dog, this only occurred in the one 30° view and in the rabbit, in none of the projections. However, the TB did remain visible for the remainder of the series in all three species whilst overlying the base of the skull. These projections were therefore potentially much more useful in the cat than the other species, and a range of angles resulted in adequate imaging of the TB therefore

allowing some tolerance in patient positioning. However, these angles do not exactly correspond with the recommended 10-20° (Hofer and others 1995).

With the mouth open, the canine and feline TB were only visible between 10 and 20°, being superimposed onto the hard palate and molar teeth at 0° (rostrocaudal) and the mandible beyond 30°. Although it has been suggested that the head be positioned so the hard palate is perpendicular to the cassette (Douglas 1987) the results of this study indicate that some angulation is required. The views in which the TB were best visualised corresponded with those advocated in previous publications (Garosi and others 2003) (Douglas 1987) although not with the 30° suggested in one report (Hoskinson 1993). These angles resulted in the TB being positioned over the air filled nasopharynx in live animals, thereby enhancing their appearance (Garosi and others 2003).

In the rabbit, opening of the jaw is limited to a maximal gape of only 20 to 25° by the TMJ capsule and also compression of soft tissue structures between the mandible and the skull (Weijs and Dantuma 1981). In addition, damage to the jaws, TMJ and masticatory muscles may result if the mouth is forced open or held open for long periods (Crossley 2003). This, combined with the long, narrow shape of the skull and mandible in this species resulted in inadequate space for projection of the TB between the maxilla and mandible. The TB was therefore not visible in these projections. Although the use of open mouth views has been suggested in the rabbit (Keeble 2006), these are mainly for dental examinations and a cotton bud placed between the incisor teeth has been suggested for the production of an open mouth lateral view of the occlusal surfaces of the cheek teeth (Harcourt-Brown 2002). A rostrocaudal open mouth view does not appear to have been documented but it is unlikely that the mouth could ever be opened far enough to allow visualisation of the TB without causing damage and therefore this view should be regarded as inappropriate for use in the rabbit.

The results of the present study suggest that the canine TB can be visualised using ventral rotational views with the mouth either open or closed, but that the open mouth views allow greater tolerance in positioning and better imaging of the TB. This corresponded with reports that the rostrocaudal open mouth view is generally best for demonstrating the TB in dogs (Gibbs 1978). In the cat, both views produced equivalent imaging although the former has been recommended due to it being easier to position in live animals (Hofer and others 1995). However, further work would be required to determine whether both are

equally as suitable for the identification of the changes associated with middle ear disease in this species. Although the rabbit TB was not projected free from superimposition onto the base of the skull at any of the ventral or dorsal angles, it was optimally imaged at 40-50° in each direction. Further work would be required to determine if either of these would be useful for assessing the middle ear in clinical cases, although the issues associated with positioning for the dorsal rotational views previously discussed are likely to make this view less useful in practice.

A major limitation of this work is that these observations were derived from individual skulls and while each was considered to be representative of its type, it is impossible to determine whether the variations observed were real or related to natural variation. Further work involving larger numbers of skulls is therefore indicated to confirm the validity of these observations.

3.4.3. Radiography of the TMJ in the dog, cat and rabbit

As with the TB, the location of the TMJ at the base of the skull in the dog and cat make their radiographic examination a challenge due to the large potential for superimposition (Schwarz and others 2002). However, the comparable TMJ anatomy between these species resulted in similar regions being visible in each of the different rotational series while the dorsal location of the TMJ in the rabbit resulted in quite different observations in this species. True lateral projections of the skull produced the greatest amount of superimposition and were regarded as being of limited value for investigation of these structures in the dog and cat (Schwarz and others 2002). The findings of the present study supported this observation in all three species.

Rotation in a lateral direction to produce the projections known as ‘nose-up’ or ‘tilted-up’ views were reported to be particularly useful for evaluation of the TMJ in the dog (Schwarz and others 2002). In the present study, the most potentially useful views in this series to examine the canine TMJ were 10 to 30° in mesaticephalic and dolichocephalic skulls, and 20 to 30° in large brachycephalic ones. These allowed the joint space and the articular surfaces of the condyloid process, mandibular fossa and retroarticular process of the lower TMJ to be projected. Lower angles favoured visualization of the joint space and higher angles the articular surfaces. The body of the retroarticular process was also clearly visualized. The higher rotational angles required for examination of brachycephalic skulls corresponded with the published recommended angle of 26.9° for this type of dog (Morgan

and Silverman 1987). Little difference was noted between the appearance of the mesaticephalic and dolichocephalic TMJ at the various angles in the present study despite them having different recommended angles of 13.6° and 10.2° respectively (Morgan and Silverman 1987). This may have been due to the equipment used only being reproducible to within 5° but it was clear that diagnostic views can be achieved at a range of angles around the recommended values. This is beneficial given the increased difficulty in the accurate positioning of live dogs, although the margin for error was less in the brachycephalic breed. Rotations beyond 30° were of less value as the molar teeth of the upper mandible moved across the lower TMJ increasingly obscuring it.

In the cat, the most useful views were 10 to 20°, which allowed visualisation of both the joint components and space of the lower TMJ. However, as with the TB, the window for visualisation was much more restricted than in the dog and therefore would require more careful positioning in a live animal. The typical cat skull is relatively wide and short therefore although the actual angles for optimum imaging of the lower TMJ were lower than those observed in the brachycephalic dog breed, the similarly restricted range of angles probably reflects the shape of the skull.

The most useful angles of rotation in this series for imaging the rabbit TMJ were considered to be the 80 and 90° (true rostrocaudal) views. In these, both TMJ were visible and the joint spaces were skylined. The dorsal location of the rabbit TMJ meant that although it avoided superimposition onto the dense bone at the base of the skull and the molar arcade, it still overlay the cranium and maxilla throughout the lower angles of rotation. In addition, the paramedian orientation of the joint meant that little information about its components was obtained until a rotation of 40 to 50° was reached. These high angles of rotation are therefore fundamentally different to the lower angles that were most useful in the dog and cat. This demonstrates the benefit of this type of anatomical study as extrapolation between species is not always possible and the influence of anatomical variations must be taken into consideration.

The features visible in the canine and feline TMJs in the long axis rotational series were again comparable, reflecting the anatomical similarities between the species. A rotational angle of at least 10° was required to project the TMJs free from one another and allow their visualization. Useful information could be obtained about the lower TMJ at most of the long axis rotational angles, although the published recommended angles are 20, 25 and

45°(Douglas 1987). Angles from 10 to 30° permitted examination of the mandibular fossa and retroarticular process while rotation beyond 40° allowed the entire caudal articular surface of the condyloid process to be visualized. This suggested that the choice of angle should be made according to the region of interest. Although the retroarticular process became superimposed onto the caudal portion of the zygomatic process at 30°, the thick bone at the base of the retroarticular process remained visible as an opaque line immediately caudal to the condyloid process. The upper TMJs were also visible through the calvarium at angles greater than 30° but were not clear due to the effects of superimposition.

The dorsal location of the TMJ in the rabbit resulted in the lower one only being projected beyond the skull and visible free from superimposition at a very small range of angles (60 to 70°) and this angle of interrogation yielded little useful information. The contralateral TMJ was also poorly visualized making these long axis rotational views of limited value for assessing the rabbit TMJ.

Dorsoventral / ventrodorsal views have been advocated as one of the recommended views for examination of the TMJ in the dog and cat, allowing the symmetry of the condyloid processes and the location of the coronoid processes to be assessed (Douglas 1987, Schwarz and others 2002). However, in this view, the medial portions of the condyloid processes were superimposed onto the calvarium and depending on the exposure settings were not always clearly visible in the cadaver head. A long axis rotational view of 70° may therefore be more beneficial in some dogs and cats to allow the entire length of the caudal articular surface to be assessed. In these views, the ventral aspect of the joint was also not visualized indicating they should be combined with at least one other view for adequate visualization of the TMJ. This corresponded with the recommendation that a minimum of one DV and two oblique views be taken in order to investigate the TMJ in small animals (Ticer and Spencer 1978, Lane 1982). In the rabbit, superimposition of the condyloid process and mandibular fossa onto the vertical ramus of the mandible in this view resulted in very little information being obtained about the TMJ and its components

At low angles of rotation in a ventral direction in the dog and cat, only the lateral and then the medial extremities of the TMJ were visualised due to superimposition onto the ramus of the mandible. However, as the angle increased the ventral and then the caudal articular surfaces could be assessed. There did not appear to be any advantage to opening the mouth

as the views were similar with the exception that the area of the articular surface being evaluated was slightly different at each angle. Rostrocaudal views are most commonly reported for evaluation of the TB in the dog but despite the TMJs being visible on them, there are currently no reports regarding their appearance in these projections. The results of this study indicate that these views can be used to visualise various parts of the articular surfaces although the higher angles of rotation appear to be most useful despite these being less useful for the TB. The TMJs in the rabbit were only visible at low rotational angles in both the ventral and dorsal series. They were skylined until 20°, beyond which they were projected onto other structures.

The views identified in the present study for optimum visualisation of the rabbit TMJ were therefore within 30° of a rostrocaudal view in either a lateral, ventral or dorsal direction and it was not well visualised in any of the long axis rotational views. Opening the mouth did not enhance visualisation of either the TB or TMJ and also must be undertaken with care in live animals, therefore open mouth views are not appropriate in this species. These observations are different to the dog and cat due to the marked differences in anatomy and location of the TMJ between these species (paramedian orientation and dorsal location relative to the dental arcade in the rabbit compared with horizontal orientation and location at the same level as the dental arcade in the dog and cat). In addition, the narrow mandibular fossa and elongated temporal process of the zygomatic arch, combined with the small size of the components in the rabbit resulted in few views that could provide useful clinical information about the joint space. Views involving a combination of angles have been used to assess the canine TMJ (Morgan and Silverman 1987) so further work would be indicated to identify any such combinations that may enhance examination of the TMJ in the rabbit. The anatomy and location of the rabbit TB however, is similar enough to the dog and cat for them to be visible using similar views.

A major limitation of this work is that these observations were derived from individual skulls and while each was considered to be representative of its type, it is impossible to determine whether the variations observed were real or related to natural variation. Further work involving larger numbers of skulls is therefore indicated to confirm the validity of these observations.

Chapter 4. Ultrasound of the tympanic bulla and temporomandibular joint in the dog, cat and rabbit.

4.1 Introduction

4.1.1. Technical aspects of ultrasound image production

The acoustic impedance of a tissue is calculated using the equation $Z = pc$ [Z = acoustic impedance, p = density, c = velocity of sound in that substance]. Fat has an acoustic impedance of 1.38 and muscle $1.7 \text{ g/cm}^2\text{sec} \times 10^{-15}$. When the ultrasound beam strikes an interface between two tissues with different acoustic impedances, a portion of the beam will be reflected and the rest is transmitted further into the patient (Curry and others 1990). The velocity of ultrasound in the body is independent of beam frequency but reflects the physical makeup of the tissue it is passing through. Most body tissues, with the exception of bone and gas, behave like liquids and so transmit sound at approximately the same velocity, accepted as 1540 m/sec (Curry and others 1990). This constant velocity allows the ultrasound machine to calculate the distance between the transducer and the interface by measuring the time interval between the ultrasound pulse and echo, then using the equation $\text{distance} = \text{velocity} \times \text{time} / 2$ (Curry and others 1990). The amplitude of the returning echo is used to allocate a shade of grey with weak echoes being darker and strong ones being white. Normal parenchymal organs and body tissues produce various shades of grey that are relatively constant between animals (Nyland and others 1995).

Bone has a high acoustic impedance ($7.8 \text{ g/cm}^2\text{sec} \times 10^{-15}$) due to its high density. At an interface between soft tissue and bone, the large difference in acoustic impedance between the tissues results in approximately 30% of the ultrasound beam being reflected back to the transducer (Herring and Bjornton 1985). This produces a hyperechoic interface on the image, representing the surface of the bone nearest the transducer. The remainder of the beam is rapidly attenuated within a short distance, mainly due to absorption, as a result of the high density and non-compressible nature of the bone (Herring and Bjornton 1985). Structures deep to the bone surface are not reached by the beam resulting in a well defined, anechoic, acoustic shadow on the image beyond the hyperechoic soft tissue - bone interface. Ultrasound is therefore limited to providing information regarding the bone surface (Risselada and others 2004). This can include contour interruptions and abnormalities in the adjacent soft tissue (Kramer and others 1997) resulting from bone tumours (Kramer and others 1997, Bakar 1999) or osteomyelitis (Reef and others 1991)

and the monitoring of fracture healing (Shepherd and Pilsworth 1994, Kramer and others 1997, Bakar 1999).

The ultrasound beam is also unable to penetrate through gas (Nyland and others 1995). Gas has a very low acoustic impedance ($0.0004 \text{ g/cm}^2\text{sec} \times 10^{-15}$) due to the low velocity at which sound waves pass through it (331 m/sec), as the molecules are far apart and easily compressed (Curry and others 1990). Approximately 99.9% of beam is reflected back to the transducer and as with bone, this produces a high amplitude echo and a hyperechoic interface on the image representing the surface of the gas nearest the transducer. Again, structures deep to the interface are not reached by the beam resulting in an anechoic area of acoustic shadowing. However, with gas, this shadow may be occupied by a series of parallel horizontal lines called 'reverberation' artefact. This results from a proportion of each returning echo being reflected back into the body, either from the transducer surface or from other interfaces within the body. The resulting multiple journeys before the echo is received by the transducer results in phantom interfaces at regular intervals from the transducer. These are particularly prominent when the beam is perpendicular to the interface and become less well defined when the beam is at an angle (Nyland and others 1995). This may be referred to as 'dirty shadowing' and must be distinguished from real structures or the contents of the gas-filled structure (Nyland and others 1995). Interrogation of gas-filled structures such as the lung will therefore also be limited to the surface unless the gas becomes replaced by a medium through which the beam can be propagated, such as the presence of peripheral lung masses or consolidation (Reichle and Wisner 2000).

When performing ultrasound examinations, it is therefore usually necessary to find 'acoustic windows' that avoid the interposition of bone or gas-filled structures between the transducer and the region of interest (Herring and Bjornton 1985). Consideration should be given to the position of the patient (Nyland and others 1995). It is usually also necessary to remove the hair overlying the region of interest by clipping and apply ultrasound gel, otherwise the beam cannot penetrate the air trapped between the hairs (Nyland and others 1995).

Appropriate transducer selection for each examination is important as this influences the resolution of the resulting ultrasound images. The 'axial' ('in-plane' or 'depth') resolution of the image is the ability to distinguish between two adjacent points located parallel with the beam and is dictated by the frequency of the transducer (Curry and others 1990). High frequency transducers produce a beam with a short wavelength (according to the equation

velocity = frequency x wavelength) and therefore good axial resolution (Curry and others 1990). However, the beam is attenuated as it passes through tissue at the rate of 1Db per cm per MHz so high frequency transducers will have poor depth of penetration. Reducing the frequency of the transducer will reduce the axial resolution but increase the depth of penetration (Curry and others 1990).

The 'horizontal' (also known as 'lateral' or 'azimuthal') resolution is the ability to distinguish between two adjacent points located perpendicular to the beam and is dictated by the width of the beam. The piezo-electric crystals are contained within rectangular transducer elements that are then aligned to form the transducer. The size of these elements dictates the width of each individual beam therefore a large number of small elements will produce an image with many lines and good horizontal resolution. Each beam travels in a parallel manner for a distance dictated by its frequency and the diameter of the element. The horizontal resolution of the beam is best in this area, which is known as the Fresnel zone. Small elements have very short Fresnel zones, after which they enter the Fraunhofer zone where the beam diverges and the horizontal resolution is reduced. This is avoided by firing the elements in groups (Curry and others 1990). Improvement of horizontal resolution can also be achieved by electronically focussing or narrowing the entire beam in the region of interest (Nyland and others 1995).

Selection of an appropriate type of transducer for the examination being performed is also important. Linear transducers require a large area of contact with the skin surface, have many elements therefore good image quality and a static beam producing optimal near field image quality. Curvilinear and microconvex transducers are linear format but with a convex face resulting in a smaller area of contact with the skin but some beam divergence reducing near field image quality. Sector transducers have a smaller number of elements therefore fewer lines per image. They produce a wedge shaped beam with poor near field image quality but the ability to image large deep structures through a small area of skin contact (Nyland and others 1995). These are most commonly used for cardiac examinations to allow imaging through the intercostal spaces (Nyland and others 1995).

4.1.2. Applications of ultrasound relating to the TB and TMJ

The human middle ear and related structures have been imaged using A and B Mode ultrasound by placing a transducer in the fluid-filled external ear canal or concha (depending on the size of the transducer) and imaging through the intact tympanic membrane (Alvord 1990). There are no reports of this approach in animals although

ultrasound examination of the tympanic membrane and middle ear cavity in dogs has been described by filling the external ear canal with saline and applying the transducer to the skin surface over the horizontal ear canal (Lee and others 2006).

There is also a report on the experimental use of ultrasound to examine the contents of the TB in canine cadavers by imaging through the thin bone wall of the TB itself (Griffiths and others 2003). This technique was reported to be able to distinguish between fluid and gas within the lumen (Griffiths and others 2003). There are no reports of this approach in humans or other species, and also no reports of the use of ultrasound in clinical cases of canine middle ear disease. However, ultrasound is currently used in human medicine for a variety of other purposes that involve the beam penetrating deep to thin layers of bone. These include Doppler flow measurements within cerebral blood vessels via the temporal bone (Aaslid and others 1982) and the identification of fluid within the paranasal sinuses through the maxillary and frontal bones (Hilbert and others 2001).

Ultrasound examination of the human TMJ (Nabeith and Speculand 1991, Stefanoff 1992, Gateno and others 1993, Long and Nyland 1999, Landes and others 2000) has been described. The technique was reported to be accurate, reproducible, non-invasive and rapidly performed (Gateno and others 1993, Landes and others 2000) although further work was advocated before it could become an accepted procedure (Payne and Nakielny 1996, Landes and others 2000). Imaging was performed from a lateral approach at varying angles (Nabeith and Speculand 1991, Landes and others 2000) with the joint in open and closed positions (Landes and others 2000). The cutis, subcutis, parotid gland, masseter muscle, lateral joint capsule (Landes and others 2000), the bony margins of the lateral pole of the mandibular condyle, the lateral cortex of the ascending ramus, the zygomatic arch and the cartilage of the tragus (Gateno and others 1993) could be identified but the medial aspect of the joint was not visible (Landes and others 2000). The disc could be identified (Nabeith and Speculand 1991, Stefanoff 1992) and was better visualised with the joint in an open position (Nabeith and Speculand 1991).

The normal equine TMJ has also been examined using ultrasound with a complete examination requiring imaging from three standard approaches (Weller and others 1999a, Rodriguez and others 2002). The parotid salivary gland, the bone margins of the mandibular condyle, mandibular fossa, articular tubercle and retroarticular process, the intra-articular disc and the joint capsule were visualised. The synovial compartments and joint ligaments were not identified while the articular cartilage was observed only in foals

(Weller and others 1999a). Ultrasound has been used to evaluate TMJ arthropathy in the horse (Weller and others 1999b).

Ultrasound is being used increasingly to evaluate the musculoskeletal system in dogs and cats (Kramer and others 1997). Several joints have been investigated in this manner (Greshake and Ackerman 1992, Reed and others 1995, Long and Nyland 1999) and the sonographic appearance of a typical joint has been described (Kramer and others 1997). However, there are currently no reports of the use of ultrasound to evaluate the TMJ in small animals.

4.1.3. Aims

The aims of the work presented in this chapter were to:

- Determine whether currently available ultrasound equipment could be used to image the canine, feline and rabbit TB and TMJ.
- Identify the optimum equipment and technique for these purposes
- Document the relevant anatomy and sonographic appearance in cadavers and live animals where possible

4.2 Material and Methods

4.2.1. Equipment

The dog and cat cadavers were imaged using a Powervision¹ ultrasound machine in conjunction with a 3.5 MHz phased array sector, a 6.5 MHz curvilinear and two 12 MHz linear transducers (footprints 5cm and 3cm) (Figure 4.2). The rabbit cadavers were imaged using this equipment and also a Diasus² ultrasound machine in conjunction with 10-22 MHz and 8-16 MHz linear transducers (4cm footprint).

4.2.2 Image production and processing

All ultrasound images were captured digitally by the respective ultrasound machines and transferred electronically to a personal computer. Paint Shop Pro 7 software (Microsoft) was used to label the resulting images.

4.2.3. Preparation of cadaver material

Ten mesaticephalic mixed breed canine, domestic breed feline and New Zealand White breed rabbit cadavers with no visible external evidence of ear, respiratory or dental disease and no abnormalities associated with the external ear, mouth or temporomandibular region were selected. The hair from each side of the head was clipped from dorsal to ventral midline over an area extending from midway along the zygomatic arch to caudal to the level of the external ear canal. Surgical spirit and ultrasound coupling medium were applied to the site to produce optimum acoustic contact between the skin surface and the transducer.

4.2.4. Ultrasound examination

The cadaver heads were placed in a lateral position and the ipsilateral TB and TMJ were examined using all the transducers and from a series of locations. The heads were then turned over and the other side examined in the same way. The images obtained were all optimised using the depth and time-gain compensation controls. The beam was focussed according to the region of interest.

In the canine and rabbit cadavers, a Spruell needle with a syringe attached was advanced along the external ear canal and through the tympanic membrane. Water or KY jelly³ was then injected into the lumen of the TB. In the feline cadavers, this technique only permitted

¹ Toshiba Medical Systems Limited, Manor Court, Manor Royal, West Sussex, RH10 2PY

² Dynamic Imaging Ltd, 9 Cochrane Square, Brucefield Industrial Park, Livingston, EH54 9DR

³ Johnson and Johnson Ltd, Maidenhead, SL63UG.

filling of the dorsal compartment of the TB with no fluid entering the ventral compartment. The Spruell needle was therefore used to guide an 18gauge 40mm needle into the dorsal compartment. This was then directed ventrally through the septum causing a cracking sound and allowed the introduction of fluid into the ventral compartment. Visualisation of this fluid and the needle within the TB allowed the identity of the TB in all three species to be confirmed. Manipulation of the mandible to open the mouth aided confirmation of the location of the TMJ and allowed it to be visualised in both closed and open positions.

The sonographic appearance of the air and fluid-filled external ear canal, air and fluid-filled TB, closed and open TMJ and surrounding structures were noted in all three species. Anatomical atlases (Crouch 1969, Barone and others 1973, Popesko 1977, Barone 1989, Popesko and others 1992, Evans 1993) in conjunction with the anatomical information and digital images obtained in Chapter 2, were used to aid in orientation of the images and identification of the structures visualized.

4.2.5. Additional Procedures

Ultrasound examination of the TB was repeated in live, unsedated animals. Two greyhounds with no history or clinical evidence of previous or current ear disease were examined in lateral and sternal recumbency using the 6.5MHz curvilinear transducer. Each TB was interrogated from a lateral and ventral approach and the sonographic appearance of the TB and the surrounding anatomy was noted. A rabbit that was presented to the University of Glasgow Small Animal Hospital with neurological signs was also examined. It was manually restrained in sternal recumbency and examined from a ventral approach using the 3cm and 5cm 12MHz linear transducers.

Figure 4.2. Ultrasound machines and transducers.



Figure 4.2.1. Powervision (Toshiba)



Figure 4.2.2. Diasus (Dynamic Imaging)

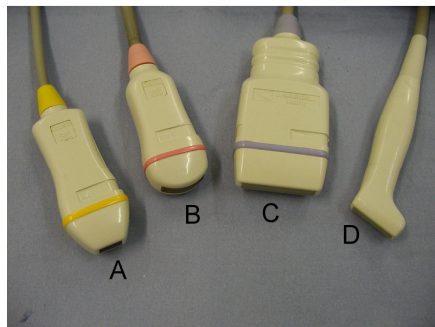


Figure 4.2.3. Toshiba transducers
A. 3.5 MHz phased array sector
B. 6.5 MHz curvilinear.
C. 12 MHz linear (5cm footprint).
D. 12 MHz linear (3cm footprint).

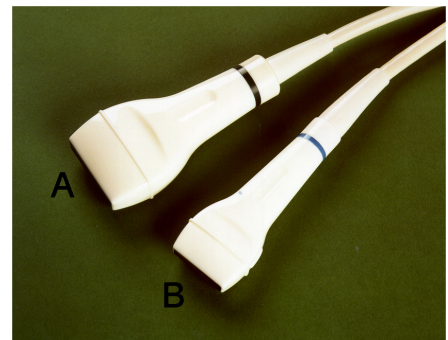


Figure 4.2.4. Diasus transducers
A. 8-16 MHz linear
B. 10-22 MHz linear

4.3. Results

4.3.1. Optimum equipment for imaging the TB

4.3.1.1 Imaging the canine TB

In canine cadavers, the 6.5MHz curvilinear transducer was considered to be the most appropriate for imaging the TB and associated structures. The size and shape of this transducer face made it easy to manipulate in the confined space of the region overlying the TB. In addition, this frequency produced good enough resolution images of the regional anatomy to aid in location of the TB while ensuring a sufficient depth of penetration for it to be adequately visualised. Problems with the other transducers included the poor near field image quality associated with the phased array sector and its low frequency that prevented adequate differentiation of relevant structures. The high frequency beam of the 12MHz transducers did not permit adequate penetration.

4.3.1.2 Imaging the feline TB

In the feline cadavers, the 3cm footprint 12MHz transducer was considered to be the most appropriate. The size of this transducer face made it easy to manipulate in the confined space of the region overlying the TB and its high frequency produced good resolution images that allowed differentiation of the relevant structures and aided in identification of the TB. The 3.5MHz phased array sector did not produce adequate resolution or near field image clarity to permit its identification. The area of contact with the skin surface required for the 5cm linear transducer resulted in a lack of manoeuvrability while the reduced near field image clarity and lower frequency of the 6.5MHz curvilinear produced suboptimal images of the relevant structures.

4.3.1.3. Imaging the rabbit TB

The 8 -16 MHz linear transducer and the 3cm 12 MHz linear transducer were deemed most appropriate for visualization of the TB in rabbit cadavers. The 10-22 MHz linear transducer did not produce adequate penetration to allow visualization of these structures while the resolution of the images produced using the 6.5 MHz curvilinear and 3.5MHz phased array sector transducers were not sufficient to allow their identification. Although the 5cm 12MHz linear transducer did allow imaging of the TB, it proved difficult to manoeuvre in the confined space.

4.3.2. Optimum transducer position for imaging the TB

4.3.2.1 Imaging the external ear canal

The external ear canal in the dog, cat and rabbit could be imaged with the transducer placed directly over it on the lateral aspect of the head. It could be examined in both long and short axis (Figure 4.3.1.1)

4.3.2.2. Imaging the TB

Two transducer positions were identified that identification of the TB. The lateral approach involved the transducer being moved ventrally from the external ear canal into a position between the caudal margin of the zygomatic arch and the wing of the atlas. This was most difficult to achieve in the rabbit due to its small size. The second position involved moving the transducer to a position ventral to the skull and directing the beam dorsally while applying moderate pressure (Figure 4.3.1.2.). This approach could be used with the transducer orientated in a longitudinal or transverse plane relative to the head or from a position midway between the two (rostralateral – caudomedial oblique). In the cat, these views were achieved by palpating the TB, placing the transducer over it and directing the beam dorsally. In the rabbit, this was achieved by placing the transducer immediately caudal to the angular process of the mandible and directing the beam accordingly. Although, the small size of the rabbit made this more difficult to achieve, with careful angulation of the beam, it was possible to image most of the TB without interference from the mastoid and jugular processes.

4.3.3. Sonographic appearance of the TB and associated structures

The skin, platysma muscle, subcutaneous fascia and fat could not be distinguished from each other and combined to form an echogenic band running across the near field of each image. This included the parotidoauricularis muscle in the rabbit.

4.3.3.1. External ear canal

Ultrasound images obtained from the external ear canal are demonstrated in Figure 4.3.2. In all three species, this appeared as a tubular structure being rectangular in long axis and oval shaped in short axis. The well-defined echogenic wall was hypoechoic relative to the adjacent tissue. The air-filled lumen was represented by a curved, central hyperechoic line that produced reverberation artefact obscuring the deeper structures. Adjacent structures visible in these views are indicated in the accompanying diagrams.

In the dog and cat, in short axis the hypoechoic mass of the temporal muscle was visible rostrally between the skin and the caudal portion of the zygomatic arch, which appeared as a hyperechoic interface with distal acoustic shadowing (Figure 4.3.2.1.). Caudally, a portion of the hypoechoic sternocephalicus muscle mass was visible between the skin and the surface of the squamous part of the temporal bone.

In the rabbit, the parotid salivary gland could not be distinguished from the surrounding fat and fascia but the styloauricular muscle could be identified rostral to the ear canal in the short axis images (Figure 4.3.2.3.). The external ear canal could be followed distally to its communication with the bony external acoustic meatus where the lumen became obscured by its bone wall (Figure 4.3.2.4.).

4.3.3.2. Lateral approach to the TB and adjacent structures

The images obtained from a lateral approach are demonstrated in Figure 4.3.3. In the dog, the TB was imaged from a lateral approach through the parotid salivary gland, which appeared as a mottled, hypoechoic, triangular shaped structure beneath the skin surface surrounded by more hyperechoic adipose tissue (Figure 4.3.3.1.). The wall of the TB nearest the transducer produced a hyperechoic convex interface and the gas contents produced either a dirty distal acoustic shadow or reverberation artefact obscuring the far and side walls of the TB, and structures deep to it.

The more ventral location of the external acoustic meatus in the cat meant that the gas-filled horizontal ear canal obscured most of the lateral aspect of the TB although a small section of the wall was visible caudally. Likewise, the TB in the rabbit could not be imaged from a lateral approach due to the presence of the bony external acoustic meatus dorsally and the thick lateral bone wall ventrally (Figure 4.3.3.2.). Further ventrally the mastoid process overlay the wall of the TB and the ramus of the mandible prevented rotation of the transducer to avoid these structures. The parotid salivary gland could still not be distinguished although the stylohyoid muscle could be identified running from the mastoid process in a ventral direction.

4.3.3.3. Ventral approach to the TB and adjacent structures

The images obtained from a ventral approach are demonstrated in Figures 4.3.4. to 4.3.6. The TB was visible from the ventral approach in all species. The bone wall produced a distinct convex hyperechoic interface with reverberation artefact or dirty shadowing obscuring the far wall and deeper structures. When imaged in short axis, the TB appeared

narrower in diameter and in the dog and rabbit had a more pointed profile than the cat, which remained rounded. The gas-filled horizontal ear canal extended from the lateral aspect of the TB in the cat and obscured deeper structures. In the rabbit, the smooth, curved bone wall of the TB and the angular shape of the mastoid process were easy to recognize in all of the ventral views. However, angulation of the beam allowed the majority of the TB to be imaged without interference from the mastoid and jugular processes. Occasionally in both feline and canine cadavers, collections of small, hypoechoic, nodular structures were identified that represented regional lymph nodes (Figure 4.3.4.1). Adjacent structures visible in these views are indicated in the figures.

4.3.3.4. Fluid-filled external ear canal

In all three species, fluid or KY jelly in the external ear canal appeared anechoic and distended the lumen. The echogenic walls remained visible but the far wall and deeper structures could also be visualised (Figure 4.3.2.2.). In the rabbit, the canal could be followed distally to its communication with the bony external acoustic meatus where the lumen became obscured by the acoustic shadowing produced by the walls even in the presence of KY jelly (Figure 4.3.2.5).

4.3.3.5. Fluid-filled TB

Prior to the introduction of fluid, when the tip of the needle was in contact with the TB wall nearest the transducer, it could be identified as a hyperechoic structure against the internal surface of the TB wall producing very localised reverberation artefact. If manipulated, the movement was detectable using real time imaging. However, when the tip was withdrawn from contact with the wall it was no longer visible.

After water or KY jelly was introduced into the canine TB, the lumen became visible as an anechoic, oval shaped region when viewed from all transducer positions, although this was easiest to achieve from the ventral approach (Figure 4.3.4.2.). The near wall of the TB still produced a convex hyperechoic interface but it was less distinct than that produced by the air-filled TB. The surface of the temporal bone that formed the far wall of the TB became visible as a concave hyperechoic interface and the beam was able to penetrate deep to it although no distinct structures could be identified. The shaft of the needle produced a hyperechoic line through the anechoic fluid. When suction was applied and the fluid aspirated, the far wall or septum, deep structures and needle were no longer identifiable and the appearance returned to that of the air-filled TB.

In the cat, the shape of the lumen and the septum when imaged from a ventral aspect varied with the orientation of the transducer. Imaging in long axis, the septum appeared as a slightly convex interface with the hypotympanum extending dorsally at the rostral and caudal ends, producing a broad, crescent shape to the lumen (Figure 4.3.5.2.). In short axis, the TB appeared more rounded and the septum was again visible, this time as a slightly concave interface with the lumen extending dorsally at its medial and lateral aspects (Figure 4.3.5.4.). Slight rostromedial – caudomedial angulation of the transducer allowed imaging midway between long and short axis, along the maximum length of the TB. A second, less distinct, convex, hyperechoic interface was visualised rostromedial to the undulating interface of the septum in this view that represented the wall of the horizontal ear canal (Figure 4.3.5.6.).

Fluid introduced only into the dorsal compartment of the feline TB could not be visualised using any of the transducer positions. Fluid within the ventral compartment could only be identified using a ventral approach. The ventral TB wall produced a finer and more clearly defined, convex hyperechoic interface than in the dog. The lumen produced an anechoic area outlining the shape of the hypotympanum and the septum bulla was visible beyond the fluid as a second convex, hyperechoic interface. No distinct structures were visible beyond the septum whether the dorsal compartment was gas or fluid-filled therefore the presence of fluid in the dorsal compartment of the feline TB could not be identified using ultrasound.

In the rabbit, the presence of KY jelly in the long axis views allowed the cranial aspect of the dorsal margin of the TB to be visualized as a concave hyperechoic interface with distal acoustic shadowing. The tympanic cavity appeared as an anechoic elongated oval shape. (Figure 4.3.6.2.). However, the caudal aspect of the lumen and dorsal wall were obscured by the well defined triangular acoustic shadow produced by the jugular process. In short axis, the medial aspect of the lumen and far wall were visible while the lateral half was obscured by the jugular process (Figure 4.3.6.4.). In the rostromedial – caudolateral oblique, the rostromedial aspect of the lumen and far wall were visualised while the caudolateral portions were obscured (Figure 4.3.6.6.). In some of the views, a convex hyperechoic line was visible running parallel with the ventral wall of the TB, which was thought to represent the bone rim at the internal margin of the external ear canal that projects a short distance into the TB lumen (Figure 4.3.6.7.).

The auditory ossicles were not identified in any of the views in any of the species.

Figure 4.3.1. Transducer positions for imaging the TB and associated structures in the dog, cat and rabbit.

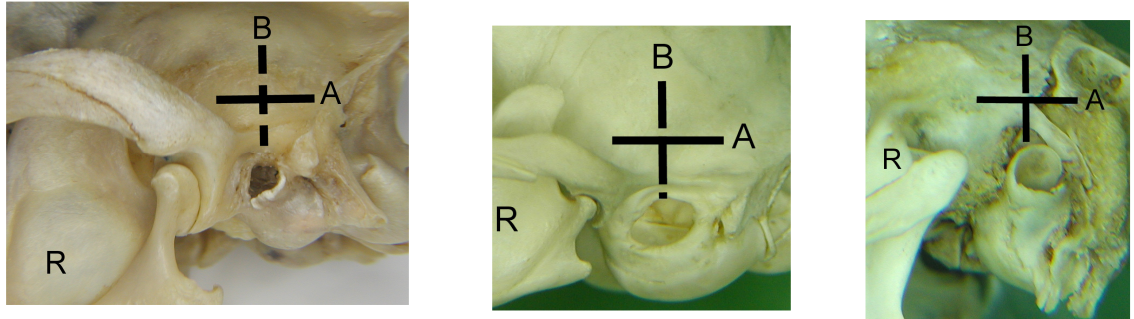


Figure 4.3.1.1. Lateral approach in the dog (left), cat (middle) and rabbit (right) for imaging the external ear canal. The transducer was orientated horizontally to produce a short axis view (A) and then rotated to a vertical position to produce a long axis view (B). Moving the transducer ventrally also allowed the TB to be examined from the lateral aspect. R = rostral.

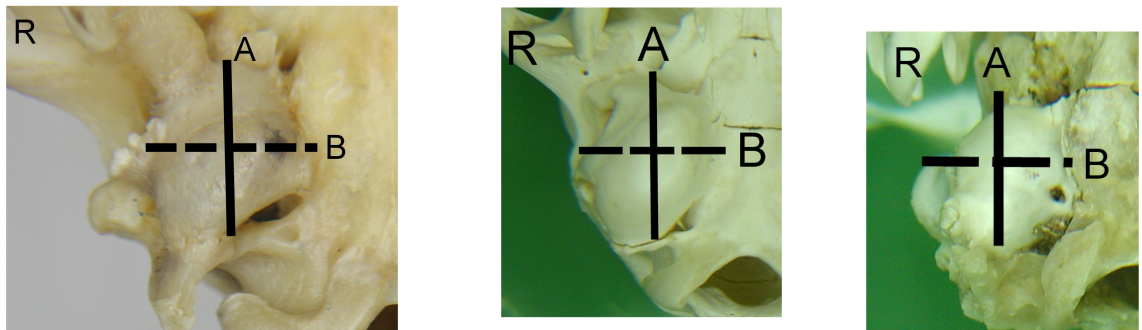


Figure 4.3.1.2. Ventral approach in the dog (left), cat (middle) and rabbit (right) for imaging the TB. The transducer was placed ventral to the skull and the beam directed dorsally. The transducer was orientated in a longitudinal (A), transverse (B) or an oblique plane between them relative to the long axis of the head. R = rostral.

<u>Label</u>	<u>Definition</u>
D	dorsal
V	ventral
R	rostral
Cd	caudal
L	lateral
M	medial
Black	acoustic shadowing deep to bone
Dark grey	fluid
Pale grey	reverberation artefact deep to gas
1	skin and subcutaneous fascia
2	external ear canal
3	zygomatic process of the temporal bone
4	temporal bone (squamous part)
5	temporalis muscle
6	sternocephalicus muscle
7	parotid salivary gland and fat
8	mastoid process
9	styloauricular muscle
10	external acoustic meatus
11	stylohyoid muscle
12	TB
13	paracondylar process
14	mandibular salivary gland
15	digastricus muscle
16	regional lymph nodes
17	far wall of TB (dog and rabbit) / septum (cat)
18	styloglossus muscle
19	sternomastoid muscle
20	longus coli muscle
21	basioccipital bone
22	horizontal ear canal
23	first cervical vertebra (C1/ atlas)
24	longissimus muscle of C1
25	inner margin of external acoustic meatus (rabbit)
*	hyoid bone
Diamond dotted line	fibrous band across digastricus muscle

The top of each image represents the transducer and the scale to the left indicates depth below the skin surface in millimetres.

Table 4.3.1. Key for anatomical features demonstrated in Figures 4.3.2. to 4.3.6. depicting the ultrasound appearance of the TB and associated structures in the dog, cat and rabbit.

Figure 4.3.2. Ultrasound appearance of the external ear canal in the dog and rabbit from a lateral approach with corresponding line diagrams. For key see Table 4.3.1

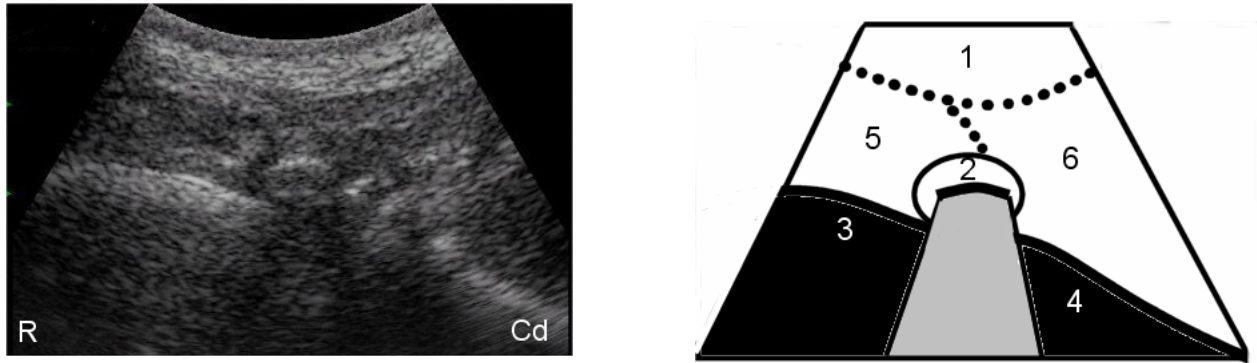


Figure 4.3.2.1. Dog. Lateral approach in a gas-filled external ear canal with the curvilinear transducer in a horizontal position.

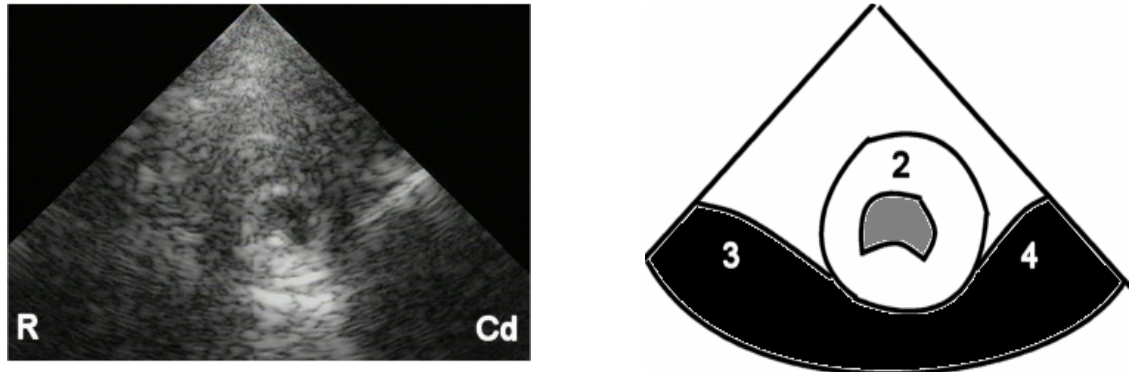


Figure 4.3.2.2. Dog. Lateral approach in a fluid-filled external ear canal with the sector transducer in a horizontal position.

Figure 4.3.2. continued. Ultrasound appearance of the external ear canal.

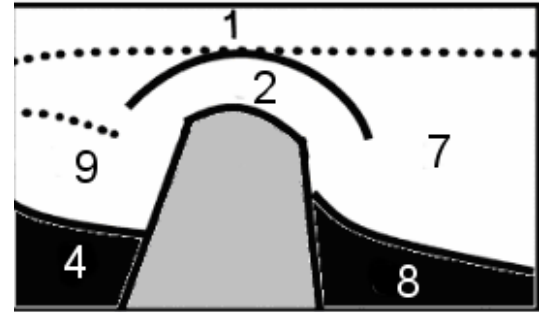
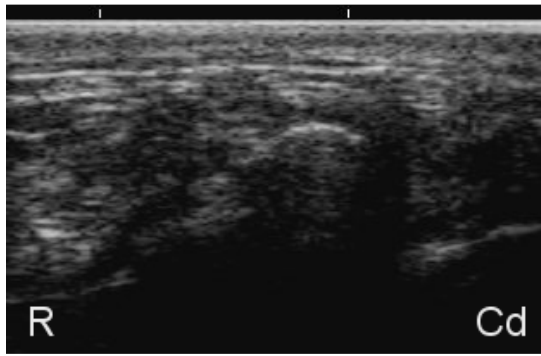


Figure 4.3.2.3. Rabbit. Lateral approach in a gas-filled external ear canal with the linear transducer in a horizontal position

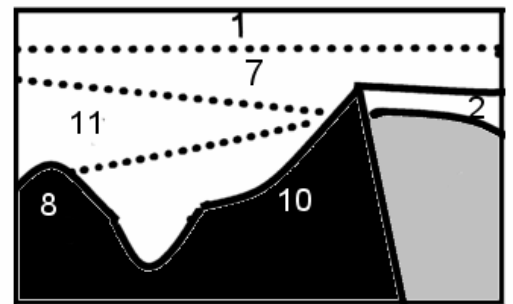
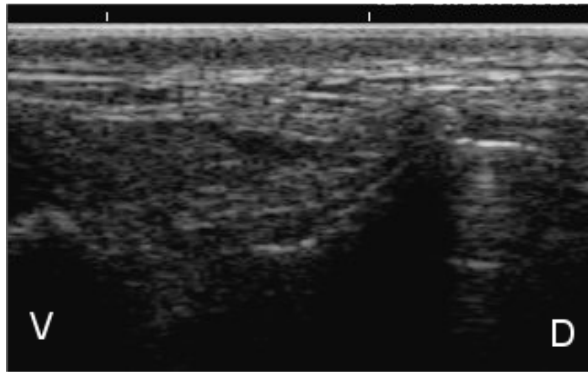


Figure 4.3.2.4. Rabbit. Lateral approach in a gas-filled external ear canal with the transducer in a vertical position.

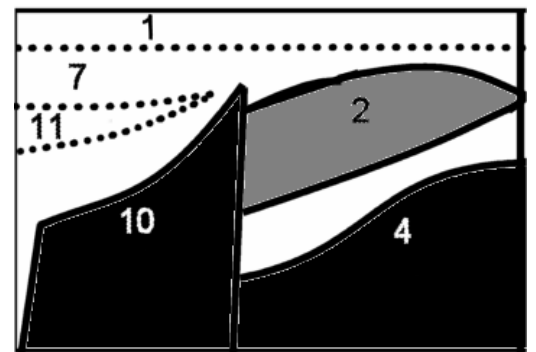
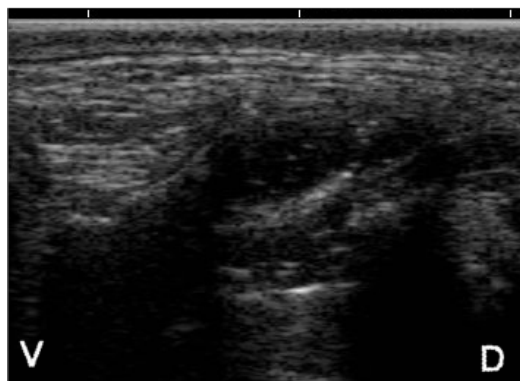


Figure 4.3.2.5. Rabbit. Lateral approach in a fluid-filled external ear canal with the transducer in a vertical position.

Figure 4.3.3. Ultrasound appearance of the gas-filled TB in the dog and rabbit from a lateral approach with corresponding line diagrams. For key see Table 4.3.1

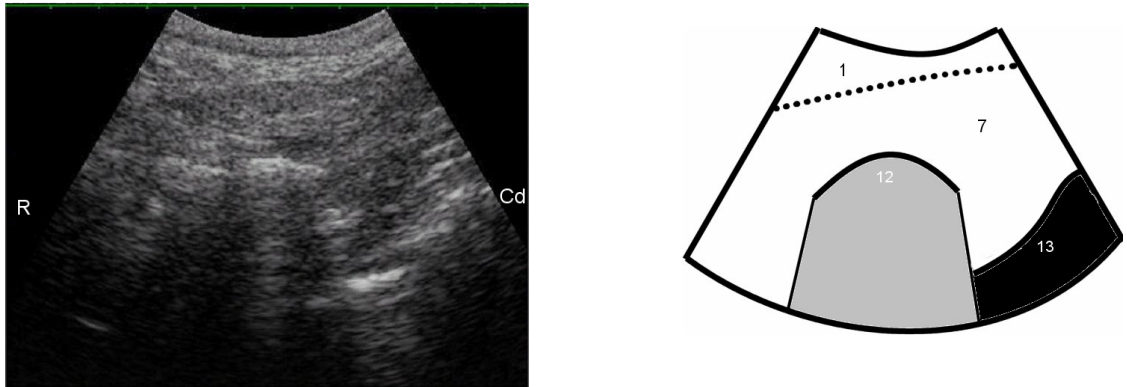


Figure 4.3.3.1. Dog. Lateral approach in a gas-filled TB with the transducer in a horizontal position

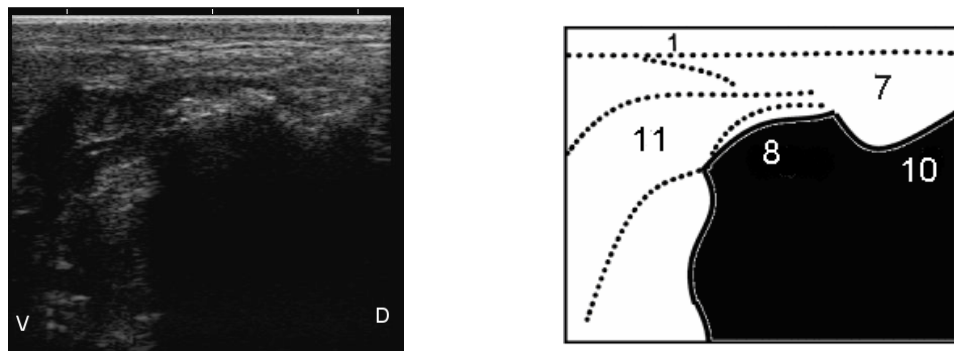


Figure 4.3.3.2. Rabbit. Lateral approach in a gas-filled TB with the transducer in vertical position.

Figure 4.3.4. Ultrasound appearance of the gas and fluid-filled TB from a ventral approach in the dog with corresponding line diagrams. For key see Table 4.3.1

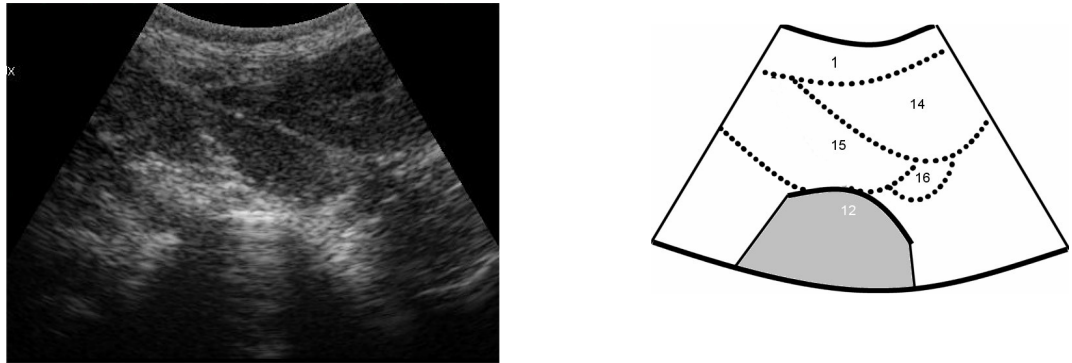


Figure 4.3.4.1. Dog. Ventral long axis approach in a gas-filled TB.

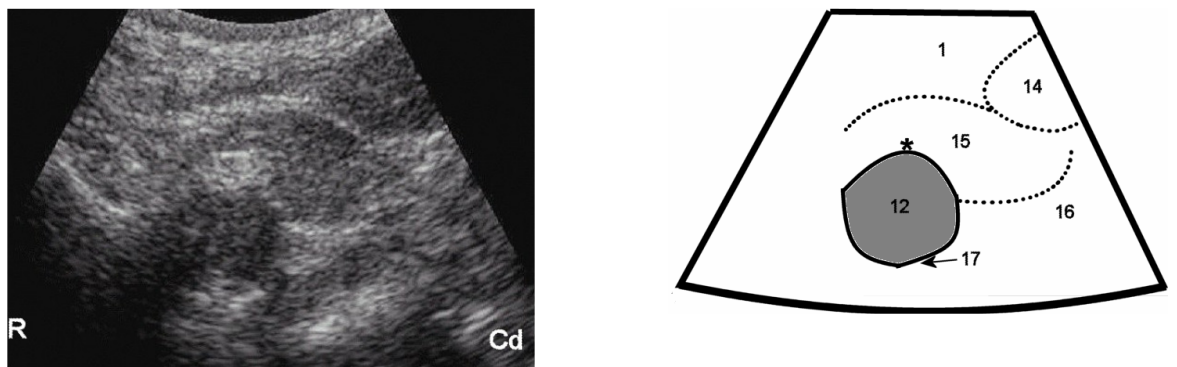


Figure 4.3.4.2. Dog. Ventral long axis approach in a fluid-filled TB.

Figure 4.3.5. Ultrasound appearance of the gas and fluid-filled TB from a ventral approach in the cat with corresponding line diagrams. For key see Table 4.3.1.

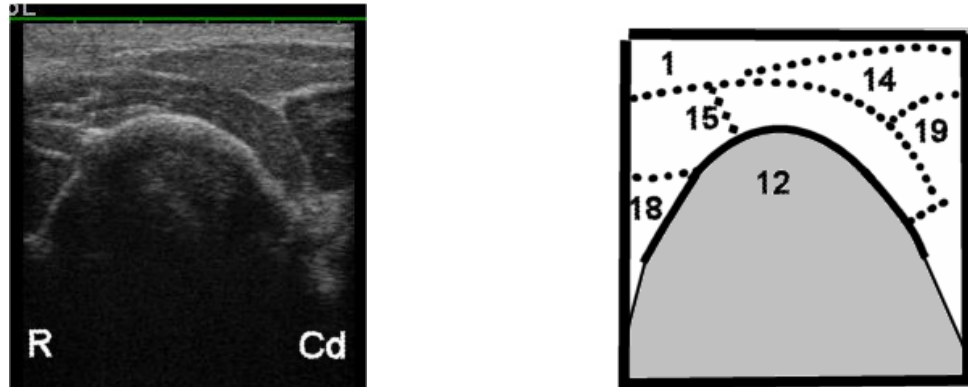


Figure 4.3.5.1. Cat. Ventral long axis approach in a gas-filled TB.

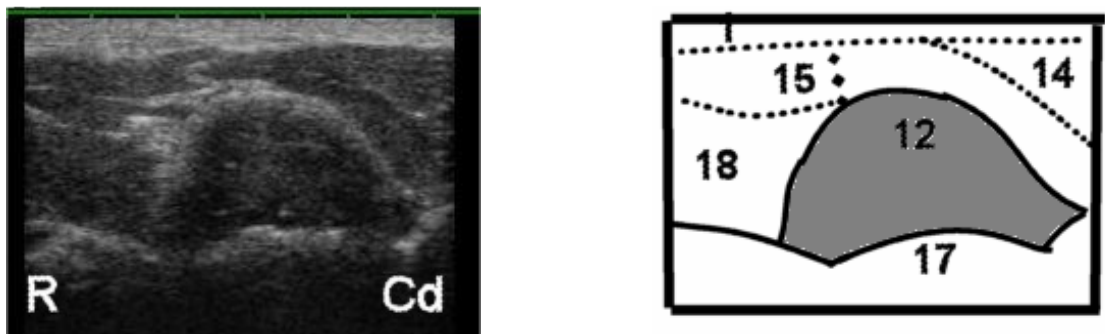


Figure 4.3.5.2. Cat. Ventral long axis approach in a fluid-filled TB.

Figure 4.3.5. continued. Ultrasound appearance of the gas and fluid-filled TB in the cat

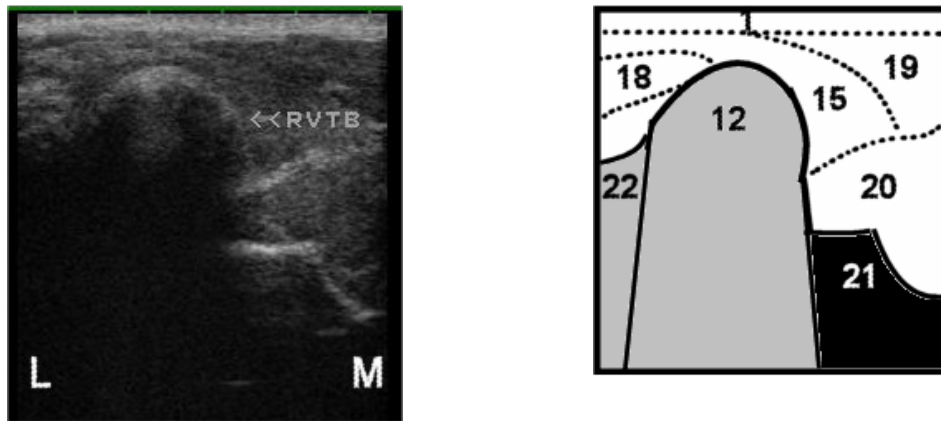


Figure 4.3.5.3. Cat. Ventral short axis approach in a gas-filled TB.
(RVTB = Ventral approach to right TB)

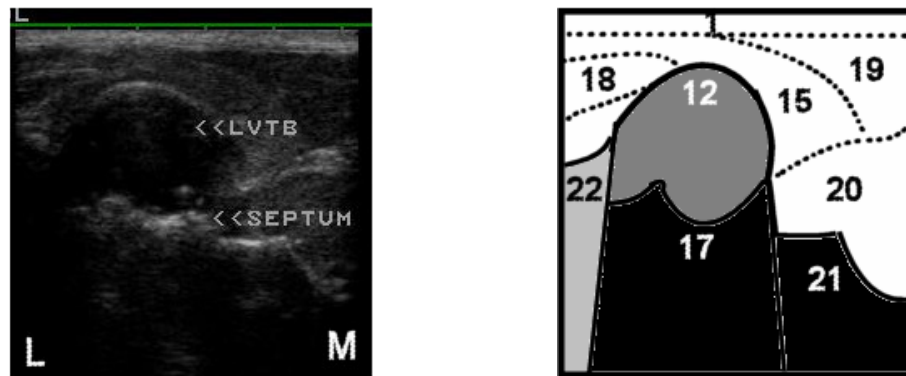


Figure 4.3.5.4. Cat. Ventral short axis approach in a fluid-filled TB.
(LVTB= Ventral approach to the left TB)

Figure 4.3.5. continued. Ultrasound appearance of the gas and fluid-filled TB in the cat

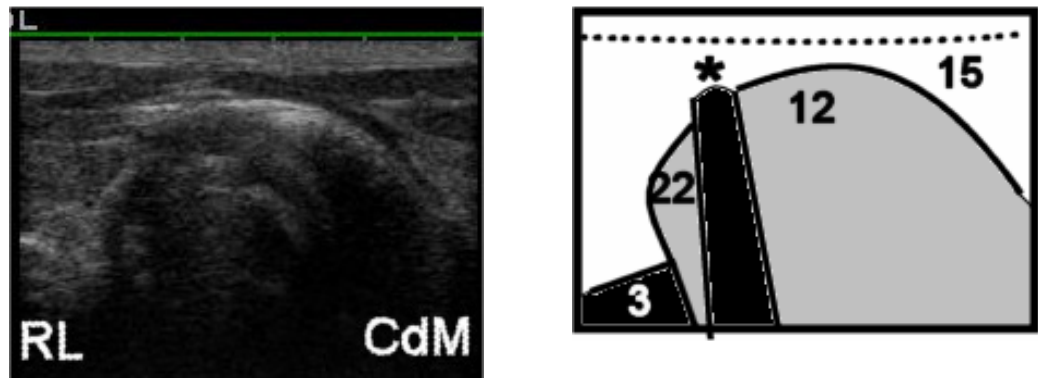


Figure 4.3.5.5. Cat. Ventral approach in a gas-filled TB with the transducer orientated in a rostralateral – caudomedial oblique direction.

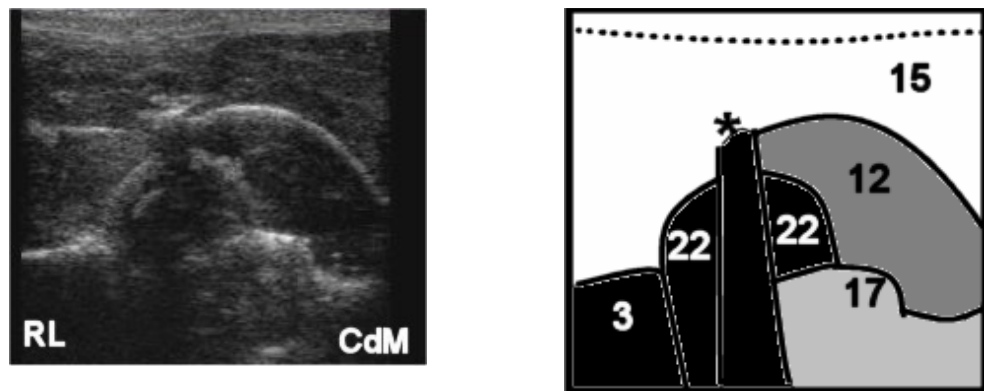


Figure 4.3.5.6. Cat. Ventral approach in a fluid-filled TB with the transducer orientated in a rostralateral – caudomedial oblique direction.

Figure 4.3.6. Ultrasound appearance of the gas and fluid-filled TB from a ventral approach in the rabbit with corresponding line diagrams. For key see Table 4.3.1

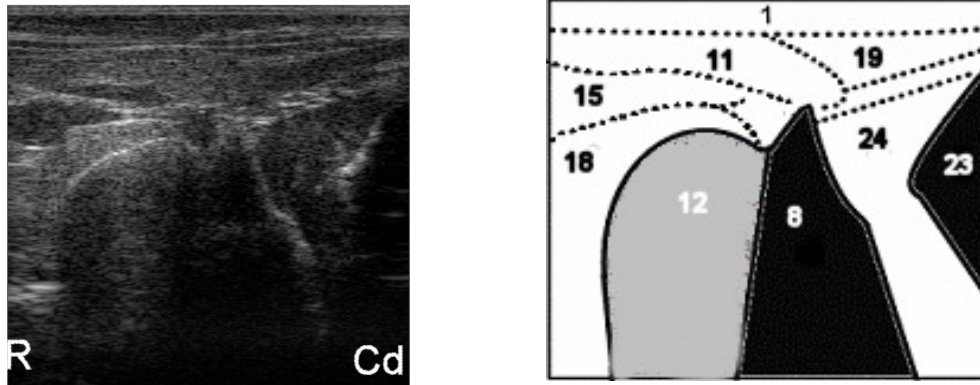


Figure 4.3.6.1. Rabbit. Ventral approach, long axis view of the gas-filled TB.

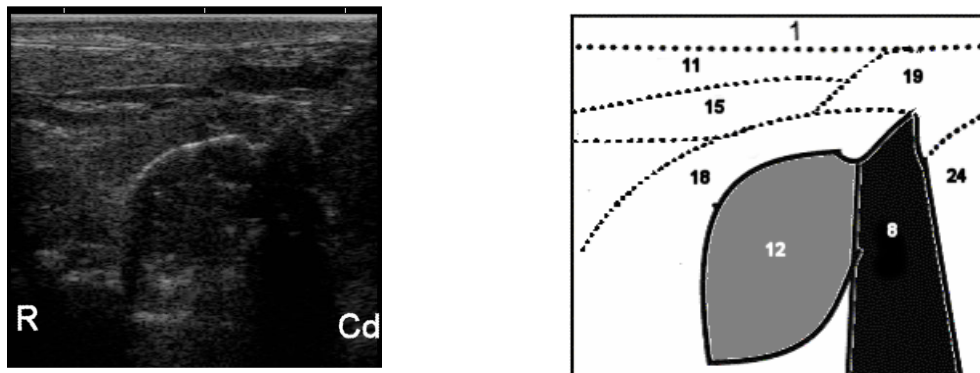


Figure 4.3.6.2. Rabbit. Ventral approach, long axis view of the fluid-filled TB.

Figure 4.3.6. continued. Ultrasound appearance of the gas and fluid-filled TB in the rabbit

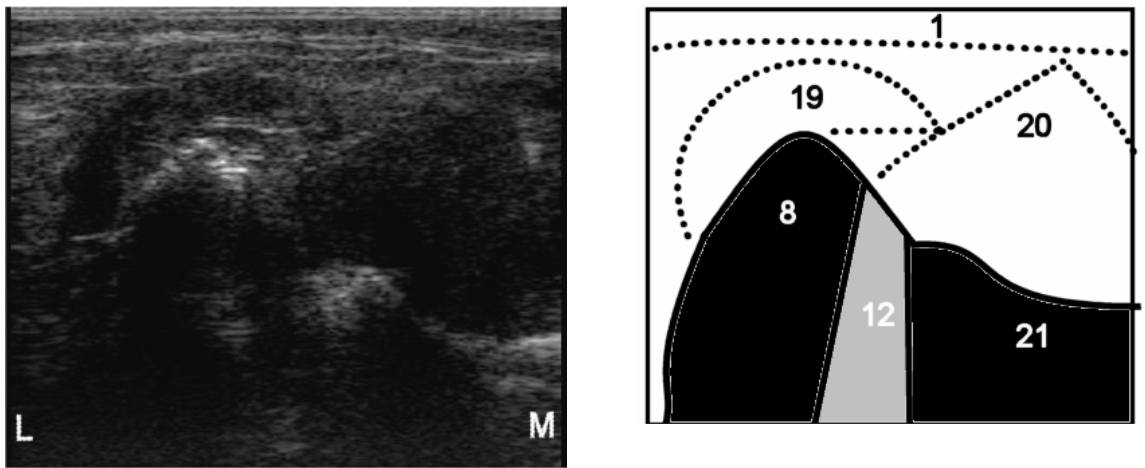


Figure 4.3.6.3. Rabbit. Ventral approach, short axis view of the gas-filled TB.

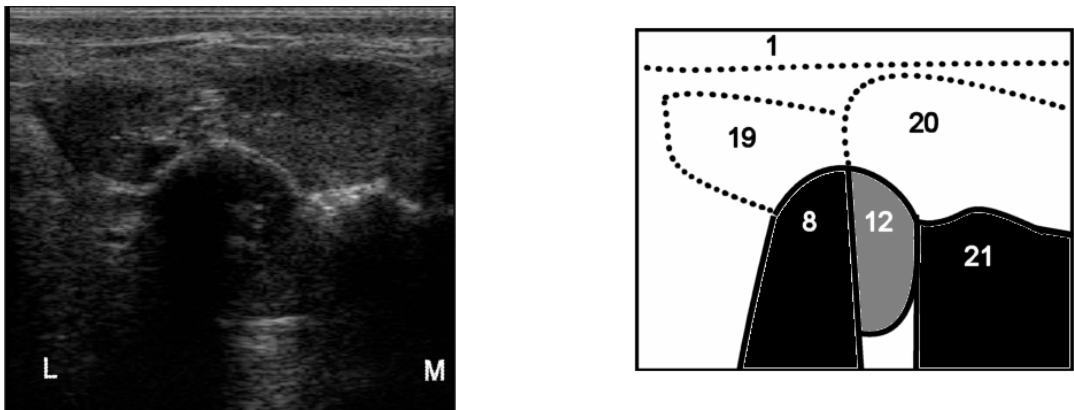


Figure 4.3.6.4.. Rabbit. Ventral approach, short axis view of the fluid-filled TB.

Figure 4.3.6. continued. Ultrasound appearance of the gas and fluid-filled TB in the rabbit

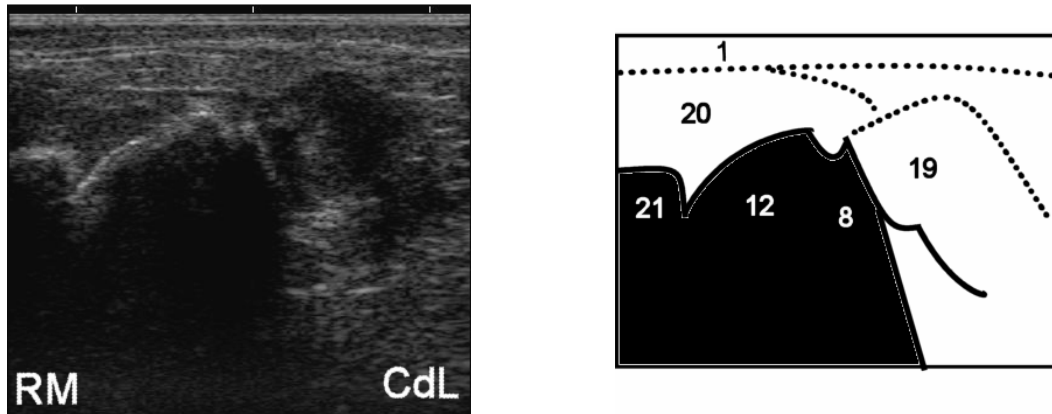


Figure 4.3.6.5. Rabbit. Ventral approach, rostromedial – caudolateral oblique view of the gas-filled TB.

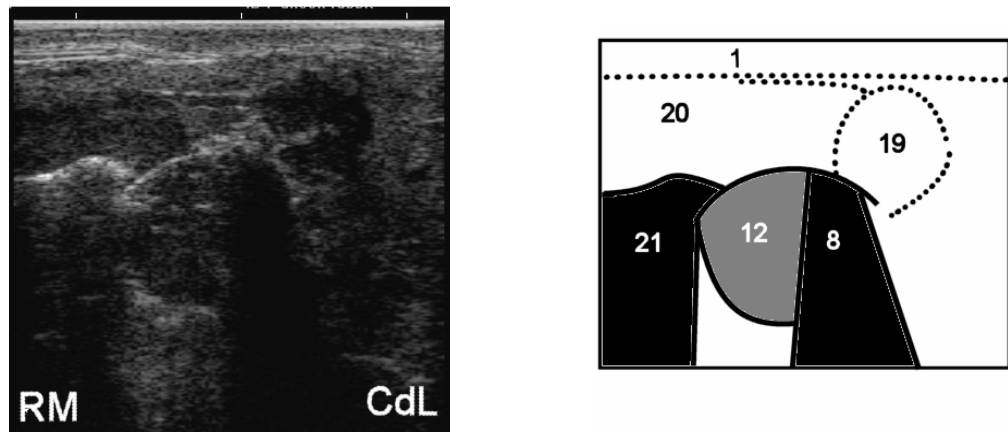


Figure 4.3.6.6. Rabbit. Ventral approach, rostromedial – caudolateral oblique view of the fluid-filled TB.

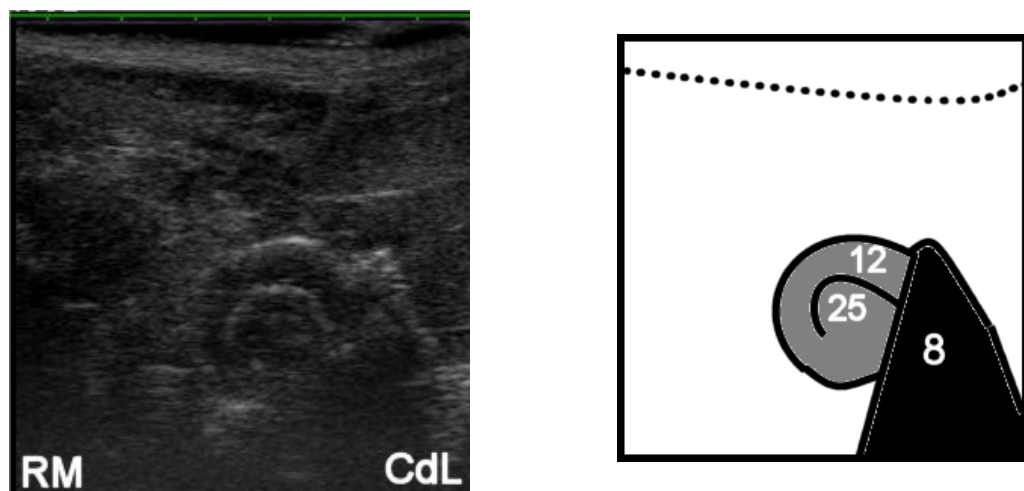


Figure 4.3.6.7. Rabbit. Ventral approach, oblique view of the fluid-filled TB demonstrating the convex interface of the inner margin of the external acoustic meatus.

4.3.4. Optimum equipment for imaging the TMJ

In all three species, both of the Powervision 12MHz linear transducers allowed the components of the TMJ to be identified. Although both produced comparable images, the 3cm one was easier to manipulate while the 5cm one produced a better overview of adjacent structures. This resulted in a complete examination of the TMJ in the cat being possible using the 3cm transducer while in the dog, a combination was more appropriate. The Diasus 8-16MHz linear transducer also provided optimal imaging of the TMJ in the rabbit. Neither the 6.5MHz curvilinear or 3.5Mhz phased array sector transducers produced adequate near field image quality or good enough resolution images to allow these small, superficial structures to be visualised in any species. The Diasus 10-22 MHz did not provide adequate depth of penetration in the rabbit.

4.3.5. Optimum transducer position for imaging the TMJ

4.3.5.1. Imaging in the dog and cat

In the dog and cat, the components of the TMJ could be imaged from lateral, caudal and rostral approaches. The lateral approach involved placing the transducer over the lateral aspect of the TMJ with the transducer orientated in a caudodorsal – rostroventral direction (Figure 4.3.7.1.). From here it was rotated to a vertical orientation. Repositioning the transducer over the lateral aspect of the mandibular fossa in a horizontal orientation. and then moving it ventrally allowed the TMJ to be imaged at different levels.

The caudal approach involved placing the transducer in a vertical position between the external ear canal and the caudal aspect of the zygomatic arch, and directing the beam rostromedially (Figure 4.3.7.2.). From here it was then moved progressively in a lateral direction to allow visualization of different areas of the condyloid process, mandibular fossa and retroarticular process.

The location of the zygomatic arch in the dog and cat prevented a true rostral transducer position being obtained. However, the TMJ could be visualized by placing the transducer as far rostral as possible and in a rostrodorsal – caudoventral orientation parallel with and just ventral to the zygomatic arch, although some pressure on the transducer was required to maintain this position. The beam was then directed caudomedially (Figure 4.3.7.3.). As the transducer was moved ventrally, lateral movement was necessary to continue to image the articular components of the TMJ, although care had to be taken to maintain the rostrocaudal angulation and not inadvertently allow the transducer to rotate into a true lateral position and therefore produce images similar to the lateral rotational series. This

was particularly the case with the cat due to its wide zygomatic arch that restricted movement rostral to the TMJ. Opening the mouth also rotated the transducer into a lateral position due to the ventral movement of the coronoid process of the mandible pushing the transducer.

4.3.5.2. Imaging in the rabbit

In the rabbit, a dorsal approach was used that involved placing the transducer on the dorsolateral aspect of the head, caudal to the orbit with the beam directed ventrally in either long or short axis relative to the head (Figure 4.3.7.4.). A rostral approach was also attempted in this species by placing the transducer rostral to the level of the mandibular fossa in short axis relative to the skull and angling the beam in a caudoventral direction (Figure 3.3.2.1.5).

4.3.6. Sonographic appearance of the TMJ

4.3.6.1. Lateral approach in the dog and cat

This approach allowed the lateral margins of the mandibular fossa, condyloid process and retroarticular process and the lateral aspect of the TMJ space to be visualised. The images obtained are demonstrated in Figures 4.3.8 and 4.3.9.

4.3.6.1.1 . Vertical transducer orientations

With the mouth closed and the transducer orientated in a caudodorsal – rostroventral direction, the lateral aspect of the caudal part of the mandibular fossa and the mid part of the condyloid process were interrogated. In this view, the beam was aligned with the condyloid crest of the mandible that was visible as a distinct hyperechoic interface running at an oblique angle across the image and producing acoustic shadowing (Figure 4.3.8.1.). In the dog it was concave but was shallower in the cat (Figure 4.3.8.2.). The masseter muscle was visible in both species as a hypoechoic structure located between the condyloid crest and the superficial fascia. The crest terminated proximally at the lateral edge of the articular surface of the condyloid process and this termination was rounded in the dog but abrupt in the cat. In the dog, a second, less distinct, convex, hyperechoic interface was present proximal to the edge of the condyloid process representing the caudal region of the small non-articular area at the lateral aspect of the dorsal surface of the condyloid process. The lateral edge of the zygomatic process of the temporal bone was visible in both species as a curved hyperechoic interface and in the dog, the tubercle at the lateral edge of the mandibular fossa produced a rounded area. The ventral aspect of the zygomatic process of the temporal bone that accommodates the caudal section of the articular surface of the

mandibular fossa fell abruptly away from the transducer into the far field of the image. The wedge shaped gap between this interface and the condyloid process represented the lateral aspect of the mid portion of the TMJ. Echogenic structures were visualised within this area representing the lateral components of the joint capsule but the intra-articular disc could not be specifically identified. The rounded protrusions associated with the lateral aspect of the condyloid process and mandibular fossa were absent in the cat so the margins on either side of the TMJ appeared much flatter and the lateral aspect of the joint narrower, so less of it was visible. Alignment of the transducer with the condyloid process in this view made it easy to recognise and then follow to the TMJ space, making this is a useful reference view to locate the TMJ at the start of an examination.

Keeping the transducer aligned with the same region of the mandibular fossa and opening the mouth resulted in the condyloid crest moving out of the image and a more caudal area of the lateral aspect of the condyloid process being visualised, producing a more rounded outline in both species (Figures 4.3.8.3. and 4.3.8.4.). The appearance of the TMJ itself did not alter noticeably in the cat and remained poorly visualised but in the dog, it became wider and more clearly visible. Opening the mouth resulted in the edge of the parotid salivary gland becoming visible as a heterogenous structure overlying the caudal aspect of the zygomatic arch in some of the images.

From this caudodorsal – rostroventral reference view, the transducer was rotated to a vertical position allowing the lateral aspect of the rostral section of the mandibular fossa and the dorsal section of the condyloid process to be visualised. With the mouth closed, in both species the zygomatic process of the temporal bone was visible as a curved hyperechoic structure and in the dog, the tubercle at the lateral margin of the mandibular fossa produced a rounded protrusion (Figures 4.3.8.5. and 4.3.8.6.). In both species, the rostral articular surface of the mandibular fossa on its ventral surface fell abruptly away from the transducer into the far field of the image, although this was more gradual than in the previous view. More of the mandibular fossa was visible in the dog than the cat. In the dog, the lateral extremity of the condyloid process produced two distinct hyperechoic bumps representing the edges of the articular and non-articular sections. The lateral aspect of the dorsal section of the TMJ appeared as broad, wedge shaped region between the mandibular fossa and condyloid process. In the cat, the lateral extremity of the dorsal articular surface of the condyloid process ended abruptly giving the TMJ a narrower triangular shape than in the dog. Ventral to the articular surface, the lateral margin of the condyloid process appeared rounded in the dog and flattened in the cat reflecting species

differences in the profile of this structure. The masseter muscle was again visible occupying the area distal to the TMJ but only a very short section of the condyloid crest was visible immediately distal to the condyloid process.

Keeping the transducer aligned with the same region of the mandibular fossa and opening the mouth resulted in the condyloid crest moving back into the image (Figures 4.3.8.7. and 4.3.8.8.). As before, this appeared as a distinct, mildly concave hyperechoic interface with a rounded end at the lateral aspect of the condyloid process in the dog and a shallower structure with an abrupt termination in the cat. The lateral margin of the condyloid process moved in a ventral direction causing a slight increase in the distance between the condyloid process and the mandibular fossa so the lateral aspect of the TMJ appeared as a broader wedge than with the mouth closed in both species although the TMJ space was still more clearly visualised in the dog.

4.3.6.1.2. Horizontal transducer orientations

Still using a lateral approach, the transducer was rotated to a horizontal orientation and moved dorsally to a position overlying the mandibular fossa on the ventral aspect of the zygomatic process of the temporal bone. In the dog, the tubercle on the lateral aspect of the mandibular fossa prevented the beam being directed along the mandibular fossa but its absence made this possible in the cat (Figure 4.3.9.1.). The condyloid process was well enclosed by the mandibular fossa in this species resulting in the lateral extremity of the condyloid process appearing as a hyperechoic focus in the centre of the image with the lateral margins of rostral and caudal sections of the mandibular fossa appearing as hyperechoic structures on either side of it. The rostral interface represented the articular process of the mandibular fossa.

Moving the transducer ventrally while still in a horizontal orientation allowed the curved lateral margin of the caudal articular surface of the condyloid process to be visualised in both species (Figure 4.3.9.2.). In the dog, the lateral protrusion of the condyloid process produced a more angular interface than in the cat but in both species the rostral non-articular surface of the condyloid process fell away from the transducer to form an arc shape. Immediately caudal to the condyloid process was the hyperechoic structure representing the lateral margin of the retroarticular process, and this was rounded in the dog but appeared more angular in the cat. The TMJ space was visualised as a thin wedge between the two structures. The open nature of the lateral aspect of the canine TMJ resulted in a reasonable amount of the joint being visualised but the close fit of the

condyloid process and the retroarticular process in the cat meant it was visible only as a narrow opening between the adjacent bone interfaces.

In more ventral locations, the condyloid crest of the mandible became responsible for the well-defined rostral hyperechoic interface rather than the condyloid process. It obscured the medial aspect of the condyloid process located beyond it and the lateral aspect of the TMJ. However, the lateral margin of the retroarticular process was still visible as a less well-defined pointed, hyperechoic structure immediately caudal to it. The condyloid process and retroarticular process in the cat were imaged at approximately the same distance from the transducer until the tip of the retroarticular process was reached when the condyloid crest appeared slightly closer to the transducer. However, in the dog, the retroarticular process was located further from the transducer at all levels. This again reflected the more enclosed nature of the feline TMJ relative to the more open canine one.

Throughout these views in both species, the masseteric fossa on the lateral aspect of the ramus of the mandible was visible as a hyperechoic interface rostral to the TMJ. The masseter muscle was identified as a hypoechoic structure between this and the skin with several hyperechoic lines representing the fibrous interfaces between its various bellies. Caudal to the TMJ, the parotid salivary gland was occasionally identified as a heterogenous, slightly hyperechoic structure under the skin. Part of the superficial masseter muscle was imaged in this region and the smaller deeper mandibuloauricularis muscle was also occasionally identified.

When the mouth was opened, the condyloid process moved rostrally and there was a slight increase in the distance between it and the margins of the mandibular fossa and retroarticular process increasing the width of the TMJ (Figure 4.3.9.3.). Moving ventrally, different areas of the condyloid process and retroarticular process were visualised but the appearance of the TMJ did not alter noticeably in either species with it remaining better visualised in the dog than in the cat. It was possible to obtain images at a greater number of locations from proximal to distal in the dog due to its larger size as reflected by the larger number of canine images in Figure 4.3.9.3. than feline ones.

4.3.6.2. Caudal approach in the dog and cat

The images obtained are demonstrated in Figure 4.3.10. From the caudal approach, with the transducer orientated as near to vertical as possible and the beam angled rostromedially, the caudal aspect of the retroarticular process could be visualised in the dog

and cat (Figure 4.3.10.1. and 4.3.10.2.). It appeared as smooth, convex hyperechoic interface continuous with the caudal aspect of the zygomatic arch that curving ventrally away from the transducer into the far field of the image. The angular process of the ipsilateral mandible appeared as a distinct, irregular, hyperechoic structure projecting into the soft tissue ventral to the retroarticular process in both species. The mandibuloauricularis muscle appearing as an echogenic area separating the angular process and the retroarticular process in the cat. The masseter muscle was visible in the regions ventral to the angular process and also dorsal to the retroarticular process. The parotid salivary gland and the masseter / mandibuloauricularis muscle were located between it and the skin in the both species.

When the TMJ was opened, the angular process moved across the image in a dorsal direction to become located between the transducer and the ventral aspect of the retroarticular process in the dog (Figure 4.3.10.3.). It also became more triangular in outline as it was imaged from a more ventral angle. In the cat it completely overlay the retroarticular process and obscured it from view.

In the dog, directing the beam progressively in a lateral direction allowed visualisation of the caudal aspect of the lateral articular surface of the condyloid process and mandibular fossa, between which the caudal aspect of the TMJ appeared as a wedge shaped area (Figure 4.3.10.4.). The mandibular fossa remained similar in appearance throughout this series but the condyloid process varied. When the transducer was aligned with the caudal aspect of the neck of the condyle, this was visible as an elongated hyperechoic interface extending ventrally from the condyloid process. As the beam moved laterally off the neck, the condyloid process progressed from an elongated through an oval to a round outline until the lateral extremity was imaged as an angular interface. Opening resulted in the area caudal to the articular surface of the condyloid process being visualised and the TMJ was reduced in width.

In the cat, the enclosed nature of the TMJ and the small size of its components meant that movement of the transducer away from the retroarticular process in lateral direction did not result in good visualisation of the TMJ space (Figure 4.3.10.5.) Opening the mouth however, allowed the TMJ to be more readily identified although the joint components were still not clearly visible. Mild alteration of the angle of the transducer by movement of the distal end medially allowed the neck of the condyle to be followed down to the level of the angular process.

4.3.6.3. Rostral approach in the dog and cat

The images obtained are demonstrated in Figure 4.3.11. From a rostral approach, with the transducer located immediately ventral to the zygomatic arch and in a rostradorsal – caudoventral orientation, the rostral margin of the lateral part of the mandibular fossa and the tubercle at the lateral margin of the mandibular fossa could be visualised in the dog as a slightly convex, hyperechoic interface (Figure 4.3.11.1.). The surrounding muscle represented the masseter muscle with several hyperechoic tendinous interfaces present within it. Since the transducer was overlying the mandibular fossa, the appearance of these structures did not alter significantly when the mouth was opened. Movement of the transducer in a ventral direction allowed the beam to be directed into the lateral area of the dorsal component of the TMJ space (Figure 4.3.11.2.). The articular surface of the condyloid process appeared as an irregular hyperechoic interface in the far field of the image and the echogenic, soft tissue components of the joint visible were visible between this and the transducer, with a depth of approximately 3.47mm. Again, opening the mouth in this position did not significantly alter the image.

Movement of the transducer in a true ventral direction resulted in the beam moving off the dorsal components of the TMJ and interrogating the non-articular rostral areas of the condyloid crest and masseteric fossa. However, slight rotation of the transducer in a lateral direction allowed the space between the condyloid process and the retroarticular process to be visualised and the soft tissue components of the joint appeared as echogenic structures (Figure 4.3.11.3.).

The wide zygomatic arch in the cat and the smaller size of the skull prevented placement of the transducer as far rostral as was achieved in the dog. The absence of the tubercle at the lateral aspect of the mandibular fossa resulted in an undulating interface in the cat representing an oblique view across the lateral aspect of the mandibular fossa (Figure 4.3.11.4.). As with the dog, the surrounding muscle represented the masseter muscle with several hyperechoic tendinous interfaces present within it.

Ventral movement of the transducer did not allow the TMJ space to be identified as in the dog due to small size of the components and the enclosed nature of the TMJ in the cat preventing the beam entering the TMJ space. Instead, the lateral extremity of the condyloid process was visible as a hyperechoic focus with hyperechoic interfaces on either side representing the rostral and caudal edges of the mandibular fossa, the latter being at the base of the retroarticular process (Figure 4.3.11.5.). When the mouth was opened, the

hyperechoic interface produced by the lateral extremity of the condyloid process was rotated out of the view but the mandibular fossa was still visible (Figure 4.3.11.6.). No soft tissue components of the joint were visible.

4.3.6.4 Dorsal approach in the rabbit

The images obtained in the rabbit are demonstrated in Figure 4.3.12. From a dorsal approach with the transducer parallel with the long axis of the head and the beam directed ventrally and slightly rostrally, the dorsal surface of the mandibular fossa could be identified as a curved, convex, hyperechoic interface caudal to the eye (Figure 4.3.12.1.). The acoustic shadow it produced obscured the rostral part of the articular surface of the condyloid process. However the rest of the dorsal surface of the condyloid process was visible extending caudal to it. The caudal section of the articular surface of the condyloid process produced a distinctive hyperechoic interface while the tapering non-articular section caudal to it was much narrower and therefore less well-defined. The surface of the temporal bone was visible in the far field of the image caudal to both these structures.

Retropulsion of the mandible resulted in the rostral articular section being located caudal to the mandibular fossa and therefore visible free from its acoustic shadow. It produced a distinctive curved hyperechoic interface (Figure 4.3.12.2.). Opening the mandible resulted in the rostral section of the articular surface of the condyloid process being visible as a distinctive curved hyperechoic structure rostral to the mandibular fossa (Figure 4.3.12.3.). The caudal section of the articular surface moved beneath the mandibular fossa and therefore was obscured from view. The caudal non-articular section of the dorsal aspect of the condyloid process remained visible caudal to the mandibular fossa but moved rostrally and ventrally. It did not produce as distinctive an interface as the articular sections. Opening and closing the mouth allowed the movement of the condyle relative to the mandibular fossa to be assessed.

From a dorsal approach but with the transducer orientated in short axis relative to the head and placed at the caudal margin of the condyloid process, the dorsal edge appeared as a narrow, angular shaped hyperechoic interface with distal acoustic shadowing (Figure 4.3.12.4). Only a small section of the condyloid process was visualised at a time and the area being interrogated altered as the transducer was moved cranially and the mouth was opened and closed (Figure 4.3.12.5.). Lateral to the condyloid process, the caudal extension of the temporal process of the zygomatic bone was also visible as a narrow hyperechoic interface with acoustic shadowing.

With the transducer placed in a position rostral to the TMJ and immediately caudal to the eye, and the beam angled caudoventrally, the rostral aspect of the condyloid process was visualised when the mouth was open. However, there were no distinctive features visible from this approach to allow orientation of the image. The structures associated with the joint space were not well defined and the intra-articular disc was not visible therefore this approach was deemed not to be of any additional benefit.

4.3.7. Additional procedures

Examination of the TB in two live dogs and a rabbit was possible without the need for sedation. Extension of the head and neck was necessary to allow positioning of the transducer in both lateral and ventral positions. The canine TB could be imaged from both the lateral and ventral positions using the 6.5 MHz transducer but the ventral approach produced more consistent images. The TB in the rabbit could be imaged from the ventral approach using both 12 MHz transducer but the smaller footprint of the 3cm one was easier to position in the confined space. The sonographic appearance of the normal canine air-filled TB and the surrounding structures were the same as that described in the cadavers. The appearance in the rabbit was also the same as that produced by the air-filled TB in the cadavers and therefore the TB were considered to be normal.

Figure 4.3.7. Transducer positions for imaging the TMJ in the dog, cat and rabbit.

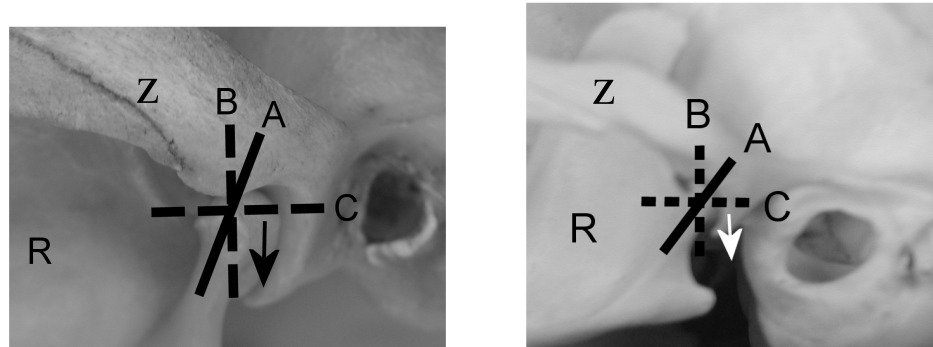


Figure 4.3.7.1. Lateral approach in the dog (left) and cat (right). The transducer was orientated in a caudodorsal – rostroventral direction (A) then rotated to vertical (B) and horizontal orientations (C) followed by movement ventrally (arrow) allowing imaging of the joint components at a series of different levels. Z=zygomatic arch. R = rostral.

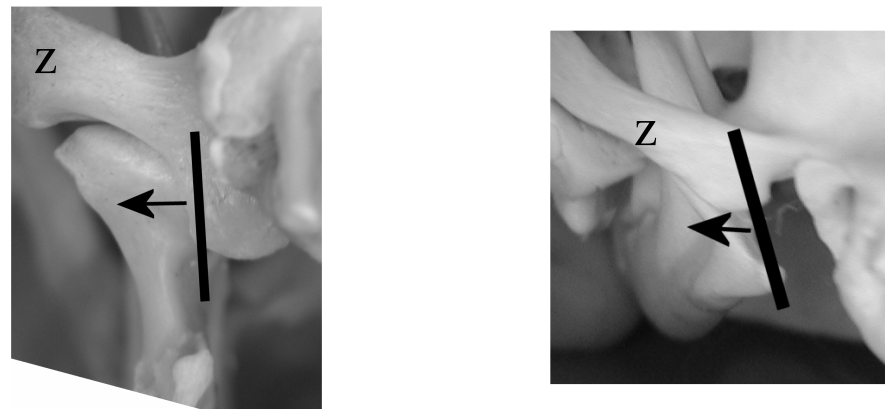


Figure 4.3.7.2. Caudal approach in the dog (left) and cat (right). The transducer was positioned vertically between the external ear canal and the caudal aspect of the zygomatic arch with the beam directed rostromedially (line), then moved progressively in a lateral direction (arrow). Z=zygomatic arch. Dorsal = top

Figure 4.3.7. continued. Transducer positions for imaging the TMJ

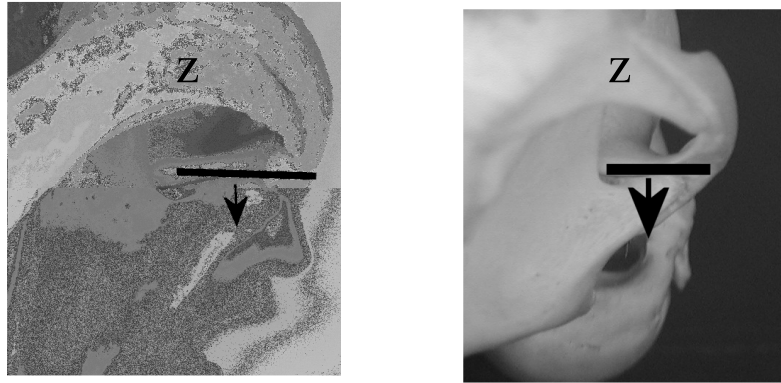


Figure 4.3.7.3. Rostral approach in the dog (left) and cat (right). The transducer was placed rostral to the TMJ, parallel with and just ventral to the zygomatic arch in a rostrodorsal – caudoventral orientation and the beam directed caudomedially (solid line). Moving the transducer ventrally (arrow) allowed imaging of the joint components at a series of different levels. Z=zygomatic arch. Dorsal = top.

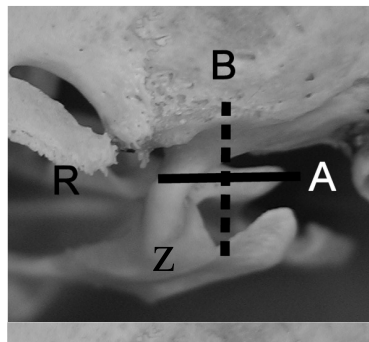


Figure 4.3.7.4.
Dorsal approach in the rabbit. The transducer was placed on the dorsolateral aspect of the head, caudal to the orbit and the beam directed ventrally in either long (A) or short axis (B) relative to the head. Z=zygomatic arch. R = rostral.



Figure 4.3.7.5.
Rostral approach in the rabbit. The transducer was placed rostral to the level of the mandibular fossa in short axis relative to the skull and the beam angled in a caudoventral direction. Z=zygomatic arch. R = rostral.

<u>Label</u>	<u>Definition</u>
D	dorsal
V	ventral
R	rostral
Cd	caudal
M	medial
L	lateral
Black	acoustic shadowing deep to bone
Dark grey	fluid (eye)
White arrows	focal zone of the beam.
*	temporomandibular joint space
1	skin and subcutaneous fascia
2	lateral aspect of mandibular fossa
3	condyloid process of mandible
4	crest of condyloid process
5	masseter muscle
6	temporal muscle
7	lateral aspect of zygomatic process of temporal bone
8	combination of parotid salivary gland, superficial masseter muscle and mandibuloauricularis muscle
9	masseteric fossa of the mandible
10	retroarticular process
11	angular process of mandible
12	neck of the condyloid process
13	temporal bone
14	eye
15	temporal muscle - superficial part (rabbit)
16	caudal extension of the temporal process of the zygomatic bone

The top of each image represents the transducer and the scale to the left indicates depth below the skin surface in millimetres.

Table 4.3.2. Key for anatomical features demonstrated in Figures 4.3.8. to 4.3.12. depicting the ultrasound appearance of the TMJ and associated structures in the dog, cat and rabbit.

Figure 4.3.8. Ultrasound appearance of the TMJ in the dog and cat from a lateral approach and vertical transducer orientations with corresponding line diagrams. For key see Table 4.3.2.

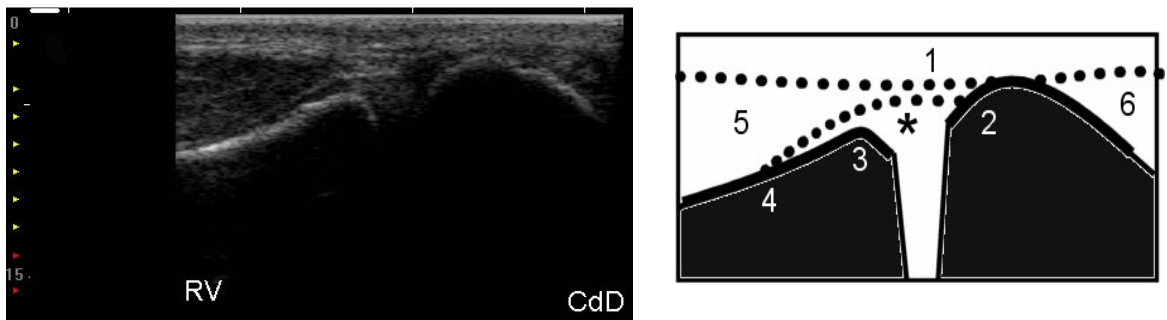


Figure 4.3.8.1. Dog. Lateral approach with the transducer in a caudodorsal – rostroventral orientation and the mouth closed.

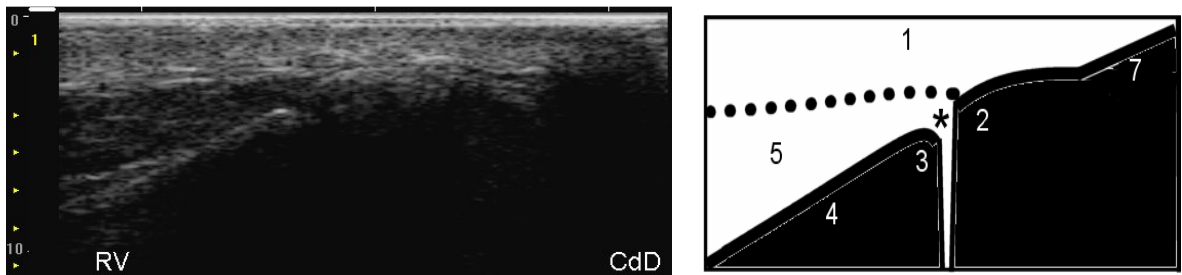


Figure 4.3.8.2. Cat. Lateral approach with the transducer in a caudodorsal – rostroventral orientation and the mouth closed.

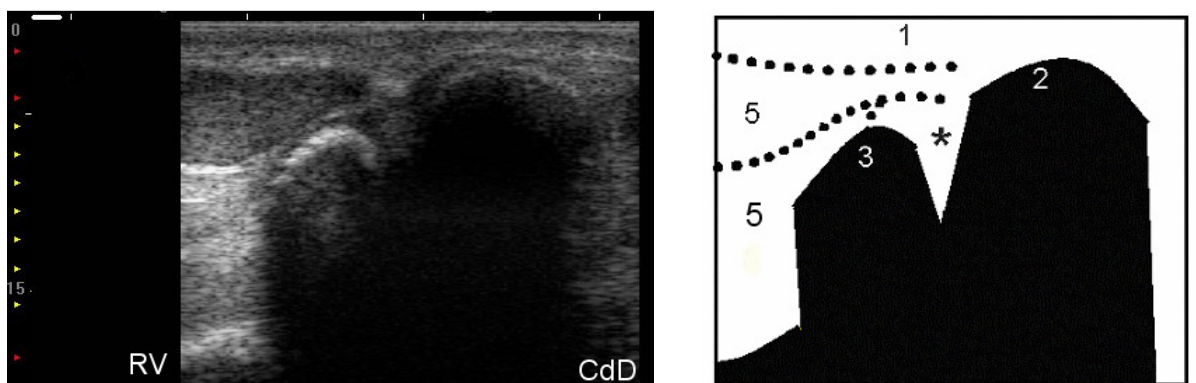


Figure 4.3.8.3. Dog. Lateral approach with the transducer in a caudodorsal – rostroventral orientation and the mouth open.

Figure 4.3.8. continued. Ultrasound appearance of the TMJ in the dog and cat from a lateral approach

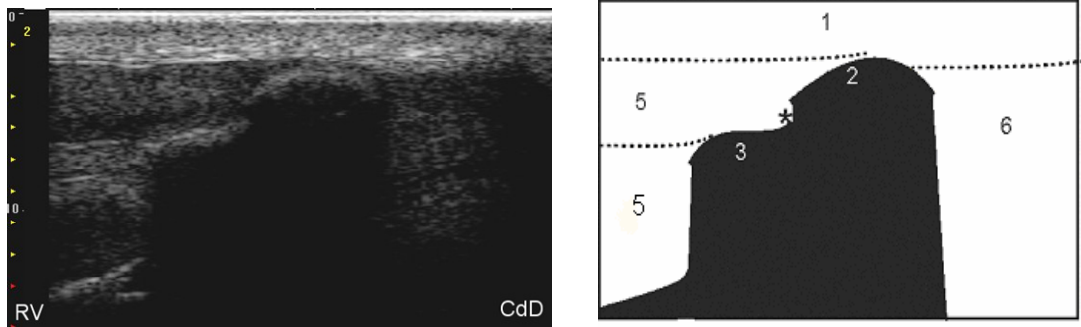


Figure 4.3.8.4. Cat. Lateral approach with the transducer in a caudodorsal – rostroventral orientation and the mouth open.

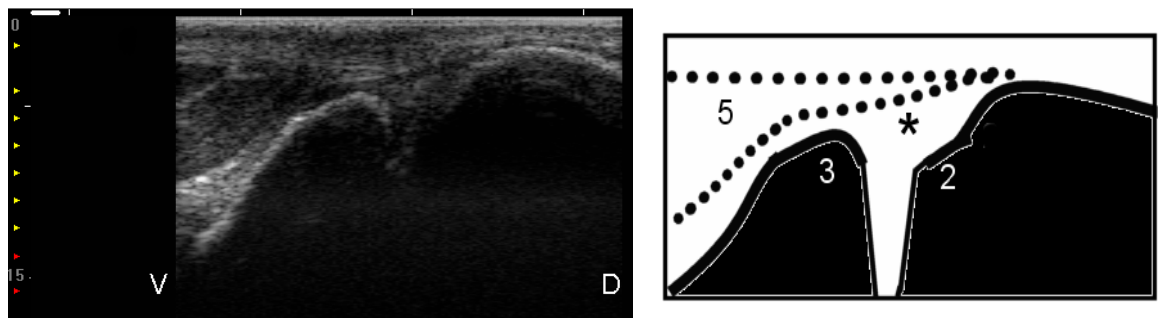


Figure 4.3.8.5. Dog. Lateral approach with the transducer in a dorsoventral orientation and the mouth closed.

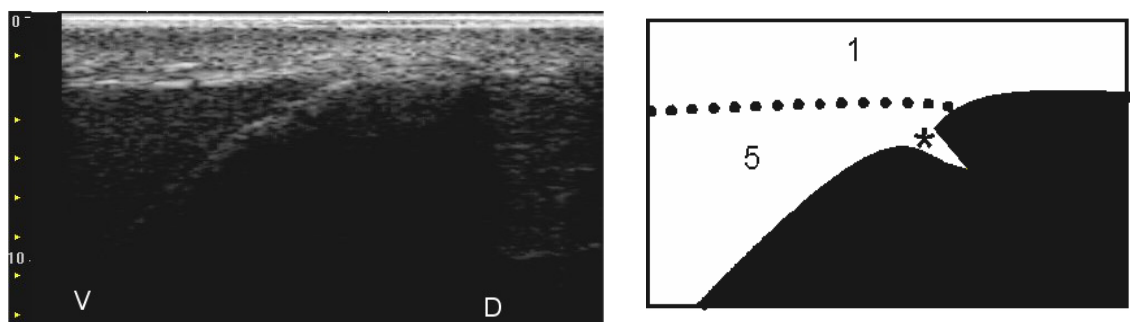


Figure 4.3.8.6. Cat. Lateral approach with the transducer in a dorsoventral orientation and the mouth closed.

Figure 4.3.8. continued. Ultrasound appearance of the TMJ in the dog and cat from a lateral approach

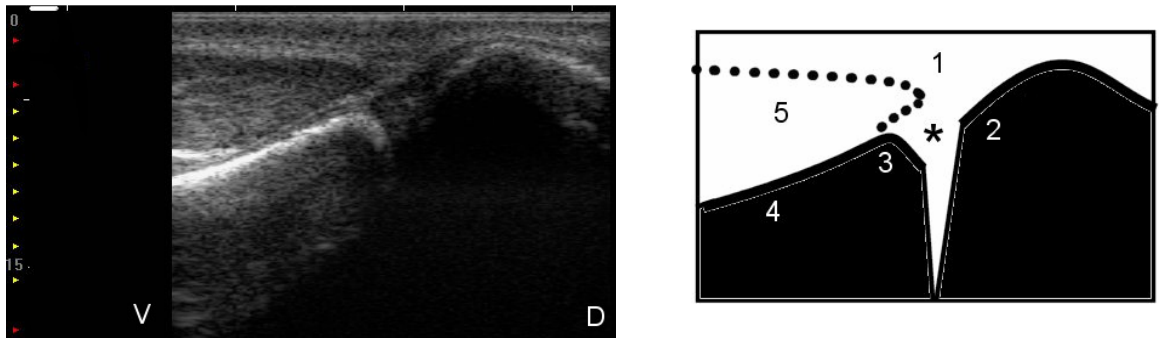


Figure 4.3.8.7. Dog. Lateral approach with the transducer in a dorsoventral orientation and the mouth open.

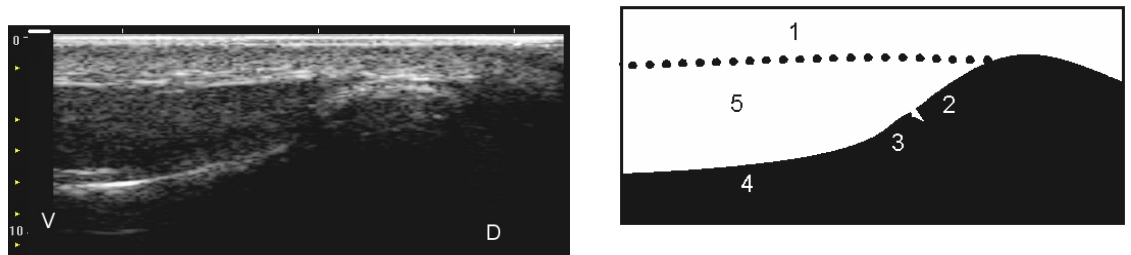


Figure 4.3.8.8. Cat. Lateral approach with the transducer in a dorsoventral orientation and the mouth open.

Figure 4.3.9. Ultrasound appearance of the TMJ in the dog and cat from a lateral approach and horizontal transducer orientations with corresponding line diagrams. For key see Table 4.3.2.

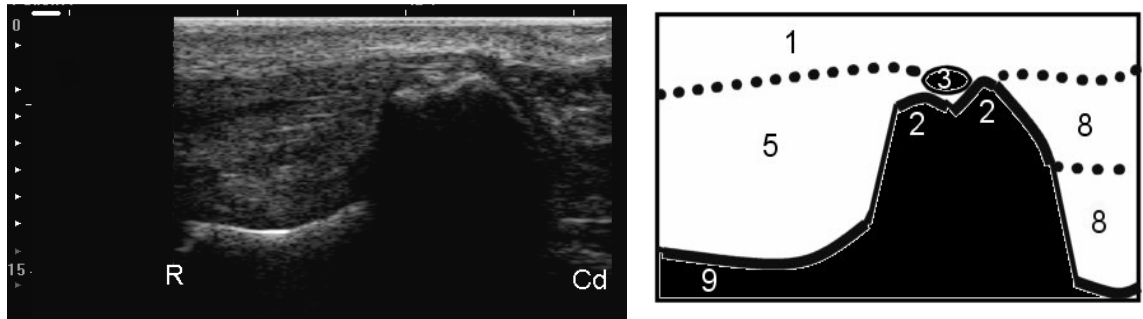


Figure 4.3.9.1. Cat. Lateral approach at the level of the MF with the transducer in a horizontal orientation and the mouth closed.

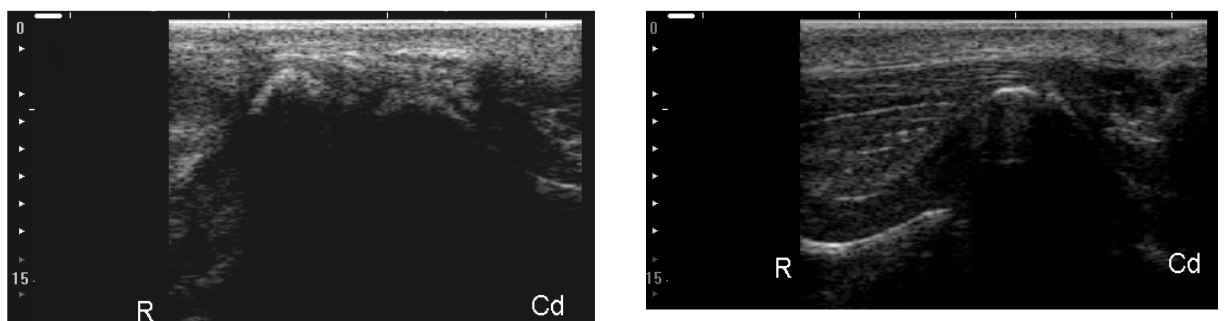
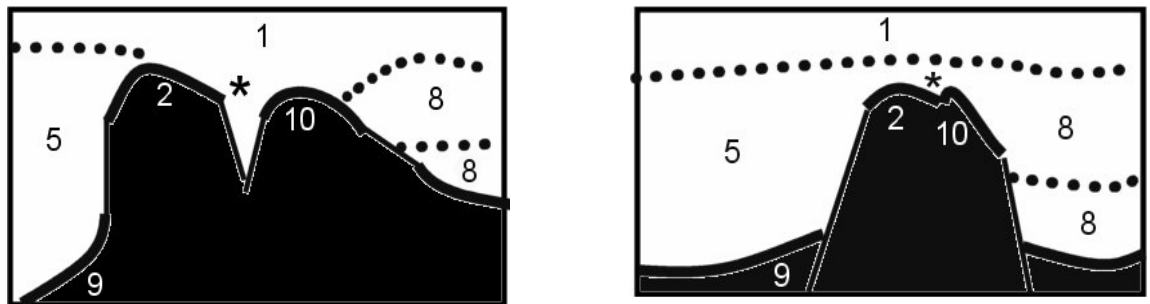


Figure 4.3.9.2. Dog (left) and cat (right). Lateral approach with the mouth closed and the transducer in a horizontal orientation being moved in a distal direction along the lateral edge of the retroarticular process.

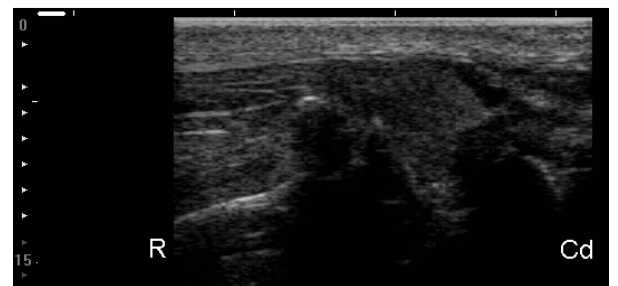
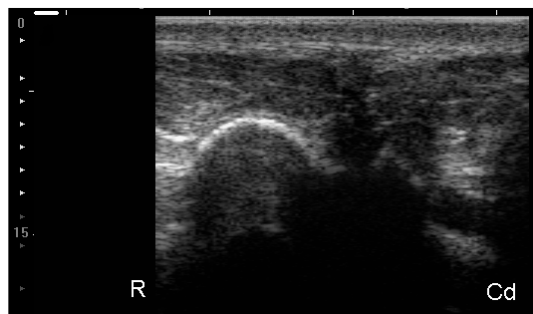
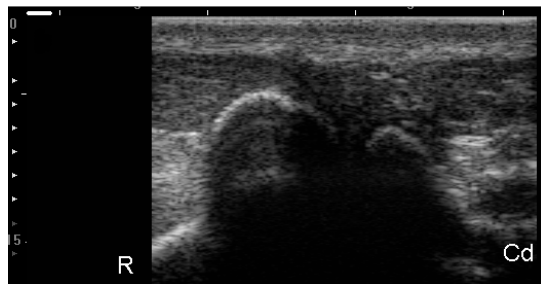
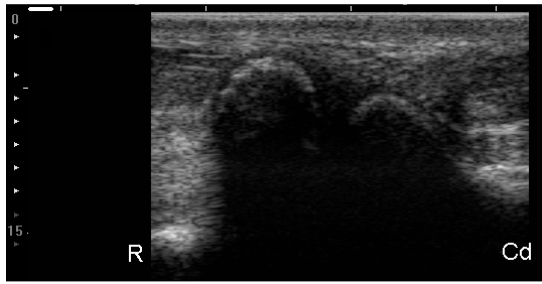


Figure 4.3.9.2. continued. Dog (left) and cat (right). Lateral approach with the mouth closed and the transducer in a horizontal orientation being moved in a distal direction along the lateral edge of the retroarticular process.

Figure 4.3.9. continued. Ultrasound appearance of the TMJ in the dog and cat from a lateral approach

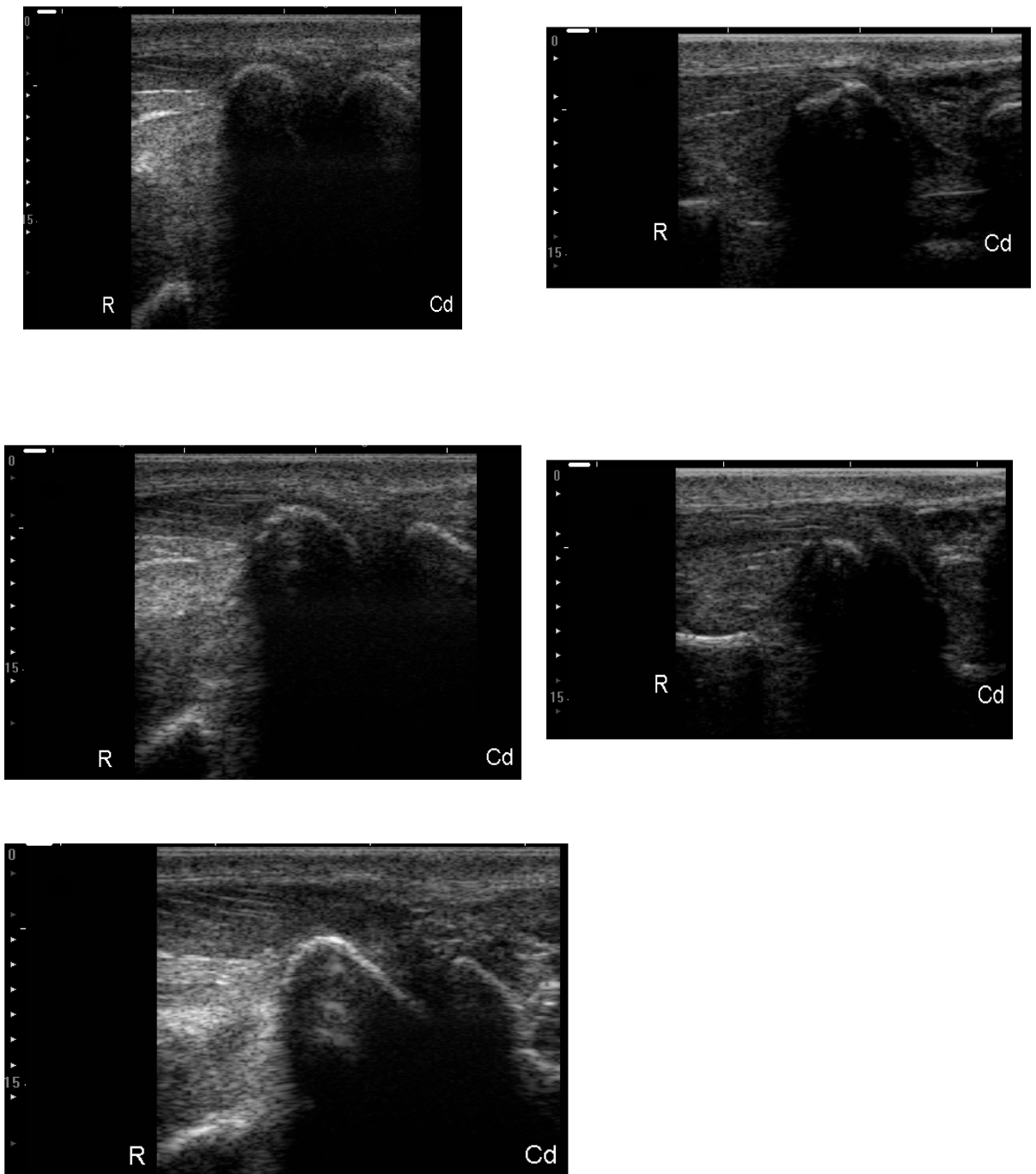


Figure 4.3.9.3. Dog (left) and cat (right). Lateral approach with the mouth open and the transducer in a horizontal orientation being moved in a distal direction along the lateral edge of the retroarticular process. For corresponding diagrams see Figure 4.3.9.2.

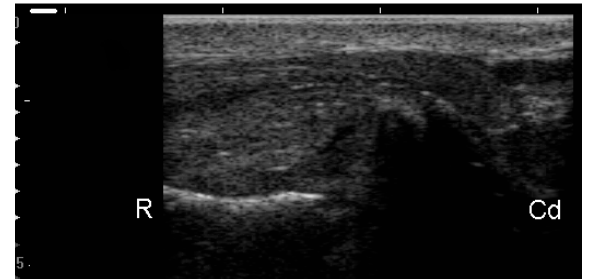


Figure 4.3.9.3. continued. Dog (left) and cat (right). Lateral approach with the mouth open and the transducer in a horizontal orientation being moved in a distal direction along the lateral edge of the retroarticular process. For corresponding diagrams see Figure 4.3.9.2.

Figure 4.3.10. Ultrasound appearance of the TMJ in the dog and cat from a caudal approach and vertical transducer orientation with corresponding line diagrams. For key see Table 4.3.2.

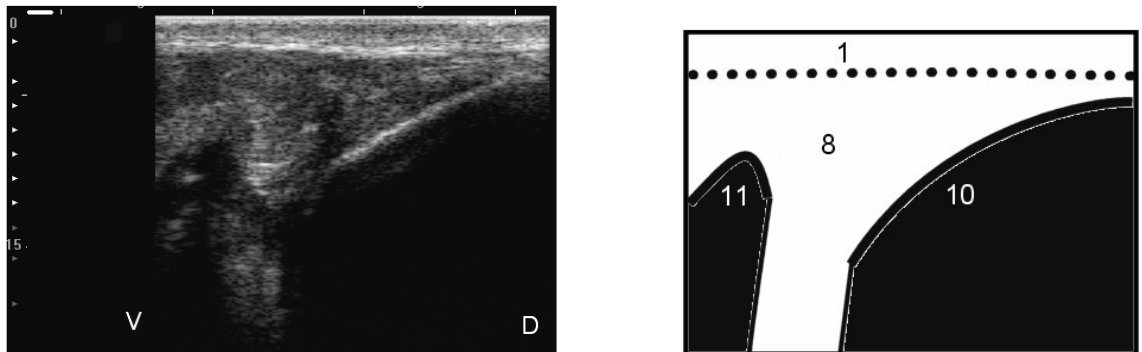


Figure 4.3.10.1. Dog. Caudal approach with the transducer in a vertical orientation and the mouth closed.

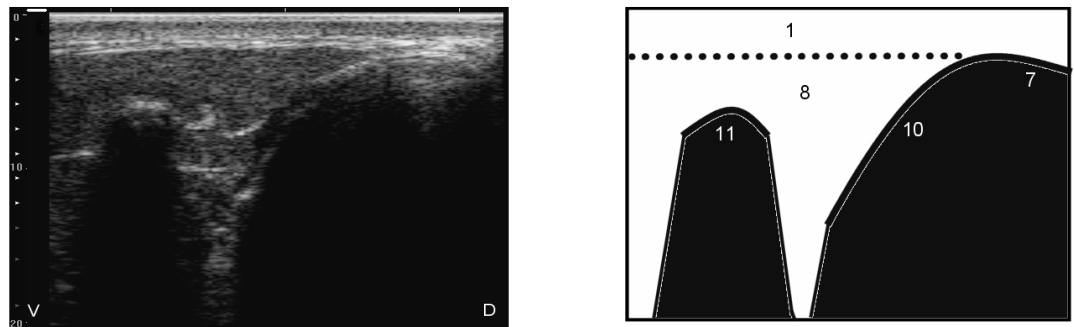


Figure 4.3.10.2. Cat. Caudal approach with the transducer in a vertical orientation and the mouth closed.

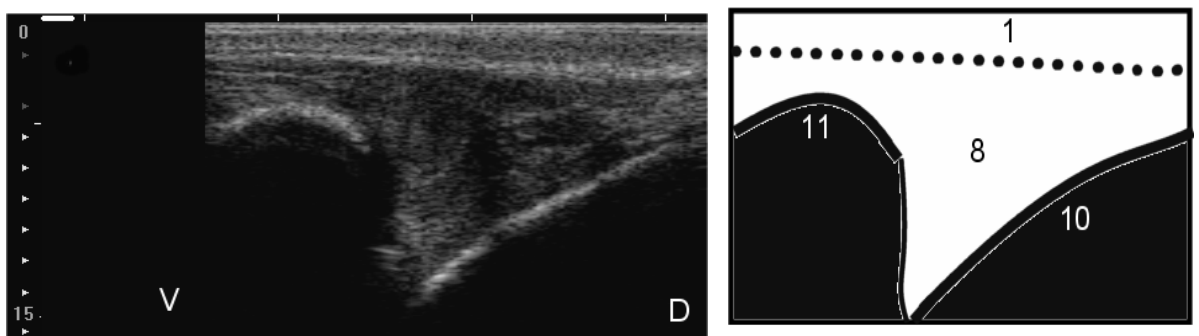


Figure 4.3.10.3. Dog. Caudal approach with the transducer in a vertical orientation and the mouth open.

Figure 4.3.10. continued. Ultrasound appearance of the TMJ in the dog and cat from a caudal approach

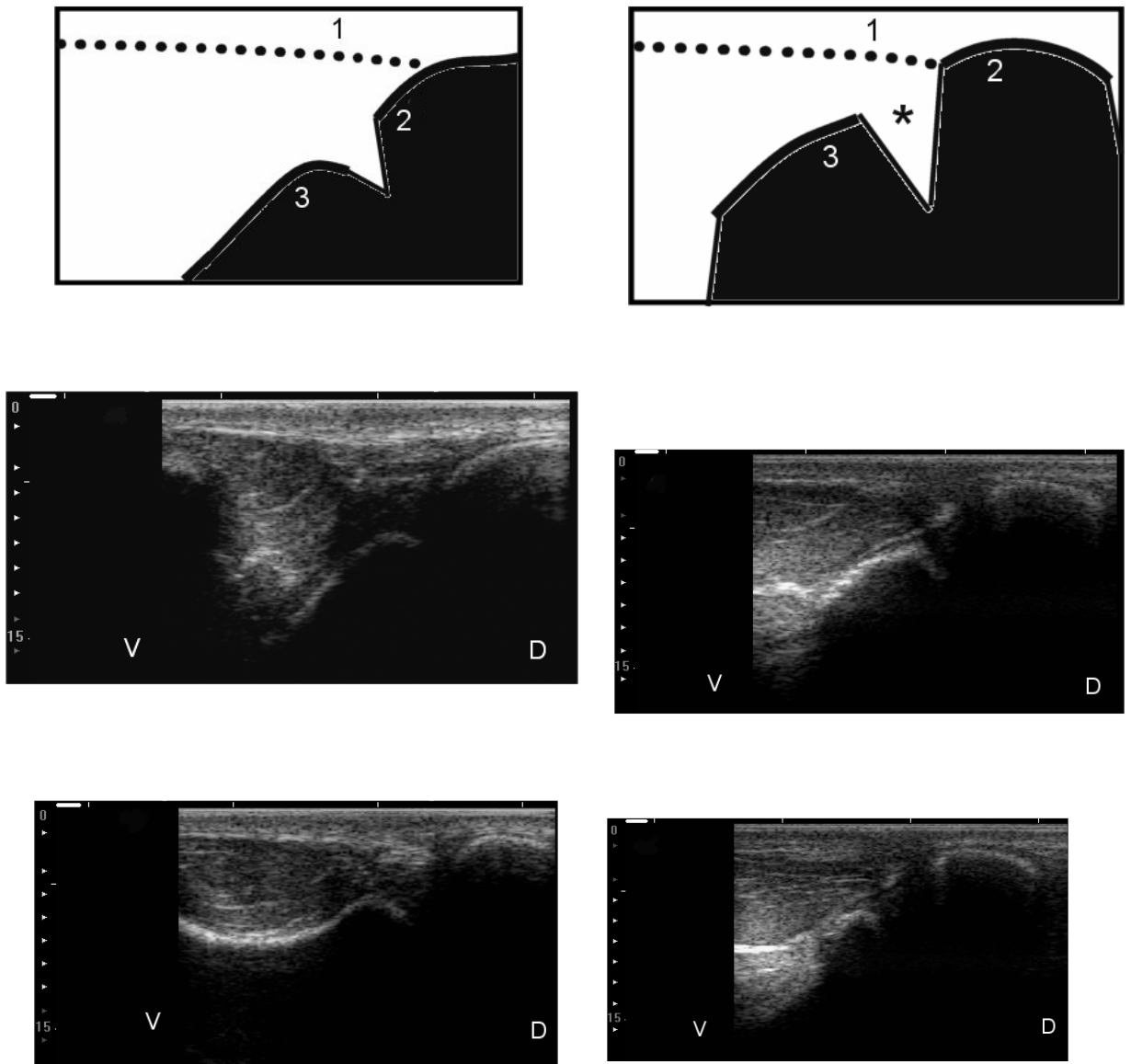


Figure 4.3.10.4. Dog. Caudal approach with the mouth closed (left) and open (right). The transducer was vertically orientated and moved in a lateral direction along the caudal edge of the MF and CP.

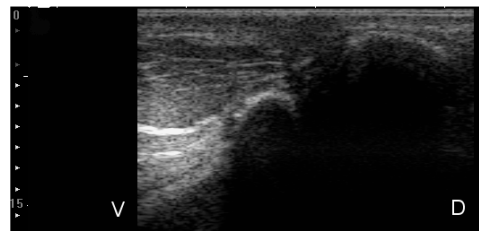
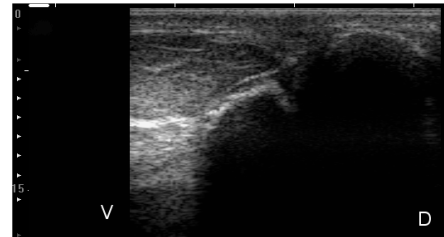
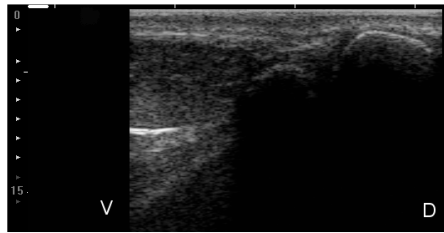
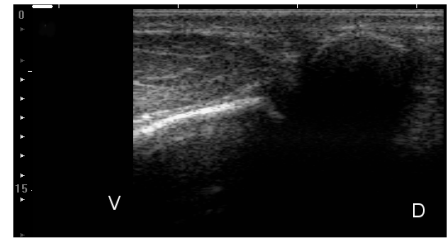
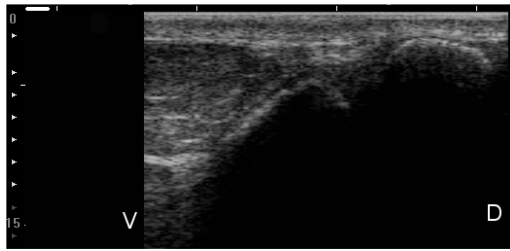


Figure 4.3.10.4. continued. Dog. Caudal approach with the mouth closed (left) and open (right). The transducer was vertically orientated and moved in a lateral direction along the caudal edge of the MF and CP.

Figure 4.3.10. continued. Ultrasound appearance of the TMJ in the dog and cat from a caudal approach

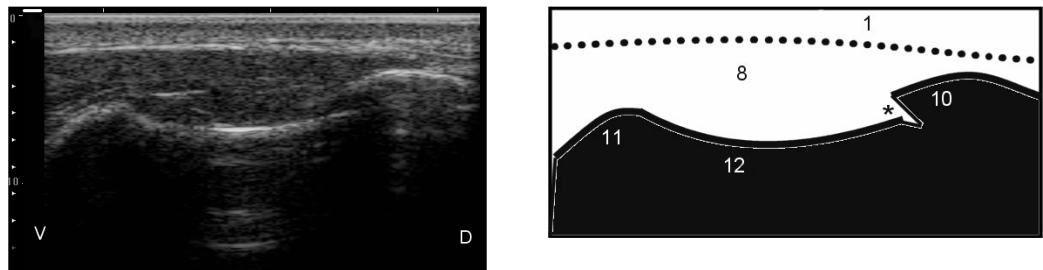
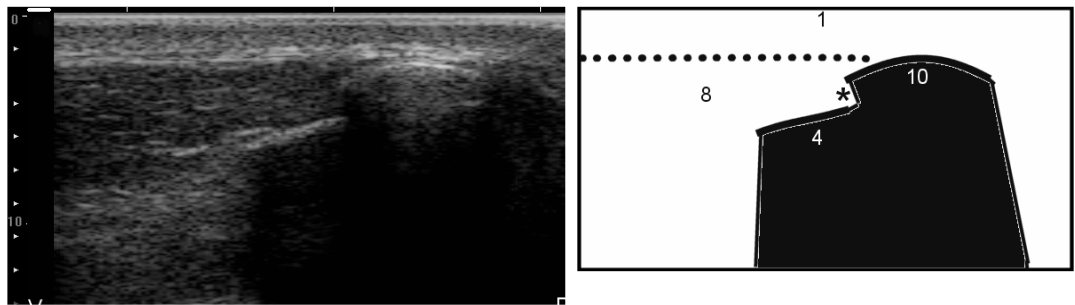
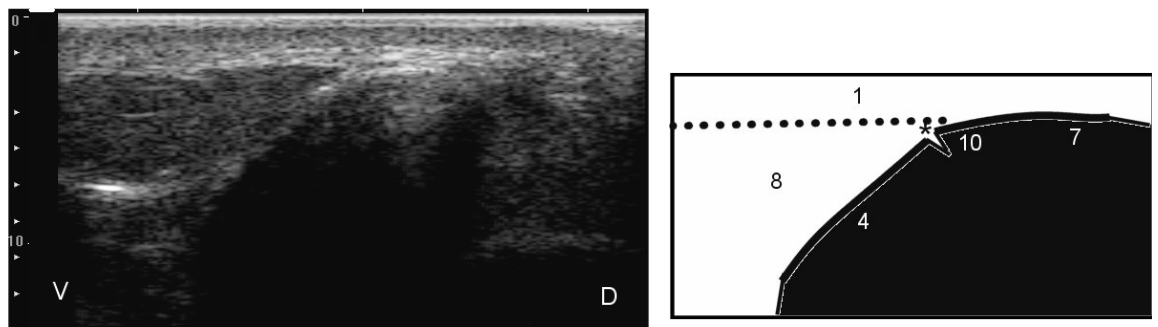


Figure 4.3.10.5. Cat. Caudal approach with the transducer in a vertical orientation and the mouth closed and open.

Figure 4.3.11. Ultrasound appearance of the TMJ in the dog and cat from a rostral approach and rostradorsal – caudoventral transducer orientation with corresponding line diagrams. For key see Table 4.3.2.

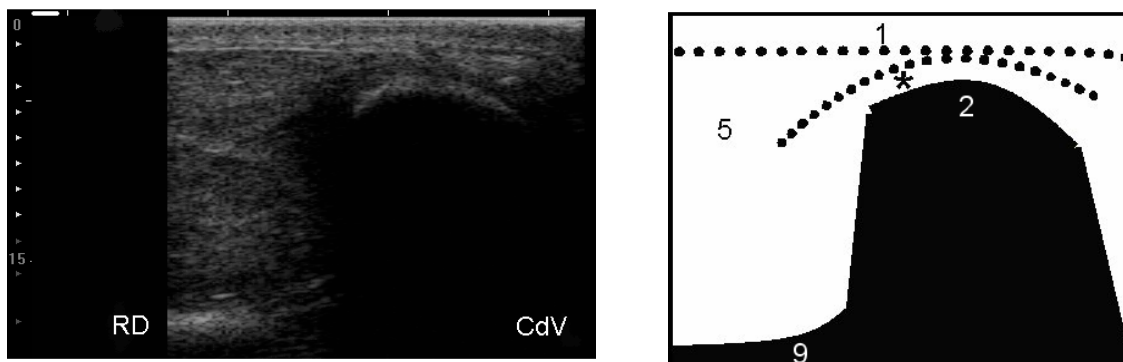


Figure 4.3.11.1. Dog. Rostral approach with the transducer in a rostradorsal – caudoventral orientation immediately ventral to the zygomatic process of the temporal bone and the mouth closed.

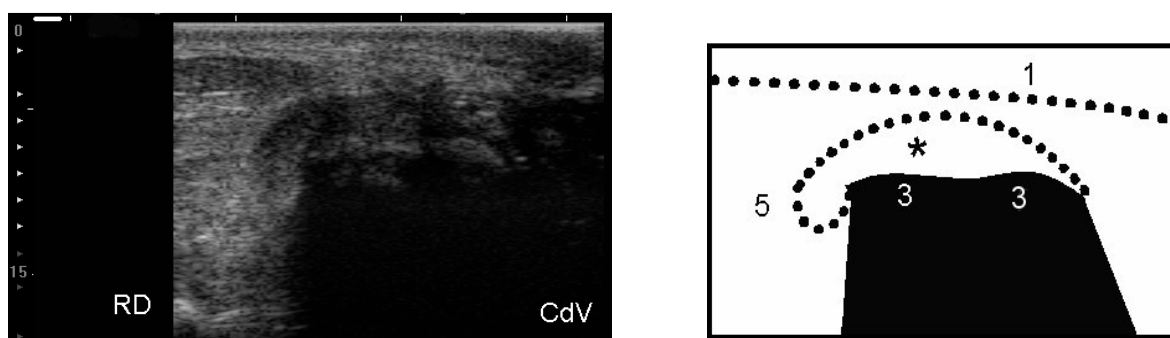


Figure 4.3.11.2. Dog. Rostral approach with the transducer in a rostradorsal – caudoventral orientation at the level of the TMJ and the mouth closed.

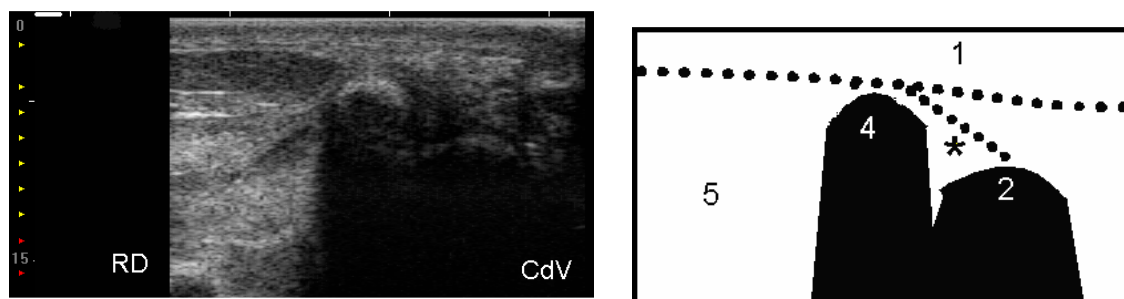


Figure 4.3.11.3. Dog. Rostral approach with distal movement of the transducer and the mouth closed.

Figure 4.3.11. continued. Ultrasound appearance of the TMJ in the dog and cat from a rostral approach

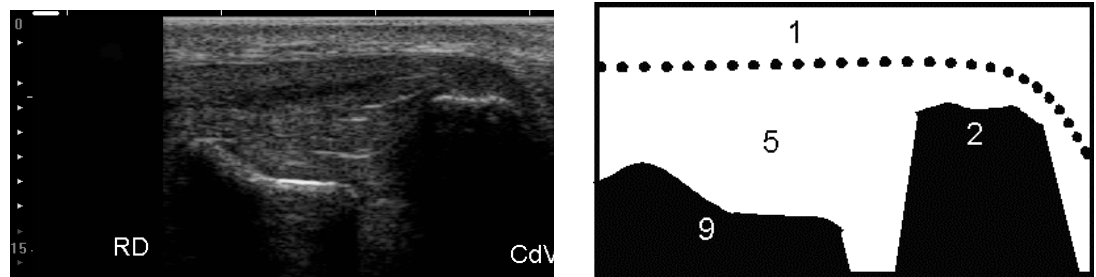


Figure 4.3.11.4. Cat. Rostral approach with the transducer in a rostradorsal – caudoventral orientation immediately ventral to the zygomatic process of the temporal bone and the mouth closed.

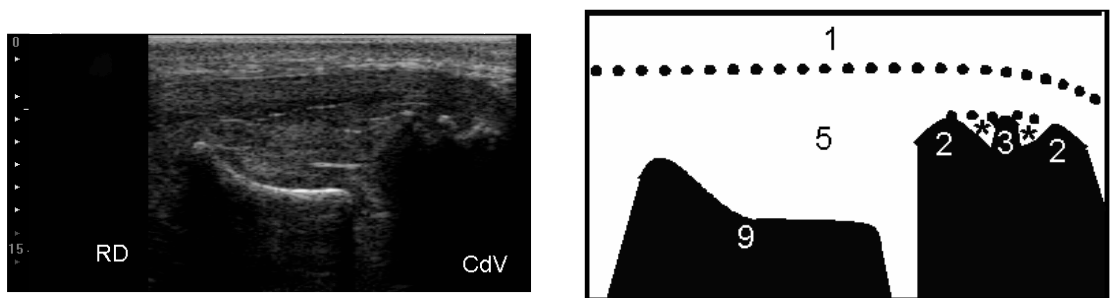


Figure 4.3.11.5 Cat. Rostral approach with the transducer in a rostradorsal – caudoventral orientation at the level of the TMJ and the mouth closed.

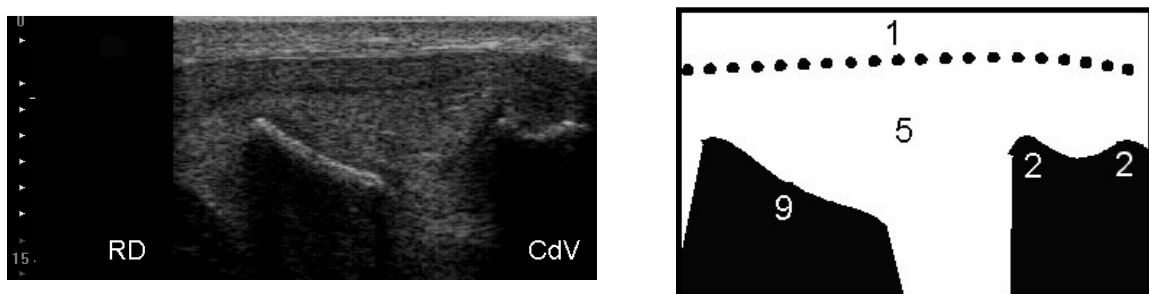


Figure 4.3.11.6 Cat. Rostral approach with the transducer in a rostradorsal – caudoventral orientation at the level of the TMJ and the mouth open.

Figure 4.3.12. Ultrasound appearance of the TMJ in the rabbit with corresponding line diagrams. For key see Table 4.3.2

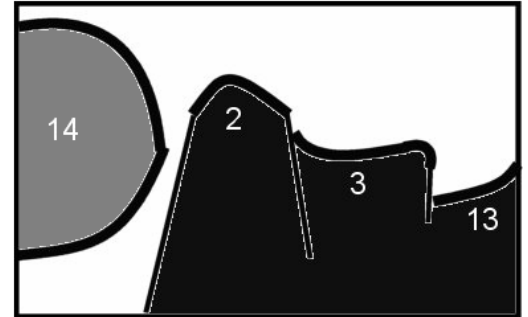


Figure 4.3.12.1 Rabbit. Dorsal approach with the transducer in long axis relative to the head and the mouth closed. .

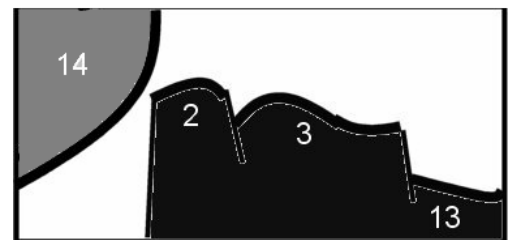
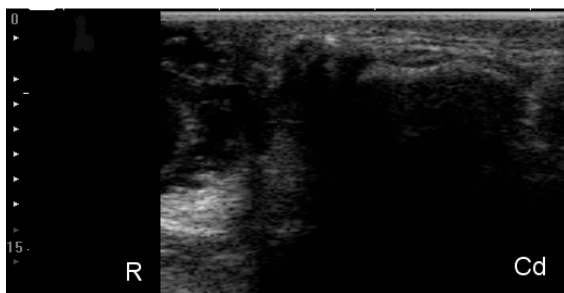


Figure 4.3.12.2 Rabbit. Dorsal approach with the transducer in long axis relative to the head and the mandible retropulsed.

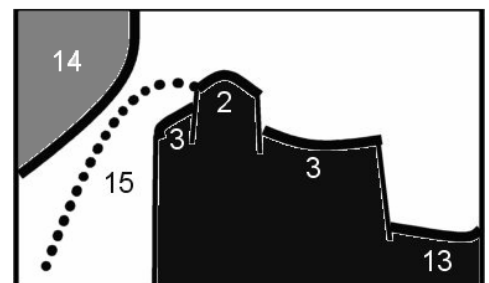
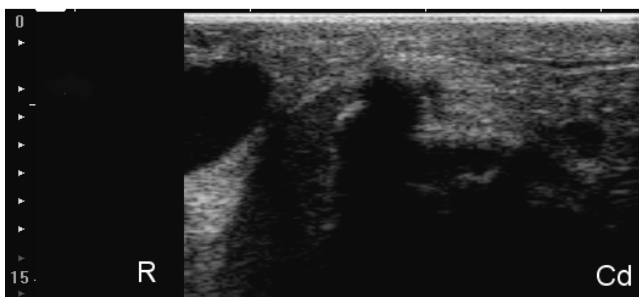


Figure 4.3.12.3. Rabbit. Dorsal approach with the transducer in long axis relative to the head and the mouth open.

Figure 4.3.12. continued. Ultrasound appearance of the TMJ in the rabbit



Figure 4.3.12.4. Rabbit. Dorsal approach with the transducer in short axis relative to the head and positioned over the caudal edge of the mandibular condyle with the mouth closed.

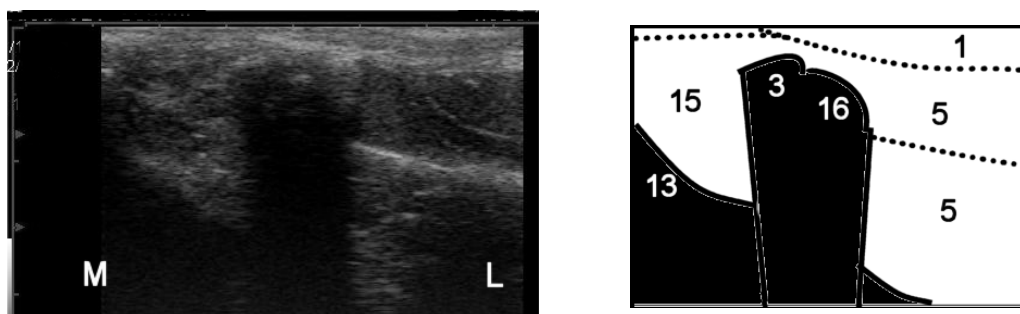


Figure 4.3.12.5. Rabbit. Dorsal approach with the transducer in short axis relative to the head and positioned immediately caudal to the mandibular fossa with the mouth closed.

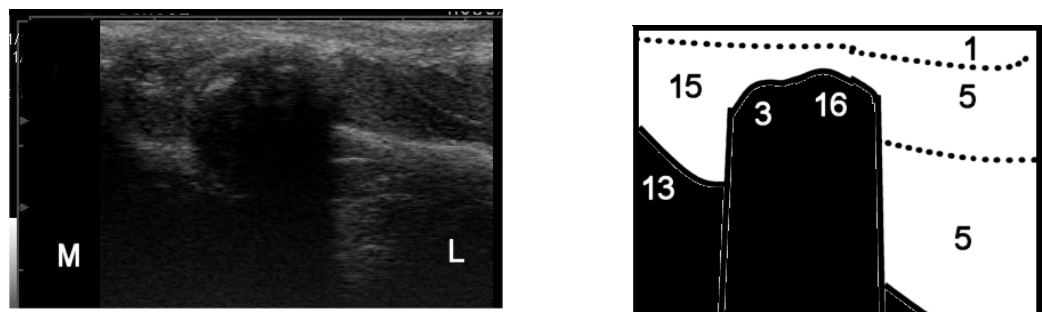


Figure 4.3.12.6. Rabbit. Dorsal approach with the transducer in short axis relative to the head and positioned immediately caudal to the mandibular fossa with the mouth open.

4.4.1. Ultrasound of the TB in the dog, cat and rabbit

The largest species being examined was the dog and the canine TB required the lowest frequency transducer (6.5 MHz) as higher ones did not provide adequate penetration. This was also the case when the canine TB was imaged through the fluid-filled external ear canal (Lee and others 2006). In a previous study, a 5MHz sector transducer operating at 3MHz was used to directly examine the TB in canine cadavers (Griffiths and others 2003). The higher frequency used in the present study resulted in better quality images and the curvilinear nature allowed characterisation of structures in the near field of the image. These were not as good resolution as those acquired in the cat and rabbit, where a 12MHz transducer was used. An 11MHz transducer was advocated for examination of the external ear canal in dogs (Lee and others 2006) but such a high frequency transducer was found to be unsuitable for examination of the canine TB in the present study.

A 12 MHz transducer was required for examination of the cat and rabbit TB, since lower frequencies did not allow adequate characterisation of this structure. In both these species, the transducer with the 3cm footprint provided the best images. Linear transducers with larger footprints are generally preferable as they provide images with better lateral resolution due to the ability to fire groups of crystals together therefore lengthening the Fresnel zone of the beam (Curry and others 1990). The transducer with the 5cm footprint also permitted more peripheral structures to be visualised on the image. However, there was insufficient space to allow manoeuvring in these species and therefore the 3cm one was deemed most appropriate. Attempts were made to image the TB in the rabbit using the very high frequency transducer (10-22MHz) in an effort to achieve even better resolution images. However, depth was the limiting factor and despite the small size of the rabbit, the TB was still too deep for identification using this transducer. This demonstrated that although it is desirable to use high frequency transducers to improve image quality, the depth of the structure being imaged will be a limiting factor in the maximum frequency that can be used.

Ultrasound has been used to image structures deep to bone interfaces in humans (Aaslid and others 1982, Hilbert and others 2001). In order to measure blood flow from the cerebral arteries in humans, low frequency transducers such as 1-2 MHz were required due to the relevant vessels being located 3.5 to 6 cm beyond the bone surface (Aaslid and others 1982). Since attenuation of the ultrasound beam as it passes through tissue increases with the frequency of the beam, these low frequencies were required to allow sufficient penetration of the beam to reach the region of interest. In contrast, when imaging the TB of

the dog, cat and rabbit, the beam was only required to travel a short distance beyond the surface of the bone in order to identify the presence of gas or fluid within the lumen, and approximately 1cm to encounter the far TB wall or septum. Therefore higher frequency transducers could be applied in these species with the added advantage of better resolution images of the regional anatomical landmarks helping identification of the TB.

The soft tissue structures and fat in the area surrounding the TB produced varying shades of grey on the resulting images reflecting their composition, as was to be expected (Nyland and others 1995). The sonographic appearance of the external ear canal has been previously reported (Lee and others 2006). In the present study, it could be visualised from a lateral approach and appeared similar in all three species.

The TB could be visualised from a lateral approach in the dog and appeared similar to that previously reported (Griffiths and others 2003). However, this was not the case in the cat or rabbit. In the cat this was due to the presence of the gas-filled horizontal external ear canal and in the rabbit the bony external acoustic meatus and mastoid process. Since the ultrasound beam cannot pass through gas or thick bone (Curry and others 1990, Herring and Bjornton 1985) the TB was obscured by acoustic shadowing using this approach in the cat and rabbit although the thick lateral wall of the TB was visible in the dog. The vertical orientation of the external acoustic meatus in the rabbit allowed the length of its lateral bone margin to be visualized, which was not possible in the dog or cat due to its horizontal orientation in these species. The parotid salivary gland was identified when imaging this region from a lateral approach in the dog and cat but in the rabbit, it could not be distinguished from the surrounding subcutaneous fat and fascia.

The TB in all species could be successfully imaged from a ventral approach. The feline TB proved much easier to locate than the dog due to its superficial nature and ease of palpation. The rabbit proved more difficult due to the confined space produced by the caudal location of the ramus of the mandible that limited manipulation of the transducer. From this approach the resulting images were similar in all three species with the exception of obvious variations in size and shape. In all cases, the ultrasound beam passed through the superficial soft tissue structures and then encountered the ventral bone wall of the TB. The large difference in acoustic impedance between these tissues resulted in approximately 30% of the beam being reflected back to the transducer producing a hyperechoic interface on the image (Herring and Bjornton 1985). However, the bone was not thick enough to attenuate the entire remainder of the beam so a proportion passed through to encounter the

gas content of the TB. Approximately 99% of the remaining beam was then reflected back towards the transducer, although a proportion of the echo would have undergone further attenuation as it passed back out through the bone interface (Curry and others 1990). This gas interface therefore contributed to the hyperechoic interface on the screen representing the ventral wall of the TB and also prevented further penetration of the beam into the TB lumen. This caused reverberation or dirty shadowing artefact and the inability to image any deeper structures such as the far TB wall.

The introduction of fluid into the TB was beneficial in confirming its identity and location. Material can be introduced into the canine and rabbit TB simply by passing a needle through the tympanic membrane and was therefore straightforward to perform (Griffiths and others 2003). However, the procedure was more difficult in the cat due to the necessity to pass the needle through the bony septum, allowing the introduction of material into the ventral compartment. Material in the dorsal compartment only was not visible using any of the transducer positions. Fluid did not appear to move between the two compartments in the cat despite repositioning of the material, which may reflect the small size of the communicating opening, the presence of surface tension in the fluid or the presence of an air trap in the empty compartment. The inability of the beam to pass through gas is further demonstrated by the tip of the needle being visible when it was in contact with the bone wall but not when it was removed even by a short distance.

When the intra-luminal gas was replaced by water or KY jelly, the proportion of the beam that penetrated the bone wall was then propagated through the fluid. This produced an anechoic region on the image beyond the ventral wall of the TB. The wall of the TB itself was less bright since it was no longer a composite of the bone and gas interfaces. The beam continued to the far wall of the TB in the dog and rabbit, and the bone septum in the cat, producing a second hyperechoic interface. This interface was concave in the dog and rabbit, and undulating in the cat, therefore could be easily differentiated from any lines resulting from reverberation artefact in the gas-filled TB as these were convex. Although theoretically structures deep to the far wall could be imaged, the amount of distortion associated with the double passage of the beam through the two bone interfaces meant that little useful information about them was obtained. In the cat, the dorsal compartment was not visible even in the presence of fluid. In the rabbit, the bone ridge around the inner margin of the external ear canal was sometimes visible as a second smaller convex interface within the fluid-filled lumen.

In the present study, the canine TB and its contents could be assessed better from a ventral approach than a lateral approach. This was contradictory to previous findings where the ventral approach was felt to be unreliable due to the anatomical complexity of the site and eventually abandoned (Griffiths and others 2003). However, the published images of the lateral approach are of too poor quality and with insufficient near field definition to determine exactly what is being imaged and whether it was truly the TB and not the fluid or air-filled horizontal ear canal (Griffiths and others 2003). Alternatively, the fluid-filled TB may have been visible due to the beam being directed along the fluid-filled external ear canal, which then acted as an acoustic window as demonstrated in another study (Lee and others 2006). This possibility was not investigated in the present study as care was taken to position the beam over the lateral wall of the TB and avoid the external ear canal.

The small size and position of the mastoid and jugular processes in the dog and cat meant that they did not interfere with imaging of the TB. However, they were present in all of the images of the rabbit TB and the inability of the beam to penetrate these structures produced acoustic shadowing that obscured the caudolateral portion of the TB lumen, even in the presence of fluid. It should be possible to differentiate between the acoustic shadowing produced by these structures and the anechoic appearance produced by fluid within the TB lumen by the ability to visualize the far wall of the fluid-filled lumen. However, the presence of these structures should be borne in mind when examining this area in the rabbit and attempts made to alter the angle of the beam to allow interrogation of as much of the TB as possible.

The ability to distinguish the presence of fluid from gas within the TB has important clinical implications since this is a common finding associated with disease of the middle ear in the dog, cat and rabbit (Gibbs 1978, Harcourt-Brown 2003, White 2003) and may be the only abnormality present in clinical cases of acute otitis media. The use of fluid and KY jelly in this study produced a distinctive anechoic appearance. However, it has been suggested that the TB in canine otitis media cases may contain denser, tenacious material that may be located in focal accumulations, making it easier to overlook (Griffiths and others 2003) and it is likely that this also applies to the cat and rabbit. However, ultrasound was able to identify mucosal thickening, focal soft tissue masses and complex fluid collections in the human sinus (Nelson and others 1990) so further work would be required to determine if this is also the case in the dog, cat and rabbit.

The present study also indicated that material located in the dorsal compartment of the feline TB cannot be detected using ultrasound. This is also likely to have implications in clinical cases since otitis media in cats commonly arises in association with a nasopharyngeal polyp and these are usually located in the dorsal compartment (Gotthelf 2004). Their presence may go undetected using this technique unless there is concurrent otitis media resulting in involvement of the ventral compartment. In clinical cases, the effect of gravity could be expected to create pooling of the fluid in the ventral region of the TB and this was observed in cases of human sinusitis where fluid was identified in the dependant portion of the maxillary sinus with an air-fluid line apparent in some cases (Nelson and others 1990). In the present study, fluid could be identified in the TB lumen with the cadavers in a lateral recumbent position, but it may be that clinical cases should be examined in sternal recumbency with the transducer applied ventrally in order to increase the chances of detecting material. Further work would be required to confirm if this is the case.

The ventral aspect of the TB wall was thin and in the present study, the ultrasound beam was able to penetrate it. However, the lateral bone wall of the canine TB was thicker and the effect of this was demonstrated by it being easier to identify fluid in the lumen from a ventral approach. In the rabbit, the beam was unable to penetrate the lateral wall of the external ear canal or the jugular process resulting in an inability to image fluid within the lumen of the external ear canal or the caudolateral portion of the TB. These observations confirm that the bone thickness will determine whether the beam can penetrate or not. New bone formation resulting in thickening of the TB wall is a common finding in the presence of chronic middle ear disease (Gibbs 1978) and therefore may influence the ability of ultrasound to identify the presence of material in the lumen in long standing cases. However, it may still be able to identify changes to the normally smooth bone wall of the TB in cases of chronic otitis media, craniomandibular osteopathy or osteomyelitis.

It has been reported that the auditory ossicles can occasionally be identified in dog in the presence of a fluid-filled TB (Griffiths and others 2003). However, they were not identified in any of the species in this study. They will not be visible in the cat due to the presence of the bone septum but theoretically should be visible in the rabbit, although it is likely that their small size will make this difficult.

In humans, the middle ear cavity has been examined by placing a small transducer in the fluid-filled external ear or concha and imaging through the intact tympanic membrane

(Alvord 1990). This approach was not possible in dogs and cats due to the presence of a vertical as well as a horizontal portion to the external ear canal. However, the introduction of fluid to the external ear canal and application of the transducer to the skin surface over the horizontal ear canal did produce an acoustic window that allowed imaging of the external ear canal and fluid-filled TB (Lee and others 2006). Potential limitations of this technique might include the inability to identify small fluid accumulations in the ventral aspect of the TB although it may be less affected by the presence of new bone formation in association with chronic otitis media. It may also have the potential to facilitate the identification of nasopharyngeal polyps in the dorsal cavity in cats. However, it was not possible to determine whether the tympanic membrane was intact or not using this technique (Lee and others 2006).

4.4.2. Ultrasound of the TMJ in the dog, cat and rabbit

The TMJ was located more superficially than the TB in all three species so the 12MHz transducer was determined to be most appropriate for imaging this structure although the optimum footprint size did vary according to the space available for manoeuvring. Again, the highest frequency transducer (10-22MHz) did not have adequate depth of penetration for use even in the rabbit. Ultrasound studies of the human TMJ have involved a range of transducer frequencies from 3.5 MHz (Nabeith and Speculand 1991) through 5.0 MHz (Gateno and others 1993) to 10-12.5MHz (Landes and others 2000). However, the studies using lower frequencies tended to be more interested in determining the location of structures relative to each other so image quality was of secondary importance, while those using higher frequency transducer did provide better images and therefore more information regarding the structures themselves. Studies of the equine TMJ have all used a 7.5MHz transducer (Weller and others 1999a, Rodríguez and others 2002) reflecting that although this region in the horse may be significantly larger than these other species it shares the same superficial location. An additional incentive to use this specific frequency in the horse stems from its widespread availability in equine practices for the examination of tendons (Weller and others 1999a).

This superficial location was also responsible for phased array sector or curvilinear format transducers in the present study being deemed less appropriate due to their poorer near field image quality when compared to the linear format (Curry and others 1990). This was reflected by all studies of the human and equine TMJ favouring linear transducers (Nabeith and Speculand 1991, Gateno and others 1993, Weller and others 1999a, Landes and others

2000, Rodríguez and others 2002) and also studies involving other joints in the dog (Long and Nyland 1999).

In humans, the TMJ was imaged from the lateral aspect with the transducer orientated in either a vertical or horizontal position (Nabeith and Speculand 1991, Gateno and others 1993, Landes and others 2000). Likewise in the horse, imaging was performed from a lateral approach and due to the anatomy of the joint, a minimum of three views were necessary to provide a complete examination (Weller and others 1999a, Rodríguez and others 2002). The horizontal location of the TMJ in the dog and cat also resulted in a lateral approach producing the views that were easiest to perform and most useful. However, in these species it was also possible to achieve caudal and slightly rostral approaches, although care was required not to revert to a lateral approach. The application of pressure on the transducer was required to maintain these approaches and therefore they are less likely to be well tolerated in conscious animals than the lateral views. The rostral views were also more difficult to achieve in the cat than the dog due to the wider zygomatic arch in this species restricting transducer placement. This may have similar implications if this technique is attempted in brachycephalic dog breeds, although further work would be required to determine if this is in fact the case. The horizontal orientation of the TMJ and the bone extension at the caudal end of the zygomatic arch in the rabbit meant that imaging from a lateral approach was not possible. A dorsal approach was used instead but did not allow as much of the joint to be examined as in the other species.

A standoff pad was used to image the equine TMJ in one study (Rodríguez and others 2002) but was only required in thin horses in another (Weller and others 1999a). In a study of the canine shoulder, standoff pads were only deemed necessary if transducers with inadequate near field image quality were used (Long and Nyland 1999). The transducers used in the present study provided good enough near field image quality without their use and there were no reports of them being used in studies of the human TMJ.

The appearance of the bony components of the TMJ in all three species conformed to that expected when imaging bony structures. The normal bone surfaces produced a smooth, even, well-defined hyperechoic interface on the image with a distal acoustic shadow that obscured all the areas of the bone beneath the surface and also deeper structures. These structures were thick enough, even in the rabbit, to prevent any through transmission of the beam. Superficial soft tissue structure produced a shade of grey on the image according to their composition. This corresponded with reports in humans and horses (Weller and others

1999a, Landes and others 2000) and also of imaging of other canine joints (Reed and others 1995, Long and Nyland 1999).

The areas of the TMJ visualised using each view were similar in the dog and cat, with obvious variations in the size and shape of the structures being interrogated. The small size of the dog and cat allowed the entire width of the TMJ to be visualised in each image while the larger size of the horse required the joint to be examined in sections (Weller and others 1999a). Using a lateral approach the lateral margins of the mandibular fossa, articular tubercle, retroarticular process and condyloid process were all visible. This corresponded with the areas visible using a similar approach in humans (Landes and others 2000) and the horse (Weller and others 1999a, Rodríguez and others 2002). The TMJ space in the dog and cat appeared as a narrow wedge shaped area that limited visualisation of structures within the joint to the lateral extremities. This was particularly the case in the cat where the mandibular fossa and retroarticular process completely enclose the condyloid process making the TMJ space very narrow. The lateral aspect of the human and equine TMJ space appeared more open although this did depend to some extent on the specific area of the TMJ being examined. This allowed penetration of the beam further into the joint space and permitted the lateral aspect of the disc to be visualised (Weller and others 1999a, Landes and others 2000, Rodríguez and others 2002). In the horse, the disc was a distinct triangular structure with a homogenous echogenicity similar to the menisci in the stifle and varied in thickness depending on the area being examined (Weller and others 1999a). The intra-articular disc is poorly developed in the dog and cat when compared to the horse and humans so it is likely that its small size combined with the narrow TMJ space prevented its visualisation

As in humans (Landes and others 2000), the lateral soft tissue components of the joint were visible in the dog and cat and the boundary between these and the surrounding soft tissue were assumed to represent the TMJ capsule. The ligaments associated with the TMJ could not be identified. In the horse, the base of the disc was continuous with the intra-articular soft tissue and the joint capsule was visible as an interface between the overlying parotid salivary gland and the disc (Weller and others 1999a). However, the lateral and caudal ligaments of the joint were completely embedded in the joint capsule and therefore not visible on ultrasound images (Weller and others 1999a) and it is likely that this was also the case in the dog and cat. No fluid was identified in either of the TMJ compartments in the horse (Weller and others 1999a) as was the case in the dog and cat. This corresponded with findings in the canine stifle where meniscal ligaments, collateral ligaments and

synovial fluid were not identified due to the small size of the structures and the small volume of fluid present in normal joints (Reed and others 1995).

The caudal approach that was possible in the dog and cat has not been reported in humans or the horse. This view allowed the retroarticular process to be assessed but provided less information about the TMJ itself and this was particularly the case with the cat due to its small size. From the rostral aspect there was only a very small window that allowed the joint itself to be assessed in the dog but the presence of the articular tubercle prevented this in the cat therefore this view is likely to be of limited value.

In the rabbit, the TMJ space was not visible from the dorsal approach due to its location beneath the zygomatic process of the temporal bone. This region of bone was too thick to allow penetration of the beam and the resulting acoustic shadowing obscured the joint. The dorsal aspect of the condyloid process was visible though, with the exception of the region engaged with the mandibular fossa, which was also obscured by the shadowing. The visible areas varied depending on whether the mouth was open and closed and with retropulsion of the mandible, it was possible to visualise most of the condyloid process. Attempts to visualise the joint space from a more rostral approach were not successful and none of the views allowed visualisation of the intra-articular disc. This structure is well represented in the rabbit and therefore technically should have been visible. However, it was firmly attached to the mandibular fossa and more loosely attached to the condyloid process. This resulted in it remaining engaged within the mandibular fossa despite repositioning the mandible and therefore it too was obscured by the shadowing produced by the zygomatic process.

Only the lateral structures of the TMJ could be assessed in the dog and cat with the medial aspect of the joint not being visible from any position. This was the same in humans (Landes and others 2000) and the horse (Weller and others 1999a). Full flexion of the stifle in one study resulted in opening of the joint and improved the ultrasonographic window for visualisation of intra-articular structures (Reed and others 1995). In humans it was reported that the disc was better visualised with the mouth open (Nabeith and Speculand 1991). Although opening the TMJ in the present study did result in different areas of the joint being interrogated in each view, it did not improve visualisation of the intra-articular features in any of the species. It did prove useful for identification of the TMJ components though and therefore it is advisable to open and close the mouth during the examination. This was particularly the case in the rabbit where it was possible to follow the movement

of the condyloid process while the mouth was being opened and closed and the rabbit demonstrated a far greater range of motion than that present in the dog and cat. Rostral movement of the mandibular condyle was identified when the mouth was opened in the horse (Weller and others 1999a) and the use of ultrasound to determine condyloid process position in humans has been advocated (Gateno and others 1993). Ultrasound has also been shown to provide considerable anatomical detail during physiological movement in humans (Landes and others 2000). However, problems were encountered in maintaining the position of the transducer when attempts were made to examine the TMJ in horses during natural mastication. For this reason, in animals, artificial manipulation of the joint under sedation may prove more beneficial. In humans, the range of movement identified in the TMJ was influenced by the presence of pain and the resulting reluctance of the subject to allow full manipulation of the jaw (Landes and others 2000). This should be taken into account if attempting to perform an ultrasound examination in an animal with TMJ abnormalities since the presence of pain is likely to reduce compliance resulting in the need for sedation.

The parotid salivary gland and masseter muscle were identified in the adjacent tissue in the dog and cat as was the case in humans (Landes and others 2000) and the horse (Weller and others 1999a). However, in the rabbit, although the masseter muscle could be identified the parotid salivary gland could not be distinguished from adjacent subcutaneous fat.

The inability of the beam to penetrate thick bone structures and image beyond the surface means that ultrasound is likely to remain an additional procedure for evaluating bone (Kramer and others 1997) and the findings of this study indicate that the TMJ of the dog, cat and rabbit are no exception. However, ultrasound has been used to identify abnormalities affecting the bone surface and new bone formation associated with TMJ osteoarthritis has been observed in an aged pony (Weller and others 1999a). In dogs, cats and rabbits, it may therefore be able to identify processes that result in changes to the bone surface including osteoarthritis, fractures, callous formation, craniomandibular osteopathy or neoplastic process. The ability to identify the components of the TMJ and relate their position to each other means it might be useful in the identification of dislocations and it has been used in humans to identify fracture dislocations of the TMJ (Landes and others 2000). The inability to penetrate beyond the lateral aspect of the joint means it is unlikely to detect the mandibular fossa and condyloid process malformations associated with TMJ dysplasia in the dog but further work would be required to demonstrate whether it could

identify the resulting incongruity between the mandibular fossa and condyloid process and also whether the caudal view could identify malformation of the retroarticular process.

Ultrasound may also be able to provide information regarding the associated soft tissue structures. In humans, ultrasound was used to identify displacement and perforation of the disc, seroma formation following contusion, capsular fibrosis and the presence of crystalline structures in the synovium (Nabeith and Speculand 1991, Landes and others 2000). In the horse, it was able to identify the soft tissue changes associated with severe joint degeneration that included narrowing of the joint space, absence of the disc and the presence of hypoechoic material around the joint delineated by an echogenic fibrous capsule and a fibrous mass around the joint (Weller and others 1999b). In this case, scintigraphy had localised the lesion but failed to characterise it and radiography had failed in both respects (Weller and others 1999b).

Chapter 5. Computed tomography of the tympanic bulla, temporomandibular joint and associated structures in the dog, cat and rabbit.

5.1 Introduction

5.1.1 Technical aspects regarding CT of the temporal region

As with radiography, CT image production relies on the differential attenuation of an X-ray beam by body tissues. The use of multiple projections allows each section of tissue to be divided into units and the total attenuation of each unit can be determined. A CT number, expressed in Hounsfield units (HU), is then allocated to each unit of tissue. This is an arbitrary number based on a scale ranging from -1000 to 4000 where water equals zero. As with radiography, gas does not attenuate the beam and therefore has the lowest value (-1000 HU) while bone attenuates a large amount and so has a high CT number (400-1000 HU) (Curry and others 1991). Allocation of a shade of gray to each CT number can then be used to build an image of the tissue located within that section. Unlike radiography, the density differences between fluid and soft tissue can be distinguished, allowing them to be allocated different CT numbers (0 versus 40-80 HU) and therefore they can be differentiated on the resulting image. Alteration of the grey scale allocated to each CT number is known as 'windowing' and can be used to enhance specific types of tissue according to the area being examined. The window level refers to the central CT number and the window width to the range of CT numbers represented in each image (Curry and others 1991).

Scanning protocols for imaging the middle ear in dogs (Hoskinson 1993, Love and others 1995, Russo and others 2002) and cats (Seitz and others 1996) have been described. Transverse images are obtained by positioning the animal in sternal recumbency with the horizontal rami of mandibles on a radiolucent pad (Hoskinson 1993), sponge trough (Russo and others 2002) or towel (Seitz and others 1996). Artefacts can be minimised by pulling the forelegs caudally to ensure that only the head is in the beam, ensuring intravenous fluid lines are outwith the gantry and using an endotracheal tube without a radio-opaque marker (Hoskinson 1993, Seitz and others 1996). The head should be taped to the table to reduce motion resulting from respiration (Hoskinson 1993).

The head is scanned from immediately rostral to the TB to just caudal to the petrous temporal bones with the entire examination being reported to take approximately 20-30 minutes (Love and others 1995, Russo and others 2002). The smallest field of view possible with high kVp and mAs settings should be used to image the TB due to their small size (Hoskinson 1993, Garosi and others 2003). Images are acquired with a slice thickness of 1-3mm (Hoskinson 1993, Love and others 1995, Barthez and others 1996, Seitz and others 1996, Russo and others 2002), although high resolution scanners produce slices between 1 and 1.5mm (Jones and others 1995). Slice can be contiguous, or with an overlap of 1mm (Hoskinson 1993, Love and others 1995). Thick slices result in better contrast resolution but partial volume artefact can make bone edges less distinct (Hoskinson 1993, Jones and others 1995). Thinner slices are noisier (Jones et al. 1995) but can aid in the identification of smaller features including the fine osseous structures of the ear (Love and others 1995, Russo and others 2002, Garosi and others 2003). However, often the equipment available limits the selection of slice thickness (Seitz and others 1996). A bone or wide window (level 200-300 HU; width 2000-3000 HU) produces an image with a large number of shades of grey and is useful in areas with good inherent contrast such as the TB, thereby optimising differentiation between areas of bone, soft tissue and air (Seitz and others 1996). A soft tissue or narrow window (level 40-50 HU; width 400-500 HU) produces a smaller number of grey shades and is superior for examining areas of low inherent contrast and therefore distinguishing between soft tissue structures (Jones and others 1995). In normal dogs and cats, the TB wall appears thicker when displayed with a narrow window (less than 250 CT HU) than with a wide window (more than 1000 HU) (Barthez and others 1996).

Acquired images of the head can be reformatted in alternative planes including sagittal, parasagittal and dorsal although these will be of poorer quality than the original in-plane images (Seitz and others 1996, Schwarz and others 2002). Helical scanning may create more artefacts and slightly less detail than conventional CT but enables better orthogonal and 3-dimensional reconstructions (Schwarz and others 2002). Likewise, overlapping slices will improve image resolution for reconstruction (Garosi and others 2003). However, it is also possible to obtain direct dorsal images by placing the animal in lateral recumbency with the neck flexed (Russo and others 2002).

CT imaging of the TMJ in dogs and cats follows similar principles to those described for the TB with a slice thickness of 1.2mm and a bed increment of 1mm being recommended (Schwarz and others 2002).

Although the administration of intravenous contrast has been advocated for the identification of inner and middle ear disease, it is not routinely performed and there do not appear to be any reports involving its use (Hoskinson 1993, Garosi and others 2003). For most conditions of the TMJ, intravenous iodine contrast is not indicated. If used, post contrast scanning should be performed using a protocol designed for imaging the brain, with a thicker slice width to reduce visible noise and to enhance contrast resolution between normal and abnormal soft tissue (Schwarz and others 2002).

5.1.2. Clinical applications of CT relating to the TB

Improvements in CT technology mean that it has now replaced multidirectional tomography for investigation of the human middle ear (Swartz 1983). The technique has been documented and the normal anatomy and variations have been described (Swartz 1983, Alexander and Caldemeyer 1998). High resolution CT allows visualisation of many structures within the human middle ear including the ossicles and their ligamentous attachments, the tensor tympani muscle and tendon and the round window. Optimum views for each have been recommended (Swartz 1983).

Although there are several publications presenting normal transverse sections of the canine and feline TB (Feeney and others 1991, George and Smallwood 1992, Hoskinson 1993, Love and others 1995, Barthez and others 1996, Seitz and others 1996, Assheuer and Sager 1997), there is currently only one publication presenting the CT anatomy of the canine middle and inner ear in any detail (Russo and others 2002) and none in cats. The TB should be symmetrical (Barthez and others 1996) and the prevailing density within the normal TB is air (Love and others 1995). Contiguous 1mm slices enabled identification of all major structures including tympanic membrane, auditory ossicles, TB, cochlea, internal acoustic meatus, semicircular canals and the vestibular window (Russo and others 2002). However, the tympanic membrane and many other small structures were not visible using 3mm slices due to partial volume artefact (Love and others 1995).

5.1.3. Applications of CT relating to the TMJ

CT evaluation of the human TMJ has been described (Suarez and others 1980). The contour and shape of the bony elements of the joint are clearly shown, with the articular space and condylar cortex being well defined, and the close relationship with the middle ear clearly evident. The disc can be visualised (Dixon 1991), with 45° oblique sections

demonstrating its thickened medial margin that can be traced into the space between the condyle and the articulating surface of the eminence (Suarez and others 1980, Dixon 1991). Difficulties in determining the position of the disc can be encountered due to the similarity in density with the surrounding soft tissue, in particular the attachment area of the lateral pterygoid muscle to the condyle (Dixon 1991) and so CT is not recommended for this purpose (Payne and Nakielny 1996). However, CT can be used to assess the spatial relationship of the joint components with each other (Minagi and others 2000). Scanning the joint in both open and closed mouth positions may also help determine the location of the disc (Dixon 1991). Exquisite anatomical detail can be obtained using a high resolution CT technique (Thompson and others 1984). Consequently in humans, CT is the method of choice for evaluating complex craniofacial trauma and investigating osseous changes and soft tissue calcifications in joints with inflammatory, developmental or neoplastic conditions (Larheim 1995, Payne and Nakielny 1996).

Transverse CT sections of the normal TMJ in horse cadavers have been published and it was reported to be an excellent imaging modality for the dense bone structures of the petrous temporal bones and joint components (Morrow and others 2000). In the dog, CT has been used to examine the elbow (Reichle and Snaps 1999) and hock joints (Gielen and others 2002), as well as the lumbosacral spine and intervertebral disc spaces in canine cadavers (Jones and others 1995). There are several publications presenting normal transverse CT sections of the canine TMJ (Feeney and others 1991, George and Smallwood 1992, Assheuer and Sager 1997) but none describe it in any detail. The use of CT to evaluate the canine and feline TMJ has been reviewed and reported that the internal soft tissue structures, including the articular cartilage and disc, joint capsule and lateral ligament were not discernable although excellent detail of the trabecular and subchondral bone was achieved (Schwarz and others 2002). Likewise, intervertebral discs are not consistently visible due to partial volume averaging during examination of the lumbosacral spine and it has been suggested that better visualisation of these structures may be possible using thinner slices (Jones and others 1995). 3-dimensional reconstructions of the canine TMJ have been performed and allowed the shape and spatial relationships of the joint components to be determined (McCormick and others 1995, Stelnicki and others 2001).

CT has been used in dogs and cats to identify fractures of the TMJ components, a mandibular osteosarcoma involving the condyloid process of the mandible and an abscess arising from the TB extending to involve the ipsilateral TMJ (Schwarz and others 2002). It has also been employed to evaluate involvement of the TMJ in a case of craniomandibular

osteopathy (Hudson and others 1994) and 3-dimensional reconstructions have been used experimentally to assess TMJ changes following mandibular distraction (McCormick and others 1995, Stelnicki and others 2001). CT was reported to be of value for evaluating TMJ disorders in horses (Dik 1994) and identified destructive TMJ disease in 2 horses (Warmerdam and others 1997) and a sheep (Warmerdam and van Weeren 1996). It has also been used to identify an avulsion fracture at the insertion of the TMJ ligaments or deep belly of the masseter muscle in a horse (Tietje and others 1996).

There appears to be only one report on the use of CT to demonstrate the normal anatomy of the rabbit head but no published images (Bochler and Kneissl 2002), and none regarding the TB or TMJ in this species.

5.1.4. Aims

The aims of the work presented in this chapter were to:

- Acquire direct transverse, sagittal and dorsal CT images of the normal and fluid-filled TB, and open and closed TMJ in dog, cat and rabbit cadavers
- Compare these images to the multiplanar anatomical sections produced in Chapter 2 and document the CT anatomy of the TB and TMJ

5.2. Materials and Methods

5.2.1. Cadaver material

Four Jack Russell Terrier dogs, four domestic breed feline and four New Zealand White rabbit cadavers with no visible external evidence of abnormalities affecting the TB or TMJ were selected from the material collected as described in Chapter 2. They were removed from the freezer and placed in running cold water for 24 hours until they had defrosted. They were then dried thoroughly.

In two cadavers of each species, ultrasound gel was introduced into the right middle ear cavity using the technique described in Chapter 4. In the cat, this was only introduced as far as the dorsal compartment so the septum remained intact. Two of each species were examined with the mouth closed and micropore tape was placed around the nose to prevent the mandible moving or the mouth opening during positioning. The other two were examined with the mouth open. In the dog this was achieved using a 5ml plastic syringe with the plunger and tip removed, placed between the canine teeth. A 2ml syringe was used in a similar way in the cat. In the rabbit, the barrel of a 2ml plastic syringe was placed across the diastema, moving the incisors approximately 1cm apart. This was as far as the mouth could be opened in this species before resistance was encountered. The heads were then wrapped in cling film to prevent leakage and contamination of the equipment or positioning devices.

5.2.2. CT equipment and procedure

An Elscint CT Twin Flash scanner (Figure 5.2.1) was used in all three species with settings of 120kV and 100mAs, a slice thickness of 1.1mm and a pitch of 0.7. The resulting in-plane resolution of the images was approximately 0.6mm.

Cadavers, with the mouth closed, were placed in a true dorsoventral position with the mandibles flat against a rectangular foam positioning block and taped in place. Cadavers, with the mouth open, were taped to the positioning block as if for a ventrodorsal radiographic view with the dorsal aspect of the head against the block. The block was then repositioned within the bore of the machine to allow direct imaging in transverse, sagittal and dorsal planes (Figure 5.2.2.). A pilot scan was performed in each cadaver and used to guide manual adjustment of the scan plane to accommodate any inconsistencies in positioning.

For transverse images, the head was positioned as for a dorsoventral or ventrodorsal radiographic view, with the long axis of the head perpendicular to the gantry. Slices were made from midway along the zygomatic arch to occipital region. Sagittal slices were obtained by rotating the positioning block through 90° so the long axis of the head remained horizontal but was now parallel with the gantry. Slices were made through the entire head from right to left. Finally, the positioning block was placed on its end so the head was positioned as if for a rostrocaudal radiographic view with the hard palate vertical and the long axis of the head still parallel with the gantry. This allowed a series of coronal or dorsal slices to be obtained through the entire head from dorsal to ventral.

5.2.3. Image analysis and reproduction

MxView software (Marconi Medical Systems, Inc) interfaced with the CT system and allowed the resulting images to be viewed using bone (level 500 HU; width 2000 HU), brain (level 35 HU; width 150 HU) and two soft tissue windows (level 45 HU; width 450 HU and level 200 HU; width 800 HU), as recommended by Jones et al. (1995) and Love et al (1995). In one canine cadaver, sagittal and dorsal reconstructions were performed from the transverse images. The series deemed to be most representative were selected for presentation.

Images were downloaded to E-film medical Imaging software (Medical Inc, Toronto) and then directly transferred digitally onto a desk top personal computer. Paint Shop Pro 7 software (Microsoft) was used to manipulate and label the resulting images.



Figure 5.2.1. Elscint Twin Flash CT scanner.



Figure 5.2.2. Rabbit cadaver head demonstrating positioning in the CT scanner.

- A. Transverse sections
- B. Sagittal sections
- C. Dorsal sections

5.3. Results

Each of the CT slice sequences took under 5 minutes to acquire and the cadaver was repositioned while the images were being reconstructed, therefore each cadaver took less than 15 minutes to image. Slight differences in size between cadavers resulted in a variable number of slices being obtained from each region in different specimens. However, all of the structures produced a similar appearance in the cadavers of each species, with some minor variations in shape and size observed. Since the areas identified remained similar throughout each series of sections obtained, only representative images have been labelled.

5.3.1. CT appearance of the gas and fluid-filled TB in the dog, cat and rabbit

In all three species, the bones of the cranium including the petrous temporal bone, auditory ossicles, TB wall and hyoid apparatus appeared hyperdense and therefore white on all the images, while gas within the lumen of the external ear canal and TB lumen appeared black. When viewed using a bone window, the soft tissue structures of the head appeared grey with fat in the fascial planes between the muscles producing hypodense streaks. Any ultrasound gel or post mortem fluid present in the external ear canal could just be distinguished from the walls of the external ear canal. Any ultrasound gel or post mortem fluid within the TB lumen, and the normal fluid associated with the inner ear, could be identified due to the adjacent bone but were isodense with the soft tissue structures beyond these.

The transverse CT images of the TB obtained in the dog, cat and rabbit using the bone window are demonstrated in Figures 5.3.1 to 5.3.3. with the key in Table 5.1.

In all three species, some partial volume artefact was observed towards the rostral and caudal extremities of the TB, resulting in apparent thickening and blurring of the wall. In the cat, the bone septum was clearly visible as a fine, curved, hyperdense line running across the TB, but was less well defined at its caudal extremity. The TB in the dog and cat were located on the ventral aspect of the skull, while they were more laterally located in the rabbit. The internal shape of the rabbit TB was elongated in a dorsoventral direction rather than the rounded shape of the dog and cat. The extensive epitympanic recess in this species could also be appreciated extending dorsally within the temporal bone.

Following the introduction of ultrasound gel into the canine TB lumen, the only areas remaining unfilled were the rostradorsal extremity, above the bone ridge formed by the inner margin of the external acoustic meatus, and the epitympanic recess around the ossicles. This distribution remained similar regardless of the position of the head. In the cat, the dorsal compartment was filled as was the epitympanic recess, again with the exception of the area around the ossicles. Although no fluid was introduced into the ventral compartment there was occasionally a small amount located at the most ventral point. Like the dog, the rostradorsal area of the rabbit TB remained unfilled although the gel did surround the ossicles and extend further dorsally into the epitympanic recess but did not completely fill this. The TB wall did not appear thickened in the presence of gel within the lumen in any of the species.

In the images of the cat, there was a small amount of post mortem fluid present in the left external ear canal at the external acoustic meatus, which resulted in a distinct air – fluid boundary at the level of the tympanic membrane (Figure 5.3.2. Slices 5 and 6). The malleus appeared as a distinct hyperdense tapering line running obliquely across the external acoustic meatus and the tympanic membrane extended from its termination to the opposite bone margin. However, in the presence of an air-filled external acoustic meatus in all three species, the tympanic membrane was not actually visible and the malleus remained visible even when the tympanic membrane had been ruptured to allow the introduction of fluid into the TB.

The sagittal images of the TB obtained in the dog, cat and rabbit using the bone window are demonstrated in Figures 5.3.4 to 5.3.6. with the key in Table 5.1. The images acquired directly were of better quality than those derived from reconstruction of the transverse images (Figure 5.3.4.1.) therefore only the directly acquired images have been presented in subsequent figures.

In the dog, the external ear canal appeared horseshoe shaped, with the ventral margin only becoming visible medial to the level of the lateral TB wall where it projected into the lumen, producing small bone ridges between the middle of the TB lumen and the caudal and rostral extremities. The malleus was visible dorsally, where the external acoustic meatus met the middle ear cavity, and was projecting from the epitympanic recess ventrally towards the location of the tympanic membrane, although this latter structure was not visible. The wall medial to the extension of the ventral margin of the external acoustic meatus remained thickest while the ventral and caudal walls were uniformly thin. The

mastoid process was visible caudal to the TB. As before, the introduction of fluid resulted in filling of the entire TB lumen with the exception of the rostral region and the epitympanic recess dorsal to the malleus.

In the cat, the caudal aspect of the TB lumen became visible at the same level as the external acoustic meatus. The septum appeared as a thin curved hyperdense line, running from the caudal ridge formed by the ventral margin of the external acoustic meatus dorsally to a point midway along the inner ear structures. The thick area of wall produced by the continuation of the ventral margin of the external acoustic meatus was restricted to the dorsolateral compartment. The wall of the ventral compartment was uniformly thin throughout. The structures of the inner ear were not as clearly visualised in the cat due to the small size and the resulting partial volume artefact causing blurring of the bone margins. The presence of a small amount of post mortem fluid at the distal end of the external ear canal in one of the cadavers again highlighted the location of the tympanic membrane although as with the dog, this was not actually visible. In this cadaver, there was a distinct gap in the dorsal edge of the septum at the lateral extremity of the promontory.

In the rabbit, the external acoustic meatus was very prominent and with medial progression, the TB lumen became visible as a semicircular area rostral and ventral to it. The malleus was visible at the ventral aspect of the extensive epitympanic recess but none of the other ossicles were identified. In the presence of fluid, the rostradorsal compartment of the TB lumen and the epitympanic recess remained empty.

The dorsal images of the TB obtained in the dog, cat and rabbit using the bone window are demonstrated in Figures 5.3.7 to 5.3.9. with the key in Table 5.1. The images acquired directly were of better quality than those obtained using reconstruction of the transverse images (Figure 5.3.7.1.) therefore only the directly acquired images have been presented in subsequent figures.

In the dog and cat, the structures of the inner ear were visualised dorsal to the level of the external acoustic meatus. However, in the rabbit the external acoustic meatus and then the extensive epitympanic recess were the most dorsal structures identified. The ossicles could be identified in these views. In the cat, the septum bulla was visible and the relationship between the dorsal and ventral compartments was clear with ventral progression, as were the differences in shape of the TB between the three species.

<u>Label</u>	<u>Description</u>
1	Tympanic bulla
2	Tympanic cavity
3	Epitympanic recess
4	Dog – bone ridge Cat – septum bulla
5	External acoustic meatus
6	Malleus
7	Incus
8	Stapes
9	Vestibular / oval window
10	Promontory
11	Cochlear / round window
12	Tympanic membrane
13	Mastoid process

Table 5.1. Anatomical features associated with the TB. Key for figures 5.3.1. to 5.3.9.

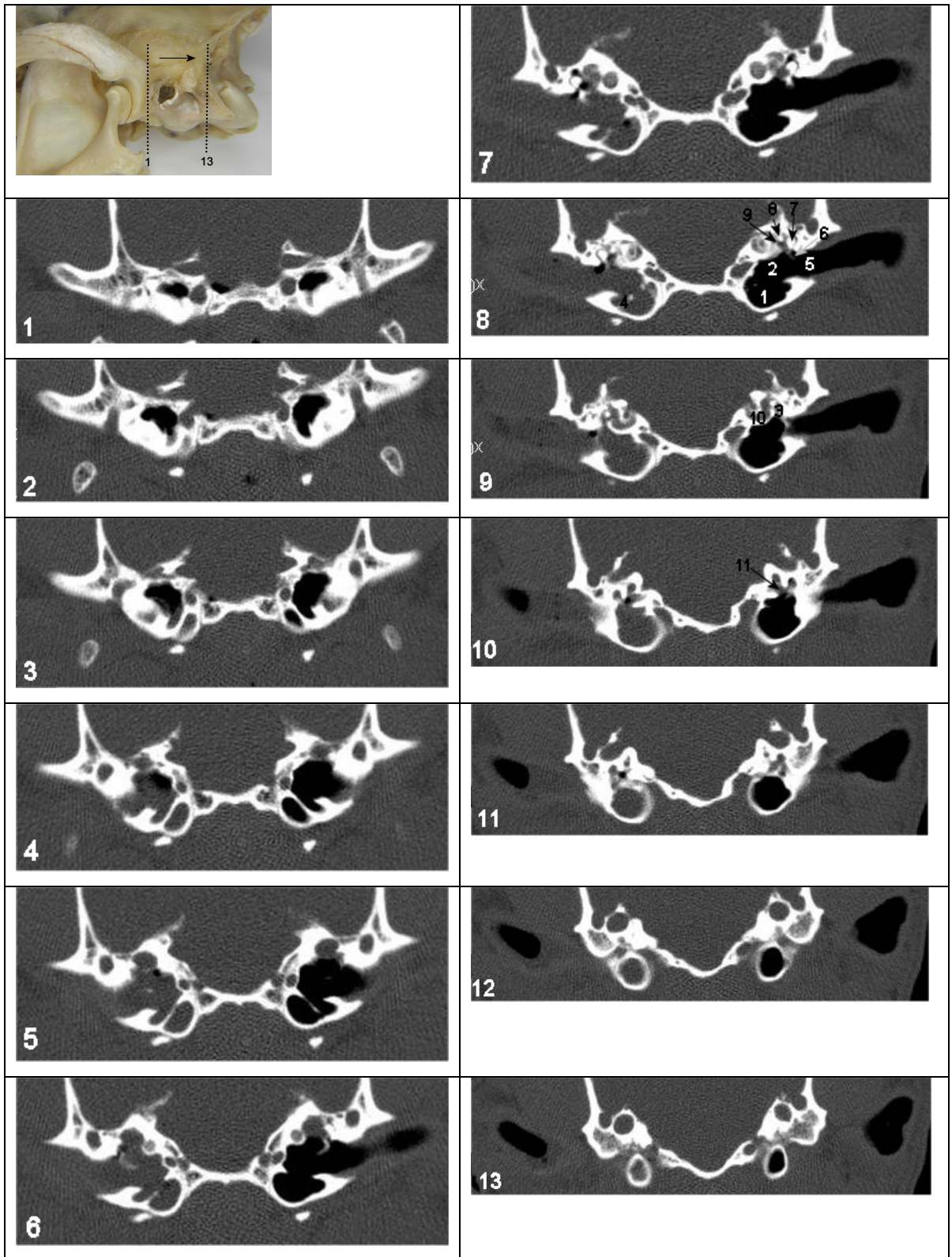


Figure 5.3.1. Transverse CT images of the gas and fluid-filled canine TB using a bone window, with the cadaver in dorsal recumbency and progressing from rostral to caudal. Dorsal is to the top and right is to the left in all images. Number in bottom left corner indicates slice number. Approximate location of the first and last slice is indicated on the pilot image. For key see Table 5.1.

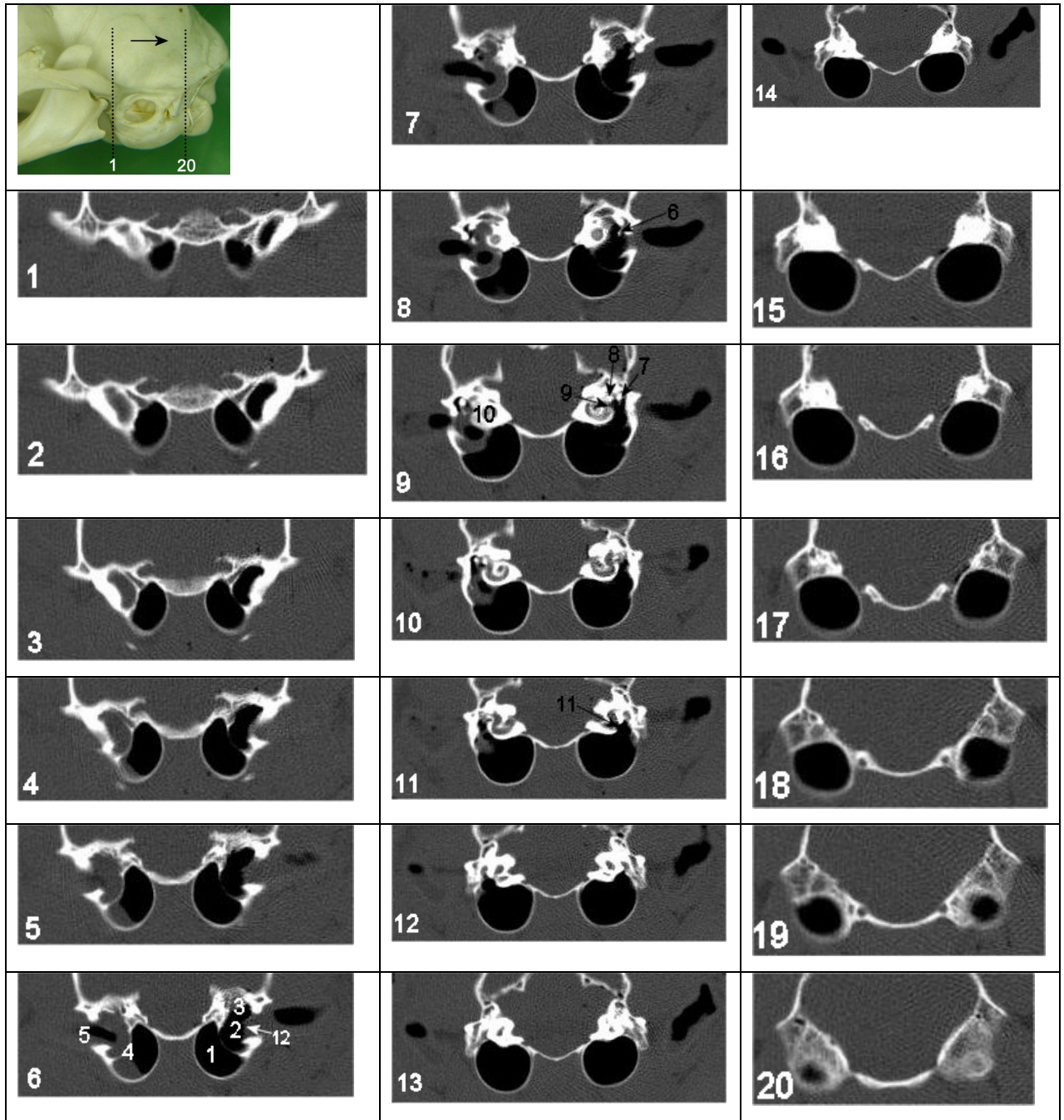


Figure 5.3.2. Transverse CT images of the gas and fluid-filled feline TB using a bone window with the cadaver in ventral recumbency, progressing from rostral to caudal. Dorsal is to the top and right is to the left in all images. Approximate location of the first and last slice is indicated on the pilot image. Number in bottom left corner indicates slice number. For key see Table 5.1.

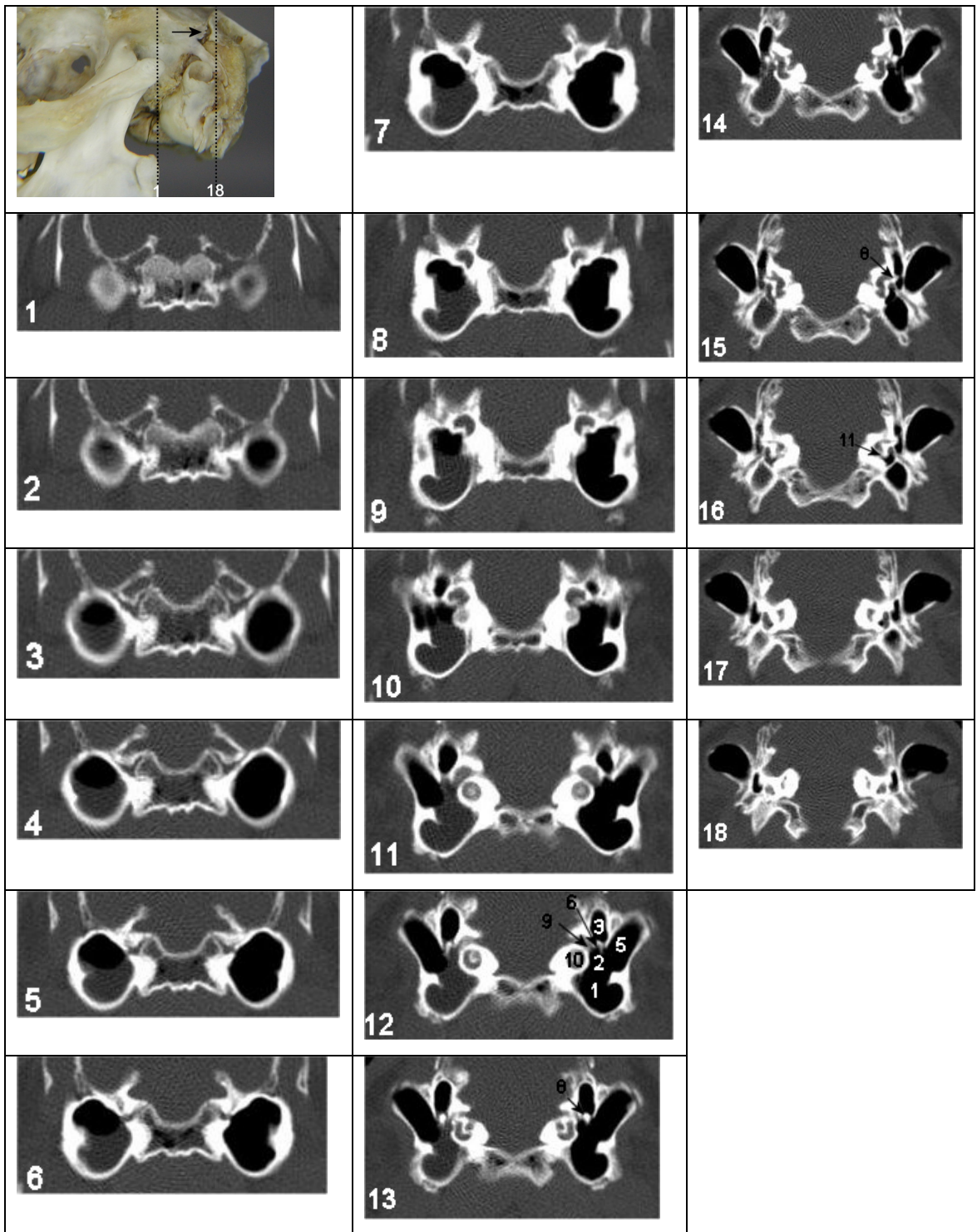


Figure 5.3.3. Transverse CT images of the gas and fluid-filled rabbit TB using a bone window with the cadaver in ventral recumbency, progressing from rostral to caudal. Dorsal is to the top and right is to the left in all images. Number in bottom left corner indicates slice number. Approximate location of the first and last slice is indicated on the pilot image. For key see Table 5.1.

Figure 5.3.4. Sagittal CT images of canine TB using a bone window. Dorsal is to the top and rostral is to the left in all images.

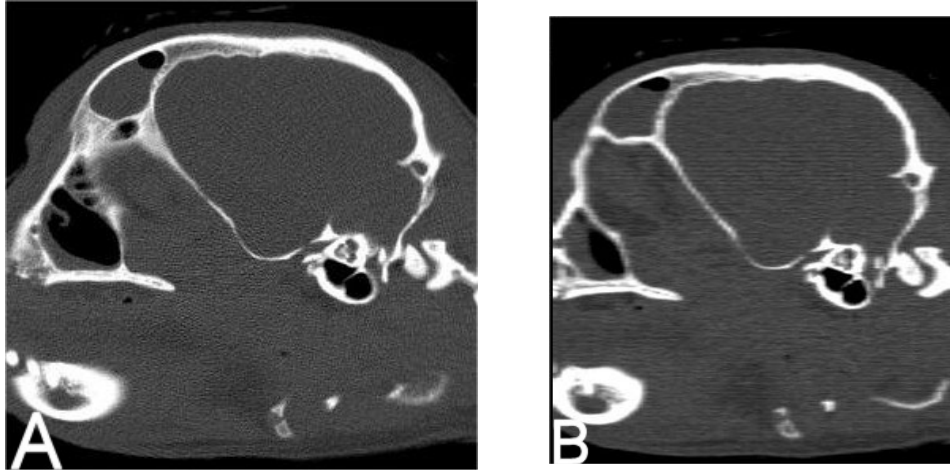


Figure 5.3.4.1. Corresponding sagittal sections through the canine TB.

A. Directly acquired. B. Reconstructed from transverse images.

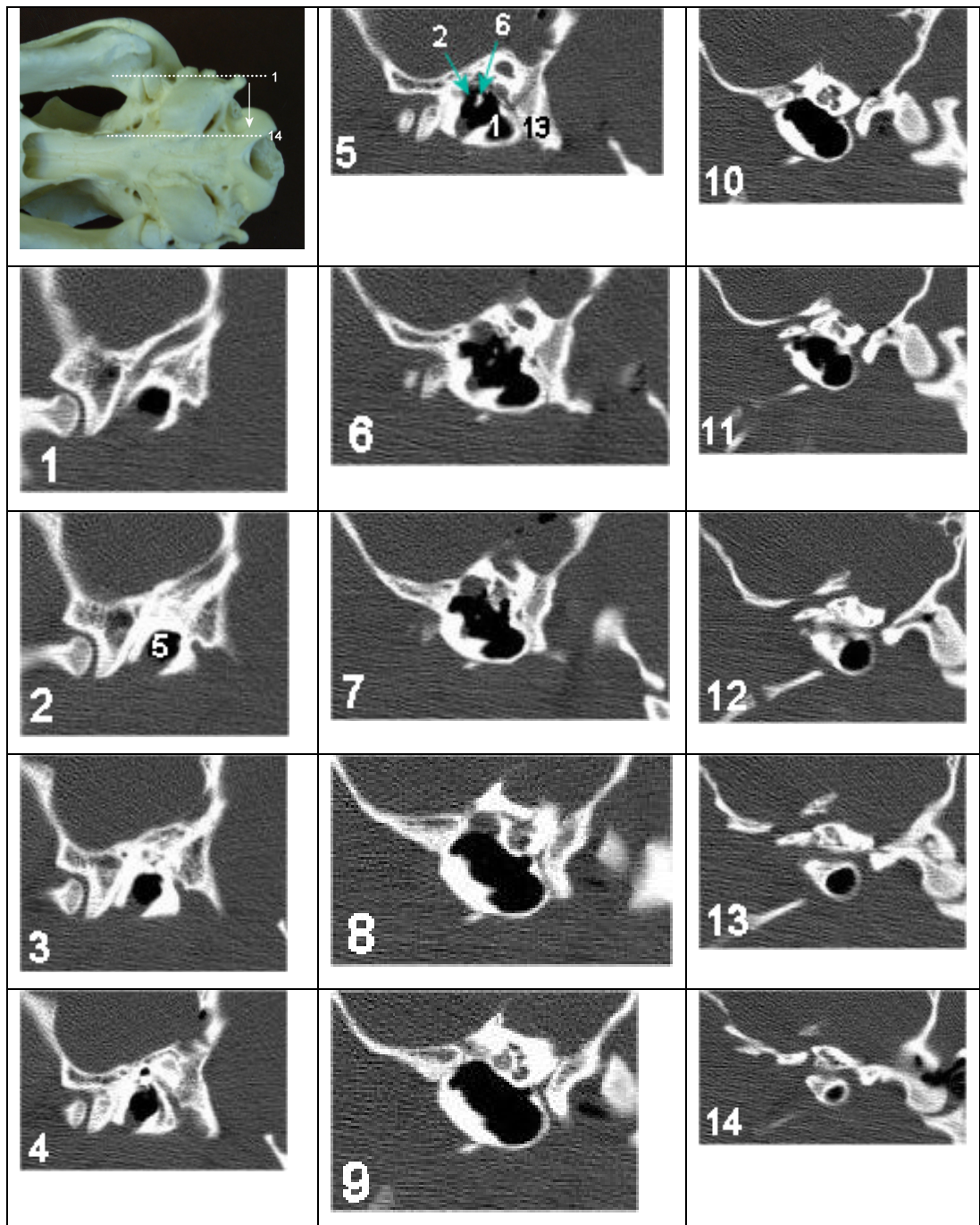


Figure 5.3.4.2. Sagittal CT images of the gas-filled canine TB with the cadaver in ventral recumbency, progressing from lateral towards midline. Number in bottom left corner indicates slice number. Approximate location of the first and last slice is indicated on the pilot image. For key see Table 5.1.

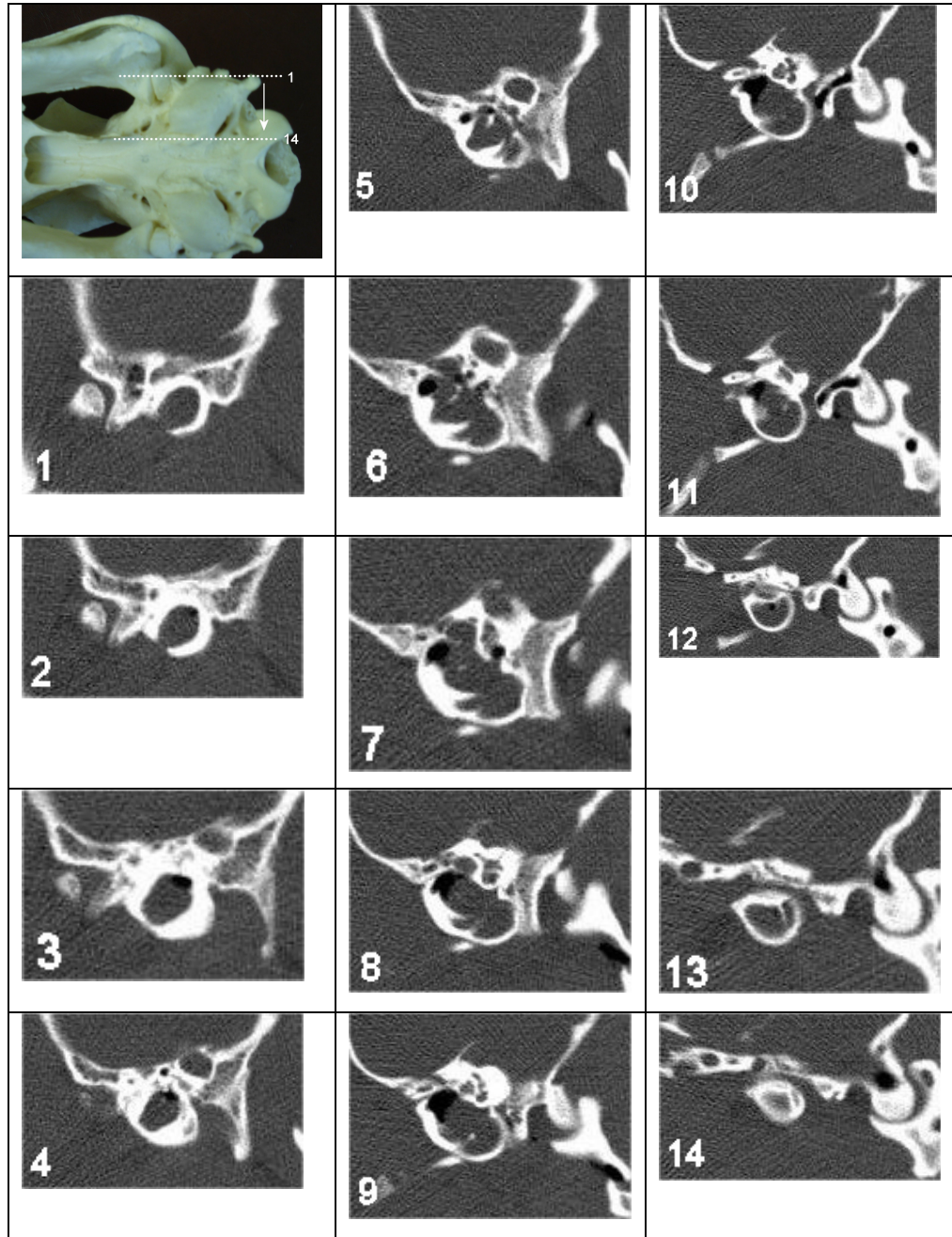


Figure 5.3.4.3. Sagittal CT images of the fluid-filled canine TB with the cadaver in dorsal recumbency. Approximate location of the first and last slice is indicated on the pilot image.

Figure 5.3.5. Sagittal CT images of the feline TB using a bone window with the cadaver in ventral recumbency, progressing from lateral towards midline. Dorsal is to the top and rostral is to the left in all images. Number in bottom left corner indicates slice number. Approximate location of the first and last slice is indicated on the pilot image. For key see Table 5.1.

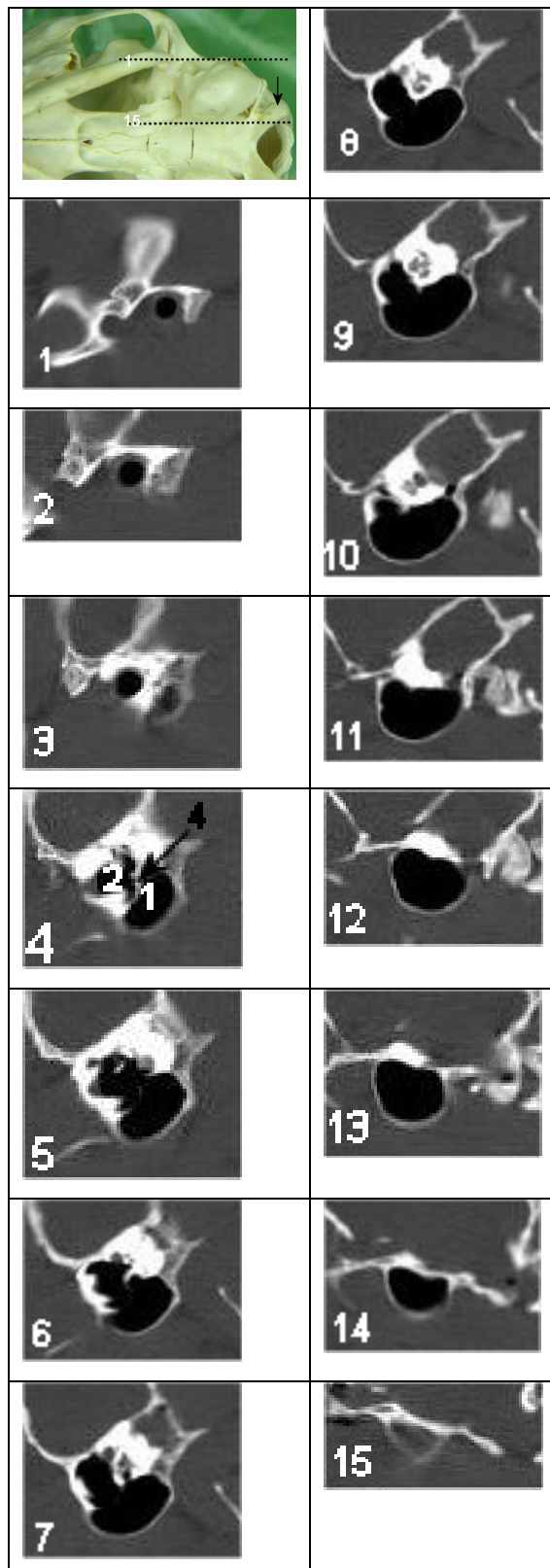


Figure 5.3.5.1. Sagittal CT images of the gas-filled feline TB

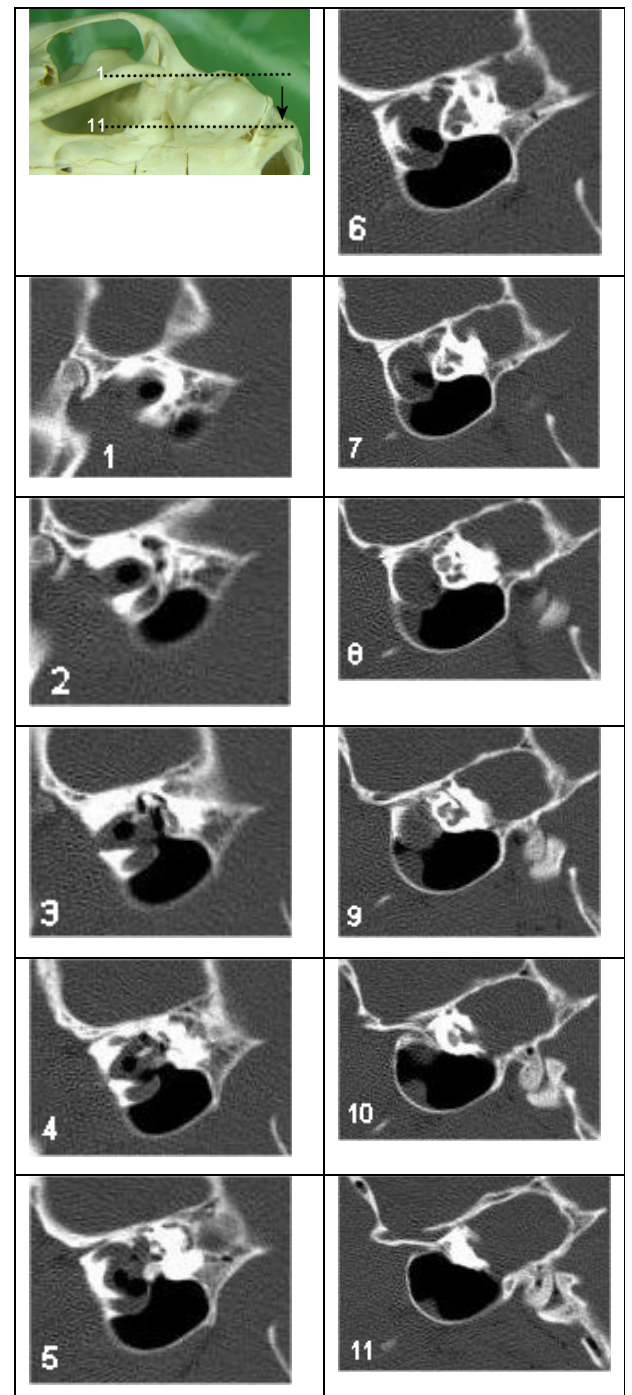


Figure 5.3.5.2. Sagittal CT images of the feline TB with a fluid-filled dorsal compartment and a small volume of fluid in the ventral compartment

Figure 5.3.6. Sagittal CT images of the rabbit TB using a bone window with the cadaver in ventral recumbency, progressing from lateral towards midline. Dorsal is to the top and rostral is to the left in all images. Number in bottom left corner indicates slice number. Approximate location of the first and last slice is indicated on the pilot image. For key see Table 5.1.

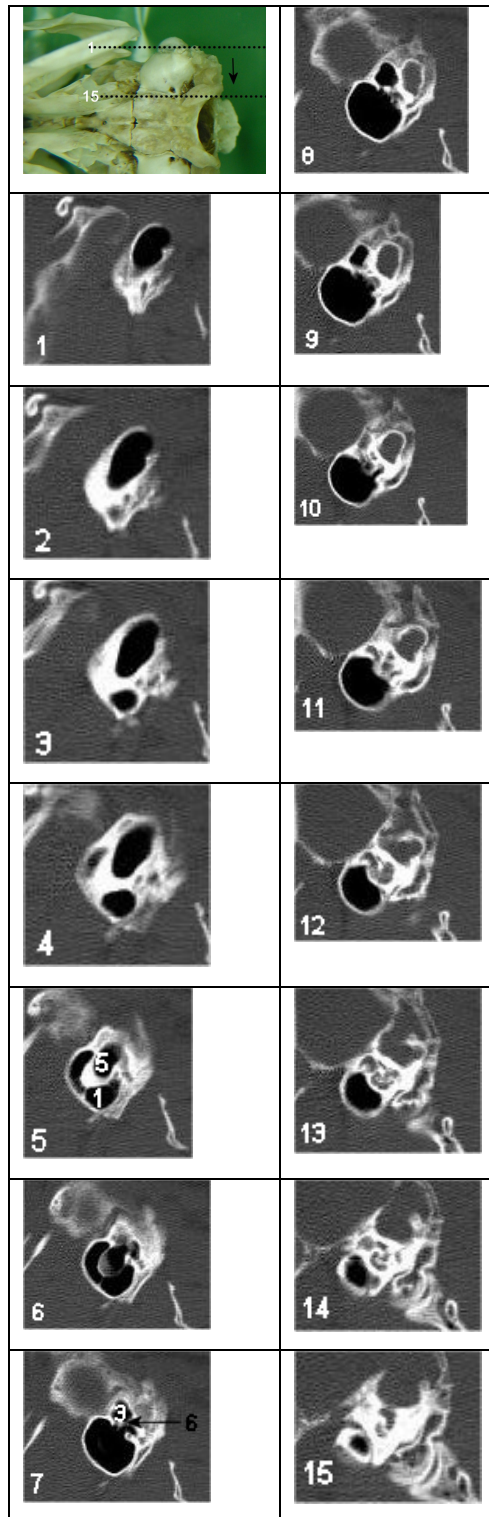


Figure 5.3.6.1. Sagittal CT images of the gas-filled rabbit TB

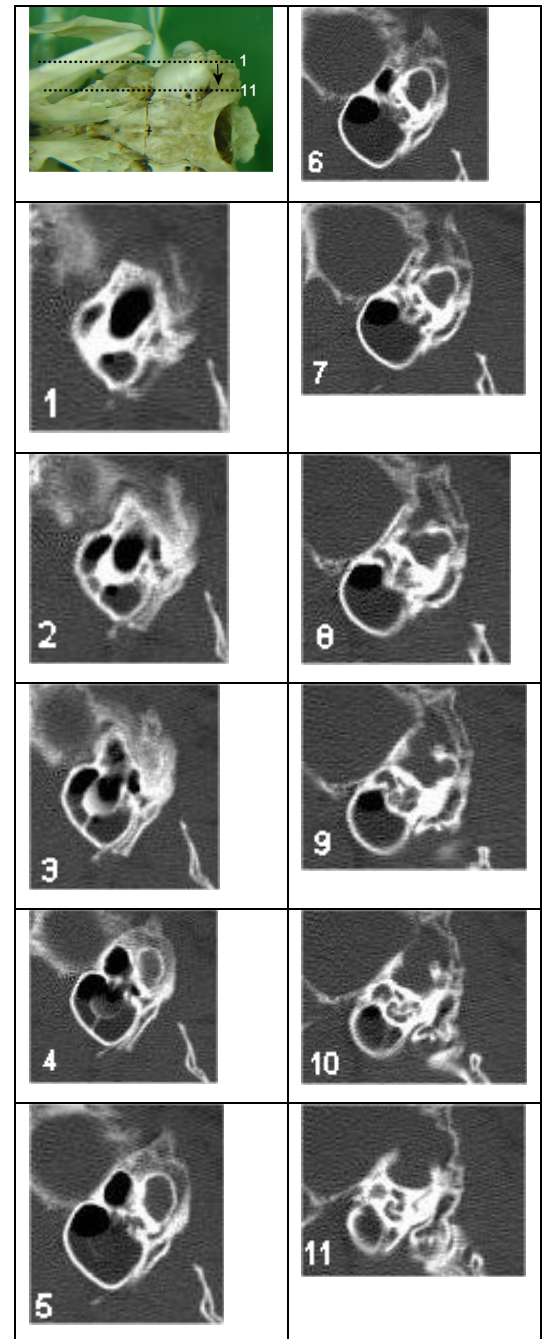


Figure 5.3.6.2. Sagittal CT images of the fluid-filled rabbit TB

Figure 5.3.7. Dorsal CT images of canine TB using a bone window. Rostral is to the top and right is to the left in all images.

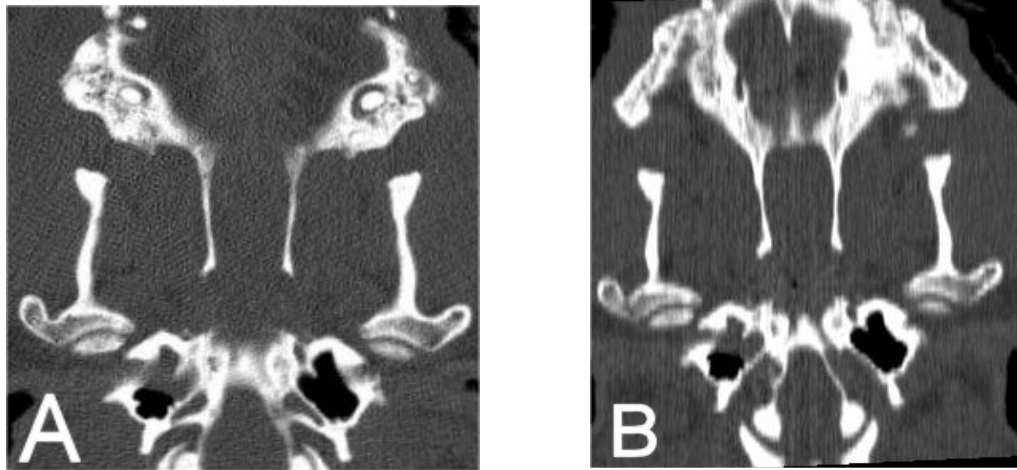


Figure 5.3.7.1. Corresponding dorsal sections through the canine TMJ.

A. Directly acquired. B. Reconstructed from transverse images.

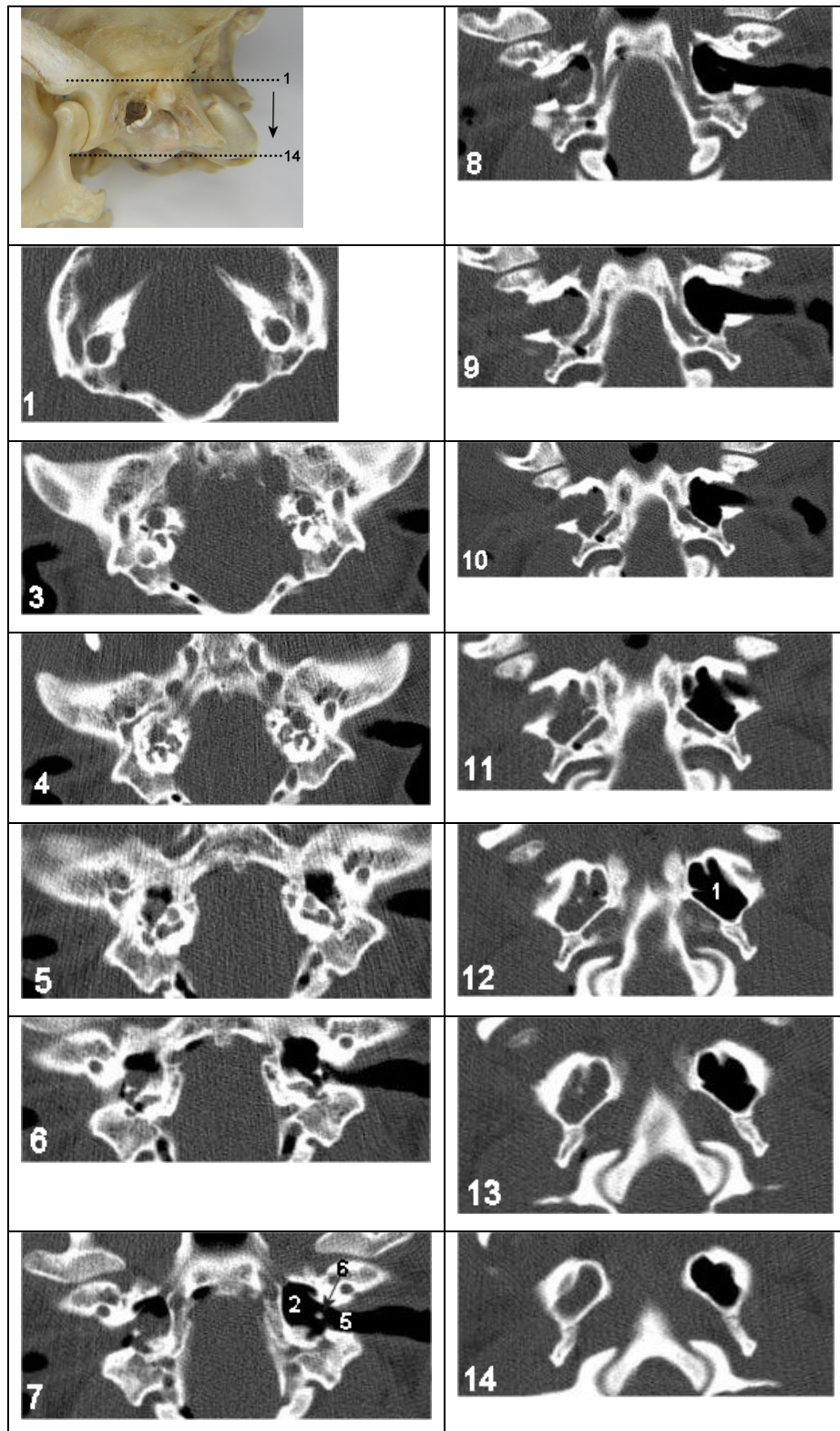
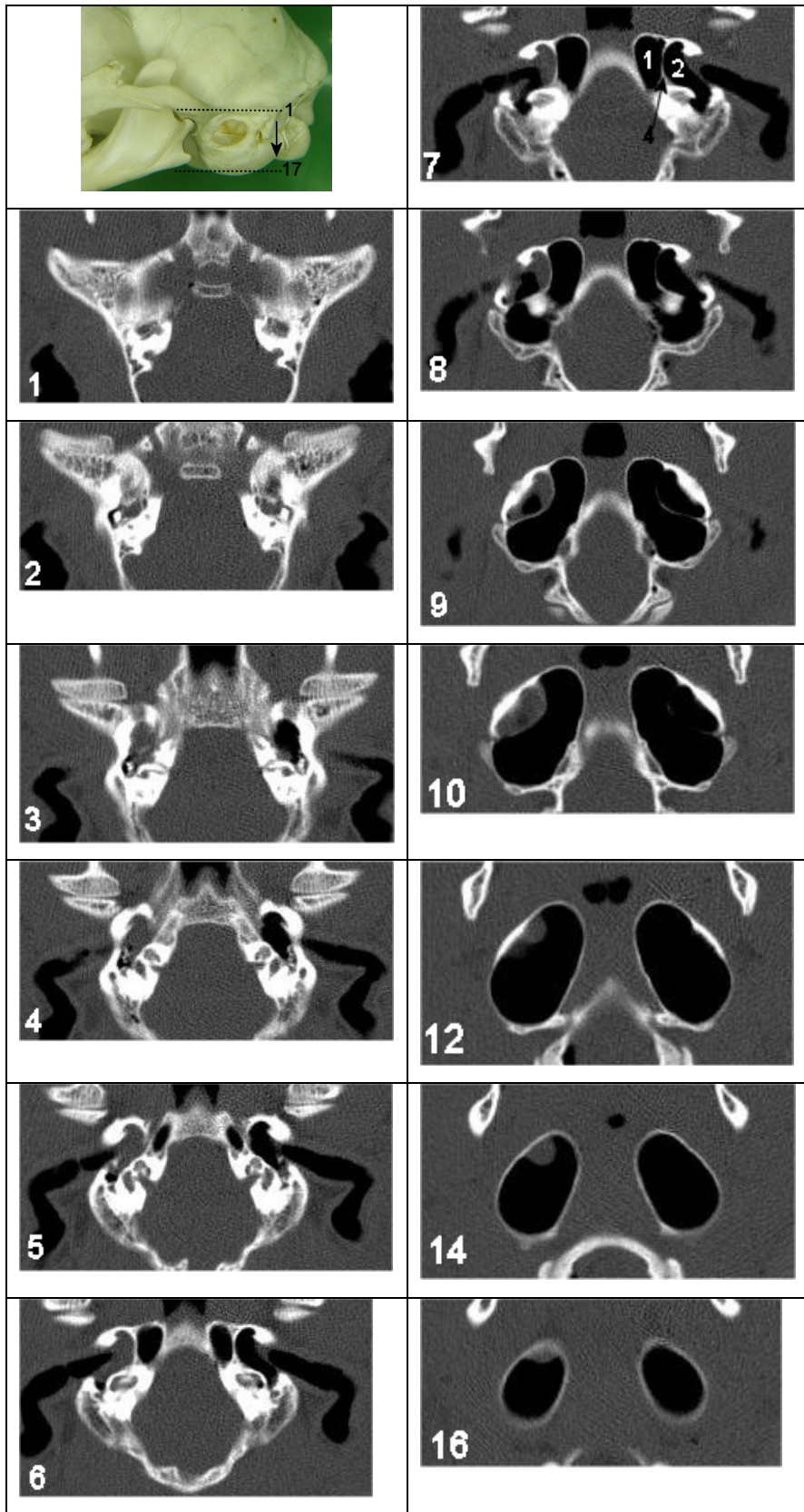


Figure 5.3.7.2. Dorsal CT images of the gas and fluid-filled canine TB with the cadaver in dorsal recumbency, progressing from dorsal to ventral. Number in bottom left corner indicates slice number. Approximate location of the first and last slice is indicated on the pilot image. For key see Table 5.1.



Figure

5.3.8.

Dorsal CT images of the gas and fluid-filled feline TB using a bone window with the cadaver in ventral recumbency, progressing from dorsal to ventral. Rostral is to the top and right is to the left in all images. Number in bottom left corner indicates slice number. Approximate location of the first and last slice is indicated on the pilot image. For key see Table 5.1.

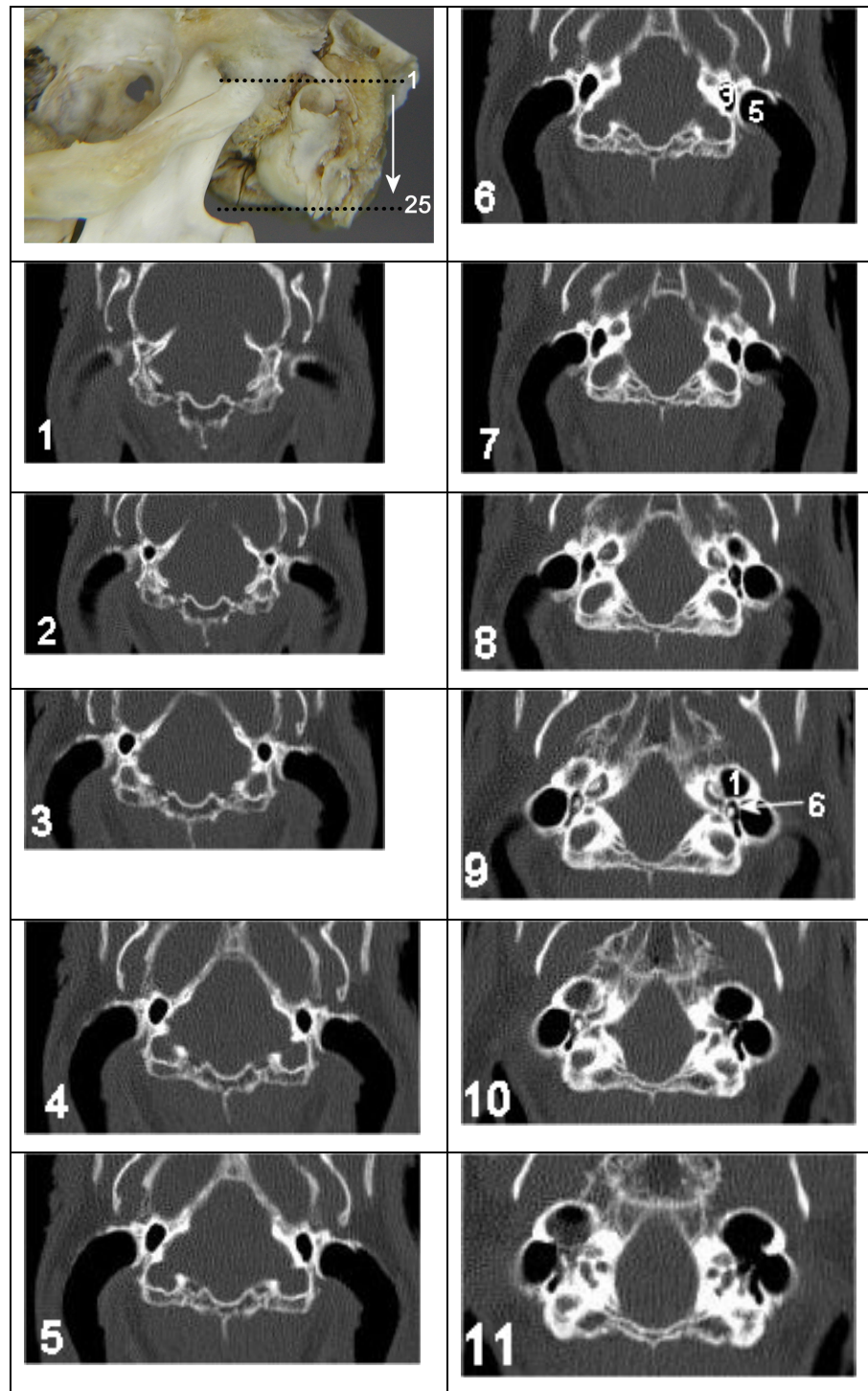
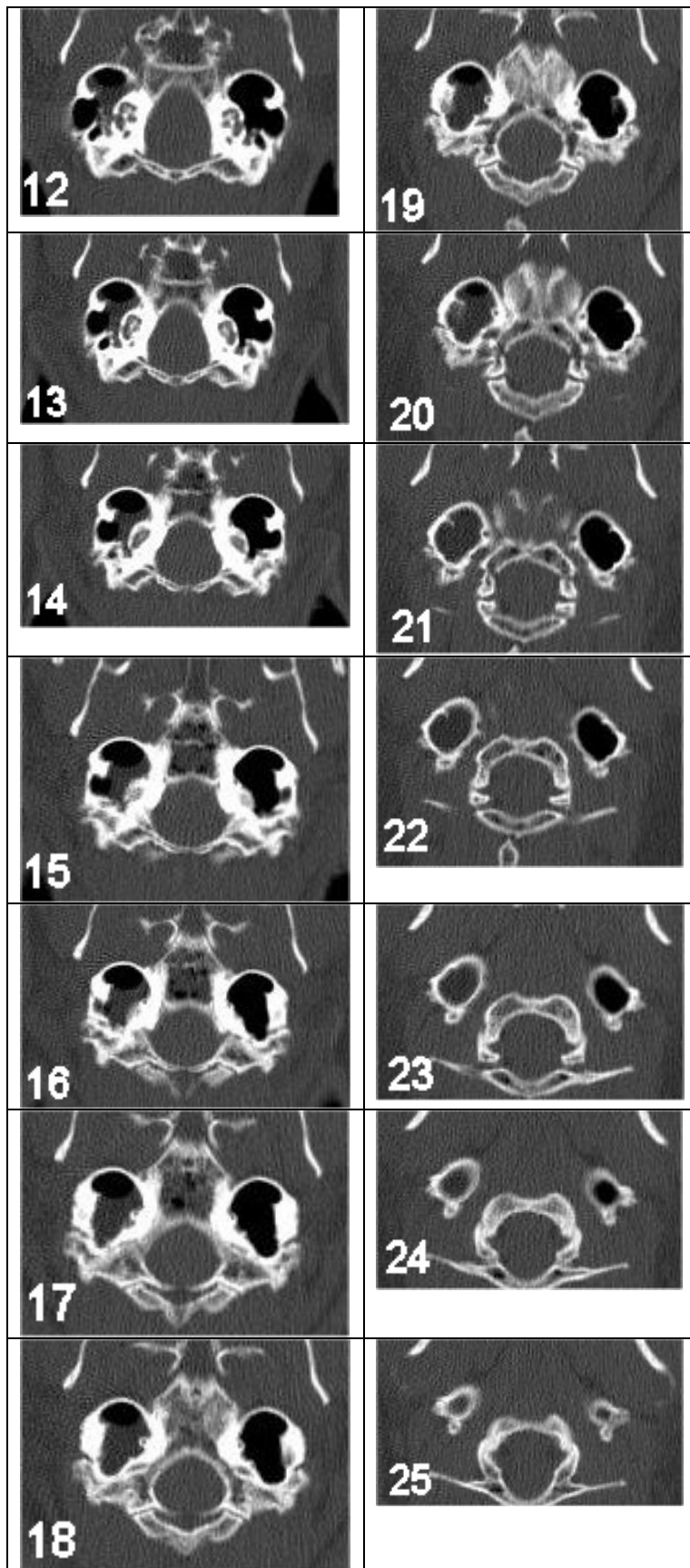


Figure 5.3.9. Dorsal CT images of the gas and fluid-filled rabbit TB using a bone window with the cadaver in ventral recumbency, progressing from dorsal to ventral. Rostral is to the top and right is to the left in all images. Number in bottom left corner indicates slice number. Approximate location of the first and last slice is indicated on the pilot image. For key see Table 5.1.

Figure 5.3.9. continued. Dorsal CT images of the gas and fluid-filled rabbit TB



5.3.2. CT appearance of the open and closed TMJ in the dog, cat and rabbit

The transverse CT images of the TMJ obtained in the dog, cat and rabbit using the bone window are demonstrated in Figures 5.3.10. to 5.3.12. with the key in Table 5.2.

The cortical bone of the zygomatic arch, mandibular fossa and condyloid process appeared uniformly hyperdense on the images but the central cancellous regions appeared less dense and speckled. In the dog and cat, the dorsal articular surface of the condyloid process and the corresponding surface of the mandibular fossa were clearly visualised with the mouth closed. The most rostral section (Fig 5.3.10. slices 2 and 3) through the closed TMJ in the dog demonstrated a defect in the lateral half of the condyloid process. This was due to the long axis of the process being orientated in a rostromedial – caudolateral direction rather than transversely, and the slightly concave rostral margin of the dorsal articular surface. The medial extremity was visible, the lateral extremity was partially within the slice but the region immediately medial to it was not, resulting in the appearance of a hypodense defect. This was not observed in the cat. The caudal and ventral articular surfaces of the condyloid process and that of the corresponding retroarticular process were not visible due to the partial volume artefact. The pit at the medial aspect of the retroarticular process was much more distinct in the dog than the cat. Using this bone window, the intra-articular fluid and soft tissue of the TMJ could not be distinguished from each other or surrounding soft tissue structures in any of the species.

With the TMJ open in the dog and cat, the same areas of the mandibular fossa were imaged but in conjunction with the caudal articular surface of the condyloid process. In the dog, this resulted in a greater angle between the lateral and medial parts of the articular surface being observed while in the cat, the surface remained horizontal. The defect at the rostral margin of the condyloid process in the dog was not visible in this series due to rotation of the condyloid process into an orientation parallel with the slice direction.

In the rabbit, the narrow mandibular fossa meant it was affected by partial volume artefact and so its articular surface could not be clearly visualised. The dorsal articular surface of the condyloid process could be identified and with the mouth closed, it was located just caudal to the level of the mandibular fossa. The dorsal surface of the condyloid process was visible in subsequent slices as it tapered caudally to the non-articular area and beyond the limit of the caudal extension of the zygomatic process. Opening the mouth in the rabbit

did not significantly alter the appearance of the TMJ components and therefore these images have not been presented.

The sagittal images of the TMJ obtained in the dog, cat and rabbit using the bone window are demonstrated in Figures 5.3.13 to 5.3.15. with the key in Table 5.2.

At the lateral aspect of the canine TMJ, the mandibular fossa appeared flattened and there was a space ventrally between it and the rounded condyloid process. The mandibular fossa became more rounded with medial progression where it and the retroarticular process matched the contour of the condyloid process well, although there was some widening of the joint space ventrally. There was a more abrupt angle between the mandibular fossa and retroarticular process towards their medial extremities. Just medial to the lateral extremity of the condyloid process there was a slight concavity on the rostral margin between it and the neck of the process, which is likely to have been responsible for the defect present in this area on the transverse images (Figure 5.3.13. Slice 5 to 7). The length of the retroarticular foramen was clearly visible in these sections.

In the cat, the lateral aspect of the mandibular fossa was more rounded than in the dog and conformed better with the shape of the condyloid process. The small size of this cadaver resulted in partial volume artefact in the centre of the TMJ that reduced visibility of the joint space in this area.

With the TMJ open, the lateral extremity of the canine condyloid process was located more laterally, as demonstrated by the more rounded shape of the corresponding zygomatic process of the temporal bone when the condyloid process was first imaged. The lateral extremity had also rotated in an anti-clockwise direction on the image and was positioned much closer to the rostral margin of the mandibular fossa, with an increased gap between the caudal articular surfaces. Medially, the condyloid process has rotated to occupy a more dorsal position so the space between it and the mandibular fossa and retroarticular process was more even with no increase ventrally. Otherwise the components appeared similar to the closed mouth views. In the cat, the larger size of this cadaver resulted in clearer images of the structures therefore representative images in this series have been labelled. Rotation of the lateral margin of the condyloid process was not as marked as that observed in the dog. Although the condyloid process had rotated within the mandibular fossa and retroarticular process, the joint space remained narrow and even. The retroarticular foramen was only just visible in these sections.

In the rabbit, the long axis of the condyloid process was visible sitting caudal to the horizontal mandibular fossa and the joint space between could be appreciated. Opening the mouth moved the condyloid process in a rostral and ventral direction relative to the mandibular fossa. Again, the small size of the structures resulted in partial volume artefact that caused blurring of the bone margins. This was particularly evident in this series due to the condyloid process of the rabbit being extremely fine in a lateromedial direction.

The dorsal images of the TMJ obtained in the dog, cat and rabbit using the bone window are demonstrated in Figures 5.3.16 to 5.3.18. with the key in Table 5.2.

In the dog, the dorsal region of the TMJ was poorly visualised, including the lateral aspect of the mandibular fossa, due to partial volume artefact but the caudal and ventral surfaces were clearly visible. Moving ventrally, the medial and lateral halves of the condyloid process became visible at the same time reflecting the horizontal and flat nature of the structure. The medial half of the caudal articular surface of the condyloid process was parallel with the corresponding area of the mandibular fossa while the lateral half could be seen to deviate away from it with resulting widening of the lateral half of the joint space. Further ventrally, the mandibular fossa was no longer visible and only the retroarticular process remained. The ventral surface of the medial half of the condyloid process remained parallel with the retroarticular process while laterally, the caudal articular surface and then the neck of the condyloid process were visible running in a rostrolateral direction. The retroarticular foramen was again clearly visible in these sections.

In the cat, the lateral aspect of the mandibular fossa was better visualised than in the dog. Again, the medial and lateral halves of the condyloid process became visible at the same time reflecting the horizontal and flat nature of the structure. The caudal margin of the condyloid process was much straighter than in the dog and did not deviate from the mandibular fossa laterally. With ventral progress the lateral structures were lost and the ventral surface of the condyloid process corresponded with the retroarticular process.

With the mouth open in the dog, the medial and lateral extremities of the condyloid process had both moved rostrally and the medial extremity was now positioned slightly beyond the medial margin of the mandibular fossa. A distinct angle was noted between the medial and lateral halves of the caudal surface of the condyloid process. The lateral part of the condyloid process became visible slightly before the medial part suggesting it had also

rotated slightly in a dorsal direction. This resulted in marked widening of the TMJ space laterally, but also some widening observed medially as the medial half of the articular surface was no longer completely parallel with the medial part of the mandibular fossa. However further ventrally, the ventral surface of the medial half of the condyloid process was again parallel with the retroarticular process while laterally, the neck of the condyloid process was visible running in a rostral direction. The medial articular surface of the condyloid process appeared slightly concave while the adjacent surface of the retroarticular process was correspondingly convex. The retroarticular process extended further ventrally than the condyloid process.

Opening the mouth in the cat resulted in the caudal margin of the condyloid process becoming slightly convex and there was a slight widening of the joint space laterally, corresponding with the rostral rotation of the lateral extremity observed in the sagittal views. Moving ventrally, the retroarticular process appeared to extend further ventrally than the limits of the condyloid process. The larger size of this cadaver resulted in clearer images of the structures therefore representative images in this series have been labelled. Again, the retroarticular foramen was only just visible in some of these views.

In the rabbit, the zygomatic process of the temporal bone became visible extending in a lateral direction. The rounded rostral margin of the condyloid process then became visible caudal to it with the joint space visible as a gap between the two structures. The condyloid process tapered in a caudal direction. With ventral progression, there was only a very small overlap between the caudal margin of the zygomatic process of the temporal bone and the cranial margin of the condyloid process suggesting that the condyloid process was located predominantly caudal rather than ventral to the mandibular fossa, as was demonstrated on the sagittal views. Further ventral progression resulted in the elongated neck of the condyloid process being visualised with the caudal extension of the zygomatic process located laterally but not extending as far caudally.

With the mouth open, the fine tapered caudal region of the condyloid process was visualised first in a position caudal to the zygomatic process of the temporal bone suggesting a location dorsal to that of the rostral region. The rostral region appeared slightly more rounded and its margins were congruent with the concavity of the mandibular fossa. There was greater overlap between the rostral part of the condyloid process and the caudal margin of the zygomatic process of the temporal bone suggesting rostral rotation of the condyloid process and a more ventral location relative to the

mandibular fossa. With ventral progression, the caudal margin of the neck of the condyloid process did not extend as far caudal to the caudal extension of the zygomatic process as with the mouth closed.

5.3.3. Effect of windowing

Typical images of the empty and fluid-filled TB and TMJ obtained using the bone, brain and soft tissue windows are demonstrated in Figure 5.3.19. The images obtained using a bone window allowed identification of cortical and cancellous bone, and also produced a clear distinction between the wall of the TB and the fluid within the lumen. The brain and soft tissue windows allowed better differentiation between the soft tissue structures of the head and the surrounding fat but none enhanced identification of the soft tissue structures associated with the TB or TMJ, or the appearance of fluid within the TB lumen. All of the bony structures of the head appeared thicker using these windows, including the walls of the TB and external ear canal, and the vertical ramus and condyloid process of the mandible. They were also associated with greater partial volume artefact and the resulting blurring of bone margins, especially in relation to the TMJ. Some streaking of the soft tissue was observed, particularly in the images obtained using the bone window, due to the presence of beam hardening artefact.

<u>Label</u>	<u>Description</u>
*	Apparent defect in lateral aspect of canine condyloid process
1	Condyloid process
2	Cat and Dog - Angular process Rabbit – vertical ramus of mandible
3	Zygomatic arch
4	Zygomatic process of the temporal bone
5	Caudal extension of the zygomatic arch (rabbit)
6	Retroarticular process
7	Squamous temporal bone
8	Pit at the medial aspect of the retroarticular process
9	Retroarticular foramen
10	Hyoid apparatus
11	External ear canal

Table 5.2. Anatomical features associated with the TMJ. Key for figures 5.3.10 to 5.3.18.

Figure 5.3.10. Transverse CT images of the canine TMJ using a bone window, progressing from rostral to caudal. Dorsal is to the top and right is to the left in all images. Number in bottom left corner indicates slice number. Approximate location of the first and last slice is indicated on the pilot image. For key see Table 5.2.

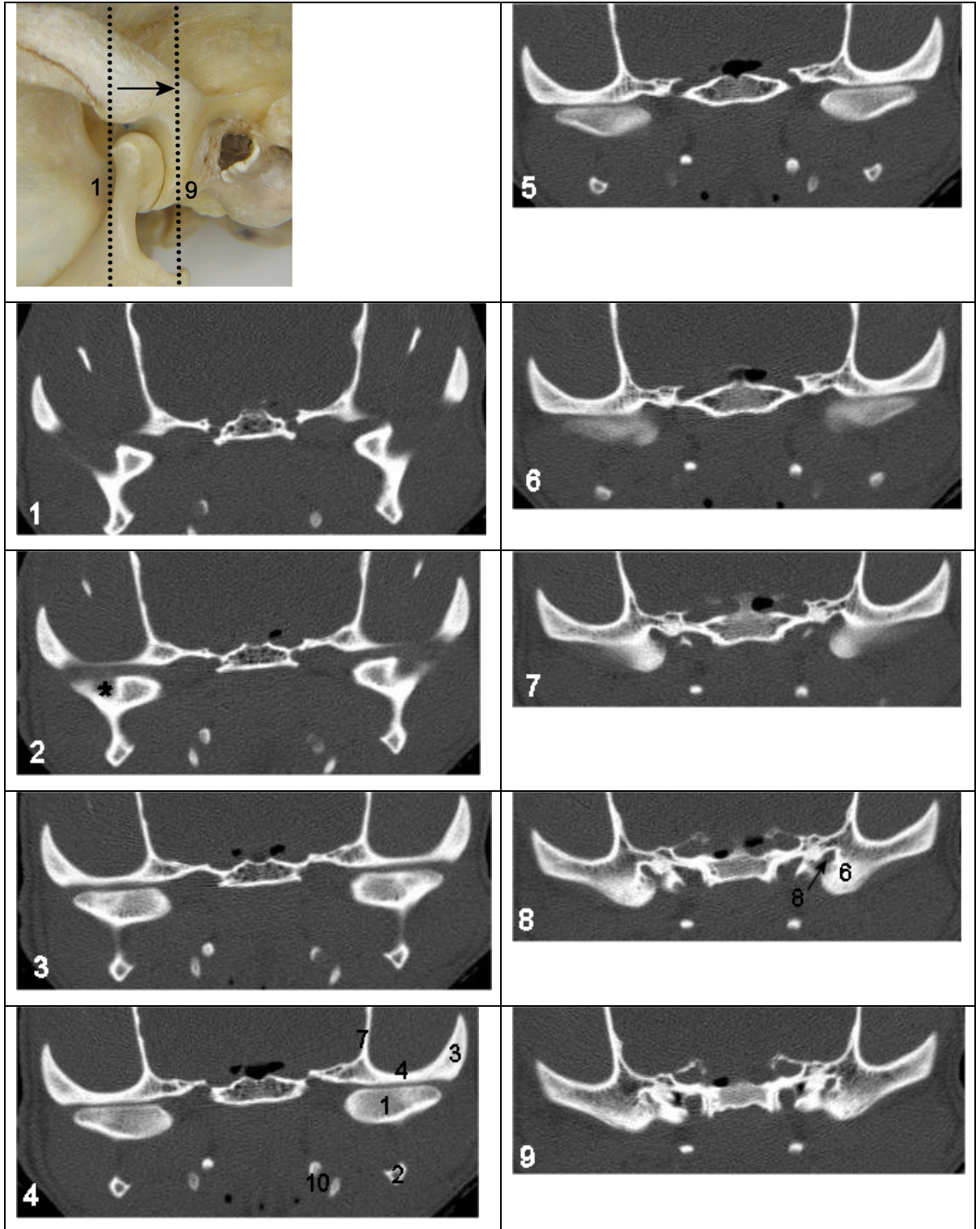


Figure 5.3.10.1. Transverse CT images of the closed canine TMJ

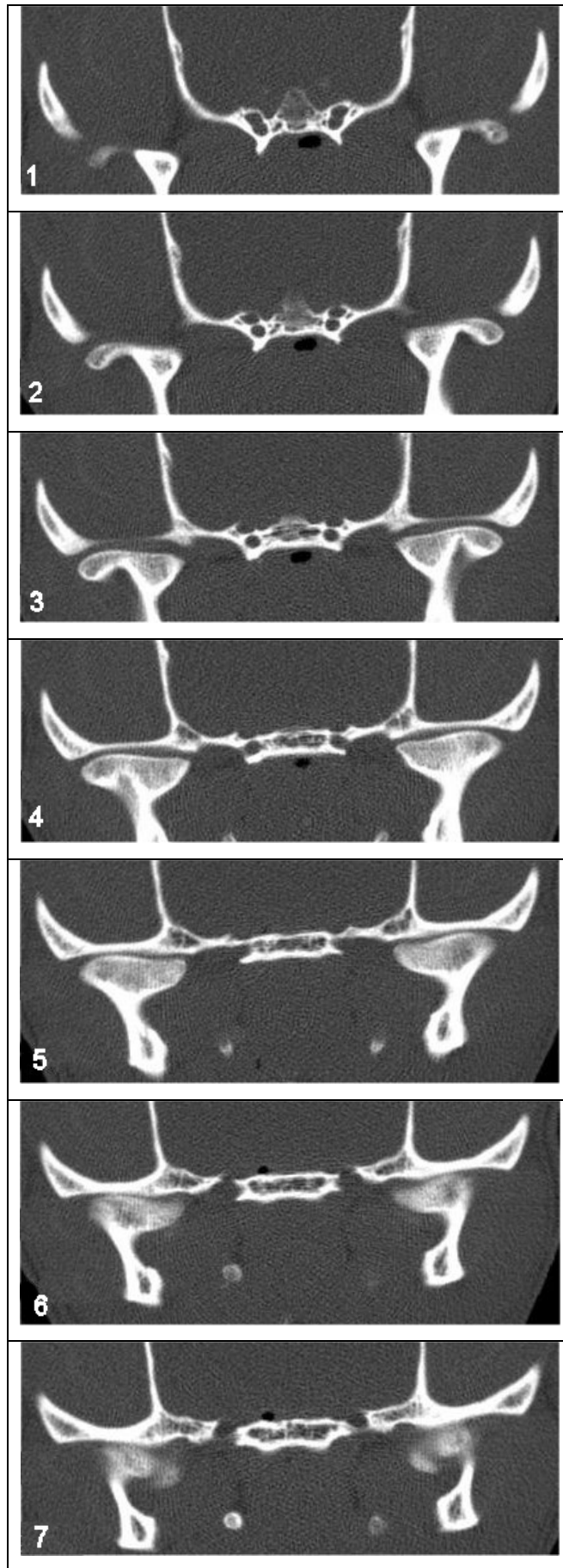


Figure 5.3.10.2. Transverse CT images of the open canine TMJ

Figure 5.3.11. Transverse CT images of the feline TMJ using a bone window, progressing from rostral to caudal. Dorsal is to the top and right is to the left in all images. Number in bottom left corner indicates slice number. For key see Table 5.2.

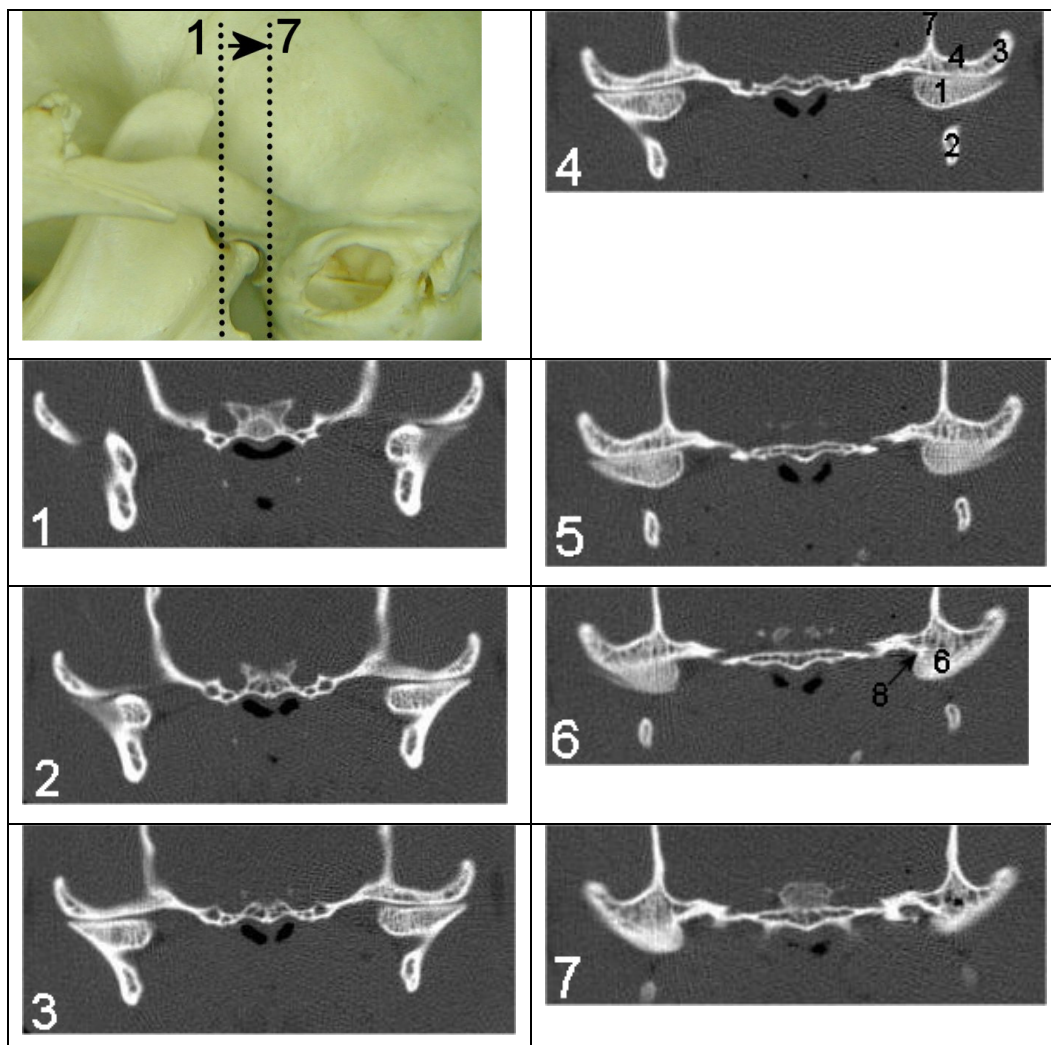


Figure 5.3.11.1. Transverse CT images of the closed feline TMJ

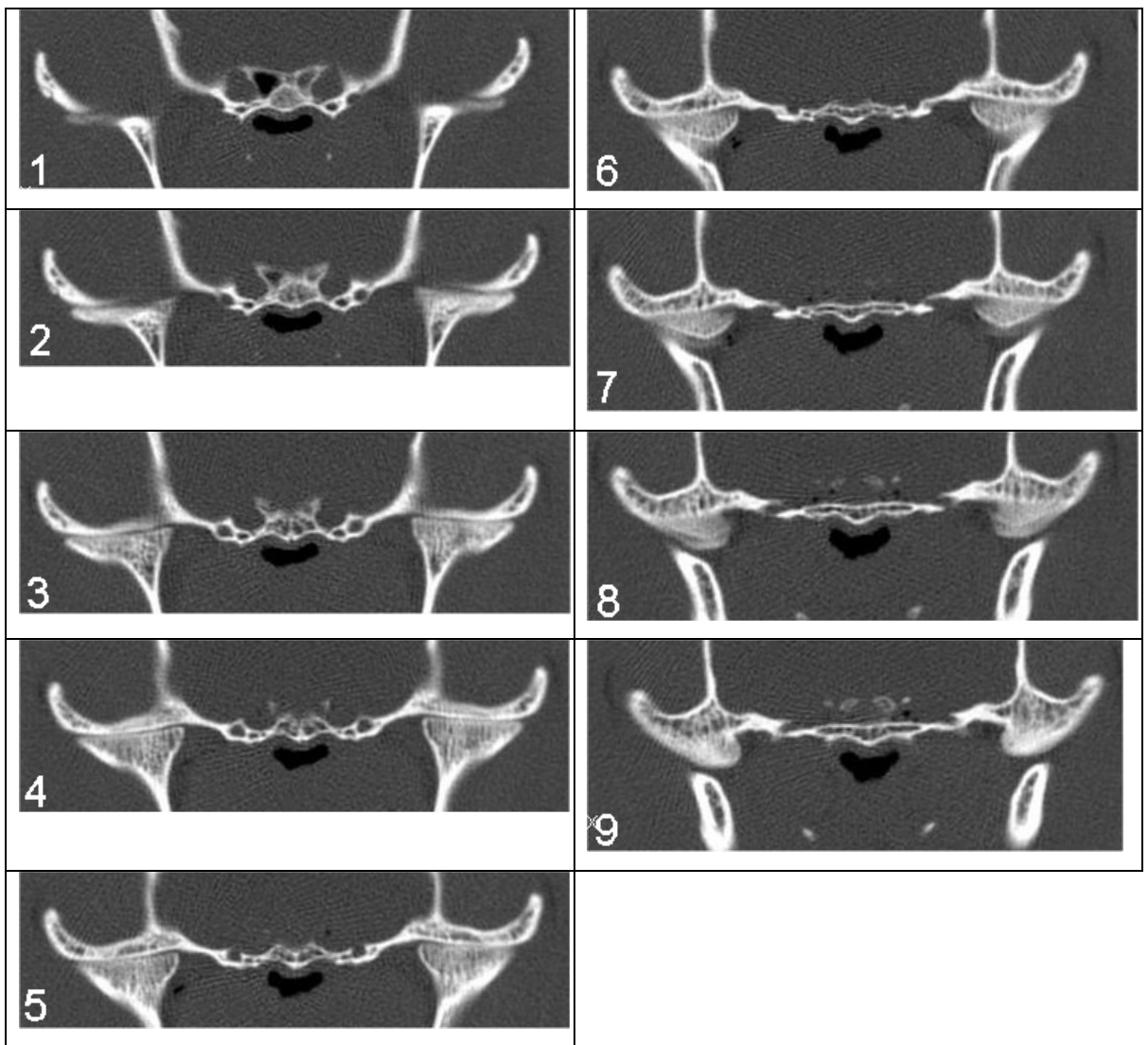


Figure 5.3.11.2. Transverse CT images of the open feline TMJ

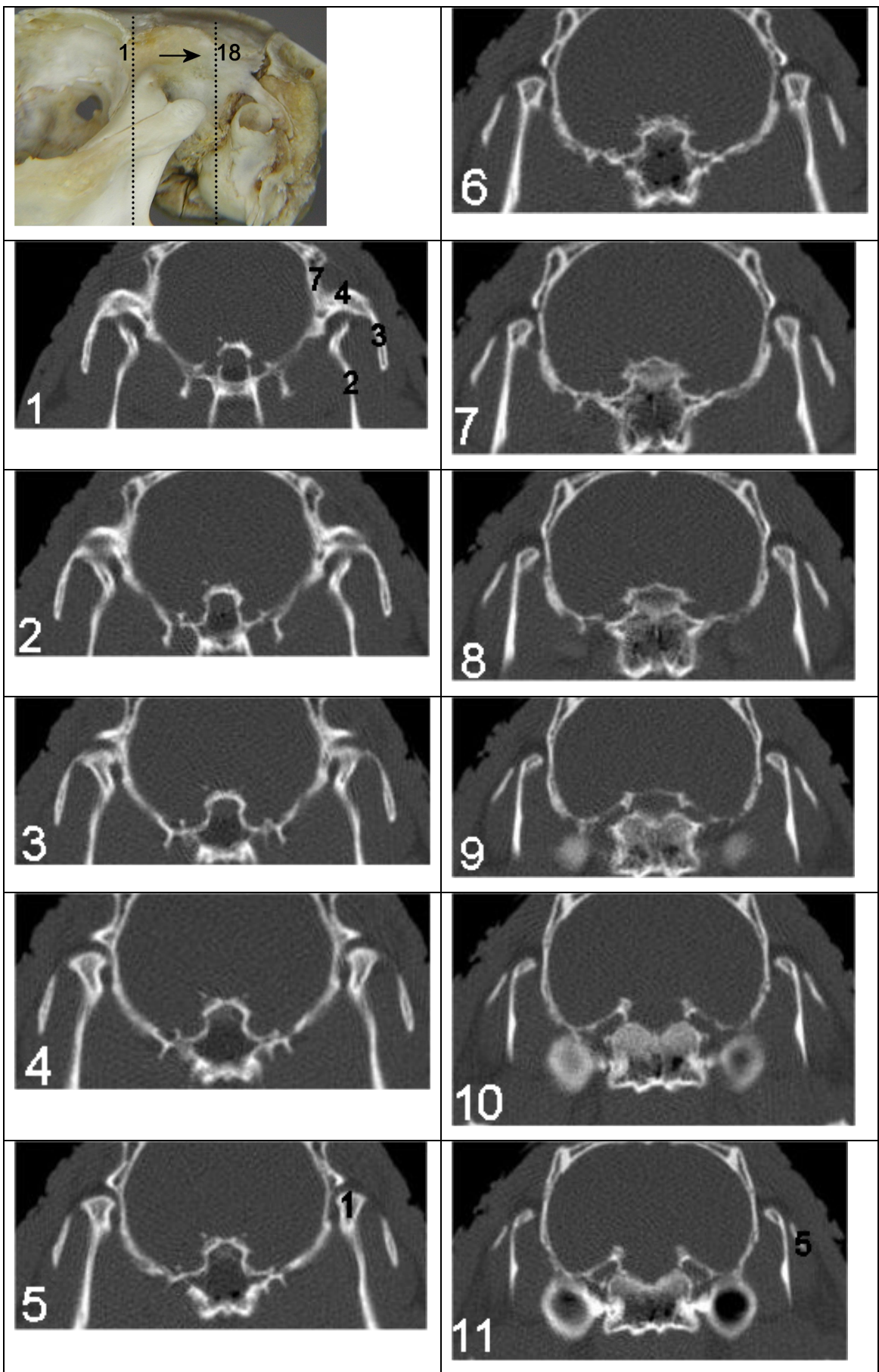


Figure 5.3.12. Transverse CT images of the closed rabbit TMJ using a bone window, progressing from rostral to caudal. Dorsal is to the top and right is to the left in all images. Number in bottom left corner indicates slice number. For key see Table 5.2.

Figure 5.3.12. continued. Transverse CT images of the closed rabbit TMJ

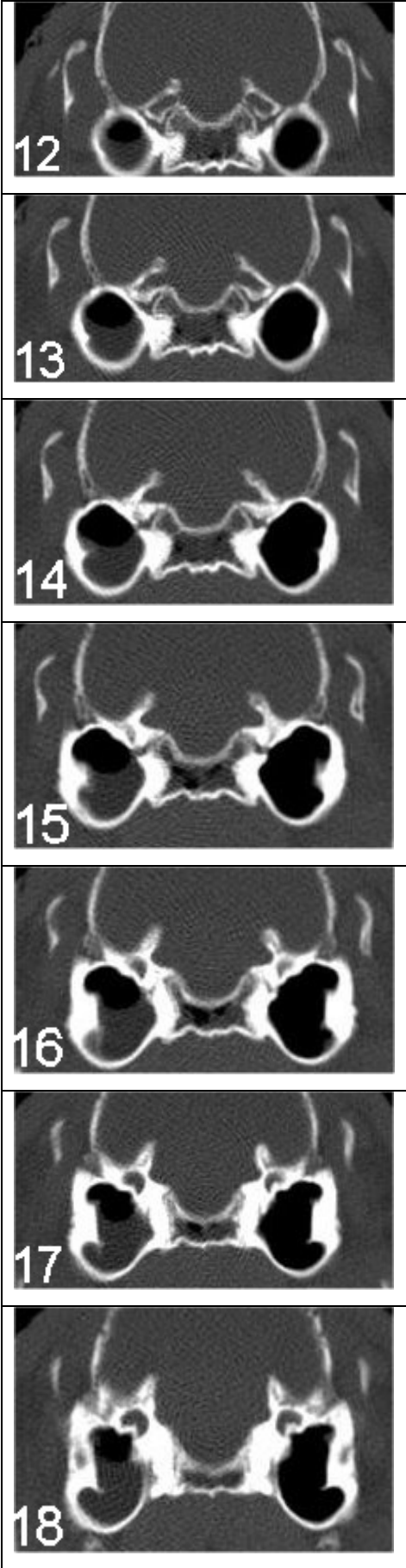


Figure 5.3.13. Sagittal CT images of the canine TMJ using a bone window, progressing from lateral towards midline. Dorsal is to the top and rostral is to the left in all images. Number in bottom left corner indicates slice number. Approximate location of the first and last slice is indicated on the pilot image. For key see Table 5.2.

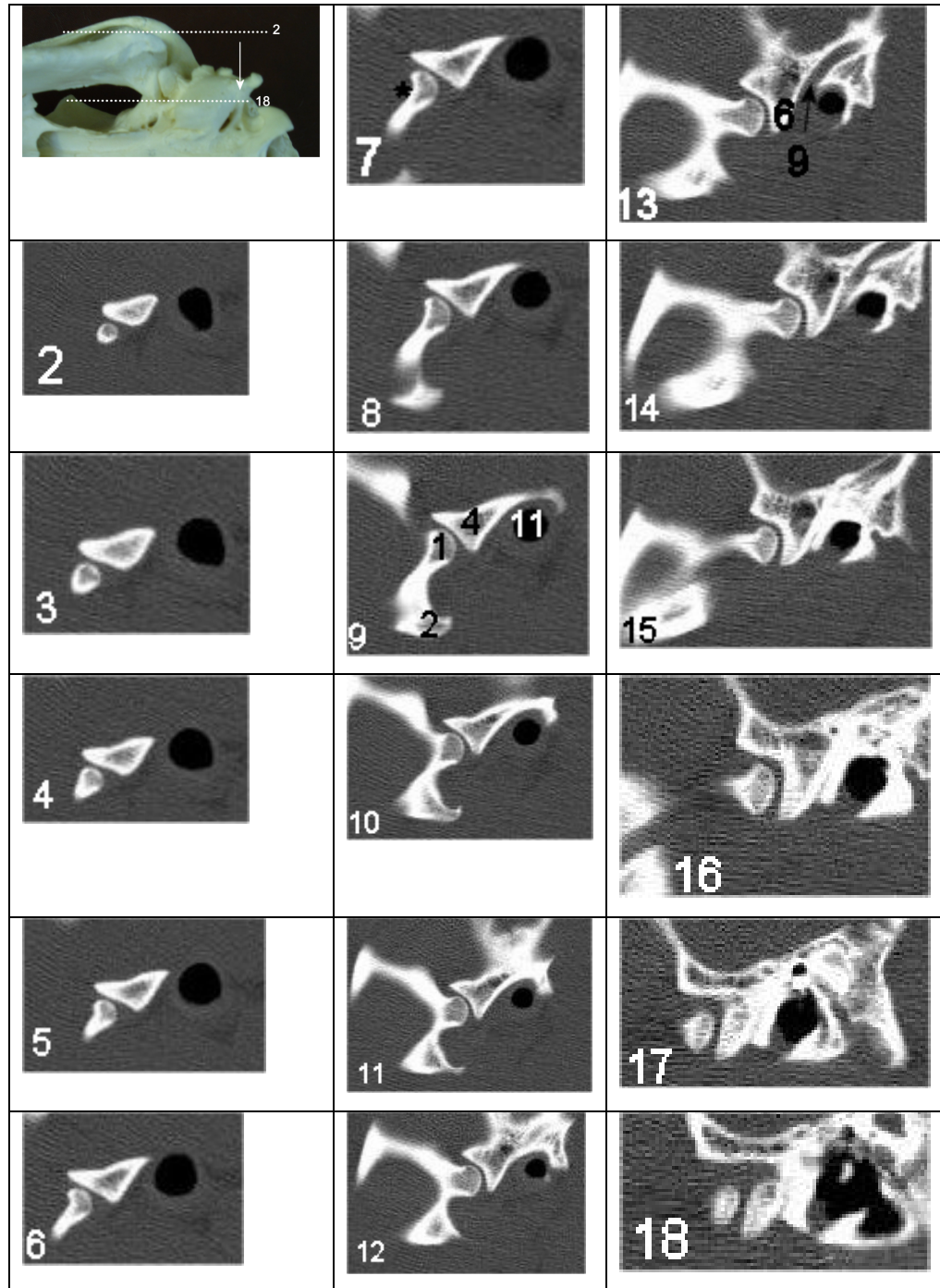


Figure 5.3.13.1. Sagittal CT images of the closed canine TMJ

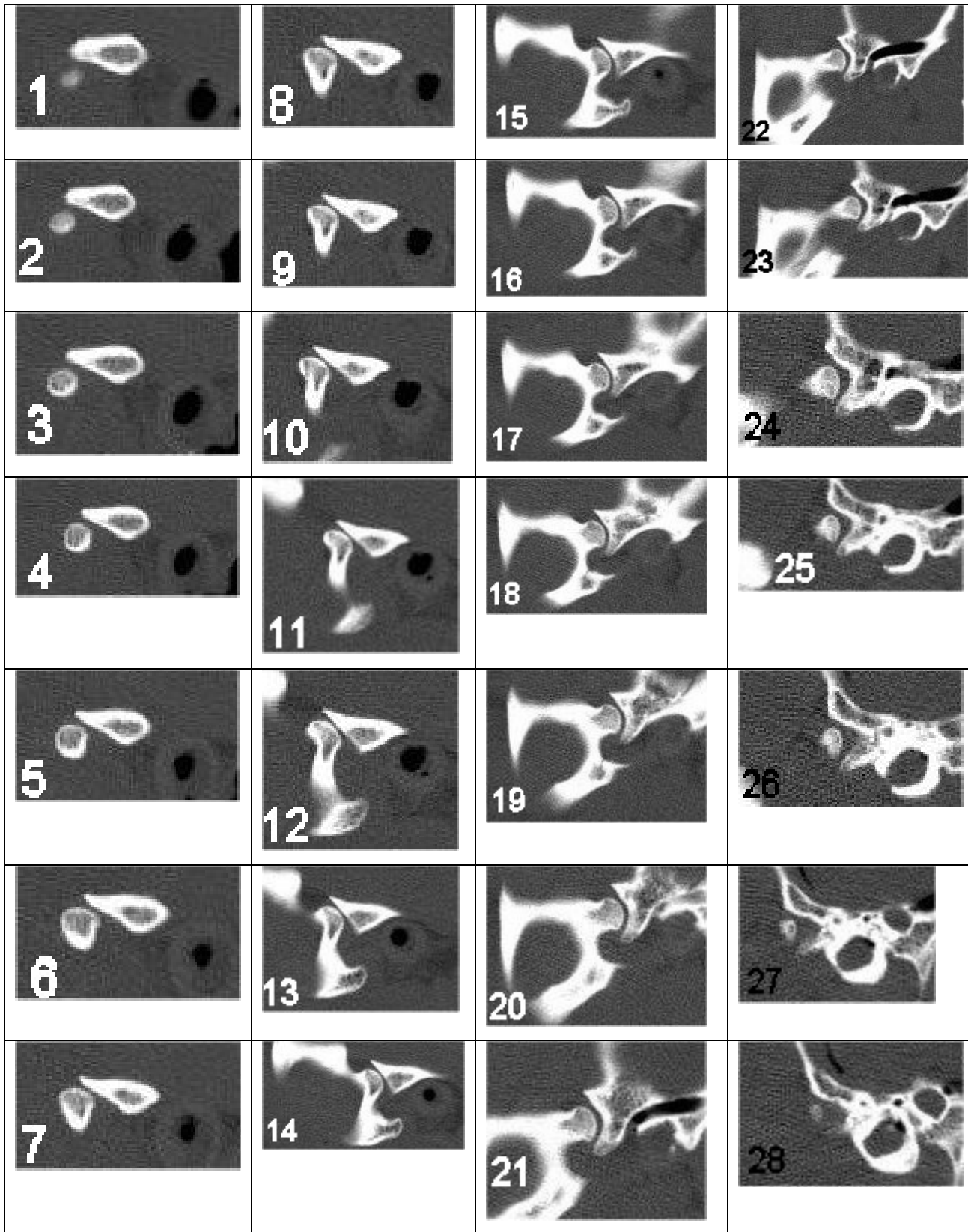


Figure 5.3.13.2. Sagittal CT images of the open canine TMJ

Figure 5.3.14. Sagittal CT images of the feline TMJ using a bone window, from lateral towards midline. Dorsal is to the top and rostral is to the left in all images. Number in bottom left corner indicates slice number. Approximate location of the first and last slice is indicated on the pilot image. For key see Table 5.2.

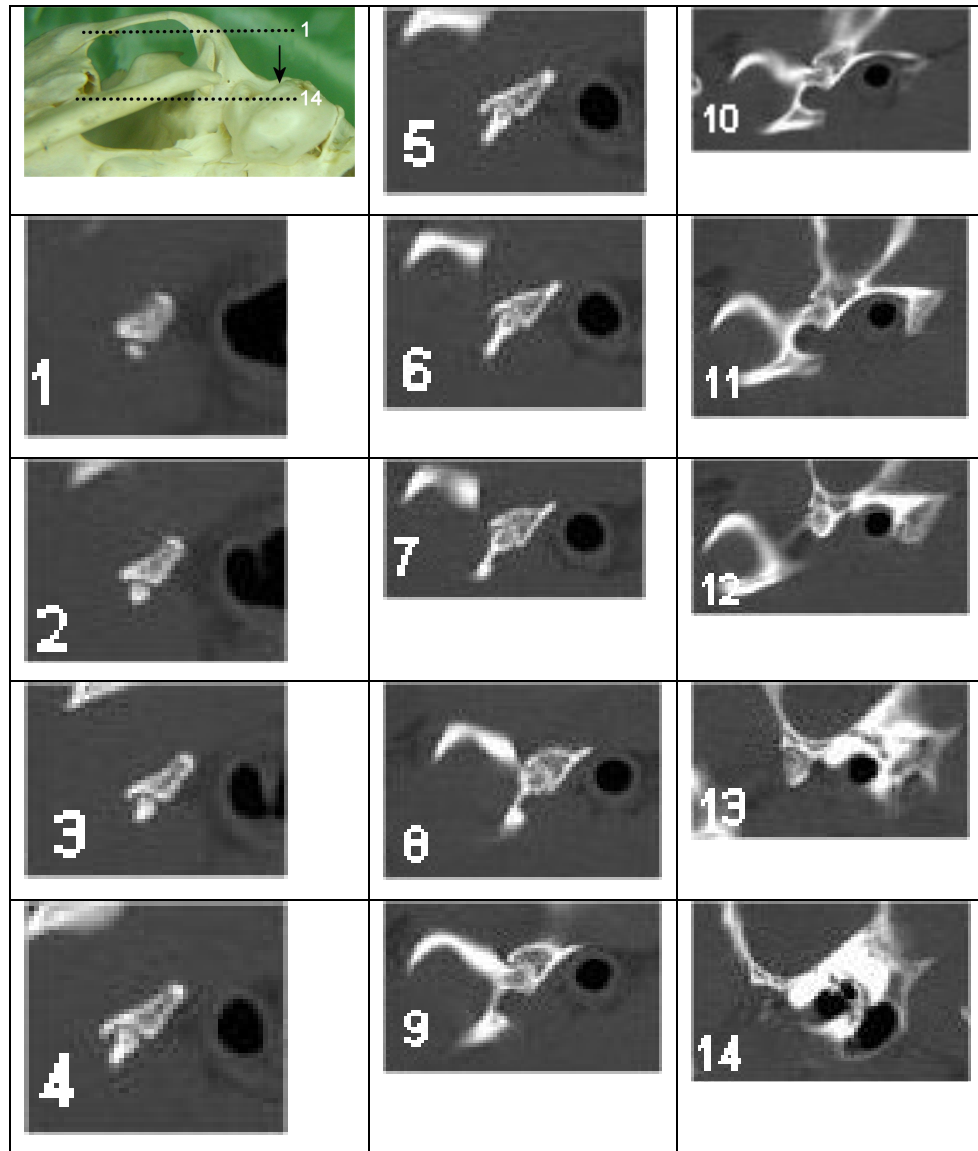


Figure 5.3.14.1. Sagittal CT images of the closed feline TMJ

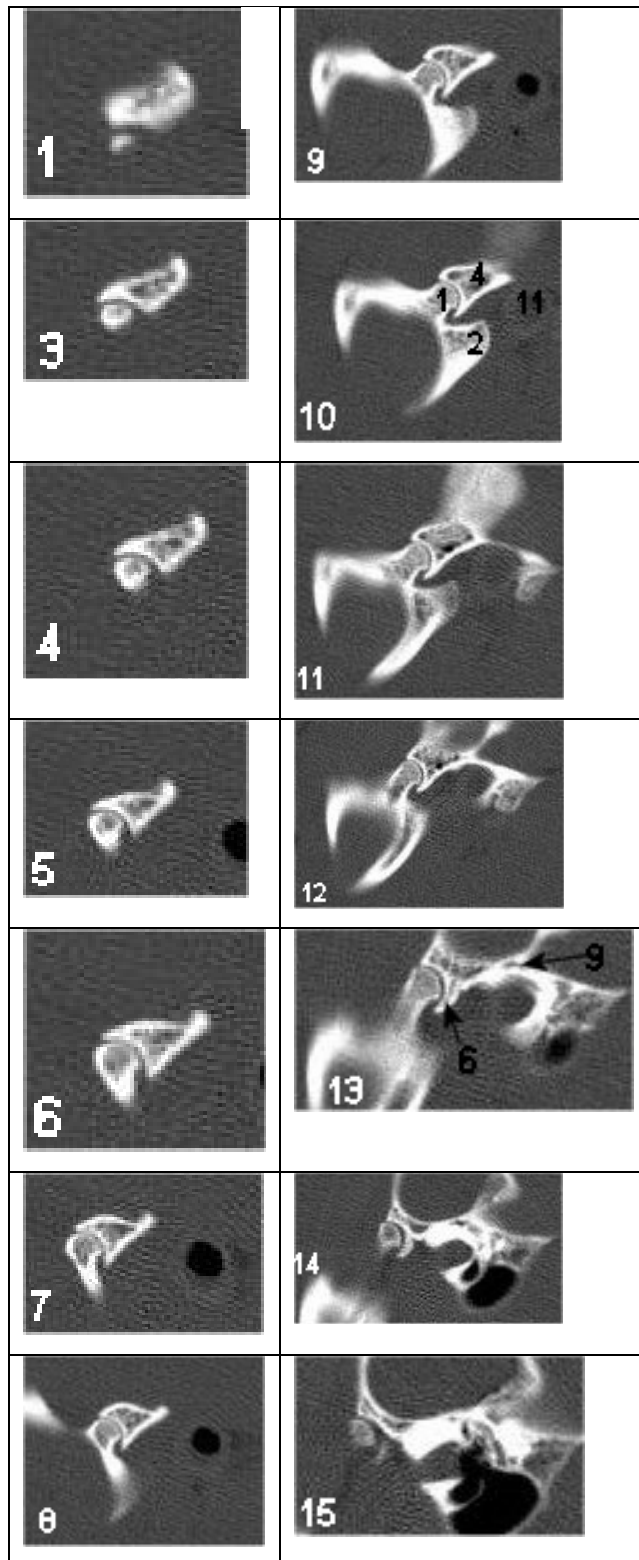


Figure 5.3.14.2. Sagittal CT images of the open feline TMJ

Figure 5.3.15. Sagittal CT images of the rabbit TMJ using a bone window, from lateral towards midline. Dorsal is to the top and rostral is to the left in all images. Number in bottom left corner indicates slice number. Approximate location of the first and last slice is indicated on the pilot image. For key see Table 5.2.

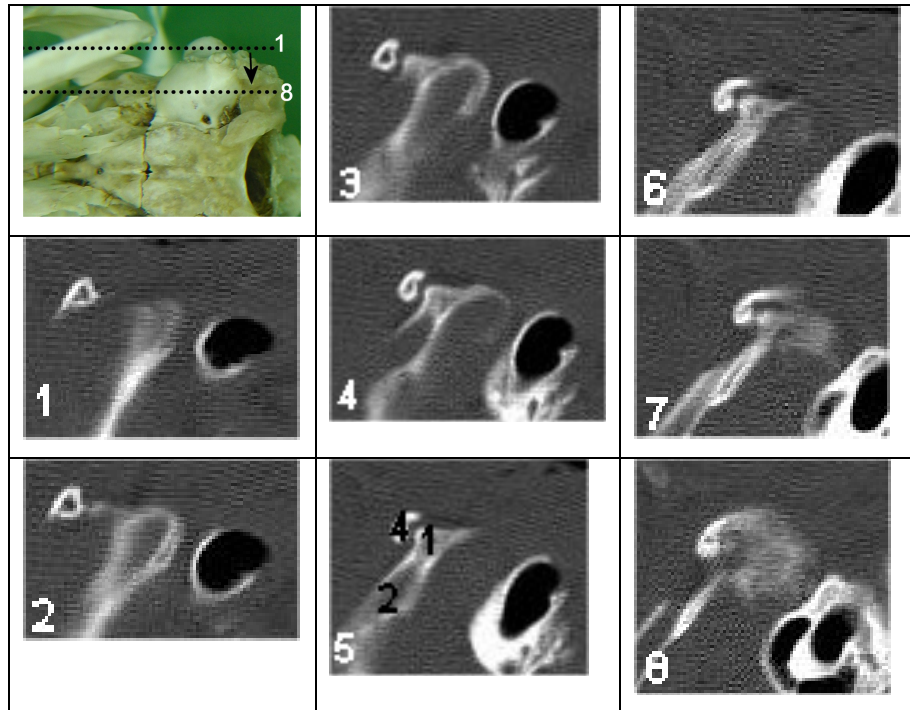


Figure 5.3.15.1. Sagittal CT images of the closed rabbit TMJ

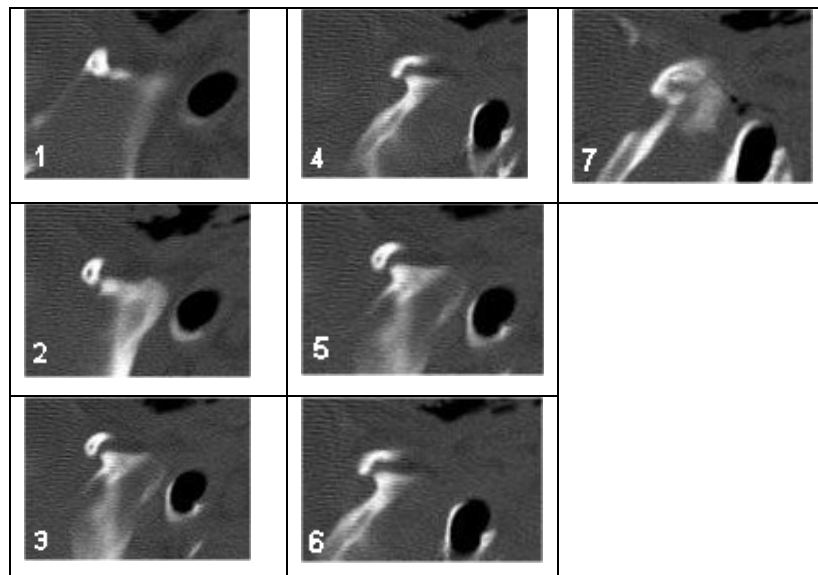


Figure 5.3.15.2. Sagittal CT images of the open rabbit TMJ

Figure 5.3.16. Dorsal CT images of the canine TMJ using a bone window, progressing from dorsal to ventral. Rostral is to the top and right is to the left in all images. Number in bottom left corner indicates slice number. Approximate location of the first and last slice is indicated on the pilot image. For key see Table 5.2.

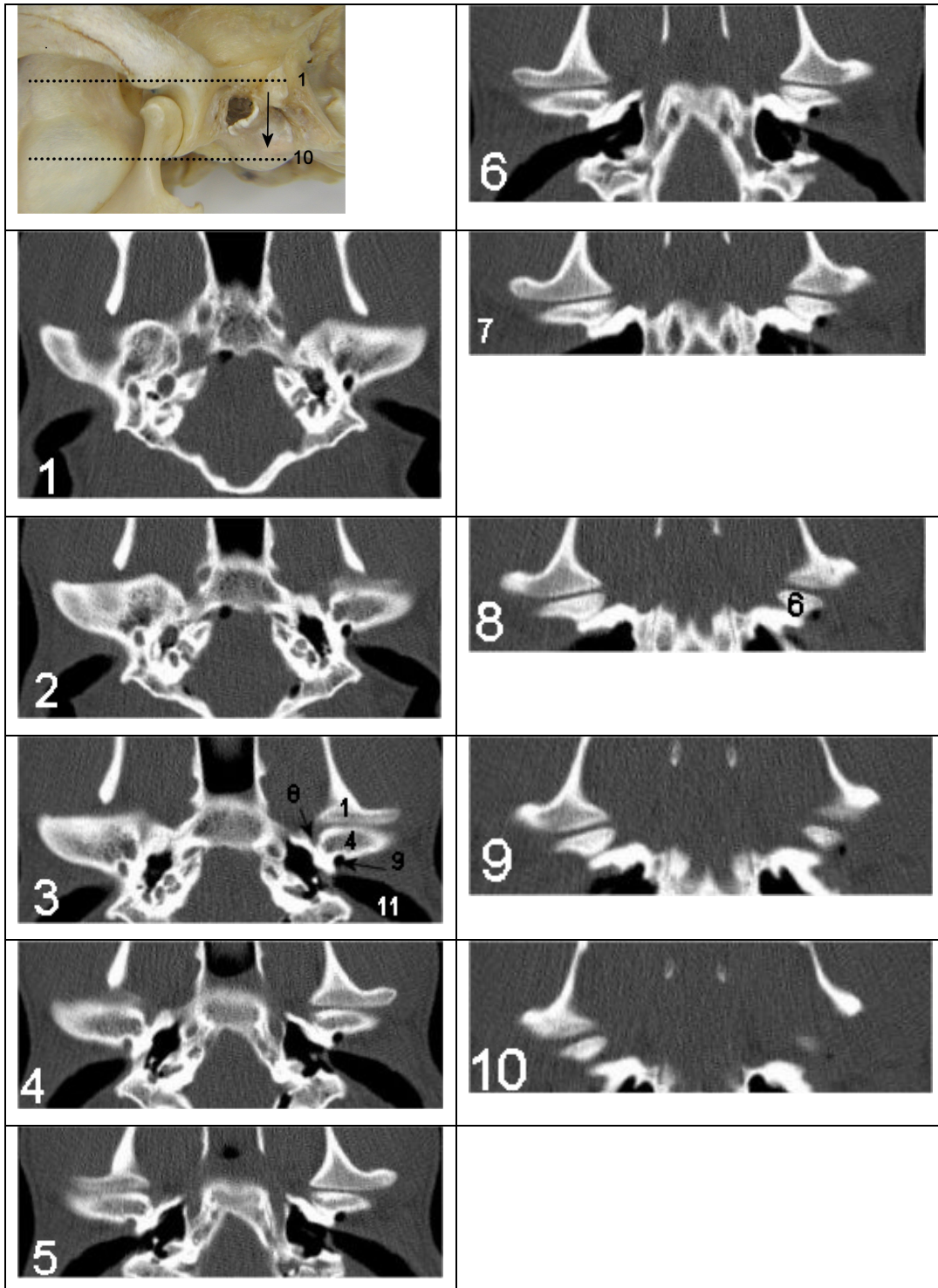


Figure 5.3.16.1. Dorsal CT images of the closed canine TMJ

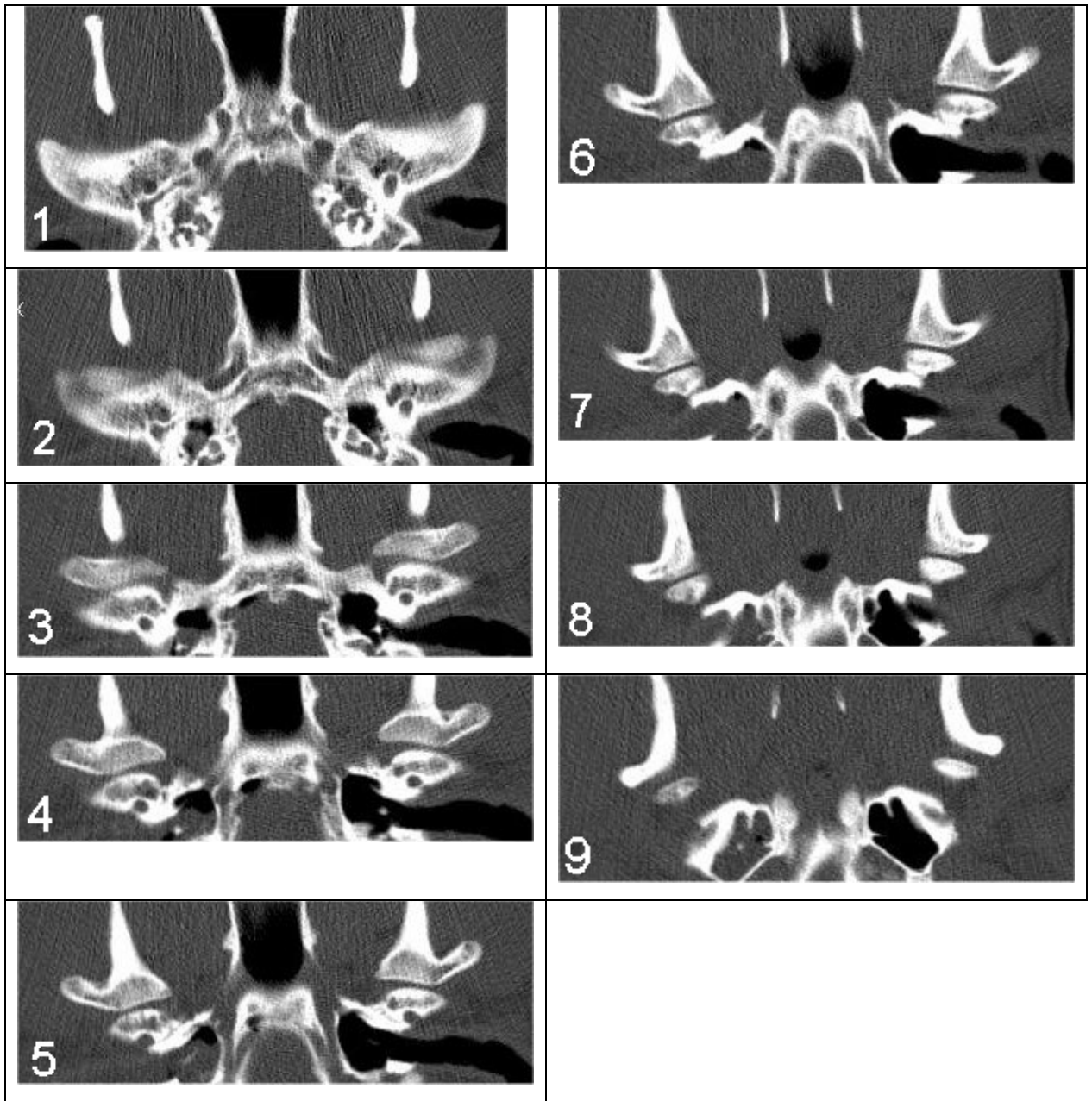


Figure 5.3.16.2. Dorsal CT images of the open canine TMJ

Figure 5.3.17. Dorsal CT images of the feline TMJ using a bone window, progressing from dorsal to ventral. Rostral is to the top and right is to the left in all images. Number in bottom left corner indicates slice number. Approximate location of the first and last slice is indicated on the pilot image. For key see Table 5.2.

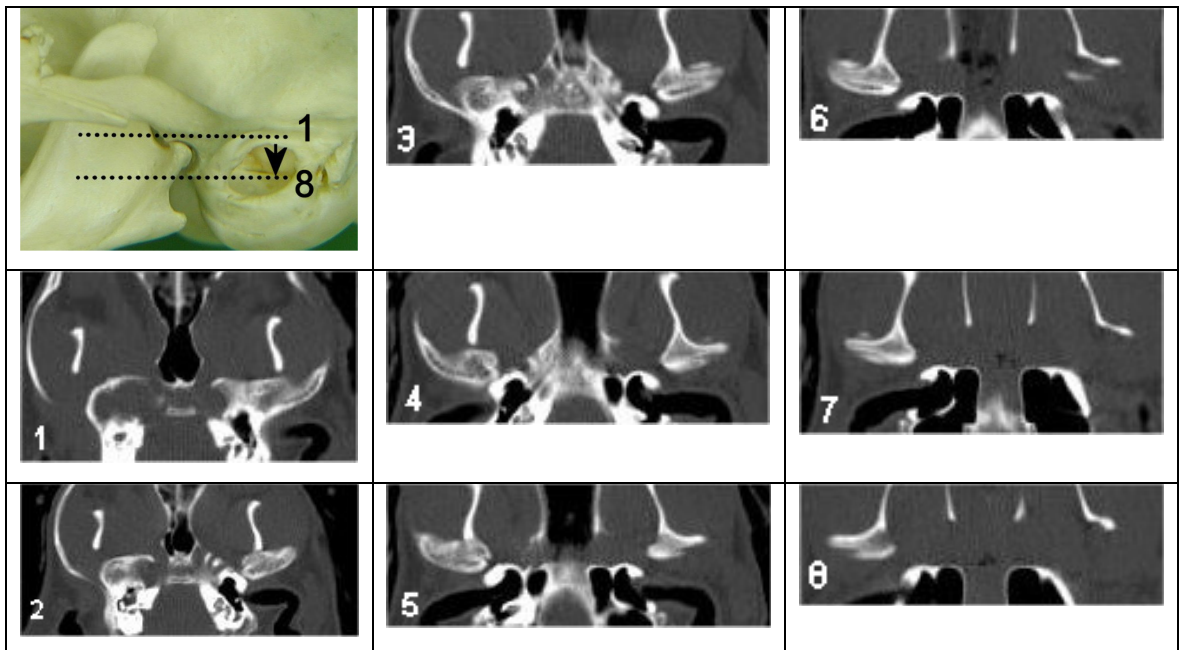


Figure 5.3.17.1. Dorsal CT images of the closed feline TMJ

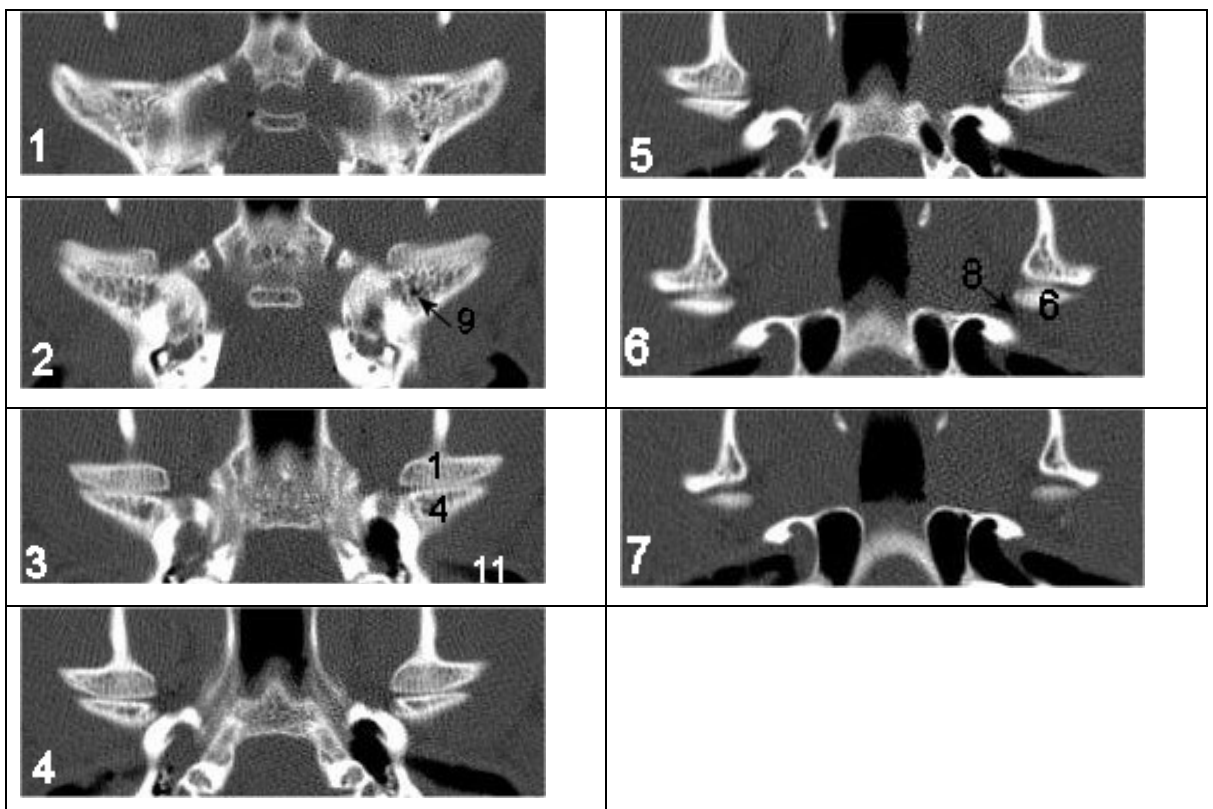


Figure 5.3.17.2. Dorsal CT images of the open feline TMJ

Figure 5.3.18. Dorsal CT images of the rabbit TMJ using a bone window, progressing from dorsal to ventral. Rostral is to the top and right is to the left in all images. Number in bottom left corner indicates slice number. Approximate location of the first and last slice is indicated on the pilot image. For key see Table 5.2.

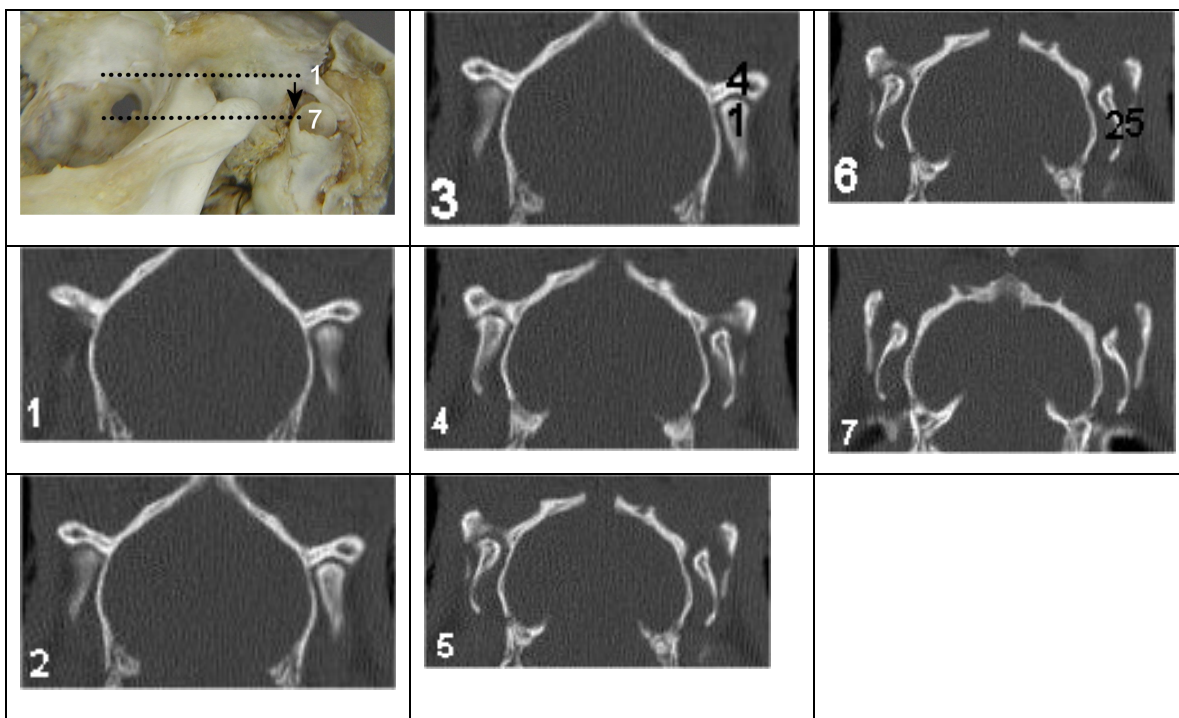


Figure 5.3.18.1. Dorsal CT images of the closed rabbit TMJ

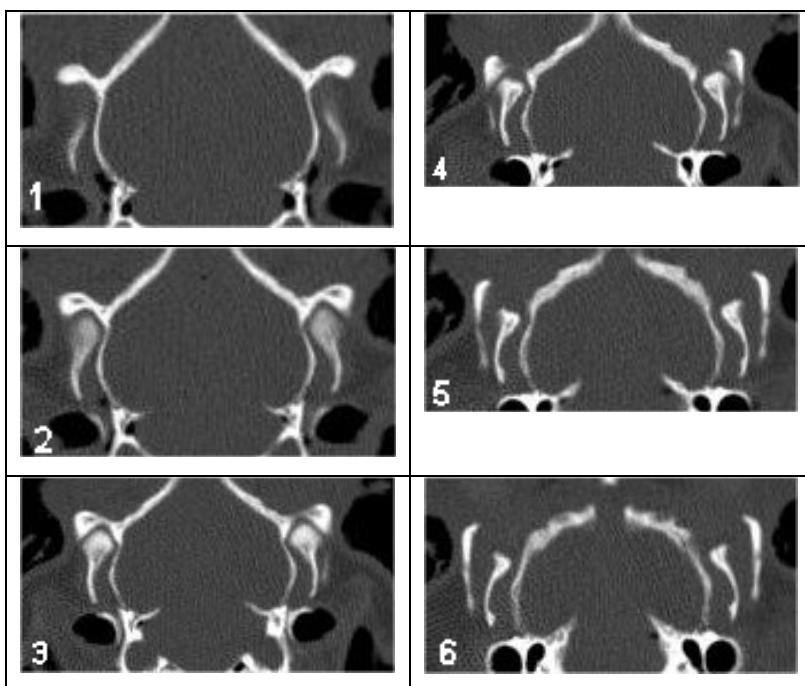


Figure 5.3.18.2. Dorsal CT images of the open rabbit TMJ

Figure 5.3.19. Transverse CT images of the empty and fluid-filled rabbit TB and TMJ viewed using different windows. A. Bone window (level 500 HU; width 2000 HU) B. brain window (level 35 HU; width 150 HU) C. Soft tissue window (level 45 HU; width 450 HU). D. Soft tissue window (level 200 HU; width 800 HU)

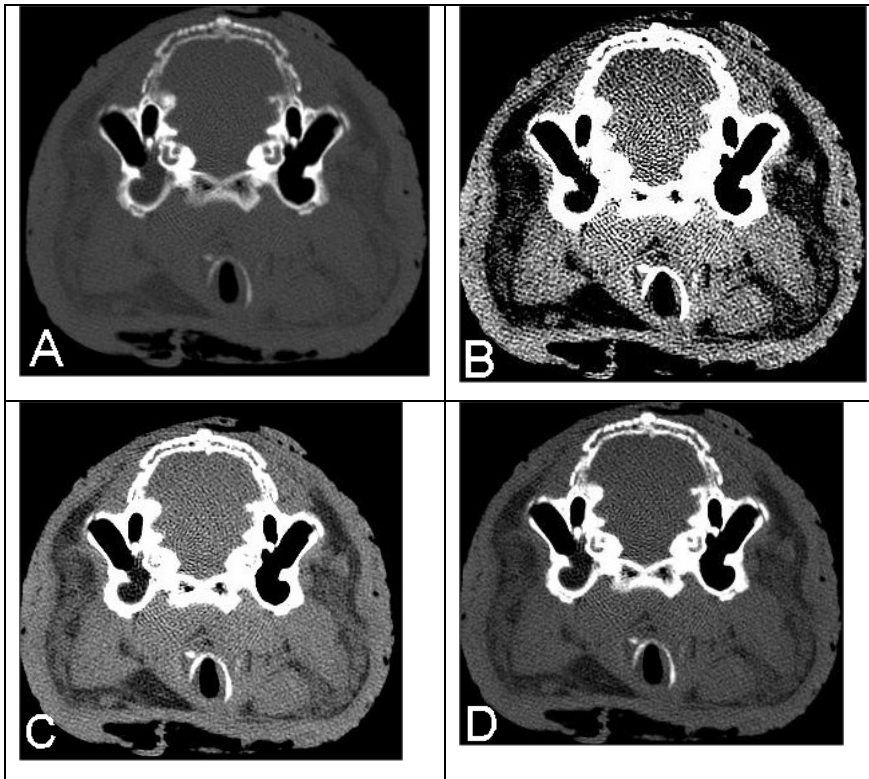


Figure 5.3.19.1. Transverse CT images of the empty and fluid-filled rabbit TB.



Figure 5.3.19.2. Transverse CT images of the closed rabbit TMJ.

5.4 Discussion

5.4.1. Material and technical considerations

Border Collie and German Shepherd cadavers were used for the work presented in previous chapters as they represented typical mesaticephalic dog breeds. However, due to time and cost constraints, it was deemed more sensible to use a smaller breed for CT imaging. Although the Jack Russell Terrier is a chondrodystrophic breed, its head remains typically mesaticephalic. While use of a non-chondrodystrophic mesaticephalic small breed may have been more appropriate, there were not many breeds within the material available that fell into this category therefore the requirement for matched material was a limiting factor.

There are ethical, financial and logistical advantages in using cadaver material for this type of study and its use is a well established practice in the medical literature (Jones and others 1995, Weller and others 1999a, Morrow and others 2000). Particular benefits in the present study included the ease of positioning to allow direct CT imaging in all three planes and the ability to use the same material for subsequent parts of the study. However, the most common problem with the use of such material is the occurrence of post mortem degeneration that may alter the appearance of the area of interest, or mimic anatomical structures or pathology (Weller and others 1999a). In the present study, the accumulation of small volumes of fluid within the normally air-filled TB lumen was observed. Similar changes were noted in post mortem CT images of the equine head, where gravity dependent fluid was encountered within the normally air-filled sinuses (Morrow and others 2000). Gas accumulation was also encountered within and around the brain and spinal cord in the present study. Air bubbles located in the epidural space and thecal sac during post mortem CT examination of the canine vertebral column have been reported (Jones and others 1995) and also within venous sinuses and veins in the equine head (Morrow and others 2000). It has therefore been recommended that examinations in cadavers be performed as soon after death as possible (Rodríguez and others 2002, Soler and others 2002). The accumulation of fluid was only observed in equine heads after 15 hours and not immediately, or at one hour, post mortem (Morrow and others 2000), suggesting a relationship with time. However, the presence of gas was noted when CT was performed both immediately and 15 hours after euthanasia but not at 1 hour (Morrow and others 2000), suggesting other factors may be associated with this.

In the present study, the imaging equipment was located in a busy veterinary hospital which limited access. It was therefore not possible to examine fresh material within a reasonable time period post mortem and so an interim preservation technique was required to prevent significant tissue degeneration. Storage at subzero temperatures was the method employed due to its simplicity and reversibility and this is a well established technique in the medical literature (Jones and others 1995). Post mortem changes affecting soft tissue structures in thawed cadaver material have been reported (Jones and others 1995) but there are no reports of any alterations in the boney structures that are the main tissue of interest when using CT to image the TB and TMJ. It is possible that damage may have occurred to the delicate bone of the inner ear structures due to expansion and contraction of the fluid-filled cavities during the freeze – thaw cycle. However, there do not appear to be any reports addressing this and no such changes were identified in the present study.

CT imaging routinely involves the acquisition of transverse sections as the required positioning of the patient in the bore of the machine is easy to achieve. The resolution of the canine transverse sections produced in the present study were superior to many older publications (George and Smallwood 1992, Love and others 1995, Assheuer and Sager 1997). This was due in part to the 1.1mm slice thickness since thin slices result in less partial volume artefact and greater resolution images (Seitz and others 1996). In two publications, 3mm thick images were presented (Love and others 1995, Assheuer and Sager 1997). This was for ‘practical and preventative reasons’ as at that time, although 1mm thickness was desirable, it required a long scan time and therefore high doses of anaesthesia and radiation (Assheuer and Sager 1997). At an earlier date, images with a slice thickness of 1.3mm were published since subsequent euthanasia of the animals meant that such welfare aspects were not a consideration (George and Smallwood 1992). However, more recently presented CT images with a slice thickness of 2.5mm are still superior to these (Garosi and others 2003) demonstrating an additional influence on image quality resulting from improvements in currently available CT equipment and software. Recently published canine images of slice thickness 1 – 1.2mm are comparable to these produced in the present study (Schwarz and others 2002, Russo and others 2002). There seem to be few published images in the cat but the images in the present study were comparable to those obtained using 1.2mm slice thickness (Schwarz and others 2002) and better than 2.5mm (Garosi and others 2003) and 1.5mm slices (Seitz and others 1996). In this latter publication, 1.5mm slices was the smallest the CT scanner could achieve, again reflecting the influence of equipment on the quality of the resulting images.

Usually following CT examinations, the transverse images are amalgamated to produce reformatted images in the sagittal and dorsal planes (Seitz and others 1996, Schwarz and others 2002). The resolution of these reformatted images depends on the resolution of the original images and also the capabilities of the software and hardware being used. Although the use of either overlapping slices or helical scanning will improve this (Schwarz and others 2002, Garosi and others 2003), the reformatted images are never as good resolution as the original transverse ones (Jones and others 1995). This is evident in published dorsal and sagittal reconstructed images in the cat (Seitz and others 1996) and the comparison between the directly acquired and reconstructed sagittal and dorsal sections in the present study.

An advantage of using cadavers in the present study was that the absence of the trunk meant the material could be easily repositioned for the direct acquisition of sagittal and dorsal sections. Although care must be taken not to kink the endotracheal tube or constrict the airway, it is possible to position anaesthetised animals for the direct acquisition of dorsal sections (Russo and others 2002). Directly acquired dorsal sections through the canine TB with a slice thickness of 1mm were of comparable quality to those produced in the present study (Russo and others 2002) although there do not seem to be any other published dorsal images in the dog. However, it would not be possible to position an anaesthetised animal in the CT scanner for the direct acquisition of sagittal sections since the length of the animal would have to be significantly less than the bore of the machine to allow centring of the region of interest. This is therefore unlikely to be an option in dogs and cats, and probably even rabbits. While the directly acquired sagittal sections produced in the present study were therefore not directly applicable to live animals, it was hoped that with extrapolation, their superior resolution would enhance the identification of anatomical structures and subsequent interpretation of conventionally reconstructed sagittal images.

CT examination of the canine TB was reported to take approximately 20-30 minutes (Love and others 1995, Russo and others 2002), which was much longer than in the present study, despite imaging of both TBs and TMJs in three different planes. Although the cadaver material was small in size, the modern CT equipment used meant that slice acquisition and image reconstruction were both performed very rapidly. The other major contributors to the duration of a CT examination are the time taken to position the patient and adjust the scan plane according to the pilot image. Since precision is required to ensure the symmetry that is important for assessment of bilateral structures such as the TB (Hoskinson 1993) and TMJ (Schwarz and others 2002), it is unlikely that the time required for these stages

can be reduced and so they now represent the rate limiting steps in the procedure. Since general anaesthesia is required to prevent patient movement during a CT examination (Love and others 1995, Seitz and others 1996), in the past it has been suggested that it is preferable to only acquire one series of images to avoid the time taken to reposition the animal and therefore reduce the length of the anaesthetic (Jones and others 1995). However, the recent reduction in acquisition and reconstruction time is likely to allow repositioning of the patient for the direct acquisition of dorsal images, if deemed necessary, without significantly compromising patient welfare.

It has been reported that CT images of the canine and feline TB and TMJ should be assessed using both bone and soft tissue windows, and those selected were recommended in previous studies (Jones and others 1995, Love and others 1995, Schwarz and others 2002). Since the structures of interest were mainly bony in nature and there was a large inherent contrast between the gas within the TB lumen and the wall, wide or bone windows were most appropriate for both. The soft tissue windows did not enhance identification of the soft tissue structures associated with either the TB or the TMJ, and so were deemed to be of limited value in their assessment.

When using the soft tissue windows, an apparent increase in thickness was observed in all of the bony structures of the head. This phenomenon has been reported to occur when using a window width of less than 1000HU to image the wall of the TB and is particularly marked in the presence of fluid within the TB lumen (Barthez and others 1996). It results from a combination of partial volume artefact, the blurring effect associated with back projection reconstruction and an increase in modulation transfer associated with lower spatial frequency objects such as bone, and increases as the window width reduces (Barthez and others 1996). The same effects will also be responsible for the apparent increase in thickness of all the bony structures of the skull in the present study due to the presence of surrounding soft tissue structures. Awareness of this artefact is necessary when interpreting CT images where the initial study may be focussed on examination of the brain, to ensure that appropriate windowing is selected for the assessment of peripheral areas (Barthez and others 1996). The lack of an apparent increase in wall thickness in the presence of a fluid-filled lumen in the present study was due to the use of a bone window with a width greater than 1000HU. Failure to select the appropriate window could result in false positive diagnoses of bulla osteitis either with or without the presence of intraluminal fluid, or false negative diagnoses when interpreting changes within the TMJ.

The presence of beam hardening artefact was also evident, particularly in the brain window images, producing a streaked appearance to the soft tissue structures. This is a common problem when using CT to image this area due to the large amount of dense bone associated with the base of the skull (Kraft and Gavin 1999).

The size of the animal being scanned can also have an influence on the quality of the images obtained and this was evident in the differences observed between the two cat cadavers presented. Although the same structures were observed in both, the smaller specimen produced images that were less clear due to the occurrence of partial volume artefact. Likewise the quality of the sagittal images obtained of the TMJ in the rabbit were affected by partial volume artefact due to the thin nature of the condyloid process in this direction. This effect could have been reduced by obtaining thinner slices in this specimen, although this is likely to have resulted in an increase in noise (Jones and others 1995). However, this demonstrates that the use of a standard imaging protocol may not be appropriate for all animals.

5.4.2. CT of the TB in the dog ,cat and rabbit

Previous publications have presented individual or representative images of the normal canine TB (George and Smallwood 1992, Assheuer and Sager 1997, Russo and others 2002, Garosi and others 2003). However, to the author's knowledge, there are no complete CT sequences of the canine TB published and no images depicting normal TB anatomy in either the cat or rabbit.

CT has been reported to identify all of the major structures of the middle ear of the dog including the tympanic membrane, the auditory ossicles and the tympanic bulla (Russo and others 2002). Although the position of the tympanic membrane could be determined in the present study relative to the malleus, the membrane itself was not identified, except in the presence of fluid in the external ear canal where it produced a distinctive angular interface between this and the air-filled tympanic cavity. This may have been due to the 1mm slices obtained in the previous study compared to the slightly thicker 1.1mm slices in the present one. However, in this previous study, it did not appear to be consistently visible and was reported to be easier to identify in dorsal than transverse images (Russo and others 2002). The auditory ossicles and the various regions of the TB could be identified in all three species in the present study, and the differences in shape and position could be appreciated. The transverse and dorsal sections appeared to be of most use for imaging the middle ear in these three species and the ability to compare with the contralateral side aided

identification of various structures. The sagittal images were felt to be of least use. Transverse and dorsal views have been reported to provide complementary views of the canine TB (Russo and others 2002).

The presence of fluid within the TB lumen neither enhanced nor obscured visualisation of any of the structures. In theory the location of fluid within the TB lumen should vary with gravity and therefore the position of the animal must be taken into consideration when interpreting images. However, this did not appear to be the case in the present study with unfilled areas remaining relatively consistent despite the position of the cadaver. Fluid tended not to fill the epitympanic recess or the rostradorsal compartment of the TB lumen. This may be due to the presence of surface tension in the gel that was used or may reflect the anatomy of the TB since the auditory tube also opens into this rostradorsal region. Ultrasound gel was selected rather than water in an effort to ensure it remained within the TB despite the repositioning required for imaging. However, it is likely that the pathological fluid associated with the presence of middle ear disease will also be relatively thick, tenacious and be affected by surface tension therefore these observations are also likely to relate to clinical cases.

One of the problems associated with the use of cadavers was the presence of post mortem fluid in the external ear canal although in this case it proved beneficial as it enhanced location of the tympanic membrane that was otherwise not visible. Unless there was post mortem fluid already present in the ventral compartment of the ear, which seems less likely since there was none present on the contralateral side, a small amount of material introduced into the dorsal compartment did pass into the ventral compartment despite the opening being small. The opening is located caudally but the location of the fluid presumably represented the effect of gravity on the material once it had passed through.

5.4.3. CT of the TMJ in the dog, cat and rabbit

Previous publications have presented individual or representative images of the normal canine TMJ (George and Smallwood 1992, Assheuer and Sager 1997). However, to the author's knowledge, there are no complete CT sequences of the canine TMJ published and no images depicting normal TMJ anatomy in either the cat or rabbit. The superior image quality obtained in the present study also allowed visualisation of additional structures in the dog including the retroarticular foramen. As image quality improves, the differentiation between previously invisible normal anatomical features and pathological changes can be a

challenge for the clinician, which is why continuing publication of normal diagnostic images using modern equipment is necessary.

In humans, CT clearly demonstrated the contour and shape of the bony elements of the TMJ, with the articular space and condylar cortex being well defined (Suarez and others 1980), and was also useful to assess the spatial relationship of the joint components with each other (Minagi and others 2000). The use of CT in the dog and cat TMJ has been reported to provide excellent detail of the trabecular and subchondral bone (Schwarz and others 2002). The same was observed in the dog, cat and rabbit in the present study. In humans, the intra-articular disc could be visualised (Suarez and others 1980, Dixon 1991), although difficulties in determining the position of the disc were encountered due to its similarity in density with the surrounding soft tissue, (Dixon 1991) and so CT was not recommended for this purpose (Payne and Nakielny 1996). The internal soft tissue structures of the canine and feline TMJ, including the articular cartilage and disc, joint capsule and lateral ligament were not be discernable (Schwarz and others 2002) and this was also the finding of the present study.

Each of the three planes allowed optimal visualisation of different areas of the TMJ. In the dog and cat, the transverse sections highlighted the dorsal components and the dorsal sections the caudal and ventral components. The sagittal sections allowed assessment of all areas of the joint space and the profile of the retroarticular process, and therefore are likely to be particularly useful in the evaluation of TMJ abnormalities in these species. The different orientation of the TMJ in the rabbit meant that the transverse section highlighted the dorsal components, the dorsal sections highlighted the rostral components and the sagittal sections highlighted both. When examining the TMJ in these species, reliance should therefore not be placed on images in one plane only, as each is likely to produce additional information. While transverse and dorsal sections can be acquired directly in live animals, it is not possible to directly acquire sagittal ones and therefore reliance must be placed on poorer quality reconstructed images.

A small, hypoattenuating area in the lateral aspect of the condyloid process was reported to be a normal anatomical variation seen on CT images of the canine TMJ but no explanation was given for this observation (Schwarz and others 2002). From the sequence of multiplanar images obtained in the present study it was clear that this was due to the shape of the rostral margin of the condyloid process and its rostromedial – caudolateral orientation resulting in the area of the condyloid process immediately medial to the lateral

extremity not being present within transverse sections through the rostral aspect of the TMJ. It is usually easier to determine the source of such features when entire sequences of thin contiguous slices in multiple planes are available rather than individual images.

The canine and feline cadavers in the present study were imaged with the mouth either completely closed or maximally open. However, due to recommendation for general anaesthesia when performing CT examinations of the head (Love and others 1995, Seitz and others 1996), most patients will be intubated and therefore the mouth will be open to varying degrees depending on the equipment used. The appearance of these structures in clinical cases is therefore likely to fall at varying stages between the two extremes presented here. Maximal opening of the rabbit mouth was not performed in the present study as this has been associated with iatrogenic damage to the TMJ and resulting post-procedural complications including anorexia (Crossley 2006). This conservative approach resulted in the minimal differences being observed between the open and closed positions in this species.

CT has been used to assess the spatial relationship of the joint components with each other (Minagi and others 2000) and this was also possible in the present study. The position of the lateral extremity of the condyloid process changed most between the closed and open positions in the dog and cat, reflecting rotation of the condyloid process within the mandibular fossa. Although this could be appreciated in all the planes, it was most evident on the sagittal images. The shape of the condyloid process associated with large rotational angles (the angle between the long axis of the mandibular condyle and the axis of rotation) has been reported to result in stretching of the lateral ligament, in turn predisposing to TMJ subluxation in the dog (Robins and Grandage 1977, Lantz and Cantwell 1986). The use of sagittal CT images in this species with the mouth closed and open may therefore have the ability to assess the distance travelled by the lateral extremity of the condyloid process. However, complete closure of the mouth will require the absence of an endotracheal tube. Given the rapid acquisition times associated with modern CT equipment, temporary extubation may be an option in some cases although further work would be required to determine if this is possible. Examination of the canine elbow can be performed under heavy sedation rather than general anaesthesia (Carerra and Trevail 2007) although for imaging the head, care would have to be taken to prevent motion resulting from respiratory movement, which could be achieved by taping the head to the table (Hoskinson 1993).

In the dorsal images of the dog, opening the mouth resulted in a greater angulation being observed between the medial and lateral halves of the condyloid process. In addition, the medial half of the condyloid process and the corresponding surface of the retroarticular process appeared slightly curved. Care should be taken to appreciate these as normal variations observed with the mouth open and not mistake them for the various abnormalities that have been reported to occur in association with TMJ dysplasia (Stewart and others 1975, Robins and Grandage 1977, Johnson 1979, Lane 1982, Stead 1984, Bennet and Prymak 1986).

Scanning the human TMJ in both open and closed mouth positions has been reported to help determine the location of the intra-articular disc (Dixon 1991) but in the present study it remained invisible throughout.

Chapter 6. Magnetic resonance imaging of the tympanic bulla, temporomandibular joint and associated structures in the dog, cat and rabbit.

6.1 Introduction

6.1.1. Technical aspects of MR image production

All hydrogen nuclei within the body spin or precess about a central axis but when placed within the magnetic field generated by an MRI unit, they all become aligned with the field. If a specific radiofrequency is then applied using a transmitter coil placed on the body surface, all of the nuclei are pulled in unison out of alignment with the magnetic field. When the radiofrequency is removed, they will progressively return to alignment with the magnetic field and the time taken for this is known as the T1 relaxation time. Individual nuclei will also revert to spinning at different rates until they are completely out of phase with each other and this interval is the T2 relaxation time. These processes occur at different rates depending on the type of tissue in which the nuclei are embedded. During this decay, the nuclei release energy in the form of a radiofrequency that can be detected by a receiver coil and provides information about the type of tissue present, which is used to build up a grey scale image of the area. Different sequences of radiofrequency application can be selected depending on the tissue type or area of interest (Thomson 1993, Tidwell 1999).

Subtle differences can be detected between areas of soft tissue making MRI ideal for the examination of such structures (Shores 1993) and more sensitive for identifying soft tissue changes than either CT or radiography (Shores 1993, Forrest 1999). The hydrogen nuclei in compact bone are not mobile and therefore not influenced by the magnetic field or applied radiofrequency. Since no signal is received back from these areas, they are depicted as black or 'signal voids' on the resulting image regardless of the sequence used. MRI is therefore less suitable for bone imaging than CT (Forrest 1999). However, bone can usually be visualised indirectly with trabecular bone being outlined by the intense signal from the marrow fat and cortical bone outlined by the marrow and surrounding soft tissue (Widmer and others 1991). There are too few nuclei in areas of gas for any signal to be detected so they too are depicted as black.

Anaesthesia is required to reduce patient movement and therefore prevent blurring of the image especially as each sequence can take several minutes to acquire (Assheuer and Sager 1997, Allgoewer and others 2000). The animal is placed in either dorsal (Allgoewer and others 2000, Garosi and others 2001) or sternal recumbency to ensure symmetry, with the head extended and held in place with a cushion (Assheuer and Sager 1997), and the forelegs pulled caudally (Allgoewer and others 2000).

For imaging of the TB, a standard small animal coil has been used and the magnetic field strength was typically 1-2.3 Tesla (Widmer and others 1991, Allgoewer and others 2000, Dvir and others 2000). Using a stronger 4 Tesla magnet provided an increased signal to noise ratio but the image was affected more by slight movements in the region of interest caused by pulsation of blood or CSF (Dayrell-Hart 1997). An examination should include T2 weighted and pre and post contrast T1 weighted acquisitions (Allgoewer and others 2000, Dvir and others 2000, Garosi and others 2000) in dorsal, sagittal and transverse planes (Dvir and others 2000), although transverse and dorsal sequences were reported as being the most useful in dogs (Bischoff and Kneller 2004) and cats (Allgoewer and others 2000). Intravenous contrast medium (gadolinium-diethylenetriamine penta-acetic acid dimeglumine / gadolinium - DPTA) was administered at a dose rate of 0.1mmol/kg in dogs (Garosi and others 2000, Garosi and others 2001) and 0.2 mmol/kg in cats (Allgoewer and others 2000). This may be useful in the presence of a mass within the TB or external ear canal and also allows clear distinction between vascularised mucosa and non-vascularised structures (Allgoewer and others 2000). Proton density weighted transverse acquisition have not been shown to provide additional information (Dvir and others 2000) although fat saturation and susceptibility techniques can be used when necessary to characterise lesions and differentiate fat from blood during evaluation of the inner ear (Dayrell-Hart 1997).

Slice thicknesses of 2-4mm have been used to image the middle ear (Allgoewer and others 2000, Dvir and others 2000). Standard imaging protocols for examination of the brain (3.5 - 5mm) do not allow the extremely small inner ear structures to be consistently visualised in their entirety (Dayrell-Hart 1997, Garosi and others 2001) and they require thinner slices to avoid partial volume artefacts (Garosi et al. 2001). To avoid problems with the increased noise associated with thin slices, volume acquisition can be used which excites the entire volume and reconstructs the data with the specified number of slices and thickness (Garosi and others 2001). Volume acquisition with a slice thickness of less than 2mm has become gold standard in humans and allows more detailed visualisation of the inner ear structures (Garosi and others 2001).

There appears to be only one report describing the use of MRI for imaging the canine TMJ (Baines and others 2002). An open 0.2 T permanent magnet was used in conjunction with a dual phased array coil. 4mm thick slices were produced with a 0.4mm gap using T1-, T2- and proton density- weighted spin echo sequences (Baines and others 2002).

6.1.2. MRI of the TB and associated structures

The use of MRI to examine the human TB has been documented (Stone and others 1983, Holliday and Reede 1989) and high resolution CT and MRI have now replaced radiography in the diagnosis of middle ear disease (Allgoewer and others 2000). MRI is reserved for use when soft tissue injuries are being evaluated since it does not visualise bone pathology satisfactorily (Robinson and others 2003). Temporal bone fractures are demonstrated only where there is displacement, with or without absence of the cortical signal void, or if fluid is present within the fracture crevice so a normal MR examination does not rule out the presence of a fracture (Holliday and Reede 1989).

In humans, the middle ear cavity was invisible on conventional MRI due to its bone boundaries and air content. The bone of the auditory ossicles and soft tissue structures including the tensor tympani muscle, stapedius muscles and the suspensory ligaments of the ossicles were too small to be readily identifiable (Holliday and Reede 1989). Despite the lack of intrinsic signal, the middle ear cleft was reliably localised within the temporal bone by its position relative to the fluid signal of the membranous labyrinth (Holliday and Reede 1989).

The appearance of the normal feline TB using MRI has been described (Allgoewer and others 2000). MRI has been used to evaluate the canine TB (Dvir and others 2000, Garosi and others 2000) but although there are publications which present normal transverse MRI sections of the canine TB (Feeney and others 1991) there do not appear to be any reports describing it in detail.

The air-filled lumen of the normal canine TB appears as a signal void, which is therefore indistinguishable from the signal void produced by the bone walls (Forrest 1999, Garosi and others 2000, Bischoff and Kneller 2004). However, in cats, the air-filled vertical and horizontal portions of the external auditory canal, both compartments of the TB and the thin separating bony lamella could be visualised (Allgoewer and others 2000). The fluid within the membranous labyrinth, semicircular ducts and cochlea of the normal inner ear

was visible as a high signal on T2 weighted image (Allgoewer and others 2000, Garosi and others 2000) that contrasts with the surrounding signal void of the bony labyrinth (Garosi et al. 2001). On transverse images this was reported to resemble the lateral silhouette of a duck (Lamb and Garosi 2000). However, visibility of these structures depended on the quality of the images, which varies with the protocol used (Dayrell-Hart 1997, Garosi and others 2001), the strength of the magnet and the amount of motion in the region of interest (Dayrell-Hart 1997).

There are currently no reports using MRI to image the TB in the rabbit.

6.1.3. MRI of the TMJ and associated structures

MRI examination of the human TMJ has been described (Drace and Enzmann 1990, Tasaki and Westesson 1993). It provided excellent delineation of anatomic detail (Landes and others 2000) and is claimed to be the only imaging modality capable of localising the disc (Larheim 1995), the appearance of which has been described (Drace and Enzmann 1990). It has therefore surpassed CT and arthrography for evaluation of this joint (Larheim 1995, Payne and Nakielny 1996). The most lateral and medial parts of the TMJ were not depicted with the same high quality of image as the central part, although this could be improved by using a smaller field of view or producing MR sections thinner than 3mm so that volume averaging of oblique structures would be reduced (Tasaki and Westesson 1993). The disc had a low signal on all pulse sequences due to its fibrous nature, which may make it difficult to distinguish from adjacent cortical bone (Payne and Nakielny 1996).

MRI has been used to examine several joints in the dog and their appearance has been described (Baird and others 1998, Snap and others 1998, Widmer and others 1991, van Bree and others 1993, Reichle and Snaps 1999, Norberg and Johnson 1999). It has also been used to visualise the vertebral column and intervertebral discs (Sether and others 1990). Although there are publications presenting normal transverse MRI sections of the canine TMJ (Assheuer and Sager 1997), there is currently only one report of evaluation of the canine TMJ using MRI and no published images.

The dorsal and transverse plane images proved to be the most useful, allowing good assessment of the shape of both the condyloid process and the mandibular fossa, and their relative positions. Due to the oblique orientation of each condyloid process relative to the common long axis of the mandibles, the sagittal plane was only useful in the midportion of

each TMJ. In these normal dogs, there was no signal from the cortical bone in any sequence and the cancellous bone was hypointense compared with the facial muscles. The articular cartilage and synovial fluid were hyperintense compared with the cortical bone but could not be distinguished from each other using these sequences. The articular disc was not demonstrated in any TMJ although this may be possible using other sequences (Baines and others 2002). There are currently no other reports of MRI imaging of the TMJ in the veterinary literature although it has been suggested that it could be used to evaluate temporomandibular joint luxations in dogs (Widmer and others 1991). There are also currently no reports using MRI to image the TMJ in the cat or rabbit.

6.1.4. Aims

The aims of the work presented in this chapter were to:

- Acquire transverse, sagittal and dorsal MR images of the normal and fluid-filled TB and the closed and open TMJ in dog, cat and rabbit cadavers
- Compare these images to the multiplanar anatomical sections produced in Chapter 2 and document the MRI anatomy of the TB and TMJ

6.2. Materials and methods

6.2.1. Cadaver material

The same cadavers were used as in Chapter 5. These consisted of four Jack Russell Terrier dogs, four domestic breed feline and four New Zealand White rabbit cadavers. Two cadavers of each species had ultrasound gel present within the right middle ear cavity. Two of each species were positioned with the mouth closed and the other two with the mouth open. The cadavers were transported directly from the CT to the MRI unit and remained wrapped in multiple layers of cling film.

6.2.2. MRI equipment

A 7 Tesla Bruker Biospin 70/30 Avance Magnetic Resonance Imaging system (Bruker, Germany) was used (Figure 6.2.1). The wrapped heads were placed into a semicircular plastic trough. Attempts were made to place them in a true dorsoventral position and they were taped in place. This was then placed within the centre of a gradient set and radiofrequency resonator combination. An actively shielded gradient set with a 200mT/m maximum gradient and a birdcage volume resonator with an internal diameter of 152mm were used for acquisition of T1 and T2 weighted images in the dog and cat and T1 weighted images in the rabbit. A smaller gradient set with a 400mT/m maximum gradient and a 72 mm internal diameter birdcage volume resonator were used for the T2 weighted imaging of the rabbit head (Figure 6.2.2.). The resonator was advanced into the magnet presenting the cadaver nose first with the long axis of the head perpendicular to the magnet and the position of the cadaver remained unaltered throughout the duration of the examination. A pilot scan was performed in each cadaver and used to guide manual adjustment of the scan plane to accommodate any inconsistencies in positioning.

A series of trial sequences were run in each species to decide on a standard protocol. Subsequently, T1 weighted images were acquired as a 3-dimensional slab FLASH (Fast Low Angle Shot) sequence producing an isotropic resolution of 312 μ m. T_E/T_R times of 5.5/30ms were used with a flip angle of 15° and three or four averages, giving a maximum acquisition time of 63 minutes. Due to a heating effect from the sequence, the T2 weighted images were acquired in multiple two dimensional blocks each consisting of 30 to 40 slices. They were RARE (Rapid Acquisition with Relaxation Enhancement) sequences with T_E/T_R values of 58.8/5000 ms and a RARE factor of eight. The in-plane resolution

was 250 μ m with a 0.5mm slice thickness and a total of 16 averages gave an overall maximum acquisition time of 50 minutes for each block

6.2.3. Image analysis and reproduction

Paravision 3.0 (Bruker) software interfaced with the MRI system and allowed the volume data sets to be downloaded digitally onto compact discs and transferred to a desk top personal computer. They were then examined using ImageJ (free internet download) software and selected images exported into Paint Shop Pro 7 (Microsoft) which was used for manipulation and labelling. The two blocks of T2 weighted images acquired in each cadaver were combined before reslicing to produce images in the sagittal and dorsal planes.

Figure 6.2.1. Bruker Biospin Avance 7T (300MHz) Magnetic Resonance Imaging system.



Figure 6.2.2. Gradient set and radiofrequency resonator combinations.

- A. Large with an internal diameter of 152mm
- B. Medium with an internal diameter of 72 mm



6.3. Results

6.3.1. Technical considerations

Acquisition of some of the images proved problematic. The emergence of an intermittent fault with the resonator resulted in several failed sequences and those that were obtained demonstrated some degree of distortion. This occurred with both T1 (Figure 6.3.3.1) and T2 weighted sequences (Figure 6.3.1.2.). Some image distortion was also sometimes encountered at the start or end of a sequence (Figure 6.3.12.2). The combination of the two T2 weighted blocks prior to reslicing therefore often produced a line down the middle of the resulting multiplanar images at the joining site (Figure 6.3.4.3). Since the sagittal and dorsal T2 images relied on reconstruction from the transverse sequences, the resulting degradation in image quality was further compounded.

Despite attempts to position the cadavers in a true dorsoventral position, some asymmetry was observed in most of the sequences and since all the multiplanar images in this study relied on reslicing, this also affected the reconstructed images. An absence of symmetry in many of images therefore hindered bilateral comparison of structures. The volumetric acquisition of the T1 weighted images meant that resolution was equivalent in all planes. However, the reconstructed T2 weighted images were affected by the slice thickness of the transverse images and therefore the sagittal and dorsal images were of poorer resolution. Distortion was also evident in the reconstructed T2 weighted images due to the slice thickness being different to the in-plane resolution, resulting in an elongated appearance. The narrow slabs of images that were therefore obtained meant that identification of adjacent anatomical structures and subsequent orientation of the images was more difficult than with the T1 weighted images. This was particularly evident due to the small size of these structures in the cat and rabbit.

In both the T1 and T2 weighted images, gas and cortical bone appeared as a signal void and therefore were black while cancellous bone produced a mottled hyperintense appearance. Any ultrasound gel present within the middle ear cavity appeared isointense with the brain and surrounding soft tissue structures on the T1 weighted images and hyperintense compared with the same structures on the T2 weighted ones. In several of the images, gas pockets were observed in and around the brain and soft tissue structures of the head as black areas.

6.3.2. MRI appearance of the gas and fluid-filled TB in the dog, cat and rabbit

The transverse MR images obtained of the gas and fluid-filled TB in the dog, cat and rabbit are demonstrated in Figures 6.3.1 to 6.3.3., the sagittal images in Figures 6.3.4 to 6.3.6 and the dorsal images in Figures 6.3.7. to 6.3.9. with the key in Table 6.1. Where the number of images in a sequence is large, intermittent or representative slices have been presented as indicated by incremental jumps in the slice sequence numbers on the images.

The fluid-filled regions of the inner ear were visible in all of the images, but distinction could not be made between the gas content of the TB, its bone walls or the adjacent bony features of the skull. It was therefore difficult to determine the extent of the lumen of the TB. In the cat, the septum bullae appeared as a fine, indistinct curved line that was most clearly visible on the T2 weighted images. The auditory ossicles were not visible but the tympanic membrane was identified in the dog as a fine, indistinct line crossing the base of the external ear canal in the dorsal images.

A small amount of material that was hyperintense compared to surrounding tissue on both T1 and T2 weighted images was identified in the ventral area of some of the empty TB, presumably due to the presence of post mortem material. The introduction of gel into the lumen allowed a distinction to be made between the lumen and the walls and therefore, although the lumen was not always completely filled, an indication of the extent of the lumen could be ascertained. It also outlined the internal bony features of the TB, the location of the septum bulla in the cat and aided placement of anatomical labels on the images. A meniscus was visible wherever there was an interface between the gel and gas, either due to incomplete filling of the TB lumen or the presence of air bubbles in the gel. The gel was not always homogenous in appearance on both T1 and T2 weighted images, being interspersed with hyperintense regions. In some images this produced a speckled appearance (Figure 6.3.4.2.) while in others there were distinct hyperintense curved lines located around the edges of the TB lumen (Figure 6.3.2.2). In some instances these were particularly prominent adjacent to the ventral TB wall or a gas interface (Figure 6.3.3.2)

<u>Label</u>	<u>Description</u>
1	Tympanic bulla
2	Tympanic cavity
3	Epitympanic recess
4	External acoustic meatus
5	Promontory
6	septum bullae – cat
7	Tympanic membrane

Table 6.1. Anatomical features associated with the TB. Key for figures 6.3.1. to 6.3.9.

Figure 6.3.1. Transverse MR images through the TB in the dog progressing from rostral to caudal. The right TB contains ultrasound gel. Dorsal is to the top and left is to the right in all images. Number in bottom left corner indicates slice number. Approximate location of the first and last slice is indicated on the pilot image. For key see Table 6.1.

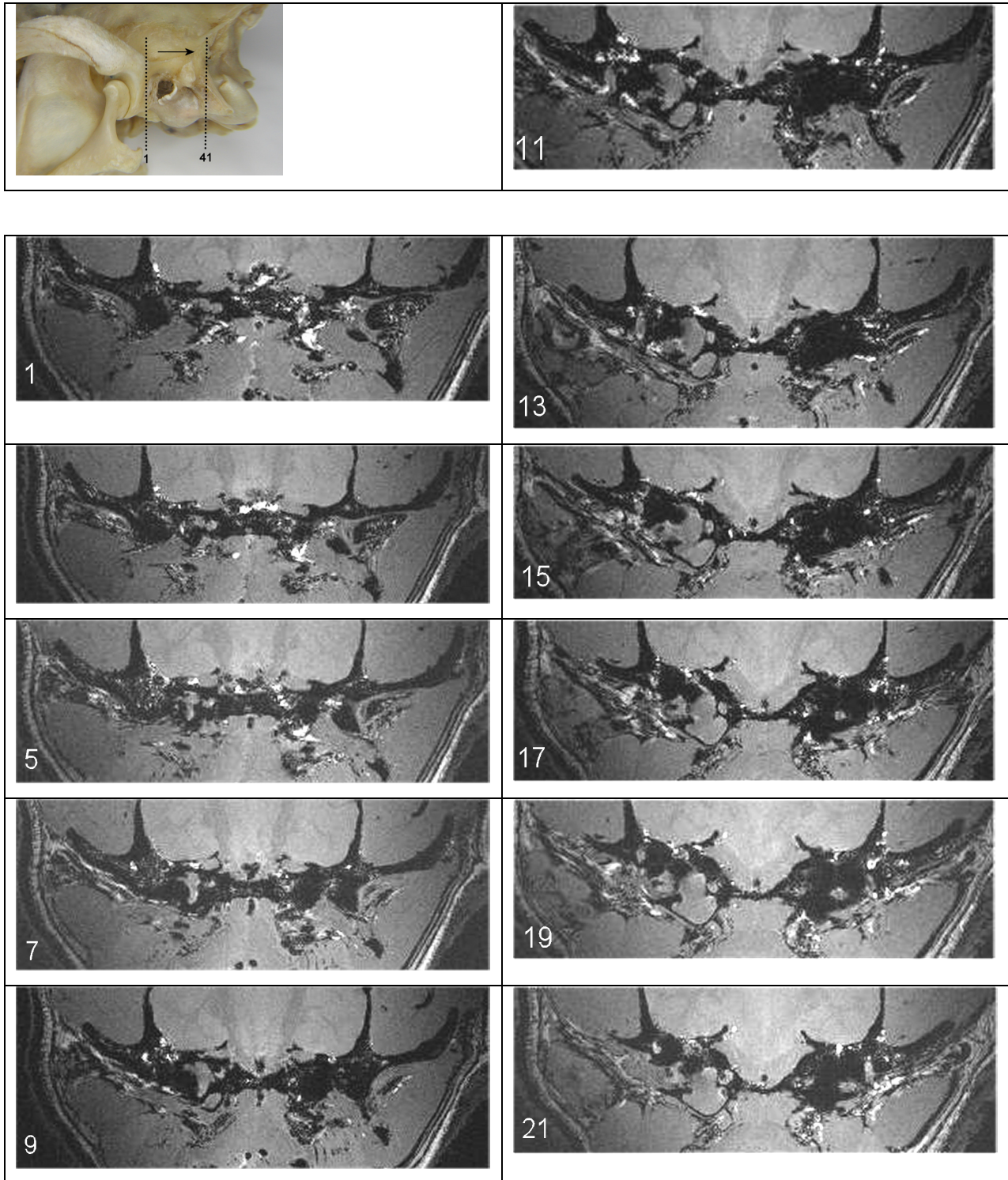
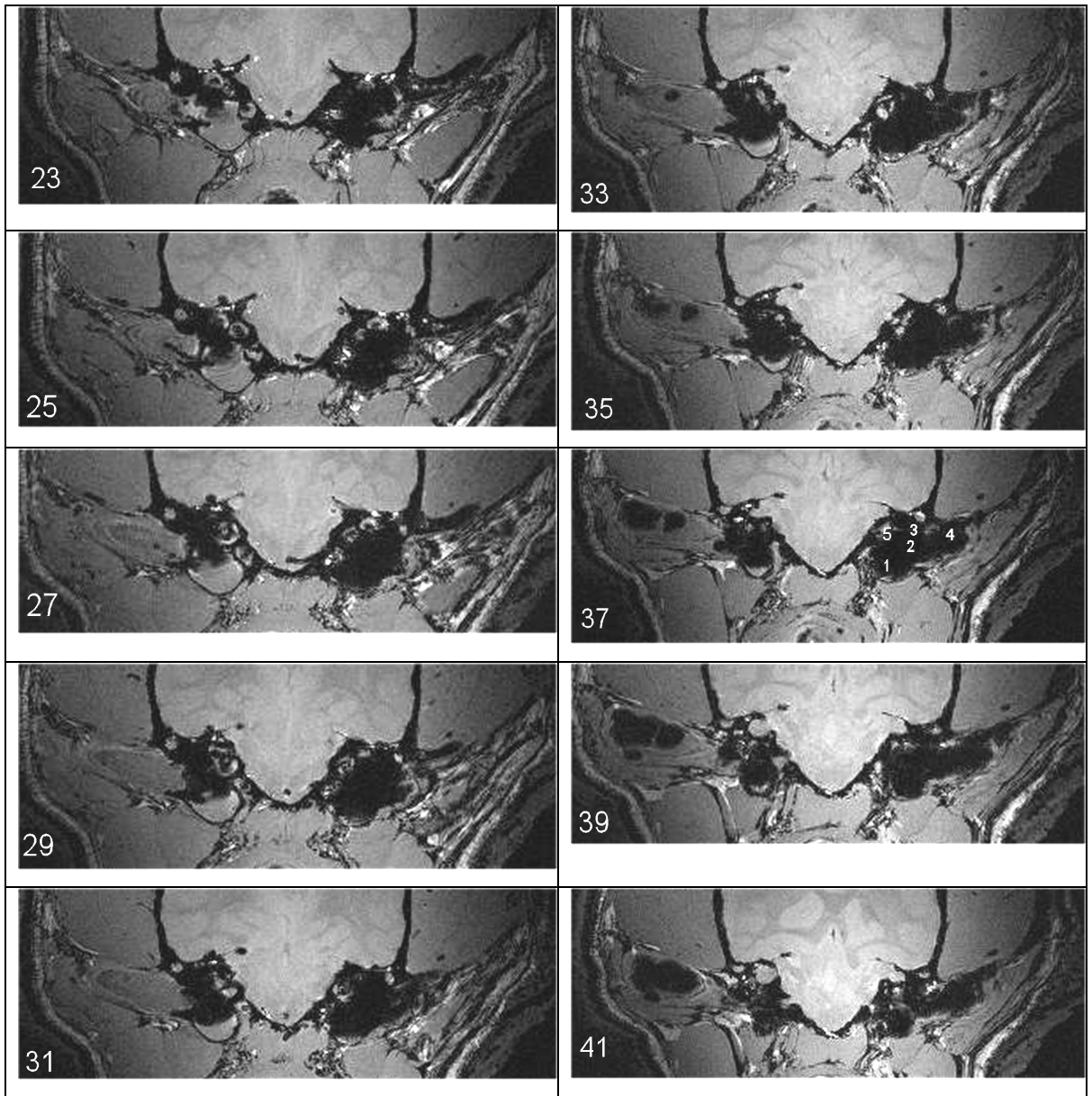


Figure 6.3.1.1. Transverse T1 weighted MR images through the gas and fluid-filled TB in the dog.

Figure 6.3.1.1 continued. Transverse T1 weighted MR images through the gas and fluid-filled TB in the dog.



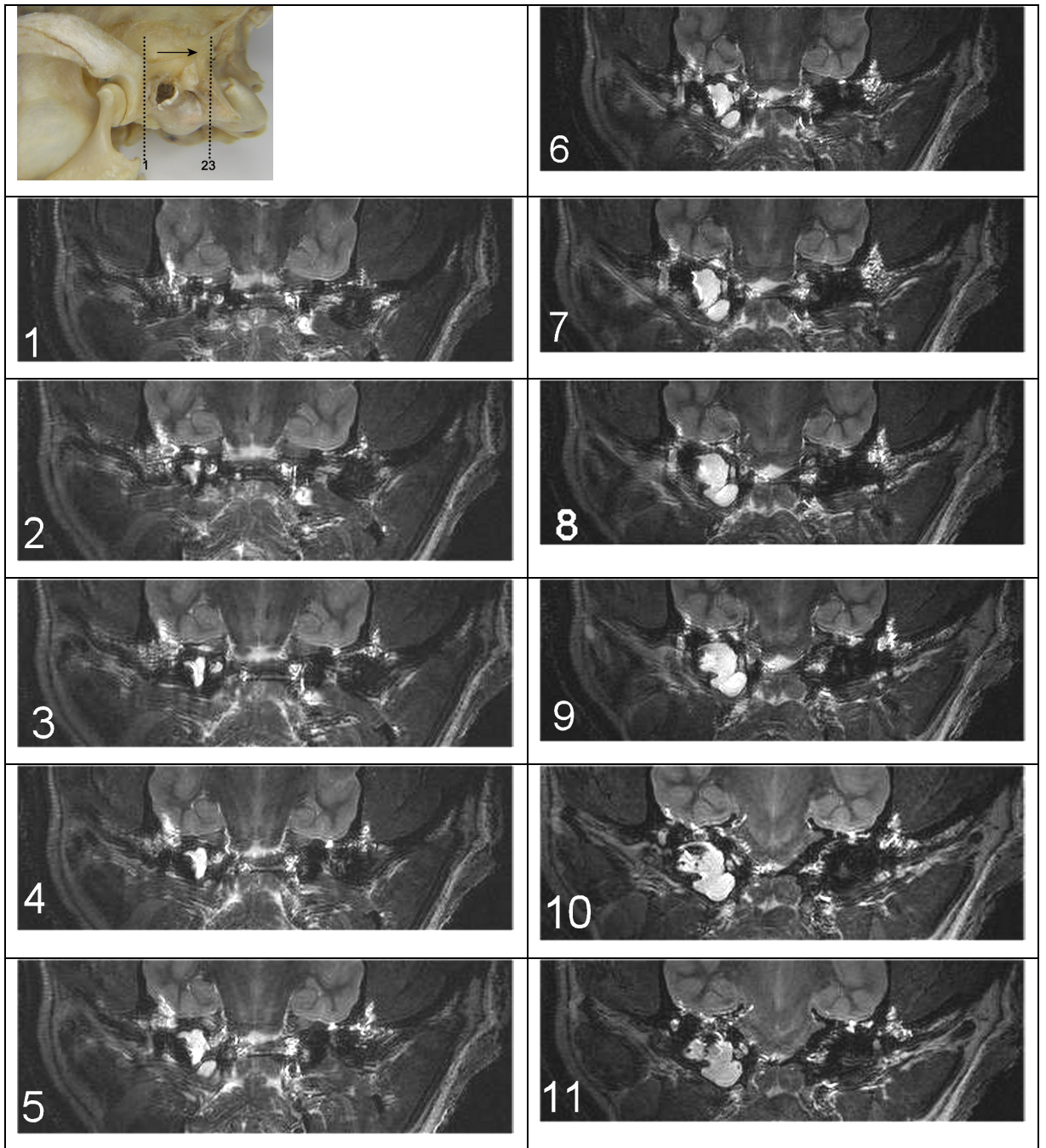


Figure 6.3.1.2. Transverse T2 weighted MR images through the gas and fluid-filled TB in the dog. Approximate location of the first and last slice is indicated on the pilot image.

Figure 6.3.1.2. continued. Transverse T2 weighted MR images through the gas and fluid-filled TB in the dog.

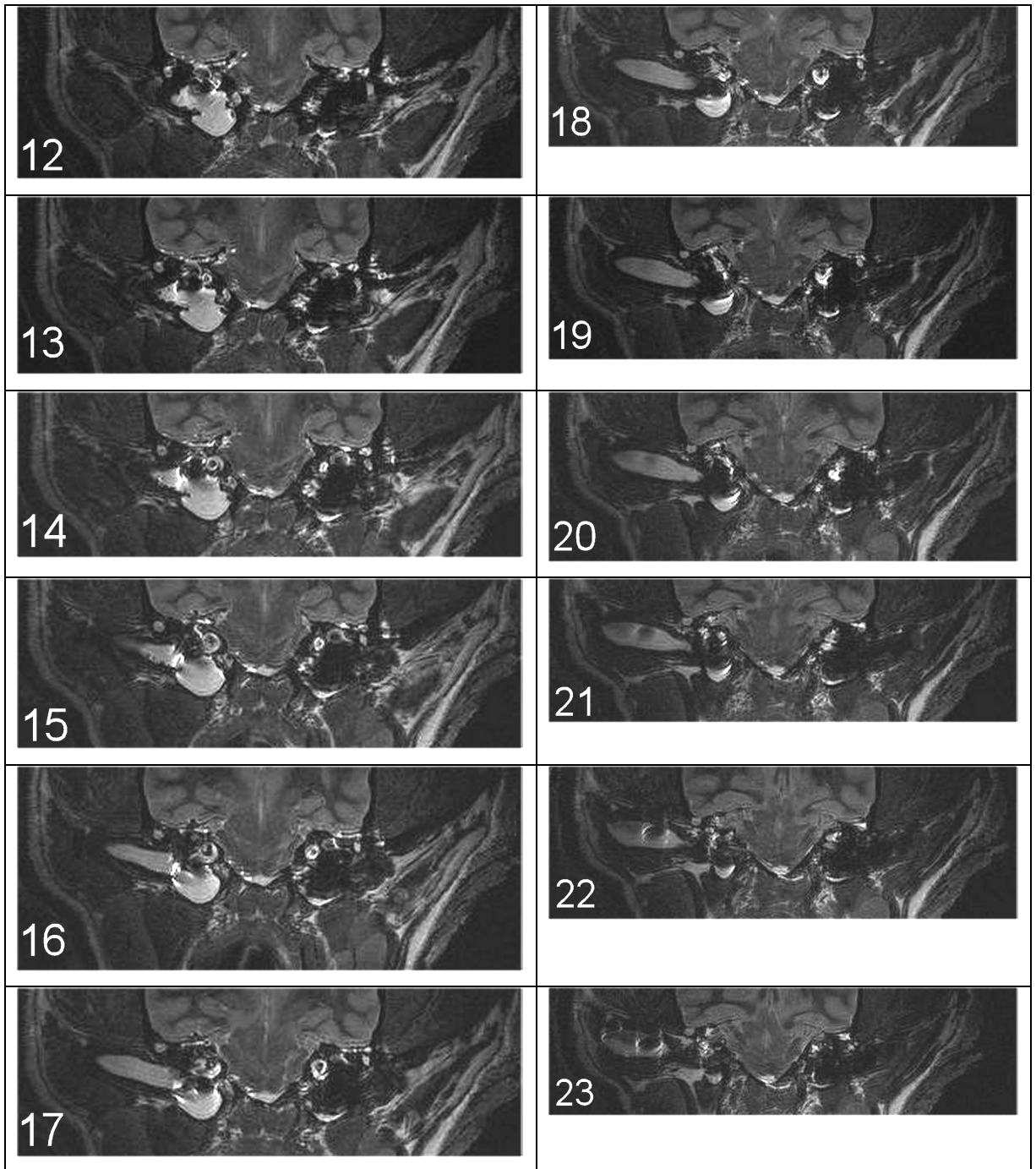


Figure 6.3.2. Transverse MR images through the TB in the cat progressing from rostral to caudal. The right TB contains ultrasound gel. Dorsal is to the top and left is to the right in all images. Number in bottom left corner indicates slice number. Approximate location of the first and last slice is indicated on the pilot image. For key see Table 6.1.

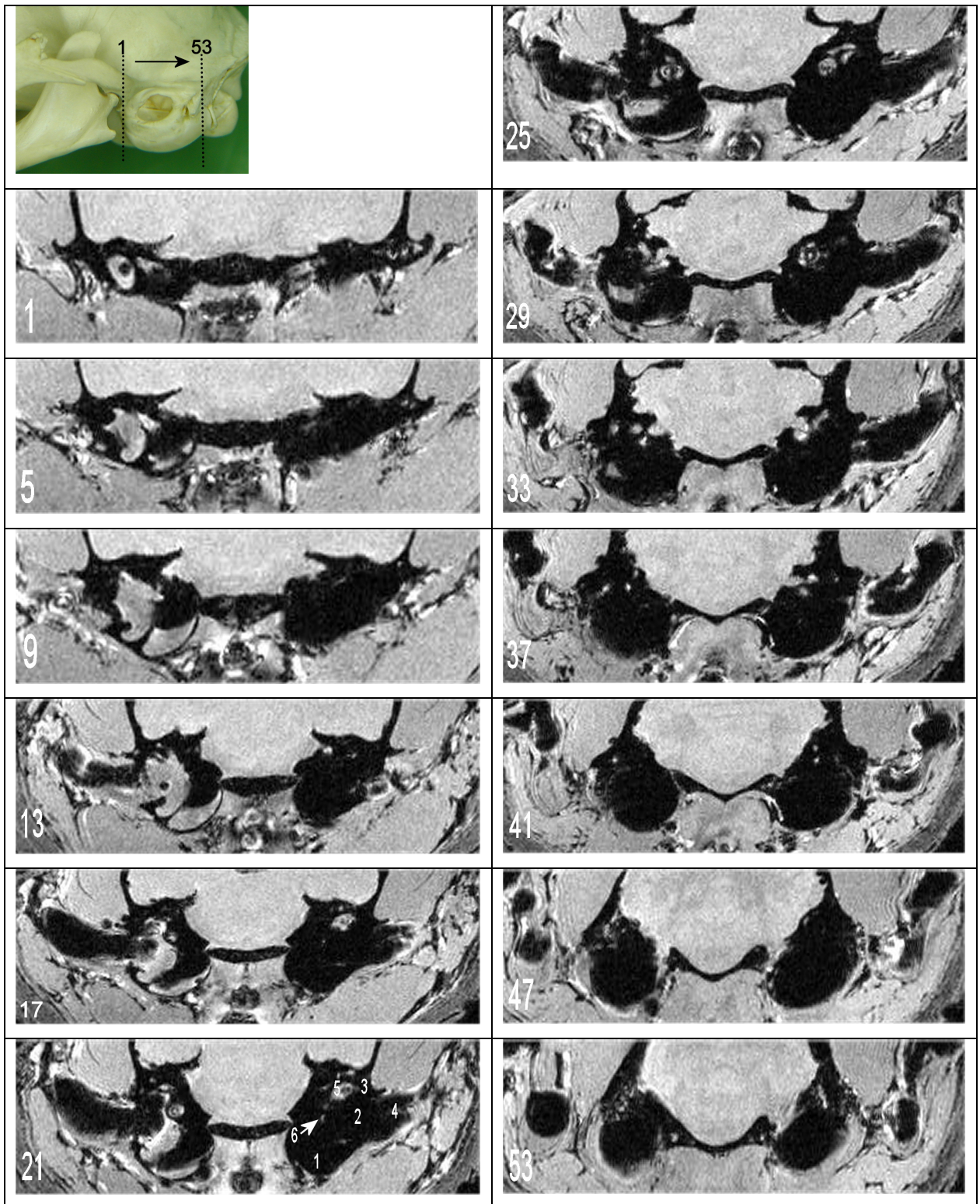


Figure 6.3.2.1. Transverse T1 weighted MR images through the gas and fluid-filled TB in the cat.

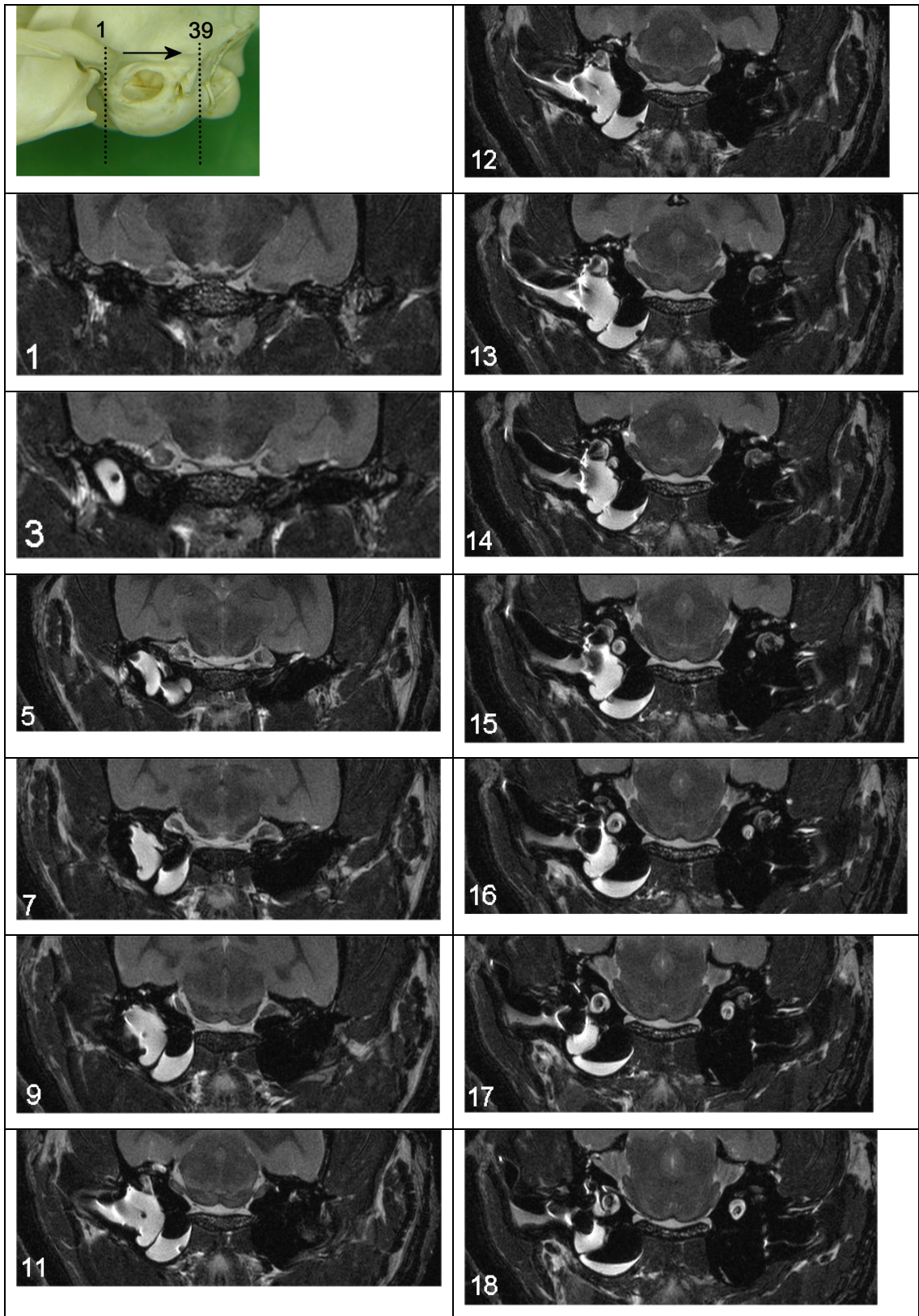


Figure 6.3.2.2. Transverse T2 weighted MR images through the gas and fluid-filled TB in the cat.

Figure 6.3.2.2. continued. Transverse T2 weighted MR images through the gas and fluid-filled TB in the cat.

Figure 6.3.3. Transverse MR images through the region of the TB in the rabbit progressing from rostral to caudal. The right TB contains ultrasound gel. Dorsal is to the top and left is to the right in all images. Number in bottom left corner indicates slice number. Approximate location of the first and last slice is indicated on the pilot image. For key see Table 6.1.

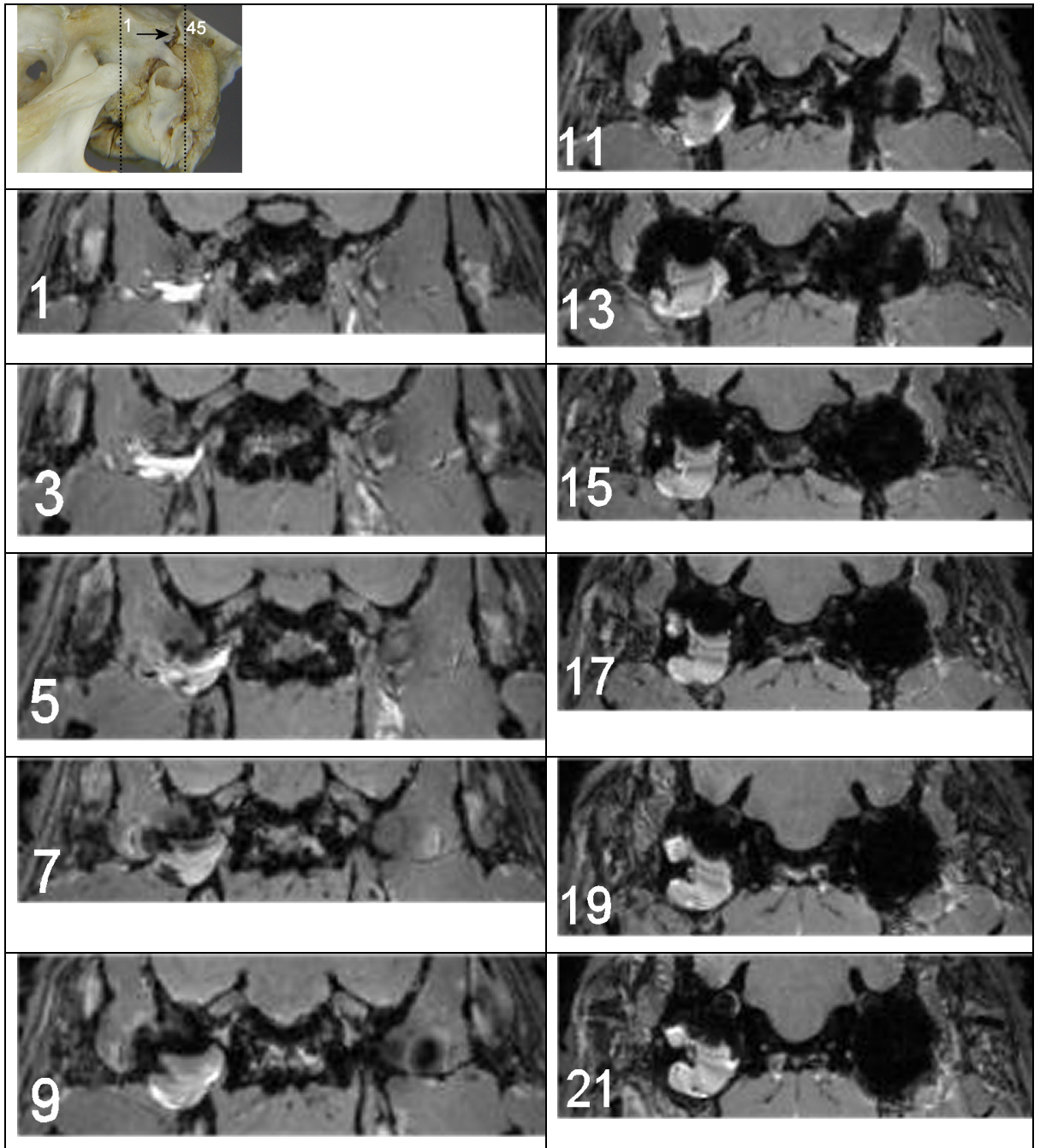
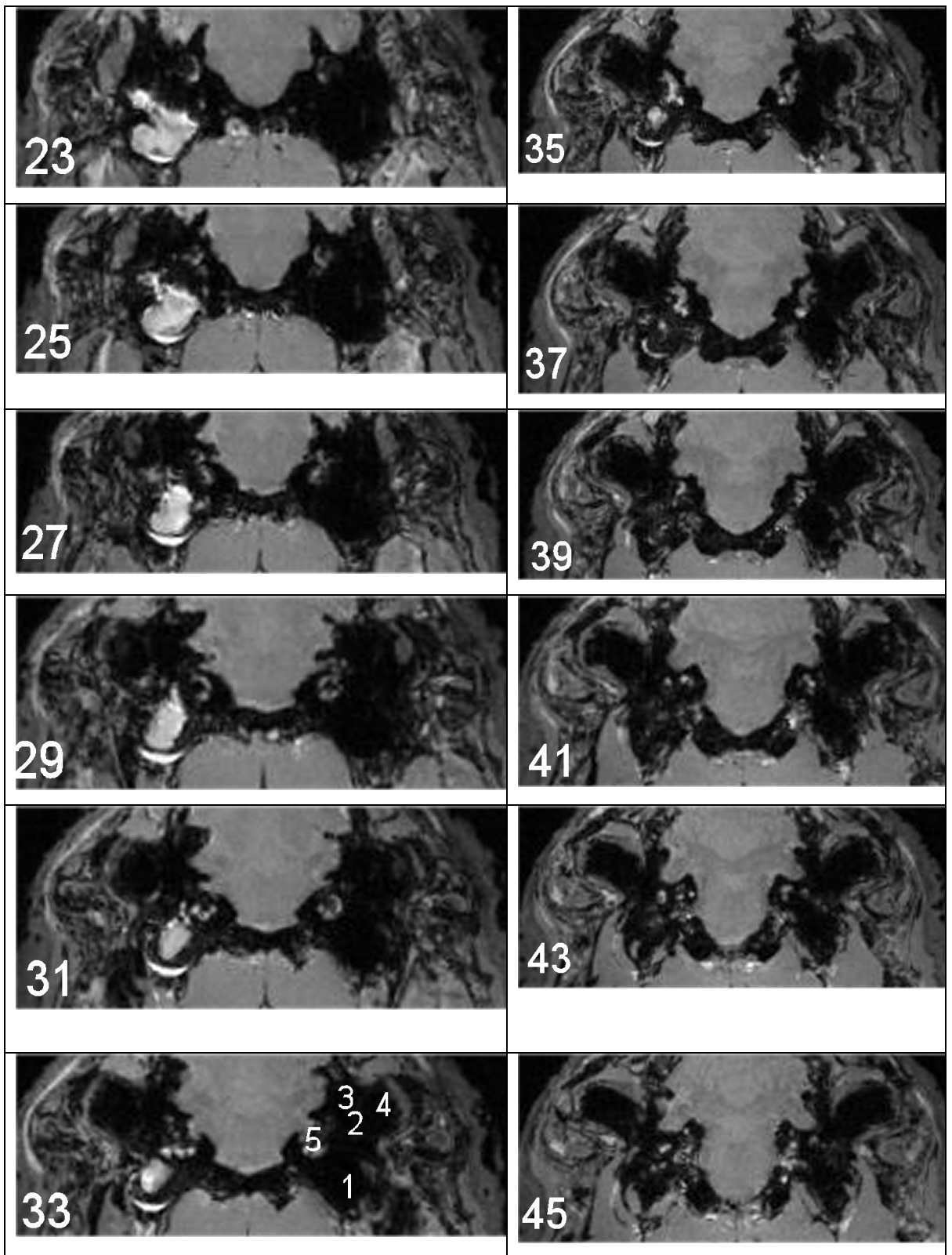


Figure 6.3.3.1. Transverse T1 weighted MR images through the gas and fluid-filled TB of the rabbit

Figure 6.3.3.1. continued. Transverse T1 weighted MR images through the gas and fluid-filled TB of the rabbit .



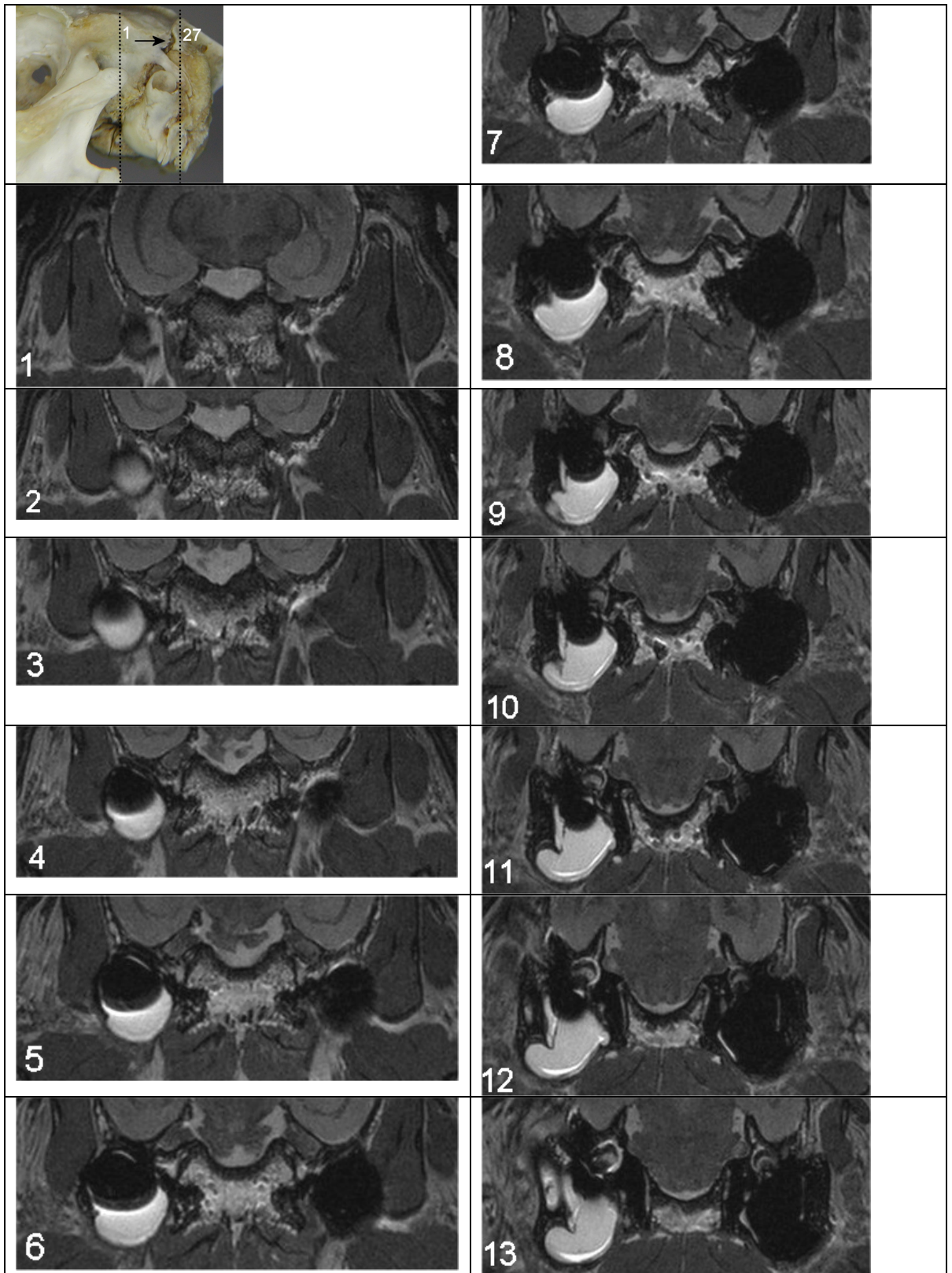


Figure 6.3.3.2. Transverse T2 weighted MR images through the gas and fluid-filled TB of the rabbit

Figure 6.3.3.2.continued. Transverse T2 weighted images through the gas and fluid-filled TB of the rabbit.

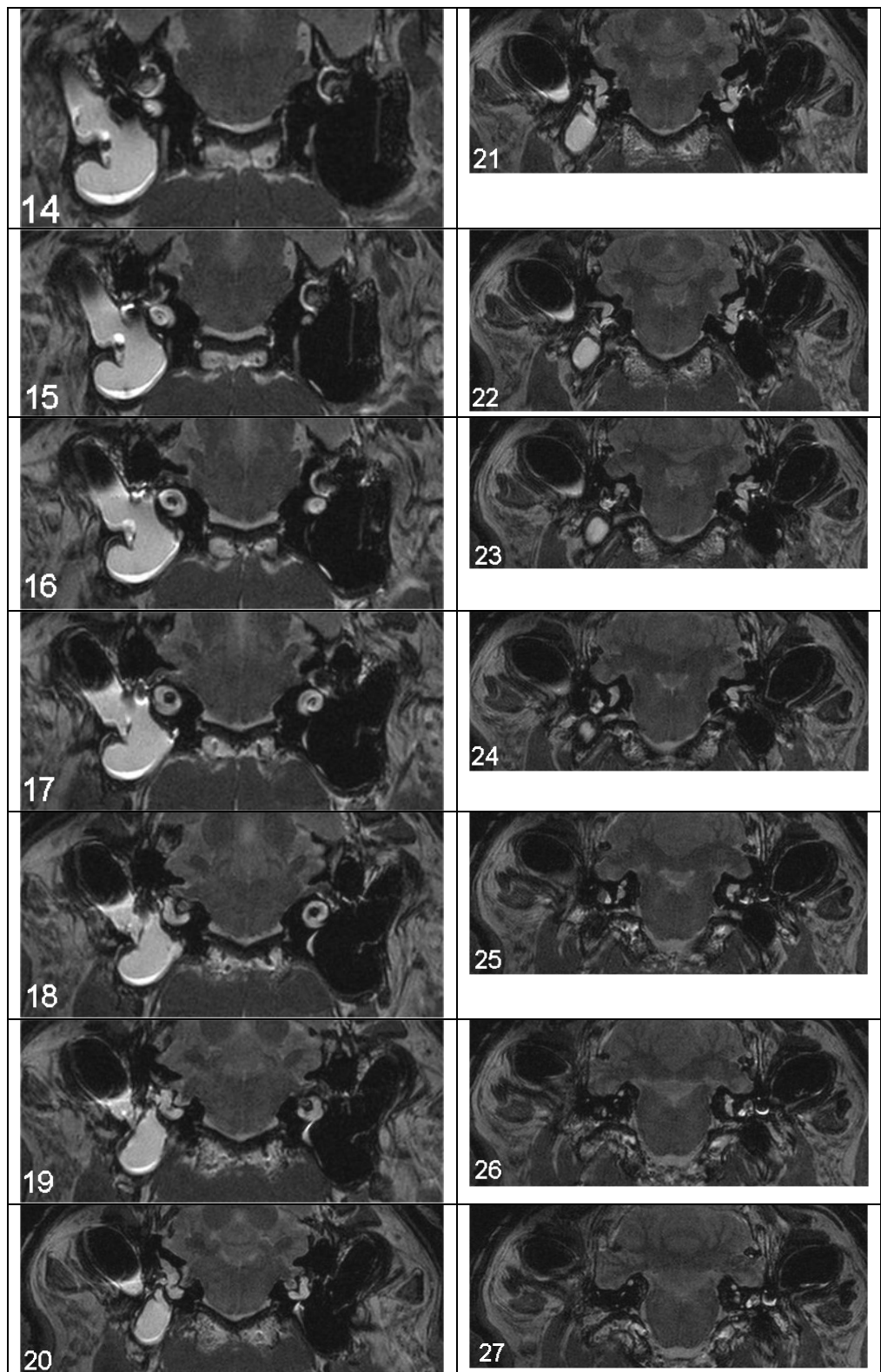


Figure 6.3.4. Sagittal MR images through the TB in the dog progressing from midline towards left. Dorsal is to top and rostral is to the left in all images. Approximate location of the first and last slice is indicated on the pilot image. For key see Table 6.1.

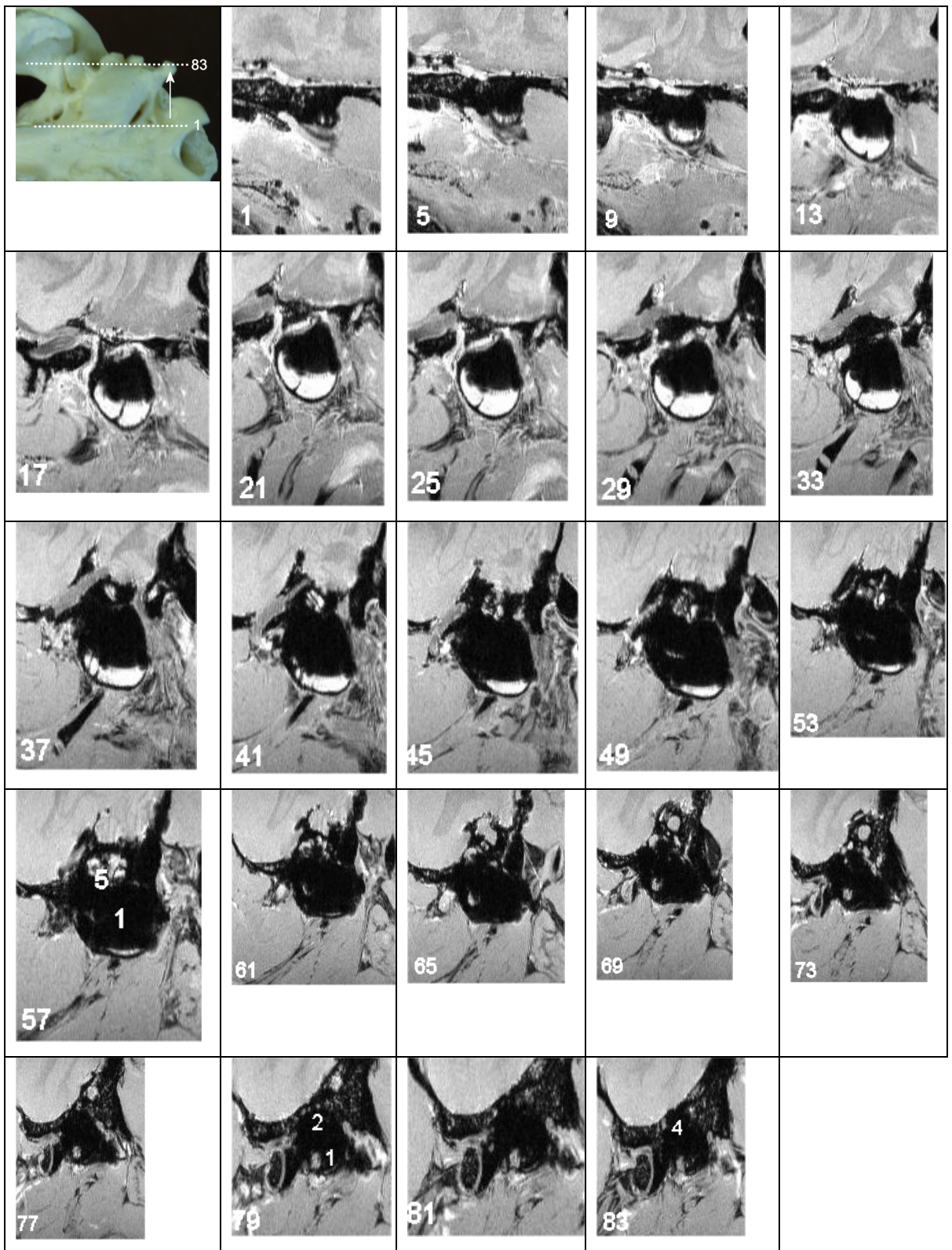


Figure 6.3.4.1. Sagittal T1 weighted MR images through the gas-filled TB in the dog.



Figure 6.3.4.2. Sagittal T1 weighted MR images through the fluid-filled TB in the dog.

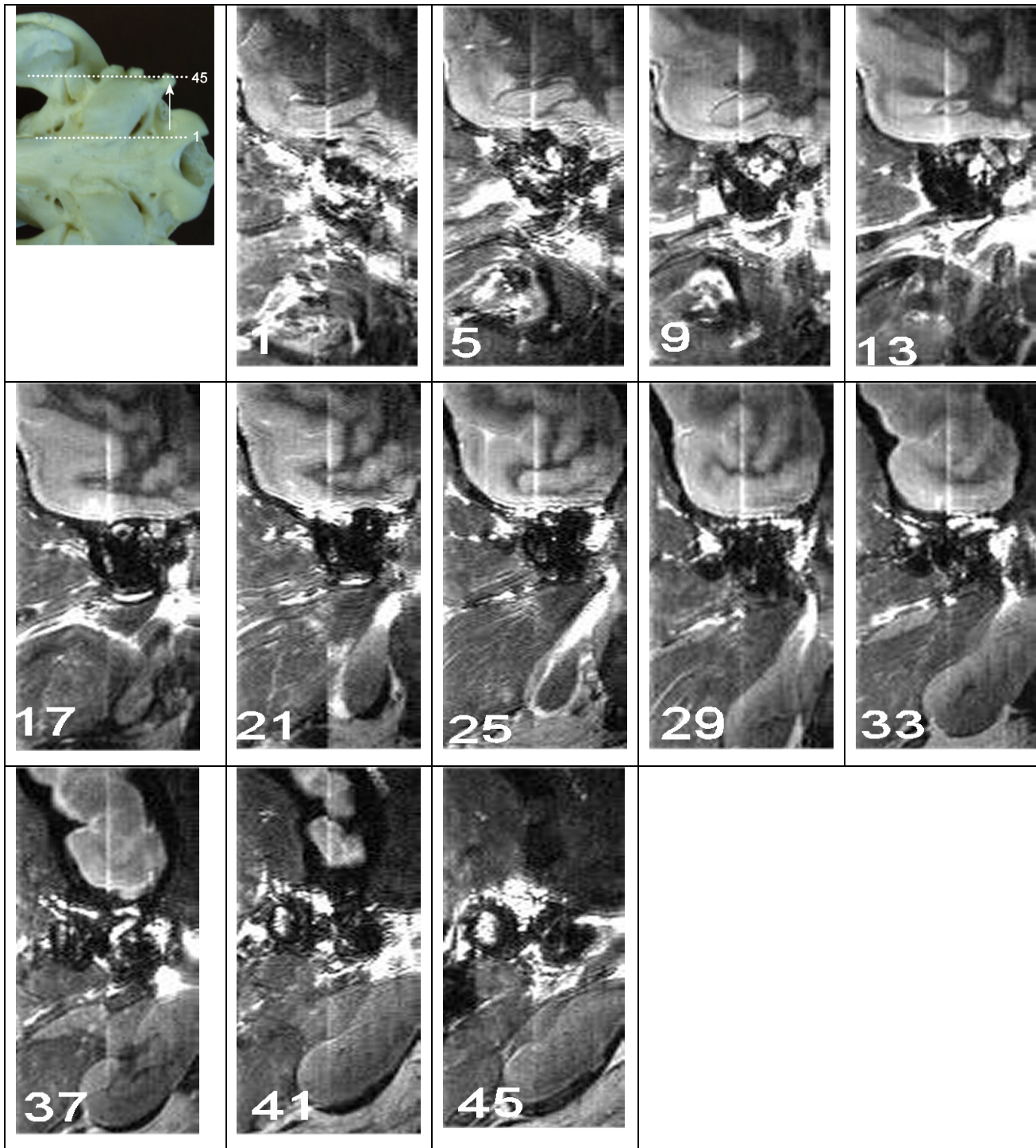


Figure 6.3.4.3. Sagittal T2 weighted MR images through the gas-filled TB in the dog. Some image distortion has resulted from an intermittent fault within the resonator.



Figure 6.3.4.4. Sagittal T2 weighted MR images through the fluid-filled TB in the dog.

Figure 6.3.5. Sagittal MR images through the TB in the cat progressing from midline towards left. Dorsal is to top and rostral is to the left in all images. Approximate location of the first and last slice is indicated on the pilot image. For key see Table 6.1.

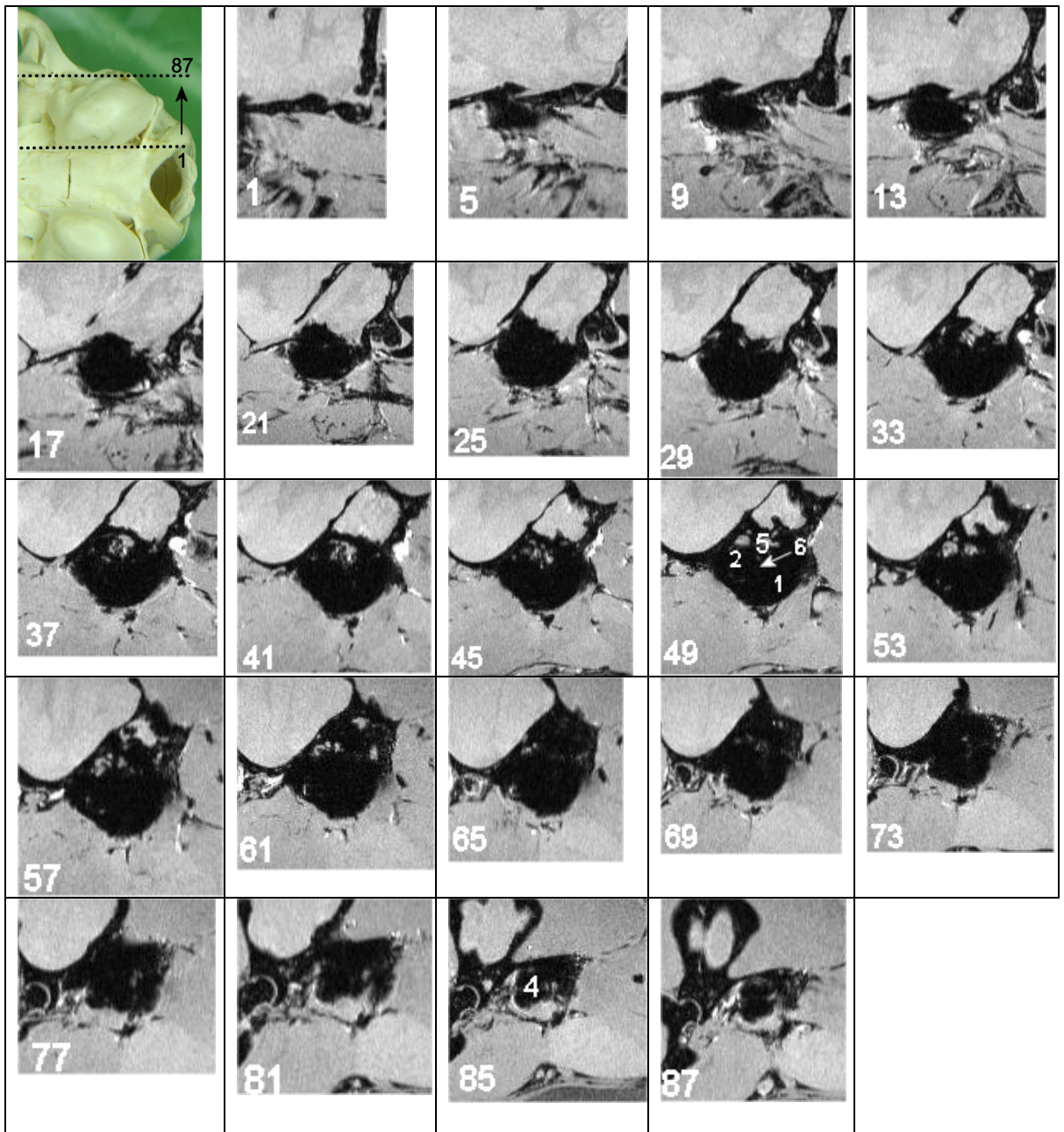


Figure 6.3.5.1. Sagittal T1 weighted MR images through the gas-filled TB in the cat.

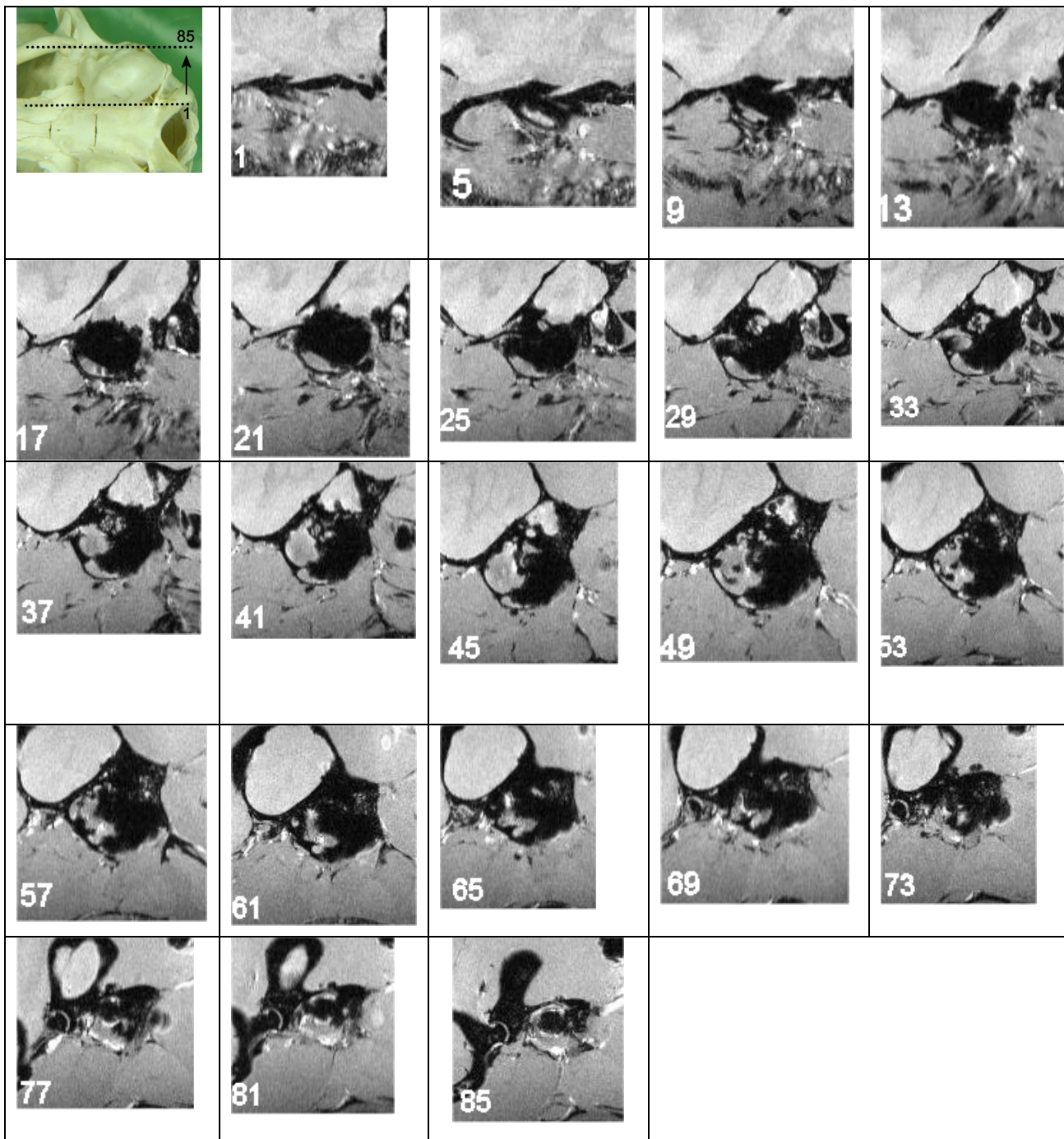


Figure 6.3.5.2. Sagittal T1 weighted MR images through the fluid-filled TB in the cat.

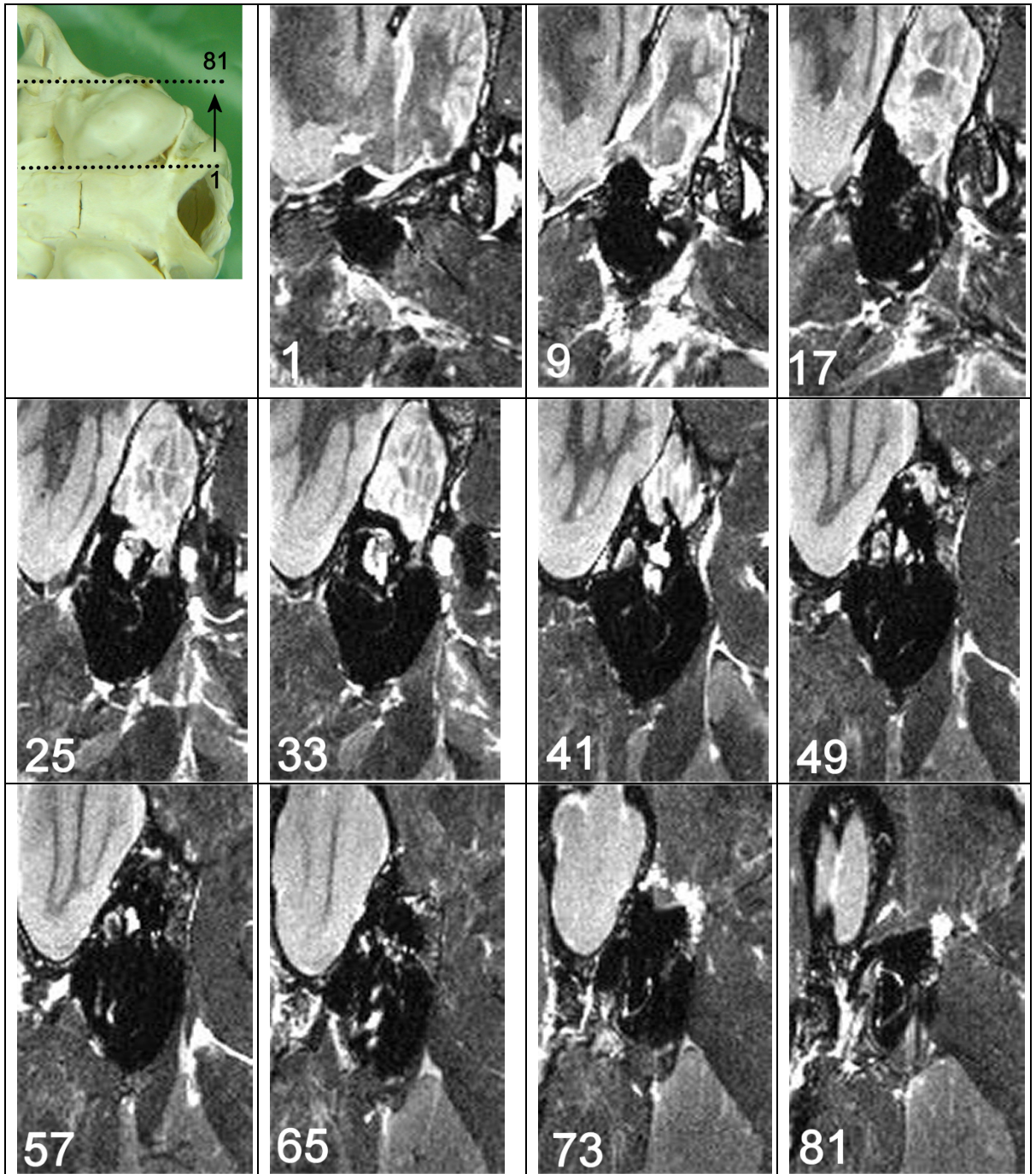


Figure 6.3.5.3. Sagittal T2 weighted MR images through the gas-filled TB in the cat. Some image distortion has resulted from an intermittent fault within the resonator.

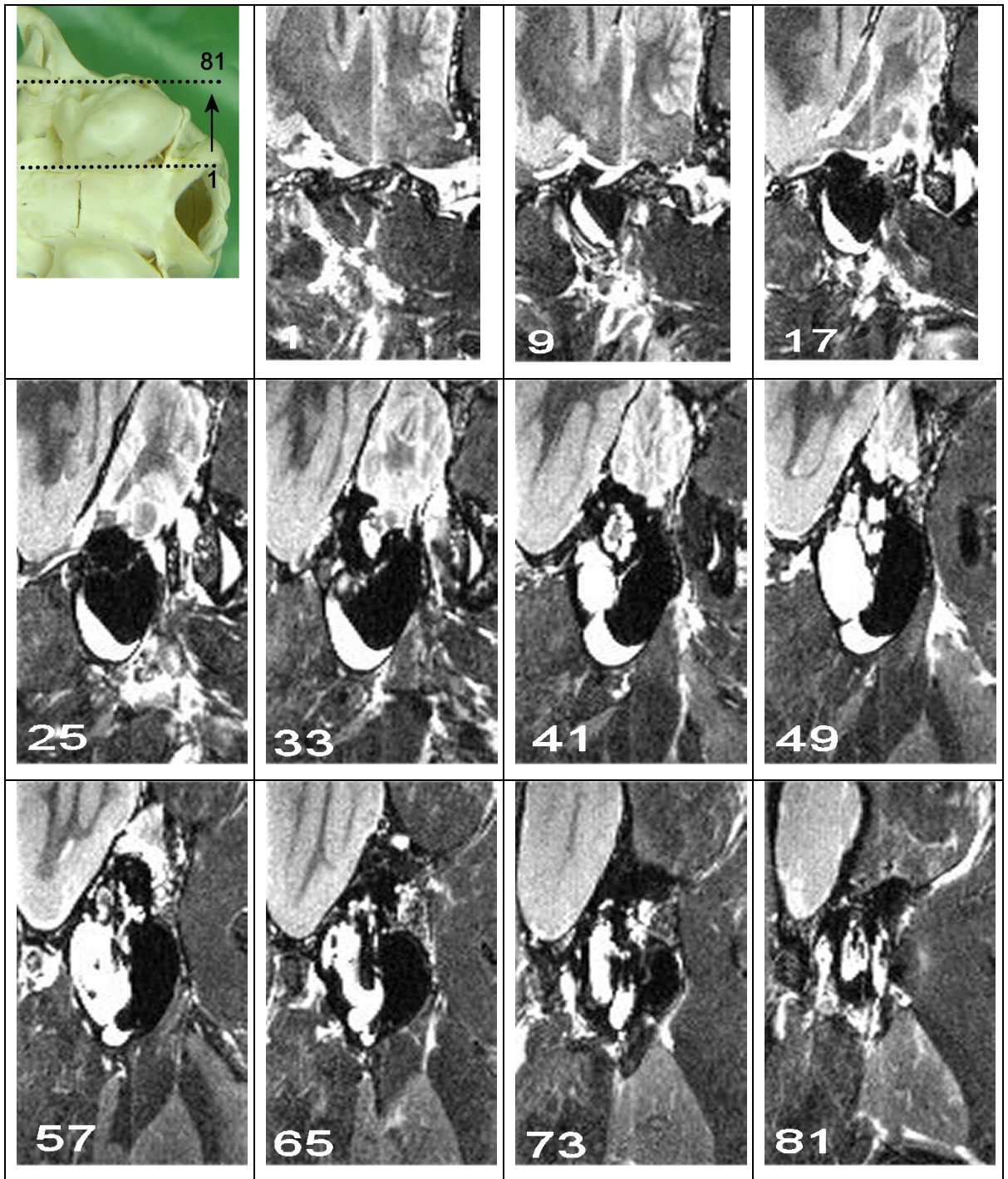


Figure 6.3.5.4. Sagittal T2 weighted MR images through the fluid gas-filled TB in the cat.

Figure 6.3.6. Sagittal MR images through the TB in the rabbit progressing from midline towards left. Dorsal is to top and rostral is to the left in all images. Approximate location of the first and last slice is indicated on the pilot image. For key see Table 6.1.

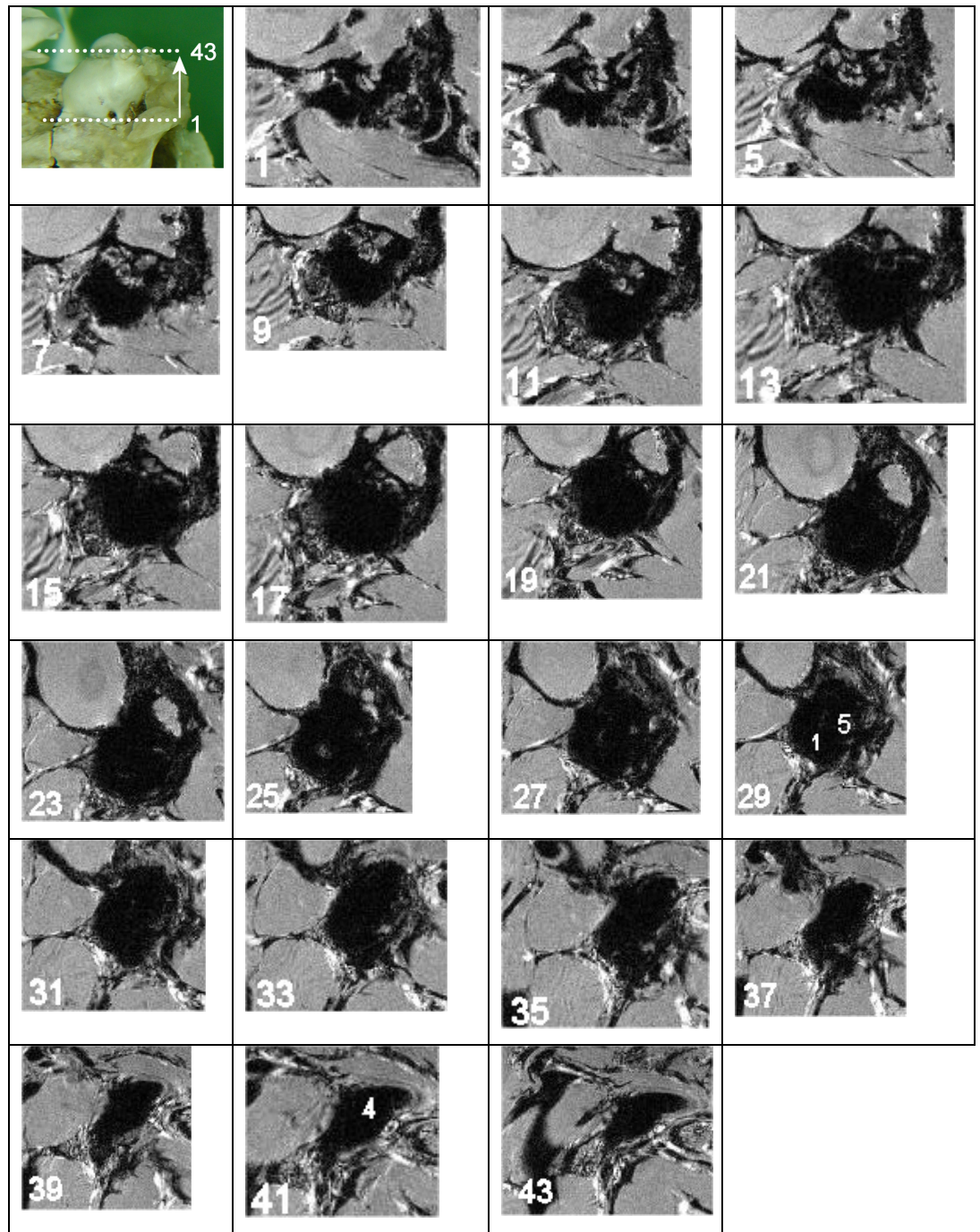


Figure 6.3.6.1. Sagittal T1 weighted MR images through the gas-filled TB in the rabbit.

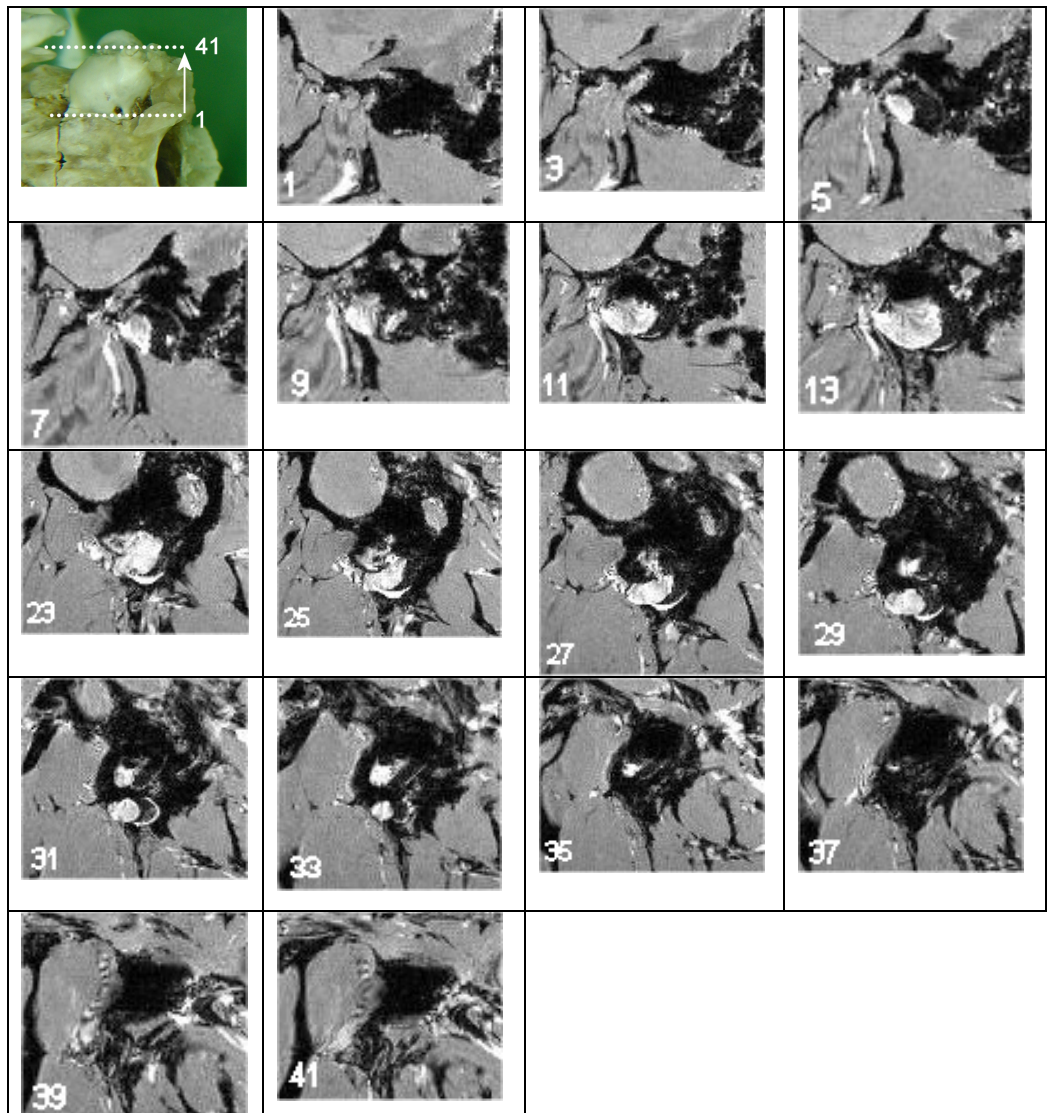


Figure 6.3.6.2. Sagittal T1 weighted MR images through the fluid-filled TB in the rabbit.

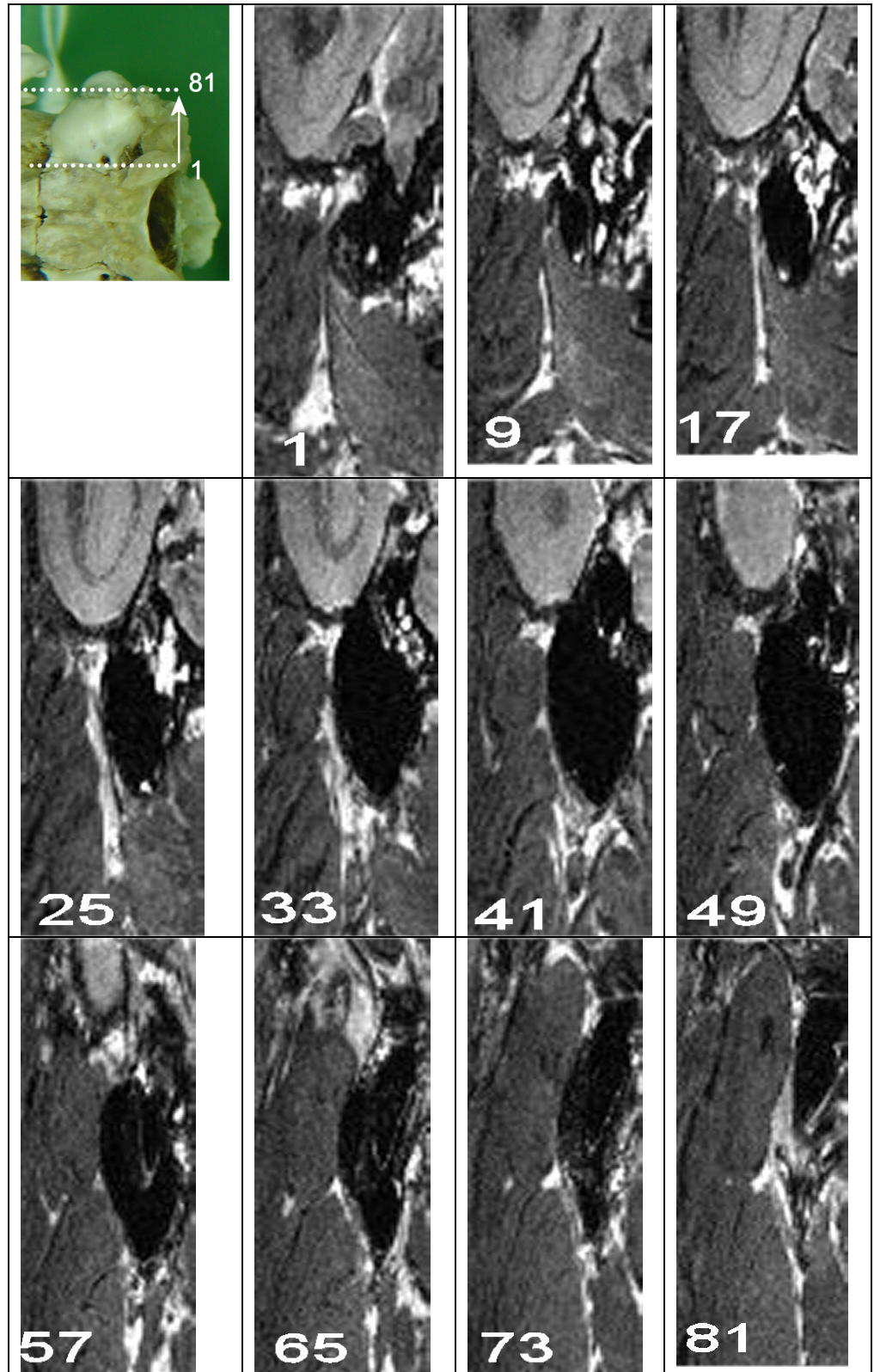


Figure 6.3.6.3. Sagittal T2 weighted MR images through the gas-filled TB in the rabbit. Some image distortion has resulted from an intermittent fault within the resonator.

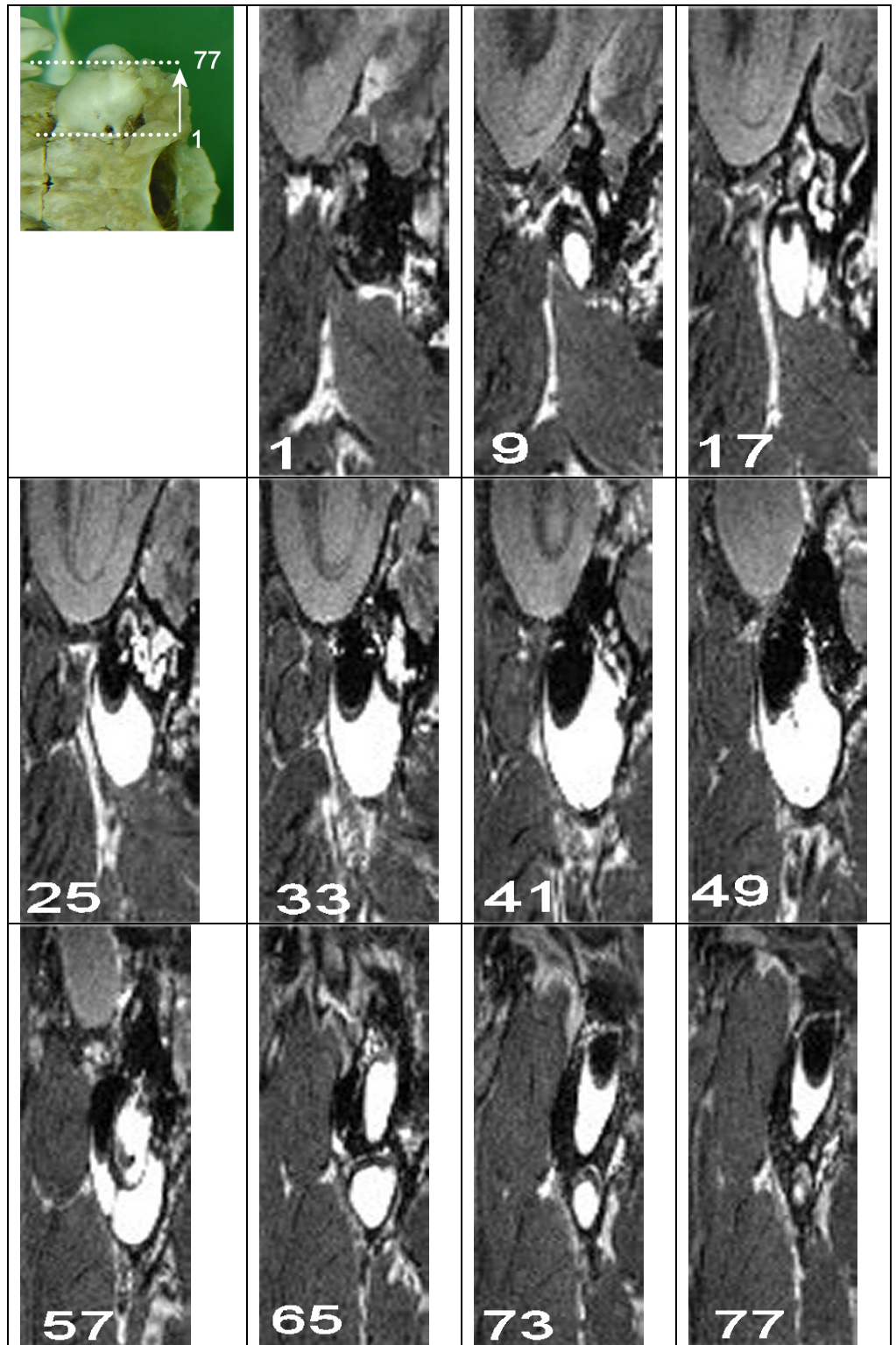


Figure 6.3.6.4. Sagittal T2 weighted MR images through the fluid-filled TB in the rabbit. Some image distortion has resulted from an intermittent fault within the resonator.

Figure 6.3.7. Dorsal MR images through the TB in the dog progressing from dorsal to ventral. The right TB contains ultrasound gel. Rostral is to the top and left is to the right in all images. Number in bottom left corner indicates slice number. Approximate location of the first and last slice is indicated on the pilot image. For key see Table 6.1.

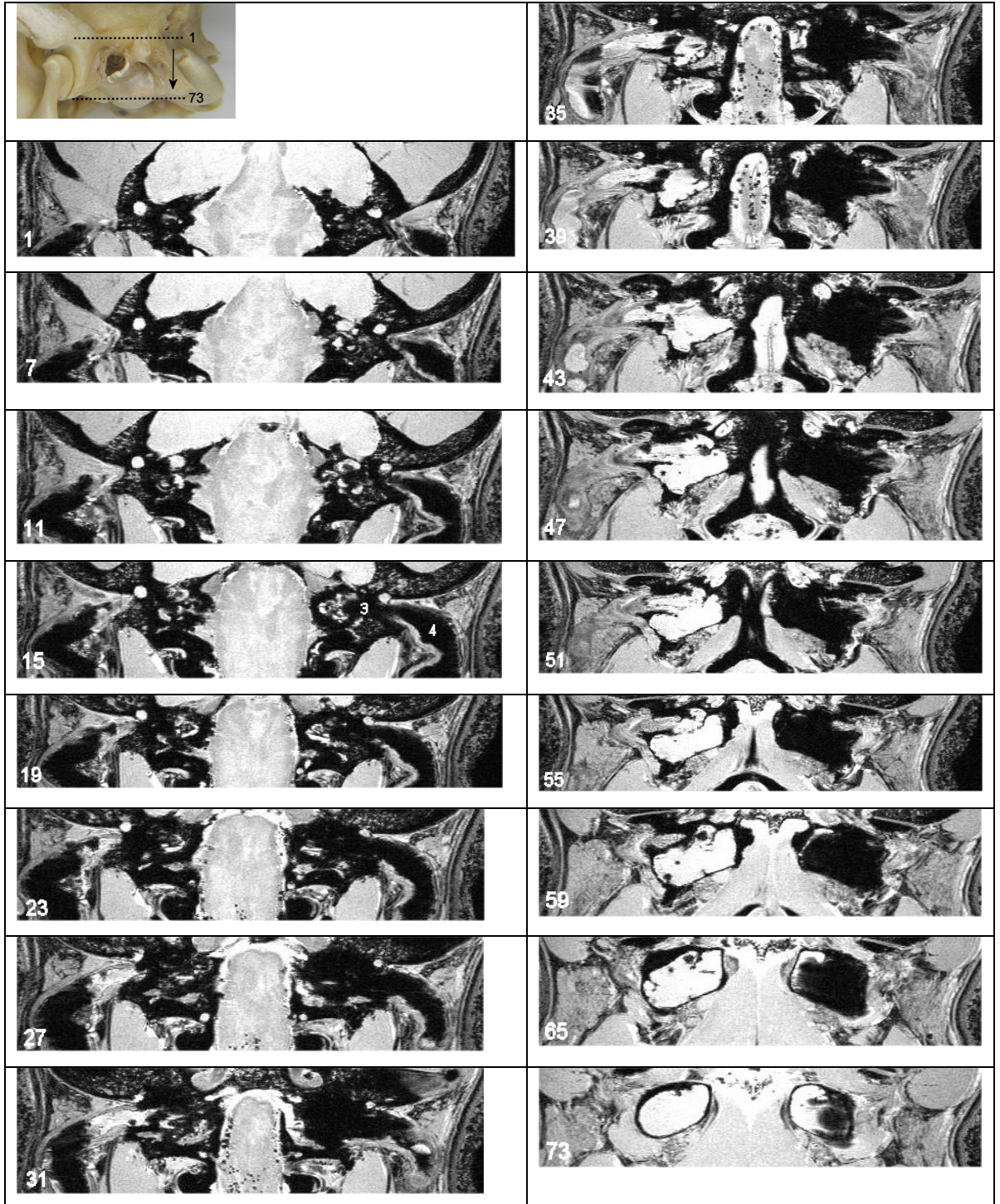


Figure 6.3.7.1. Dorsal T1 weighted MR images through the gas and fluid-filled TB in the dog.

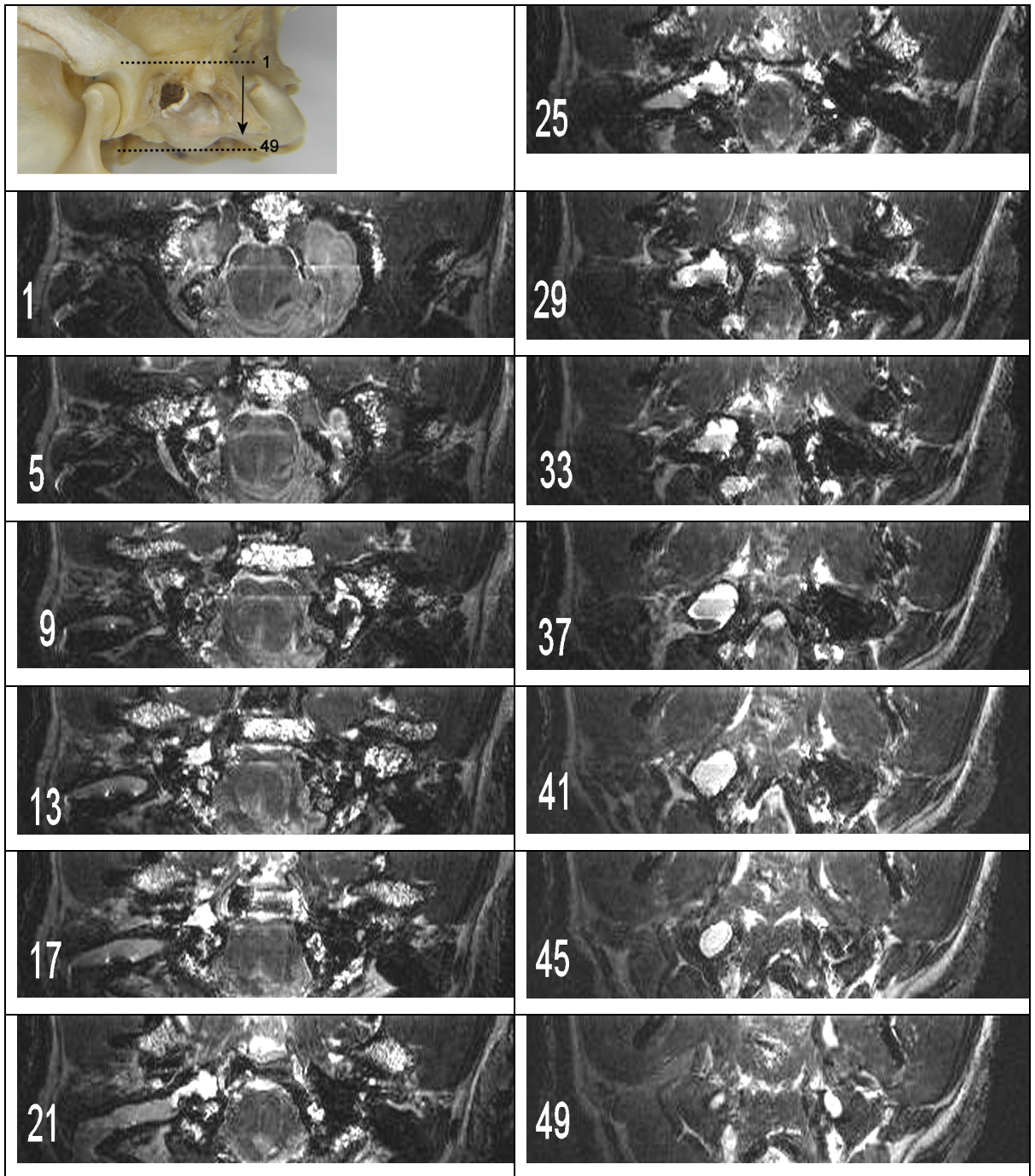


Figure 6.3.7.2. Dorsal T2 weighted MR images through the gas and fluid-filled TB in the dog.

Figure 6.3.8. Dorsal MR images through the TB in the cat progressing from dorsal to ventral. The right TB contains ultrasound gel. Rostral is to the top and left is to the right in all images. Number in bottom left corner indicates slice number. Approximate location of the first and last slice is indicated on the pilot image. For key see Table 6.1.

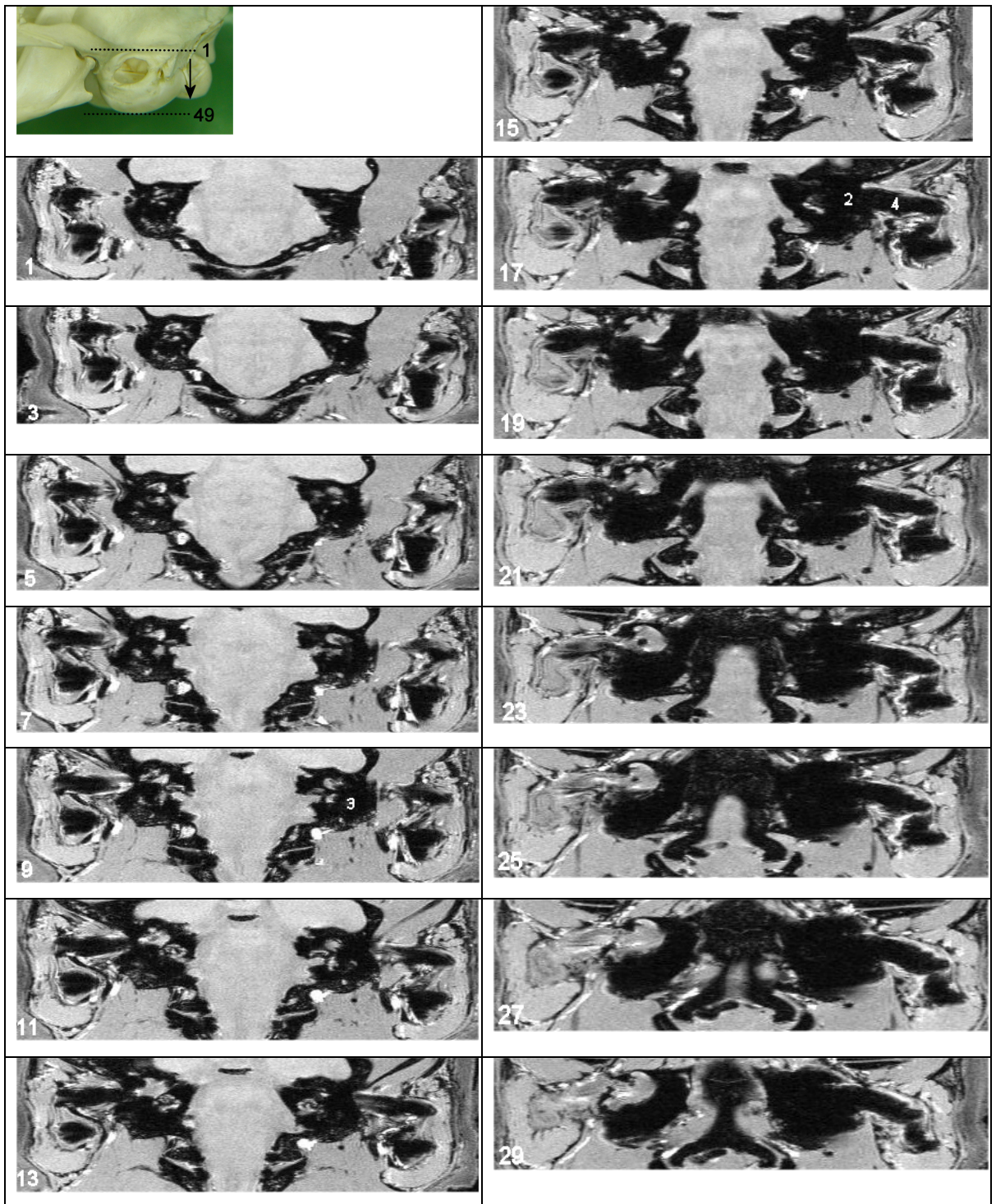
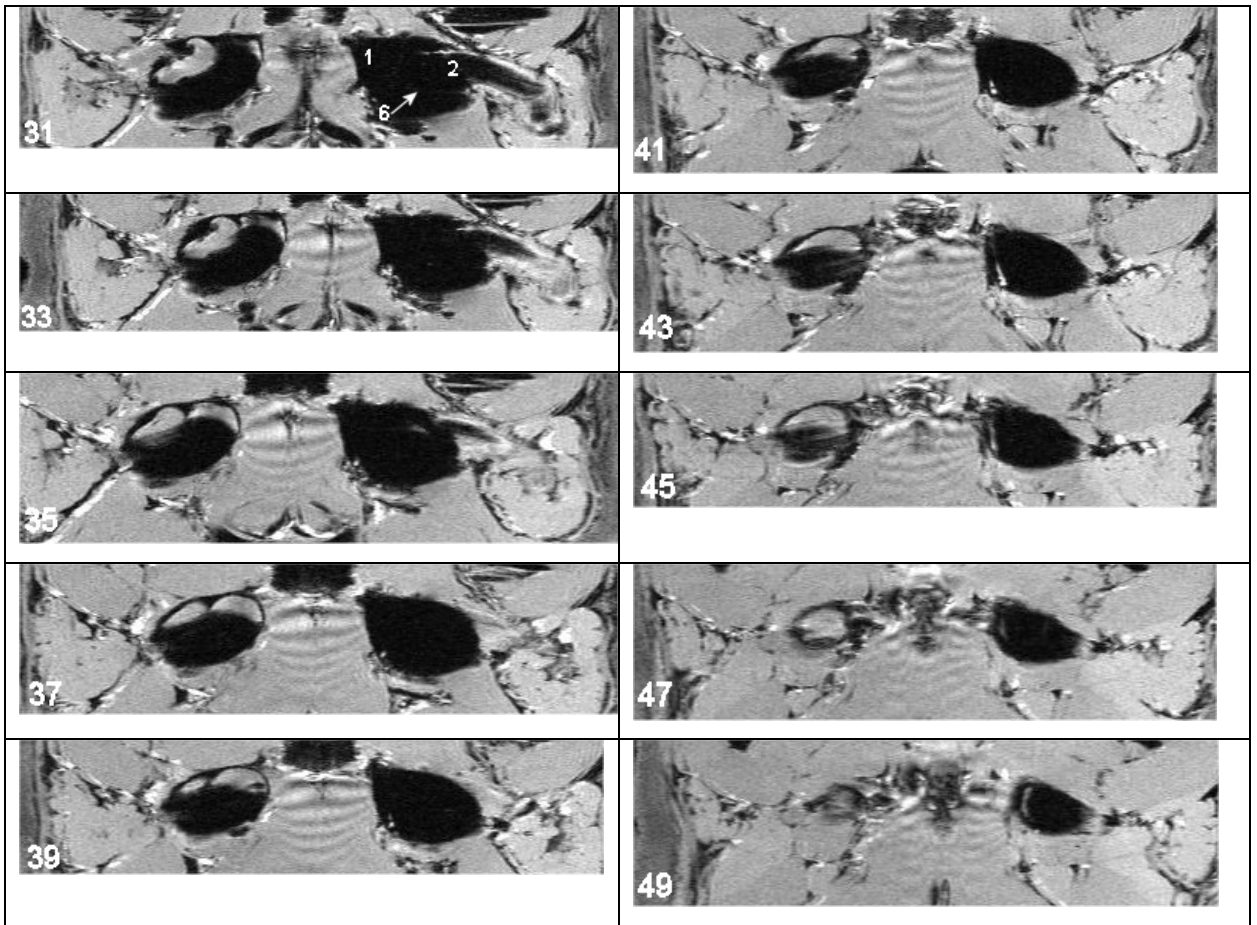


Figure 6.3.8.1. Dorsal T1 weighted MR images through the gas and fluid-filled TB in the cat.

Figure 6.3.8.1. continued. Dorsal T1 weighted MR images through the gas and fluid-filled TB in the cat.



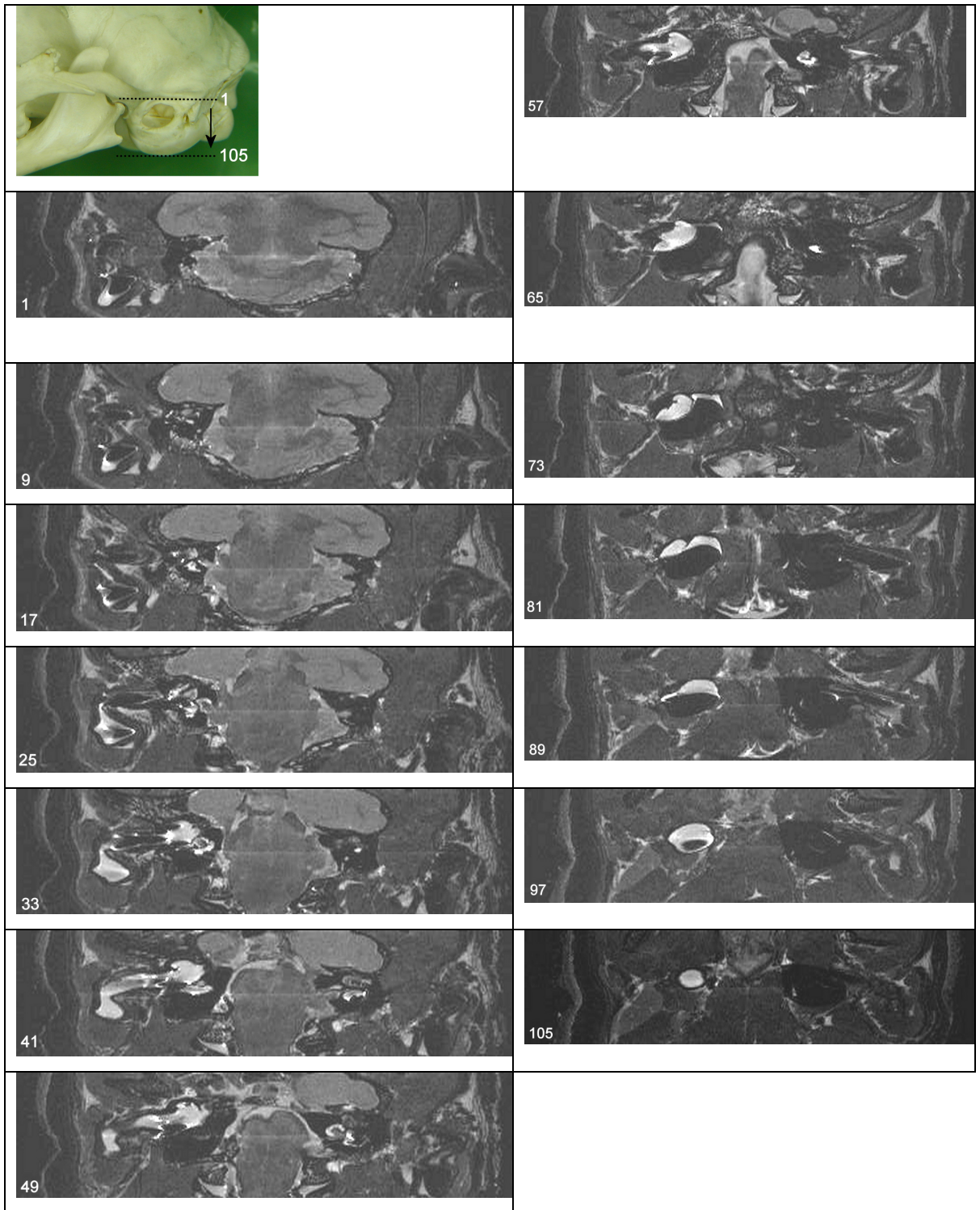


Figure 6.3.8.2. Dorsal T2 weighted MR images through the gas and fluid-filled TB in the cat.

Figure 6.3.9. Dorsal MR images through the TB in the rabbit progressing from dorsal to ventral. The right TB contains ultrasound gel. Rostral is to the top and left is to the right in all images. Number in bottom left corner indicates slice number. Approximate location of the first and last slice is indicated on the pilot image. For key see Table 6.1.

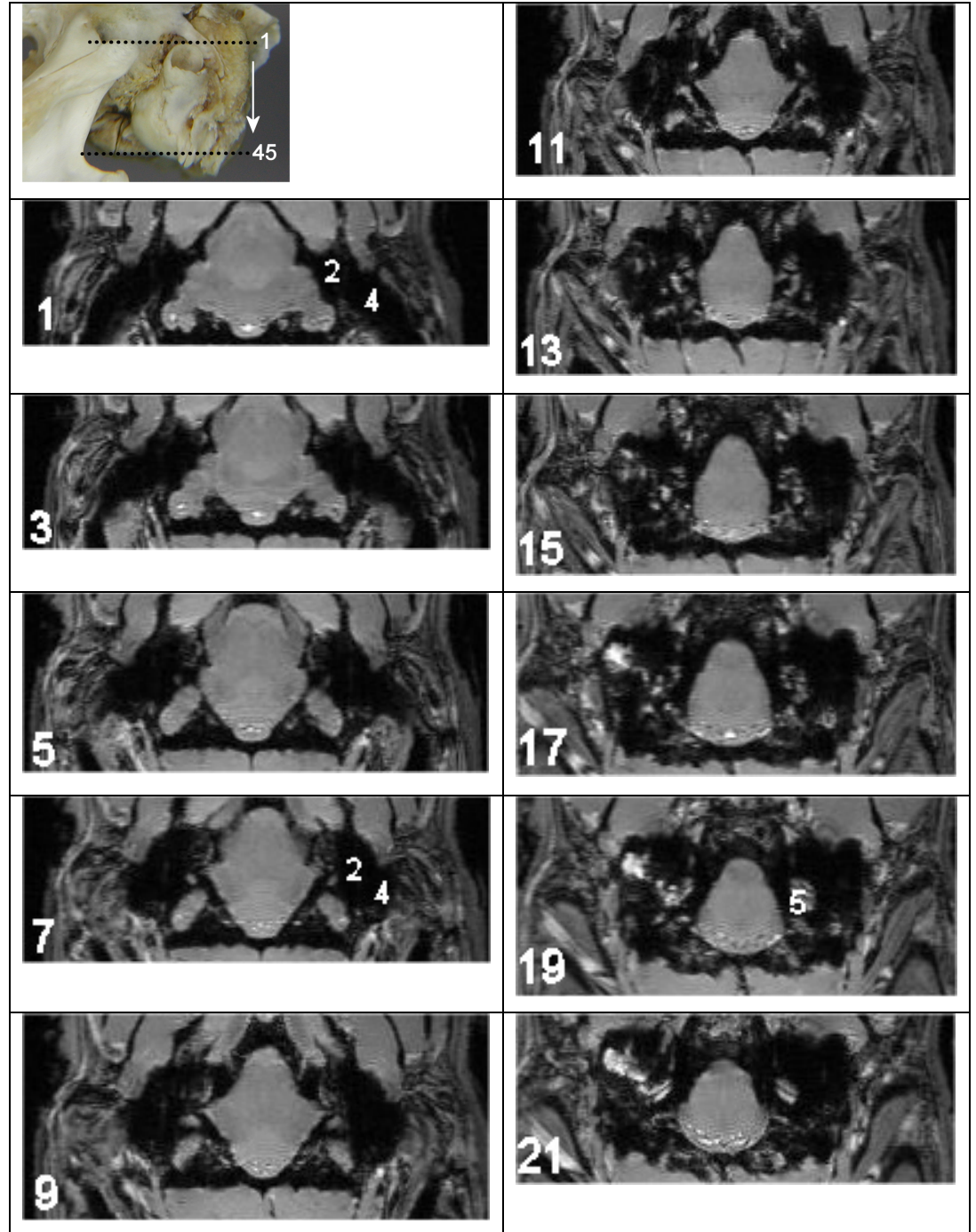
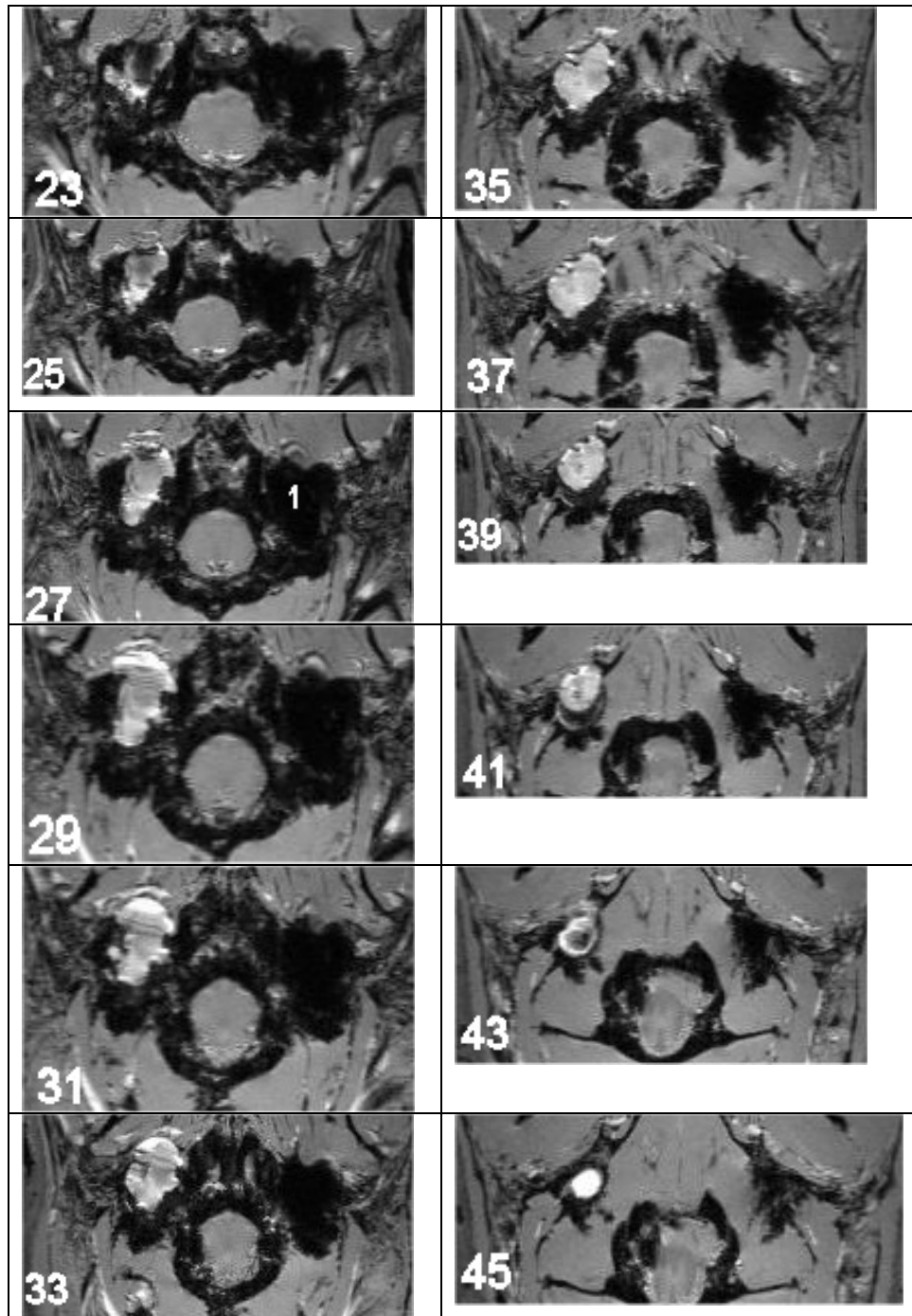


Figure 6.3.9.1. Dorsal T1 weighted MR images through the gas and fluid-filled TB in the rabbit.

Figure 6.3.9.1. continued. Dorsal T1 weighted MR images through the gas and fluid-filled TB in the rabbit.



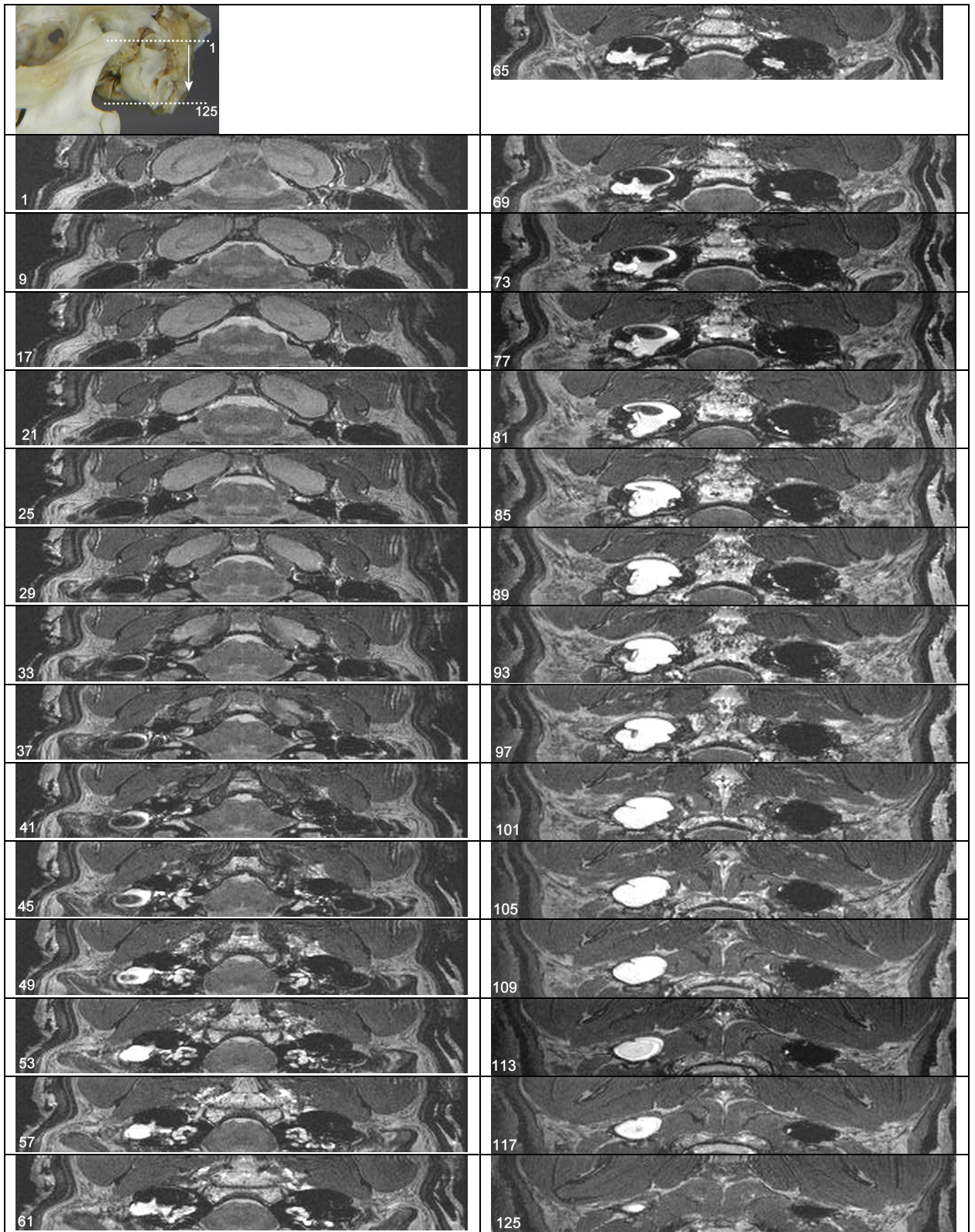


Figure 6.3.9.2. Dorsal T2 weighted MR images through the gas and fluid-filled TB in the rabbit. Some image distortion has resulted from an intermittent fault within the resonator.

6.3.3. MRI appearance of the closed and open TMJ in the dog, cat and rabbit

The transverse MR images obtained of the closed TMJ in the dog, cat and rabbit are demonstrated in Figures 6.3.10 to 6.3.12., the sagittal images in Figures 6.3.13 to 6.3.15 and the dorsal images in Figures 6.3.16. to 6.3.18. with the key in Table 6.2. Where the number of images in a sequence is large, intermittent or representative slices have been presented as indicated by incremental jumps in the slice sequence numbers on the images. The images of the open TMJ did not add any information to that already ascertained in Chapter 5 and therefore have not been presented.

The bony components of the TMJ were well delineated in the T1 weighted images due to the contrast between the signal void of the cortical bone and the adjacent soft tissue structures. The central cancellous regions of the zygomatic arch and condyloid process were also clearly visible as speckled regions of hyperintense signal interspersed with the signal void associated with mineralised material.

In the transverse sections, the dorsal articular surface of the condyloid process and the corresponding surface of the mandibular fossa were outlined in both the dog and cat. In the rostral sections, the shape of the canine condyloid process resulted in the presence of a prominent defect due to the medial half and lateral extremities being located in the slice but the rest of the lateral half being outwith it. This was present to a lesser degree in the cat where the majority of the lateral half of the condyloid process was absent from the rostral sections. In the caudal sections, the pit at the medial aspect of the retroarticular process was prominent in the dog and less so in the cat. Likewise, the retroarticular foramen carrying the retroarticular vein produced a prominent defect in the zygomatic arch in the dog but was not visible in the cat.

The margins of the joint space were well demarcated on the T1 weighted images in the dog and the lateral ligament could be identified. The medial attachments of the joint capsule to the mandibular fossa and the pit at the medial aspect of the retroarticular process were also visible. Immediately adjacent to the mandibular fossa and condyloid process were layers that were isointense with the surrounding soft tissue. Between these was a slightly hypointense layer that was present throughout the extent of the joint space. Rostrally, there appeared to be another isointense layer within the hypointense one producing a striated appearance. It was not clear which of these layer represented the articular cartilage, the synovial fluid and the intra-articular disc. In the cat, the TMJ space was very narrow and

uniformly isointense. The lateral attachments of the joint were not clearly defined but the medial ones were visible.

In the rabbit, a similar striated appearance to the dog was present within the joint space immediately caudal to the level of the mandibular fossa and again, it was not clear which of these layers represented the articular cartilage, the synovial fluid and the intra-articular disc.

In the sagittal T1 weighted images in the dog and cat, the dorsal and caudal articular surfaces of the condyloid process were visible along with the corresponding surfaces of the mandibular fossa and retroarticular process. The rostral and ventral extent of the joint capsule were clearly visible as were its lateral and medial attachments. The middle of the joint space appeared as a uniformly isointense area but medially and laterally individual layers were again visible. In the cat the joint was very narrow with the mandibular fossa closely conforming to the contour of the condyloid process and the space appeared uniformly isointense throughout. In the rabbit, the relationship between the condyloid process and mandibular fossa was clearly visible in these sections, with the former located slightly caudal and ventral to the latter, and a relatively small region of association between the articular surfaces. There was an isointense line running the length of the dorsal aspect of the condyloid process but the corresponding line associated with the mandibular fossa appeared to meet with it half-way along the length of the process. Rostral to this was a triangular, striated region, but it was not clear whether this represented the disc or an amalgamation of it and the intra-articular fluid.

In the dorsal images, the only articular surfaces clearly visible in the dog and cat were the medial aspect of the caudal surface of the condyloid process and the corresponding surface of the retroarticular process. The extent of the joint capsule in the dog was visible as a halo around the condyloid process and again, this took the form of two isointense layers with a central hypointense one. The medial and lateral attachments of the capsule were not evident in these views. The joint in the cat was very narrow and the space appeared uniformly isointense throughout. In the rabbit, the slice immediately dorsal to each condyloid process demonstrated an oval shaped hypointense structure caudal to the mandibular fossa that may have represented the disc.

In the T2 weighted images there was better distinction between the cortical and cancellous bone but poorer visualisation of the joint components, with the exception of the medial attachments that produced a hyperintense appearance in the caudal sections. There was a large amount of distortion evident in the sagittal T2 weighted sequences in the cat and rabbit due to the effects of image reconstruction.

<u>Label</u>	<u>Description</u>
*	Apparent defect in lateral aspect of canine condyloid process
1	Condyloid process
2	Cat and Dog - Angular process Rabbit – vertical ramus of mandible
3	Zygomatic arch
4	Zygomatic process of the temporal bone
5	Caudal extension of the zygomatic arch (rabbit)
6	Retroarticular process
7	Squamous temporal bone
8	Pit at the medial aspect of the retroarticular process
9	Retroarticular foramen
10	Intra-articular disc

Table 6.2. Anatomical features associated with the TMJ. Key for figures 6.3.10 to 6.3.18.

Figure 6.3.10. Transverse MR images through the closed TMJ in the dog progressing from rostral to caudal. Dorsal is to the top and left is to the right in all images. Number in bottom left corner indicates slice number. Approximate location of the first and last slice is indicated on the pilot image, or key see Table 6.2.

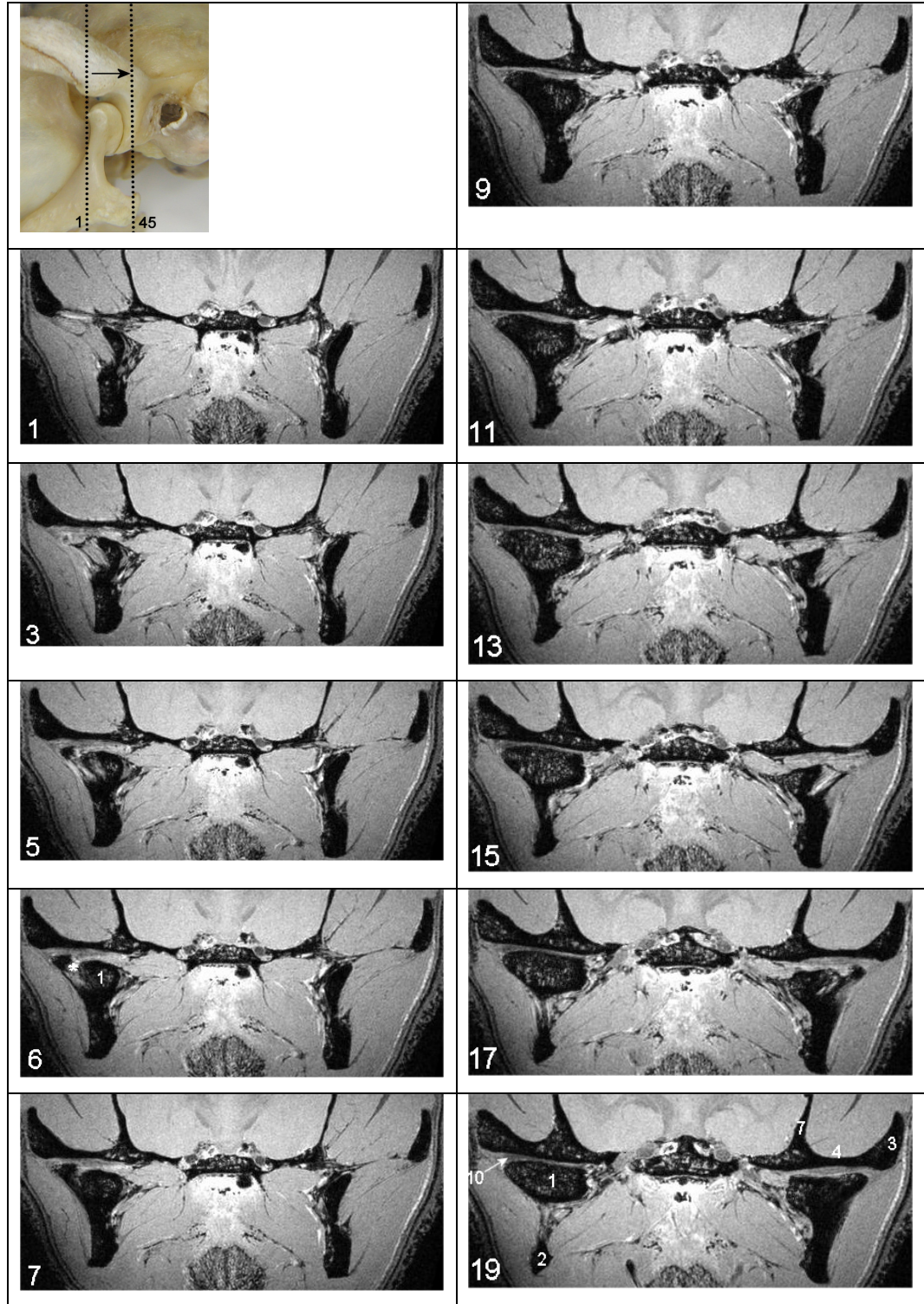
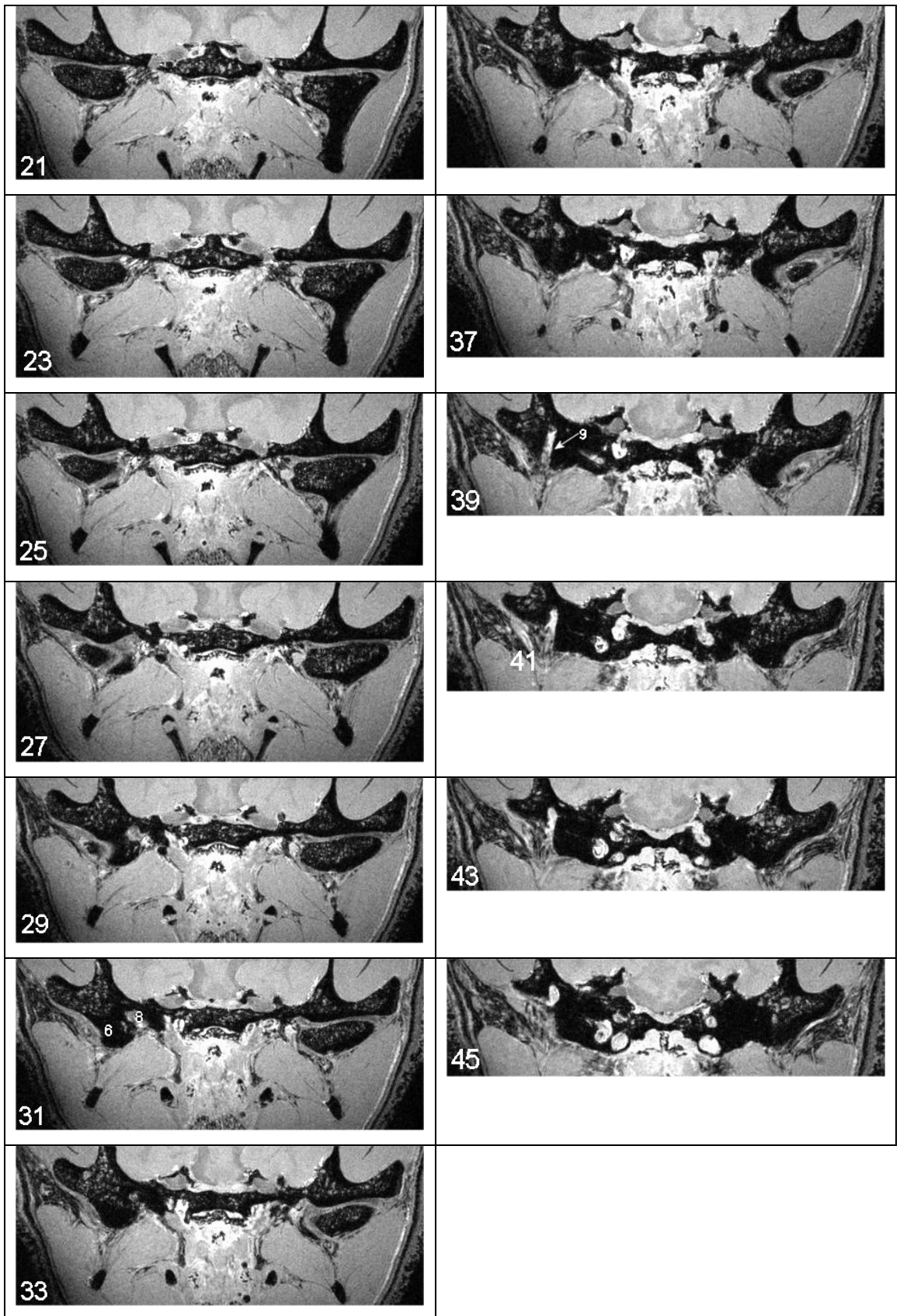


Figure 6.3.10.1. Transverse T1 weighted MR images through the closed TMJ in the dog

Figure 6.3.10.1. continued. Transverse T1 weighted MR images through the closed TMJ in the dog



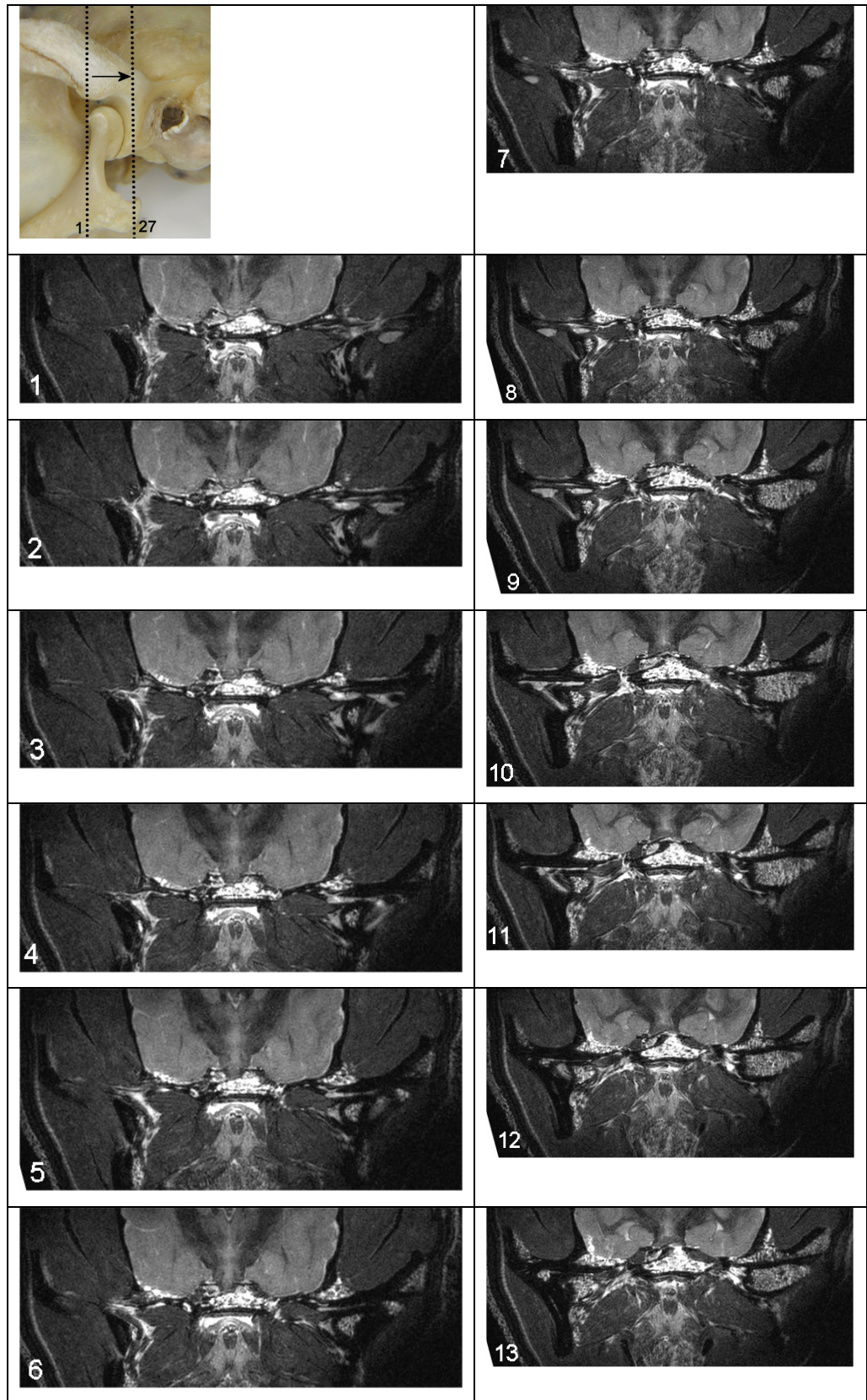


Figure 6.3.10.2. Transverse T2 weighted MR images through the closed TMJ in the dog.

Figure 6.3.10.2. continued. Transverse T2 weighted MR images through the closed TMJ in the dog.

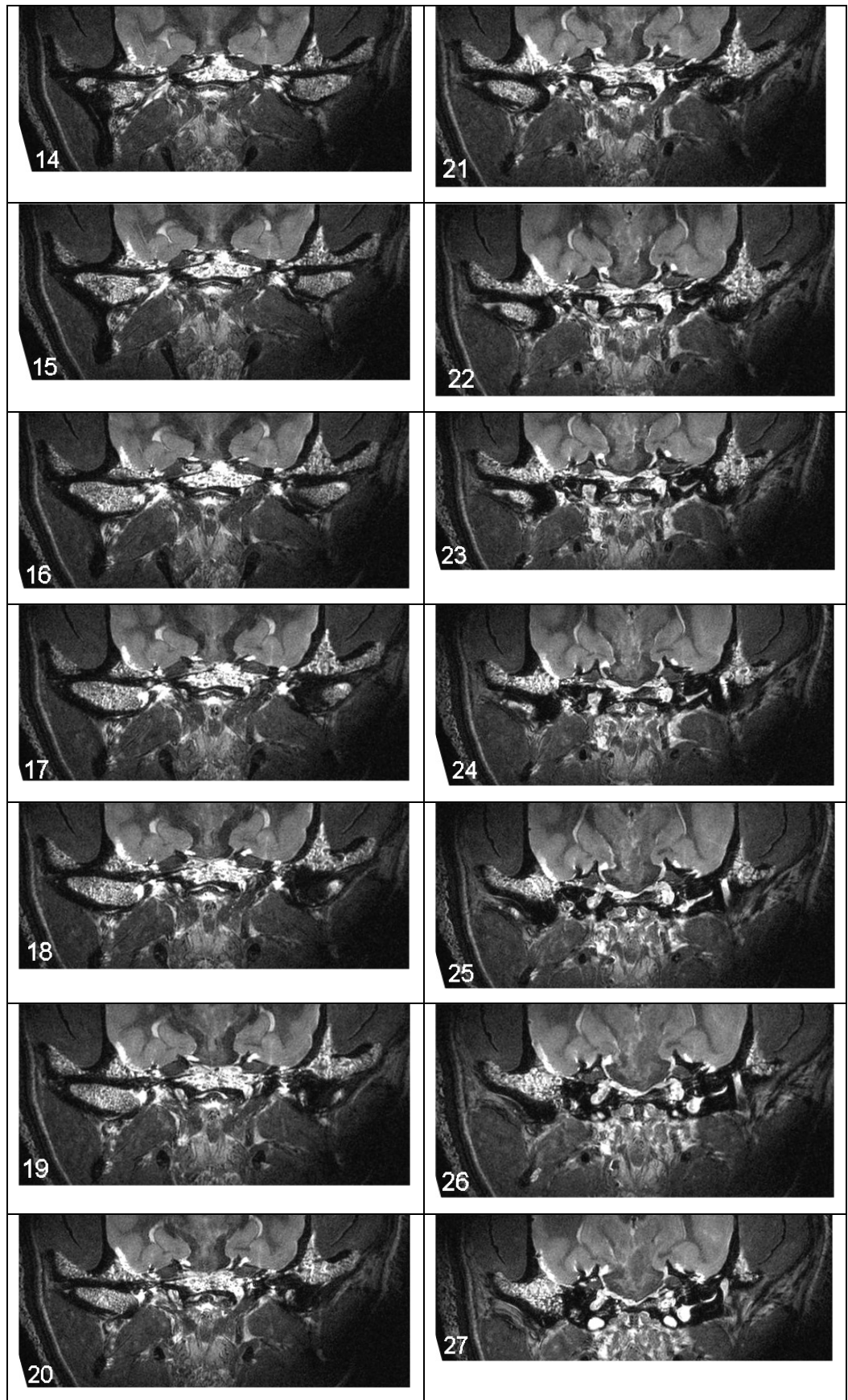


Figure 6.3.11. Transverse MR images through the closed TMJ in the cat progressing from rostral to caudal. Dorsal is to the top and left is to the right in all images. Number in bottom left corner indicates slice number. Approximate location of the first and last slice is indicated on the pilot image. For key see Table 6.2.

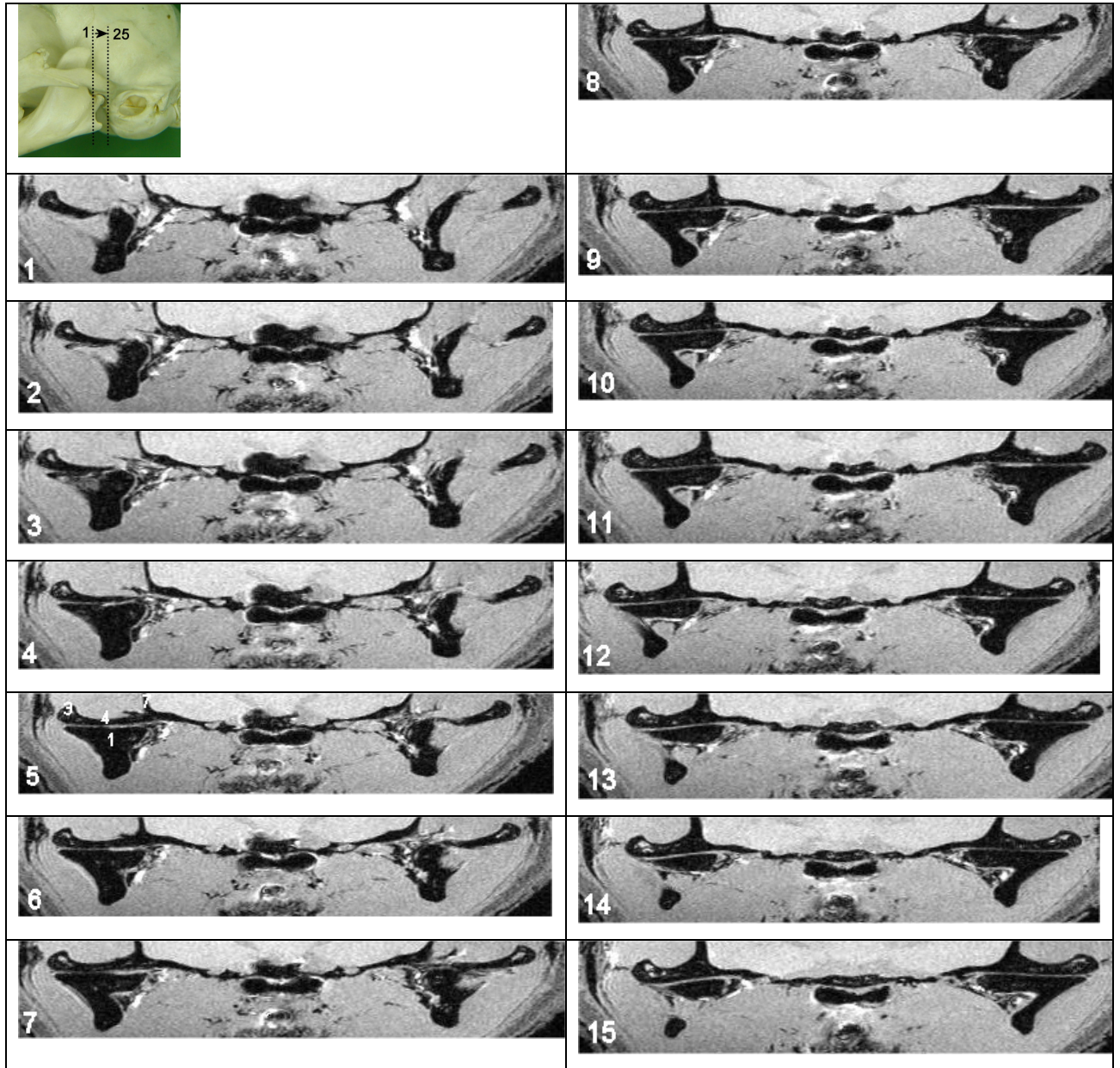
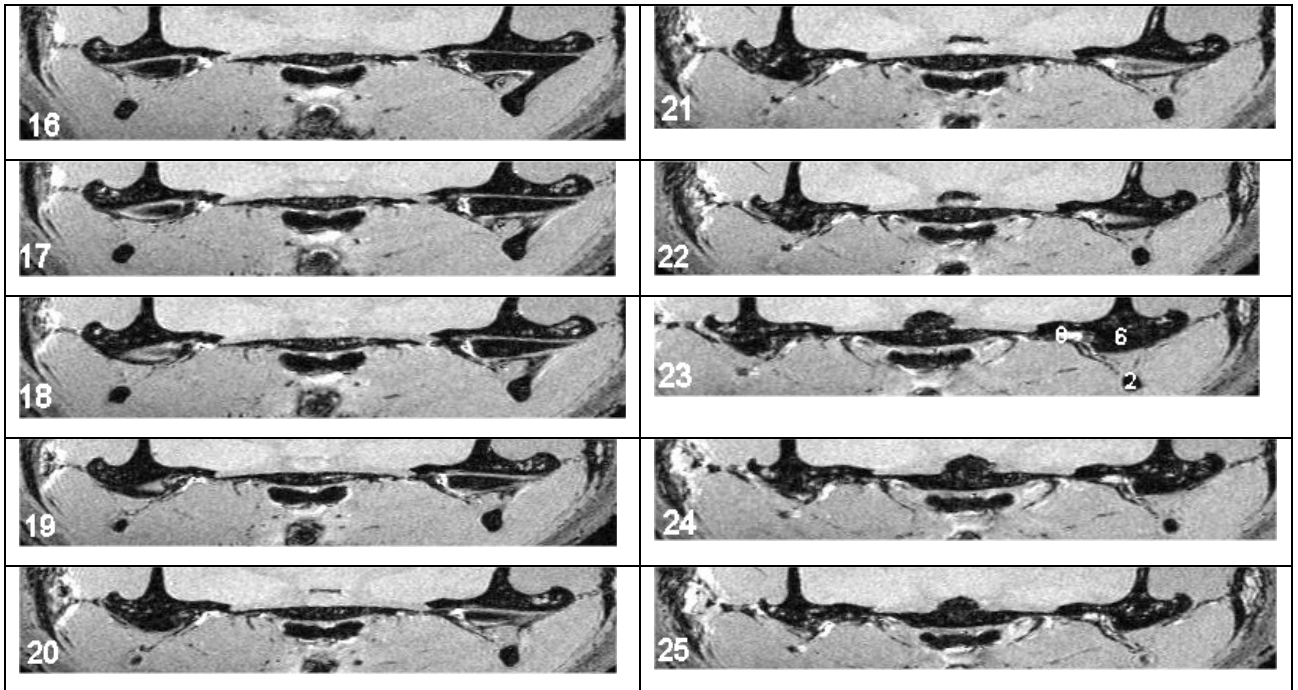


Figure 6.3.11.1. Transverse T1 weighted MR images through the closed TMJ in the cat.

Figure 6.3.11.1. continued. Transverse T1 weighted MR images through the closed TMJ in the cat.



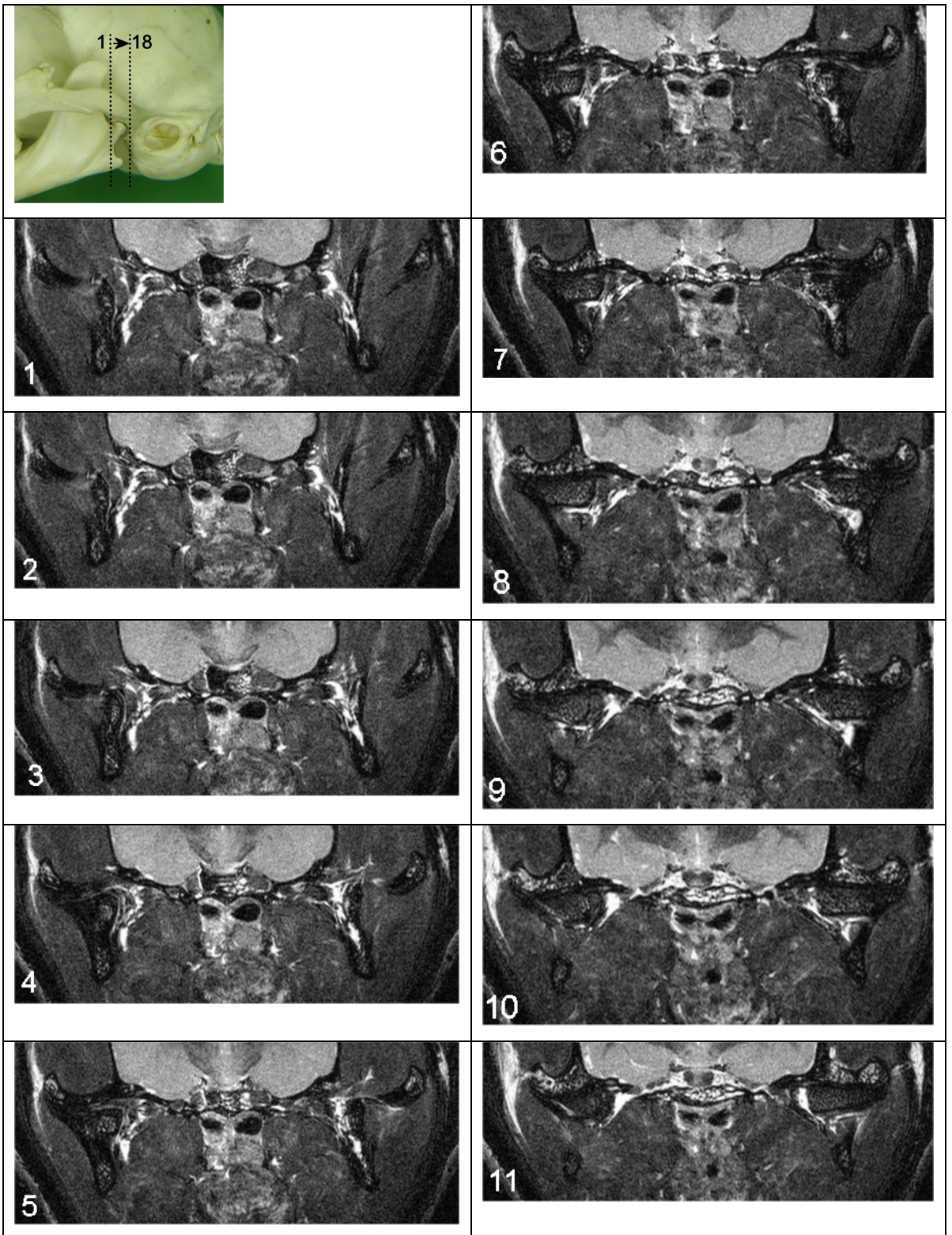


Figure 6.3.11.2. Transverse T2 weighted MR images through the closed TMJ in the cat.

Figure 6.3.11.2. continued. Transverse T2 weighted MR images through the closed TMJ in the cat.

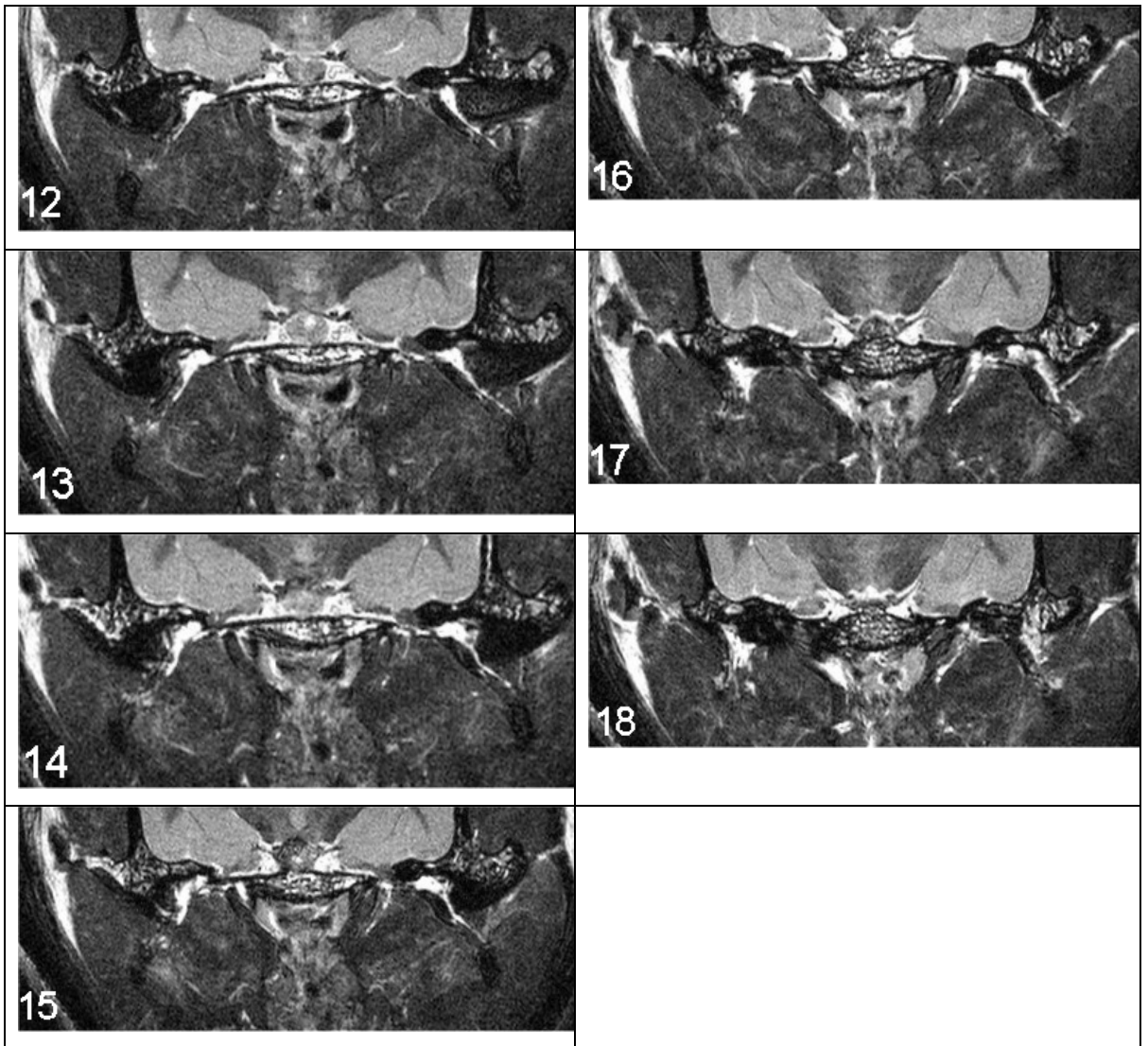


Figure 6.3.12. Transverse MR images through the closed TMJ in the rabbit progressing from rostral to caudal. Dorsal is to the top and left is to the right in all images. Number in bottom left corner indicates slice number. Approximate location of the first and last slice is indicated on the pilot image. For key see Table 6.2.

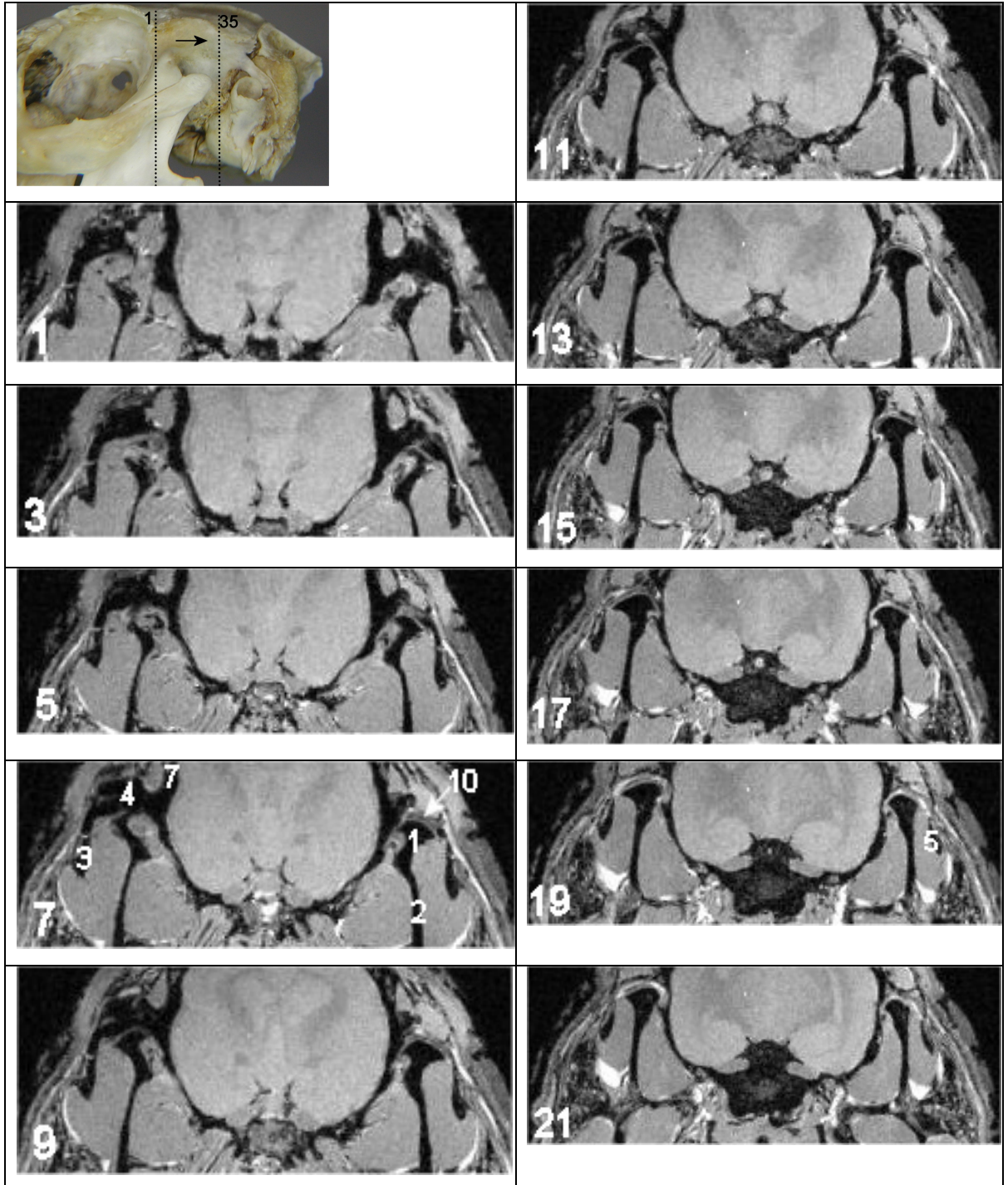
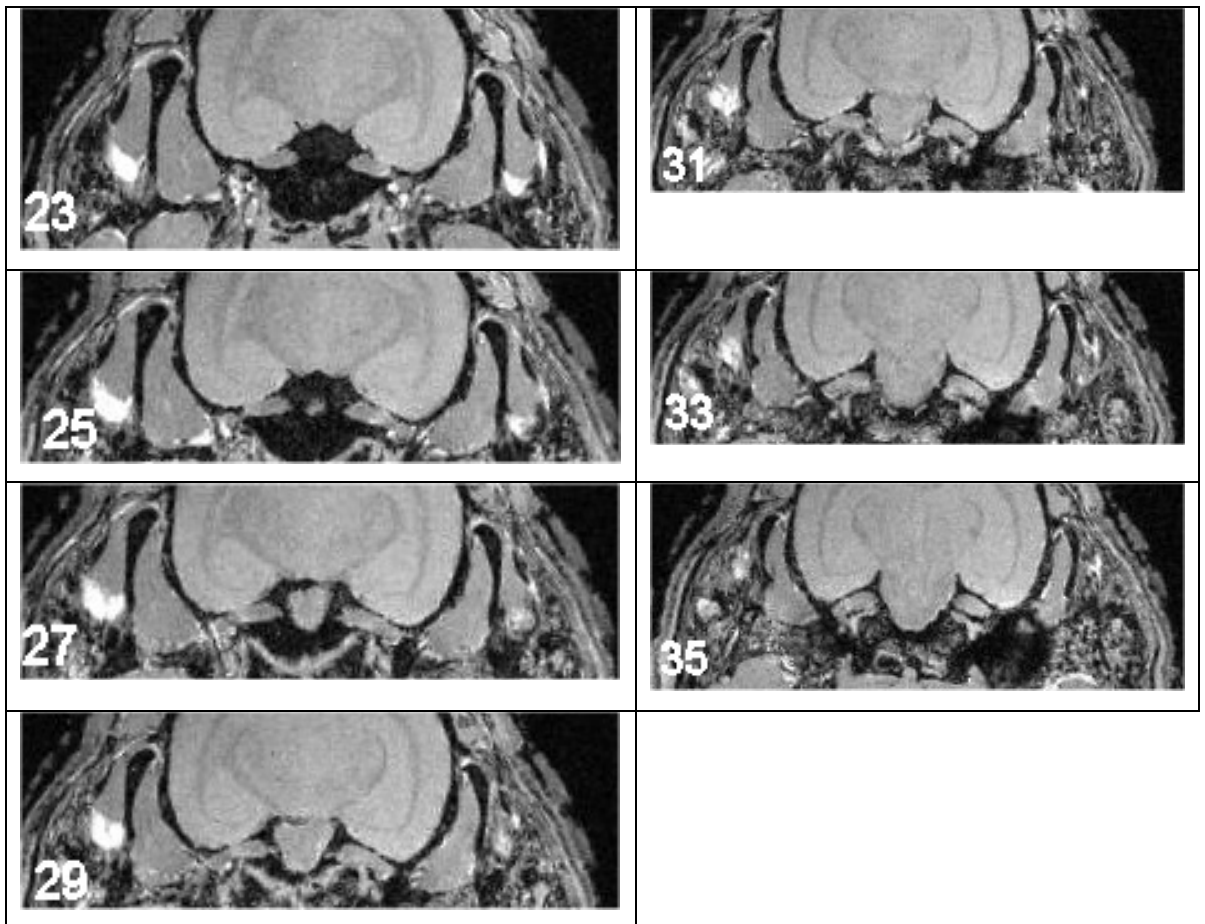


Figure 6.3.12.1. Transverse T1 weighted MR images through the closed TMJ in the rabbit

Figure 6.3.12.1. continued. Transverse T1 weighted MR images through the closed TMJ in the rabbit



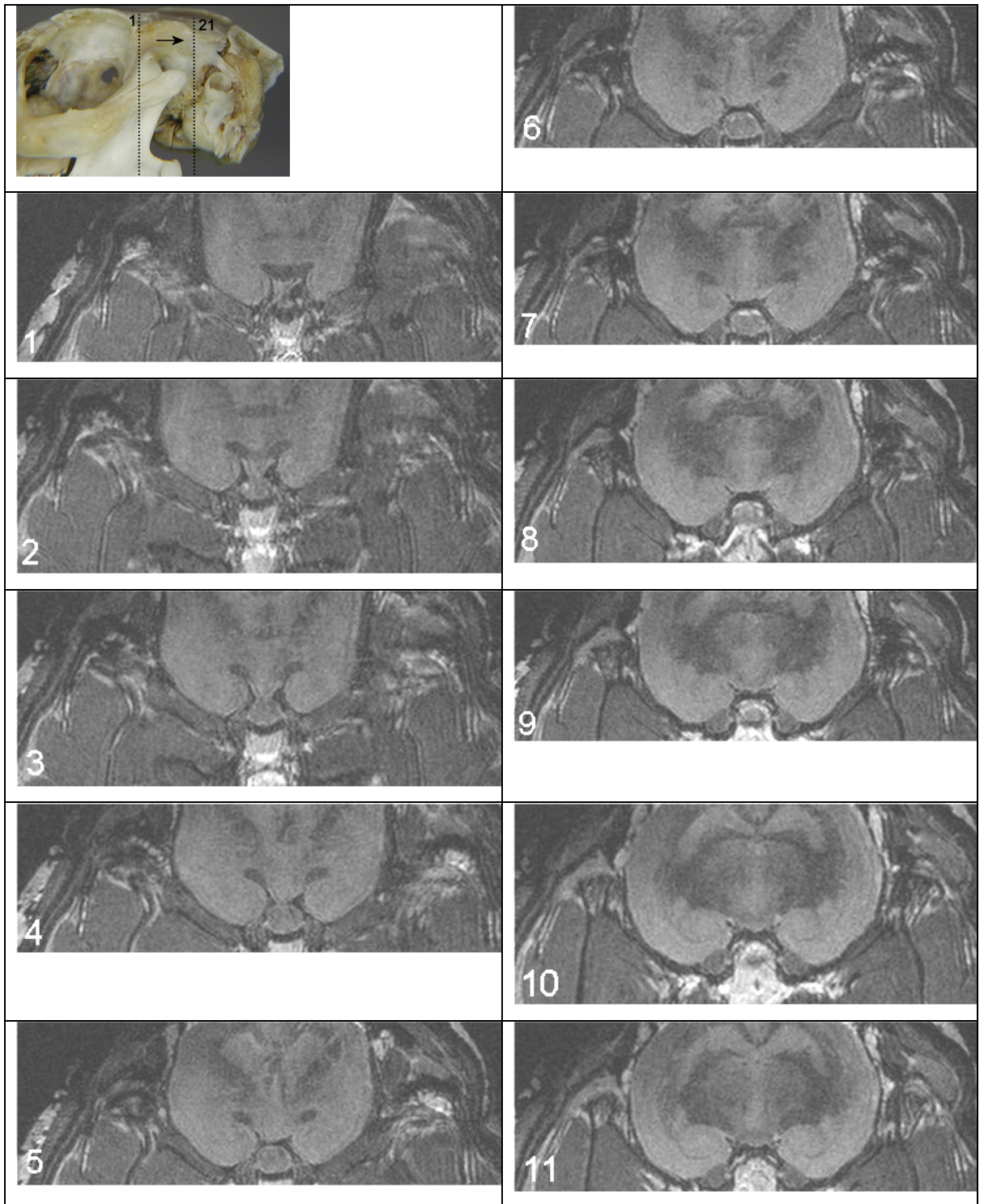


Figure 6.3.12.2. Transverse T2 weighted MR images through the closed TMJ in the rabbit

Figure 6.3.12.2 continued. Transverse T2 weighted MR images through the TMJ in the rabbit

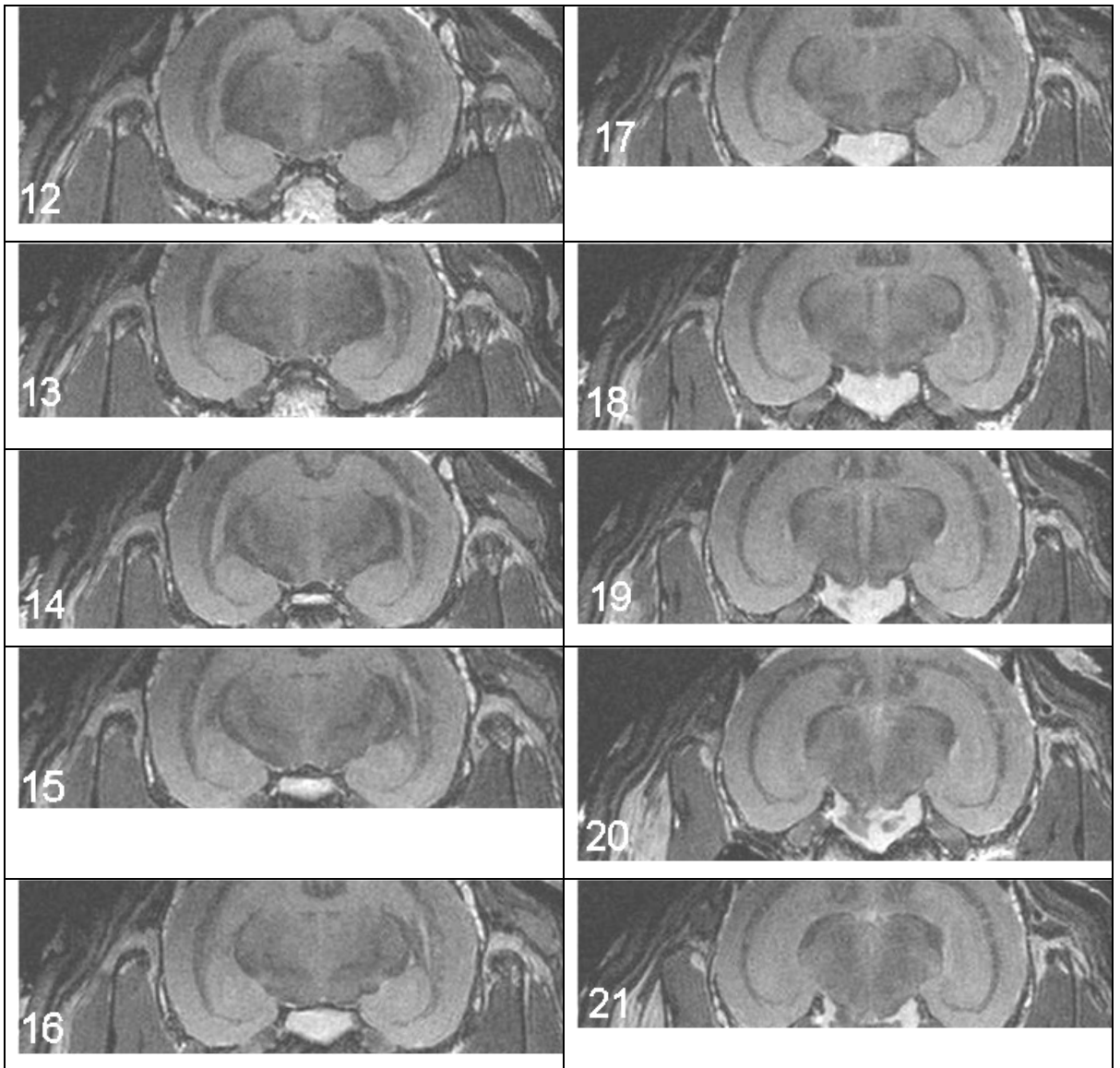


Figure 6.3.13. Sagittal MR images through the closed TMJ in the dog progressing from midline towards left. Dorsal is to top and rostral is to the left in all images. Number in bottom left corner indicates slice number. Approximate location of the first and last slice is indicated on the pilot image. For key see Table 6.2.

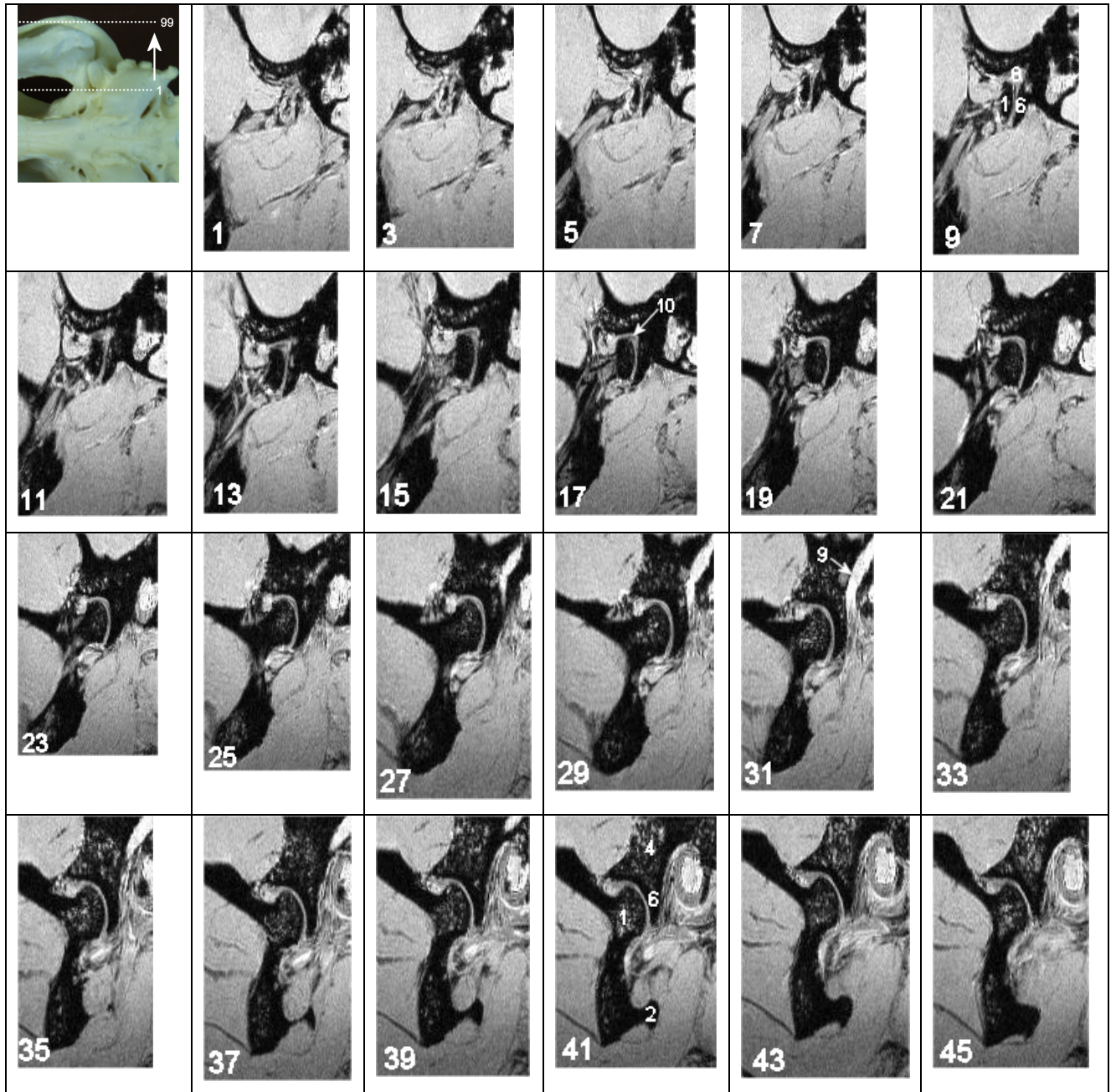
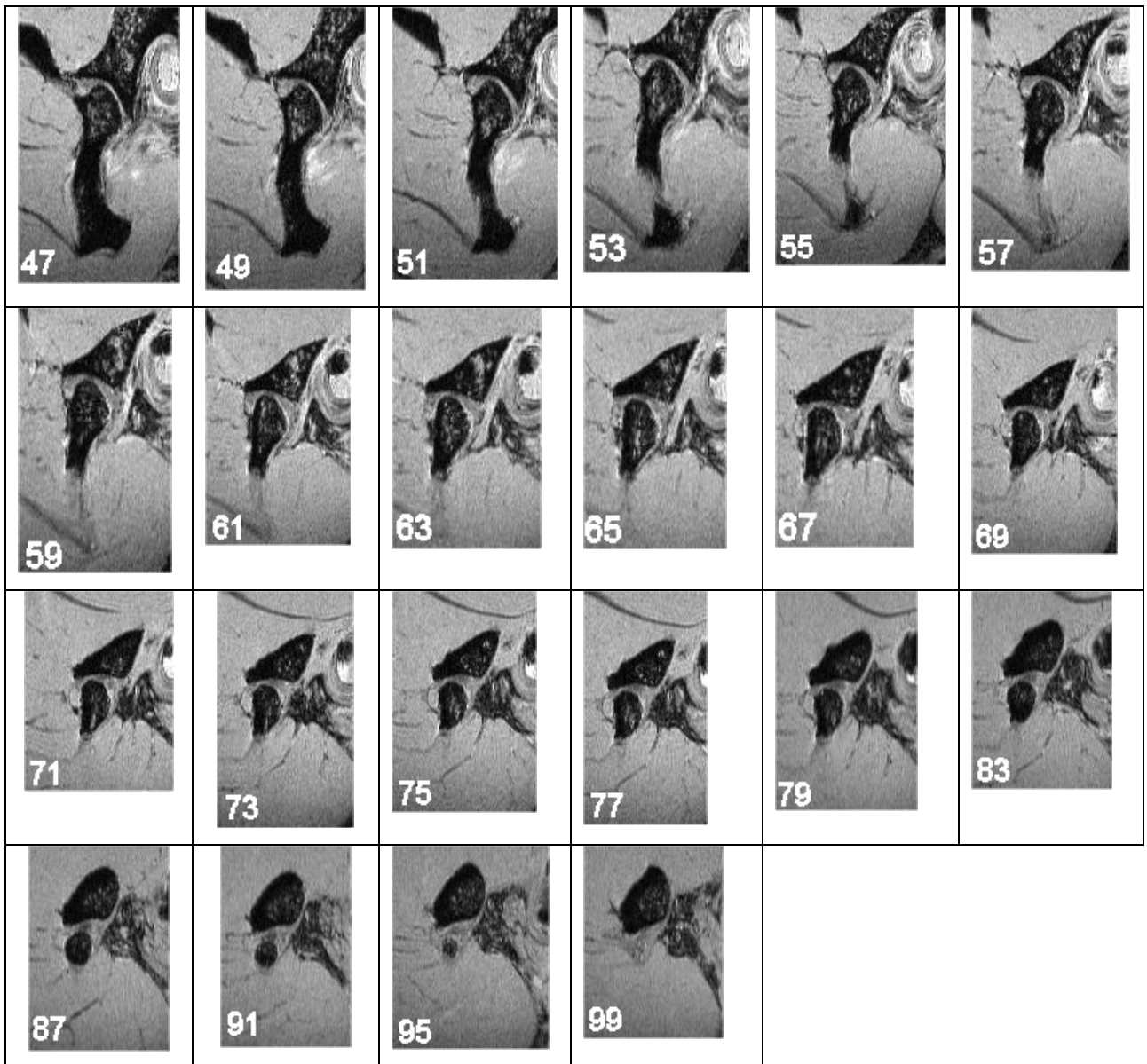


Figure 6.3.13.1. Sagittal T1 weighted MR images through the closed TMJ in the dog.

Figure 6.3.13.1. continued. Sagittal T1 weighted MR images through the closed TMJ in the dog.



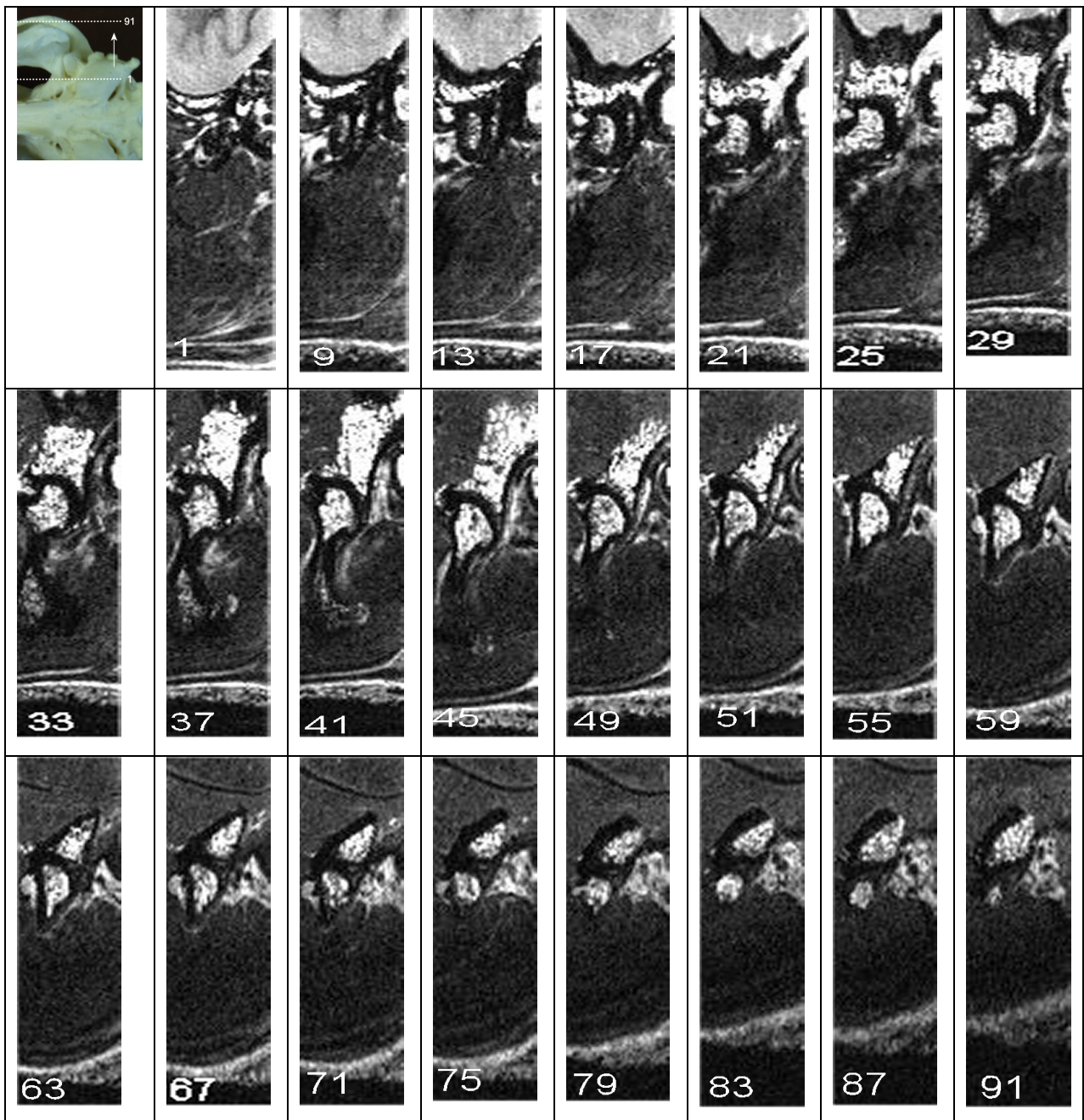


Figure 6.3.13.2. Sagittal T2 weighted MR images through the closed TMJ in the dog. Some image distortion has resulted from an intermittent fault within the resonator.

Figure 6.3.14. Sagittal MR images through the TMJ in the cat progressing from midline towards left. Dorsal is to top and rostral is to the left in all images. Number in bottom left corner indicates slice number. Approximate location of the first and last slice is indicated on the pilot image. For key see Table 6.2.

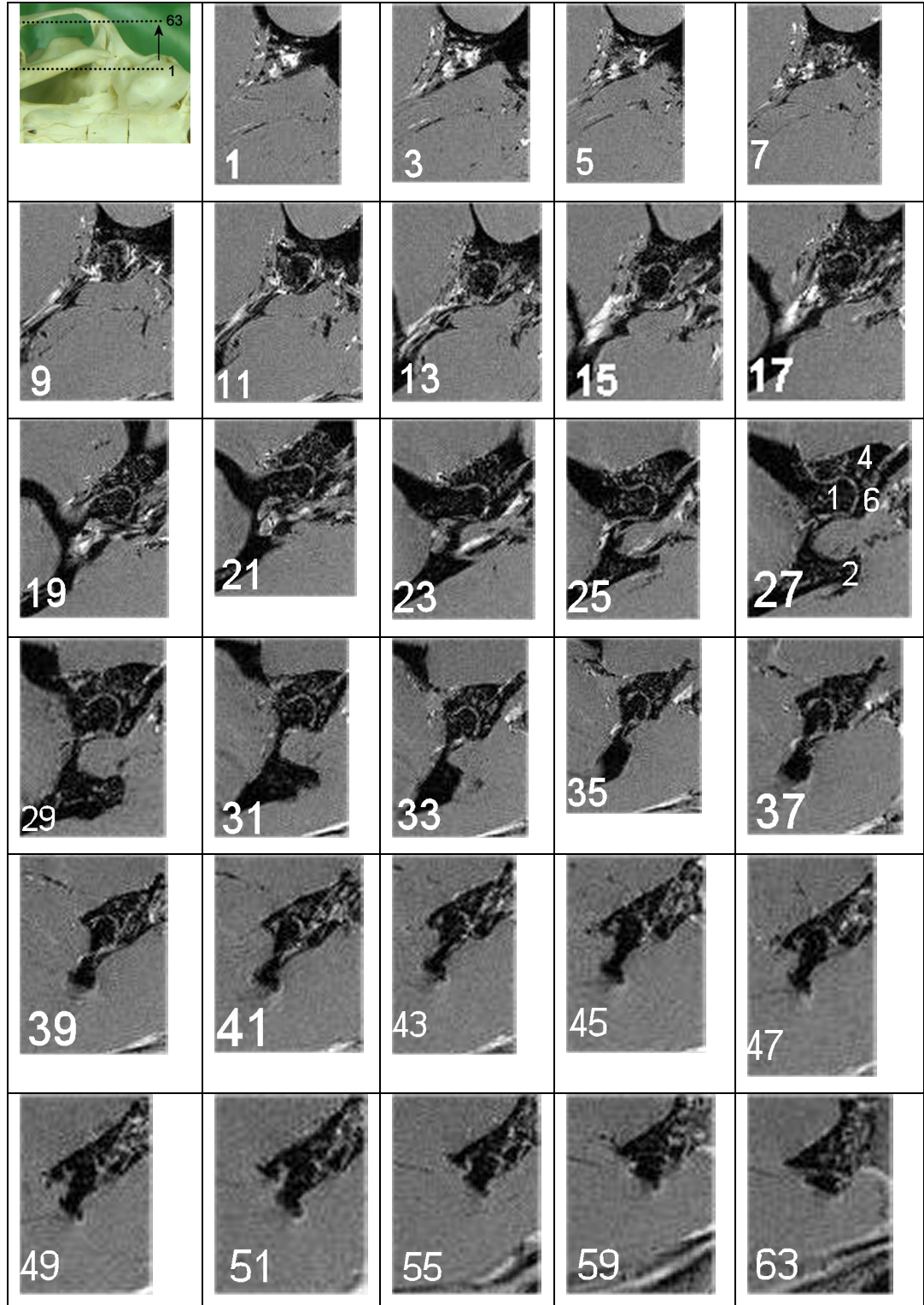


Figure 6.3.14.1. Sagittal T1 weighted MR images through the closed TMJ in the cat.

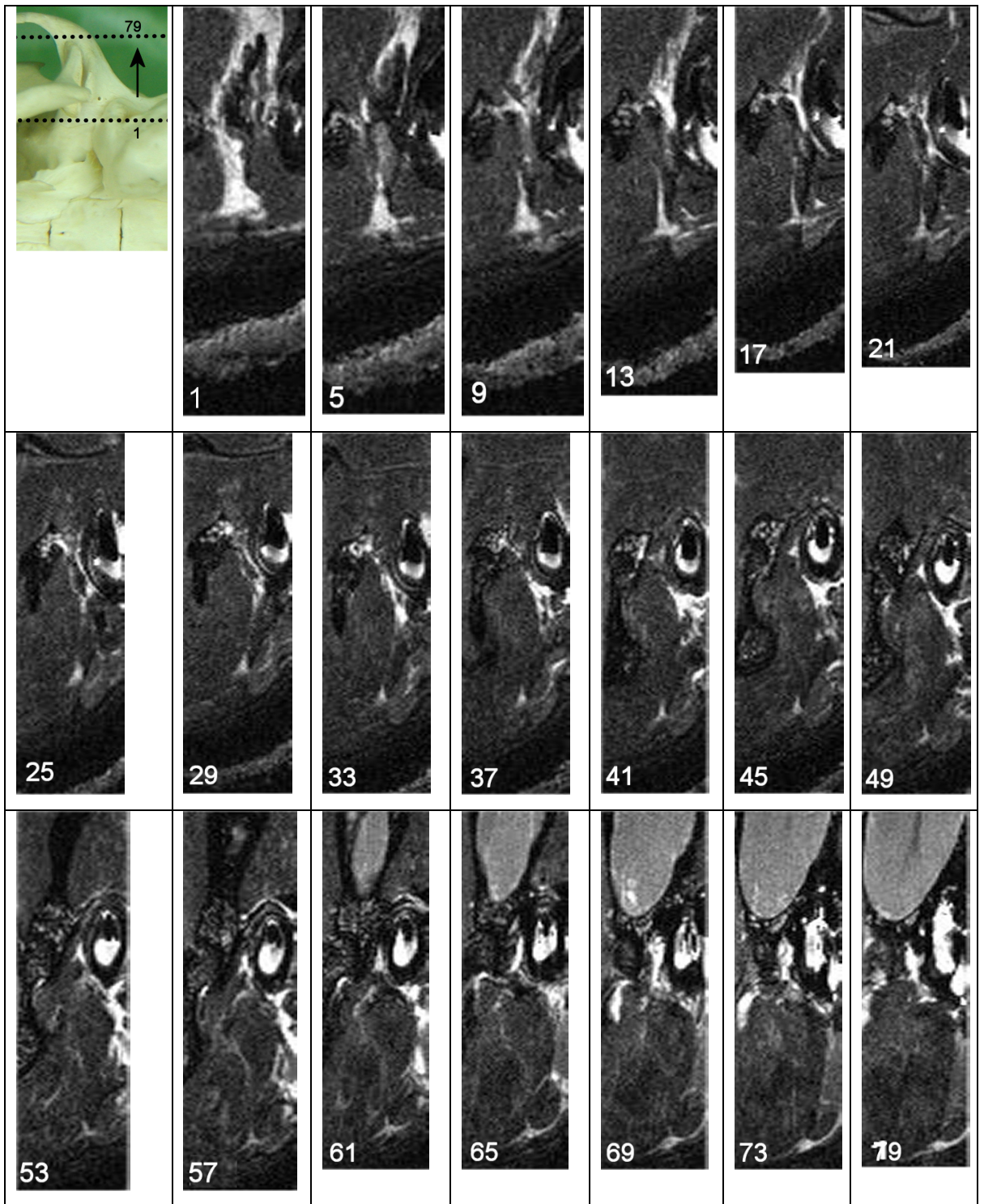


Figure 6.3.14.2. Sagittal T2 weighted MR images through the closed TMJ in the cat.

Figure 6.3.15. Sagittal MR images through the TMJ in the rabbit progressing from midline towards left. Dorsal is to top and rostral is to the left in all images. Number in bottom left corner indicates slice number. Approximate location of the first and last slice is indicated on the pilot image. For key see Table 6.2.

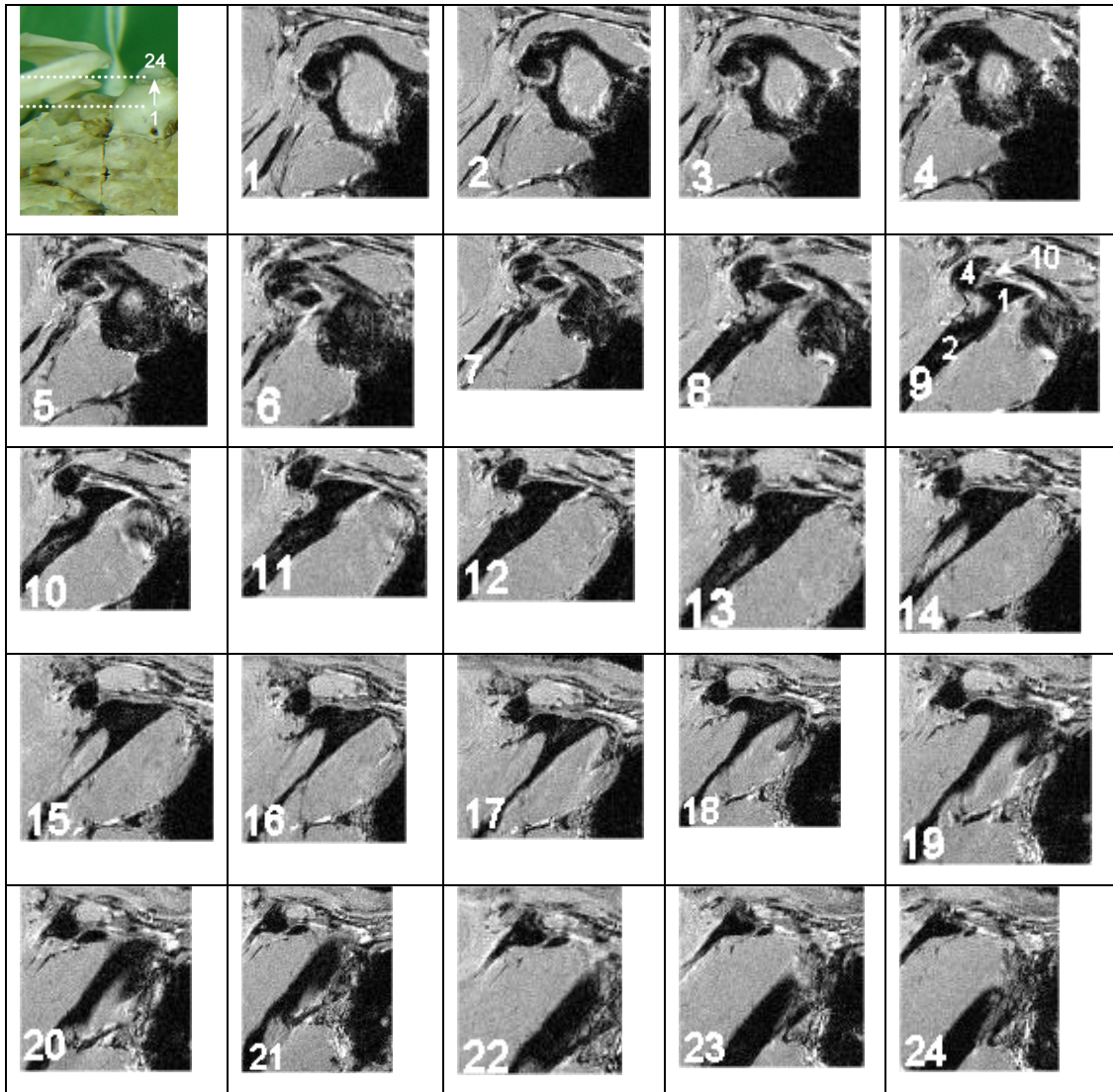


Figure 6.3.15.1. Sagittal T1 weighted MR images through the closed TMJ in the rabbit

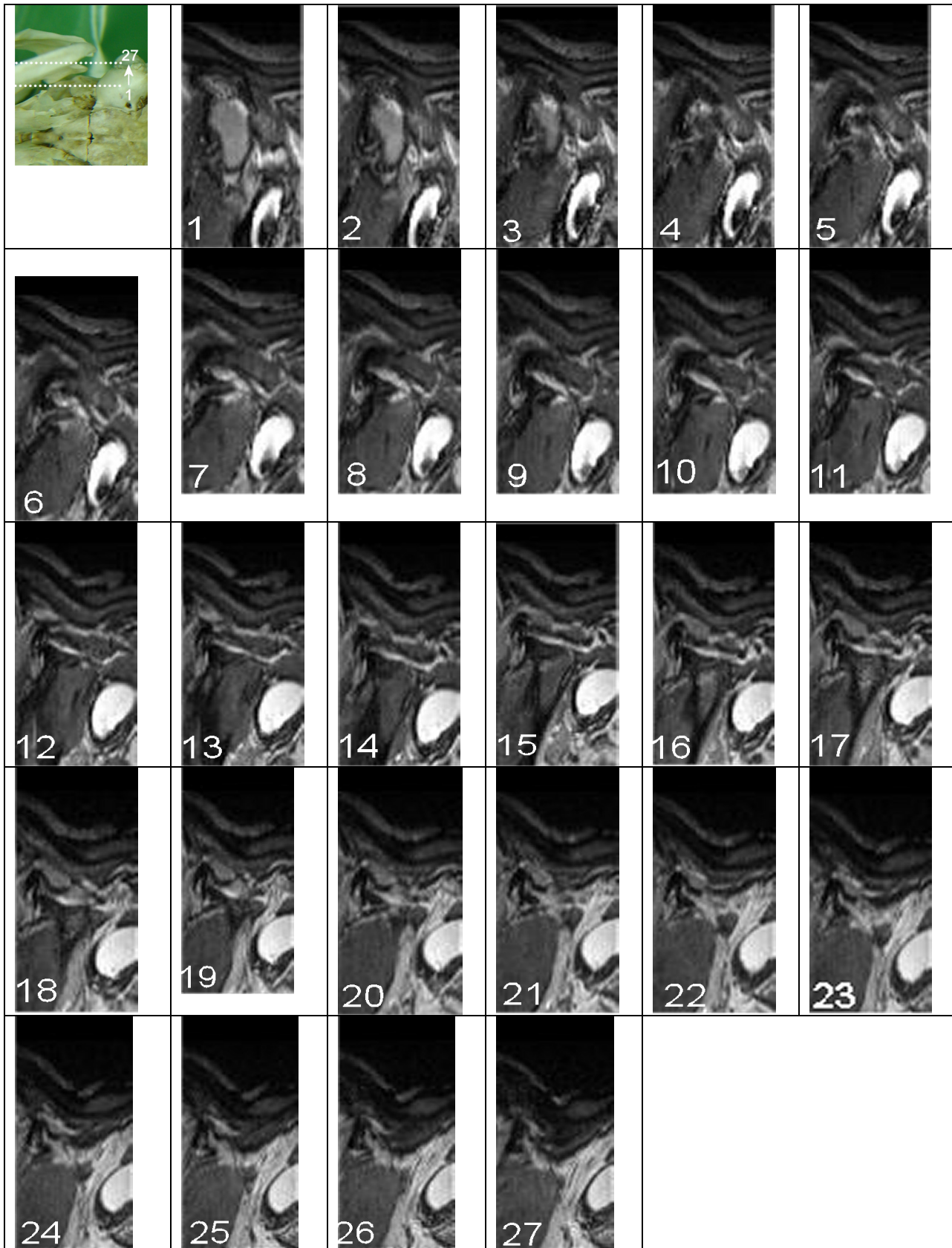


Figure 6.3.15.2. Sagittal T2 weighted MR images through the TMJ in the rabbit.

Figure 6.3.16. Dorsal MR images through the closed TMJ in the dog progressing from dorsal to ventral. Rostral is to the top and left is to the right in all images. Number in bottom left corner indicates slice number. Approximate location of the first and last slice is indicated on the pilot image. For key see Table 6.2.

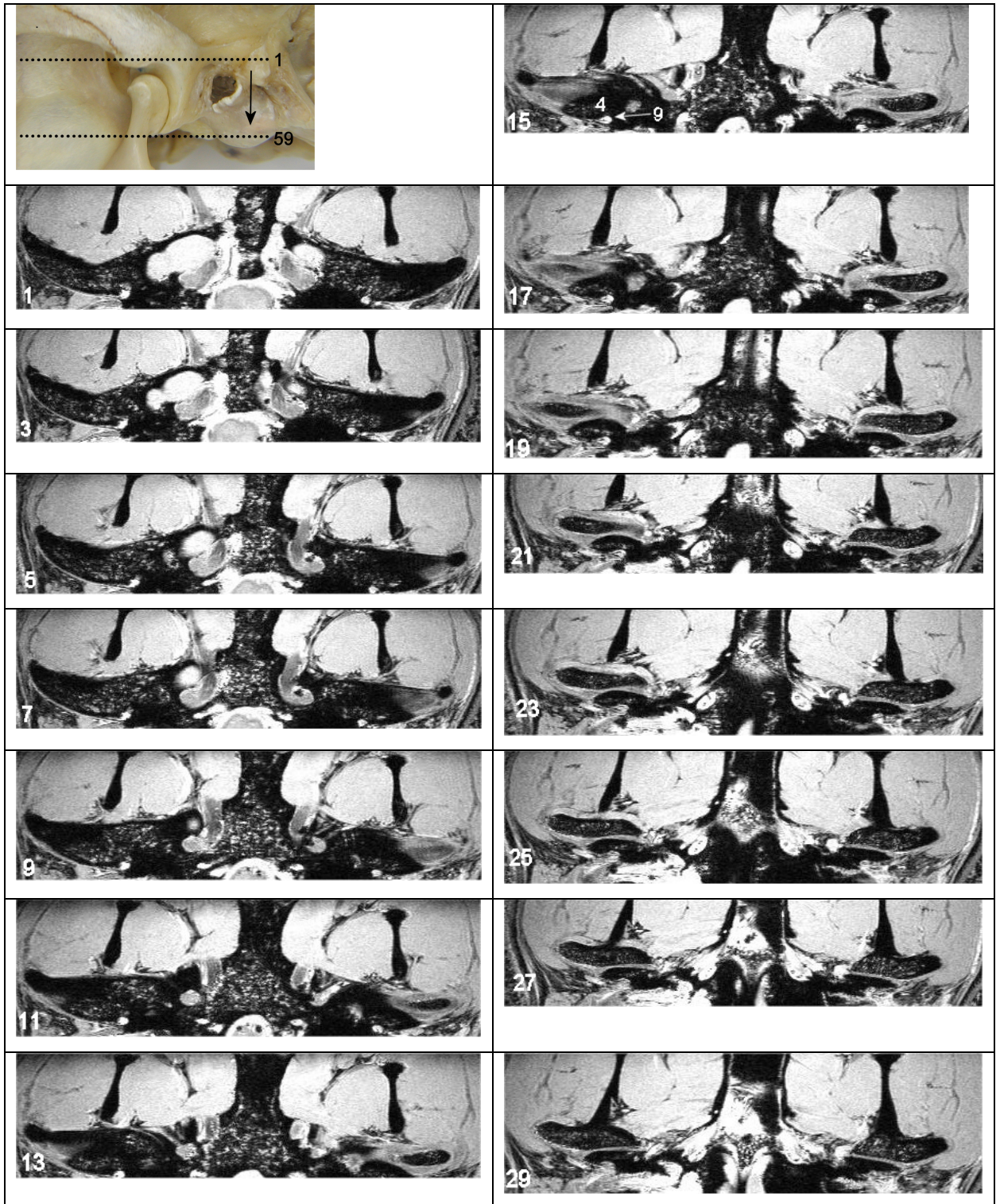
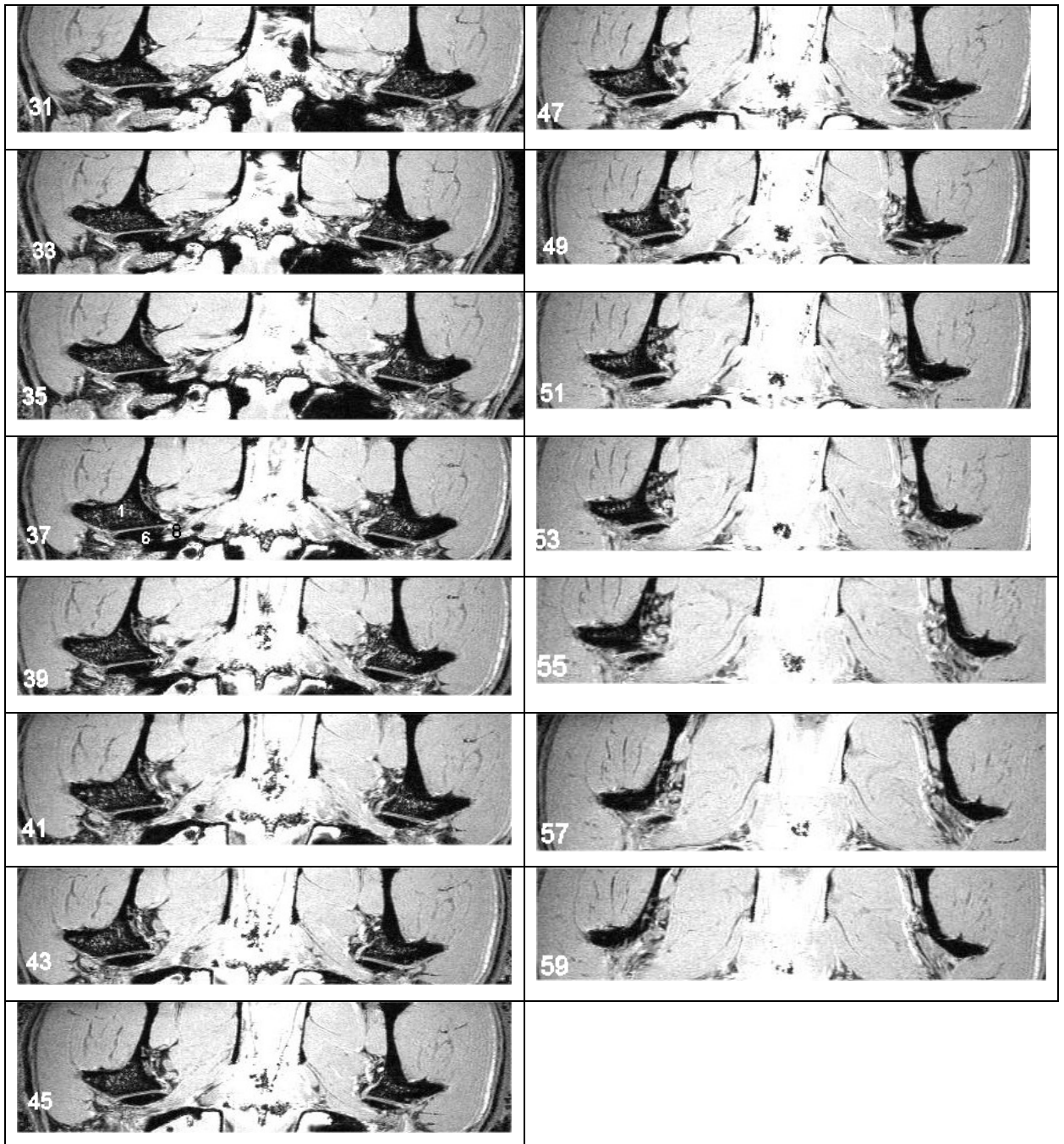


Figure 6.3.16.1. Dorsal T1 weighted MR images through the closed TMJ in the dog.

Figure 6.3.16.1. continued. Dorsal T1 weighted MR images through the closed TMJ in the dog.



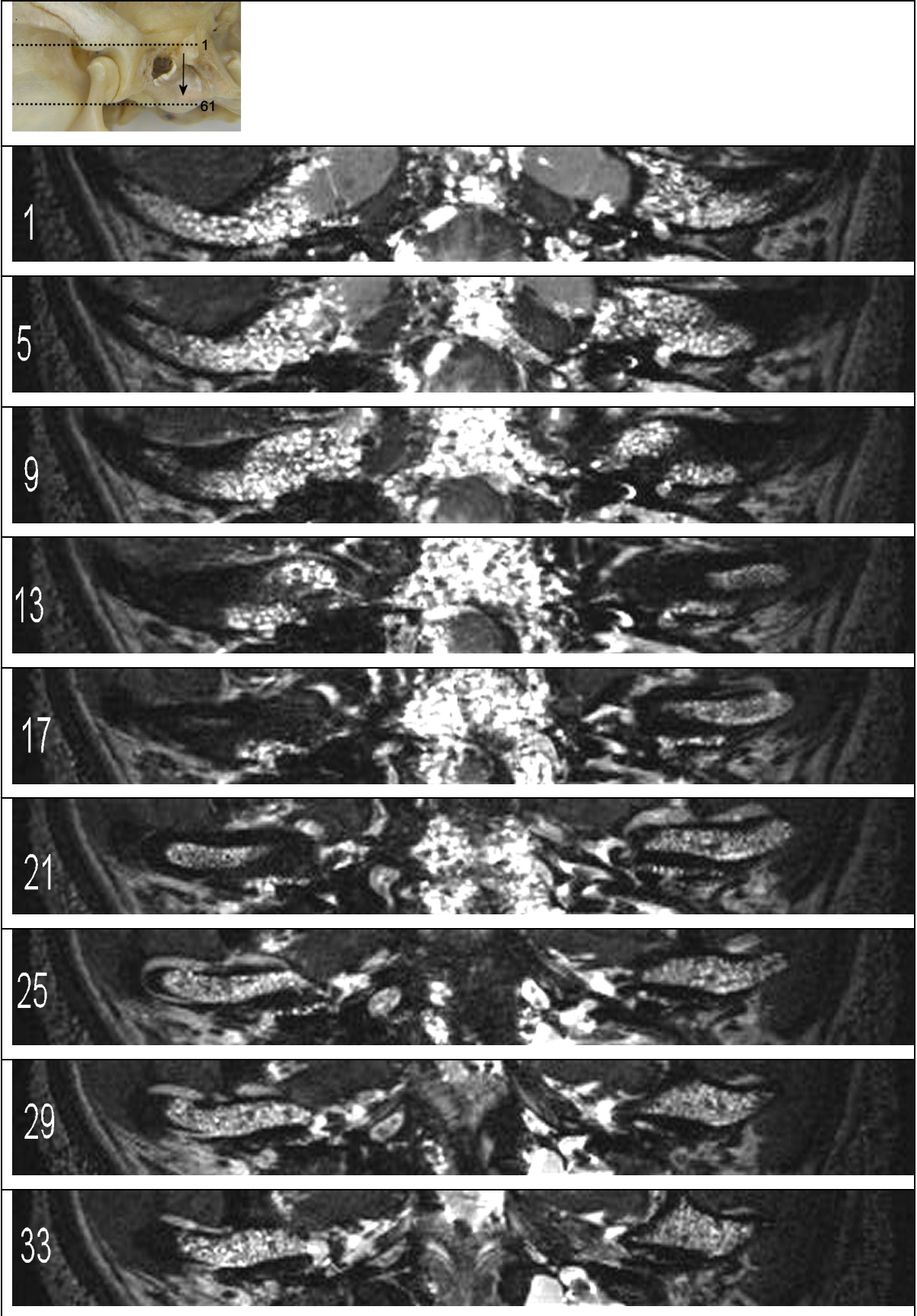


Figure 6.3.16.2. Dorsal T2 weighted MR images through the closed TMJ in the dog

Figure 6.3.16.2. continued. Dorsal T2 weighted MR images through the closed TMJ in the dog.

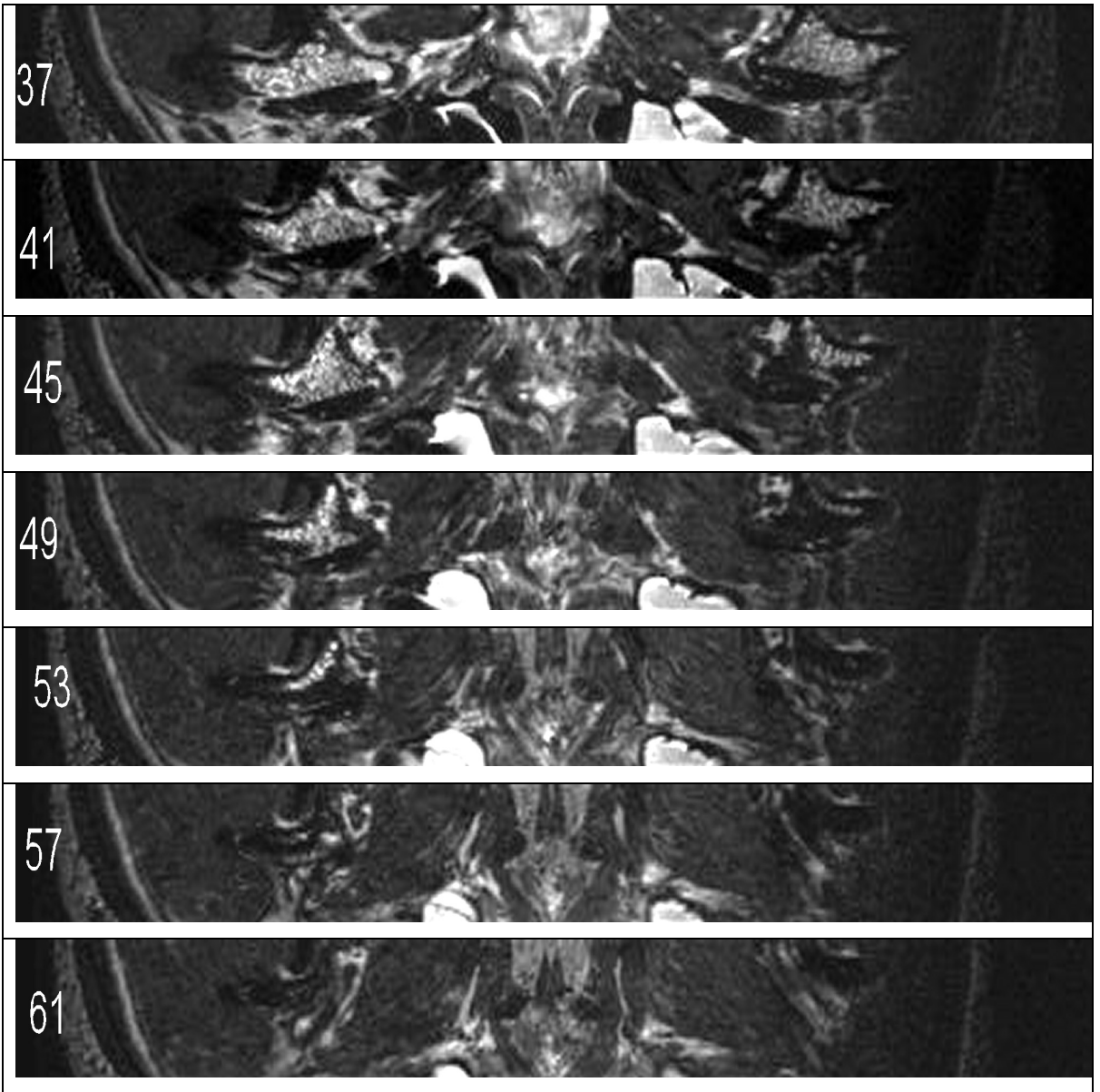


Figure 6.3.17. Dorsal MR images through the closed TMJ in the cat progressing from dorsal to ventral. Rostral is to the top and left is to the right in all images. Number in bottom left corner indicates slice number. Approximate location of the first and last slice is indicated on the pilot image. For key see Table 6.2.

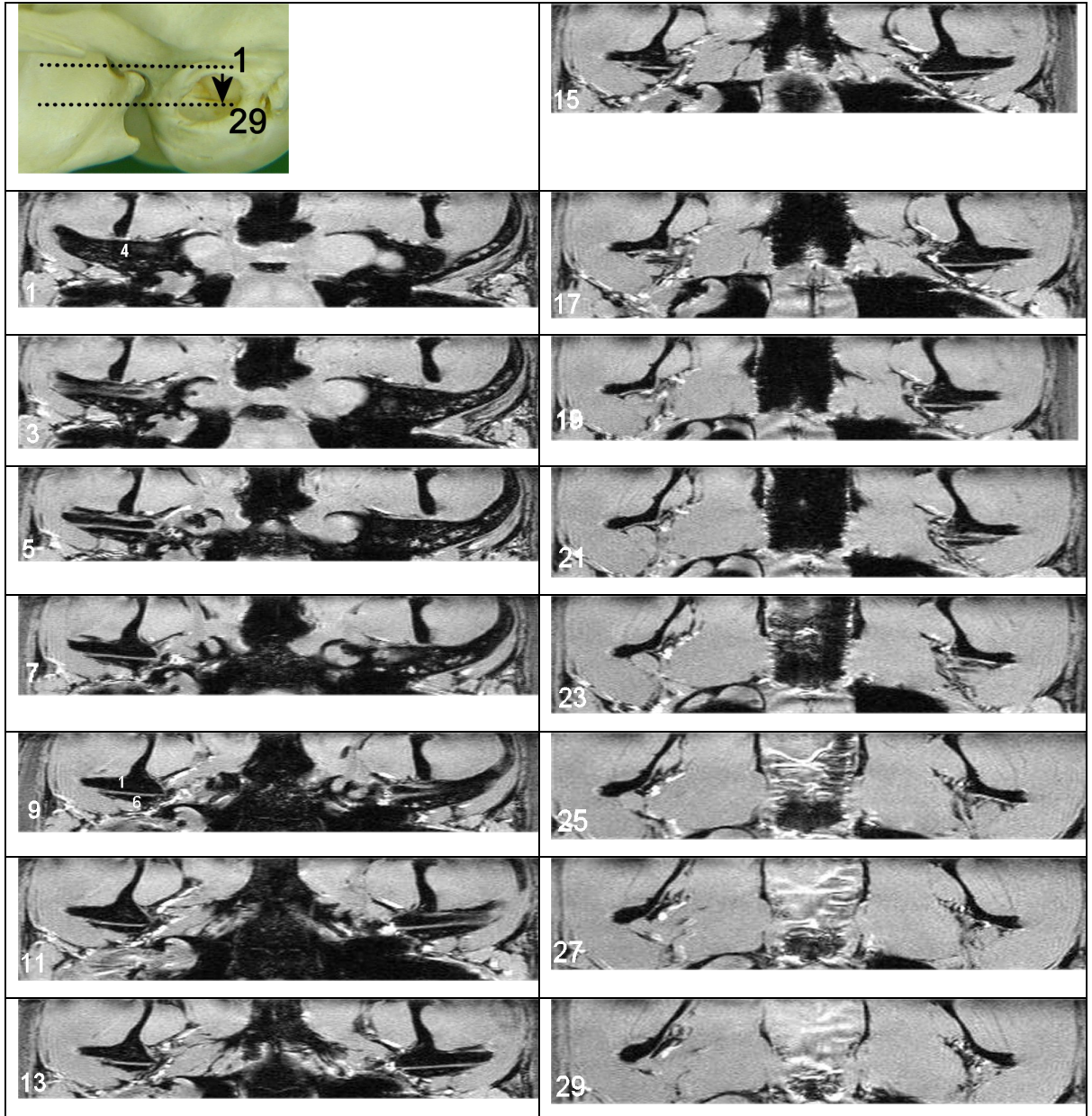


Figure 6.3.17.1. Dorsal T1 weighted MR images through the closed TMJ in the cat

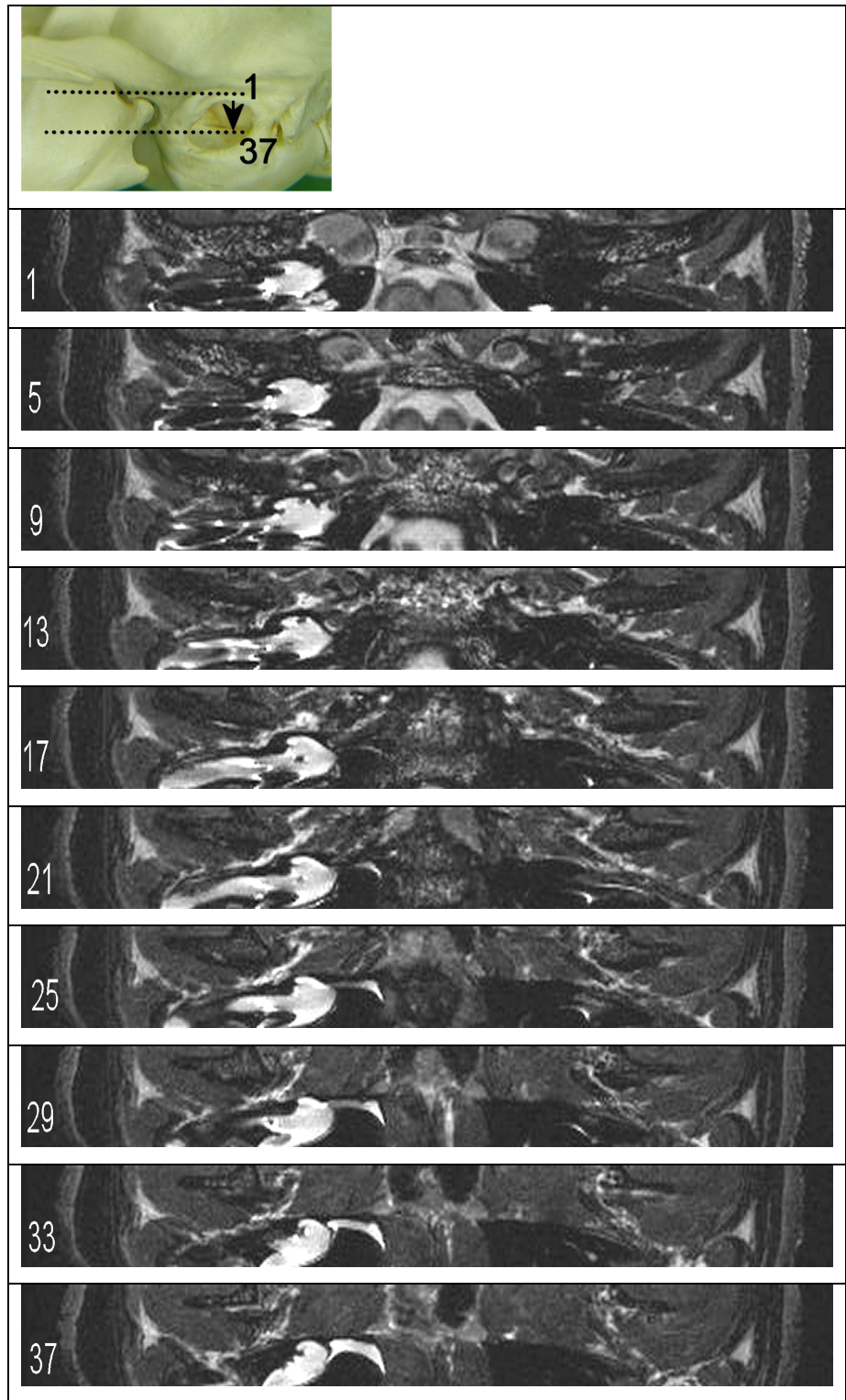


Figure 6.3.17.2. Dorsal T2 weighted MR images through the closed TMJ in the cat. Some image distortion has resulted from an intermittent fault within the resonator.

Figure 6.3.18. Dorsal MR images through the closed TMJ in the rabbit progressing from dorsal to ventral. Rostral is to the top and left is to the right in all images. Number in bottom left corner indicates slice number. Approximate location of the first and last slice is indicated on the pilot image. For key see Table 6.2.

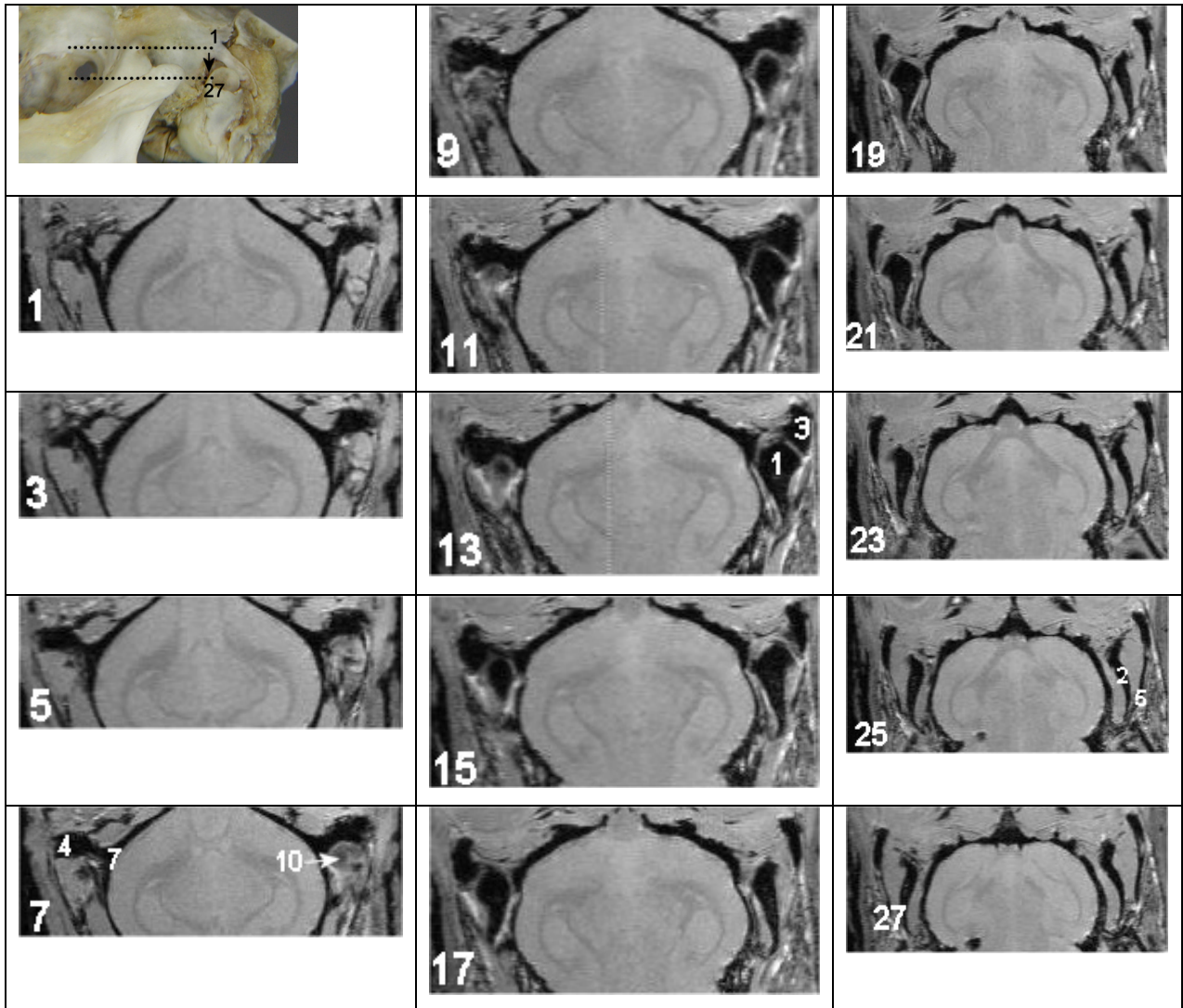


Figure 6.3.18.1. Dorsal T1 weighted MR images through the closed TMJ in the rabbit

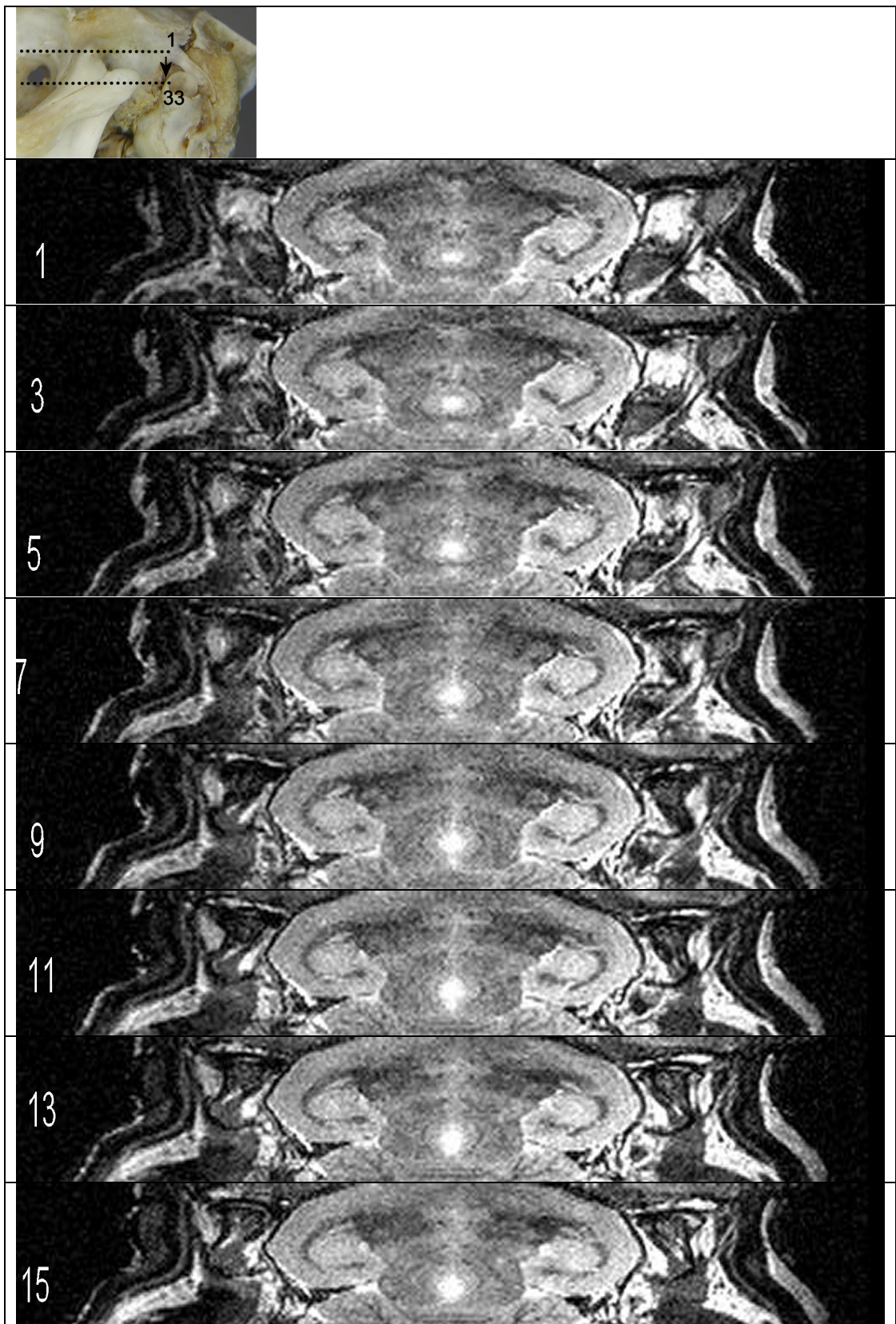
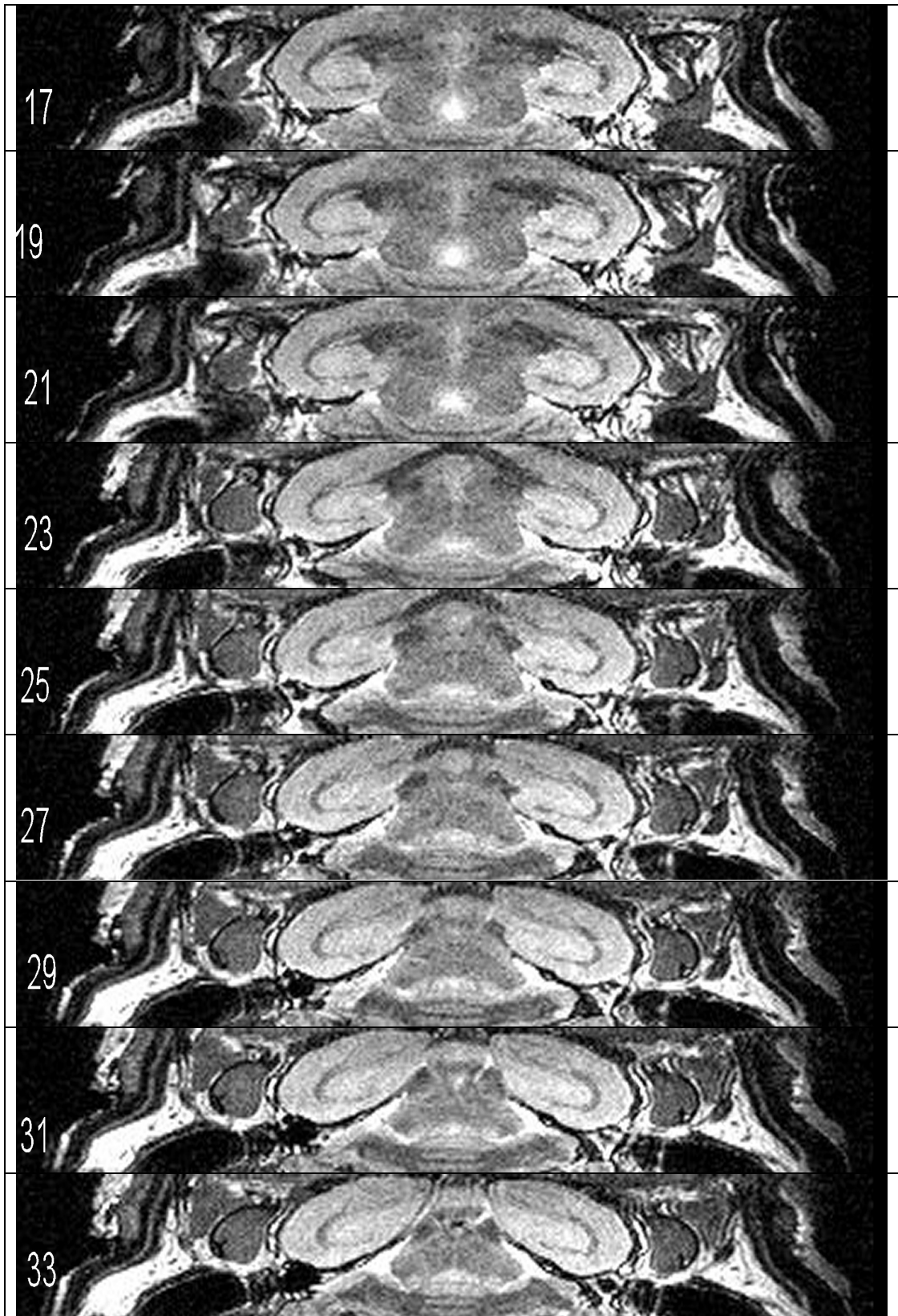


Figure 6.3.18.2. Dorsal T2 weighted MR images through the closed TMJ in the rabbit. Some image distortion has resulted from an intermittent fault within the resonator.

Figure 6.3.18.2. continued. Dorsal T2 weighted MR images through the closed TMJ in the rabbit. Some image distortion has resulted from an intermittent fault within the resonator.



6.4. Discussion

6.4.1. Material and technical considerations

The strength of the magnets used for previous studies of the canine and feline head have ranged from 1 – 4 Tesla (Widmer and others 1991, Dayrell-Hart 1997, Dvir and others 2000, Allgoewer and others 2002), making the 7 Tesla magnet used in this study significantly stronger. The advantage of this was the production of superior resolution images with higher signal to noise ratio than those obtained using more conventional equipment. While the images presented in this study are therefore not directly comparable with conventionally acquired MR images, it was hoped that with extrapolation, their superior resolution would enhance the identification of anatomical structures and subsequent interpretation of these images. However, while use of a 4 Tesla magnet was also reported to provide an increased signal to noise ratio, the image was affected more by slight movements in the region of interest caused by pulsation of blood or cerebrospinal fluid (Dayrell-Hart 1997). The use of cadavers in the present study meant this was not a problem but this would have to be borne in mind if this equipment was used to examine live animals.

The MRI equipment normally used for clinical veterinary imaging is the same as that in human medicine and is therefore designed to accommodate an adult human. This means that all regions of small animal patients can be imaged while in larger species such as the horse, imaging is limited to extremities including the head, neck and limbs (Tucker and Farrell 2001, Tucker and Sande 2002). MRI requires a gradient set and radiofrequency resonator combination to accompany the patient into the magnet. This, combined with the much smaller bore of the 7 Tesla magnet when compared to conventional equipment, meant that the maximum diameter of the material that could be imaged was limited to 152mm. This was adequate to accommodate the experimental animals that the equipment is mainly used for including mice, rats and rabbits. The cat and rabbit cadavers in the present study therefore fitted comfortably, but the canine cadavers were limited to small breeds. As discussed in Chapter 5, a lack of non-chondrodystrophic mesaticephalic small breed dogs within the available material limited selection of breed type to the Jack Russell Terrier, a chondrodystrophic mesaticephalic breed.

One problem associated with the use of cadavers was the presence of post mortem changes. There were gas pockets observed in the brain and soft tissues of some of the cadavers which appeared as black areas of signal void on the images. Since the heads had been removed at the level of the cervical region, it was possible that gas had tracked

rostrally between the fascial planes of the neck and along the spinal canal. Although the material had been stored at sub zero temperature, it was also possible that tissue decomposition had occurred either prior to freezing or after thawing, especially given that technical considerations meant the material underwent CT examination prior to MRI. Although the cadaver was initially at room temperature, it was surrounded by multiple layers of cling film to protect the equipment and also encased within the gradient set and radiofrequency resonator combination. This would have insulated the cadaver and prevented heat loss to the surroundings. The heat generated throughout the scans may have speeded up decomposition of the material with the resulting formation of gas pockets, or caused the expansion of existing ones, and therefore exacerbated the changes.

The MR signal obtained from soft tissues within the body can be influenced by many factors, one of which is temperature (Mullin 2007). In live animals, homeostatic mechanisms will dissipate heat and therefore the tissue will remain at constant body temperature. However, for the reasons already outlined, it was likely that the temperature of the cadaver material varied throughout the examination. The appearance of the soft tissue structures may therefore not correspond directly with those obtained using similar sequences in live animals. In the present study the build up of heat was particularly problematic in the canine T2 weighted images. While this is also not desirable in live animals due to the potential for tissue damage, heat will be better dissipated in live tissue than cadavers. MRI has been reported to have no known detrimental biological effects (Larheim 1995) and tissue heating has not been reported as a problem in clinical cases. Furthermore, this equipment has been used to image the head region of live rats under experimental conditions with no adverse effect to the animals (Farr and others 2006). The problems encountered in the present study were therefore most likely due to the use of cadaver material in combination with the long scanning times. However, in addition to the length of anaesthesia, this may represent a reason why such prolonged acquisition times may be inappropriate for use in live animals. MRI is very sensitive to differences in soft tissue composition (Tidwell 1999) so the potential for post mortem alterations in the signal intensity produced by various structures must also be borne in mind when imaging cadavers rather than live animals.

MRI has a high dependence on equipment and technical factors, all of which are not yet completely understood. A problem was encountered in the present study that was thought to be due to an intermittent fault within the resonator, resulting in either complete failure of the sequence or marked distortion of the images. Geometric distortion has been reported to

result from magnetic field inhomogeneity (Forrest 1999) and this may have been responsible for the distortion that was also observed at the ends of some of the T2 weighted sequences. This was the first time that dogs and cats had been imaged using this equipment therefore there were no standard imaging protocols in place prior to the study. In addition, the volume of canine material was at the maximum that could be accommodated by the machine. The use of cadavers to perform pilot examinations using new equipment may therefore be indicated so as to avoid compromising patient welfare by prolonging anaesthesia time while establishing protocols and identifying potential problems.

The length of the examination and the noise associated with the application of the radiofrequency mean that general anaesthesia is required when performing MRI in live animals to reduce patient movement and subsequent blurring of the image (Assheuer and Sager 1997, Allgoewer and others 2000). The duration of the anaesthetic is therefore a limiting factor in clinical cases and each sequence is typically restricted to four to five minutes, giving a total examination time of between 30 and 45 minutes (Carerra and Trevail 2007). However, the time taken to perform each sequence is dependent on several factors that are usually also linked to image quality. Since this was the primary objective in the present study, the acquisition times were well in excess of those used clinically. This was possible due to the use of cadavers so duration of anaesthetic was not a consideration but these sequences are unlikely to be suitable for use in live animals.

Standard imaging protocols for examination of the brain (3.5 - 5mm) do not allow the extremely small inner ear structures to be consistently visualised in their entirety (Dayrell-Hart 1997, Garosi and others 2001) and thinner slices are required to avoid partial volume artefacts (Garosi and others 2001). Slice thicknesses of 2-4mm have therefore been recommended for use to investigate the middle ear (Allgoewer and others 2000, Dvir and others 2000). Image quality was the main prerogative in the present study, therefore the 312 μ m and 250 μ m slices obtained for the T1 and T2 weighted images respectively were well in excess of these recommendations. The large number of averages obtained contributed to the increased signal to noise ratio and therefore superior image quality but also resulted in long acquisition times. In the present study, these were three to four for the T1 and 16 for the T2 weighted images, compared to the two reported in clinical cases (Allgoewer and others 2000).

Routine MR examinations should include imaging in dorsal, sagittal and transverse planes (Dvir and others 2000). Direct imaging in all three planes is possible using MRI and can be

achieved without repositioning the patient (Widmer and others 1991, Shores 1993, Forrest 1999). However, the acquisition of three slice series will significantly increase the length of the examination. To reduce scan times, the transverse slices can be amalgamated and used to produce reformatted images in sagittal and dorsal planes. The resolution of these reformatted images depends on the resolution of the original images and also the capabilities of the software and hardware being used but are never as good as the original transverse images. The only advantage is that the reconstructions can be performed after the scan and so reduce examination and anaesthesia time.

Imaging of the head in clinical cases of middle ear disease should include pre and post contrast T1, and T2 weighted acquisitions (Allgoewer and others 2000, Dvir and others 2000, Garosi and others 2000), since T1 weighted images are superior for demonstrating regional anatomy while T2 weighted ones favour the identification of fluid. Each sequence must be acquired individually therefore again contributing to the overall examination time.

The T1 weighted images in the present study were obtained using a three dimensional volumetric acquisition, which allowed the data to be acquired as a block rather than as individual slices. This resulted in isotropic resolution so the block could then be sectioned in any plane without a loss of resolution. Image quality in all three planes was therefore comparable and of 312 μ m, which was better resolution than that of the reformatted T2 weighted images. In live animals, the acquisition of a three dimensional volume will take a shorter time than the direct acquisition of images in multiple planes therefore reducing anaesthesia time. Volume acquisition reduces the problems resulting from the increased noise associated with thin slices and in combination with a slice thickness of less than 2mm has become gold standard in humans, allowing more detailed visualisation of the inner ear structures (Garosi and others 2001).

The acquisition of the T2 weighted images in blocks as a series of two dimensional slices meant that reconstruction was necessary to create the multiplanar views. The resolution of these images was limited by slice thickness (0.5mm or 500 μ m), which resulted in poorer image quality than the transverse images (250 μ m) and the corresponding T1 weighted images (312 μ m). This disparity between the in-plane resolution and slice thickness resulted in the production of elongated T2 weighted images. Although software could be used to interpolate the data and create a more anatomically correct image, this would require either the creation or omission of pixels and therefore the depiction of the signal

intensity obtained from the structures would no longer be accurate. In addition, the width of the slab of images made orientation of the images more difficult as less of the surrounding anatomy was visible. The reconstructed T2 weighted images in the present study were therefore of significantly poorer quality than the originals and this limited the appreciation of anatomical structures on them.

Accurate patient positioning is important to allow comparison of bilateral symmetry, especially in transverse and dorsal images (Assheuer and Sager 1997, Allgoewer and others 2000, Garosi and others 2001). However, this is often difficult to achieve as demonstrated by the presence of asymmetry affecting most of the images in the present study despite the use of cadavers, which should have made positioning easier. The semicircular shape of the plastic trough into which the cadavers were placed may have contributed so the use of a flat surface that would ensure the mandibles remained parallel may be preferable. Although judicious placement of the slice sequences on pilot images can compensate for some asymmetry in the patients position, any reconstructed image subsequently acquired from the data set will also be affected as demonstrated in this study.

6.4.2. MRI of the TB in the dog, cat and rabbit

In humans, the middle ear cavity was invisible on conventional MRI due to its bone boundaries and its air content (Holliday and Reede 1989). Likewise in dogs, the air-filled lumen of the normal TB was reported to appear as a signal void, which was therefore indistinguishable from that produced by the bone walls (Forrest 1999, Garosi and others 2000, Bischoff and Kneller 2004). This corresponded with the appearance of the gas-filled TB in all species in the present study. In cats, the air-filled vertical and horizontal portions of the external auditory canal, both compartments of the TB and the thin separating bony lamella could be visualised (Allgoewer and others 2000). Although the septum bulla could be localised in this study, it was not clearly or consistently visible in all views. The tympanic membrane could be identified in the dorsal images but again was not clearly or consistently imaged, although its appearance when visible, was similar to that previously documented in the dog (Assheuer and Sager 1997, Owen and others 2004). The auditory ossicles could not be identified in any of the images.

Material was identified in the middle ear cavity of 7% of dogs undergoing MRI for the investigation of neurological signs and of these, 41% were not associated with middle ear disease (Owen and others 2004). The fluid encountered in the TB lumen of live animals was most commonly localised in the dependent part of the TB. It was hyperintense relative

to the brain on T2 weighted images and isointense (Allgoewer and others 2000, Garosi and others 2003, Owen and others 2004) or hyperintense on T1 weighted images (Owen and others 2004). Air bubbles were observed as well-defined, rounded signal voids (Owen and others 2004) and there was usually an obvious meniscus (Garosi and others 2003). This corresponded with the appearance and location of the ultrasound gel, any post mortem fluid and gas bubbles encountered in the cadavers in the present study.

In many instances, the MR appearance of fluid identified within the TB lumen was reported to be heterogenous (Allgoewer and others 2000, Owen and others 2004). Focal areas of varying intensity have also been encountered within such fluid that were thought to represent areas with a different composition or concentration of material (Hammond 2007). It has been reported that in chronic cases of middle ear disease, progressive dehydration of fluid resulting in an increasing protein concentration may lead to an increase in signal on T1 and a decrease on T2 weighted images (Owen and others 2004). However, there does not appear to be a correlation between the signal characteristics of the material and the diagnosis (Owen and others 2004). Despite the ultrasound gel used in the present study being of a uniform consistency, it also produced a heterogenous appearance in some of the images. MRI may have identified subtle variations in the composition of the gel or the ventral location of some of the hyperintense regions may have reflected the presence of post mortem fluid prior to the introduction of the gel. However, the location of many of these regions adjacent to the curved ventral surface of the TB wall or the meniscus at a gas interface may also imply that these are artificial signals, although further work would be required to determine if this is the case. The presence of a narrow hyperintense rim has been described in some cases of otitis media (Allgoewer and others 2000, Garosi and others 2000, Owen and others 2004) and while this is usually observed following gadolinium contrast administration (Allgoewer and others 2000, Owen and others 2004) the results from the present study suggest that a curved hyperintense line adjacent to the TB wall may also be artefactual.

The presence of fluid within the TB lumen improved its visualisation by outlining the internal margin and the extent of the lumen relative to the surrounding bone. It also enhanced determination of the location of the septum bulla in the cat. In humans, MRI was able to image the auditory ossicles in the presence of serous fluid within the middle ear cavity due to their resulting delineation (Duprez and others 2002) but not in the normal air-filled state (Holliday and Reede 1989).

Transverse and dorsal sequences were reported as being the most useful for imaging the TB in cats as they allowed comparison of both sides (Allgoewer and others 2000). However, this relies heavily on patient positioning to ensure symmetry and as the results of the present study indicate, this can be difficult to achieve. The intention in the present study had been to use the fluid-filled TB in these images to ascertain the extent of the gas-filled lumen TB relative to the surrounding bone on the contralateral side, but this did not prove to be possible in most instances. Each of the planes demonstrated different features associated with the TB but the lack of contrast between the bone wall and the contents meant that the information obtained in the normal state was relatively limited in both T1 and T2 weighted sequences. However, fluid in the lumen could be clearly identified using both sequences indicating that they will both be beneficial in the investigation of animals with middle ear disease. The usefulness of each view in the present study was also limited by image quality indicating that if 3-dimensional volumetric data acquisition is not possible, then direct acquisition of images in each plane is far superior to relying on image reconstruction.

6.4.3. MRI of the TMJ in the dog, cat and rabbit

MRI has been reported to provide excellent delineation of TMJ anatomy in humans (Landes and others 2000). Although T1, T2 and proton density weighted sequences have been reported for imaging of the canine TMJ (Baines and others 2002), in the present study the T1 weighted images provided the best anatomical detail in all three species. In the T2 weighted images, the intra-articular space was difficult to distinguish from the adjacent cortical bone of the mandibular fossa and condyloid process and therefore these sequences were felt to be of more limited value.

In humans, MRI was reported to be the only imaging modality capable of localising the intra-articular disc (Larheim 1995) and it had a low signal on all pulse sequences due to its fibrous nature, which was reported to make it difficult to distinguish from adjacent cortical bone (Payne and Nakielny 1996). In dogs, the articular cartilage and synovial fluid were reported to be hypointense compared to the cortical bone but could not be distinguished from each other and the disc was not visible (Baines and others 2002). In the present study, some parts of the joint space in the dog and rabbit appeared uniformly isointense compared to the surrounding soft tissue structures (hypointense relative to cortical bone) and it was likely that, as in this previous report, these represented a combination of the articular cartilage and synovial fluid. However, in some images in the dog and rabbit, a central hypointense area was also visible. The joint space in these species is separated by the disc

into dorsal and ventral chambers each containing synovial fluid (Barone 1989, Caporn 1995), therefore it is likely that this area represented the disc surrounded by fluid. In the dog, the disc was best visualised in the transverse and sagittal images while in the rabbit, it was easiest to identify in the sagittal and dorsal planes.

In the dog, the intra-articular disc is not particularly well developed and is thinner centrally than peripherally (Shengyi and Yinghua 1991). This would explain why it was only visualised at the lateral and medial aspects of the joint but not centrally. The rabbit has a better developed intra-articular disc than in the dog due to its herbivorous diet and it is saddle shaped, again being relatively thick peripherally with a central indentation (Weijs and Dantuma 1981, Barone 1989). Although it conforms to the condyloid and glenoid articular surfaces (Weijs and Dantuma 1981), it does not cover the rostral portion of the condyloid process (Barone 1989) and this was evident in the sagittal and dorsal images in the present study. The mandibular fossa in the cat better conforms with the shape of the condyloid process than in the dog or rabbit (Caporn 1995). The resulting narrow joint space was evident in this study and made it very difficult to examine the intra-articular region. As determined in Chapter 2, the cat has only a thick membrane rather than a disc (Gillbe 1973) therefore it was not surprising this was not visible. The intra-articular disc in humans is easy to identify and assess using standard MRI protocols, allowing discal pathology and inflammatory conditions to be diagnosed (Larheim 1995, Landes and others 2000). However, the actual size of the disc in dogs and rabbit is much smaller so although it has been located in the present study, meaningful assessment of its position and structure in clinical cases is likely to be limited. The joint capsule in all three species has extensive peripheral attachments to adjacent structures and these could also be appreciated on the images in the present study, particularly medially and laterally (Scapino 1965, Gillbe 1973, Ström and others 1988, Barone 1989).

Chapter 7. Comparison of imaging modalities for the investigation of otitis media in the dog, cat and rabbit.

7.1 Introduction

7.1.1 Otitis media

Otitis media, or inflammation of the middle ear cavity occurs in the dog, cat and rabbit. Although it can arise via different routes, in the dog it is most commonly associated with the spread of inflammation across the tympanic membrane secondary to chronic or severe external ear canal disease (Neer and Howard 1982, Shell 1988, Little and others 1991a). In the cat it is more likely due to ascending infection through the auditory tubes from nasopharyngeal viral infections (White 2003) and may be associated with the presence of nasopharyngeal polyps although it is not clear whether they are the cause or sequel (Parker and Binnington 1985, Kapatkin and others 1990, Trevor and Martin 1993). In the rabbit, it most commonly occurs secondary to respiratory infection with *Pasteurella multocida* (Kpodekon 1983). The most significant complications of otitis media are the progression to otitis interna or extension to involve the brain (Neer and Howard 1982, Kpodekon 1983). Early diagnosis and treatment is therefore warranted to prevent such potentially serious secondary complications. Pathological changes associated with otitis media include the presence of thickened mucosa, inflammatory fluid or pus within the TB lumen and thickening of the TB wall (Flatt and others 1977, Little and others 1991a, White 2003). Acute changes observed in dogs with experimentally induced otitis media and in rabbits with naturally occurring disease were mucosal inflammation and the presence of intraluminal fluid (Smith and Webster 1925, Tojo and others 1985).

7.1.2. Radiography in the investigation of otitis media

Conventional radiography is commonly used in the evaluation of dogs and cats with ear disease. Although routine evaluation usually includes a combination of views (Gibbs 1978, Douglas 1987, Kapatkin and others 1990, Remedios and others 1991, Hoskinson 1993, Farrow 1994, Love and others 1995, Sullivan 1995, Owens and Biery 1998), dorsoventral or ventrodorsal and in particular rostrocaudal open mouth views, were reported as being the most useful (Gibbs 1978, Love and others 1995). The rostrocaudal open mouth view can be difficult to perform in the cat due to the positioning involved so a rostro 10° ventral-dorsocaudal oblique or 10° ventrodorsal view has been suggested as an alternative for use

in this species (Hofer and others 1995, Owens and Biery, 1998). As in the dog and cat, lateral and dorsoventral radiographic views are considered standard for examination of the rabbit skull (Harcourt-Brown 1995, Harcourt-Brown, 2003). A variety of other views have also been suggested depending on the area under investigation (Harcourt-Brown 1995, Crossley 1995, Harcourt-Brown, 2003) but none that are specific for the TB.

There is currently no consensus regarding the diagnostic accuracy of radiography in cases of otitis media (Remedios and others 1991, Love and others 1995, Rohleder and others 2006). The results from previous imaging studies of canine otitis media are presented in Table 7.1. Radiography has been reported to commonly underestimate the severity of canine middle ear disease (Shell 1988, Hoskinson 1993), especially in early cases or when bony changes are absent (Shell 1988). In cadavers, radiography only had a sensitivity of 80% and specificity of 65% for the identification of TB fluid in the absence of bone changes (Griffiths and others 2003) and so probably contributes most in the evaluation of patients with chronic or recurrent disease (Hoskinson 1993). False negative radiographic findings have been reported in dogs with otitis media (Remedios and others 1991, Love and others 1995, Rohleder and others 2006) and cats with nasopharyngeal polyps (Allgoewer and others 2000) due to the absence of chronic changes or suboptimal image quality (Remedios and others 1991). False positive results were only reported in one study (Rohleder and others 2006) therefore positive radiographic findings can be regarded as highly sensitive in the diagnosis of otitis media (Remedios and others 1991, Love and others 1995), although negative findings do not rule it out (Remedios and others 1991) since early changes may be too subtle for detection (Love and others 1995, Rohleder and others 2006). This has been confirmed in dogs with experimentally induced otitis media where only 14% (1/7) of cases of less than 10 days duration demonstrated a detectable increase in opacity of the TB while at 15-20 days duration, 87.5% (7/8) were identifiable radiographically (Tojo and others 1985).

Radiographic changes associated with otitis media in dogs and cats can include an increased opacity within the TB; thickening, blurring or irregularity of the osseous margins; erosion of the ventral wall; expansion and distortion of the TB or sclerosis of the petrous temporal bone (Lawson 1957, Spruell 1964, Bistner 1967, Rose 1977, Gibbs 1978, Farrow 1985, Sanchez and others 1987, Hoskinson 1993, Farrow 1994, Love and others 1995, Barthez and others 1996). Rarely, severe lesions can extend into adjacent soft tissue

(Spruell 1964) or involve neighbouring structures such as the temporomandibular joint (Schwarz and others 2002) and may result in partial obstruction of the pharynx (Sanchez and others 1987). Conditions such as osteomyelitis that cause destruction of TB wall may not be distinguishable from malignant neoplasia (Farrow 1994). In rabbits changes include increased density within the TB (Wolvekamp and Oschwald 1991, Beed 1997) that may be bilateral (Wolvekamp and Oschwald 1991), and thickening of the bone (Beed 1997).

7.1.3. Sonographic investigation of otitis media.

Ultrasound has been used to identify the presence of fluid placed within the middle ear cavity of canine cadavers by imaging through the thin bone wall of the TB (Griffiths and others 2003). This technique was reported to be able to distinguish between fluid and gas within the lumen with greater accuracy than radiography (Griffiths and others 2003) (see Table 7.1). However, this appears to be the only report of this approach in any species and there are no reports of its use in clinical cases of middle ear disease.

Study	Sensitivity (%)	Specificity (%)	PPV (%)	NPV (%)
Remedios and others 1991*				
Radiography	75 (12/16)	100 (3/3)	100 (12/12)	40 (3/4)
Love and others 1995*				
Radiography	66 (12/18)	100 (9/9)	100 (12/12)	60 (9/15)
Computed tomography	83 (15/18)	88 (8/9)	94 (15/16)	73 (8/11)
Rohleder and others 2006*				
Radiography	55 (16/29)	72 (13/18)	76 (16/21)	50 (13/26)
Computed tomography	86 (25/29)	89 (16/18)	93 (25/27)	80 (16/20)
Griffiths and others 2003 ⁺				
Radiography	80 (16/20)	65 (13/20)	70 (16/23)	76 (13/17)
Ultrasound	100 (20/20)	100 (20/20)	100 (20/20)	100 (20/20)

Table 7.1. Sensitivity, specificity, positive (PPV) and negative predictive values (NPV) from previous imaging studies of the canine TB. * indicates clinical studies. ⁺ indicates cadaver study. Due to the presence of an error, the radiography results for Rohleder and others (2006) have been recalculated and therefore are slightly different to those appearing in the original publication.

7.1.4. CT in the investigation of otitis media

High resolution CT is the method of choice for examination of middle ear structures in humans (Czerny and others 1997) and CT evaluation of pathology involving these structures has been reported (Ali and others 1993, Alexander and Caldemeyer 1998). It can accurately diagnose ear disease while providing an efficient use of resources at low risk to the patient (Twemlow 1991). CT is the procedure of choice for the detection of osseous abnormalities of the temporal bone, bony changes associated with soft tissue masses in the temporal bone (Holliday and Reede 1989) and the investigation of conductive hearing loss (Maroldi and others 2001). It provides more specific information regarding the soft tissue within the middle ear than radiographic procedures (Swartz 1983), although it may not be able to differentiate inflammatory from granulation tissue (Holt and Walker 1997). The use of two CT projections to distinguish dependent fluid from non-dependent soft tissue opacities has been suggested (Swartz 1983) and it also remains the 'gold standard' for the detection and delineation of temporal bone fractures (Holliday and Reede 1989).

The use of CT in the diagnosis of canine middle ear disease (Forrest 1999) and otitis media has been advocated (Remedios and others 1991, Hoskinson 1993) and images published (Hoskinson 1993, Love and others 1995). It has also been used to evaluate canine otoliths (Ziemer and others 2003), feline nasopharyngeal polyps (Seitz and others 1996), an abscess extending from the ipsilateral TB (Schwarz and others 2002) and for investigation of craniomandibular osteopathy involving the TB in a dog (Hudson and others 1994). There are only two studies evaluating CT for the diagnosis of canine otitis media (Love and others 1995, Rohleder and others 2006).

The criteria used to evaluate the middle ear using CT are the same as for radiographs (Love and others 1995). Transverse and dorsal plane images allow comparison between sides (Allgoewer and other 2000) while midsagittal or parasagittal reconstructed images are beneficial in identifying the extent of nasopharyngeal polyps in cats (Seitz and others 1996). The presence of fluid within a normally air-filled cavity produces opacification while partial filling is easily recognised by the gravity dependent location of the fluid and the presence of a horizontal air-fluid interface (Morrow and others 2000). However, the presence of fluid within the TB causes an apparent increase in thickness of the TB wall so care must be taken when identifying this change on images (Barthez and others 1996).

The sensitivity of CT in the diagnosis of otitis media was greater than for radiography but the specificity varied (Love and others 1995, Rohleder and others 2006) (see Table 7.1). The benefits of CT were deemed in one study to be too marginal to support its use as a screening tool, although it was suggested as being beneficial in cases where clinical signs were indicative of otitis media but radiographs were negative (Love and others 1995). More recently though, CT has become accepted for the evaluation of middle ear disease in veterinary practice (Garosi and others 2003).

In dogs with otitis externa, the changes observed using CT images were the same as on radiographs (Hoskinson 1993, Barthez and others 1996). Abnormalities of the inner ear are rarely if ever, evident on CT and artefacts caused by the petrous portion of the temporal bone limit examination of the caudal fossa to rule out a brain lesion in the presence of confusing vestibular signs (Garosi and others 2001).

7.1.5. MRI in the investigation of otitis media

The use of MRI in a variety of human middle ear related diseases including otitis media has been described and the identification and characterisation of inflammatory or neoplastic soft tissue abnormalities within the temporal bone is reported to be easier with MRI than CT due to lack of bone artefact (Stone and others 1983).

MRI currently represents the gold standard for the veterinary diagnosis of middle ear disease (Griffiths and others 2003). The MRI changes in cases of canine otitis interna (Garosi and others 2000, Garosi and others 2001), media (Dvir and others 2000, Garosi and others 2000, Garosi and others 2001) and externa (Dvir and others 2000), and feline middle ear disease including nasopharyngeal polyps (Allgoewer and others 2000), have been reported. MRI identified neoplastic lesions affecting the inner or middle ear in dogs with peripheral vestibular disease (Garosi and others 2001) and a malignant melanoma in a cat (Allgoewer and others 2000). It is reported to be more sensitive than radiography and more specific than either radiography or CT for the identification of otitis media in the dog and cat, the sensitivity and specificity of these other techniques being particularly compromised in the presence of early or mild changes (Dvir and others 2000) (see Table 7.1).

Using MRI, soft tissue within the TB lumen can be differentiated from fluid as it is visible on both T1 and T2 weighted images and there will be no air-fluid line (Dvir and others

2000). Material within the canine TB was reported to be hyperintense on T2 and isointense with neural tissue on T1 with a hyperintense rim on post contrast T1 (Garosi and others 2000, Garosi and others 2001). In the cat, it was inhomogenous and on T2 weighted images either hyperintense to muscle suggesting it had a high water content which would be compatible with mucosal swelling and / or fluid retention or isointense to the cerebrum and hypointense to the CSF (Allgoewer and others 2000). In another dog, the TB was lined with 2-5mm thick, uneven mucosa with only a small area of central residual air (Dvir and others 2000). On T2 weighted images this mucosa appeared laminated with hyperintense layers indicating a high fluid content consistent with hypervascular tissue, oedema or granulation tissue, and hypointense layers suggesting fibrous tissue indicating chronic changes (Dvir and others 2000).

The TB wall was visible as a fine hypointense line due to the adjacent soft tissue rather than air (Dvir and others 2000). However no abnormalities were identified in the TB wall or the adjacent petrous temporal bones in cases of otitis media in dogs or cats despite the presence of radiographic changes (Allgoewer and others 2000, Dvir and others 2000, Garosi and others 2001).

In cases with otitis externa, the external ear canal was narrowed and lined with 2-4mm soft tissue, the top layer of which was hyperintense in both T1 and T2 weighted images, but more so on T1, indicative of thickened epithelium (Dvir and others 2000). The tissue below appeared hypointense on both T1 and T2, but more so on T2, indicative of fibrous tissue associated with chronic changes. At the medial end of the canal was a hyperintense, thickened hyperplastic membrane obstructing the canal which was thought to be the remains of the tympanic membrane (Dvir and others 2000).

MRI has been used to identify otitis interna in the dog (Garosi and others 2000, Garosi and others 2001) and can also help identify the presence of a brain lesion (Dvir and others 2000). In humans, chronic inflammation can result in fibrous obliteration of the fluid-containing spaces of the inner ear and therefore an absence of the normal high signal (Garosi and others 2000). This absence has also been associated with the presence of otitis interna in dogs (Garosi and others 2000, Garosi and others 2001). However, the normal signal was not always visible in unaffected ears suggesting a lack of sensitivity in the currently utilised MRI protocols (Garosi and others 2001). Contrast enhanced MRI of the

inner ear has been described in humans and may be useful to identify abnormalities such as labyrinthitis. Contrast enhancement on T1 weighted images has been reported in 6 dogs with peripheral vestibular signs indicating otitis interna (Garosi and others 2001) and 2 dogs with 'old dog vestibulitis' (Dayrell-Hart 1997).

7.1.6. Aims

The aims of the work presented in this chapter were to:

- Create a crude cadaver model of one of the major features of acute otitis media, namely fluid accumulation within the middle ear cavity, in the dog, cat and rabbit
- Use this model to assess the relative accuracy of different radiographic views, ultrasound and CT for the identification of fluid within the TB of these species
- Investigate the application of these techniques in live clinical cases of canine otitis media

7.2. Materials and methods

7.2.1. Comparison of imaging techniques in cadavers

7.2.1.1 Preparation of cadaver material

Thirty-three canine cadavers representing a variety of breeds, 42 domestic breed cats and 42 New Zealand White rabbits were selected from the cadavers collected as outlined in Chapter 2. Numbers were determined by availability of material. They were removed from the freezer and placed in cold running water for 24hours until they had defrosted and were then dried thoroughly. All were checked to ensure there was no external evidence of ear or respiratory disease and no abnormalities associated with the external ear or temporal region. Each of them was then labelled with a unique number that accompanied it throughout the study.

A crude model of acute otitis media was created based on the technique used in Chapter 4 whereby fluid was inserted into the TB lumen to confirm the location of the TB on ultrasound images. Ultrasound coupling gel was used and a random number of the TB in each species group were filled. In the dog and rabbit cadavers, this was performed by advancing a Spruell needle along the external ear canal and through the tympanic membrane. Approximately 3-5 ml of gel was then introduced into the middle ear cavity. In the canine cadavers and 17 of the rabbit cadavers, this procedure was only performed in the ears that were filled. In 25 rabbit cadavers, a Spruell needle was passed through the tympanic membrane in both ears whether they were filled or not as a control.

In the cat, the Spruell needle was used to guide an 18gauge 1.5inch needle into the dorsal compartment of the TB. This was then directed ventrally through the septum, causing a cracking sound, and allowed the introduction of approximately 1ml of gel into the ventral compartment. The same needle insertion procedure was followed on all TB whether filled or left empty to eliminate interpretation of fluid-filled TB based on the presence of septal damage. In all species, care was taken to try and avoid concurrent filling of the external ear canal with gel and also contamination of gel onto the hair coat.

Specimens were examined in batches of four and each specimen was examined using radiography, ultrasound and CT in the course of a single day, as outlined below. Following completion of the imaging procedures the cadavers were returned to cold storage at -20°

until frozen. Using the location of the external ear canals as a guide, they were then sectioned transversely at the level of the TB using a bandsaw. The content of each TB was recorded as fluid or gas-filled.

7.2.1.2. Radiography

This was the first procedure to be performed and used the radiographic equipment described in Chapter 3. Time constraints on access to the machine meant that the positioning device created in Chapter 3 could not be used so the cadavers were manually positioned using foam wedges where appropriate.

In the canine cadavers, rostrocaudal open mouth radiographic views were made using exposure settings of 60-66kV and 16 mAs. The heads were secured in a vertical position with the nose pointing towards the X-ray tube and the hard palate and sagittal plane at an angle of 10-20° to the beam as demonstrated in Figure 7.2.1. The jaws were taped open, the tongue was taped to the mandible and the beam was centred on the base of the tongue.

In the feline cadavers, exposure settings of 53kV and 4mAs were used and two projections were produced. A rostrocaudal open mouth view was performed with the heads secured in a vertical position and the nose pointing towards the X-ray tube, in a similar manner to the dog. The hard palate was positioned at an angle 10-20° to the beam with the skull resting on the occiput, and a theoretical line joining the medial canthi of the eyes aligned parallel to the cassette. The mouth was held open with a plastic speculum between the upper and lower left canine teeth. The X-ray beam was centered on the base of the tongue, which was extended rostrally and ventrally and taped in position. A rostro 30° ventro-caudodorsal or ventrodorsal oblique view was then performed with the dorsal aspect of the head resting against a sloped foam wedge, in a similar manner to the rabbit demonstrated in Figure 7.2.2. The hard palate was at an angle of approximately 30° from the vertical, the mouth remained closed and the beam was centred at midline, level with the caudal aspect of the mandible.

In the rabbit cadavers, exposure settings of 57kV and 3.2 mAs were used and four projections were produced, resulting in three views being obtained of each TB. The cadavers were positioned using foam wedges as demonstrated in Figure 7.2.2. A dorsoventral view was obtained by resting the head on the mandibles and centering the

beam on the midline of the head at the level of the external ear canals. A rostro 40° ventro-caudodorsal oblique view was performed by resting the dorsal aspect of the head against a sloped foam wedge so that the hard palate was at an angle of 40° from the vertical. The beam was centred in midline level with the caudal aspect of the mandible. The left and right latero 40° ventro-laterodorsal oblique views were obtained by placing the head into a 90° 'V' shaped trough of foam wedges. The dorsal and right or left side of the head respectively, were in contact with the wedges and the nose and philtrum were used as a reference for the correct angle positioning. The beam was centered over the lower TB.

X-ray marking tape (X-Rite Tape, X-Rite, Inc., Grandville, MI) was used to identify the specimen number in all radiographs and a primary left / right marker was also used. The films were divided into groups by species and projection and each group filed in a separate envelope.

7.2.1.3. Ultrasound imaging

All of the cadaver heads were examined using a Powervision ultrasound machine (Toshiba). A 6.5MHz curvilinear transducer was used to examine the dog heads and a 12MHz linear transducer with a 3cm footprint for the cat and rabbit heads. The hair from each side of the cadaver head was clipped from the region overlying the external ear canal down to the ventral midline. Surgical spirit, then ultrasound coupling medium, were applied to the site to produce optimum acoustic contact between the skin surface and the transducer. Each TB was examined with the cadavers in a sternally recumbent position and the transducer in lateral and ventral positions as described in Chapter 4.

All of the heads were examined by the author (sonographer A), an experienced veterinary sonographer and Diplomat of the Royal College of Veterinary Surgeons (RCVS) and the European College of Veterinary Diagnostic Imaging (ECVDI). Three other sonographers each examined the heads of one species. Sonographer B examined the canine heads, sonographer C the feline ones and sonographer D the rabbit ones. These were veterinary undergraduate students who had no prior experience of using ultrasound but had received an introductory training session in that species prior to the study. The specimen number was entered into the ultrasound machine at the start of each examination and left / right markers added to the screen throughout the procedure as appropriate. The operators were all blinded as to which ears had been filled and also the results of the other examinations. All of the examinations were carried out in isolation and there was no discussion of the

findings. The images were interpreted at the time of the examination and the contents of each TB were recorded as being either gas or fluid-filled. Images of each TB were also captured digitally directly onto the hard drive of the ultrasound machine then transferred electronically onto a personal computer using an optic disc.

7.2.1.4. Computed tomography

CT was performed using an Elscint Exel 2400 elite CT scanner in all of the cat and rabbit cadavers but only 25 of the canine heads due to unexpected limitations on access to the equipment. The cadavers were each placed on the bed resting on their mandibles with their noses directed into the gantry. The specimen number was entered into the CT machine at the start of each examination and a head in/face down setting applied to ensure correct placement of left/right markers on each image. The TB and air-filled external ear canals were identified on the survey views and used as landmarks to plan the location of the slices. In the dog, a single transverse slice with a width of 2.5 mm was made through the TB. On the basis of these results, two transverse sections were performed in the cat and rabbit. These were 2.5mm slices with a 5 mm bed increment in the cat and 1.0mm slices with a 5mm bed increment in the rabbit.

Images were viewed using a window (center of 400-500 HU and a width of 2000-2500 HU), printed using a Kodak Ektascan 2180 Laser Printer and placed in envelopes according to species.

7.2.1.5. Interpretation of radiographs and CT images

The radiographs and CT images were interpreted independently by two experienced radiologists. Radiologist A was a Diplomat of the RCVS and ECVDI while radiologist B was a veterinary diagnostic imaging resident who became a Diplomat of the ECVDI towards the end of the study. The radiologists were blinded as to which ears had been filled and also to the results of the other examinations. The CT images and each radiographic projection group were read independently and it was noted whether each TB appeared to be air or fluid-filled. In the rabbit, the dorsoventral and rostrocaudal views, the dorsoventral and oblique view and the rostrocaudal and oblique view were then interpreted together before all three views were interpreted together.

7.2.1.6. Statistical analysis of results

The accuracy, sensitivity, specificity, positive and negative predictive values for each of the techniques in each of the species was calculated using the chi square analysis and the formulae presented in Table 7.2.1 and as described by Altman (1977). Kappa analysis (k) was performed to determine the inter-observer variance in the interpretation of the radiographs, ultrasound and CT images as described by Altman (1977). The levels of agreement are demonstrated in Table 7.2.2.



Figure 7.2.1. Radiographic positioning of the canine cadaver head for the rostrocaudal open mouth view.

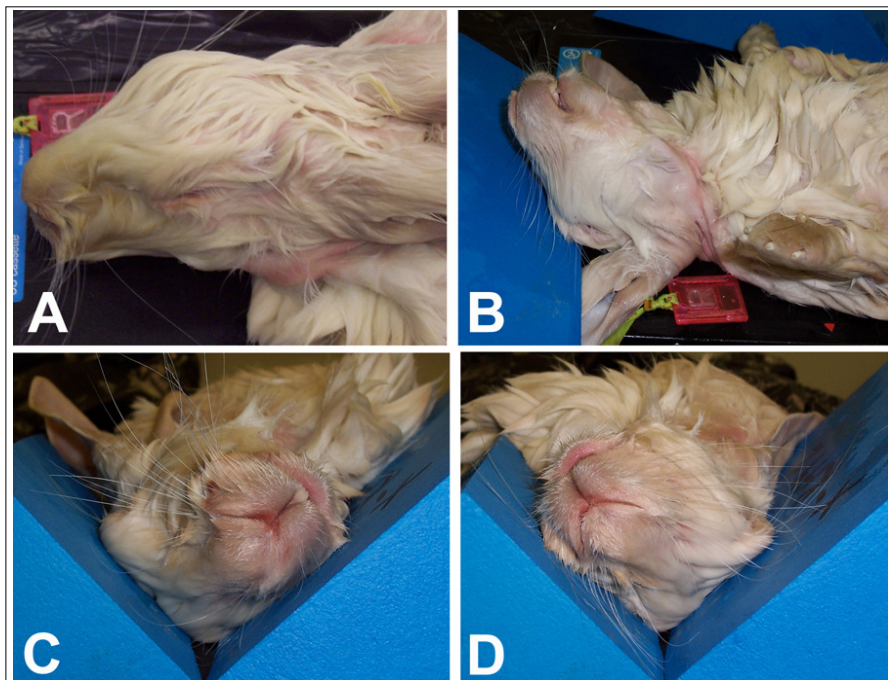


Figure 7.2.2. Radiographic positioning of the rabbit head using foam wedges.

A. Dorsoventral view

B. Rostro-40°C ventro-caudodorsal view oblique view

C. Left lateral 40° ventro-laterodorsal oblique view

D. Right lateral 40° ventro-laterodorsal oblique view

Parameter	Formula
Accuracy =	$\frac{\text{Number of correct diagnoses (gel or air-filled TB)}}{\text{Total number of diagnoses}}$
Sensitivity =	$\frac{\text{Number of true positives (gel filled TB) identified}}{\text{Total number of true positive (gel filled TB) present}}$
Specificity =	$\frac{\text{Number of true negatives (air-filled TB) identified}}{\text{Total number of true negatives (air-filled TB) present}}$
Positive predictive value =	$\frac{\text{Number of true positives (gel filled TB)}}{\text{Total number of positive diagnoses}}$
Negative predictive value =	$\frac{\text{Number of true negatives (air-filled TB)}}{\text{Total number of negative diagnoses}}$

Table 7.2.1. The formulae used to calculate the accuracy, sensitivity, specificity, positive and negative predictive values for each of the techniques (Altman 1997).

K value	correlation
<0.2	minimal agreement
0.2-0.4	poor agreement
0.4-0.6	moderate agreement
0.6-0.8	good agreement
>0.8	excellent agreement

Table 7.2.2. The levels of agreement for Kappa analysis (k) performed to determine the inter-observer variance in interpretation of the imaging procedures carried out.

7.2.2. Comparison of imaging techniques in canine otitis media cases

7.2.2.1. Case selection

Approval was obtained from the University of Glasgow ethics committee prior to this part of the study commencing. Twenty-nine dogs with chronic otitis externa and suspected otitis media that presented to University of Glasgow Small Animal Hospital were entered into this study with informed owner consent. Imaging was performed as part of the normal diagnostic evaluation of these cases.

7.2.2.2. Diagnostic Imaging

Ultrasound examination was performed in all of the cases by sonographer A. The animals were prepared as outlined previously in section 7.2.1.3. and examined in both lateral and sternal recumbency either without sedation or following pre-medication prior to general anaesthesia for further diagnostic workup. A Toshiba Powervision ultrasound machine with a 6.5MHz curvilinear transducer was used. Patient details were entered onto the machine at the start of each examination and appropriate right/left markers added throughout. The examinations were all recorded on Super VHS videotape.

General anaesthesia was induced immediately prior to further imaging in all cases. Radiographic examination was performed using the radiographic equipment described in Chapter 3, manual patient positioning and a table top technique. Optimum exposure factors were determined for each case based on the depth of tissue being penetrated in conjunction with the exposure chart for the machine. Four projections were produced in each case. A dorsoventral view was performed by placing the patient in sternal recumbency, resting the head symmetrically on the mandibles and centering the beam in the middle of the head at the level of the external ear canal. A rostrocaudal open mouth view was obtained by placing the patient in dorsal recumbency and positioning the head and beam as described in section 7.2.1.2. The endotracheal tube was removed immediately prior to exposure and replaced following it. Right and left rostro 20-30° latero-caudolateral oblique views were then performed by placing the animal in right and left lateral recumbency respectively. The nose was raised to the required angle using a foam wedge and the beam centered over the TB nearest the cassette. These oblique views were assessed for superimposition by the contralateral bulla and repeated following repositioning if necessary. This resulted in three views being obtained of each TB. Patient details and left/right markers were present on each film.

CT was performed during the same anaesthesia with the patients in sternal recumbency and using the same equipment and positioning described previously in section 7.2.1.4. Six sequential transverse 2.5mm slices with 2.5mm bed increments were taken through both TB in each case.

Following imaging, appropriate treatment was instigated in each case depending on the findings. The radiographs and CT images were collected, labelled and stored until adequate numbers were obtained for the study to be concluded.

7.2.2.3. Image interpretation and statistical analysis

Ultrasound images were interpreted by sonographer A at the time of the examination. At the end of the study, the videotapes of the examinations were reviewed independently by sonographer C. Sonographer C had participated in the feline cadaver study and received a short training session in the dog. Assessment of the radiographs and CT images were performed following completion of the study by radiologists A and B. Image interpretation of each TB was based on the appearance of the walls and the content of the lumen. Both sonographers and radiologists were blinded as to the case details and the results of the other examinations.

The rostrocaudal open mouth radiographic views were considered independently (RCdOM). The dorsoventral and rostro 20-30° latero-caudolateral oblique views were combined and assessed together (DV & RLOblique). On a different occasion, all three views were considered together by each radiologist (All views). Finally all three views were assessed by consent between both radiologists (All views - Cons). The CT images were assessed initially by each radiologist and then consensually. The results of consensual CT assessment were considered to be the 'gold standard' for this study. Subjective assessment of the severity of CT changes was graded 0 (negative), 1 (mild), 2 (moderate) or 3 (severe).

The level of inter-observer agreement was assessed using kappa analysis statistic (Altman 1997). The levels of agreement are demonstrated in Table 7.2.2. The associations between ultrasonographic, radiographic and CT findings were examined using univariable binary, univariable ordinal or multivariable binary logistic regression as appropriate with a significance value of $p < 0.05$ (Minitab, Minitab Inc).

7.2.3. Investigation of the TB in two Cavalier King Charles Spaniels

Following completion of the clinical study, two Cavalier King Charles Spaniels (CKCS) were presented to the University of Glasgow Small Animal Hospital with neurological signs. Chiari-like syndrome was suspected so an MRI examination was performed using the 1.5Tesla mobile clinical unit and revealed the presence of material within the TB lumen. Ultrasound was performed using the equipment described in Chapter 4 following which surgery was performed to drain the TB. The clinical notes from both of these cases have been removed from the archives and cannot be located so no further clinical information is available.

7.3. Results

7.3.1. Cadaver study

7.3.1.1. Cadaver material

Sixty-six canine TB (33 cadavers) were examined using ultrasound and radiography, 50 of which were also examined using CT. After sectioning with the bandsaw, the findings in five TB (four different cadavers) did not correspond with whether the ear had been filled or not and these TB were excluded from the study. Four of these TB were meant to have been filled but were empty after sectioning while one had not been filled but subsequently was found to contain a significant volume of fluid. Of the remaining 61 TB, 31 had been filled while 30 remained empty. The results from both TB in 29 cadavers remained in the study. Unilateral filling had been performed in 15 of these cadavers and the other 14 had TB that were bilaterally identical (six full and eight empty).

Eighty-four feline TB (42 cadavers) were examined using all modalities. Nine TB (in seven different cadavers) were excluded from the study on the basis of the findings following sectioning. Two of these demonstrated significant damage to the TB that had presumably occurred ante-mortem but had not been identified during the selection process. A further two were almost empty despite supposedly being filled, while five demonstrated post mortem changes that included the accumulation of varying amounts of fluid within the TB. Of the remaining 75 TB, 36 had been filled while 39 remained empty. The results from both TB in 35 cadavers remained in the study. Twenty-four heads were unilaterally filled and the remaining eleven heads were bilaterally identical (five full and six empty).

Eighty-four rabbit TB (42 cadavers) were examined using all modalities. Four TB (in two cadavers) were excluded from the study based on the findings following sectioning. Fluid was absent in two despite filling and a significant amount of post mortem fluid was present in two that were supposedly empty. Of the remaining 80 TB, 47 had been filled while 33 remained empty. Twenty-eight heads were unilaterally filled and the remaining 12 were bilaterally identical (three full and nine empty).

7.3.1.2. Diagnostic Images

7.3.1.2.1. Radiography

Radiographs from a cadaver head of each species are demonstrated in Figure 7.3.1. These demonstrate the typical radiographic appearance of fluid and gas-filled TB using these views. The presence of gel in all species resulted in a diffuse, subtle increase in soft tissue opacity throughout the TB lumen. This was particularly evident when compared with the more lucent lumen of the contralateral gas-filled TB. The damage to the septum bullae of the cat was not clearly evident in any of the radiographs.

In the rostrocaudal open mouth views of the dog and cat skulls, the normal air-filled TB appeared as a distinctive hemispherical structure projecting from the ventral surface of the temporal bone and overlying the soft tissue of the pharynx. The surrounding bone wall was smooth, thin and complete with a radiolucent lumen. In the cat, the septum was visible as a thin curved bone, which divided TB transversely into dorsal and ventral compartments. The rostro 10° ventro-caudodorsal oblique view in the cat projected the TB between the petrous temporal bone rostrally and the occipital condyles caudomedially. Most of the ventral compartment was clearly visible overlying the soft tissue of the neck. Although the dorsal compartment was superimposed onto the occipital bone it was still clearly visible as it remained free from the dense bone of the petrous temporal region. The septum was again clearly visible separating the two areas.

The dorsoventral view in the rabbit projected the caudal aspect of the TB onto the dense petrous temporal bone but the rostral portions were more clearly visible with the wall appearing as a thin curved radio-opaque line. The rostro 40° ventro-caudodorsal oblique view projected the TB caudal to the mandible and directly over the petrous temporal bone. The walls appeared thick and less of the lumen was visible. The left latero 40° ventro-laterodorsal oblique view projected almost the entire right TB free from superimposition on the skull. The bone tube of the external acoustic meatus was projected end-on and therefore appeared as a distinctive radio-opaque circular structure with a more lucent lumen that overlay the dorsal aspect of the TB lumen, therefore enhancing its visualisation.

7.3.1.2.2. Ultrasound

Ultrasound images from a cadaver head of each species are demonstrated in Figure 7.3.2. These demonstrate the typical sonographic appearance of fluid and gas-filled TB using a ventral long axis approach. The near wall of the empty TB reflected a portion of the beam to produce a hyperechoic convex interface. The remainder of the beam was then reflected from the surface of the gas within the lumen, which contributed to the hyperechoic interface and also produced a 'dirty' distal acoustic shadow. In some air-filled TB ring down artefact was also noted. The far and side walls of the TB were obscured as were structures located deep to it.

In the presence of gel, the portion of the beam penetrating the TB wall was propagated through the lumen, which appeared as an anechoic oval shaped region beyond the hyperechoic interface of the near wall. In the dog and rabbit, the far wall of the TB became visible as a concave hyperechoic interface, which could be easily differentiated from the convex lines representing ring down artefact produced by the gas-filled TB. In the cat, it was the septum rather than the far wall of the TB that became visible through the fluid.

7.3.1.2.3. CT

CT images from a cadaver head of each species are demonstrated in Figure 7.3.3 and demonstrate the typical CT appearance of fluid and gas-filled TB. In all three species, the bone wall of the TB appeared as a smooth, well defined, hyperdense structure. The bony septum in the cat was evident as a curved hyperdense line crossing the TB obliquely. The normal gas-filled lumen appeared black. Gel produced a homogenous, hypodense fluid opacity occupying the lumen and the presence of any gas bubbles within it appeared as black areas.

Figure 7.3.1. Radiographs of canine, feline and rabbit cadaver heads with a fluid-filled left TB and a gas-filled right TB. L = left; R=right



Figure 7.3.1.1. Canine cadaver.
Rostrocaudal open mouth view

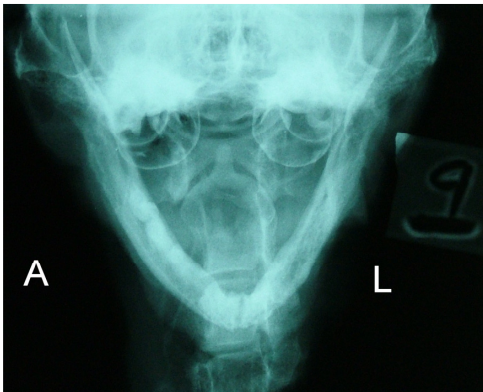


Figure 7.3.1.2. Feline cadaver.
A: Rostrocaudal open mouth view
B: Rostro 30° ventro-caudodorsal oblique view



Figure 7.3.1. continued. Radiographs of canine, feline and rabbit cadaver heads with a fluid-filled left TB and a gas-filled right TB. L = left

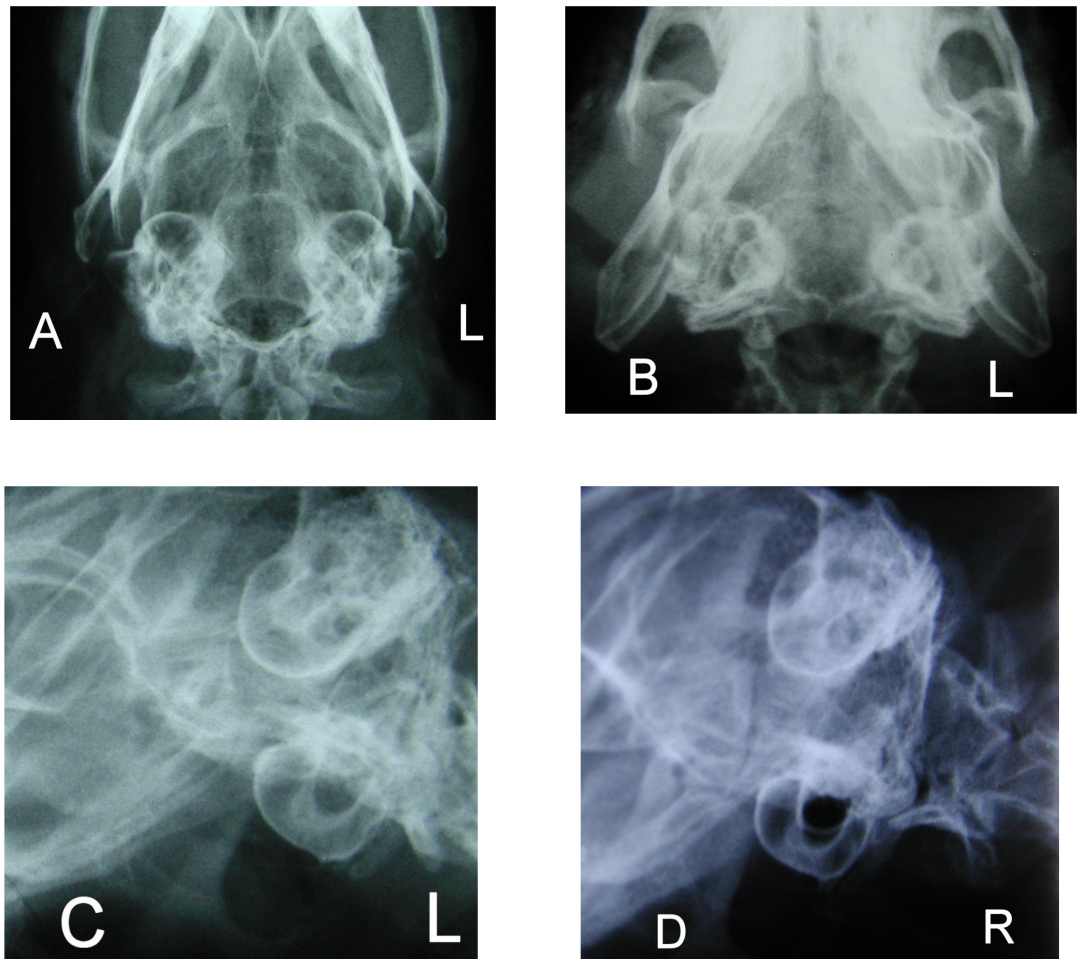


Figure 7.3.1.3. Rabbit cadaver.

A: Dorsoventral view

B: Rostro 40° ventro-caudodorsal oblique view

C: Left latero 40° ventro-laterodorsal oblique view

D: Right latero 40° ventro-laterodorsal oblique view

Figure 7.3.2. Ultrasound images of canine, feline and rabbit cadaver heads with a fluid-filled left TB and a gas-filled right TB. L = left; R=right

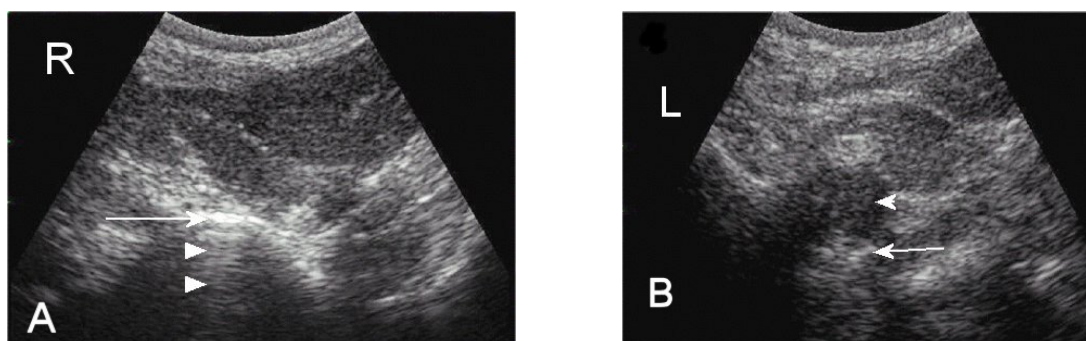


Figure 7.3.2.1. Canine cadaver. Long axis views from a ventral approach

A: Gas-filled TB. Arrow heads = reverberation artefact in the lumen.

Arrow = ventral wall of TB

B: Fluid-filled TB. Arrow head =anechoic fluid within lumen. Arrow = far wall of TB.

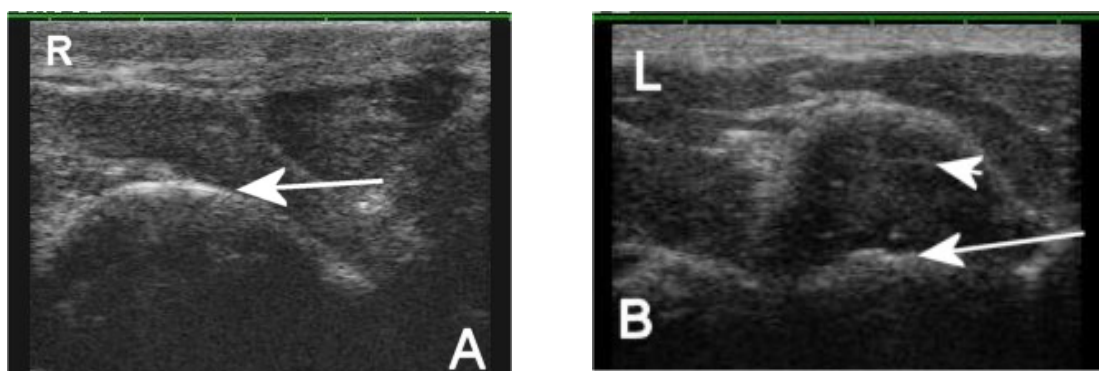


Figure 7.3.2.2. Feline cadaver. Long axis views from a ventral approach

A: Gas-filled TB. Arrow = ventral wall of TB

B: Fluid-filled TB. Arrow head =anechoic fluid within lumen.

Arrow = far wall of TB.

Figure 7.3.2. continued. Ultrasound images of canine, feline and rabbit cadaver heads with a fluid-filled left TB and a gas-filled right TB. L = left; R=right

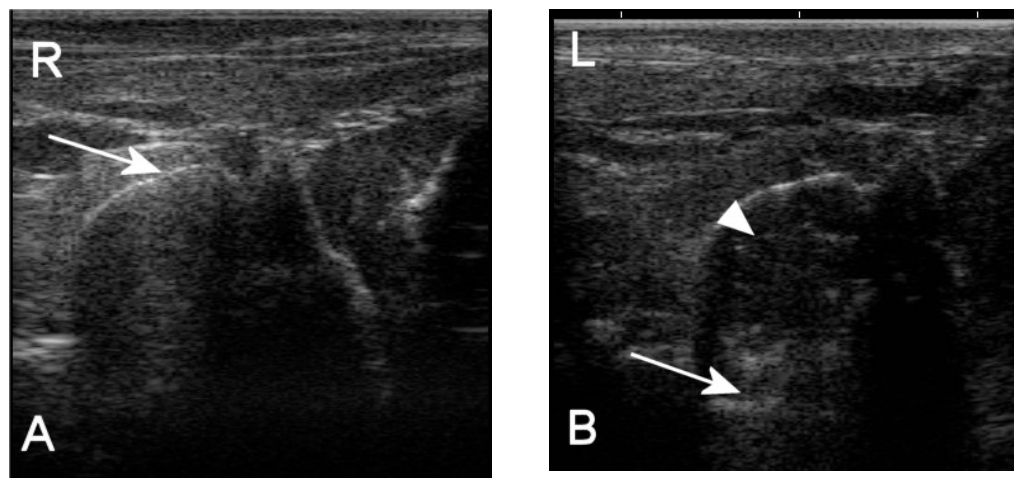


Figure 7.3.2.3. Rabbit cadaver. Long axis views from a ventral approach

A: Gas-filled TB. Arrow = ventral wall of TB

B: Fluid-filled TB. Arrow head =anechoic fluid within lumen.

Arrow = far wall of TB.

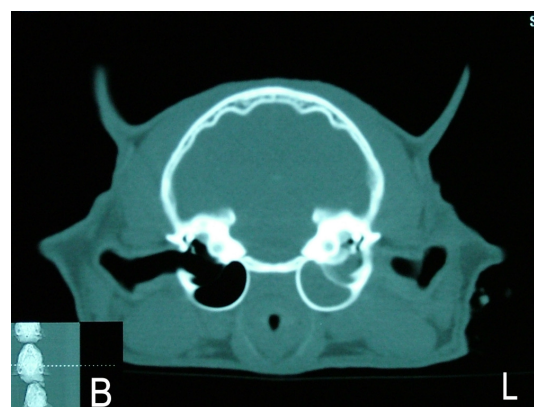
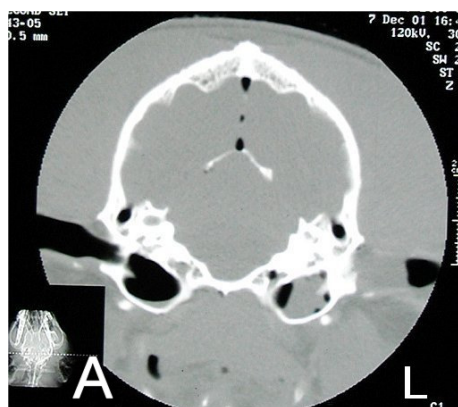


Figure 7.3.3. CT images of cadaver heads with a fluid-filled left TB and a gas-filled right TB.

L = left; R = right

A: Canine

B: Feline

C: Rabbit

7.3.1.3. Statistical analysis

7.3.1.3.1. Canine cadavers

The accuracy, sensitivity, specificity, positive and negative predictive values for each of the techniques in the dog are presented in Table 7.3.1. There was moderate agreement between the radiologists' interpretation of the radiographs ($k=0.6$), a moderate agreement ($k=0.5$) between the sonographers' results and perfect agreement ($k=1$) for interpretation of the CT images.

Of the 15 heads that were unilaterally filled, 6 of these (40%) were correctly identified by radiologist A, 6 (40%) by radiologist B, 12 (80%) by sonographer A and 10 (67%) by sonographer B. In the 14 heads that had bilaterally identical TB (six full and eight empty), 6 (43%) were correctly identified by radiologist A, 3 (21%) by radiologist B, 9 (64%) by sonographer A and 8 (57%) by sonographer B.

7.3.1.3.2. Feline cadavers

The accuracy, sensitivity, specificity, positive and negative predictive values for each of the techniques in the cat are presented in Table 7.3.2. There was good agreement between the radiologists' interpretation of the rostrocaudal open mouth views ($k=0.68$) and their interpretation of the ventrodorsal oblique views ($k=0.76$). There was excellent agreement ($k=0.89$) between the sonographers' results and perfect agreement ($k=1$) for interpretation of the CT images.

Of the 24 heads that were unilaterally filled, all of these were correctly identified by both radiologists on the ventrodorsal oblique view and both sonographers. Only 21 (87.5%) were correctly identified using the rostrocaudal open mouth view by radiologist A and 19 (80%) by radiologist B, with either the wrong TB or both TB being identified as full. In the eleven heads that had bilaterally identical TB (five full and six empty), the rostrocaudal open mouth view as interpreted by radiologist A correctly identified this in five (45%) and by radiologist B in eight (73%) including all the full ones. The ventrodorsal oblique view interpreted by radiologist A only correctly identified three (27%) which were all bilaterally empty while the same view interpreted by radiologist B correctly identified eight (73%), again including all five full ones. Nine (82%) were correctly identified by both sonographers, with A identifying all six empty ones and C all five full ones.

7.3.1.3.3. Rabbit cadavers

The accuracy, sensitivity, specificity, positive and negative predictive values for each of the techniques in the rabbit are presented in Table 7.3.3. There was excellent agreement between the radiologists' interpretation of the dorsoventral views ($k=0.82$), good agreement for the ventrodorsal oblique views ($k=0.65$) and moderate agreement for the lateral oblique views ($k=0.5$). Good agreement was observed between radiologists when the views were combined ($k=0.75, 0.77, 0.8$ and 0.75), with the combination of the dorsoventral and ventrodorsal obliques producing a result verging on excellent ($k=0.8$). There was an excellent agreement ($k=0.89$) between the sonographers' results and again perfect agreement ($k=1$) for the interpretation of the CT images.

Of the 28 heads that were unilaterally filled, 25 (90%) were correctly identified by radiologist A and 23 (82%) by radiologist B using the dorsoventral view, 22 (79%) by radiologist A and 23 (82%) by radiologist B using the ventrodorsal oblique view and 18 (64%) and 22 (79%) respectively using the latero 40° ventro-laterodorsal oblique view. Twenty-seven (96%) were correctly identified by sonographer A and 26 (93%) by sonographer D. In the twelve heads that had bilaterally identical TB (three full and nine empty), the dorsoventral view as interpreted by radiologist A was able to correctly identify six (50%), including all the bilaterally full TB, while radiologist B correctly identified seven (58%). Radiologist A correctly identified seven (58%) using the ventrodorsal oblique view, which included none of the bilaterally full TB, while radiologist B identified four (33%). Using the latero 40° ventro-laterodorsal oblique view radiologist A identified seven (58%) correctly, again including all of the bilaterally full TB, and radiologist B six (50%). Eleven (92%) were correctly identified by sonographer A, including all the bilaterally full TB, and all were correctly identified by sonographer D.

Canine	Accuracy (%)	Sensitivity (%)	Specificity (%)	PPV (%)	NPV (%)	k value
RCdOM – Rad A	56	60	52	55	57	
RCdOM – Rad B	56	57	55	55	57	0.6
Sonographer A	82	90	74	77	88	
Sonographer B	75.5	80	74	75	80	0.5
CT A	83	67	100	100	74	
CT B	83	67	100	100	74	1.0

Table 7.3.1. Accuracy, sensitivity, specificity, positive (PPV) and negative predictive values (NPV), and inter-observer agreement (k=kappa) calculated for each of the techniques used to identify fluid within the TB in canine cadavers. RCdOM = rostrocaudal open mouth view. Rad = radiologist.

Feline	Accuracy (%)	Sensitivity (%)	Specificity (%)	PPV (%)	NPV (%)	K value
RCdOM – Rad A	83	83	82	83	82	
RCdOM – Rad B	74	72	77	79	71	0.68
VDOblique – Rad A	87	86	87	88	85	
VDOblique – Rad B	82	75	90	90	76	0.76
Sonographer A	96	85	100	100	93	
Sonographer B	96	100	92	92	100	0.89
CT A	100	100	100	100	100	
CT B	100	100	100	100	100	1

Table 7.3.2. Accuracy, sensitivity, specificity, positive (PPV) and negative predictive values (NPV), and inter-observer agreement (k=kappa), calculated for each of the techniques used to identify fluid within the TB in feline cadavers. RCdOM = rostrocaudal open mouth view. VDOblique = rostro 10° ventro-caudodorsal or ventrodorsal oblique view. Rad = radiologist.

Rabbit	Accuracy (%)	Sensitivity (%)	Specificity (%)	PPV (%)	NPV (%)	k value
DV– Rad A	77.5	77.8	80	85.4	71.8	
DV– Rad B	81.25	79	85	88	74	0.82
VDOblique – Rad A	73.75	71.1	80	84.2	66.7	
VDOblique – Rad B	81.25	77	88	90	73	0.65
LVOblique – Rad A	76.25	68.9	88.6	91.2	67.4	
LVOblique - RadB	81.25	83	79	85	76	0.5
DV & VDOblique – Rad A	78.75	82.2	77.1	84.1	75	
DV & VDOblique – Rad B	86.25	81	94	95	78	0.8
DV & LVOblique – Rad A	78.75	82.2	74.3	84.1	72.2	
DV & LVOblique – Rad B	83.75	81	88	90	76	0.75
VDOblique & LVOblique – Rad A	83.75	88.9	77.1	87	79.4	
VDOblique & LVOblique – Rad A	82.5	85	79	85	79	0.77
All views – Rad A	85	84.4	85.7	92.7	77	
All views – Rad B	85	85	85	89	80	0.75
Sonographer A	97.5	100	95	95	100	
Sonographer B	97.5	95	100	100	95.5	0.89
CT A	100	100	100	100	100	
CT B	100	100	100	100	100	1

Table 7.3.3. Accuracy, sensitivity, specificity, positive (PPV) and negative predictive values (NPV), and inter-observer agreement (k=kappa), calculated for each of the techniques used to identify fluid within the TB in rabbit cadavers. DV = dorsoventral view. VDOblique = rostro 40° ventro-caudodorsal or ventrodorsal oblique view. LVOblique = latero 40° ventro-laterodorsal oblique view. Rad = radiologist.

7.3.2. Clinical case series study

Fifty-eight ears were assessed in 29 dogs. Based on the results from the consensual interpretation of the CT images, 27 (46.6%) TB were considered abnormal. Twenty-three of these had content changes and 21 had wall changes on the CT images.

The results for accuracy, sensitivity, specificity, positive predictive value, negative predictive value and interobserver agreement (kappa) for the combined identification of TB wall and lumen changes using each of the imaging procedures performed are summarised in Table 7.3.4. Inter-observer agreement was highest for CT assessment, but was still only moderate ($k=0.58$). Levels of inter-observer agreement for radiographic views were poor, with the exception of the combination of the dorsoventral view lateral oblique views, which was moderate ($k=0.46$). Inter-observer agreement between sonographers was minimal. Inter-observer agreements for the independent identification of TB wall and content changes for each of the techniques is demonstrated in Table 7.3.5. Agreement was better for lumen content changes using CT and wall changes on all of the radiographic views. Sonographer B did not identify any wall changes therefore agreement between the sonographers for this parameter could not be calculated. This will also have influenced the combined result presented in Table 7.3.4.

The univariable binary logistic regression analysis of the association between consensus CT and radiographic assessments is demonstrated in Table 7.3.6. There was a significant association between the radiographic identification of both content and wall changes and the subsequent identification of similar changes on CT. This was further increased when the identification of both content and wall changes were combined. Table 7.3.7 demonstrates the univariable binary logistic regression analysis of the association between consensual CT and radiologist A's interpretation of each radiographic view, with radiologist B's results in Table 7.3.8. There was a significant correlation between all of the views and the CT results for both radiologists. However, when interpreted by radiologist A, the rostrocaudal open mouth view appeared particularly good for the identification of bone changes and the combination of views for soft tissue changes, while these provided the poorest results when interpreted by radiologist B.

The association between consensus CT and sonographer A's interpretation is demonstrated in Table 7.3.9. Sonographer B's results were not included in this calculation due to the inability to identify wall changes. There was no correlation between the sonographic identification of content changes and subsequent CT findings but there was with regard to wall changes and therefore the combination of the findings. There was no correlation between the consensus radiographic and sonographer A's results for any of the features as demonstrated in Table 7.3.10.

The multivariable binary logistic regression analysis of the association between consensus CT, consensus radiographic and sonographer A's results are demonstrated in Table 7.3.11. Consensual CT assessment of content and wall changes was significantly associated with both radiographic and sonographic interpretation indicating that the CT outcome was best predicted by a combination of radiographic and sonographic findings but only when both content and wall changes were included.

The univariable ordinal regression analysis of the association between the consensual CT grade and the consensual radiographic and sonographer A's assessment is demonstrated in Table 7.3.12. Detection of radiographic changes was significantly associated with increasing severity of disease as was the identification of content changes on ultrasound and the combination of content and wall changes.

Imaging technique	Accuracy (%)	Sensitivity (%)	Specificity (%)	PPV (%)	NPV (%)	k value
RCdOM – Rad A	62	67	58	58	67	
RCdOM – Rad B	76	70	81	76	76	0.25
DV & RLOblique – Rad A	76	96	58	67	95	
DV & RLOblique – Rad B	83	82	84	82	84	0.46
All views – Rad A	64	78	52	59	73	
All views - RadB	81	82	81	79	83	0.32
All views (Cons)	76	85	68	70	84	
Sonographer A	64	74	55	59	77	
Sonographer B	57	37	74	56	72	0.16
CT A	88	85	90	89	88	
CT B	88	85	90	89	88	0.58

Table 7.3.4. Accuracy, sensitivity, specificity, positive (PPV) and negative predictive values (NPV), and inter-observer agreement (k=kappa), calculated for the identification of combined TB wall and lumen changes in canine cases of otitis media, compared with the ‘gold standard’ of consensual CT interpretation. RCdOM = rostrocaudal open mouth view. DV = dorsoventral view. RLOblique = rostro 20-30° latero-caudolateral oblique view. Rad = radiologist. Cons = consensual interpretation.

Imaging technique	k value	Imaging technique	k value
<u>TB contents</u>		<u>TB wall</u>	
RCdOM	0.28	RCdOM	0.67
DV & RLOblique	0.22	DV & RLOblique	0.48
All views	0.37	All views	0.53
Ultrasound	0.23	Ultrasound	*
CT	0.82	CT	0.44

Table 7.3.5. Inter-observer agreement (k=kappa), calculated for the independent identification of TB wall and lumen changes using each of the imaging techniques. RCdOM = rostrocaudal open mouth view. DV = dorsoventral view. RLOblique = rostro 20-30° latero-caudolateral oblique view. * not calculated as sonographer B found no abnormal wall changes

Variable	OR	95% CI	p value
CT(Cons) content versus All views (Cons) content	10.07	2.67-38.02	0.001
CT(Cons) wall versus All views (Cons) wall	11.08	2.74-44.75	0.001
CT(Cons) content and wall versus All views (Cons) content and wall	12.07	3.29-44.38	<0.001

Table 7.3.6. Univariable binary logistic regression analysis of the association between consensual CT and radiographic interpretation. (Cons) = consensual. OR = odds ratio. CI = confidence interval. Significance $p < 0.05$.

Variable	OR	95% CI	p value
CT (Cons) content versus Rad A - RCdOM content	5.33	1.61-17.64	0.006
Rad A - DV & RLOblique content	7.84	2.27-27.08	0.001
Rad A - All views content	64.00	11.63-352.17	<0.001
CT (Cons) wall versus Rad A - RCdOM wall	49.08	8.97-268.46	<0.001
Rad A - DV & RLOblique wall	14.40	3.96-52.39	<0.001
Rad A - All views wall	14.25	3.98-50.98	<0.001
CT (Cons) wall and content versus Rad A - RCdOM content and wall	18.00	4.81-67.39	<0.001
Rad A - DV & RLOblique content and wall	18.20	4.87-68.05	<0.001
Rad A - All views wall content and wall	41.40	8.91-192.27	<0.001

Table 7.3.7. Univariable binary logistic regression analysis of the association between consensual CT and radiologist A's interpretation of each radiographic view. OR = odds ratio. CI = confidence interval. Significance $p < 0.05$. RCdOM = rostrocaudal open mouth view. DV = dorsoventral view. RLOblique = rostro 20-30° latero-caudolateral oblique view. Rad = radiologist. Cons = consensual interpretation.

Variable	OR	95% CI	p value
CT (Cons) content versus			
Rad B - RCdOM content	5.50	1.72-17.57	0.004
Rad B - DV & RLOblique content	5.50	1.72-17.57	0.004
Rad B - All views content	3.08	1.01-9.34	0.047
CT (Cons) wall versus			
Rad B - RCdOM wall	7.00	1.88-26.10	0.004
Rad B - DV & RLOblique wall	10.82	2.19-53.51	0.003
Rad B - All views wall	11.67	2.84-47.89	0.001
CT (Cons) wall and content versus			
Rad B - RCdOM content and wall	3.39	1.10-9.80	0.033
Rad B - DV & RLOblique content and wall	4.85	1.36-17.31	0.015
Rad B - All views wall content and wall	3.33	1.06-10.48	0.039

Table 7.3.8. Univariable binary logistic regression analysis of the association between consensual CT and radiologist B's interpretation of each radiographic view. OR = odds ratio. CI = confidence interval. Significance $p < 0.05$. RCdOM = rostrocaudal open mouth view. DV = dorsoventral view. RLOblique = rostro 20-30° latero-caudolateral oblique view. Rad = radiologist. Cons = consensual interpretation.

Variable	OR	95% CI	p value
CT(Cons) content versus			
Sonographer A content	1.75	0.52-5.89	0.366
CT(Cons) wall versus			
Sonographer A wall	3.39	1.11-10.35	0.032
CT(Cons) content and wall versus			
Sonographer A content and wall	3.47	1.14-10.57	0.029

Table 7.3.9. Univariable binary logistic regression analysis of the association between consensual CT and sonographers A's interpretation. (Cons) = consensual. OR = odds ratio. CI = confidence interval. Significance $p < 0.05$.

Variable	OR	95% CI	p value
All views (Cons) content versus Sonographer A content	1.48	0.41-5.32	0.547
All views (Cons) wall versus Sonographer A wall	1.59	0.56-4.56	0.385
All views (Cons) content and wall versus Sonographer A content and wall	1.62	0.56-4.65	0.374

Table 7.3.10. Univariable binary logistic regression analysis of the association between consensual radiographic and sonographers A's interpretation. (Cons) = consensual. OR = odds ratio. CI = confidence interval. Significance $p < 0.05$.

Variable	OR	95% CI	p value
CT (Cons) content versus All views (Cons) content Sonographer A content	9.95	2.62-37.76	0.001
CT (Cons) wall versus All views (Cons) wall Sonographer A wall	11.6	2.7-49.82	0.001
CT (Cons) content and wall versus All views (Cons) content and wall Sonographer A content and wall	13.03	3.29-51.67	<0.001
	3.95	1.05-14.85	0.042

Table 7.3.11. Multivariable binary logistic regression analysis of the association between consensual CT, and consensual radiographic and sonographers A's interpretation. (Cons) = consensual. OR = odds ratio. CI = confidence interval. Significance $p < 0.05$.

Variable	OR	95% CI	p value
CT (Cons) grade versus			
All views (Cons) content	12.57	3.77-41.94	<0.001
All views (Cons) wall	9.28	2.84-30.39	<0.001
All views (Cons) content and wall	11.59	3.26-41.22	<0.001
CT (Cons) grade versus			
Sonographer A content	3.38	1.09-10.46	0.035
Sonographer A wall	2.25	0.83-6.09	0.111
Sonographer A content and wall	3.69	1.25-10.85	0.018

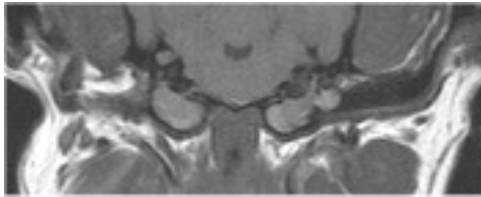
Table 7.3.12. Univariable ordinal regression analysis of the association between increasing CT grade and radiographic and sonographers A's results interpretation. (Cons) = consensual. OR = odds ratio. CI = confidence interval. Significance $p < 0.05$.

7.3.3. Investigation of the TB in two Cavalier King Charles Spaniels

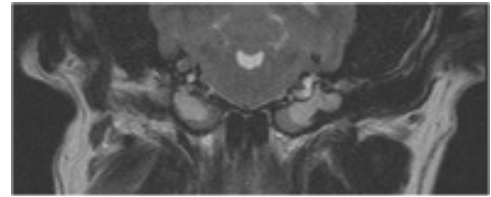
The MR images from these cases are presented in Figure 7.3.4. In case one, the lumen of both TB were completely filled with material. This produced two different intensities on the image with the material located towards the ventromedial aspect of the lumen being hypointense compared to the remainder of the fluid. However, both regions were relatively homogenous and there was a distinct boundary between them. This was particularly evident on the T2 weighted transverse image. In case two, one TB lumen was full while the other contained only a small amount of fluid located caudally. The material in this case appeared homogenous on the T2 weighted images but slightly heterogenous in the T1 weighted ones.

The typical ultrasound appearance of the three full TB in these cases is presented in Figure 7.3.5. The material produced a more echogenic appearance on the ultrasound image than that associated with the presence of ultrasound gel. However, it remained relatively homogenous and still permitted penetration of the beam such that the far wall of the TB could be visualised as a concave, hyperechoic interface. The small volume of fluid within the fourth TB was not identified during the ultrasound examination and produced the appearance typical of an empty TB, as demonstrated in Chapter 4.

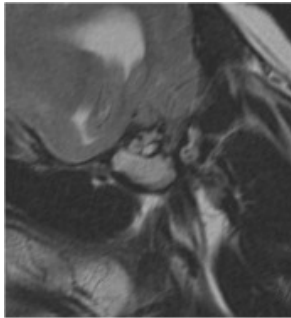
Following surgery, the appearance of the material removed from the TB lumen is demonstrated in Figure 7.3.6. Analysis of the material will have yielded further information regarding its composition but these results have been lost with the case records. Both cases recovered well in the short term but information regarding longer term follow-up is also absent.



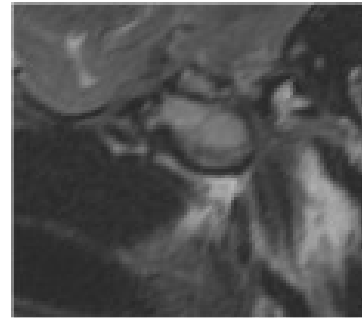
Case 1. T1 weighted transverse image



Case 1. T2 weighted transverse image



Case 1. T2 weighted sagittal image left TB



Case 1. T2 weighted sagittal image right TB



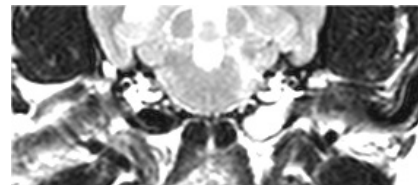
Case 1. T1 weighted dorsal image



Case 1. T2 weighted dorsal image



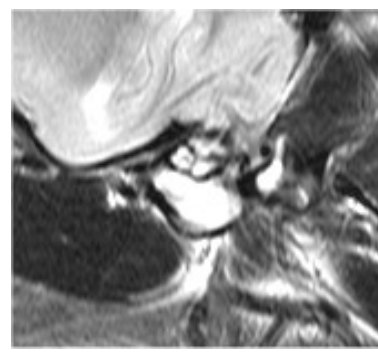
Case 2. T1 weighted transverse image



Case 2. T2 weighted transverse image



Case 2. T1 weighted sagittal image left TB



Case 2. T2 weighted sagittal image left TB

Figure 7.3.4. Images of the TB in CKCS undergoing MRI examination for the investigation of neurological signs thought to be associated with Chiari-like syndrome.

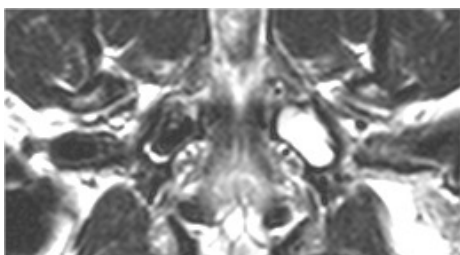
Figure 7.3.4. continued. Images of the TB in CKCS undergoing MRI examination for the investigation of neurological signs thought to be associated with Chiara-like syndrome.



Case 2. T2 weighted sagittal image right TB



Case 2. T2 weighted sagittal image right TB



Case 2. T2 weighted dorsal image

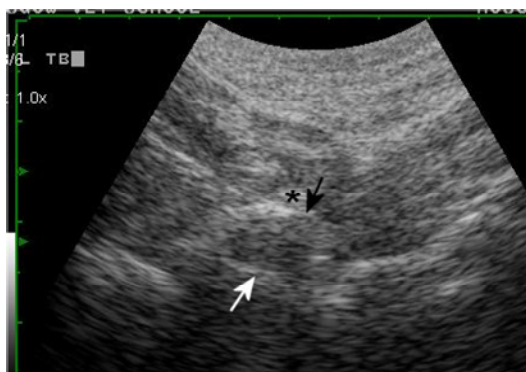


Figure 7.3.5. Ultrasound image of the left TB of a Cavalier King Charles Spaniel with fluid in the TB lumen identified during an MRI examination. Black arrow = near TB wall; White arrow = far TB wall; * = stylohyoid bone



Figure 7.3.6. The material that was subsequently removed from the TB.

7.4. Discussion

7.4.1. Material and technical considerations

The presence of fluid within the TB lumen is a common change associated with acute otitis media and often occurs prior to the development of more chronic secondary changes involving the wall (Smith and Webster 1925, Geary 1965, Gibbs 1978, Tojo and others 1985). The introduction of material into the TB lumen of dog and rabbit cadavers was a very straightforward procedure to perform and provided a crude model for this condition in these species, characterised by the presence of material within the TB lumen in the absence of wall changes. The need to penetrate the septum in the cat made the procedure a bit more difficult to perform and resulted in iatrogenic damage to the structure although the external wall remained unaffected and therefore the model was still felt to be appropriate in this species also.

The use of cadavers in place of live animals to produce images of normal structures and investigate imaging phenomenon can be justified on ethical, financial and logistic grounds (Jones and others 1995, Barthez and others 1996, Weller and others 1999a, Morrow and others 2000). Fluid has been introduced through the intact tympanic membrane and into the TB lumen of normal, live dogs to investigate ultrasound examination of the middle ear cavity (Lee and others 2006). However, in the present study it was felt that the performance of such an invasive and undoubtedly painful procedure could not be justified in live dogs or rabbits when an acceptable cadaver alternative existed. The additional damage induced in the feline model means that this procedure will never be justifiable for use in live animals.

One potential problem with the use of cadaver material however, is the lack of clinical history (Tasaki and Westesson 1993). In the present study, TB damage was present in two cats that was not identified during the selection procedure and was only revealed on sectioning, resulting in exclusion from the study. This highlights the importance of employing control measures to ensure that the cadaver material selected is consistent and representative.

Ultrasound gel is viscous and designed to adhere to surfaces. This was used to fill the TB rather than water in an effort to ensure that the TB remained full throughout the series of examinations, despite repeated handling and repositioning of the heads. Although this was effective in most of the cadavers, the gel was absent from four canine, two feline and two

rabbit TB by the time of freezing, most likely due to leakage out through the perforated tympanic membrane. In addition, unfilled canine, feline and rabbit TB had also accumulated a significant volume of fluid by the time of freezing presumably as a result of post mortem change. This represented another of the problems associated with the use of cadavers where post mortem change can alter the appearance of the area of interest, or mimic anatomical structures or pathology (Weller and others 1999a). Examinations in fresh cadavers should be performed as soon after death as possible (Rodríguez and others 2002, Soler and others 2002). However, access to the imaging equipment used in the present study was limited due to its location in a busy veterinary hospital and the most efficient way to perform this study was therefore to prepare and examine the material in batches. It was then necessary to freeze the accumulated material until the relevant part of the study to prevent marked post mortem tissue degeneration. The results of this study highlight the importance of incorporating control measures to ensure that the material remains in a consistent state throughout the duration of the study period. However, the majority of the material remained suitable for inclusion in the study thereby justifying the use of cadaver material for this purpose.

Another consideration in this type of study is that the same procedure must be performed in all material so that any conclusions reached are based strictly on the stated criteria and are not influenced by the observation of incidental findings. The amount of gel introduced into the TB lumen was limited to reduce the chances of accumulation in the external ear canal that might have provided extraneous information to the observers as to whether the TB had been filled or not. Likewise, the septum bulla was penetrated in all cats and both tympanic membranes punctured in a number of rabbits whether the TB was filled or not to ensure all material would appear the same.

7.4.2. Technical considerations of the diagnostic imaging procedures

Fluid and soft tissue produce the same opacity on radiographs (Curry and others 1990). The presence of a wet hair coat in animals being radiographed can therefore result in an increased opacity or streaking on the resulting image. The performance of an ultrasound examination requires the elimination of air between the transducer and skin surface and this is usually achieved by clipping a patch of hair and then thorough wetting of the skin surface by the application of ultrasound gel (Nyland and others 1995). Contamination of adjacent hair is likely during the examination and complete physical removal of the gel

after the examination has been completed is impossible. Since ultrasound gel is fluid based, it also has the potential to produce artefacts on subsequent radiographs that could interfere with interpretation. For this reason, radiography was always performed prior to the ultrasound examination in this study. Although ultrasound gel will produce similar artefacts on CT images, the sectional formation of the images means it will not be superimposed over the area of interest and is therefore unlikely to interfere with interpretation of the images.

The radiographic views selected for use in this chapter were based on those recommended in the literature for the investigation of clinical cases of otitis media and also those that can be easily and repeatably positioned in live animals. The rostrocaudal open mouth view is generally considered best for demonstrating the TB in dogs as it is easy to position and allows comparison of both TB on a single film free from superimposition onto the dense petrous temporal bone (Gibbs, 1978, Love and others 1995). A rostro 10° ventral-dorsocaudal oblique view was also performed in the cat cadavers as this is reportedly easier to perform in this species (Hofer and others 1995). Besides the dorsoventral view, there are no specific projections recommended for investigation of the TB in rabbit. Based on the findings in Chapter 3, the rostro 10° ventral-dorsocaudal oblique view was unlikely to be of use in the rabbit so the rostro 40° ventro-caudodorsal oblique was selected as being the nearest equivalent. The latero 40° ventro-laterodorsal oblique views were selected as being among the most useful of the long axis views. These views proved easy to position using wedges and there was some flexibility in the exact degree of angulation required which should facilitate positioning in live animals. The lower TB was projected free from superimposition and the end-on projection of the external acoustic meatus enhanced visualisation of the TB lumen.

The intention was to completely fill each TB with ultrasound gel and this produced a distinctive anechoic appearance on the ultrasound images with a uniform distribution that permitted through transmission of the beam and visualisation of the far wall of the TB. However, it has been suggested that the TB in canine otitis media cases may contain denser, tenacious material that may be located in focal accumulations, making it easier to overlook (Griffiths and others 2003) and it is likely that this also applies to the cat and rabbit. However, ultrasound was able to identify mucosal thickening, focal soft tissue masses and complex fluid collections in the human sinus (Nelson and others 1990) so it

seems likely that it will be able to identify the fluid associated with otitis media in the dog, cat and rabbit although further work would be required to confirm this. Another potential limitation in the cat is the inability to image the contents of the dorsal compartment using this technique, as determined in Chapter 4. This is also likely to have implications in clinical cases since otitis media in cats commonly arises in association with a nasopharyngeal polyp and these are usually located in the dorsal compartment (Gotthelf 2004). Their presence may therefore go undetected using this technique unless there is concurrent otitis media and accumulation of material in the ventral compartment. Although in the present study, fluid could be identified in the TB lumen with the cadavers in a lateral recumbent position, it may be that in clinical cases, animals should be examined in sternal recumbency with the transducer applied ventrally in order to increase the chances of material being identified although further work would be required to confirm this.

On the pilot CT images, the gas-filled external ear canals were used as landmarks to guide placement of the slices. However, given the association between the presence of otitis externa and otitis media, particularly in the dog (Shell 1988), this may not always be possible in clinical cases. Slice thicknesses of 1-3mm have been recommended for CT imaging of the TB (Hoskinson 1993, Love and others 1995, Barthez and others 1996, Seitz and others 1996, Russo and others 2002), with thinner slices aiding the identification of smaller structures (Love and others 1995, Russo and others 2002). Slices 1mm thick were reported to allow identification of all major structures (Russo and others 2002) while the tympanic membrane and other small structures were not always visible using 3mm slices due to partial volume artefact (Love and others 1995). In the present study, 2.5mm slices were adequate for the dog and cat TB but the smaller size of the rabbit prompted the use of 1mm slices.

Although contiguous slices are required for a complete clinical examination of the TB (Russo and others 2002), it was felt that one slice would be adequate to distinguish between the presence of fluid and gas within the canine TB lumen. However, the gel was not imaged in eight TB due to incomplete filling and location of the gel outwith the slice leading to false negative results. It was therefore decided to increase the number of slices to two in the cat and rabbit, which proved adequate, given the subsequent 100% agreement between the CT images and bandsaw findings in these species. The time required to perform a complete CT examination of the TB is approximately 20-30 minutes and

multiple slices are required to image the entire 3-dimensional structure (Love and others 1995). The use of a minimal number of slices in the present study therefore reduced time and cost implications, since CT is often charged per slice.

7.4.3. Comparison between the imaging modalities in cadavers

7.4.3.1. Radiography

The influence of the observer on image interpretation is a factor that must be considered when comparing diagnostic imaging procedures. Kappa analysis allows us to determine how well the results obtained by different observers agree beyond that which we would expect by chance (Altman 1997). On the radiographs in the present study, the mild increase in soft tissue opacity within the TB lumen produced very subtle changes that could not always be differentiated from the superimposed soft tissue. Interpretation of these changes was subjective, which is evident by there only being moderate agreement between the radiologists' interpretation of the radiographs in the dog, despite both radiologists being experienced. In the cat however, a good correlation was obtained for both views, suggesting that the changes observed must be clearer in this species. Agreement in the rabbit varied from moderate to excellent depending on the view, indicating that changes were most evident on the dorsoventral views and least on the lateral oblique views. Various combinations of the views produced good inter-observer agreement suggesting that this compensated for the less obvious changes on the lateral oblique views but also reduced the influence of the clearer changes observed on the dorsoventral views.

It is important to be able to objectively compare the results obtained using different procedures. Although the accuracy is easy to calculate, it does not provide much information about the relative merits of each one. The sensitivity of a diagnostic test is the proportion of true positives which are correctly identified by the test or the chances of diseased patients producing positive results while the specificity is the proportion of true negatives correctly identified (Altman 1997). However, when using a diagnostic test in a clinical context, the result of the test is all that is known. It is therefore more important to know how good the test is at identifying abnormalities or what proportion of cases with abnormal findings are truly abnormal. The positive predictive value provides this information while the negative predictive value tells us how many cases with normal findings are truly unaffected (Altman 1997). The positive and negative predictive values

also allow us to determine the false positive and negative rates for each procedure for comparison with other reports.

The problems associated with relying on such subtle changes for interpretation is reflected by radiography emerging as the least accurate method for identifying the presence of fluid within all three species in the present study, despite the experience of both radiologists. In the dog, the results were lower than those in two clinical studies (Remedios and others 1991, Love and others 1995). Discrepancy with these reports may have resulted from the use of a single view compared to the series recommended for the investigation of clinical cases of otitis media (Douglas 1987). However, it may also reflect the stage of the disease process. Although opacification of the TB was the most common radiographic finding reported in dogs and cats with otitis media (12/16), in only one animal was this finding not accompanied by a change in thickness of the TB wall (Remedios and others 1991). Most of the findings associated with the radiographic diagnosis of otitis media are associated with chronic changes resulting from long standing and sustained inflammation (Tojo and others 1985). The changes being relied upon in the present study were designed to mimic an acute state of the disease prior to the occurrence of wall changes and so were likely to be more difficult to identify. This indicates that radiographic studies will not consistently allow the identification of fluid in the absence of bony changes and that radiography is therefore unlikely to be of use in most acute cases of otitis media which is in agreement with a previous report (Farrow 1985). However, the results in the present study were also lower than those reported in a similar cadaver study, which also employed a single rostrocaudal open mouth view in cadavers with no bone changes, and the reason for the discrepancy between these results is not known (Griffiths and others 2003).

The radiographic results obtained in the cat and rabbit were similar and were superior to those obtained in the dog both in the present and previous studies (Griffiths and others 2003). This suggests that the presence of fluid in the TB was easier to identify radiographically in cats and rabbits than in dogs. Although the reason for this remains unclear, the bone wall of the TB is thinner in the cat than the dog and there is also a reduced thickness of overlying soft tissue. This may have allowed the subtle increase in opacity to become more apparent in this species.

The rostrocaudal open mouth view can be difficult to perform in the cat due to the positioning involved, so a rostro 10° ventral-dorsocaudal oblique view has been suggested for use in this species instead (Hofer and others 1995). Both views produced similar results in the present study, with those for the rostro-10° ventral-caudodorsal oblique view being marginally better than those of the rostrocaudal open mouth view. Since this latter view is easier to perform, the results of this study would support its use in place of the more traditional rostrocaudal open mouth view.

Dorsoventral radiographic views are considered standard for examination of the rabbit skull (Harcourt-Brown 1997, Harcourt-Brown 2002) and a variety of other views have been suggested depending on the area under investigation (Crossley 1995, Harcourt-Brown 1995, Harcourt-Brown 2003), although none that are specific for the TB. The results obtained from the three views used in the rabbit in the present study were similar and none emerged as significantly better or worse than the others. All were easy to position indicating all are appropriate for investigation of the TB in this species. Combinations of the views did improve results slightly but again no specific combination appeared significantly better than the others. The combination of all three views did not surpass the accuracy of the combinations of only two views. This suggests that while there is merit in producing a series of views, as is recommended in the dog, there is no specific view or combination that is likely to be more useful than the others.

There were both false negative and positive radiographic findings in all species in the present study and in the dog, these were higher than those reported in clinical studies (Remedios and others 1991, Love and others 1995, Rohleder and others 2006). Although the quality of a radiographic study, including poor patient positioning, asymmetry, malpositioning of the tongue, poor collimation, poor centering and inappropriate exposure factors can contribute to the false negative rate (Farrow 1985, Remedios and others 1991), the use of cadavers and an established technique in the present study meant these should not have caused a problem. False negative results in clinical studies are usually attributed to the animals not being affected chronically enough to be detected radiographically. In one study this was supported by them all having a relatively short clinical history (Remedios and others 1991) and in another, by changes identified surgically which were too subtle to be detected radiographically (Love and others 1995, Rohleder and others 2006). The false negative rate in the former study was 25% but was likely to have been underestimated due

to the retrospective nature meaning that other radiographically negative animals probably existed that did not undergo surgical exploration and therefore went undiagnosed (Remedios and others 1991). False positive results were less common and only reported in one study where they were attributed to the individual observer and how they assessed mild disease (Rohleder and others 2006).

It has been reported that since involvement of the TB in disease processes is usually unilateral, comparing the two sides will make the identification of abnormalities easier (Thrall 2002). In the present study, one radiologist was able to differentiate the presence of fluid from air in the dog more consistently when there was unilateral filling while the other identified unilateral and bilateral changes with approximately the same degree of accuracy. Both radiologists were better at identifying unilateral than bilateral changes in all the views in the cat and rabbit, although this was more marked in one radiologist than the other. The rostrocaudal open mouth view in the cat appeared to be better than the rostro-10° ventral-caudodorsal oblique view for the identification of unilateral changes in the cat while the rostro-40° ventral-caudodorsal oblique view appeared to be poor for the identification of bilateral changes in the rabbit, particularly where both TB were full. This indicates that the ability to compare both sides is likely to improve the accuracy of the interpretation, especially in the presence of unilateral changes, although this is also likely to be dependent on the individual operator. It has been suggested that comparison with the radiographs of a normal animal is more beneficial in improving diagnoses (Farrow 1985) and this is substantiated by the improved identification of unilateral changes where a normal air-filled TB is present for comparison.

7.4.3.2. Ultrasound

The sonographic appearance of normal and fluid-filled canine TB was similar to that previously reported (Griffiths and others 2003). The moderate inter-observer agreement between sonographers when imaging the canine cadavers suggests that, as with radiography, interpretation of the sonographic changes observed in this species was relatively subjective. This result may also reflect the inexperience of one of the operators. Ultrasound produced better results in the dog than radiography, which was consistent with the findings of a previous report (Griffiths and others 2003). False negative results may have resulted from incomplete filling of the TB or the presence of pockets of air within the gel. The reason for the false positive results was not determined although care must be

taken to distinguish the hyperechoic lines produced by reverberation artefact from the far wall of the TB. Despite the inexperience of one of the sonographers (B) they were still more accurate at differentiating between fluid and air in the TB lumen than both radiologists suggesting the appearances were more straightforward to differentiate using ultrasound than radiography. This also confirmed that it was possible to rapidly learn how to perform a sonographic evaluation of the TB in this species and interpret the images to an adequate degree of competency. The results obtained by the experienced sonographer (A) in the present study were comparable with those obtained using a single CT slice. Comparable results have also been obtained between ultrasound and CT for the identification of fluid in the sinuses of humans with paranasal sinusitis (Hilbert and others 2001).

However, the ultrasound results did not match the 100% reported in a previous similar study (Griffiths and others 2003). This report employed a lateral approach to the TB that was not found to be possible in the present study (as outlined in Chapter 4) and no indication was made as to how much fluid was introduced into the TB lumen. Based on these observations, the author suspects that in this previous study, it was the presence of fluid in the external ear canal, resulting from filling of the TB, that was identified rather than fluid within the TB lumen itself, and that this may be responsible for the disparity in results between the two studies.

The inter-observer agreement between the sonographers when examining the feline and rabbit cadavers was excellent. This may suggest that the sonographic distinction between fluid and gas within the TB in these species was more clear-cut than in the dog and also less subjective than the changes observed radiographically. This is also reflected by the ultrasound results obtained in the cat and rabbit being better across the board than those obtained in the dog and the inexperienced sonographers C and D obtaining marginally better and comparable results with experienced sonographer A respectively. The superficial location of the TB in these species allowed a high frequency transducer to be used and the resulting improvement in image resolution may have contributed to this finding. The thinner TB wall in these species and shorter distance for the beam to travel across the lumen may have resulted in better visualisation of the septum in the cat and the far wall in the rabbit, which were major factors in helping determine the presence of fluid. The mastoid process overlying the rabbit TB also produced a distinctive appearance that

facilitated identification of the TB in this species, making it easy to orientate the image and therefore determine if the far wall was visible or not. Although these results approached those of a previous similar study in dogs, they still did not match them (Griffiths and others 2003).

In the cat, the sonographer with the most experience (A) produced only false negative errors (reflected in sensitivity and negative predictive values of 85% and 93%) while the less experienced sonographer (B) produced only false positive errors (reflected in their specificity and positive predictive values of 92%). However, the opposite was observed in the rabbit whereby experienced sonographer A produced only false positive errors (specificity and positive predictive values of 95%) while the less experienced sonographer (D) produced only false negative errors (sensitivity and negative predictive values of 95%). This suggests that there may have been subtle differences in weighting of the criterion used by each operator in reaching a diagnosis, although further investigation would be necessary to determine this.

In the dog and the cat, both sonographers were able to differentiate fluid and air-filled TB more consistently when there was unilateral filling than when the contents of both were the same. This suggested that comparison played a useful role in the interpretation of the images. The excellent results obtained in the rabbit meant it was not possible to determine if the presence of unilateral changes influenced the results in any way in this species.

7.4.3.3. CT

In the present study, CT slices emerged as the gold standard for differentiating the presence of fluid from gas in the TB. The presence of gel produced a very distinctive appearance on the CT images and differentiation between it and air was straightforward as demonstrated by the 100% agreement between the radiologists interpretation of the images in all three species. CT consistently produced the best inter-observer correlations throughout the study suggesting that interpretation of images must be more objective than with either radiography or ultrasound.

CT also produced the best results across the board in all three species despite being limited to a minimal number of slices that did not constitute a complete CT examination. Two slices proved adequate in the cat and rabbit, producing perfect correlation between CT

images and post mortem finding. However, the single slice obtained in the dog resulted in eight false negative results due to incomplete filling resulting in the location of the ultrasound gel outwith the slice. In clinical cases, false negative findings have been reported in association with changes of either the epithelium or bone wall of the TB which were too mild to identify (Love and others 1995). There were no false positive results in the present study, therefore the presence of fluid was indicative, as reflected by the positive predictive values. False positive results using CT has been reported due to exuberant ear canal epithelium bulging through the tympanic membrane, producing a soft tissue opacity apparently located within the TB lumen (Love and others 1995) while in another study it was related to the individual observers assessment of mild disease (Rohleder and others 2006).

Although a complete series of slices is recommended to allow full examination of the TB and associated structures (Love and others 1995), the results of this study suggest that a minimum of two slices can be used to accurately identify the presence of fluid in the lumen. Interestingly, it was predominantly the left ear in which the presence of gel was missed (6/8) which may reflect variations in the filling technique of a right handed operator.

7.4.4. Comparison between imaging techniques in canine otitis media cases

The inter-observer agreements for all of the imaging modalities in this part of the study were poorer than those obtained in the cadavers, presumably reflecting the range of changes encountered in the clinical cases and therefore a greater degree of subjectivity in their interpretation when compared to the more clear-cut full or empty status of the cadavers. In general, CT agreement was best for content changes, which is not surprising since apparent wall thickness has been shown to be influenced by window setting and the presence of intraluminal fluid (Barthez and others 1996). Likewise, the better agreement for wall changes on all of the radiographic views was to be expected given the acceptance that radiography is better for imaging bone than soft tissue (Curry and others 1990).

The CT results were not perfect but were comparable with those obtained in other clinical studies (Love and others 1995, Rohleder and others 2006), again reflecting the potential for the presence of a range of subtle changes in clinical cases. Although CT is not absolutely sensitive or specific for the detection of middle ear disease in the dog (Garosi and others

2003, Rohleder and others 2006), it was selected for use as the gold standard in this study as it is presently the optimum technique available for imaging the TB. High resolution CT is the method of choice for examination of middle ear structures in man (Czerny and others 1997) and CT or MRI are now commonly accepted for evaluation of middle ear disease in veterinary practice (Garosi and others 2003). An additional attempt was made to maximise the accuracy of the 'gold standard' CT diagnosis by using consensual interpretation with two radiologists to remove the effects of inter-observer variation. As with previous studies, interpretation was based on transverse images only (Love and others 1995, Garosi and others 2003, Rohleder and others 2006) therefore further work would be indicated to determine whether the provision of multiplanar images would affect the results obtained. Surgical findings were not used as the 'gold standard' in the present study since this would have limited case inclusion to those proceeding to surgery based on imaging or clinical findings, and therefore was felt to not accurately reflect the diagnostic challenge faced by practitioners. In addition, it has been demonstrated that surgical findings do not necessarily correspond with histopathology (Rohleder and others 2006).

The results of the radiographic assessment of the clinical cases were better than those obtained in the cadaver study, reflecting the presence of changes potentially affecting the TB wall as well as the lumen. This observation is supported by the better correlation between the radiographic identification of wall changes than content changes with subsequent CT findings (Table 7.3.6). The odds ratio is a way of comparing whether the probability of a certain event is the same for two groups (Altman 1997). In the present study it indicted the chances of changes identified using each imaging technique being associated with the presence of corresponding changes on subsequent examinations, with higher values indicating a greater likelihood. A greater correlation still was obtained when content and wall changes were combined suggesting that although wall changes may be easier to identify radiographically, it is important not to overlook the presence of luminal changes in the overall assessment. In a previous study the presence of luminal material rather than wall changes were found to be associated with the presence of middle ear pathology but only when the severity of the disease was high (Rohleder and others 2006).

The radiographic results in the present study were generally poorer than in previous reports (Remedios and others 1991, Love and others 1995, Rohleder and others 2006). This may have reflected the use of CT rather than surgery as the gold standard, resulting in the

retention of cases with subtle enough changes that would not have warranted progression to surgery in the previous studies. This is further supported by the significant association between increasing severity of disease and the ability to identify both wall and content changes on the radiographs (Table 7.3.12.). A lower severity of disease has been reported to decrease the observer's diagnostic certainty (Rohleder and others 2006) and this is also reflected in the poor inter-observer agreement in the present study.

Although all of the radiographic views demonstrated a correlation with subsequent CT findings, differences for each were observed between radiologists, therefore none emerged as being of particular benefit and the combination of all three views did not always produce the best results (Table 7.3.7. and 7.3.8.). In addition, radiologist A displayed a tendency to over interpret the results as demonstrated by the lower sensitivity and positive predictive values indicating false positive results. These were only reported in one previous study where they were also attributed to the individual observer in the assessment of mild disease leading to the suggestion that further evaluation of the effects of observer experience be investigated (Rohleder and others 2006). This indicates that the radiologist interpreting the images is likely to have an effect on the results and also the optimum views that should be performed.

This study showed that it was possible to perform an ultrasound examination of the middle ear cavity in live clinical canine cases without the need for sedation or general anaesthesia. There was a significant difference between the results for sonographer A and B with very poor agreement between them. The possible causes for this include the relative inexperience of sonographer B and the reliance on videocassette recordings for assessment. Consensual ultrasonography was not possible at the time of performing the ultrasound, and was also not thought to be a feasible replication of the practice situation where usually one person performs and evaluates the scan. This is unlike radiography and CT where interpretation can be carried out after the examination by one or more people, a situation especially likely in difficult cases. The need for interpretation at the time of the study and the difficulties in rendering meaningful information from another sonographer's images or videotape are limitations of ultrasound and make the results very dependent on the experience and skill of the operator (Reed and others 1995, Long and Nyland 1999). It is therefore necessary to have a thorough knowledge of the relevant regional anatomy since accurate interpretation of images depends directly on the differentiation between normal

and abnormal anatomy at the time of the examination (Nyland and others 1995, Long and Nyland 1999). The results of the present study indicate that training is not a substitute for actually performing the examination.

The results from the sonographic assessment of the clinical cases were poorer than those obtained in the cadaver study. This presumably reflected the reliance on a characteristic appearance in the cadavers, resulting from complete filling of the TB in the presence of normal walls. However, the appearance of the TBs in the clinical study were much more variable. In cases where the TB was only partially full, identification of the material relied on it being located against the wall nearest the transducer as the presence of any gas between it and the wall caused it to be obscured by the resulting acoustic shadow. The animals were examined in sternal recumbency to increase the chances of such material moving under gravity to a location where it could be identified. When identified, this material resulted in an irregular area of separation between the bone wall and the gas interface but the far wall of the TB remained obscured. This type of appearance was often difficult to differentiate from the dirty acoustic shadowing produced by an empty TB or from mild irregularities in the wall and is reflected in the lack of significant correlation between content changes identified using ultrasound and those subsequently present on CT examination (Table 7.3.10). This is also supported by the observation that ultrasound was better able to detect changes to the TB contents as the severity of disease progressed and therefore the contents became easier to identify (Table 7.3.12). However, the sonographic detection of wall changes was significantly correlated with those identified on CT examination (Table 7.3.10). Changes to the bone wall of the TB were identified on ultrasound as a loss of the smooth outline and an altered contour with reduced penetration of the beam. The absence of the characteristic appearance of the TB wall was therefore a good indicator of the presence of disease. It is also likely that the presence of wall changes hampered adequate assessment of the contents and therefore contributed to the poorer results obtained for the assessment of luminal changes.

Although there was no direct correlation between the radiographic and ultrasound results, their combination did produce significantly better correlation with subsequent CT results suggesting that using both techniques together can provide a more accurate assessment of the canine TB than either of them alone. This indicates that ultrasound does have a role to

play in the assessment of middle ear disease in the dog but may not be as useful in acute cases as the cadaver study suggested.

7.4.5. Investigation of the TB in two Cavalier King Charles Spaniels

Fluid within the TB was occasionally observed unexpectedly in dogs undergoing CT (Barthez and others 1996) and MRI (Owen and others 2004) of the brain and likewise, in the two CKCS in the present study where MRI was performed for the investigation of neurological signs that were thought to be associated with the presence of Chiari-like syndrome. Brachycephalic breeds appear to have a predisposition to the accumulation of fluid in the middle ear cavity (Owen and others 2004). It has been suggested that this results from their excessive, redundant pharyngeal tissue and consequent narrowing of the pharynx interfering with the function of the auditory tubes (Owen and others 2004, Dennis 2006). This theory is supported by the induction of secretory otitis media following experimental obstruction of the auditory tube in dogs (Tojo and others 1985). The presence of fluid within the TB has therefore been reported as a common non-clinical finding on MRI of the CKCS and Boxer (Dennis 2006).

Primary secretory otitis media, a condition similar to 'glue ear' in children has also been reported in dogs, and predominantly the CKCS (Cox and others 1989, Stern-Bertholtz and others 2003). The diagnostic imaging observations in the two CKCS cases in the present study were thought to be consistent with this diagnosis. Although the exact cause is as yet unknown, auditory tube dysfunction is thought to result in formation of a mucoid plug within the TB lumen, either unilaterally or bilaterally. The clinical signs can be indistinguishable from cervical disc, central nervous system or middle ear disease (Stern-Bertholtz and others 2003) and therefore in the present study were probably attributable to this condition rather than the Chiari-like syndrome that was originally suspected.

One of the cases demonstrated bilateral filling of the TB and the fluid produced a distinctive two-tone appearance on the MR images, particularly the T2 weighted ones. This implied that the fluid was non-uniform and that the ventrally located regions may have had a different composition to the other areas. It has been reported that in chronic cases of middle ear disease, progressive dehydration of fluid results in a rising protein concentration that may lead to an increase in signal intensity on T1 and a decrease on T2 weighted images (Owen and others 2004), which would correspond with the ventrally located fluid

in this case. The other case demonstrated unilateral filling of the TB and only a small volume of fluid in the contralateral ear. The fluid appeared heterogenous on T1 weighted images and homogenous on T2 weighted ones, which also corresponded with previous reports (Allgoewer and others 2000, Owen and others 2004). However, despite the uniform nature of the ultrasound gel used in Chapter 6, its appearance on the MR images was also heterogenous. This suggests that further work is required to determine exactly what influences the signal intensity and uniformity of fluid located within the middle ear cavity, and whether the variations observed are real or artificial.

All three completely filled TB were identified using ultrasound. The fluid was more echogenic than the ultrasound gel used in Chapter 4 reflecting the difference in composition. However, it did still allow penetration of the beam to the far wall of the TB thereby producing the characteristic appearance of a fluid-filled TB. Although results from analysis of the material were not available in these cases, the material removed from previous cases has been reported as being predominantly mucoid in nature (Stern-Bertholtz and others 2003), which would be consistent with the ultrasound appearance. This further confirms the potential role that ultrasound has in the investigation of middle ear disease in the dog.

Chapter 8. Anatomical variations observed in the canine and rabbit skull.

8.1. Introduction

The skull of the domestic dog demonstrates a range of size and shape that is far greater than any other mammalian species (Evans 1993). Variations in size tend to reflect the overall size of the dog while variations in shape most commonly involve the facial region with three distinct groups, dolichocephalic, mesaticephalic and brachycephalic, reflecting the relative proportions of the facial region to the rest of the skull (Evans 1993). Cat and rabbit skulls also demonstrate breed and individual variations in size and shape, with the existence of relatively dolichocephalic and brachycephalic cat breeds (Oriental and Persian respectively) and brachycephalic rabbit breeds (Netherland Dwarf) (Pond and Ralieggh 1979, Mettler 1992). The effect of these variations on the anatomy of the temporal region of the skull and in particular the TB and TMJ is not well reported.

Chondrodystrophy is a disturbance in development of the cartilage primordia of long bones leading to arrested growth or dwarfism, whereby the head and trunk are essentially normal but the limbs are short (Stedman 2006). The bones of the skull are also affected although the location and severity of changes throughout the skeleton varies between species (Sawin and others 1959). Severe chondrodystrophy is lethal at, or soon after birth, but in the dog, there are several breeds including the Cavalier King Charles Spaniel (CKCS), Dachshund, Bassett Hound and Jack Russell where chondrodystrophy is a normal breed characteristic. Chondrosytophy has also been reported in the New Zealand White rabbit in associated with the presence of the Dachs gene (Sawin and others 1959).

Dysplasia is the abnormal development or growth of a cell, tissue or organ (Schwarz 1993). Dysplasia of the TMJ has been reported in the Irish Setter, Basset Hound, Boxer, Golden Retriever, Labrador and Bernese Mountain Dog as isolated cases with most of the population demonstrating normal TMJ anatomy (Stewart and others 1975, Robins and Grandage 1977, Johnson 1979, Lane 1982, Stead 1984, Bennet and Prymak 1986). However, radiographic changes consistent with TMJ dysplasia have also been described in American Cocker Spaniels and Dachshunds in the absence of clinical signs (Hoppe and Svalastoga 1980, Vollmerhaus and others 1996, Vollmerhaus and Roos 2003). The

underlying cause of TMJ dysplasia in the dog is not known although many theories have been suggested (Robins and Grandage 1977, Johnson 1979).

A variety of radiographic features have been recorded in cases of TMJ dysplasia (Stewart and others 1975, Robins and Grandage 1977, Johnson 1979, Lane 1982, Stead 1984, Bennet and Prymak 1986). Varying degrees of change have also been observed and the condition may not always be bilateral (Hoppe and Svalastoga 1980). It has been suggested that the resulting shape of the condyloid process can cause excessive movement of the lateral aspect of the condyle and stretching of the lateral ligament, thereby leading to laxity of the joint and that this can be assessed by measurement of the rotational angle (Robins and Grandage 1977, Lantz and Cantwell 1986).

Radiography has been used to evaluate all reported cases of TMJ dysplasia in the dog and there are currently no reports of the use of CT or MRI in its identification. According to the human literature, currently there is no 'gold standard' imaging modality for the assessment of TMJ function (Landes and others 2000).

8.1.1. Aims

The aims of the work presented in this chapter were to:

- Describe the anatomical variations observed in the TMJs of the CKCS skulls in Chapter 2.
- Evaluate the radiographic changes associated with this condition in CKCS and also describe the appearance using other imaging modalities.
- Attempt to determine how widespread these changes are in the CKCS population presented to the University of Glasgow Small Animal Hospital for diagnostic imaging
- Measure the rotational angle of the mandibular condyle in affected dogs to determine if any correlation exists with this condition.
- Describe the anatomical variations observed in the rabbit skulls in Chapter 2

8.2. Materials and Methods

8.2.1. CKCS cadaver material

From the information available, it was not possible to differentiate consistently between Cavalier King Charles Spaniels and King Charles Spaniels and so both have been included in the term CKCS.

Three of the 50 emascerated canine skulls studied in Chapter 2 were from CKCS and in each, marked variations were noted in the anatomy of the TMJ when compared with those of the other skulls. The conformation of the components of the TMJ in each CKCS skull was assessed and described. The rotational angle of each mandibular condyle was measured as described in Chapter 2.

CKCS cadavers were sourced from the donations received by the University of Glasgow Veterinary Anatomy unit as outlined in Chapter 2. The heads were removed at the mid cervical region and stored at -20°C until required.

8.2.2. Diagnostic imaging of CKCS cadavers

The emascerated skulls with the least and most marked changes were radiographed at a selection of lateral and long axis rotational angles using the equipment described in Chapter 3.

The heads from the CKCS cadavers were thawed and radiographed. A dorsoventral and right and left latero $10-30^{\circ}$ rostro – laterocaudal oblique views were taken of the TMJs. The appearance of the joints was assessed and the rotational angles were measured from the dorsoventral view. CT and MRI was performed in one CKCS cadaver head using the equipment and technique described in Chapters 5 and 6. A three dimensional CT reconstruction was also created.

8.2.3. Review of CKCS cases

All of the CKCS which had undergone either radiography, CT or MRI of the skull at the University of Glasgow Veterinary School Small Animal Hospital between 1991 and 2006 were identified. Radiography and CT were performed using the equipment described in Chapters 3 and 5. MRI was performed using a 1.5 Tesla mobile clinical MRI unit. In each

case, the reason for the examination, the images produced and the appearance of the TMJs were noted. The rotational angles were measured where dorsoventral radiographs were present.

8.2.4. Rabbit cadaver material and diagnostic imaging

Ten emascerated rabbit skulls were prepared for use in Chapter 2 and in four, the base of the skull appeared different to the rest. The appearance of this region in these skulls was assessed and described.

Following CT and MR imaging of the rabbit cadavers in Chapters 5 and 6, one demonstrated a similar anomaly in the anatomy of the base of the skull. The CT and MRI appearance of this skull was described. 3-dimensional CT reconstructions were performed in this head and a normal one for comparison.

8.3 Results

8.3.1. Anatomy and radiography of emascrated CKCS skulls

The appearance of the bony components of the TMJ in two of the emascrated CKCS skulls is demonstrated in Figure 8.3.1. The dentition of the three CKCS skulls in the anatomical collection indicated that they were adult and the TMJ in all of them were considered to be markedly different to those observed in the control group, as described in Chapter 2. The retroarticular processes were short, thickened and blunt ending. The articular surfaces of the medial aspect of the mandibular fossa and the retroarticular process were convex in a mediolateral direction. When the mandibular fossa was viewed from the lateral aspect, a straight line or at best a shallow concavity was formed between the rostral margin of the mandibular fossa and the tip of the retroarticular process. The articular surface of the lateral aspect of the mandibular fossa was short but present.

The ventral articular surface of the condyloid process of the mandible was shortened and reflected the shape of the corresponding regions of the mandibular fossa and retroarticular process. The dorsal, caudal and ventral regions of the medial articular surface were all concave, which produced a beak shape to the medial extremity although the severity of these changes varied between the skulls. The lateral region of the condyloid process had a more rounded profile than normal and the lateral articular surface did not extend to the margin of the condyloid process but terminated at varying distances along the condyle where it formed a rounded protrusion. These features produced an undulating caudal margin to the condyle.

The radiographic appearance of these skulls is demonstrated in Figure 8.3.2. On dorsoventral radiographs of the skull with the most marked changes, the marked concavity of the medial articular surface of the condyloid process and the beak shape of the medial extremity were clearly visualised. In the skull with the mildest changes however, the condyloid process appeared relatively normal on the dorsoventral view, with the exception of a mild concavity of the medial articular surface and a slight convex protrusion on the lateral caudal articular surface representing its premature termination. True lateral views demonstrated retroarticular processes which were either absent or appeared very short with rounded rather than pointed margins, although the rest of the structures associated with the joints were not clearly visible due to superimposition.

Lateral rotation of 10 to 30° demonstrated an abnormal shape to the end-on appearance of the condyloid process as a result of the deficient ventral articular surface not producing the normal curved caudoventral margin and the medial margin producing an angular one in its place. This was most marked in the worst affected skulls where the lateral articular surface was projected beyond the reduced medial one. The mandibular fossae were shallow or mildly convex and the retroarticular processes were short and blunt ended with convex articular surfaces.

Long axis rotation through 20° to 30° confirmed the absence of the tip of the retroarticular process and the reduced length of its lateral margin resulted in the presence of a notch between it and the caudal aspect of the condyloid process instead of the normal smooth curve. Flattening or convexity of the middle of the mandibular fossa was observed and the shape of the fossa was not congruent with that of the condyloid process so the joint space diverged caudally. The concavity of the medial articular surface in the worst affected cases became visible in the upper condyloid process at 30° and the lower condyle at 55°. At rotations beyond 30°, the hypoplastic retroarticular process failed to produce as marked an opaque, curved line as in normal skulls. At a rotation of 70°, the entire caudal articular surface of both condyloid processes could be assessed, although they were superimposed over the bones of the skull.

8.3.2. Radiography, CT and MRI of the CKCS cadavers

The radiographs obtained from the CKCS cadaver heads are demonstrated in Figure 8.3.3. The appearance of the TMJs was similar to that described in the CKCS emascerated skulls and demonstrated in Figure 8.3.2. The changes on the dorsoventral view were limited to the presence of a concave medial articular surface on the condyloid processes. However, rotation of the skull in a long axis direction, to produce a latero 70° ventral-laterodorsal oblique view, aided the identification of more subtle changes in the contour of the caudal articular surface. The latero 10-30° rostro – laterocaudal oblique views also allowed the contour of the condyloid process to be assessed in addition the length and profile of the retroarticular process.

The CT images obtained from the CKCS cadaver are demonstrated in Figure 8.3.4. The results from Chapter 5 indicated that sections viewed using a bone window were optimum

for examination of the TMJ therefore only these images have been presented. Transverse CT images demonstrated a marked concavity in the centre of the mandibular fossa compared to the straight horizontal surface in the normal TMJ. The dorsal articular surface of the condyloid process was congruent with that of the mandibular fossa resulting in an undulating margin with a marked difference between the shape of the lateral and medial halves. Laterally, the articular surface was convex, corresponding with the concavity of the mandibular fossa while medially it was concave to accommodate the thicker mandibular fossa in this area.

At the rostral margin of the TMJ, the hypodense defect in the lateral half of both condyloid processes was more marked than in the normal TMJ, indicating that the lateral extremity of the condyloid process was extending further rostrally than the adjacent regions. This was confirmed on the sagittal sections where the concavity of the rostral margin between the lateral part of the condyloid process and the neck of the condyle was more marked than in the normal dog. This defect was more prominent on the right than the left in both series indicating the presence of asymmetrical changes.

In the sagittal sections, the lateral region of the mandibular fossa appeared to be located in a more dorsal position relative to the condyloid process when compared to the caudodorsal position observed in the normal dog. The condyloid process was more rounded than normal and projected ventral to the level of the mandibular fossa. With medial progression, the articular surface of the mandibular fossa remained flattened and the retroarticular process appeared poorly developed, failing to not extend caudal to the condyloid process. The margin of the condyloid process became flattened and angular in this region resulting in marked incongruity of the joint space, with the mandibular fossa and retroarticular process failing to encase the condyloid process.

As in the control population of skulls, the dorsal articular surfaces and lateral half of the mandibular fossa were not visualised in the dorsal sections. However, the lateral extremity of the condyloid process became visible before the medial regions indicating that it was located further dorsally than normal, which corresponded with its appearance on the transverse views. Moving ventrally, the angle observed between the medial and lateral halves of the caudal margin of the condyloid process was similar to that of the normal dog with the TMJ open. While in the normal dog these margins remained flat, in the CKCS the

outline of the lateral extremity was very rounded and the medial half was distinctly concave. This corresponded with a convexity of the surface of the retroarticular process resulting in the medial half of the TMJ remaining congruent.

The 3-dimensional reconstruction of the CKCS TMJ is shown in Figure 8.3.4.4. The retroarticular process appeared shorter than normal but otherwise the external appearance of the TMJ was relatively unremarkable. Sectioning of the volume would have been required for the variations to become evident. Separation of the condyloid process and mandibular fossa was attempted to reveal the true extent of the changes but the undulating joint space between these structures meant that this was not possible.

The MR images obtained from the CKCS cadaver are illustrated in Figure 8.3.5. The results from Chapter 6 indicated that T1 weighted images were superior to T2 weighted ones for imaging the components of the TMJ and therefore only these images have been presented. The areas of the TMJ imaged and the changes in shape of the components observed in each of the planes was similar to the corresponding CT images. The defect in the rostral aspect of the lateral half of the condyloid process was particularly prominent in the transverse images, appearing as a hyperintense circular area surrounded by the signal void produced by the cortical bone.

In both CT and MR images, the changes were readily identified in transverse and sagittal images but more difficult to assess in dorsal ones.

8.3.3. Review of clinical cases

Twenty six adult CKCS had undergone a radiographic examination of the skull between 1991 and 2001, the details of which are presented in Table 8.3.1. Only two were radiographed specifically for investigation of the TMJ while the rest were radiographed for a variety of reasons. These two cases were the only ones in which a prospective radiographic diagnosis of TMJ dysplasia was made although the final clinical diagnoses were of masticatory myositis and stomatitis.

Fifteen of these cases demonstrated conformational variations affecting both TMJs that could be consistent with a diagnosis of bilateral dysplasia. Five cases had views which only allowed examination of one of the TMJs, although in each case the joint under

interrogation demonstrated similar anatomical variations. In a further six cases, the views available were not sufficient to allow adequate examination of the TMJ and so a conclusion could not be reached. Examples of the typical radiographic appearance of the TMJs in these cases are demonstrated in Figure 8.3.6.

All of the adequately visualised joints demonstrated short, blunt ending or absent retroarticular processes, flat or convex mandibular fossae and angular condyloid processes. A range of severity was noted with most demonstrating changes similar to those observed in the least affected of the emascrated skulls although two cases had a marked concavity of the medial articular surface similar to the worst affected skull and one case had one TMJ which was more severely affected than the other.

Fourteen adult CKCS had undergone a CT examination of the skull between 2001 and 2006. None of these were specifically for investigation of the TMJ. Technical problems with the CT data archiving computer system meant that that the original data from the examinations could not be accessed and reliance was therefore placed on the archived images from each case. In all instances, only transverse images had been printed for archiving. In ten cases, the region of interest was the brain therefore only images produced using various soft tissue and brain windows were available, which did not allow adequate visualisation of the TMJ components to assess their shape and configuration. In the four cases where the TB were being investigated, the images were produced using bone windows and therefore allowed assessment of the TMJ. In all four of these cases, the transverse images demonstrated a concave medial articular surface and beak shaped medial extremity of the condyloid process with corresponding convex shape of the mandibular fossa. The retroarticular process could not be assessed in these views due to partial volume artefact. Examples of the typical CT appearance of these TMJs are demonstrated in Figure 8.3.7.

Forty-eight adult CKCS had undergone an MRI examination of the head between 2004 and 2006. None of these were specifically for investigation of the TMJ. The archived sequences reflected the region of interest but in general, the TMJs were included in any T1 and T2 weighted transverse and dorsal sections that were present. Sagittal sequences did not tend to extend far enough laterally for inclusion of the TMJ.

The slice thickness resulted in the TMJ being imaged in an average of two slices in each direction. The appearance therefore reflected the specific areas that were present in each section. All of the transverse images demonstrated some degree of concavity of the medial articular surface and a beak shaped medial extremity of the condyloid process with corresponding convex shape of the mandibular fossa. There was also occasionally a hyperintense region present within the lateral half of the condyoid process. The retroarticular process was not well imaged in these views. In the dorsal images, when the caudal articular surface of the condyloid process was present, the lateral extremity was very rounded while the medial half was distinctly concave. However, this was not consistently visible in these views and in some cases the condyloid process merely appeared slightly mis-shapen. The transverse images were therefore regarded as being better than the dorsal ones for the identification of changes, especially in more subtle cases. Examples of the typical MRI appearance of these TMJs are demonstrated in Figure 8.3.8.

8.3.4. Rotational angles

The rotational angles measured from the dorsoventral radiographs of the 3 skulls, 4 cadaver heads and 19 clinical cases are demonstrated in Table 8.3.2.

Figure 8.3.1. Gross appearance of the TMJ in CKCS skulls.



Figure 8.3.1.1. and 8.3.1.2. Ventral view of the mandibular fossa and retroarticular process in two CKCS skulls.

Arrow: short, thick and blunt ended retroarticular processes.

* : convex medial articular surface of the mandibular fossae



Figure 8.3.1.3. and 8.3.1.4. Caudodorsal view of the condyloid processes in two CKCS skulls.

> : premature termination of the lateral articular surface of the condyloid processes

>> : concave medial articular surface

Figure 8.3.2. Radiographic appearance of the TMJ in emascrated CKCS skulls.



Figure 8.3.2.1. Dorsoventral view of the skull with the mildest changes.

> : premature termination of the lateral articular surface of the condyloid process

>> : concave medial articular surface

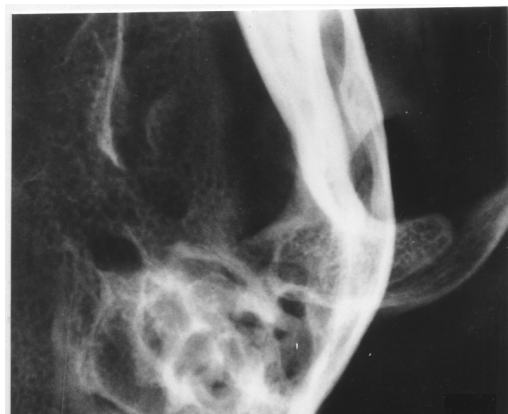


Figure 8.3.2.2. Dorsoventral view of the skull with the most marked changes. Note the marked concavity of the medial articular surface and the beak shape of the medial extremity.



Figure 8.3.2.3. Latero 20° rostral - laterocaudal oblique view of the skull with the mildest changes. Note the short retroarticular process, the flat mandibular fossa and the angular appearance of the condyloid process due to the deficient medial margin.

Figure 8.3.2. continued. Radiographic appearance of the TMJ in emascerated CKCS skulls.

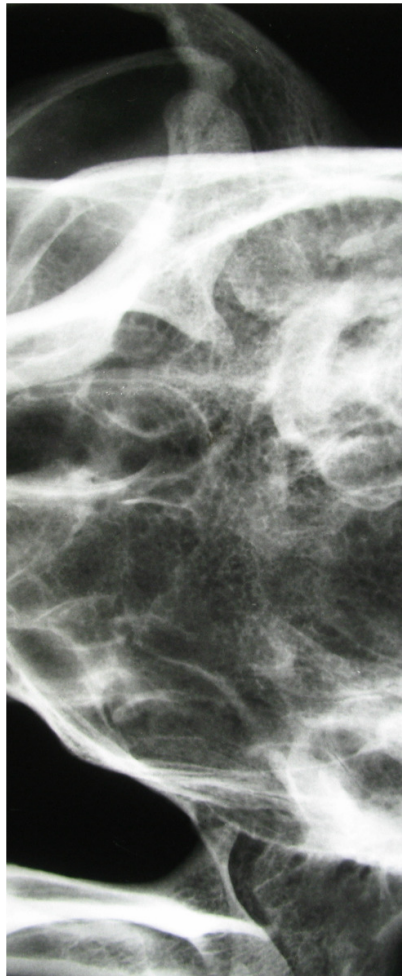


Figure 8.3.2.4. Latero 70° ventral-laterodorsal oblique view of the skull with the most marked changes. Note how the profiles of the caudal articular surface of both condyloid processes are clearly visible.

Figure

nce of the TMJ in CKCS cadavers.

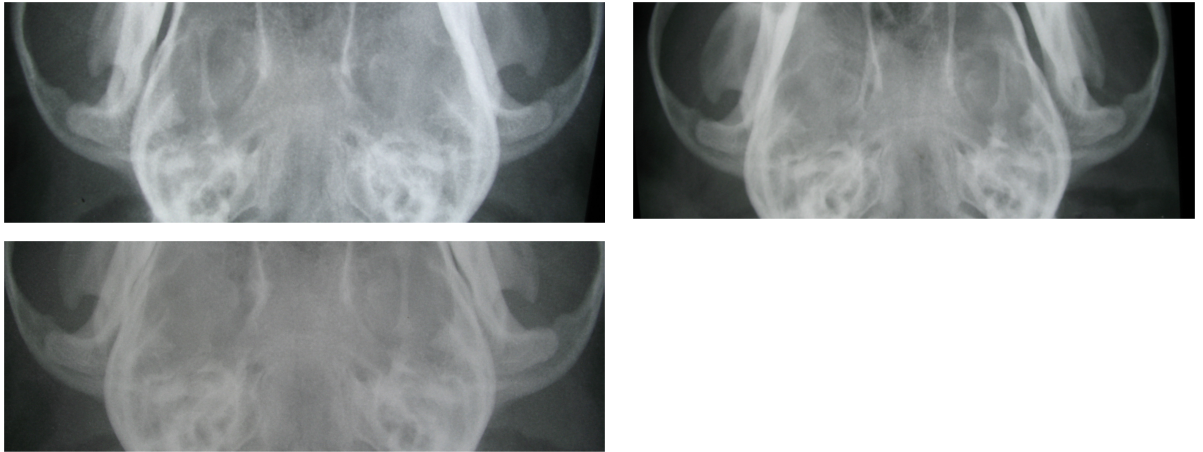


Figure 8.3.3.1. Examples of dorsoventral views.

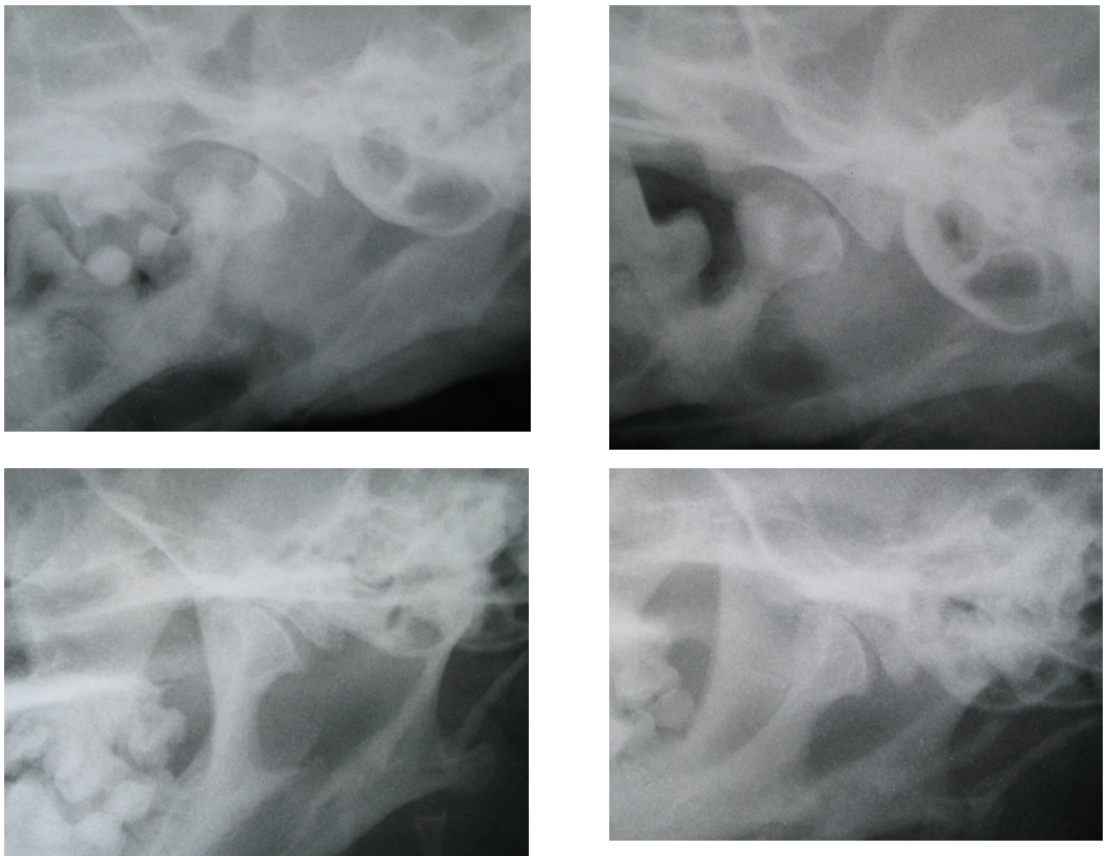


Figure 8.3.3.2. Examples of latero 20° rostro – laterocaudal oblique views.

Figure 8.3.3. continued. Radiographic appearance of the TMJ in CKCS cadavers.

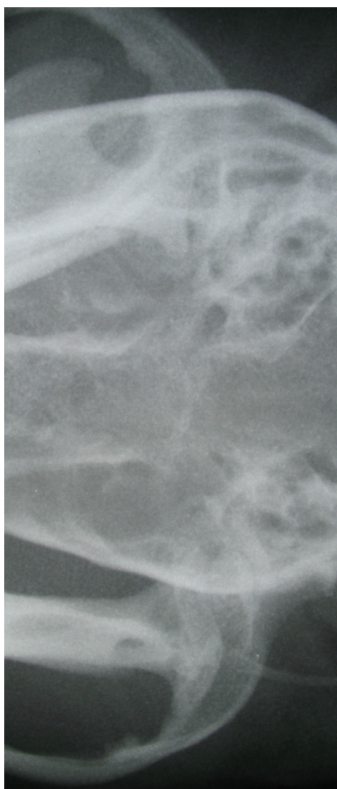


Figure 8.3.3.3. Example of a latero 70° ventral-laterodorsal oblique view.

Figure 8.3.4. CT images through the TMJ in a CKCS cadaver viewed using a bone window.

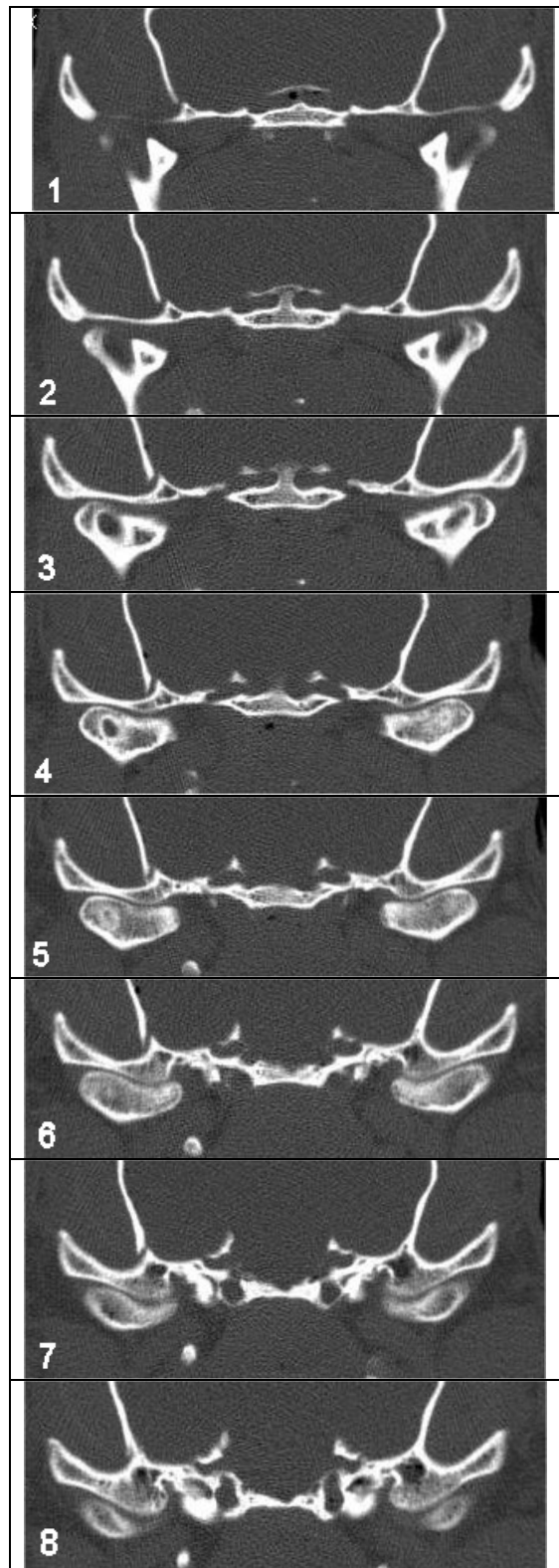


Figure 8.3.4.1. Transverse CT images progressing from rostral to caudal. Dorsal is to the top and right is to the left in all images. Number in bottom left corner indicates slice number.

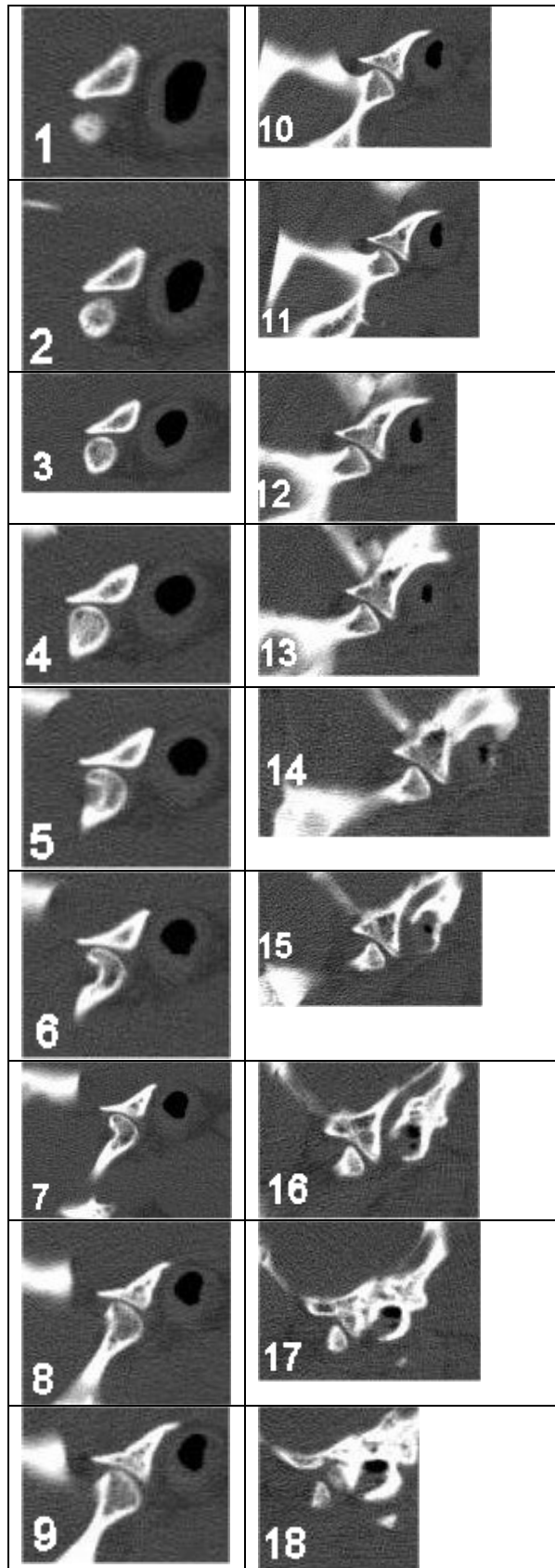


Figure 8.3.4.2. Sagittal CT images progressing from lateral towards midline. Dorsal is to the top and rostral is to the left in all images. Number in bottom left corner indicates slice number.

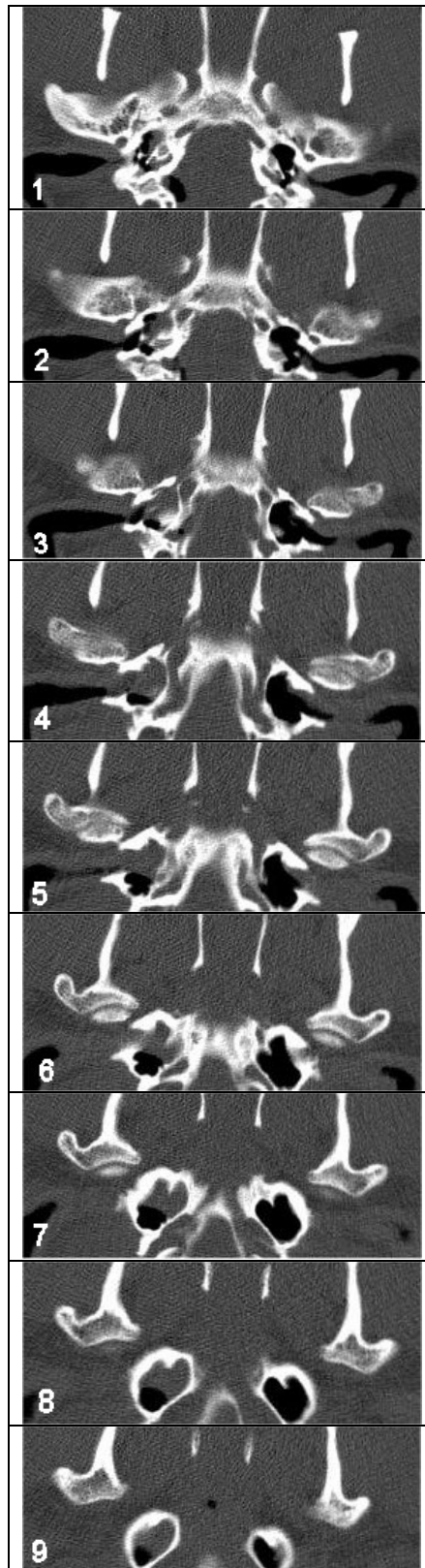


Figure 8.3.4.3. Dorsal CT images progressing from dorsal to ventral. Rostral is to the top and right is to the left in all images. Number in bottom left corner indicates slice number.

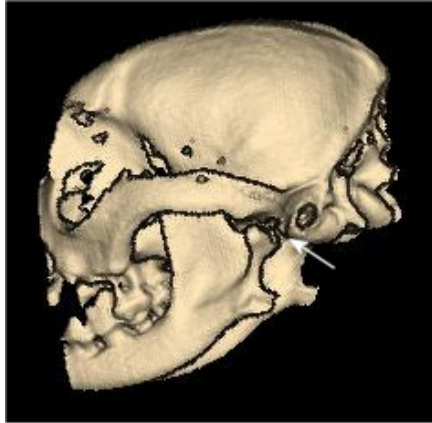


Figure 8.3.4.4. Three dimensional CT reconstruction of the TMJ in a CKCS cadaver demonstrating incomplete development of the retroarticular process (arrow)

Figure 8.3.5. T1 weighted MRI sections through the TMJ of a CKCS cadaver.

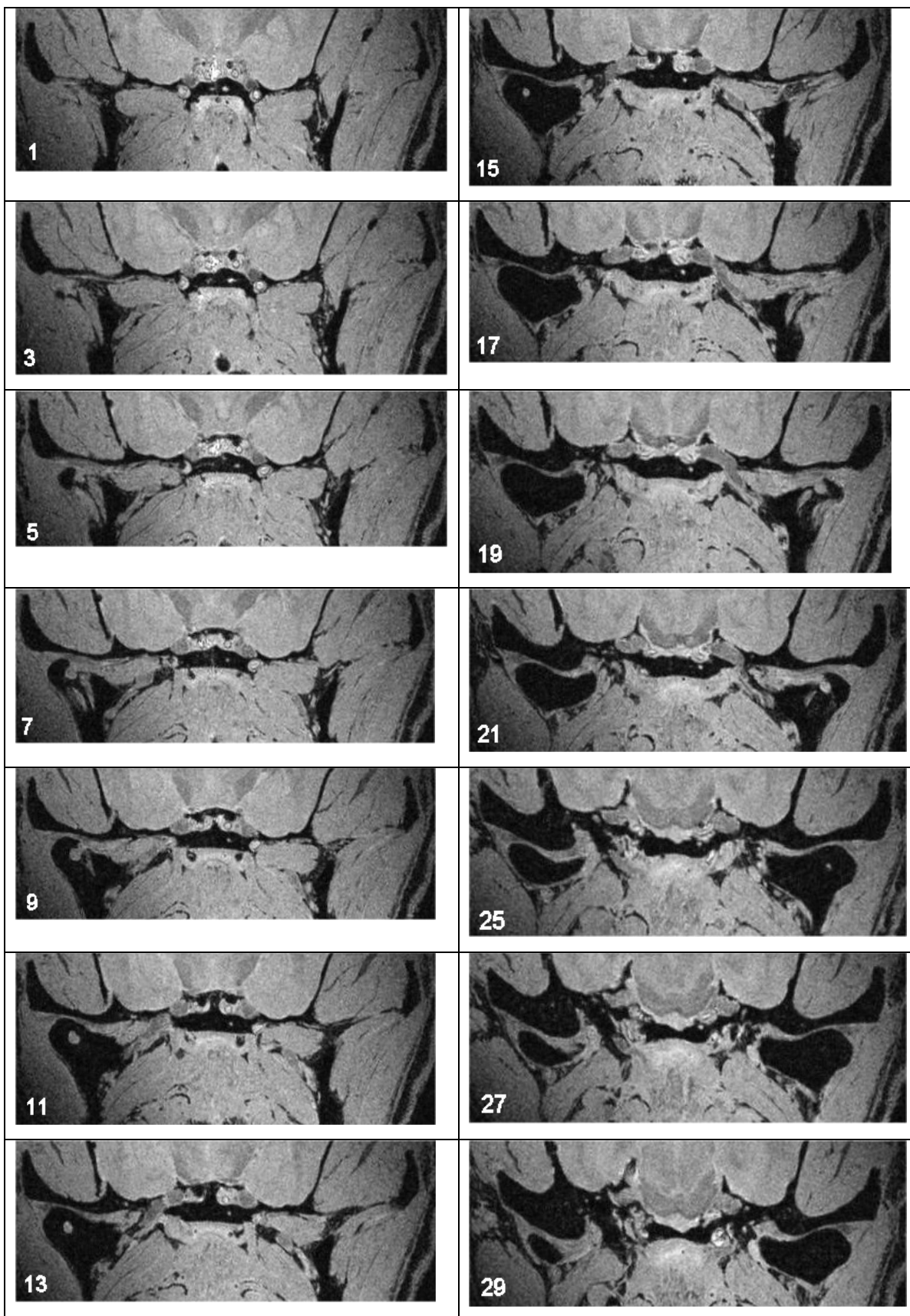
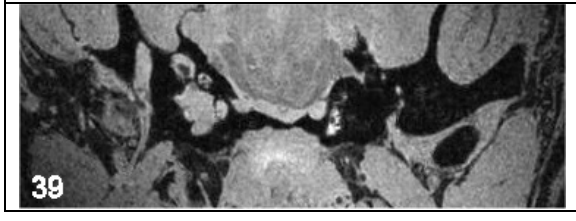
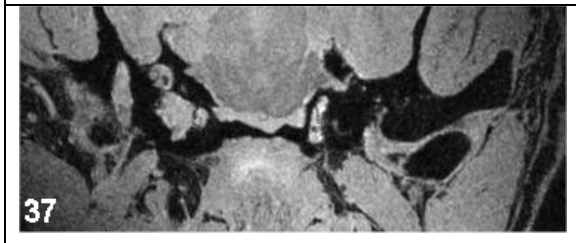
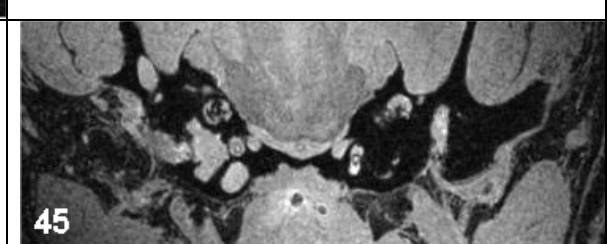
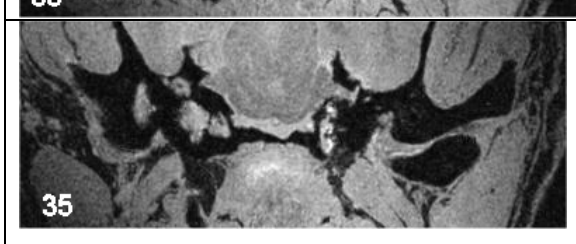
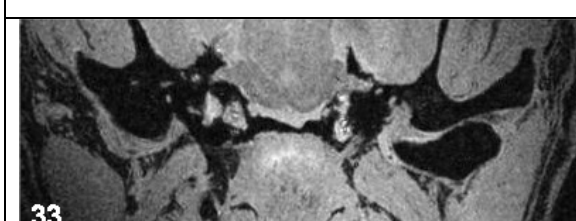
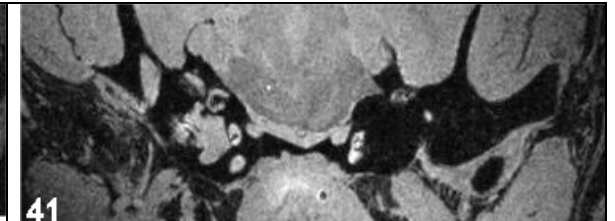
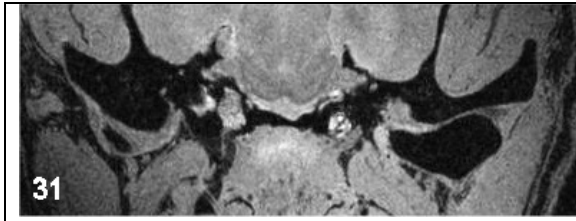


Figure 8.3.5.1. Transverse images progressing from rostral to caudal. Dorsal is to the top and right is to the left in all images. Number in bottom left corner indicates slice number.

Figure 8.3.5.1 continued. Transverse T1 weighted MRI sections through the CKCS TMJ.



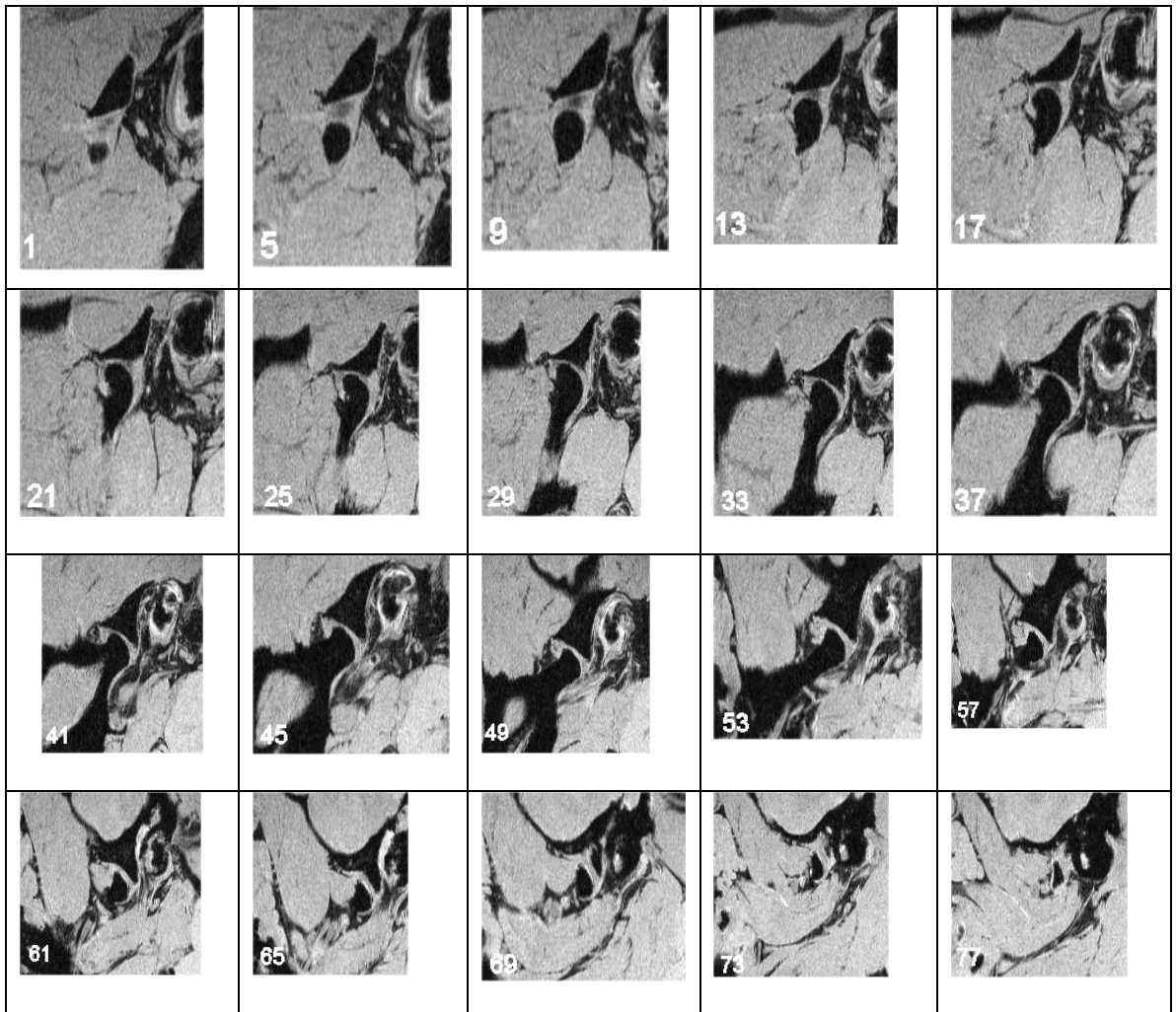


Figure 8.3.5.2. Sagittal images progressing from lateral towards midline. Dorsal is to the top and rostral is to the left in all images. Number in bottom left corner indicates slice number.

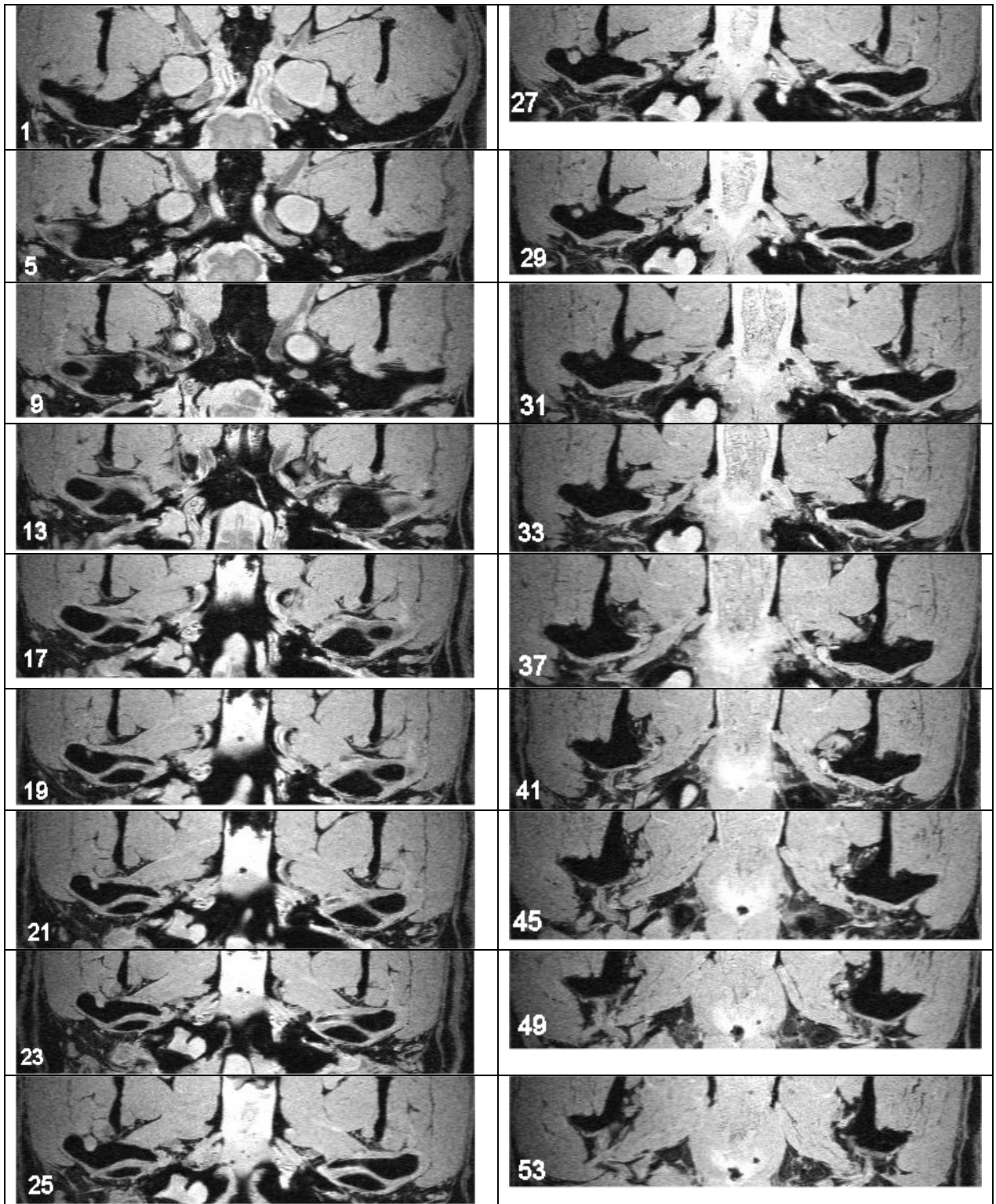


Figure 8.3.5.3. Dorsal images progressing from dorsal to ventral. Rostral is to the top and right is to the left in all images. Number in bottom left corner indicates slice number.

No.	Reason for Radiography	Views	Conclusion
1	orbital mass	DV	Both joints abnormal
2	mandibular fracture	DV / LAT	Both joints abnormal
3	hemiparesis	DV / LAT	Both joints abnormal
4	facial paralysis/ vestibular signs	DV / 2 x Lat oblique	Both joints abnormal
5	dysphagia	DV / 2 x Lat oblique	Both joints abnormal
6	head tilt	DV / LAT / RCdOM	Both joints abnormal
7	nasal discharge	DV / LAT / 2 x Lat oblique	Both joints abnormal
8	dysphagia	DV / 2 x Lat oblique	Both joints abnormal
9	unable to open mouth	DV / 2 x Lat oblique	Both joints abnormal
10	otitis	DV / RCdOM	Both joints abnormal
11	not stated	2 x Lat oblique	Both joints abnormal
12	not stated	2 x Lat oblique	Both joints abnormal
13	not stated	RCdOM / 2 x Lat oblique	Both joints abnormal
14	not stated	2 x Lat oblique	Both joints abnormal
15	paraparesis	2 x Lat oblique	Both joints abnormal
16	facial paralysis / head tilt	DV / 1 x Lat oblique	Visible joint abnormal
17	ataxia	DV / LAT / Lat oblique	Visible joint abnormal
18	mandibular fracture	DV / LAT	Visible joint abnormal
19	not stated	1 x Lat oblique	Visible joint abnormal
20	respiratory noise	LAT	Visible joint abnormal
21	swollen face	DV / LAT	Non - diagnostic
22	orbital swelling	DV / LAT	Non - diagnostic
23	chronic otitis	DV	Non - diagnostic
24	otitis	DV	Non - diagnostic
25	otitis	DV	Non - diagnostic
26	deafness	DV	Non - diagnostic

Table 8.3.1. Details of adult CKCS that had undergone a radiographic examination of the skull between 1991 and 2001. DV = Dorsoventral ; LAT = Lateral ; RCdOM = Rostrocaudal open mouth ; Lat oblique = latero 10-30° rostro – laterocaudal oblique

Figure 8.3.6. Examples of typical radiographs obtained in live CKCS dogs undergoing radiography of the head for the investigation of a variety of clinical conditions.



Figure 8.3.6.1. Dorsoventral view.

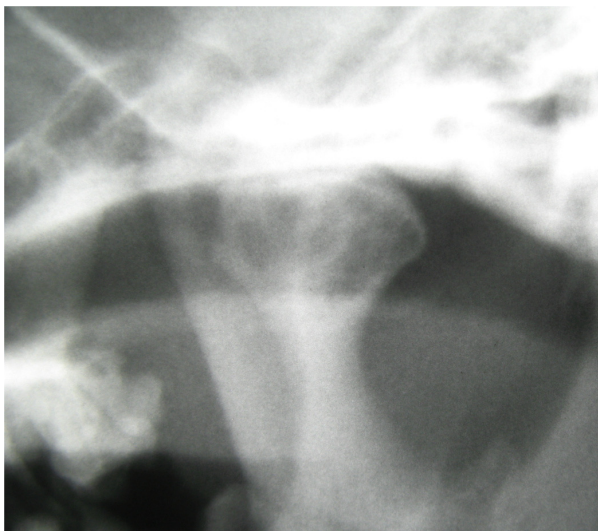
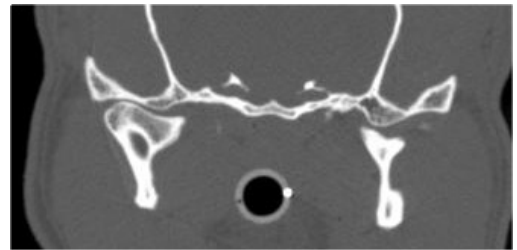
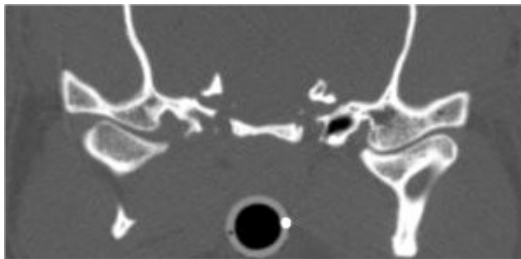
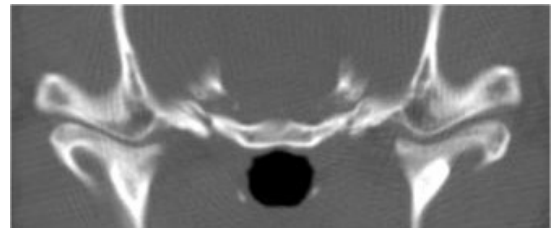
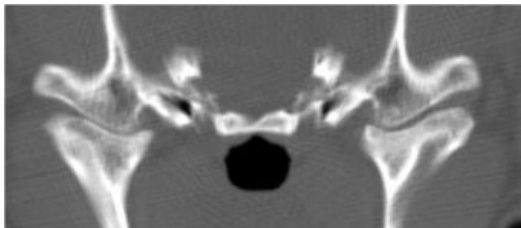


Figure 8.3.6.2. Latero 20° rostro – laterocaudal oblique view.

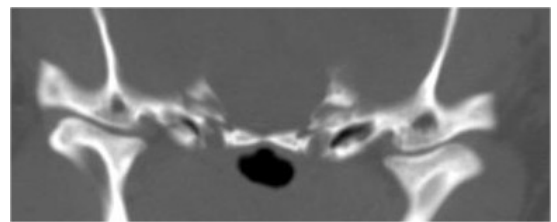
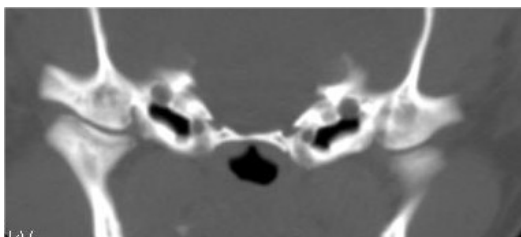
Figure 8.3.7. Examples of typical transverse sections through the TMJ of live CKCS dogs undergoing CT of the head for the investigation of a variety of clinical conditions. Images are viewed using a bone window. Dorsal is to the top and right is to the left in all images.



Case 1

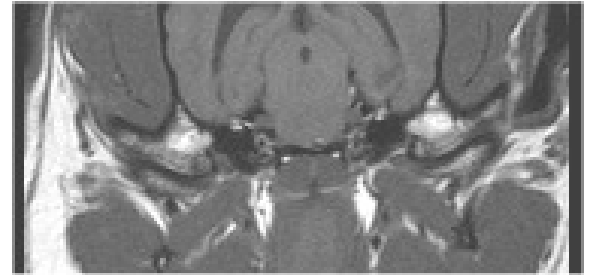


Case 2

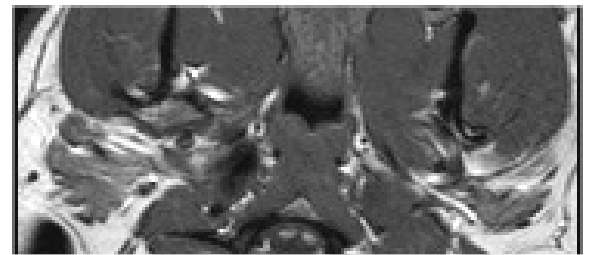
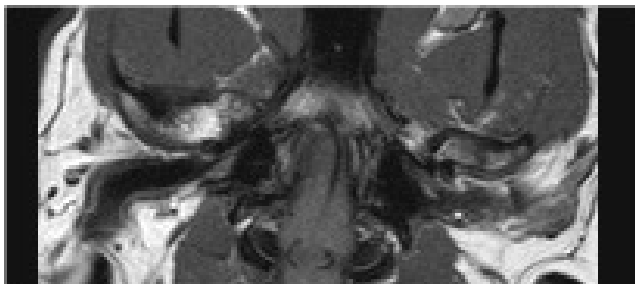


Case 3

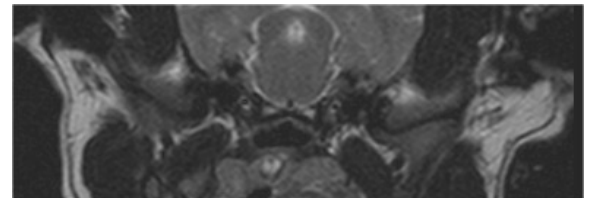
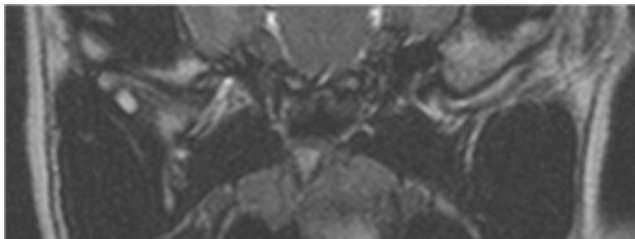
Figure 8.3.8. Examples of typical MR images through the TMJ of live CKCS dogs undergoing MRI of the head for the investigation of a variety of clinical conditions.



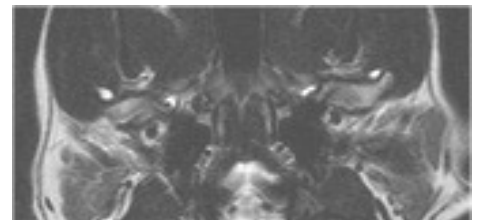
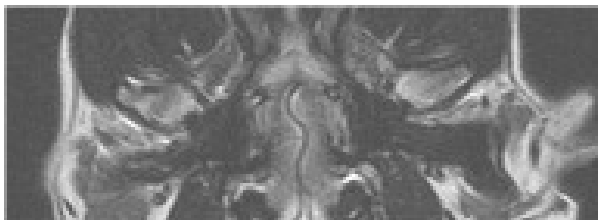
T1 weighted transverse sections



T1 weighted dorsal sections



T2 weighted transverse sections



T2 weighted dorsal sections

	Angle (°)	
	Left	Right
Skull 1	15	10
Skull 2	19	22
Skull 3	30	30
Head 1	17	18
Head 2	24	25
Head 3	23	24
Head 4	22	24
Case 1	28	25
Case 2	20	20
Case 3	23	25
Case 4	22	20
Case 5	22	24
Case 6	25	25
Case 7	10	14
Case 8	25	24
Case 9	29	25
Case 10	23	28
Case 16	20	23
Case 17	23	24
Case 18	25	23
Case 21	19	19
Case 22	25	24
Case 23	20	24
Case 24	24	22
Case 25	21	25
Case 26	19	19
Mean (SD)	22 (4.3)	22.5 (4.1)

Table 8.3.2. The rotational angles measured from the dorsoventral radiographs of CKCS.

SD = standard deviation

8.3.5. Anatomical observations in the emascerated rabbit skulls.

Although the bony anatomy of the rabbit TB and TMJ was the same in all specimens examined, some variation was noted in the conformation of the base of the skull, as demonstrated in Figure 8.3.9. In the majority of the skulls, the suture between the basioccipital and basisphenoid bones, or spheno-occipital synchondrosis, was obvious and open. However, in a small proportion of skulls, this was not visible despite the other sutures of the skull being similar in appearance to the normal skulls. The base of the skull was shorter in these specimens and, although the foramen magnum was of a similar size and shape to the normal skulls, when the skull was viewed from a ventral aspect, a larger proportion of it was visible indicating rostral rotation of the occipital bone. From the lateral aspect, the TB appeared to be located closer to the caudal extension of the zygomatic process than in the others skull and the caudal border of the skull was angled in a rostral direction.

In one skull, the spheno-occipital synchondrosis was not visible and the base of the skull was markedly asymmetrical, being longer on the left than the right with a distinct twisted appearance to the bone. Again, a larger proportion of the foramen magnum was visible from the ventral aspect than in the normal skulls and it too appeared asymmetrical. The right TB was located further rostral than the left as demonstrated by the shorter distance between it and the caudal extension of the zygomatic process when the skull was viewed from the right lateral aspect compared to the left side. The rostral angulation of the caudal border of the skull was also greater when the skull was viewed from the right compared to the left.

8.3.6. CT and MRI appearance of anatomical variations in the rabbit skull.

Examples of the CT images obtained in a normal rabbit cadaver head and one demonstrating these changes are presented in Figure 8.3.10. On the midline sagittal CT images of the normal rabbit, the spheno-occipital synchondrosis was visible as a vertical hypodense space between the bones. In the abnormal one it appeared as a hyperdense line between the adjacent bones with no space. Moving laterally, the brain case was also relatively small in this skull when compared with the normal head. This was apparently due to the caudal border of the occipital region being at a more acute angle. The angle between the occipital condyles and the first cervical vertebra was also sharper in this skull. Three dimensional reconstructions of normal and abnormal cadaver heads were performed but the

difference in the conformation of the base of the skull could not be identified from any aspect.

Examples of the MR images obtained in a normal rabbit cadaver head and one demonstrating these changes are presented in Figure 8.3.11. Again, the sphenoccipital synchondrosis was visible in the normal cadaver, this time as a vertical hyperintense area between the bones. In the abnormal one it was not visible and the signal voids produced by the adjacent bones appeared confluent. This region of bone appeared more convex than in the normal cadaver resulting in a reduced height of the caudal fossa.

Figure 8.3.9. Anatomical variations observed in rabbit skulls.

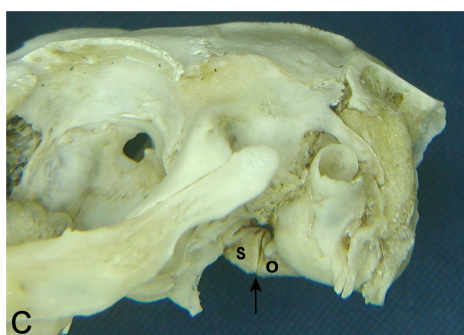
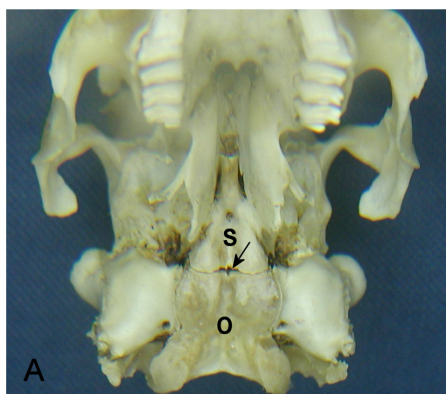


Figure 8.3.9.1. Appearance of a normal rabbit skull.

A. Ventrorostral aspect. B. Ventral aspect.
C. Lateral aspect.

o = basioccipital bone

s = basisphenoid bone

arrow = spheno-occipital synchondrosis

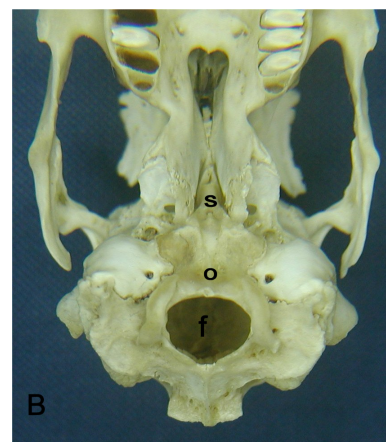
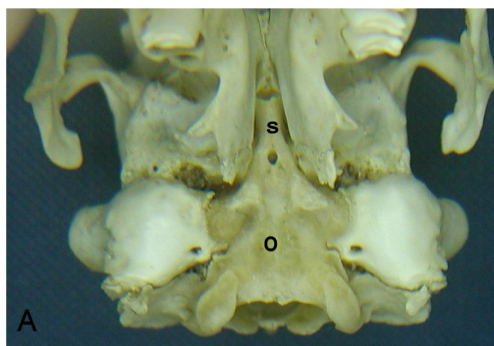


Figure 8.3.9.2. Appearance of an anatomical variation observed in three rabbit skulls.

A. Ventrorostral aspect. B. Ventral aspect.
C. Lateral aspect.

o = basioccipital bone

s = basisphenoid bone

f = foramen magnum

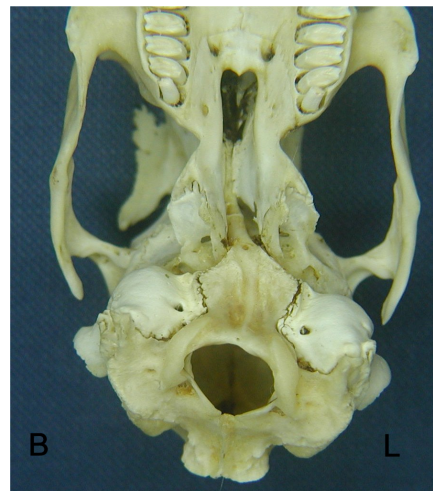
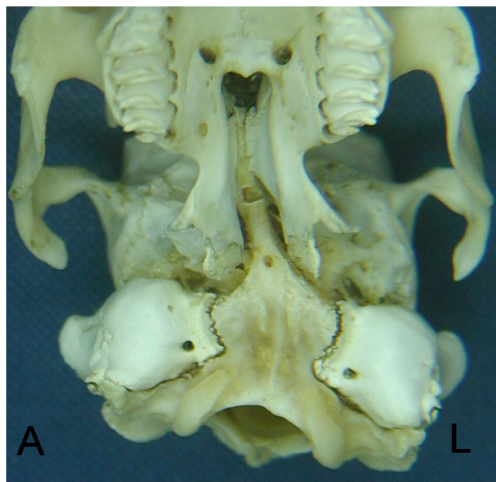


Figure 8.3.9.3. Appearance of an anatomical variation observed in one rabbit skull.
A. Ventrorostral aspect. B. Ventral aspect. C. Left lateral aspect. D. Right lateral aspect
L = left side * = caudal extension of zygomatic process

Figure 8.3.10. Sagittal CT images through a rabbit cadaver, viewed using a bone window. Rostral is to the right and dorsal to the top of the images. Arrow = spheno-occipital synchondrosis

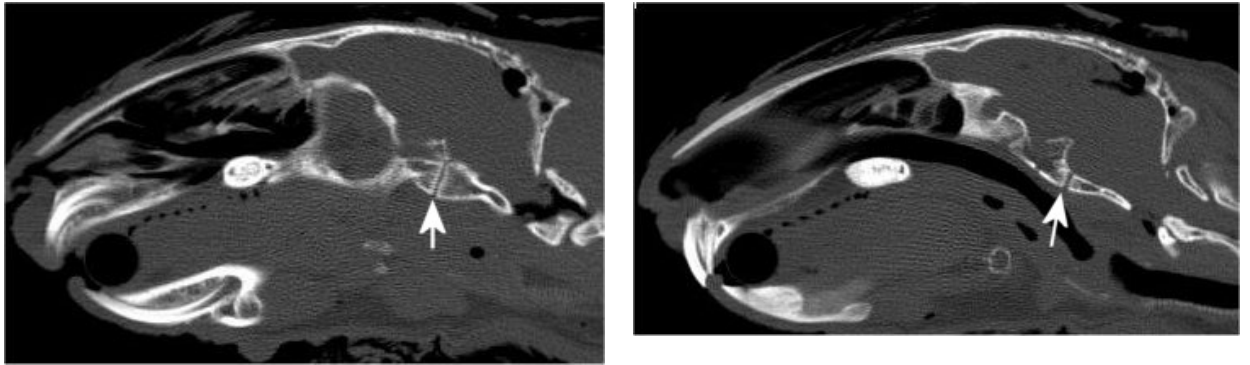


Figure 8.3.10.1. Examples of midline and para-sagittal sections of a normal rabbit cadaver head.

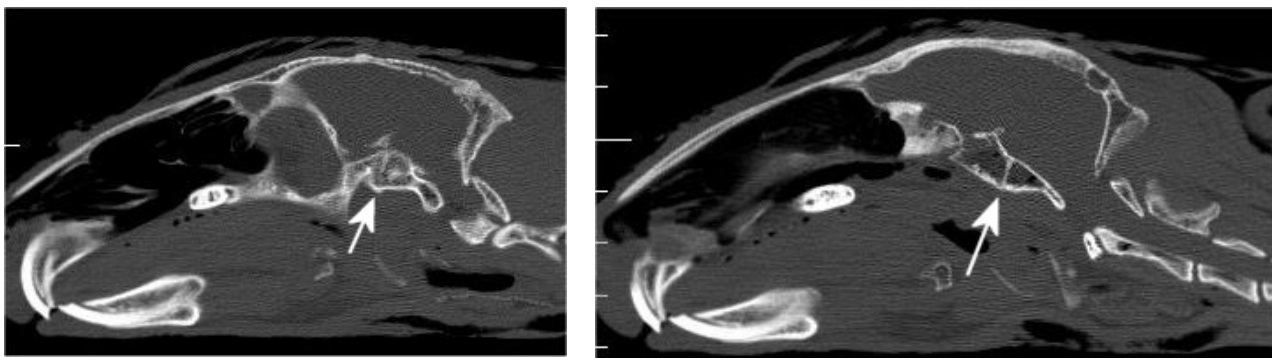


Figure 8.3.10.2. Examples of corresponding midline and para-sagittal sections through a rabbit cadaver head demonstrating anatomical variation.

Figure 8.3.11. Sagittal T1 weighted MR images through a rabbit cadaver. Rostral is to the right and dorsal to the top of the images. Arrow = spheno-occipital synchondrosis

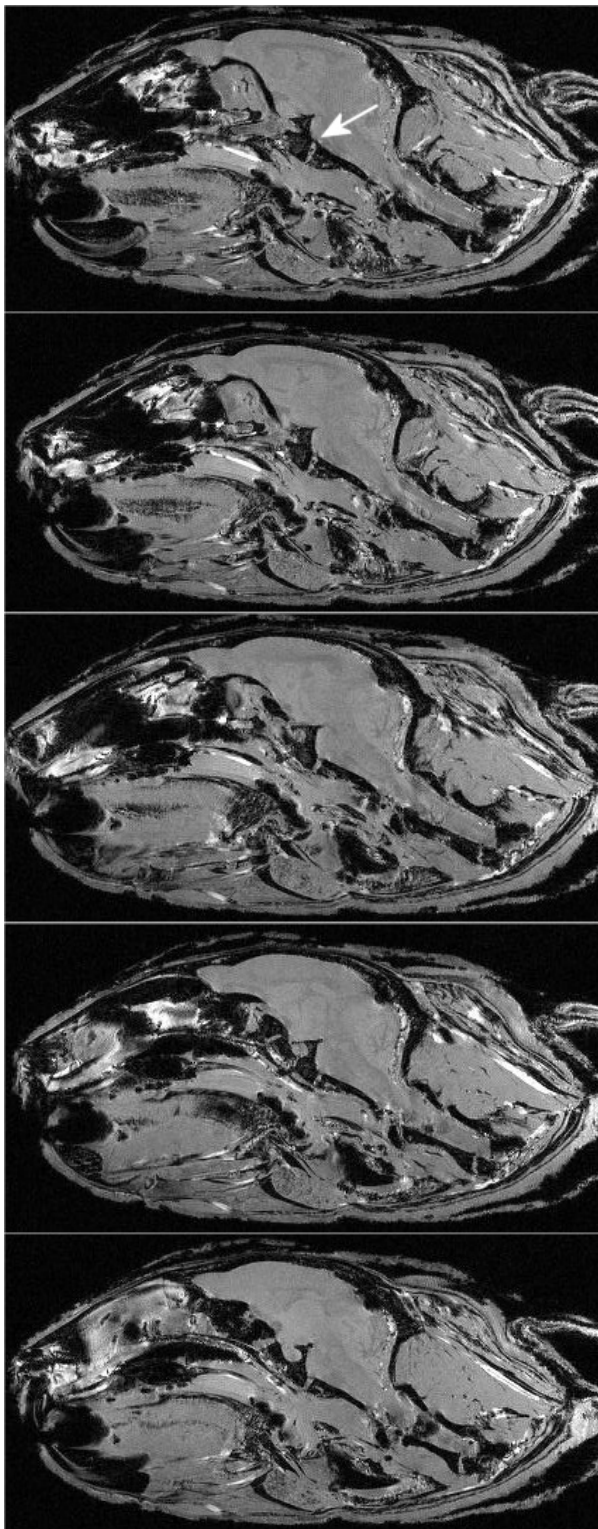


Figure 8.3.11.1. Examples of sequential midline and para-sagittal sections of a normal rabbit cadaver head.

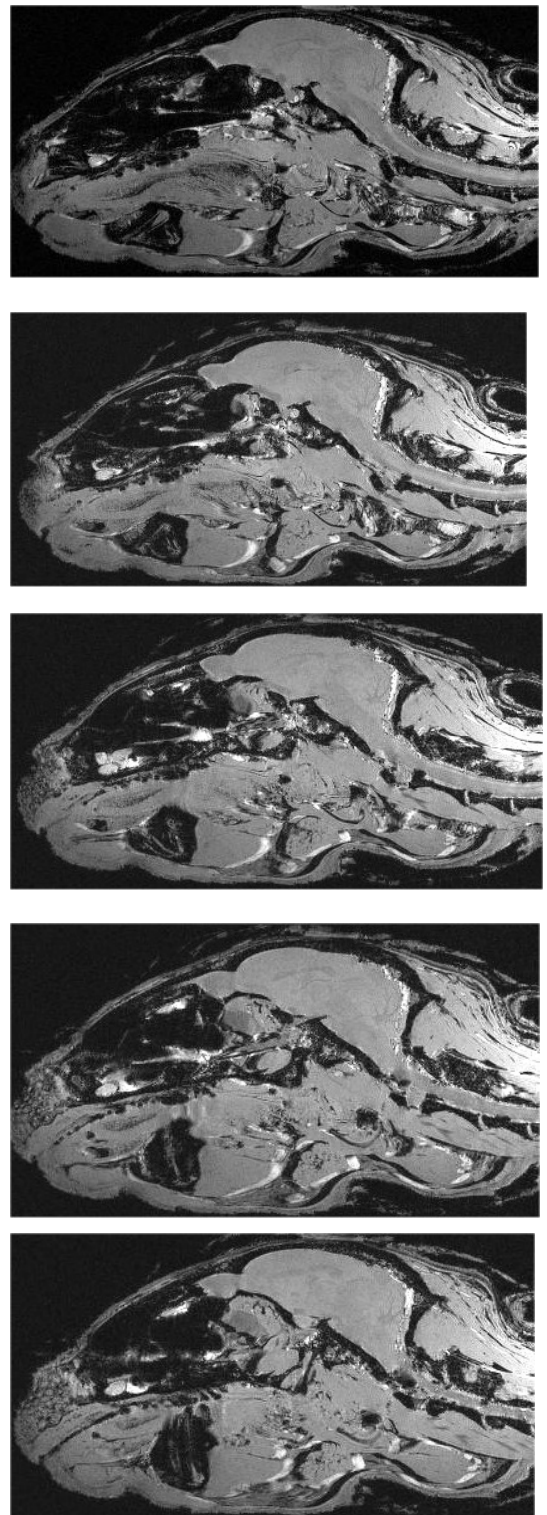


Figure 8.3.11.2. Corresponding sections of a rabbit demonstrating an anatomical variation in the base of the skull.

8.4 Discussion

8.4.1. TMJ dysplasia in CKCS

The normal anatomic and radiographic appearance of the canine TMJ has been described (Scapino 1965, Ström and others 1988, Evans 1993, Caporn 1995, Owens and Biery 1998, Schwarz and others 2002, Thrall 2002). The changes encountered in the anatomy of the CKCS in the present study were considered to be consistent with the presence of TMJ dysplasia. Although classically associated with the Irish Setter and Bassett Hound, TMJ dysplasia has been observed in a variety of breeds including the Boxer, Labrador Retriever, Golden Retriever and Bernese Mountain dog (Stewart and others 1975, Robins and Grandage 1977, Johnson 1979, Lane 1982, Stead 1984, Bennet and Prymak 1986). The condition has also been described in the American Cocker Spaniel and Dachshund, in what appears to be a different clinical context and it is with this group that these previously unreported observations in the CKCS correspond most closely (Hoppe and Svalastoga 1980, Vollmerhaus and others 1996, Vollmerhaus and Roos 2003).

A variety of features have been recorded in cases of TMJ dysplasia including shallow mandibular fossae; deficient temporal articular surfaces; thickened, enlarged, hypoplastic or absent retroglenoid processes; divergent, claw shaped joint spaces; flattened or small mandibular condyles; abnormally shaped condylar articular surfaces and abnormal angulation or location of the condyloid processes (Stewart and others 1975, Robins and Grandage 1977, Johnson 1979, Lane 1982, Stead 1984, Bennet and Prymak 1986). The abnormalities observed in the CKCS in the present study differ from these reports in that a range of dysplastic changes were noted. The skull with the longest retroarticular process had the most concave mandibular fossa and the one with the shortest retroarticular process had the most convex mandibular fossa suggesting that elongation of the retroarticular process and concavity of the mandibular fossa may be related, although there were insufficient skulls in the study to confirm this observation. The articular surfaces of the condyloid process mirrored those of the mandibular fossa suggesting that these structures may have an influence on the development of each other. The ventral articular surface of the condyloid process only extended as far as the ventral margin of the shortened retroarticular process and the degree of convexity of the medial aspect of the mandibular fossa produced a corresponding concavity of the condyle. The length of the lateral aspect of the mandibular fossa was related to the area where the corresponding articular surface of

the condyloid process terminated. These observations suggest that the development of the condyloid process and mandibular fossa must progress concurrently regardless of the fact that the upper and lower mandibles are developmentally independent despite being counterparts, as demonstrated in brachycephalic breeds (Evans 1993). The abnormalities reported in Dachshund skulls corresponded closely with observations in the present study, where varying degrees of concavity of the medial aspect of the articular surface of the condyloid process and premature termination of the lateral aspect producing an undulating caudal margin were also reported (Vollmerhaus and Roos 2003). American Cocker Spaniels were also reported as showing varying degrees of dysplastic changes including bilateral flattening of the glenoid cavity and hypoplasia of the retroarticular process (Hoppe and Svalastoga 1980). This condition was reported to be bilateral in six related dogs and unilateral in another two unrelated ones (Hoppe and Svalastoga 1980). Likewise in the present study, the changes observed were not always bilaterally symmetrical although there was no information available to determine if the animals from which the material was obtained were related in any way.

The dysplastic changes identified in the CKCS cadavers and cases in the present study were retrospective and were not associated with clinical signs. Only two dogs underwent diagnostic imaging specifically for problems associated with opening or closing the mouth, and these were the only dogs in which a prospective diagnosis of TMJ dysplasia was made. However, the changes observed were comparable with those of the other asymptomatic dogs. Also, the eventual clinical diagnoses reached were unrelated to the TMJs and subsequently treated successfully so the contribution of these abnormalities to the clinical presentation of the dogs must be questioned. Likewise, TMJ dysplasia in American Cocker Spaniels was also discovered during the investigation of another condition and in Dachshunds during an unrelated study, so neither were associated with clinical signs (Hoppe and Svalastoga 1980, Vollmerhaus and others 1996, Vollmerhaus and Roos 2003). TMJ dysplasia occurs in most breeds as an isolated event with the majority of the population having normal TMJ anatomy (Johnson 1979, Hazewinkel and others 1993). However, none of the CKCS TMJs that could be adequately assessed in the present study were considered normal. These observations suggest that these changes may represent a breed variation for the CKCS. Since there appear to be striking similarities between the Dachshund, American Cocker Spaniel and CKCS, these may form a group where dysplastic changes can be regarded as a normal breed feature.

The underlying cause of TMJ dysplasia in the dog is not known although many theories have been suggested. These include it being a primary problem with either congenital or acquired aetiologies, or that the dysplastic changes develop as a result of other factors such as the effect of rapid growth in chondrodystrophied breeds, inferior prognathism or laxity of the mandibular symphysis (Robins and Grandage 1977, Johnson 1979). This condition has been observed in more than one animal in litters of Bassett Hounds which suggested a hereditary component in this breed (Stewart and others 1975). The absence of dysplastic changes in any of the larger brachycephalic breeds in the present study suggested that size must be an influence if brachycephalism is involved. However, neither Bassett Hounds nor Dachshunds are brachycephalic making its involvement less likely. The Bassett Hound, Dachshund, CKCS and American Cocker Spaniel are all naturally chondrodystrophic and although the characteristic changes are the presence of short limb bones and a normal sized skull and trunk, concurrent changes in the skull bones have been reported in a number of different species (Sawin and others 1959). However, these tend to involve the base of the skull and the occipito-vertebral articulation and there do not appear to have been any reports regarding abnormal development of the TMJ. Chondrodystrophy affects bones that form from endochondral ossification while the components of the TMJ form from the viscerocranium by a combination of endochondral and intramembranous ossification (Evans 1993).

The most characteristic clinical sign associated with TMJ dysplasia is reported to be open mouth jaw locking due to laxity of the joint, allowing impingement of the coronoid process on the zygomatic arch, where it becomes trapped in a position lateral to it (Robins and Grandage 1977, Johnson 1979). However, in the Boxer, Labrador Retriever and Golden Retriever, displacement of the coronoid process was not observed and jaw locking was thought to arise from secondary osteoarthritic changes associated with the joints. In another dog, the presenting signs were of jaw pain and dysphagia, and open mouth jaw locking was not a feature (Bennet and Prymak 1986). The absence of clinical signs in the present study despite the presence of severe dysplastic changes remains unexplained (Robins and Grandage 1977). Widening of the joint space has been reported in most of the previous examples of TMJ dysplasia but this was not noted in radiographs in the present study (Johnson 1979, Stead 1984, Bennet and Prymak 1986). This may suggest that bony changes observed in the CKCS are not associated with marked laxity of the joint, possibly

due to compensatory soft tissue changes or conformation of the condyloid process to the abnormal shape of the mandibular fossa. In Dachshunds, the interarticular disc has been reported to be of abnormal shape and thickness and this may compensate for bony dysplasia by outweighing the incongruence of the joint (Vollmerhaus and others 1996). The contribution of surrounding soft tissue structures to the function of the joint was reinforced by two dogs with clinical signs in the absence of radiographic abnormalities and in one, a selective masticatory myositis was hypothesised to be the cause of the jaw locking (Lantz and Cantwell 1986, Hazewinkel and others 1993).

Alternatively, the broad zygomatic arch in the CKCS may make it difficult for the coronoid process to become located lateral to it despite the presence of joint laxity. However, this is unlikely since open mouth jaw locking can arise without the coronoid process becoming involved with the zygomatic arch (Bennet and Prymak 1986). Secondary degenerative joint disease is a likely consequence of dysplastic joints and has been reported in association with TMJ dysplasia where in some dogs it appeared to cause the open mouth jaw locking (Stead 1984, Bennet and Prymak 1986). There was no evidence of degenerative changes in any CKCS TMJ in the present study, suggesting these changes are not associated with marked laxity.

The radiographic changes reported in association with TMJ dysplasia in Irish Setters and Bassett Hounds included enlarged, rostrally located retroarticular processes, a deficient dorsal temporal articular margin producing a misshapen mandibular fossa and a widened, irregular joint space. The only significant differences appeared to be in the shape of the mandibular condyles where the Irish Setter was described as having a medial articular surface that occupied more than half of the condyloid process and protruded beyond the mandibular fossa, while those in the Bassett Hounds were reported to be smaller than normal (Stewart and others 1975, Robins and Grandage 1977, Johnson 1979). The published dorsoventral radiograph of TMJ dysplasia in a Basset Hound was characterized by a marked concavity of the medial articular surface similar to that observed in the present study (Robins and Grandage 1977). The radiographic changes in the Boxer, Golden Retriever and Labrador Retriever are less well described and include increased obliquity of the mandibular condyles, shallow mandibular fossae and wide, irregular joint spaces (Bennet and Prymak 1986). However osteophyte formation was described on the

retroarticular processes in these dogs and also in a Bassett Hound (Stead 1984, Bennet and Prymak 1986).

In the present study, the severity of the dysplastic changes influenced the radiographic views in which they could be identified. The most common view present was the dorsoventral, but only TMJs which had marked concavity of the medial aspect of the condyloid process or a rounded protrusion at the premature termination of the lateral articular surface could be identified in this view. It was difficult to conclusively distinguish mild concavity, flattening or unevenness of the caudal articular surface from a normal variations. However, not all of the dorsoventral radiographs were positioned symmetrically and rotation in a long axis direction appeared to enhance assessment of the shape of the caudal articular surface of the condyloid process, particularly in the presence of subtle changes. True lateral views were also of marginal value due to superimposition of the TMJs and the only feature which could be noted conclusively was absence of the retroarticular process. Lateral oblique views were the most useful for identification of subtle abnormalities. They permitted each joint to be examined individually and the length of the retroarticular process to be assessed. The shape of the mandibular fossa was apparent and this allowed the significance of the shape of the condyloid process on the dorsoventral view to be more accurately assessed. The most consistent changes identified in these views were a short or absent retroarticular process in association with flattening of the mandibular fossa and an angular appearance to the condyloid process resulting from its deficient medial margin. These observations suggested that a straight dorsoventral view may not be sufficient to identify subtle changes and that a combination of views should be used, with the lateral oblique appearing to be the most useful. This corresponded with the recommendation that the best radiographic views to make for assessment of the TMJs are a lateral oblique view of each joint and a dorsoventral (Lane 1982).

The appearance of TMJ dysplasia on CT and MRI images has not been previously reported although a Beagle undergoing CT for the investigation of a mass arising from the middle ear was reported to have very curved articulating TMJ surfaces that were similar to those observed in the Dachshund (Schwarz and others 2002). The changes observed in the CT and MR images in the present study corresponded with those observed grossly and radiographically. The transverse sections allowed assessment of the contour of the condyloid process and corresponding mandibular fossa, while sagittal sections also allowed

the shape and length of the retroarticular process to be evaluated. The undulating nature of the joint components resulted in the impression of congruence in the transverse and dorsal sections while the sagittal ones alone demonstrated the true degree of incongruence throughout the entire joint space. The dorsal sections were considered to be of least value as they only identified concavity of the medial articular surface of the condyloid process in cases with marked changes. The 3-dimensional reconstructions did not allow assessment of the internal components of the joint but did allow the retroarticular process to be examined therefore may be useful if only transverse sections are available since the retroarticular process can be difficult to assess in these images.

Retrospective studies are limited by the availability of archived material, reflecting the area of interest during the original examination. The lack of appropriate radiographic views in some cases prevented all of the joints from being adequately assessed. Assessment of CT and MR images were easiest in the cadavers where contiguous slices were acquired, meaning that all regions of the joints could be examined. The slice thickness and increment of archived images influenced retrospective assessment of these structures, due either to their incomplete representation or to the effects of partial volume artefact. Although sagittal MR sections were deemed to be useful for assessment of joint congruity, none of the archived sequences extended laterally enough to incorporate the TMJs. Likewise, in Chapter 6 it was determined that T1 weighted MR images were best for imaging the TMJ but in many cases only T2 weighted ones were available, although the changes still tended to be marked enough for identification. In the case of CT, images stored using brain or soft tissue windows did not allow adequate visualisation of the joints and only those saved using a bone window could be used. Suboptimal positioning that hindered assessment of bilateral symmetry was encountered in all three modalities, although in the case of the dorsoventral radiographs, it was actually advantageous. Given the problems with suboptimal positioning arising in chapters 5 and 6 when cadavers were used, it was not surprising that this also occurred when positioning live clinical cases.

An increase in the obliquity of the condyloid processes has been reported in several dogs with TMJ dysplasia and open mouth jaw locking, although the actual angle was not always measured (Bennet and Prymak 1986, Robins and Grandage 1977, Johnson 1979, Lantz and Cantwell 1986, Hazewinkel and others 1993). Large angles are thought to result in excessive movement of the lateral aspect of the condyle which leads to stretching of the

lateral ligament and in turn subluxation (Robins and Grandage 1977, Lantz and Cantwell 1986). The rotational angle, which is angle between the long axis of the condyloid process and the medial portion of the articular surface, has been measured in normal dogs. In a study of 35 dogs representing 18 different breeds the mean angle of the right condyloid process was 13.8° with a standard deviation (SD) of 5.0 and the left was 15.2° SD 5.1 (Hazewinkel and others 1993). In Chapter 2, the rotational angle was measured in 38 dogs of 22 different breeds where the mean angle of the right condyloid process was 16.8° SD 4.8 and the left was 15.9° SD 5.2. Although neither study included enough dogs to establish normal breed values, the six Boxers in Chapter 2 demonstrated larger angles of obliquity than the other breeds present. The mean angle of their right condyloid process was 22.8° SD 4.7 and the left 22.8° SD 3.4, which probably accounted for the higher overall mean value. With the exception of Boxers, a value of less than 20° was consistent with a normal TMJ.

The mean angle of the right and left condyloid processes in the CKCS was 22.5 SD 4.1 and 22.0 SD 4.3 respectively, which was similar to the average values obtained for the normal Boxers in Chapter 2. The angles of the condyloid processes in the CKCS increased with severity of the dysplastic changes and values of above 20° were calculated for 77% of them. The remaining dogs did not have values markedly different from those of the normal mandible in other breeds previously reported and in Chapter 2 (Hazewinkel and others 1993). Only one dog with open mouth jaw locking in the absence of radiographic changes was reported to have a larger angle than normal dogs of the same breed, while the rest of the dogs in the study did not (Hazewinkel and others 1993). This overlap between values in dogs with and without clinical signs or radiographic changes suggests this the rotational angle is not a reliable indicator of joint laxity and supports the hypothesis that surrounding soft tissue has an effect on joint function (Lantz and cantwell 1986, Hazewinkel and others 1993). Although the angle of the condyloid process increases with severity of bony changes, a large angle does not necessarily mean the joint is dysplastic therefore the shape of the joint components is of greater significance than the angle of the condyle. As bony changes become marked, they become easier to identify on diagnostic images. However, if during diagnostic imaging changes consistent with TMJ dysplasia are identified in the CKCS, American Cocker Spaniel or Dachshund then they are unlikely to be associated with the clinical signs being investigated.

8.4.2. Variations in rabbit skull anatomy

The anatomical variations associated with the base of the rabbit skull observed in this study appeared to imply a premature closure of the spheno-occipital synchondrosis. This resulted in shortening of the base of the skull and rostral rotation of the occipital bone, foramen magnum and TB. The asymmetry observed in one specimen could have resulted from one section of the suture closing before the other half. The rabbits used in this study were age matched and this was confirmed by the appearance of the other skull sutures being the same in all the emasculated specimens.

Chondrodystrophy has been observed in the New Zealand White rabbit in the presence of the Dachs gene (Sawin and others 1959). This affects the bones of the skull and limbs that form by endochondral ossification from cartilage precursors, and in the skull, the spheno-occipital synchondrosis is most vulnerable (Sawin and others 1959). In normal rabbits, bony fusion, transforming the synchondrosis into a synostosis, occurs late in life or not at all, while in Dachs rabbits, it can occur as early as within a few weeks of birth. Asymmetry associated with uneven closure has also been reported (Sawin and others 1959). The appearance reported in these skulls was very similar to that encountered in the present study. However, Dachs rabbits demonstrate the disproportionate dwarfism associated with their chondrodystrophic state, while the ones used in the present study were clinically normal and of normal physical proportions. Further work would therefore be required to determine why such marked changes were noted in the bones of the skull in the absence of other skeletal abnormalities and the role of this, or other genes in this process. It would also be of interest to determine whether this also occurs in other rabbit breeds, in particular the brachycephalic Netherland Dwarf and other dwarf breeds.

Further work would also be required to determine if these changes are associated with concurrent alterations in the brain or spinal cord in this species, and if they are ever associated with clinical signs. There are two stages of growth of the skull, the first being rapid expansion of the brain case followed by slow, prolonged growth resulting in elongation of the cranium and face (Sawin and others 1959). Despite the premature closure of the spheno-occipital synchondrosis, in Dachs rabbits, concurrent delayed closure of the caudal components of the cranial base (between the basioccipital and exoccipital, and exoccipital and supraoccipital bones) suggest that the brain is likely to remain unaffected by the retardation in size of the endochondral bones (Sawin and others 1959). However,

further changes in Dachs rabbits were also reported at the occipito-atlanto-axial region including abnormalities of spacing, accessory ossification centres and aberrations in fusion of components (Sawin and others 1962). Occipital dysplasia is common in CKCS and seen sporadically in other small dog breeds (Dennis 2006). The resulting malformation of the occipital bone, can cause a reduction in size of the caudal fossa and crowding at the foramen magnum leading to syringohydromyelia and hydrocephalus similar to Chiari syndrome in humans (Dennis 2006). However, it is not always associated with neurological signs and therefore has been reported as a normal morphological variation in brachycephalic breeds (Thrall 2002). Neurological problems are often encountered in the rabbit (Keeble 2006) and it may be that animals with underlying anatomical variations such as those observed in the present study are predisposed to such conditions.

Chapter 9. General Discussion

Dogs, cat and rabbits are currently the three most popular companion animals in the United Kingdom (Nicholson, 2001, Meredith 2006, PFMA 2006). Although radiography remains the most common veterinary diagnostic imaging modality, diagnostic ultrasound is now widespread in general practice (Nyland and others 1995). The availability of CT and MRI is also increasing (Dennis 2006), particularly with the introduction of mobile services, and recent advances in computer hardware and software have resulted in a significant improvement in image quality across the board. The quality of the images produced in the present study were superior to many older publications (George and Smallwood 1992, Love and others 1995, Seitz and others 1996, Assheuer and Sager 1997). However, the accurate interpretation of the resulting images still relies on an appreciation of normal regional anatomy and how it appears using each of the techniques (Nyland and others 1995). As image quality improves, there is therefore a continuing need for anatomical studies to identify and characterise features that were previously unidentified or can now be visualised in greater detail. The use of cadavers in such studies is well established (Jones and others 1995) but may be associated with the presence of artefactual post mortem changes (Jones and others 1995, Weller and others 1999, Morrow and others 2000). Although this was also observed in the present study, it did not significantly influence the results obtained and therefore the use of cadavers remains a valid alternative to the use of live animals and their associated ethical, welfare and logistical issues (Jones and others 1995).

The temporal bone in the dog, cat and rabbit comprises three parts. Of these, the tympanic part forms the TB, housing a large portion of the middle ear, while the squamous part gives rise to a zygomatic process that articulates with the mandible to form the TMJ (Weijs and Dantuma 1981, Little and Lane 1986, Barone 1989, Evans 1993, Caporn 1995). While the TB of the dog and cat are well described, there are no reports specifically regarding the TB of the rabbit. The bony and soft tissue anatomy of the TB was generally similar between the species although each had features specific to them. Their location on the ventral surface of the base of the skull was constant but variations in shape and relative size were observed between the species, being most prominent and projecting furthest ventrally in the cat. The mastoid and paracondylar processes in the rabbit were very prominent and overlay the caudal aspect of the TB wall while the mastoid process was almost absent in the cat.

Likewise, the external ear canal formed an extensive bone tube in the rabbit but in the cat was merely a ring of bone. The dog demonstrated a distinctive bone ridge at the base of the external ear canal that was extended in the cat to form a complete bony septum dividing the TB lumen into dorsal and ventral compartments. The epitympanic recess in the rabbit was extensive, extending in a dorsal direction medial to the external ear canal.

The TMJ anatomy of the dog and cat was similar reflecting their carnivorous nature (Evans 1993, Capron 1995). Both were transversely orientated and level with the molar arcade. However, the joint in the cat was relatively featureless compared with the dog and demonstrated better congruity between the articular surfaces. A distinctive intra-articular disc was identified in the dog while there was merely a fibrous sheet in the cat. The herbivorous nature of the rabbit resulted in a fundamentally different anatomy to the TMJ, being located dorsal to the molar arcade and orientated rostrocaudally. There was poor congruity between the articular surfaces with compensation in the form of a well developed, intra-articular disc.

It is useful to have normal specimens available for comparison when interpreting diagnostic images and the production of multiplanar anatomical sections are beneficial for use in conjunction with the sectional images produced by ultrasound, CT and MRI (George and Smallwood 1992, Assheuer and Sager 1997, Weller 1999, Harcourt-Brown 2003, Morrow and others 2003). However, preservation of fresh material can be problematic given the health and safety implications associated with the production, storage and use of conventional formalin based preservation methods (Health and Safety Executive 2002). Plastination is a relatively new technique that addresses many of these issues (Miklošová and Sivrev 1999, Whittaker 2007). Although there is a need for investment in the appropriate equipment and compliance with the health and safety aspects of each stage of the process, it proved to be a relatively straight forward procedure to perform. The resulting material was of high quality with little tissue distortion and completely safe to handle and store, making it ideal for teaching and comparison with multiplanar diagnostic images.

Many radiographic views are recommended for investigation of the TB and TMJ in the dog and cat (Douglas and others 1987, Farrow 1994, Owens and Biery 1998, Schwarz and others 2002) but there are currently few specific reports in the rabbit (Harcourt-Brown 2003). The comparable location and anatomy of the TB between the three species meant it

could be visualized in similar views and the TB nearest the cassette was best imaged at low angles of rotation in lateral and long axis directions. This corresponded with the current recommendations in dogs and cats (Douglas and others 1987, Farrow 1994, Owens and Biery 1998) and indicated that these views were also appropriate in the rabbit. From ventral angles of rotation, the canine TB was best visualised with the mouth open while in the cat it could be imaged with the mouth either closed or open. This confirmed reports that a rostro 10° ventral-dorsocaudal oblique view may be used in place of a rostrocaudal open mouth view in this species (Hofer and others 1995) but also demonstrated that this is not applicable to the dog. The open mouth views were not appropriate for use in the rabbit although the TB could be visualised with the mouth closed in this series and also by rotation in a dorsal direction.

The TMJ nearest the cassette in the dog and cat were also best imaged at low lateral and long axis angles of rotation, again corresponding with the recommended views (Douglas and others 1987, Farrow 1994, Owens and Biery 1998, Schwarz and others 2002). Various components could also be examined in the ventral rotational views and this has not been previously reported. The fundamental differences in the anatomy and location of the rabbit TMJ meant that it proved difficult to visualise in these views and the best ones proved to be low angles of rotation from a rostrocaudal position in either a lateral, ventral or dorsal direction. These results indicate that extrapolation of views between species is not always possible and that anatomical studies such as this are necessary in the determination of appropriate views.

Although ultrasound is now routinely used for a range of examinations in veterinary practice, there is only one report of its use for imaging the TB in canine cadavers (Griffiths and others 2003) and none in live animals or other species. It has been used to image the equine TMJ (Weller and others 1999a, Weller and others 1999b) but again, there are no reports in other species. These structures could be imaged using conventional ultrasound equipment in the dog cat and rabbit. Although high frequency transducers proved optimum in the cat and rabbit, these are becoming increasingly available in general practice suggesting that these examinations could potentially be performed outwith referral centres. A lower frequency transducer was required in the dog due to the larger size and therefore greater depth of penetration required of the beam, but also resulted in poorer image quality. The size and shape of the TB varied on the images according to the anatomical differences

observed between the species, with the feline TB being most prominent, superficial and therefore easiest to identify. The ultrasound beam was able to penetrate the thin ventral TB wall and distinguish between the presence of gas and fluid in the lumen in all three species, corresponding with the previous report in the dog (Griffiths and others 2003). In the presence of fluid, the far wall of the TB became visible in the dog and rabbit, and the septum in the cat. The prominent mastoid process in the rabbit produced a distinctive appearance that aided identification of the TB but also obscured a large proportion of the lumen so care was required when determining luminal changes in this species.

As in the horse, (Weller and others 1999a, Weller and others 1999b) the bone surfaces of the lateral aspect of the TMJ components could be visualised in the dog and cat from a series of different angles. Unlike the horse though, the small size of these species meant that none of the soft tissue components of the joint could be identified. Despite both being herbivores, the TMJ anatomy in the rabbit differed significantly from the horse therefore examination was limited to a dorsal approach. The mandibular fossa was not visible due to its location on the ventral surface of the zygomatic process of the temporal bone but the location of the condyloid process caudal to the mandibular fossa meant that its dorsal articular surface could be examined. Again though, none of the soft tissue components of the joint could be identified. This suggests that ultrasound is likely to be of limited benefit in clinical evaluation of the TMJ although it could potentially identify changes involving the lateral structures in the dog and cat and the dorsal aspect of the condyloid process in the rabbit.

Many referral centres now have CT machines and there are many reports of its use for imaging the TB in dogs and cats (Hoskinson 1991, Love and others 1995, Seitz and others 1996). Although it is also recommended for imaging the TMJ in these species (Schwarz et al. 2002), there appear to be few reports and none for either structure in the rabbit. Most CT images are acquired in the transverse plane with subsequent reconstruction in the dorsal and sagittal planes (Tidwell 1999) although it is possible to position anaesthetized animals for the direct acquisition of dorsal sections (Russo et al. 2002). The directly acquired images in the present study were of better quality than reconstructions and the rapid sequence acquisition associated with modern CT equipment indicates that the examination time is not excessively lengthened by the additional direct acquisition of dorsal sections. Although it has been recommended that the TB and TMJ be assessed using both bone and

soft tissue windows (Love and others 1995, Schwarz and others 2002), soft tissue windows in the present study were found to be of limited value and therefore bone windows appear most appropriate. The bony components of the TB and TMJ and the gas-filled TB lumen were well visualised in all three species. In keeping with the observations of Russo and others (2002), the transverse and dorsal sections appeared to be of most use for imaging the middle ear, and the ability to compare with the contralateral side aided identification of the various structures. The presence of fluid did not significantly influence the images obtained of the TB and the same structures could be identified in both states.

In the case of the TMJ, each of the multiplanar series allowed a different area of the joint to be examined. In the dog and cat, the transverse sections highlighted the dorsal components and the dorsal sections the caudal and ventral components. The sagittal sections allowed assessment of all areas of the joint space and the profile of the retroarticular process, and therefore are likely to be particularly useful in the evaluation of TMJ abnormalities in these species. The orientation of the TMJ in the rabbit meant that the transverse section highlighted the dorsal components, the dorsal sections highlighted the rostral components and the sagittal sections highlighted both. Opening the mouth altered the regions that could be assessed in each sequence but the soft tissue components of the TMJ could not be distinguished from adjacent structures in any view or position despite opening and closing the mouth being reported to help determine the location of the intra-articular disc in humans (Dixon 1991). A small hypoattenuating area in the rostral aspect of the lateral half of the canine condyloid process on transverse CT images has been reported as a normal anatomical variation (Schwarz and others 2002). The present study indicated that this was due to the shape and orientation of the rostral margin of the condyloid process resulting in the area immediately medial to the lateral extremity not being present within transverse sections through the rostral aspect of the TMJ.

The use of MRI for imaging of the middle ear in the dog and cat (Allgoewer and others 2000, Dvir and others 2000, Garosi and others 2000) has been reported but there appears to be only one report of its use to image the canine TMJ (Baines and others 2002) and none in the cat and rabbit. The 7 Tesla MRI unit used in this study had a significantly stronger magnet than those used routinely for clinical examinations, allowing a greater signal to noise ratio and consequent improvement in image quality. However, it was also a non-standard unit that had not been used for imaging this type of material previously, therefore

technical problems were encountered with the examinations and subsequent image production. This supports the use of cadavers in place of clinical cases when performing preliminary examinations to establish protocols using new equipment.

MRI allows direct imaging in all three planes without repositioning the animal, which is not possible using CT (Widmer and others 1991, Shores 1993, Forrest 1999). However, the examination of CT images using different windows can be performed after completion of the scan while each type of MRI sequence must be obtained individually. MRI sequences take longer to produce than a corresponding CT one (Dennis 2006) therefore the overall length of the examination will also be greater and this was borne out by the results in the present study. The 3-dimensional volumetric acquisition of the T1 weighted images resulted in isotropic resolution and therefore multiplanar images of comparable quality with a single sequence. However, the concentric slab acquisition of transverse T2 weighted images and subsequent multiplanar reconstruction produced distortion and degradation in image quality and therefore was not a substitute for direct multiplanar image acquisition.

As with CT (Russo and others 2002), transverse and dorsal sequences were reported to be most useful for imaging the middle ear (Allgoewer and others 2000) as they allowed comparison of both sides. However, this relied heavily on symmetrical patient positioning and as the results of the present study indicate, this can be difficult to achieve. The TB walls, gas-filled lumen and adjacent bony regions of the skull were indistinguishable on all the images, as previously reported (Forrest 1999, Allgoewer and others 2000, Garosi and others 2000, Bischoff and Kneller 2004), so the information obtained about this region in its normal state was limited. However, also in keeping with previous reports, the normal inner ear fluid was clearly visible on both T1 and T2 weighted images, (Allgoewer and others 2000, Garosi and others 2000, Garosi and others 2001) and therefore provided a landmark for orientation. Although imaging of the tympanic membrane in dogs (Assheuer and Sager 1997, Owen and others 2004), and the bone septum in cats (Allgoewer and others 2000) has been documented, neither were clearly nor consistently visible in the present study. The presence of fluid within the lumen enhanced identification of the boundaries and internal features of the TB, suggesting that this technique is likely to be of more benefit in the diseased state. This corresponded with a previous report where MRI was able to image the auditory ossicles in humans, but only in the presence of serous fluid within the middle ear cavity which allowed precise delineation of the structures (Duprez

and others 2002). Variations in signal intensity were observed within the fluid and while this has been observed in clinical cases with pathological middle ear fluid accumulations (Allgoewer and others 2000, Owen and others 2004), the uniformity of the material used in the present study suggested it may have been artefactual.

The dorsal and transverse plane images were reported to be the most useful for MR imaging of the canine TMJ, allowing good assessment of the shape of both the condyloid process and the mandibular fossa, and their relative positions (Baines and others 2002). In the present study, as with the CT images, different regions of the joint were best visualised in each of the planes in each of the species and therefore all were deemed useful. The canine TMJ has been imaged using T1, T2 and proton weighted sequences (Baines and others 2002) but in the present study, the T1 weighted images produced better distinction between the components and therefore were most appropriate in all three species. Soft tissue structures including the intra-articular disc could be identified in some of the T1 weighted images in the dog and rabbit but not in the cat, reflecting the relative prominence of this structure in these species. In the dog, the disc was best visualised in the transverse and sagittal images while in the rabbit, it was easiest to identify in the sagittal and dorsal planes. The area of the joint in which it was visible reflected its anatomy. This structure was not discernable on the T2 weighted images but the extensive peripheral attachments of the joint capsule in all three species (Scapino 1965, Gillbe 1973, Ström and others 1988, Barone 1989) could be appreciated on both sequences, particularly medially and laterally. This presumably reflects the superior image quality in the present study since the disc was not visible in a previous canine study (Baines and others 2002).

The introduction of fluid into the middle ear cavity of cadavers as an aid to identification of the TB on diagnostic images also presented a crude model of acute otitis media. CT proved to be the best method for identifying the presence of middle ear fluid in dog, cat and rabbit cadavers and also in live clinical cases of canine otitis media, where it can be considered as a 'gold standard' technique, along with MRI (Garosi and others 2003). A complete CT examination of the TB should utilize contiguous slices (Love and others 1995, Russo and others 2002) but in the present study, a minimum of two slices accurately identified the presence of fluid in cadavers and six slices in the clinical cases produced results comparable with other clinical studies (Love and others 1995, Rohleder and others 2006).

Often the only radiographic changes in acute cases is the presence of fluid within the TB lumen and this can be challenge to identify diagnostically (Smith and Webster 1925, Geary 1965, Gibbs 1978). The radiographic changes identified in the canine cadavers in this study were also very subtle, as reflected by the results being poorer than for the other species and there only being a moderate inter-observer agreement. The results were also poorer than those obtained in the clinical study, presumably reflecting the use of a single view rather than the recommended series (Douglas 1987) and the presence of secondary changes in live cases producing more obvious changes. This is supported by the significant correlation between the radiographic identification of wall changes and subsequent CT findings, and the association between increasing severity of disease and the ability to identify both wall and content changes. However, the range of changes present in clinical cases is reflected in a poorer inter-observer agreement. These findings correspond with a previous report stating that radiographic studies are unlikely to be of use in most acute cases of canine otitis media as they will not consistently identify fluid in the absence of bony changes (Farrow 1985). The results obtained in the clinical study were also lower than previous clinical studies (Remedios and others 1991, Love and others 1995) and may reflect the choice of an alternative gold standard to produce a more representative clinical situation.

The radiographic results and inter-observer agreements obtained in the cat and rabbit were superior to these obtained in the dog both in the present and a previous cadaver study (Griffiths and others 2003), suggesting that the presence of fluid in the TB was easier to identify radiographically in these species. Further work would be required to determine whether this observation also applies to clinical cases. In the cat, the rostro 10° ventral-dorsocaudal oblique view did prove easier to position than the rostrocaudal open mouth view and also produced similar radiographic results therefore confirming the suggestion of Hofer and others (1995), that this is a suitable alternative in this species. All of the views employed in the rabbit were easy to position and no single view or combination emerged as particularly beneficial suggesting that while there is merit in producing a series of views, as is recommended in the dog (Douglas 1987), no specific recommendations can be made for this species.

It has been suggested that comparison with the radiographs of a normal animal is more beneficial in improving diagnoses than bilateral comparison within the same animal (Farrow 1985). Allowing for some operator variation, this is generally substantiated by the

results of the present study whereby the radiologists were better able to identify unilateral changes in all views, presumably due to the presence of a normal gas-filled TB for comparison.

The sonographic appearance of normal and fluid-filled TB in canine cadavers was similar to that previously reported (Griffiths and others 2003). However, the specific approach employed could not be reproduced in the present study and probably accounts for the disparity in results observed. Ultrasound produced better results than radiography in the cadavers, although the moderate inter-observer agreement suggested that the sonographic changes observed were still relatively subjective. Sonographic assessment of the TB could be performed in live clinical cases of otitis media but the poor inter-observer agreement reflected the manner in which one set of results was obtained and demonstrated that although the technique could be learned rapidly to a high degree of accuracy, training was not a substitute for actually performing the examination. The TB in two cases of primary secretory otitis media in CKCS were similar to those observed in the cadavers, with complete filling of the lumen and a normal wall. However, the appearance encountered in the clinical study was much more variable due to incomplete filling of the lumen and the presence of wall changes. Loss of the characteristic appearance of the TB wall was a good indicator of the presence of disease but also hampered adequate assessment of the contents, although changes to both the wall and content became easier to identify as the severity of the disease progressed. Although ultrasound was not as good as radiography for the identification of otitis media in dogs, the combination of the two modalities significantly improved the results suggesting that ultrasound does have a potential role in the evaluation of this condition.

In the cat and rabbit cadavers, the results for ultrasound were better than radiography across the board and the inter-observer agreement was excellent. This suggested that the sonographic distinction between fluid and gas within the TB in these species was more clear-cut than in the dog, but may also have reflected the use of a high frequency transducer. All sonographers were able to differentiate fluid and air-filled TB more consistently when there was unilateral filling rather than when the contents of both were the same, suggesting that comparison also plays a useful role in this imaging modality. Further work would be required to determine if this examination can be performed in live

clinical cases of otitis media in the cat and rabbit, and whether these results can be repeated, However, the superior results obtained in these species make it likely.

The changes encountered in the anatomy of the CKCS in the present study were considered to be consistent with the presence of TMJ dysplasia. Most cases of TMJ dysplasia occur sporadically in a variety of breeds and are associated with specific clinical signs that often includes open mouth jaw locking (Stewart and others 1975, Robins and Grandage 1977, Johnson 1979, Lane 1982, Stead 1984, Bennet and Prymak 1986). However, in the present study, these changes were encountered in every available anatomical specimen and clinical case with adequate diagnostic images suggesting that it is widespread within the population. It was also not associated with clinical signs and therefore could be considered as a normal anatomical variation in this breed. A similar situation is described in the American Cocker Spaniel and Dachshund including the demonstration of varying degrees of dysplastic changes that are not necessarily symmetrical (Hoppe and Svalastoga 1980, Vollmerhaus and others 1996, Vollmerhaus and Roos 2003). Although the underlying cause of TMJ dysplasia is not known (Robin and Grandage 1977, Johnson 1979), a hereditary component has been suggested (Stewart and others 1975) and the chondrodystrophied nature of the American Cocker Spaniel, Dachshund and CKCS is also likely to play a part. The influence of brachycephalism appears less convincing since this does not apply to the Dachshund and larger brachycephalic breeds demonstrated normal TMJ anatomy.

Only marked changes could be identified on dorsoventral radiographs, although inadvertent asymmetrical positioning often aided the identification of milder alterations in the caudal articular surface of the condyloid process. Lateral oblique views were the most useful for identification of subtle changes and allowed assessment of the retroarticular process. This corresponded with recommendations that a dorsoventral and lateral oblique views of each joint are best for assessment of the TMJs (Lane 1982). Transverse CT and MRI sections allowed assessment of the contour of the condyloid process and corresponding mandibular fossa, while sagittal sections also allowed the shape and length of the retroarticular process to be evaluated. These alone demonstrated the true degree of incongruence throughout the entire joint space. The dorsal sections were considered to be of least value and 3-dimensional reconstructions provided no extra information. This differs from a previous

report where transverse and dorsal images were recommended for examination of the canine TMJ (Baines and others 2002).

The angle between the long axis of the condyloid process and the medial portion of the articular surface, also known as the rotational angle (Hazewinkel and others 1993), increased with the severity of the dysplastic changes observed in the CKCS in the present study. However, there was an overlap between these CKCS and dogs of other breeds with normal TMJ anatomy as documented in Chapter 2 and a previous report (Hazewinkel and others 1991). This suggests that the rotational angle is not a reliable indicator of joint laxity and that the shape of the joint components is of greater significance.

As with the CKCS, the anatomical variations encountered in a proportion of the rabbits in this study were identified as incidental findings and were not associated with clinical signs. The premature closure of the spheno-occipital synchondrosis was easy to identify in the emasculated skulls and sagittal CT and MR images, but were not readily appreciable in other imaging planes. Although these changes have been reported to occur in association with the Dachs gene in New Zealand White rabbits (Sawin and others 1959), these specimens did not demonstrate any of the other characteristic chondrodystrophic features associated with its presence. Further work would therefore be indicated to determine whether another gene was responsible and also whether this is present within other rabbit breeds. Such malformations are common in specific breeds of dog where they may or may not be associated with clinical signs (Thrall 2002, Dennis 2006), but given the relatively high incidence of neurological problems encountered in rabbits (Keeble 2006), it would be of benefit to determine whether some of the cases might have underlying anatomical variations that would predispose them to such conditions.

Although the quality of diagnostic images is constantly improving, there are many factors that will influence a clinicians' choice of technique. Such considerations include the cost of CT and MRI examinations, which will be greater than radiography and ultrasound, and access to equipment, which may be more limited. Radiography and CT both utilize ionizing radiation for image production and MRI requires a magnetic field, both of which must be used in accordance with the relevant health and safety regulations. Accurate patient positioning and immobility are necessary for CT, MRI and many radiographic views therefore these procedures require the use of general anaesthesia which may be a

restriction in sick animals. Ultrasound is generally well tolerated in unsedated animals and has many advantages over these other modalities in terms of cost and availability. However, most important is selection of the most appropriate procedure according to the anatomical area or condition under investigation. Studies such as this are vital to determine which single or combination of imaging techniques should ideally be selected, demonstrate the appearance of the structures being examined and provide an indication of the type of clinical information likely to be obtained. As technology advances, there is a continual need to revisit previously published work and conclusions to ensure that recommendations remain current and optimal. This equips clinicians with the knowledge to be able to make the best decision based on all the options available to them and obtain the maximum amount of information from the resulting images.

Reference List

- Aaslid, R., Markwalder, T. M. & Nornes, H. 1982. Noninvasive transcranial Doppler ultrasound recording of flow velocity in basal cerebral arteries. *Journal of Neurosurgery* 57: 769-774.
- Alexander, A. E. & Caldemeyer, K. S. 1998. Clinical and surgical application of reformatted high-resolution CT of the temporal bone. *Neuroimaging Clinics of North America* 8: 631-650.
- Ali, Q. M., Ulrich, C. & Becker, H. 1993. Three-dimensional CT of the middle ear and adjacent structures. *Neuroradiology* 35: 238-241.
- Allgoewer, I., Lucas, S. & Schmitz, S. A. 2000. Magnetic resonance imaging of the normal and diseased feline middle ear. *Veterinary Radiology and Ultrasound* 41: 412-418.
- Altman, D. G. 1997. Some common problems in medical research. In Altman, D. G. (Ed) *Practical Statistics for Medical Research* (pp. 396-439). London: Chapman & Hall.
- Alvord, L. S. 1990. Uses of ultrasound in audiology. *Journal of the American Academy of Audiology* 1: 227-235.
- American College of Veterinary Radiology website 2006. History. <http://www.acvr.org/general/history/index.html>.
- Anderson, M. A., Orsini, P. G. & Harvey, C. E. 1996. Temporomandibular ankylosis: treatment by unilateral condylectomy in two dogs and two cats. *Journal of Veterinary Dentistry* 13: 23-25.
- Arnautovic, I. & Osman, F. 1985. Anatomical studies on the auditory ossicles of the cat and rabbit. *Assuit Veterinary Medical Journal* 15: 53-57.
- Assheuer, J. & Sager, M. 1997. MRI and CT atlas of the dog. Berlin: Blackwell Science.
- Baines, E. A., Sales, J. I., Baines, S. J. & Herrtage, M. E. 2002. Magnetic resonance imaging of the canine temporomandibular joint. *Proceedings of the 9th annual conference of the European Association of Veterinary Diagnostic Imaging, Archena, Spain*. 85.
- Baird, D. K., Hathcock, J. T., Rumph, P. F., Kincaid, S. A. & Visco, D. M. 1998. Low-field magnetic resonance imaging of the canine stifle joint: normal anatomy. *Veterinary Radiology and Ultrasound* 39: 87-97.
- Bakar, Z. A. 1999. An ultrasonographic study of musculoskeletal injuries and mammary gland tumour in small animals. PhD thesis: University of Glasgow.
- Barone, R. 1989. Anatomie comparée des mammifères domestiques. Paris: Éditions Vigot.
- Barone, R., Pavaux, C., Blin, P. C. & Cuq, P. 1973. Atlas of rabbit anatomy. Paris: Masson.

- Barthez, P. Y., Koblik, P. D., Hornof, W. J. & Wisner, E. R. 1996. Apparent wall thickening in fluid filled versus air filled tympanic bulla in computed tomography. *Veterinary Radiology and Ultrasound* 37: 95-98.
- Beed, B. J. 1997. Respiratory disease and the Pasteurella complex. In Hillyer, E. V. & Quesenbery, K. E. (Eds) *Ferrets, rabbits and rodents. Clinical medicine and surgery* (pp. 189-201). Philadelphia: W.B.Saunders.
- Bennet, D. & Prymak, C. 1986. Excision arthroplasty as a treatment for temporomandibular dysplasia. *Journal of Small Animal Practice* 27: 361-370.
- Bergan, T. & Langanke, J. 1996. Model experiments to detect abscesses with ultrasonography in carcasses of pigs. *Fleischwirtschaft* 76: 130-131.
- Bermejo Fenoll, A., Gonzalez Sequeros, O. & Gonzalez Gonzalez, J. M. 1992. Histological study of the temporomandibular joint capsule: theory of the articular complex. *Acta Anatomy* 145: 24-28.
- Bischoff, M. G. & Kneller, S. K. 2004. Diagnostic imaging of the canine and feline ear. *Veterinary Clinics of North America : Small Animal Practice* 34: 437-458.
- Bistner, S. 1967. What is your diagnosis? *Journal of the American Veterinary Medical Association* 150: 1385-1387.
- Bjotvedt, G. & Geib, L. W. 1981. Otitis media associated with Staphylococcus epidermidis and Psoroptes cuniculi in a rabbit. *Veterinary Medicine, Small Animal Clinician* 76: 1015-1016.
- Bloch, F., Hanson, W. W. & Packard, M. 1946. Nuclear induction. *Physical Review* 69: 127.
- Block, M. S., Unhold, G. & Bouvier, M. 1988. The effect of diet texture on healing following temporomandibular joint discectomy in rabbits. *Journal of Oral and Maxillofacial Surgery* 46: 580-588.
- Bochler, A. & Kneissl, S. 2002. Computed tomographic anatomy of the head of the rabbit. *Proceedings of the 9th annual conference of the European Association of Veterinary Diagnostic Imaging. Archena, Spain.* 97.
- Bradley, R. L., Noone, K. E., Saunders, G. K. & Patnaik, A. K. 1985. Nasopharyngeal and middle ear polypoid masses in five cats. *Veterinary Surgery* 14: 141-144.
- Bruyette, D. S. & Lorenz, M. D. 1993. Otitis externa and otitis media: diagnostic and medical aspects. *Seminars in Veterinary Medicine and Surgery (Small Animal)* 8: 3-9.
- Buckingham, S. H. W. & Jeffcott, L. B. 1991. Osteopenic effects of forelimb immobilisation in horses. *Veterinary Record* 128: 370-373.
- Budinger, T. F. & Lauterbur, R. C. 1984. Nuclear magnetic resonance technology for medical studies. *Science* 226: 288-298.

- Bydder, G. M., Steiner, R. E., Young, I. R., Hall, A. S., Thomas, D. J., Marshall, J., Pallis, C. A. & Legg, N. J. 1982. Clinical NMR imaging of the brain: 140 cases. *American Journal of Roentgenology* 139: 215-236.
- Caporn, T. M. 1995. Traumatic temporomandibular joint luxation: Comparative anatomy of the temporomandibular joint. *Veterinary Comparative Traumatology and Orthopaedics* 8: 58-60.
- Carerra, I. & Trevail, T. 2007. Personal communication. *Division of Companion Animal Studies, University of Glasgow*.
- Cho, B. K. & Irudayaraj, J. M. K. 2003. Foreign object and internal disorder detection in food materials using noncontact ultrasound imaging. *Journal of Food Science* 68: 967-974.
- Clow, H. & Young, I. R. 1978. Britain's brains produce first NMR scans. *New Scientist* 80: 588.
- Cox, C. L., Slack, R. W. T. & Cox, G. J. 1989. Insertion of a transtympanic ventilation tube for the treatment of otitis media with effusion. *Journal of Small Animal Practice* 30: 517-519.
- Crocker, D. E., Webb, P. M., Costa, D. P. & Boeuf, B. J. 1998. Protein catabolism and renal function in lactating northern elephant seals. *Physiological Zoology* 71: 485-491.
- Crossley, D. A. 2003. Oral biology and disorders of lagomorphs. *Veterinary Clinics of North America : Exotic Animal Practice* 6: 629-659.
- Crossley, D. A. 2006. Personal communication. *DaCross Services DaCross.com*.
- Crossley, D. A. 1995. Dental disease in rabbits. *Veterinary Record* 137: 384.
- Crouch, J. E. 1969. Text Atlas of Cat Anatomy. Philadelphia: Lea & Febiger.
- Curie, J. & Curie, P. 1880. Development par pression de l'electricite polaire dans les cristaux hemidres a faces inclinees. *Compte Rendue de 'Acadamie Scientifique, Paris* 91: 294-295.
- Curry, T. S., Dowdey, J. E. & Murry, R. C. 1990. Christensen's Physics of Diagnostic Radiology. London: Williams & Wilkins.
- Cywa-Benko, K., Krawczyk, J., Wezyk, S., Knapik, J., Bielinska, H. & Rosinski, A. 1999. Efficiency of various techniques for in vivo estimation of meatiness in geese. *Roczniki Naukowe Zootechniki* 26: 143-152.
- Czerny, C., Turetschek, K., Duman, A. & Imhof, A. 1997. CT and MRI of the middle ear. *Der Radiologe* 37: 945-953.
- Damadian, R. V. 1974. Apparatus and method for detecting cancer in tissue. *United States Patent* no. 3789832.
- Dayrell-Hart, B. L. 1997. MR imaging of the vestibular apparatus of the dog. *Proceedings of the 15th annual conference of the American College of Veterinary Internal Medicine* 606-607.

- Deeb, B. J. 1997. Respiratory disease and the Pasteurella complex. In Hillyer, E. V. & Quesenbery, K. E. (Eds) *Ferrets, rabbits and rodents. Clinical medicine and surgery* (pp. 189-201). Philadelphia: W.B.Saunders.
- Dennis, R. 2006. Skull - general. In Barr, F. J. & Kirberger, R. M. (Eds) *BSAVA manual of canine and feline musculoskeletal imaging* (pp. 173-191). Quedgeley: British Small Animal Veterinary Association.
- Dik, K. J. 1994. Computed tomography of the equine head. *Veterinary Radiology and Ultrasound* 35: 236.
- Dixon, D. C. 1991. Diagnostic imaging of the temporomandibular joint. *Temporomandibular Disorders and Orofacial Pain* 35: 53-74.
- Douglas, S. W. 1987. Canine Radiography: Skeletal System - Skull. In Douglas, S. W. (Ed) *Principles of Veterinary Radiology* (pp. 177-196). Philadelphia: Bailliere Tindall.
- Drace, J. E. & Enzmann, D. R. 1990. Defining the normal temporomandibular joint: closed-, partially open-, and open-mouth MR imaging of asymptomatic subjects. *Radiology* 177: 67-71.
- Duprez, T., Menten, R., Saint-Martin, C., Deggouj, N., Decat, M. & Cosnard, G. 2002. Imaging the middle-ear ossicles in humans: CT or MRI? *Paediatric Radiology* 32: 102-103.
- Dussik, K. T., Dussik, F. & Wyt, L. 1947. Auf dem wege zur hyperphonographic des gehirnes. *Wiener Medizinische Wochenschrift* 97: 425-429.
- Dvir, E., Kirberger, R. M. & Terblanche, A. G. 2000. Magnetic resonance imaging of otitis media in a dog. *Veterinary Radiology and Ultrasound* 41: 46-49.
- EAVDI - British and Irish Division website 2006. History. <http://www.vet.gla.ac.uk/EVDI/ea-bed.htm#history>.
- Ellenport, C. R. 1975. General Introduction. In R. Getty. (Ed) *Sisson and Grossman's The Anatomy of the Domestic Animals*. (pp. 3-5). London: W.B.Saunders.
- Eom, K., Lee, H. & Yoon, J. 2000. Canalographic evaluation of the external ear canal in dogs. *Veterinary Radiology and Ultrasound* 41: 231-234.
- European Magnetic Resonance Forum website 2003. A short history of magnetic resonance imaging from a European viewpoint. <http://www.emrf.org/FAQs%20MRI%20History.html>.
- Evans, H. E. 1993. *Miller's Anatomy of the Dog*. Philadelphia: W.B. Saunders.
- Farhat, A. & Chavez, E. R. 2000. Comparative performance, blood chemistry, and carcass composition of two lines of Pekin ducks reared mixed or separated by sex. *Poultry Science* 79: 460-465.
- Farr, T. D., Carswell, H. V. O., Gallagher, L., Condon, B., Fagan, A. J., Mullin, J. & Macrae, I. M. 2006. 17beta-Estradiol treatment following permanent focal ischemia does not influence recovery of sensorimotor function. *Neurobiology of Disease* 23: 552-562.

- Farrow, C. S. 1985. Radiographic characterization of osteomyelitis of the tympanic bulla in a dog. *Modern Veterinary Practice* 66: 871-874.
- Farrow, C. S. 1992. Known case conference. *Veterinary Radiology and Ultrasound* 33: 262-263.
- Farrow, C. S. 1994. The Head. In Farrow, C. S. (Ed) *Radiology of the Cat*. (pp. 1-30). Mosby.
- Feeney, D. A., Fletcher, T. F. & Hardy, R. M. 1991. Atlas of correlative imaging anatomy of the normal dog: ultrasound and computed tomography. London: W.B.Saunders.
- Field, I. C., Bradshaw, C. J. A., McMahon, C. R., Harrington, J. & Burton, H. R. 2002. Effects of age, size and condition of elephant seals (*Mirounga leonina*) on their intravenous anaesthesia with tiletamine and zolazepam. *Veterinary Record* 151: 235-240.
- Fingland, R. B., Gratzek, A., Vorhies, M. W. & Kirpensteijn, J. 1993. Nasopharyngeal polyp in a dog. *Journal of the American Animal Hospital Association* 29: 311-314.
- Flatt, R. E., DeYoung, D. W. & Hogle, R. M. 1977. Suppurative otitis media in the rabbit: prevalence, pathology, and microbiology. *Laboratory Animal Science* 27: 343-347.
- Forrest, L. J. 1999. The head : excluding the brain and orbit. *Clinical Techniques in Small Animal Practice* 14: 170-176.
- Fossum, T. W. 2002. Surgery of the ear. In Fossum, T. W. (Ed) *Small animal surgery* (pp. 230). St.Louis: Mosby.
- Fox, J. G., Norberg, R. F. & Myers, D. D. 1971. The relationship of *Pasteurella multocida* to otitis media in the domestic rabbit (*Oryctolagus cuniculus*). *Laboratory Animal Science* 21: 45-48.
- Gao, D. C., Xu, X. F., Xu, L. & Qi, X. L. 1995. *Psoroptes cuniculi* parasitism of the middle and inner ear of rabbits. *Chinese Journal of Veterinary Science* 15: 198-199.
- Garosi, L. S., Dennis, R., Penderis, J., Lamb, C. R., Targett, M. P., Cappello, R. & Delauche, A. J. 2001. Results of magnetic resonance imaging in dogs with vestibular disorders: 85 cases (1996-1999). *Journal of the American Veterinary Medical Association* 218: 385-391.
- Garosi, L. S., Dennis, R. & Schwarz, T. 2003. Review of diagnostic imaging of ear diseases in the dog and cat. *Veterinary Radiology and Ultrasound* 44: 137-146.
- Garosi, L. S., Lamb, C. R. & Targett, M. P. 2000. MRI findings in a dog with otitis media and suspected otitis interna. *Veterinary Record* 146: 501-502.
- Gateno, J., Miloro, M., Hendler, B. H. & Horrow, M. 1993. The use of ultrasound to determine the position of the mandibular condyle. *Journal of Oral and Maxillofacial Surgery* 51: 1081-1086.
- Geary, J. C. 1965. Radiographic aspects of otitis media. *Auburn Veterinarian* 121: 71-73.

- George, T. F. & Smallwood, J. E. 1992. Anatomic atlas for computed tomography in the mesencephalic dog: head and neck. *Veterinary Radiology and Ultrasound* 33: 271-240.
- Getty, R., Foust, H. L., Presley, E. T. & Miller, M. E. 1956. Macroscopic anatomy of the ear of the dog. *American Journal of Veterinary Research* 17: 364-375.
- Gibbs, C. 1977. The head. Part II. Traumatic lesions of the mandible. *Journal of Small Animal Practice* 18: 51-54.
- Gibbs, C. 1978. The head III: Ear disease. *Journal of Small Animal Practice*. 19: 539-545.
- Gibbs, C. & Hinton, M. H. 1981. Radiological examination of the rabbit. I. The head, thorax and vertebral column. *Journal of Small Animal Practice* 22: 687-703.
- Gielen, I., van Bree, H., van Ryssen, B., de Clercq, T. & de Rooster, H. 2002. Radiographic, computed tomographic and arthroscopic findings in 23 dogs with osteochondrosis of the tarsocrural joint. *Veterinary Record* 150: 442-447.
- Gillbe, G. V. 1973. A comparison of the disc in the craniomandibular joint of three mammals. *Acta Anatomy* 86: 394-409.
- Gotthelf, L. N. 2004. Diagnosis and treatment of otitis media in dogs and cats. *Veterinary Clinics of North American : Small Animal Practice* 34: 469-487.
- Green, R. W. 1996. Small Animal Ultrasound. Philadelphia: Lippincott - Raven.
- Greshake, R. J. & Ackerman, N. 1992. Ultrasound evaluation of the coxofemoral joints of the canine neonate. *Veterinary Radiology and Ultrasound* 33: 99-104.
- Griffith, J. M. & Henry, W. L. 1973. A real - time system for two-dimensional echocardiography. *Proceedings of the 26th annual conference of Engineering in Medicine and Biology* 15: 422.
- Griffiths, L. G., Sullivan M, O'Neill, T. & Reid, S. W. J. 2003. Ultrasonography versus radiography for detection of fluid in the canine tympanic bulla. *Veterinary Radiology and Ultrasound* 44: 210-213.
- Hall, E. M. 1966. Editorial: Current teaching of veterinary radiology at undergraduate level. *Journal of the American Veterinary Radiology Society* 7: 2-3.
- Hammond, G. 2007. Personal communication. *Royal (Dick) School of Veterinary Studies, University of Edinburgh*.
- Harcourt-Brown, F. 2003. Textbook of Rabbit Medicine. Oxford: Butterworth Heineman.
- Harcourt-Brown, F. M. 1995. A review of clinical conditions of pet rabbits associated with their teeth. *Veterinary Record* 137: 341-346.
- Harvey, C. E. & Goldschmidt, M. H. 1978. Inflammatory polypoid growths in the ear canal of cats. *Journal of Small Animal Practice* 19: 669-677.
- Hathcock, J. T. & Stickle, R. L. 1993. Principles and concepts of computed tomography. *Veterinary Clinics of North America : Small Animal Practice* 23: 399-415.

- Hazewinkel, H. A., Koole, R. & Voorhout, G. 1993. Mandibular coronoid process displacement; signs, causes, treatment. *Veterinary Comparative Traumatology and Orthopaedics* 6: 29-35.
- Health and Safety Executive 1998. Ionising Radiation Regulations Act. .
- Health and Safety Executive 2002. Control of Substances Hazardous to Health Regulations. .
- Henry, J. G., Mundt, G. N. & Hughes, W. F. 1956. Ultrasonics in ocular diagnosis. *American Journal of Ophthalmology* 41: 488.
- Herring, D. S. & Bjornton, G. 1985. Physics, facts, and artifacts of diagnostic ultrasound. *Veterinary Clinics of North America: Small Animal Practice* 15: 1107-1122.
- Hilbert, G., Vargas, F., Valentino, R., Gruson, D., Chene, G., Bebear, C., Gbikpi-Benissan, G. & Cardinaud, J. P. 2001. Comparison of B-mode ultrasound and computed tomography in the diagnosis of maxillary sinusitis in mechanically ventilated patients. *Critical Care Medicine* 29: 1337-1342.
- Hofer, P., Meisen, N., Bartholdi, S. & Kaser-Hotz, B. 1995. A new radiographic view of the feline tympanic bullae. *Veterinary Radiology and Ultrasound* 36: 14-15.
- Holliday, R. A. & Reede, D. L. 1989. MRI of mastoid and middle ear disease. *Radiologic Clinics of North America* 27: 283-299.
- Holt, D. E. & Walker, I. 1997. Radiographic appearance of the middle ear after ventral bulla osteotomy in five dogs with otitis media. *Veterinary Radiology and Ultrasound* 38: 182-184.
- Holtz, W. 1982. Pregnancy detection in swine by pulse mode ultrasound. *Animal Reproduction Science* 4: 219-226.
- Hoppe, F. & Svalastoga, E. 1980. Temporomandibular joint dysplasia in American Cocker Spaniels. *Journal of Small Animal Practice* 21: 675-678.
- Hoskinson, J. J. 1993. Imaging techniques in the diagnosis of middle ear disease. *Seminars in Veterinary Medicine and Surgery (Small Animal)* 8: 10-16.
- Huang, G. T., Rosowski, J. J., Flandermeyer, D. T., Lynch, T. J. & Peake, W. T. 1997. The middle ear of a lion: Comparison of structure and function to domestic cat. *Journal of the Acoustical Society of America* 101: 1532-1549.
- Hudson, J. A., Montgomery, R. D., Hathcock, J. T. & Jorboe, J. M. 1994. Computed tomography of craniomandibular osteopathy in a dog. *Veterinary Radiology and Ultrasound* 35: 94-99.
- Indrieri, R. J. & Taylor, R. F. 1984. Vestibular dysfunction caused by squamous cell carcinoma involving the middle ear and inner ear in two cats. *Journal of the American Veterinary Medical Association* 184: 471-473.
- Jackson, J. A. & Langham, W. H. 1968. Whole-body NMR spectrometer. *Review of Scientific Instrumentation* 39: 510-513.

- Johnson, K. A. 1979. Temporomandibular joint dysplasia in an Irish Setter. *Journal of Small Animal Practice* 20: 209-218.
- Jones, J. C., Vartee, R. E. & Bartels, J. E. 1995. Computed tomographic anatomy of the canine lumbosacral spine. *Veterinary Radiology and Ultrasound* 36: 91-99.
- Junqueira, L. C., Carneiro, J. & Long, J. A. 1986. The Sense Organs. In Junqueira, L. C., Carneiro, J. & Long, J. A. (Eds) *Basic Histology* (pp. 201-233). California: Lange Medical Publications.
- Kapatkin, A. S., Matthiesen, D. T., Noone, K. E., Church, E. M., Scavelli, T. E. & Patnaik, A. K. 1990. Results of surgery and long term follow-up in 31 cats with nasopharyngeal polyps. *Journal of the American Animal Hospital Association* 26: 387-478.
- Kealy, K. 1992. Veterinary radiology, a historical perspective. *Veterinary Radiology and Ultrasound* 33: 5-7.
- Keeble, E. 2006. Common neurological and musculoskeletal problems in rabbits. *In Practice* 28: 212-218.
- Keech, M. A., Stephenson, T. R., Bowyer, R. T., Bellenberghe, V. V. & Hoef, J. M. 1998. Relationships between blood-serum variables and depth of rump fat in Alaskan moose. *Alces* 34: 173-179.
- Kirk, H. 1932. X-rays in small animal practice. *Veterinary Record* 12: 171.
- Koblick, P. D. & Berry, C. R. 1990. Dorsal plane computed tomographic imaging of the ethmoid region to evaluate chronic nasal disease in the dog. *Veterinary Radiology and Ultrasound* 31: 92-97.
- Konig, T., Grashorn, M. A. & Bessei, W. 1998. Estimation of breast meat yield in living broilers using B-scan sonography. Second report: accuracy of the method. *Archiv fur Geflugelkunde* 62: 121-125.
- Kossof, G., Fry, F. J. & Eggleton, R. C. 1971. Application of digital computer to control ultrasonic visualisation equipment. *Ultrasonographica Medica* 1: 33-40.
- Kpodekon, M. 1983. Pathology and pathogenesis of aural and encephalitic complications of pasteurellosis in farmed rabbits. *Annales de Recherches Veterinaires* 14: 225-232.
- Kraft, S. 2002. CT and MRI Reading List. www.acvr.vcdavis.edu/societ/ctmr/ctmr.html.
- Kraft, S. & Gavin, P. R. 1999. Intracranial neoplasia. *Clinical Techniques in Small Animal Practice* 14: 112-123.
- Kramer, M., Gerwing, M., Hach, V. & Schimke, E. 1997. Sonography of the musculoskeletal system in dogs and cats. *Veterinary Radiology and Ultrasound* 38: 139-149.
- Kraus, M. S., Mahaffey, M. B., Girard, E., Chambers, J. N., Brown, C. A. & Coates, J. R. 1997. Diagnosis of C5-C6 spinal luxation using three dimensional computed tomographic reconstruction. *Veterinary Radiology and Ultrasound* 38: 39-41.

- Kumar, A., Welti, D. & Ernst, R. R. 1975. NMR Fourier zeugmatography. *Journal of Magnetic resonance* 18: 69-83.
- Kumar, B. V. D., Rajashekar, G. & Rao, P. S. 2000. Vestibular syndrome in a rabbit. *Indian Veterinary Journal* 77: 268-269.
- Lamb, C. & Garosi, L. S. 2000. Images in medicine: Two little ducks went swimming one day. *Veterinary Radiology and Ultrasound* 41: 292.
- Lamb, C. R., Stowater, J. L. & Pipers, F. S. 1988. The first twenty-one years of veterinary diagnostic ultrasound: A bibliography. *Veterinary Radiology and Ultrasound* 29: 37-45.
- Landes, C., Walenzik, H. & Klein, C. 2000. Sonography of the temporomandibular joint from 60 examinations and comparison with MRI and axiography. *Journal of Cranio-Maxillofacial Surgery* 28: 352-361.
- Lane, J. G. 1982. Disorders of the canine temporomandibular joint. *Veterinary Annual* 22: 175-187.
- Langevin, P. 1924. De l'emploi des ondes ultrasonores pour le son. *Publications Speciale de Bureau Hydrographic International, Monaco* 3: 11.
- Lantz, G. C. & Cantwell, H. D. 1986. Intermittent open mouth jaw locking in 5 dogs. *Journal of the American Veterinary Medical Association* 188: 1403-1405.
- Larheim, T. A. 1995. Current trends in temporomandibular joint imaging. *Oral Surgery Oral Medicine Oral Pathology Oral Radiology and Endodontics* 80: 555-576.
- Lauterbur, P. C. 1973. Image formation by induced local interactions: examples of employing nuclear magnetic resonance. *Nature* 242: 190-191.
- Lauterbur, P. C. 1974. Magnetic resonance zeugmatography. *Pure and Applied Chemistry* 40: 149-157.
- Lawson, D. D. 1957. Otitis media in the cat. *Veterinary Record* 69: 643-647.
- Lee, J., Eom, K., Seong, Y., Lee, H., Park, J., Lee, J., Jang, K., Lee, K., Oh, T., Lee, S., Yoon, J., Lee, H., Choi, H., Lee, Y. & Chang, D. 2006. Ultrasonographic evaluation of the external ear canal and tympanic membrane in dogs. *Veterinary Radiology and Ultrasound* 47: 94-98.
- Lemattre, M., Lemattre, P. & Lemaire, F. 1999. Standing tree quality assessments using ultrasound. *Acta Horticulturae* 496: 269-277.
- Lewis, R. E. 1960. The proposed radiographic facilities for the Purdue Veterinary School. *Journal of the American Veterinary Radiology Society* 2: 32-33.
- Lindhahl, I. L. 1966. Detection of pregnancy in sheep by means of ultrasound. *Nature* 212: 642-643.
- Little, C. J. L. & Lane, J. G. 1986. The surgical anatomy of the feline bulla tympanica. *Journal of Small Animal Practice* 27: 371-378.

- Little, C. J. L., Pearson, G. R. & Lane, J. G. 1989. Neoplasia involving the middle ear cavity of dogs. *Veterinary Record* 124: 54-57.
- Little, C.J.L., Lane, J.G. & Pearson, G.R. 1999a. Inflammatory middle ear disease of the dog: the pathology of otitis media. *Veterinary Record* 128: 293-296.
- Little, C.J.L., Lane, J.G., Gibbs, C. & Pearson, G.R. 1999b. Inflammatory middle ear disease of the dog: the clinical and pathological features of cholesteatoma, a complication of otitis media. *Veterinary Record* 128: 319-322.
- Liu, S. K., Dorfman, H. D. & Patnaik, A. K. 1974. Primary and secondary bone tumours in the cat. *Journal of Small Animal Practice* 15: 141-156.
- Long, C. D. & Nyland, T. G. 1999. Ultrasonographic evaluation of the canine shoulder. *Veterinary Radiology and Ultrasound* 40: 372-379.
- Love, N. E., Kramer, R. W., Spodnik, G. J. & Thrall, D. E. 1995. Radiographic and computed tomographic evaluation of otitis media in the dog. *Veterinary Radiology and Ultrasound* 36: 375-379.
- Ludwig, G. D. & Struthers, F. W. 1949. Considerations underlying the use of ultrasound to detect gall stones and foreign bodies in the tissues. *United States Navy Medical Research Institute Report* 4: 1-27.
- Maroldi, R., Farina, D., Palvarini, L., Marconi, A., Gadola, E., Menni, K. & Battaglia, G. 2001. Computed tomographic and magnetic resonance imaging of pathologic conditions of the middle ear. *European Journal of Radiology* 40: 78-93.
- Martin, N., Sterkers, O. & Nahum, H. 1990. Chronic inflammatory disease of the middle ear cavities: Gd-DTPA-enhanced MR imaging. *Radiology* 176: 399-405.
- McCormick, S. U., McCarthy, J. G., Grayson, B. H., Staffenberg, D. & McCormick, S. A. 1995. Effects of mandibular distraction on the temporomandibular joint: Part 1, Canine study. *Journal of Craniofacial Surgery* 6: 358-363.
- Meomartino, L., Fatone, G., Brunetti, A., Lamagna, F. & Potena, A. 1999. Temporomandibular ankylosis in the cat: a review of seven cases. *Journal of Small Animal Practice* 40: 7-10.
- Meredith, A. 2006. Rabbits. <http://www.aquavet.i12.com/Rabbit.htm>. Royal (Dick) School of Veterinary Studies, University of Edinburgh.
- Mettler, M. 1992. Origin and history. In Mettler, M. (Ed) *The proper care of dwarf rabbits*. (pp. 7-72). New Jersey: TFH Publications Inc.
- Miklošová, M. & Sivrev, D. 1999. Plastination - A teaching and research tool. *Folia Veterinaria* 43: 104-107.
- Milan, J. 1972. Digital storage display of two - dimensional ultrasonic scans. *Journal of Physics and Medical Biology* 17: 440.
- Minagi, S., Sato, T., Kishi, K., Natsuaki, N. & Akamatsu, Y. 2000. Comparative study of the temporomandibular joint space in maximum intercuspation and canine edge-to-edge

- positions in deep bite and non-deep bite subjects. *Journal of Oral Rehabilitation* 27: 517-521.
- Mishra, K. C. 1995. Incidence and management of ear mite infestations in rabbits. *Indian Veterinary Journal* 72: 861-863.
- Morgan, J. P. & Silverman, S. 1987. *Techniques of Veterinary Radiography*. Iowa State University Press.
- Morrow, K. L., Park, R. D., Spurgeon, T. L., Stashak, T. S. & Arceneaux, B. 2000. Computed tomographic imaging of the equine head. *Veterinary Radiology and Ultrasound* 41: 491-497.
- Mullin, J. 2007. Personal communication. *7 Tesla MRI Unit, University of Glasgow Institute for Comparative Medicine*.
- Nabeith, Y. B. & Speculand, B. 1991. Ultrasonography as a diagnostic aid in temporomandibular joint dysfunction. A preliminary investigation. *International Journal of Oral and Maxillofacial Surgery* 20: 182-186.
- Neer, T. M. & Howard, P. E. 1982. Otitis media [dog]. *Compendium on Continuing Education for the Practicing Veterinarian* 4: 410.
- Nelson, R. J., Perry, S., Hames, T. K. & Pickard, J. D. 1990. Transcranial Doppler ultrasound studies of cerebral autoregulation and subarachnoid hemorrhage in the rabbit. *Journal of Neurosurgery* 73: 601-610.
- Nicholson, M. 2001. The history of the BRC. www.thebrc.org/index.html British Rabbit Council Website.
- Non-destructive Testing Resource Center website 2006. History of Radiography. <http://www.ndt-ed.org/EducationResources/CommunityCollege/Radiography/Introduction/history.htm>.
- Nordberg, C. C. & Johnson, K. A. 1999. Magnetic resonance imaging of normal canine carpal ligaments. *Veterinary Radiology and Ultrasound* 40: 128-136.
- Nyland, T. G., Mattoon, J. S. & Wisner, E. R. 1995. Physical principles, instrumentation and safety of diagnostic ultrasound. In Nyland, T. G. & Mattoon, J. S. (Eds) *Veterinary Diagnostic Ultrasound* (pp. 3-18). Philadelphia: W.B. Saunders.
- Onslow, R. 2007. About the AHT - History. <http://www.aht.org.uk/> Animal Health Trust website.
- Owen, M. C., Lamb, C. R., Lu, D. & Targett, M. P. 2004. Material in the middle ear of dogs having magnetic resonance imaging for investigation of neurological signs. *Veterinary Radiology and Ultrasound* 45: 149-155.
- Owens, J. M. & Biery, D. N. 1998. The Skull. In Owens, J. M. & Biery, D. N. (Eds) *Radiographic Interpretation for the Small Animal Clinician*. (pp. 105-114). London: Williams and Wilkins.

- Parker, N. R. & Binnington, A. G. 1985. Nasopharyngeal polyps in cats: Three case reports and a review of the literature. *Journal of the American Animal Hospital Association* 21: 473-478.
- Patrick, F. E. 2002. A review of fracture fixation as it affects the small animal pelvis: an anatomic, ultrasonographic, cross-sectional and retrospective radiographic study. PhD thesis: University of Glasgow.
- Payne, M. & Nakielny, R. A. 1996. Temporomandibular Joint Imaging. *Clinical Radiology* 51: 1-10.
- Percy, D. H. & Barthold, S. W. 2001. Rabbit bacterial infections. In Percy, D. H. & Barthold, S. W. (Eds) *Pathology of Laboratory Rodents and Rabbits* (pp. 260-283). Ames: Iowa State University Press.
- Pet Food Manufacturer's Association website 2003. www.pmf.com.
- Piyasena, P., Mohareb, E. & McKellar, R. C. 2003. Inactivation of microbes using ultrasound: a review. *International Journal of Food Microbiology* 87: 207-216.
- Pond, G. & Raleigh, I. 1979. A standard guide to cat breeds. London: MacMillan London Ltd.
- Popesko, P. 1977. Atlas of topographical anatomy of the domestic animals. Philadelphia: WB Saunders.
- Popesko, P., Rajtová, V. & Horák, J. 1992. A colour atlas of anatomy of small laboratory animals. London: Wolfe Publishing.
- Porter, M. 1991. Therapeutic ultrasound. *Journal of Equine Veterinary Science* 11: 357-362.
- Preston, R. C. & Shaw, A. 2001. Recommended ultrasound field safety classification for medical diagnostic devices. Middlesex: National Physics Laboratory.
- Pryer, A. A. 1931. The uses and limitations of X-rays in horse practice. *Veterinary Record* 11: 899.
- Purcell, E. M., Torrey, H. C. & Pound, R. V. 1946. Resonance absorption by nuclear magnetic moments in a solid. *Physical Review* 69: 37-38.
- Pym, R. A. E., Popovic, B. & Boderó, D. A. V. 1998. Selection for breast meat yield in Japanese quail (*Coturnix coturnix japonica*) using real time ultrasound. *Proceedings of the 6th World Congress on Genetics Applied to Livestock Production, Armidale, Australia*. 290-293.
- Rai, R. B., Singh, D. & Singh, R. N. 1986. Otitis in rabbits-etiopathological studies. *Indian Veterinary Medical Journal* 10: 243-244.
- Reed, A. L., Payne, J. T. & Constantinescu, G. M. 1995. Ultrasonographic anatomy of the normal canine stifle. *Veterinary Radiology and Ultrasound* 36: 315-321.
- Reef, V. B. 1998. Equine Diagnostic Ultrasound. Philadelphia: W.B.Saunders.

- Reef, V. B., Reimer, J. & Reid, C. F. 1991. Ultrasonographic findings in horses with osteomyelitis. *Proceedings of the 37th Annual Convention of the American Association of Equine Practitioners*. 381-391.
- Reichle, J. K. & Snaps, F. 1999. The Elbow. *Clinical Techniques in Small Animal Practice* 14: 177-186.
- Reichle, J. K. & Wisner, E. R. 2000. Non-cardiac thoracic ultrasound in 75 feline and canine patients. *Veterinary Radiology and Ultrasound* 41: 154-162.
- Remedios, A. M., Fowler, J. D. & Pharr, J. W. 1991. A comparison of radiographic versus surgical diagnosis of otitis media. *Journal of the American Animal Hospital Association* 27: 183-188.
- Rhodes, W. H. 1960. Foreward. *Journal of the American Veterinary Radiology Society* 2.
- Richardson, L. F. 1912a. Apparatus for warning a ship at sea of its nearness to large objects wholly or partly underwater. *British Patent* 1125.
- Richardson, L. F. 1912b. Apparatus for warning a ship of its approach to large objects in the fog. *British Patent* 9423.
- Rinck, P. A., Bielke, G. & Meves, M. 1984. Modified spin-echo sequence in tumor diagnosis. *Magnetic Resonance in Medicine* 1: 236.
- Riser, W. H., Parkes, L. J. & Shirer, J. F. 1967. Canine craniomandibular osteopathy. *Journal of the American Veterinary Radiology Society* 8: 23-30.
- Risselada, M., Kramer, M. & van Bree, H. 2004. Approaches for ultrasonographic evaluation of long bones in the dog. *Veterinary Radiology and Ultrasound* 44: 214-220.
- Robins, G. & Grandage, J. 1977. Temporomandibular joint dysplasia and open mouth jaw locking in the dog. *Journal of the American Veterinary Medical Association* 171: 1072-1076.
- Robinson, S., Pekkola, J. & Baumgartner, W.-D. 2003. CT reveals overlooked temporal bone injuries. *Diagnostic Imaging Europe* 19: 22-27 + 55.
- Rodríguez, M. J., Agut, A., Latorre, R. & Gil, F. 2002. Ultrasonographic imaging and anatomic sections of the normal equine temporomandibular joint. *Proceedings of the 9th annual conference of the European Association of Veterinary Diagnostic Imaging, Archena, Spain*. 118.
- Rohleder, J. J., Jones, C. J., Duncan, R. B., Larson, M. M., Waldron, D. D. & Tromblee, T. 2006. Comparative performance of radiography and computed tomography in the diagnosis of middle ear disease in 31 dogs. *Veterinary Radiology and Ultrasound* 47: 45-52.
- Rose, W. R. 1977. Small animal clinical otology: radiology. *Veterinary Medicine, Small Animal Clinician* 72: 1508-1511.
- Russo, M., Covelli, E. M., Meomartino, L., Lamb, C. R. & Brunetti, A. 2002. Computed tomographic anatomy of the canine inner and middle ear. *Veterinary Radiology and Ultrasound* 43: 22-26.

- Saito, K., Nakaji, S., Umeda, T., Shimoyama, T., Sugawara, K. & Yamamoto, Y. 2003. Development of predictive equations for body density of sumo wrestlers using B-mode ultrasound for the determination of subcutaneous fat thickness. *British Journal of Sports Medicine* 37: 144-148.
- Sanchez, I., Hathcock, J. T. & Henderson, R. A. 1987. What is your diagnosis? *Journal of the American Veterinary Medical Association* 191: 731-732.
- Sandersen, C., Guyot, H., Vandeputte, S., Carstanjen, B., Amory, H. & Rollin, F. 2003. Speed of sound measurements in the evaluation of bone properties in Holstein-Friesian cows: a preliminary study. *Acta Veterinaria Scandinavica Supplementum* 2: 149.
- Sawin, P. B., Ranlett, M. & Crary, D. D. 1959. Morphogenetic studies of the rabbit. XXV. The sphenoccipital synchondrosis of the Dachs (chondrodystrophy) rabbit. *American Journal of Anatomy* 105: 257-280.
- Sawin, P. B., Ranlett, M. & Crary, D. D. 1962. Morphogenetic studies of the rabbit. XXIX. Accessory ossification centres at the occipito-vertebral articulation of the Dachs (chondrodystrophy) rabbit. *American Journal of Anatomy* 111: 239-257.
- Scapino, R. 1965. The third joint of the canine jaw. *Journal of Morphology* 116: 23-50.
- Schnelle, G. B. 1994. *Veterinary Radiology*. Philadelphia: North America Veterinarian Inc.
- Schwarz, C. 1993. *The Chambers Dictionary*. London: Chambers Harrop Publishers Ltd.
- Schwarz, T., Sullivan, M. & Hartung, K. 2000. Radiographic anatomy of the cribriform plate (*Lamina cribrosa*). *Veterinary Radiology and Ultrasound* 41: 220-225.
- Schwarz, T., Weller, R., Dickie, A. M., Konar, M. & Sullivan, M. 2002. Imaging of the canine and feline temporomandibular joint: A review. *Veterinary Radiology and Ultrasound* 43: 85-97.
- Seitz, S. E., Losonsky, J. M. & Marretta, A. M. 1996. Computed tomographic appearance of inflammatory polyps in three cats. *Veterinary Radiology and Ultrasound* 37: 99-104.
- Sether, L. A., Nguyen, C., Yu, S. N., Haughton, V. M., Ho, K. C., Biller, D. S., Strandt, J. A. & Eurell, J. C. 1990. Canine intervertebral disks: correlation of anatomy and MR imaging. *Radiology* 175: 207-211.
- Shell, L. G. 1988. Otitis media and otitis interna etiology, diagnosis and medical management. *Veterinary Clinics of North America : Small Animal Practice* 18: 885-899.
- Shengyi, T. & Yinghua, X. 1991. Biomechanical properties and collagen fiber orientation of TMJ discs in dogs: Part 1. Gross anatomy and collagen fiber orientation of the discs. *Journal of Craniomandibular Disorders: Facial and Oral Pain* 5: 28-34.
- Shepherd, M. C. & Pilsworth, R. C. 1994. The use of ultrasound in the diagnosis of pelvic fractures. *Equine Veterinary Education* 6: 223-227.
- Shively, M. J. 1979. Xeroradiographic anatomy of the domesticated rabbit (*Oryctolagus cuniculus*) Part I: Head, thorax and thoracic limb. *The Southwestern Veterinarian* 32: 219-233.

- Shores, A. 1993. Magnetic resonance imaging. *Veterinary Clinics of North America: Small Animal Practice* 23: 427-459.
- Sicher, H. 1962. Temporomandibular articulation concepts and misconceptions. *Journal of Oral Surgery* 20: 281-284.
- Smallwood, J. E., Shively, M. J. & Rendano, V. T. 1985. A standardized nomenclature for radiographic projections used in veterinary medicine. *Veterinary Radiology* 26: 2-9.
- Smith, D. T. & Webster, L. T. 1925. Epidemiological studies on respiratory infections of the rabbit. VI Etiology of otitis media. *Journal of Experimental Medicine* 41: 275-283.
- Snaps, F. R., Saunders, J. H., Park, R. D., Daenen, B., Balligand, M. H. & Dondelinger, R. F. 1998. Comparison of spin echo, gradient echo and fat saturation magnetic resonance imaging sequences for imaging the canine elbow. *Veterinary Radiology and Ultrasound* 39: 518-523.
- Snyder, S. B., Fox, J. G. & Soave, O. A. 1973. Subclinical otitis media associated with *Pasteurella multocida* infections in New Zealand white rabbits (*Oryctolagus cuniculus*). *Laboratory Animal Science* 23: 270-272.
- Soler, M., Agut, A., Larorre, R., Murciano, J. & Gil, F. 2002. Plastinated sections of the canine stifle joint used as a tool for the interpretation of magnetic resonance imaging. *Proceedings of the 9th annual conference of the European Association of Veterinary Diagnostic Imaging*. Archena, Spain. 90.
- Spruell, J. S. A. 1964. Treatment of otitis media in the dog. *Journal of Small Animal Medicine* 5: 107-152.
- Stead, C. 1984. The temporomandibular joint. In Houlton, J. & Collison, R. (Eds) *BSAVA Manual of Small Animal Arthrology* (pp. 326-327). Cheltenham BSAVA.
- Stedman, T. L. 2006. *Stedman's Medical Dictionary*. Philadelphia: Lippincott, Williams and Wilkins.
- Stefanoff, V. I. 1992. Ultrasound imaging of the TMJ disc in asymptomatic volunteers. *Journal of Cranio-Maxillofacial Surgery* 20: 337-340.
- Steiss, J. E. 2000. Physical therapy modalities: therapeutic ultrasound and phonophoresis. *Compendium on Continuing Education for the Practicing Veterinarian* 22: 690-693.
- Stelnicki, E. J., Stucki-McCormick, S. U., Rowe, N. & McCarthy, J. G. 2001. Remodelling of the temporomandibular joint following mandibular distraction osteogenesis in the transverse dimension. *Plastic and Reconstructive Surgery* 107: 647-658.
- Stern-Bertholtz, N., Sjoström, L. & Wallin Håkanson, N. 2003. Primary secretory otitis media in the Cavalier King Charles Spaniel: a review of 61 cases. *Journal of Small Animal Practice* 44: 253-256.
- Stewart, W. C., Baker, G. J. & Lee, R. 1975. Temporomandibular subluxation in a dog: a case report. *Journal of Small Animal Practice* 16: 345-349.

- Stone, E. A., Goldschmidt, M. H. & Littman, M. P. 1983. Squamous cell carcinoma of the middle ear in a cat. *Journal of Small Animal Practice* 24: 647-651.
- Ström, D., Holm, S., Clemensson, E., Haraldson, T. & Carlsson, G. E. 1988. Gross Anatomy of the craniomandibular joint and masticatory muscles of the dog. *Archives of Oral Biology* 33: 597-604.
- Suarez, F. R., Bhussry, B. R., Neff, P. A., Huang, H. K. & Vaughn, D. 1980. A preliminary study of computerised tomographs of the temporomandibular joint. *Compendium on Continuing Education* 1: 217-222.
- Suckow, M. A., Brammer, D. W., Rush, H. G. & Chrisp, C. E. 2002. Biology and diseases of rabbits. In Fox, J. G., Anderson, L. C., Loew, F. M. & Quimby, F. W. (Eds) *Laboratory Animal Medicine* (pp. 339-340). Orlando: Academic Press.
- Sullivan M. 1989. Temporomandibular ankylosis. *Journal of Small Animal Practice* 30: 401-405.
- Sullivan, M. 1995. The head and Neck - The ear and temporo-mandibular joints. In Lee, R. (Ed) *Manual of Small Animal Diagnostic Imaging* (pp. 21-23). Cheltenham: BSAVA.
- Swartz, J. D. 1983. High-resolution computed tomography of the middle ear and mastoid. Part I: Normal radioanatomy including normal variations. *Radiology* 148: 449-454.
- Tanaka, E., Tanaka, M. & Miyawaki, Y. T. K. 1999. Viscoelastic properties of canine temporomandibular joint disc in compressive load-relaxation. *Archives of Oral Biology* 44: 1021-1026.
- Tasaki, M. M. & Westesson, P. L. 1993. Temporomandibular joint: diagnostic accuracy with sagittal and coronal MR imaging. *Radiology* 186: 723-729.
- Temple, R. S., Stonaker, H. H., Howry, D., Posakony, G. & Hazaleus, M. H. 1956. Ultrasonic and conductive methods for estimating fat thickness in live cattle. *Proceedings of the American Society of Animal Production (Western Section)* 7: LXX-1-LXX-5.
- Thompson, H. & Irvine, R. 2007. Personal communication. *Division of Pathological Sciences, University of Glasgow*.
- Thompson, J. R., Christiansen, E., Hasso, A. N. & Hinshaw, D. B. 1984. Temporomandibular joints: high resolution computed tomographic evaluation. *Radiology* 150: 105-110.
- Thomson, C. E., Kornegay, J. N., Burn, R. A., Drayer, B. P., Hadley, D. M., Levesque, D. C., Gainsburg, L. A., Lane, S. B., Sharp, N. J. H. & Wheeler, S. J. 1993. Magnetic resonance imaging - a general overview of principles and examples in veterinary neurodiagnosis. *Veterinary Radiology and Ultrasound* 34: 2-17.
- Thrall, D. E. 2002. *Textbook of Veterinary Diagnostic Radiology*. Philadelphia: W.B. Saunders.
- Ticer, J. W. & Spencer, C. P. 1978. Injury of the feline temporomandibular joint: Radiographic signs. *Journal of the American Veterinary Radiology Society* 19: 146-156.

- Tidwell, A. S. 1999. Advanced imaging concepts: A pictorial glossary of CT and MRI technology. *Clinical Techniques in Small Animal Practice* 14: 65-111.
- Tietje, S., Becker, M. & Böckenhoff, G. 1996. Computed tomographic evaluation of head diseases in the horse: 15 cases. *Equine Veterinary Journal* 28: 98-105.
- Tojo, M., Matsuda, H., Fukui, K., Sasai, H. & Baba, E. 1985. Experimental induction of secretory and purulent otitis media by surgical obstruction of the eustachian tube in dogs. *Journal of Small Animal Practice* 26: 81-89.
- Toyras, J., Nieminen, M. T., Kroger, H. & Jurvelin, J. S. 2002. Bone mineral density, ultrasound velocity, and broadband attenuation predict mechanical properties of trabecular bone differently. *Bone* 31: 503-507.
- Trevor, P. B. & Martin, R. A. 1993. Tympanic bulla osteotomy for treatment of middle-ear disease in cats: 19 cases (1984-1991). *Journal of the American Veterinary Medical Association* 202: 123-128.
- Tucker, R. L. & Farrell, E. 2001. Computed tomography and magnetic resonance imaging of the equine head. *Veterinary Clinics of North America : Equine Practice*. 17: 131-144.
- Tucker, R. L. & Sande, R. D. 2001. Computed tomography and magnetic resonance imaging of the equine musculoskeletal conditions. *Veterinary Clinics of North America : Equine Practice* 17: 145-157.
- Twemlow, S. 1991. Computerised tomography: its role in the assessment of ear disease. *Radiography Today* 57: 22-26.
- Valente, A. L. S., Cuenca, R., Zomora, M., Parga, M. L., Lavin, S., Alegre, F. & Marco, I. 2007. Normal multi-detector computed tomography of the vertebral column and coelomic structures of the loggerhead sea turtle (*Caretta caretta*). *The Veterinary Journal* In press.
- van Bree, H., Degryse, H., van Ryssen, B., Ramon, F. & Desmidt, M. 1993. Pathological correlations with magnetic resonance images of osteochondrosis lesions in canine shoulders. *Journal of the American Veterinary Medical Association* 202: 1099-1105.
- Vollmerhaus, B. & Roos, H. 2003. Die transversale Kieferbewegung (translationsbewegung) des Hundes, zugleich ein Hinweis auf die Kiefergelenkdysplasie beim Dachshund. *Anatomia, Histologia, Embryologia: Veterinary Medicine Series C* 25: 145-149.
- Vollmerhaus, B., Roos, H. & Brunberg, L. 1996. Anatomic basis and radiological findings of the temporomandibular joint in Dachshunds. *Kleintierpraxis* 41: 787-792.
- Warmerdam, E. P. L., Klein, W. R. & van Herpen, B. P. J. M. 1997. Infectious temporomandibular joint disease in the horse: computed tomographic diagnosis and treatment of two cases. *Veterinary Record* 141: 172-174.
- Warmerdam, E. P. L. & van Weeren, P. R. 1996. Computed tomography and treatment of chronic temporomandibular joint arthritis in a sheep- a case study. *Veterinary Quarterly* 18: S94-S96.

- Weijjs, W. A. & Dantuma, R. 1981. Functional anatomy of the masticatory apparatus in the rabbit (*Oryctolagus cuniculus L.*). *Netherlands Journal of Zoology* 31: 99-147.
- Weller, R., Taylor, S., Maierl, J., Cauvin, E.R. & May, S.A. 1999a. Ultrasonographic anatomy of the equine temporomandibular joint. *Equine Veterinary Journal* 31: 529-532.
- Weller, R., Cauvin, E.R., Bowen, I.M. & May, S.A. 1999b. Comparison of radiography, scintigraphy and ultrasonography in the diagnosis of a case of temporomandibular joint arthropathy in a horse. *Veterinary Record* 144: 377-379.
- White, R. A. S. 2003. Middle ear. In Slatter, D. (Ed) *Textbook of Small Animal Surgery* (pp. 1757-1767). Philadelphia: Elsevier Science.
- Whitelock, R. G., Dyce, J. & Houlton, J. E. F. 1997. A review of 30 tumours affecting joints. *Veterinary Comparative Traumatology and Orthopaedics* 10: 146-152.
- Whittaker, G. E. 2007. Plastination. www.humanbiology.curtin.edu.au/plastination.html Curtin University School of Biomedical Sciences website.
- Widmer, W. R., Buckwalter, K. A., Braunstein, E. M., Visco, D. M. & O'Connor, B. L. 1991. Principles of magnetic resonance imaging and application to the stifle in dogs. *Journal of the American Veterinary Medical Association* 198: 1914-1922.
- Wikipedia 2006a. History of CT. http://en.wikipedia.org/wiki/Computed_tomography The Free Encyclopedia.
- Wikipedia 2006b. MRI. <http://en.wikipedia.org/wiki/MRI> The Free Encyclopedia.
- Wild, J. J. 1950. The use of ultrasonic pulses for the measurement of biological tissues and the detection of density changes. *Surgery* 27: 183-188.
- Williamson, H. D. 1978. The new photography - A short history of veterinary diagnostic radiology. *Veterinary Record* 103: 84-87.
- Wolvekamp, P. & Oschwald, C. 1991. Small Mammals : Rabbit. In Rubel, Isenbugel & Wolvekamp. (Eds) *Atlas of Diagnostic Radiology of Exotic Pets.* (pp. 30-33). London: Wolfe Publishing Limited.
- Wright, J. W., Wright, J. W. & Hicks, G. 1982. Polytomography and congenital anomalies of the ear. *Annals of Otology, Rhinology and Laryngology* 91: 1-4.
- Zhao BoSen.Basir, O. A. & Mittal, G. S. 2003. Detection of metal, glass and plastic pieces in bottled beverages using ultrasound. *Food Research International* 36: 513-521.
- Zhou, Y. C., Wang, J., Zhang, B. & Su, Y. Q. 2002. Ultrasonic immunization of sea bream, *Pagrus major*, with a mixed vaccine against *Vibrio alginolyticus* and *V. anguillarum*. *Journal of Fish Diseases* 25: 325-331.
- Ziemer, L. S., Schwarz T & Sullivan M 2003. Otolithiasis in 3 dogs. *Veterinary Radiology and Ultrasound* 44: 28-31.
- Zook, B. C., Hitzelberg, R. A., Fike, J. R. & Bradley, E. W. 1981. Anatomy of the beagle in cross-section: head and neck. *American Journal of Veterinary Research* 42: 844-849.